SYNTHESIS OF KAINIC ACID DERIVATIVES AND THEIR APPLICATION AS KAINATE RECEPTORS PROBES

by

Zhenlin Tian

B.Sc., Hubei University of Technology, 2010
M.Sc., East China University of Science and Technology, 2013

A thesis submitted in partial fulfillment of
the requirements for the degree of

DOCTOR OF PHILOSOPHY

in
THE COLLEGE OF GRADUATE STUDIES
(Chemistry)

THE UNIVERSITY OF BRITISH COLUMBIA
(Okanagan)

July 2019

The following individuals certify that they have read, and recommend to the College of Graduate Studies for acceptance, a thesis/dissertation entitled:

Synthesis of kainic acid derivatives and their application as kainate receptors probes

submitted by Zhenlin Tian in partial fulfillment of the requirements of

the degree of Doctor of Philosophy in Chemistry .

Dr. Fred Menard, Department of Chemistry, UBC Okanagan

Supervisor

Dr. Paul Shipley, Department of Chemistry, UBC Okanagan

Supervisory Committee Member

Dr. Isaac T.S. Li, Department of Chemistry, UBC Okanagan

Supervisory Committee Member

Dr. Gregory Dake, Department of Chemistry, UBC Vancouver

University Examiner

Dr. Jeffrey Keillor, Department of Chemistry and Biomolecular Sciences, University of Ottawa

External Examiner

Abstract

Kainate receptors play important roles in the central nervous system. However, investigating their role in physiology is hampered by the current lack of tools to study them in dynamic cellular contexts. This thesis describes the synthesis of C4-kainoids and their derivatives, which are designed to serve as chemical probes to study kainate receptors in neurobiology.

Chapter 1 provides a brief introduction of kainate receptors' roles in central nervous systems and an overview of existing probes for glutamate receptors.

Chapter 2 presented a comprehensive structure/activity analysis for efficient KARs ligands. This chapter reviews all reported kainic acid analogs that have been biologically tested and identifies systematic trends in biological activity of these analogs. These trends combined with protein crystallographic studies led us to identify structural guidelines that must be respected to design the next generation of efficient ligands for kainate receptors. These guidelines informed our synthetic design of the kainoid chemical probes presented in subsequent chapters.

Chapter 3 focuses on the development of a synthetic strategy of kainic acid analogs that: (1) is short, (2) is high-yielding and scalable, and (3) allows easy variation of substituents at the C4 position of kainic acid. It resulted in a general stereoselective synthesis of 4-substituted kainoids: kainic acid and its natural isomers were synthesized in 8 to 11 steps from the commercially available 4-hydroxyproline. The sequence also enables a late-stage modification of C4 substituents with sp^2 nucleophiles. Stereoselective steps include a cerium-promoted nucleophilic addition and a palladium-catalyzed reduction. A 10-step route to a carboxylic acid derivative was also established to enable ready functionalization of the C4 position. This work represents the first unified synthetic route to C4 derivatives of kainic acid.

Chapter 4 describes the synthesis of kainoid derivatives that bear a fluorescent moiety that is used to visualize kainate receptors in living cells. A key intermediate from our general synthesis was exploited to create a novel alkynyl kainoid at the C4 position. This alkynyl kainoid was then coupled with a sulfo-Cy5-azide linker chain using a copper-catalyzed reaction to construct a fluorescent probe. *In vitro* fluorescence imaging performed by confocal microscopy with this far-red fluorescent probe confirmed the capability of labeling kainate receptors. This work reports the synthesis and use of the first fluorescent probe for kainate receptors.

Chapter 5 describes the synthesis of two photo-controllable agonists for kainate receptors: a photocaged and a photoswitchable kainoids. First, our synthesis of one of the most potent unnatural

kainoids (phenylkainic acid) was modified to install a photo-cleavable group on the nitrogen atom. The coumarin-type photo-cleavable group can be removed rapidly upon blue light irradiation, which results in the irreversible release of the agonist to trigger kainate receptor activity. Second, a kainoid derivative was synthesized where the C4 side chain integrates an azobenzene that can be isomerized between its *cis* or *trans* configuration using light. From the structural analyses presented in Chapter 2, only the *trans*-azobenzene form should be able to bind to kainate receptors. Since this photo-isomerization is reversible using visible light (i.e., photoswitch), this kainoid probe can serve as an on/off switch to control the ion conductance of kainate receptors in cells. Kinetic studies by UV-Vis and ^{1}H NMR spectroscopy confirmed that the photoswitch does isomerize upon irradiation.

Overall, a set of new chemical tools for kainate receptors is reported that expands the range of means to perform neurobiological experiments. Along the way, a practical synthetic route to new analogs of kainic acid was established. The compounds presented in this thesis are now being used by colleagues and collaborators to answer questions about the role of kainate receptors in neurons and glial cells that cannot be addressed using current neurobiology methods.

Lay Summary

Kainate receptors (KARs) are crucial for maintaining the function of neurons in the brain. However, the lack of tools that can target KARs has prevented the progress of research about the physiological role of these receptors in neurons. Accordingly, my project aimed at developing chemical biology tools that can solve the limitations of KARs research. First, I developed a set of guidelines to design better chemical tools. Next, I developed a unified strategy to build the tools using organic synthesis. With further modifications, I developed a method to create three types of chemical tools that can be used to probe the activity of KARs in cells: a fluorescent kainoid, a photocaged kainoid, and a photoswitchable kainoid. These probes all have in common that they use light either track, activate, or control KARs in living cells. My compounds will accelerate the research on kainate receptors in neurobiology, which will help find treatments for neurodegenerative diseases.

Preface

This research project was conceived equally by Zhenlin Tian and Dr. Menard, with contributions also provided by Briana Clark and Simon Edelmann. As outlined below, the results of this thesis have led to, or are in the process of being written for, five publications in peer-reviewed journals. Zhenlin Tian wrote all of the manuscripts, including this dissertation.

Chapter 2

Zhenlin Tian, Brianna Clark, Frederic Menard. **Kainic acid-based agonists of glutamate receptors – Structural design guidelines emerge from a SAR analysis**. *ACS Chemical Neuroscience* **2019** (Under review).

Zhenlin Tian and Dr. Menard defined the scope of the manuscript. Zhenlin Tian: (1) conducted the literature search and structure analysis of all the reported kainoids; (2) compared the bioactivities of kainoids systematically; (3) wrote the manuscript and prepared the figures with the help of Dr. Menard; (4) assembled and compiled the tables listing all literature assays in the supplementary information files. Brianna Clark and Dr. Menard researched, analyzed and created the gene sequence alignments.

Chapter 3

Zhenlin Tian, Frederic Menard. **Synthesis of kainoids and C4 derivatives**. *Journal of Organic Chemistry* **2018**, 83, 6162.

Zhenlin Tian and Dr. Menard defined the scope of this manuscript. Zhenlin Tian: (1) conducted the synthetic experiments for all the compounds included in this paper; (2) conducted all characterization experiments, including NMR, IR and MP; (3) processed and analyzed all data the experimental data; (4) wrote the manuscript and prepared the submission with the help of Dr. Menard.

Chapter 4

Zhenlin Tian, Frederic Menard. **An affinity probe for kainate receptors**, *Journal of the American Chemical Society* (manuscript in preparation).

Zhenlin Tian and Dr. Menard defined the scope of this manuscript. Zhenlin Tian: (1) conducted the synthetic experiments for all the compounds included in this paper; (2) performed all

characterization experiments, including NMR, IR and MP; (3) conducted molecular biology experiments, including plasmid propagation and transfection; (4) carried out the confocal imaging experiments in living cells with the help of Dr. Menard; (5) processed and analyzed all data the experimental data; (6) wrote the manuscript and prepared the submission with the help of Dr. Menard.

Chapter 5

Zhenlin Tian, Simon Edelmann, Frederic Menard. **A coumarin-caged kainoid as a blue-light releasable agonist for kainate receptors.** (manuscript in preparation).

Zhenlin Tian and Dr. Menard defined the scope of this manuscript. Zhenlin Tian: (1) conducted the synthetic experiments with the help of Simon Edelmann for several precursor synthesis; (2) performed all characterization and photochemistry experiments; (3) processed and analyzed all data the experimental data; (4) wrote the manuscript and prepared the submission with the help of Dr. Menard and Simon Edelmann for reviewing.

Zhenlin Tian, Frederic Menard. **A visible light switchable agonist for kainate receptors**. (manuscript in preparation).

Zhenlin Tian and Dr. Menard defined the scope of this manuscript. Zhenlin Tian: (1) conducted the synthetic experiments for all the compounds involved; (2) performed all characterization and photochemistry experiments; (3) processed and analyzed all data the experimental data; (4) wrote the manuscript and prepared the submission with the help of Dr. Menard.

Table of Contents

Abbreviations

General Abbreviations in Schemes:

aq	aqueous
atm	atmosphere
c	concentration
cat.	catalytic/catalyst
conv.	conversion
δ	chemical shift
Δ	heat
d	day(s) (e.g., 2 d)
dr	diastereomeric ratio
ee	enantiomeric excess
eq	equation
equiv.	molar equivalent(s)
EDG	electron donating group
EWG	electron withdrawing group
h	hour(s) (e.g., 3 h)
h□	light irradiation
min	minute(s)
MS	molecular sieves
NMR	nuclear magnetic resonance
quant.	quantitative yield
R_f	retardation factor
rt (rt)	room temperature (22 °C)
sat.	saturated
UV	ultraviolet
Vis	visible
NOE	nuclear Overhauser effect
LED	light-emitting diode
CNS	central nervous system
PLC	phospholipase C
PKC	protein kinase C
LBD	ligand binding domain
SAR	structure–activity relationship
KAR	kainate receptor
GluR	glutamate receptor

Chemical Abbreviations

Ac	acetyl
AcOH	acetic acid
Ac_2O	acetic anhydride
Ar	aryl
Boc	*tert*-butoxycarbonyl
Bu	butyl
t-Bu	*tert*-butyl
Bz	benzoyl
Cbz	benzyloxycarbonyl
Cy	cyclohexyl
Pf.	9-Phenyl-9-fluorenyl
dba	dibenzylideneacetone
DCM	dichloromethane
DCE	1,2-dichloroethane
DIPEA	*N,N'*-diisopropylethylamine
Diox.	1,4-dioxane
DMSO	dimethylsulfoxide
TMSCl	trimethylsilyl chloride
Et	ethyl
Bu	butyl
Et_3N	triethylamine
Et_2O	diethyl ether
EDCI	1-ethyl-3-(3-dimethylaminopropyl) carbodiimide
DMAP	4-dimethylaminopyridine
HOBT	hydroxybenzotriazole
Pf	9-phenyl-9-fluorenyl
DMP	Dess–Martin periodinane
TBTA	tris(benzyltriazolylmethyl)amine
DECM	7-(diethylamino)coumarinyl
MNI	4-Methoxy-7-nitroindolinyl
EtOAc	ethyl acetate
Hex	hexanes
MCPBA	*m*-chloroperoxybenzoic acid
Me	methyl
MeCN	acetonitrile
MeOH	methanol
Ph	phenyl
i-Pr	isopropyl
py	pyridine
p-Ns	4-nitrobenzenesulfonyl
R	undefined substituent
TFA	trifluoroacetate
THF	tetrahydrofuran
TLC	thin layer chromatography
TMS	trimethylsilyl
Tf	trifluoromethansulfonyl
Ts	tosyl
AMPA	α -amino-3-hydroxy-5-methyl-4-isoxazolepropionic acid
NMDA	*N*-Methyl-D-aspartic acid
KA	kainic acid
DA	domoic acid
PhKA	phenylkainic acid
GABA	γ -aminobutyric acid
Glu	Glutamic acid
DMA-DMF	*N,N*-dimethylformamide dimethyl acetal
CNQX	6-cyano-7-nitroquinoxaline-2,3-dione
PFQX	6-pyrrolyl-7-trifluoromethyl-quinoxaline- 2,3-dione
Cy5	cyanine 5

List of Schemes

List of Figures

List of Tables

Acknowledgments

I would like to thank my supervisor, Dr. Frederic Menard, for patient guidance in chemistry learning and assistance on the troubleshooting for the research projects. I appreciate your continuing support during my Ph.D. learning. And a huge thanks to your great efforts on bio-experiments and manuscript publication.

I am grateful to Dr. Vojtech Kapras for insightful discussions. Thanks to Dr. Zandberg and Matt Noestedem for HPLC and mass spectrometry analyses. Thanks to Simon Edelmann for the synthesis of precursors. Thanks to Mitra Tabatabaee for the help with biological experiments, also to Brianna Clark for the gene analysis of kainate receptors project.

A huge thanks to my committee members, Dr. Paul Shipley and Dr. Issac Li. Thanks, Dr. Shipley for NMR support and guidance. Thank you to Dr. Li for excellent suggestions on the biological experiments.

To my collaborators, Zongjie Wang, Dr. Xian Jian and Morgan A. Alford, thank you for your efficient work and productivity on the projects. And thanks for allowing me to be involved in the novel materials projects.

I gratefully acknowledge UBC for the financial support of University Graduate Fellowships and Graduate Dean's Thesis Fellowship. Also, thanks to UBC for the travel grants that enabled me to attend chemistry conferences and have chances to access the Canadian Chemistry community. Great thanks to Dr. Sandra Mecklenburg for offering the opportunity of teaching assistantships and the access to instruments in undergraduate labs.

Dedication

To Beibei Chen, my wife, thank you for your patience, resilience and selfless support during these four years. I appreciate your continuous learning to adapt to the local work and life. It is one of the most important driving forces for me cracking all the difficulties in my projects. Please forgive my absence during your holidays due to experiments. Without you, I would not be able to finish my Ph.D.

献给我的爱人–陈贝贝，以及我的父亲母亲。

Zhenlin Tian

Kelowna, March 2019

Chapter 1

Introduction

Ionotropic glutamate receptors (iGluRs) are glutamate-gated ion channels that mediate the principal excitatory neurotransmission in the brain (Figure 1–1).[1] They are categorized into three subgroups based on their sensitivity to agonists: α-amino-3-hydroxy-5-methyl-4-isoxazole propionic acid (AMPA), *N*-methyl-D-aspartate (NMDA), and kainate or kainic acid (KA).[1] Each iGluR subtype has modular domains that assemble into tetramers to form ligand-gated ion channels; they include an amino-terminal domain (ATD), a ligand-binding domain (LBD), a transmembrane domain (TMD), and a carboxy-terminal domain (CTD, Figure 1–1c).[2]

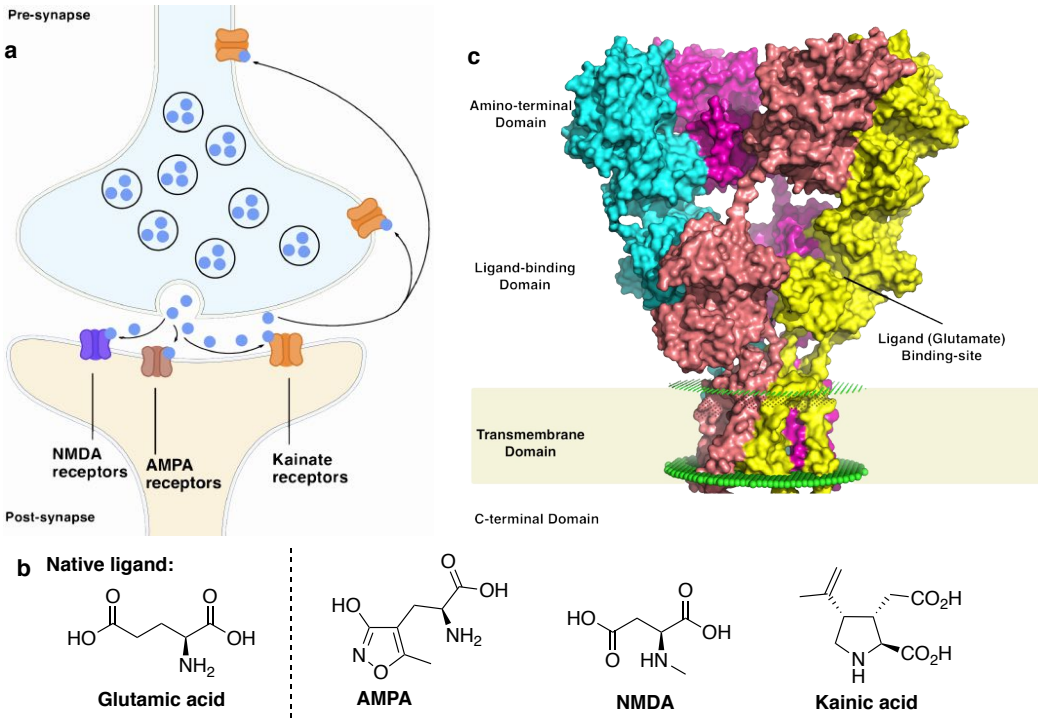

Figure 1–1. (A) In neurons, iGluRs are present at both the pre- and post-synapse.[3] (B) Naturally occurring agonists of iGluRs: AMPA, NMDA, and kainic acid. (C) A functional iGluR protein is composed of four monomers that assemble to create a central channel pore to allow passage of cationic ions through the cell membrane.[4]

In mammals, cationic ion channels of iGluRs open upon glutamate binding to generate synaptic currents for neuron communication.[2] These events induce long-term potentiation (LTP) and long-term depression (LTD), which are fundamental to learning and memory formation.[5] The dysfunction of GluRs leads to neurological disorders and neurodegenerative diseases. Over the past three decades, scientists have done extensive studies on the molecular mechanism of iGluRs. A variety of X-ray crystallography and cryogenic electron microscopy (cryo-EM) studies of GluRs have been reported.[2,6,7] They show that conformational changes underlying activation and desensitization occur mainly in the LBD and ion channel regions. Upon binding of glutamate, the clamshell closure of the LBD imparts a rotation of the pore helices, which opens GluRs for Ca^{2+} inflow. In other words, the conformational change of LBD leads to the open state of iGluRs.[8] This model can also predict the conformation changes of iGluR domains that lead to different functional states.[8,9]

However, the exact regulation pathways of different iGluRs members remain uncertain. The expression level and trafficking of iGluRs in CNS is another factor that impacts neurotransmission.[5] There is now extensive evidence confirming that expression of GluRs can be activity-induced in either positive or negative feedback. For instance, immature synapse models have been shown to display NMDARs-mediated currents only,[10] but an AMPA-type response was observed after being subjected to LTP.[11] This rapid unsilencing of synapses was caused by AMPARs "appearing" at initially AMPARs-void postsynapses.[12] This finding has sparked interest in differential GluRs expression and trafficking events at synaptic termini.[5] The basic mechanism of this trafficking is thought to involve phosphorylation and dephosphorylation of GluRs with their subsequent insertion at synapse sites. However, due to the lack of tracking tools, the molecular mechanisms governing the movement of GluRs in and out of synapse boutons are still elusive.[13]

1.1 Distinct role of kainic acid receptors in CNS

Among the ionotropic family of glutamate receptors (iGluR), the AMPA and NMDA receptors have been studied the most. In contrast, the role of kainic acid-sensitive receptors (KAR) in CNS is still not well understood.[14] There are five subtypes of KAR proteins (Table 1–1).[15] For consistency, only the more recent nomenclature will be used in this thesis, i.e., GluK1-5.

Unlike AMPA and NMDA receptors that are located on the postsynaptic bouton, KARs are present at *both* the pre- and post-synapse—although higher densities are found at the pre-synapse.[16] This ubiquitous feature allows KARs to contribute to several functions: presynaptic modulation of excitatory and inhibitory currents, postsynaptic depolarization of excitatory

synapses, refinement of synaptic strength (during development and synaptic plasticity), and enhancement of neuronal excitability. The bidirectional modulation role of KARs at synapses has also been confirmed in mossy fibers and CA3 region of the hippocampus.[16] This dual role affects the balance between excitation and inhibition in the neuronal network and has important implications for cognition.[16]

Table 1–1. NC-IUPHAR* nomenclature of kainic acid receptors. The receptor used in this thesis is shown in bold.

Receptor Family	NC-IUPHAR subunit nomenclature	Previous + unofficial names	Human gene
Kainate receptors	GluK1	GluR5	*GRIK1*
	GluK2	**GluR6**	***GRIK2***
	GluK3	GluR7	*GRIK3*
	GluK4	GluR KA1	*GRIK4*
	GluK5	GluR KA2	*GRIK5*

* NC-IUPHAR: Nomenclature Committee of the International Union of Pharmacology on receptor and drug classification.

The predominant presynaptic localization of KARs suggests that they can facilitate excitatory synaptic plasticity. In early research on GluK2 and GluK3 knockouts mice models, both rapid activation and long-term potentiation (LTP) were impaired in mossy fibers.[17] The same effect was observed by blocking KARs in mossy fibers: LTP was significantly blocked by the selective antagonist LY382884 (Figure 1–2). Surprisingly, this LTP could be still induced by cyanquixaline (CNQX), a non-selective antagonist of AMPARs and KARs.[3,18] These results show that wide-spectrum antagonists are unable to prevent LTP phenomena.[19] As LY382884 is selective for the GluK1 subtype, it suggests that LTP is induced primarily by GluK1. Similarly, Contractor *et al.* have demonstrated that LTP is not abolished in GluK2 knockout mice, while GluK1-deficient mice showed normal LTP at synapses.[5] While much evidence supports a crucial role for KARs in synaptic plasticity, there is no clear explanation for this difference observed in subtype function.[3,19]

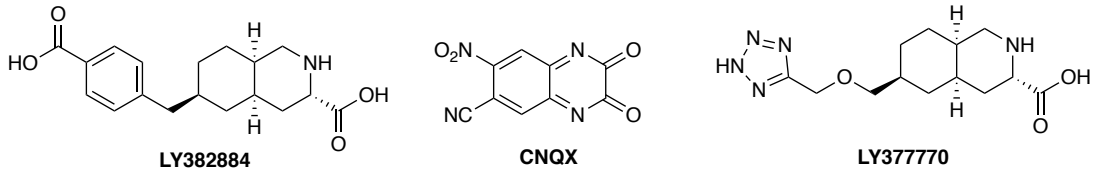

Figure 1–2. Common antagonists used in GluRs neurobiology research.

Besides the regulation roles in ionotropic pathways, KARs are also involved in a metabotropic modulation that is distinct from AMPARs and NMDARs.[19] Studies suggest that KARs can trigger downstream neuron cell signals through an unconventional metabotropic mechanism involving G

protein and secondary messengers (Figure 1–3a). This signaling inhibits gamma-aminobutyric acid (GABA) at pre-synapses, correlates with G protein activation, phospholipase C (PLC) and protein kinase C (PKC) activity, and is followed by signaling modes in dorsal root ganglion neurons. This activity is independent of Ca^{2+} ion flux,[19] but the molecular mechanisms underlying this signaling are unknown. This proposed pathway raises important questions, such as how do KARs activate G proteins and trigger downstream effects. Regardless of the exact mechanisms, an increasing number of physiological functions seem to be regulated by KARs through this unconventional signal. So far, this putative dual signaling appears to be a feature unique to KARs.

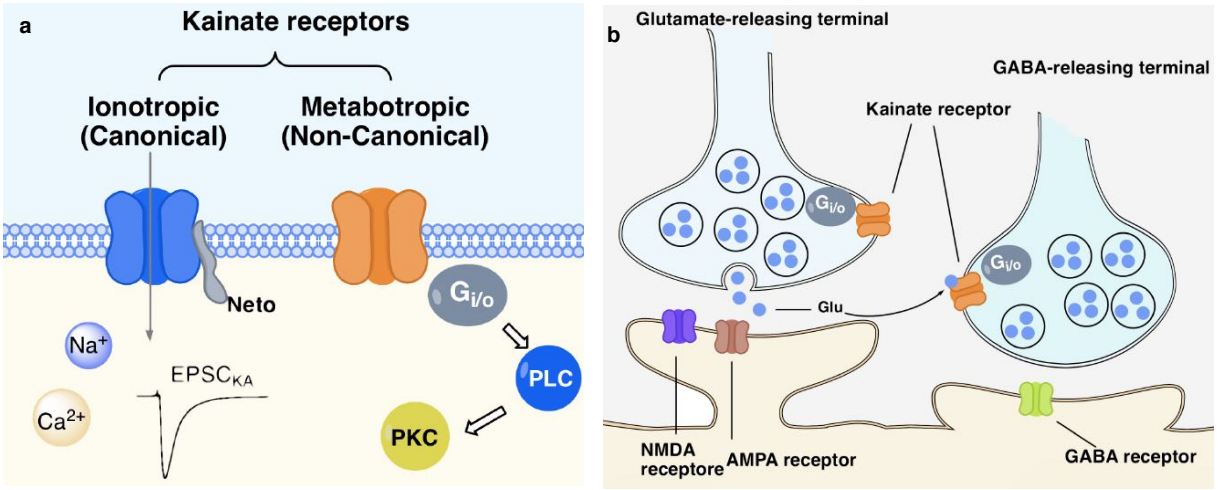

Figure 1–3. Two proposed kainate receptor-mediated signalling pathways. (A) Kainate receptors (KARs) can act via ionotropic and metabotropic pathways.[20] Neto1 and Neto2 auxiliary subunits co-assemble with KARs to modulate their function. In the hippocampus, Neto1 enhances the amplitude and prolongs the kinetics of KAR-mediated currents at synapses between mossy fibers–CA3 pyramidal cells.[21] (B) Kainate receptors-mediated modulation of Glu and GABA release in hippocampus.[16] ESPC: excitatory postsynaptic current. Neto: Neuropilin and tolloid-like protein.

KARs also play important roles in the mediation of GABA transmission in the CNS (Figure 1–3b). Early research has shown that activation of KARs by glutamate in the hippocampus leads to the release of GABA.[16] For example, KAR agonists enhanced the action potential-independent GABA release in both CA1 interneurons and pyramidal cells. The diversity of the select KAR functions presented above offer a glimpse at to why they appear involved in so many neurological diseases. Finding compounds that can modulate KAR activity is an attractive medicinal goal.

1.2 Therapeutic potential of kainic acid receptors

Neuropathology studies have shown that KARs are involved in acute and chronic neurodegenerative diseases, including epilepsy, pain and psychiatric disorders.[20,22] Among these

diseases, KARs have been most prominently associated with epilepsy. This is likely due to the excitatory/inhibitory imbalances caused by abnormal KARs activity.

KAR & epilepsy. It is well known that kainic acid (KA) injection in animal models produces epilepsy symptoms. In fact, KA is routinely used to model epileptic diseases[22] and to evaluate neuroprotective drugs.[23] Moreover, the elimination of GluK2 in knockout mice reduces their seizures after KA injection. These reports indicate that KARs contribute to overexcitability in neurons, which can cause epilepsy. Antagonists of GluK1, e.g., LY377770 and LY382884, demonstrated the ability to prevent the development of epileptic activities in hippocampal slices (Figure 1–2). These agonists reduced seizures both in *vitro* and *vivo*.

KARs & pain. KARs are also expressed in dorsal root ganglion (DRG) and dorsal horn neurons, where they play roles in sensory transmission and pain. For instance, GluK5 is the only ionotropic GluR expressed in DRG and may be involved in nociception in DRG neurons (pain transmission). [19] While pain perception is not a disease per say, chronic pain (persistent recurrent pain) is now a prevalent debilitating neurological disorder. Biological assays with KAR antagonists support their involvement in pain sensation. For example, in a paw-licking experiment induced by formalin, the KAR antagonist LY382884 decreased the pain response in rodents. Similarly, *GRIK1* knockout animal models showed mitigation of pain-associated behaviours.[19] Additional experimental data that are beyond the scope of this review also support a role for KARs in neurophysiological pathologies.

KARs & other disorders. Genetic epidemiology has identified several correlations between KARs and neuropsychiatric disorders. For instance, aberrant GluK4 function has been found to be linked to schizophrenia in some populations. GluK2 and GluK3 are associated with the obsessive-compulsive disorder. GluK3 was also found to be associated with depression, and GluK2 to be associated with autism.[22] However, these epidemiological studies are limited to suggestive correlations, further experimental research is required to identify a causative link to human disease. A recent genetic study also found that loss-of-function mutations in GluK2 correlated with non-syndromic autosomal recessive mental retardation in a consanguineous family, thereby suggesting that GluK2 receptors are essential to brain function in humans.[22] The above genetic associations with neurodevelopmental disorders are consistent with KARs playing an important role in the development/stability of neuronal circuitry. [19] These intriguing associations still await confirmation from molecular and cellular studies, yet they offer clear research opportunities with applications to human disease.

1.3 Limitations in research on kainic acid receptors

Current KAR research relies on agonist and antagonist-induced cell models, and on gene knock-out animal models.[24] The potent agonist neurotoxin kainic acid (KA) is widely used to mimic the effect of glutamate in neurodegenerative models, as well as to distinguish KARs activity from AMPARs and NMDARs.[25]

Kainic acid is typically used in cells or tissues by bath perfusions or by local micro-injections. In animals, the injection of KA leads to seizures, followed by deficiencies in short-term memory and long-term learning, and by depression-like behaviours.[24] In neurons, KA causes an excessive Ca^{2+} influx that eventually induces acute neuron death. The Ca^{2+} influx also increases oxidative stress in neuron cells (via positive feedback loops of reactive oxygen species).[26] In microglia, KA triggers an inflammatory-like response that causes their deleterious activation, leading to outcomes that resemble Parkinson and Alzheimer's diseases.

While KARs' phenotypic role in neurodegenerative diseases has been explored extensively with *GRIK* gene knockout models, our understanding of their biochemical role in these diseases is still superficial.[27] Most current biological methods rely on recombinant gene manipulations and prevent the precise spatio-temporal control of KARs. Moreover, since these techniques can only be used in animal models, their translation to clinical research is also very limited.[24] More importantly, distinguishing the individual contributions of the three classes of GluRs is difficult; a challenge made even greater for KA and AMPA receptors due to the high homology of their binding site for glutamate. Indeed, besides the kainoid neurotoxins, there is still no agonist or antagonist that is selective for KARs over AMPARs.[22]

1.4 Precedents on biosensors and switchable probes for GluRs

A few biosensors have been reported to study iGluRs in neurons. For example, Hamachi *et al.* reported fluorescent probes based on PFQX as selective ligand to label AMPARs in cells (Ax488-5s, Figure 1–4).[28,29] Similarly, Stromgaard *et al.* employed ariotoxin-636 to visualize glutamate channels in hippocampal neurons.[30] These molecules solve two limitations of biological alternatives: they enable the real-time tracking of *native* glutamate receptors in neurons by simple bath application, that is, without genetic modification.

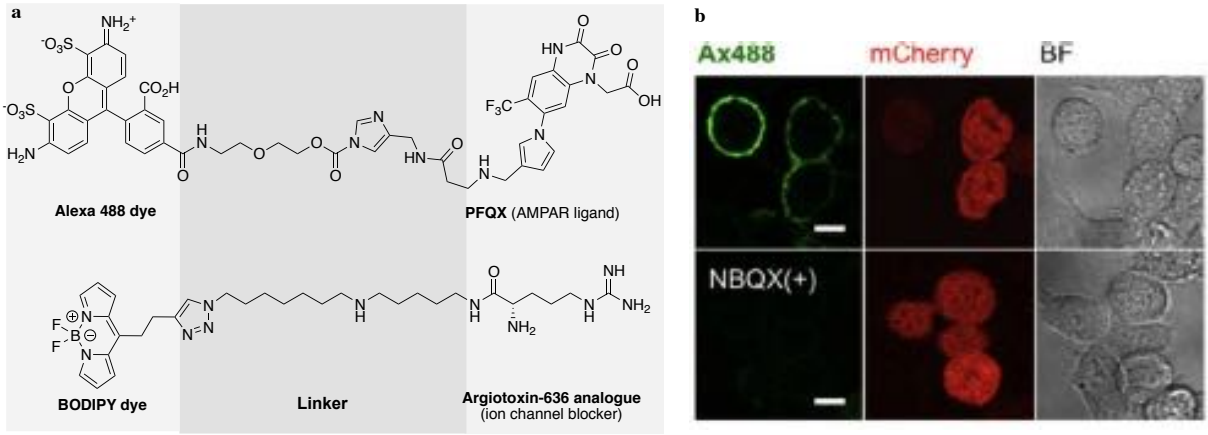

Figure 1–4. Examples of reported fluorescent probes for iGluRs. (A) Structures of **Ax488-5s** and **iGluR probe-1**. (B) Representative fluorescence imaging of AMPA-sensitive GluRs in living cells using Ax488-5s (green dye); mCherry was used as transfection marker for AMPARs.[28]

With the advent of modern photochemistry, new photoactive pharmacology tools have been emerging in ion channels research.[31] The more established photoactive chemical tools for iGluRs study are the photo-caged glutamates pioneered by Ellis-Davies (Figure 1–5).[32-34] For example, the MNI-Glu and DECM-Glu photo-caged compounds were invented by assembling glutamate and a photolabile protecting group. These molecules enable the photo-inducible activation of iGluRs. Upon local light irradiation, the caged glutamate can be released with spatial precision. These photo-caged glutamates have been widely used in neurobiology as tools to activate select neurons or tissues. An important limitation of these compounds is that they release glutamate which by definition activates all GluRs. While useful for physiological studies, these compounds do not allow one to study the contributions of individual classes of ion channels.

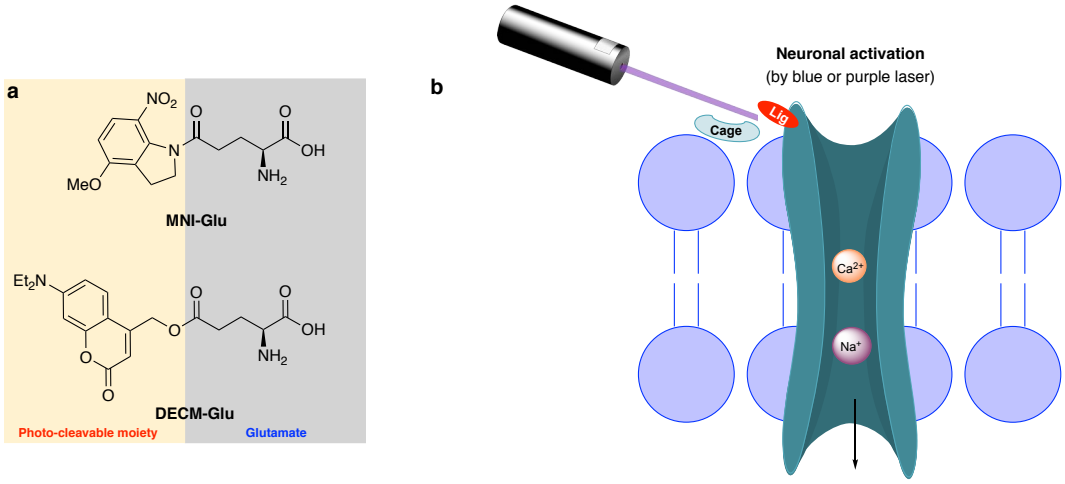

Figure 1–5. (A) Examples of photocaged glutamate molecules. (B) Upon light irradiation, the photosensitive MNI or DECM moieties (photocages) are cleaved and yield the parent carboxylates as formal hydrolysis products equivalents.

Photocaged glutamates are "turn-on" chemical probes: the formation of the active agonist is irreversible once the protecting group is cleaved. A complementary type of chemical probes are *photo-switches*: they rely on an agonist that can be turned on/off reversibly with light. Examples of "photo-switches" for GluRs are depicted in Figure 1–6a. The photoswitch component of the molecules is an azobenzene sidechain attached to known GluRs ligands. Light irradiation triggers a reversible *cis*/*trans* isomerization of the azo double bond. In GluRs, the binding site of the agonists possessed a narrow channel that can only accommodate the *trans*-azobenzene sidechain; consequently, the reversible photoswitching of the *cis*/*trans* sidechain controls the activation ↔ deactivation mode of the receptor.

Due to their well characterized binding site, several photoswitches have been developed for iGluRs.[34,35] For instance, ligands that exert selectivity towards AMPARs, such as AMPA or ShuBQX, were modified with azobenzene components and have been demonstrated to reversibly control AMPAR activation in living systems.[35-37] Furthermore, *in vivo* experiments with photoswitchable compounds in zebrafish suggest that they can even trigger photo-dependent behaviours.[38]

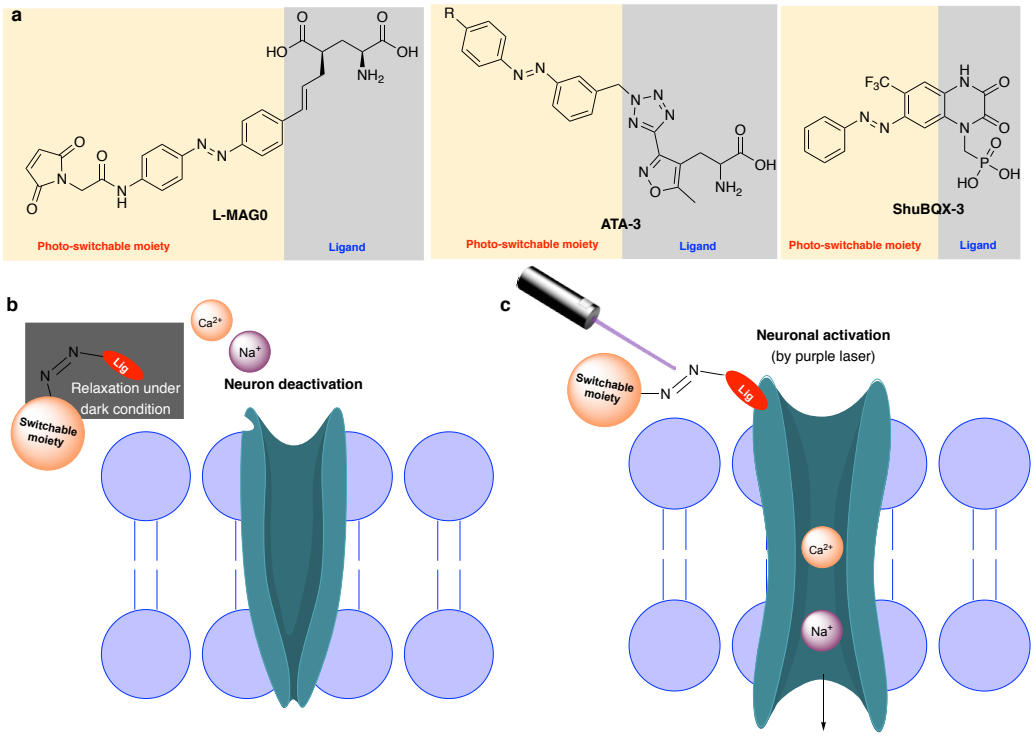

Figure 1–6. Photoswitches for GluRs modulation. (A) Examples of reported GluR photoswitches. (B) The *cis* configuration of the azobenzene in the photoswitches prevents proper binding of the ligand. (C) The *trans* configuration of the azobenzene sidechain matches the LBD's channel and allows the ligand to reach its high affinity binding pocket. Thermodynamically, the azobenzene group prefers to exist in the *trans* configuration under dark condition (thermal), and *cis* confirmation under purple light irradiation (photochemical).

1.5 Thesis overview

While chemical probes have been reported to study GluRs generally, or AMPARs selectively, no tool exists yet that enables the selective visualization or control of KARs. The objective of my research is thus to develop chemical probes to study KARs in living cells without needing the recourse to genetic modifications. Ideally, a set of probes will allow the fluorescence imaging of KARS, and a different set will enable the selective activation or inactivation of KARs. As common structural features, they consist of a ligand, a linker, and a functional moiety (Figure 1–7a). The ligand that will impart selectivity for the KARs—over the NMDA or AMP receptors—is the high affinity neurotoxin kainic acid. This thesis will focus on two types of probes: affinity probes for the visualization of KARs and photo-pharmacological tools for KAR control.

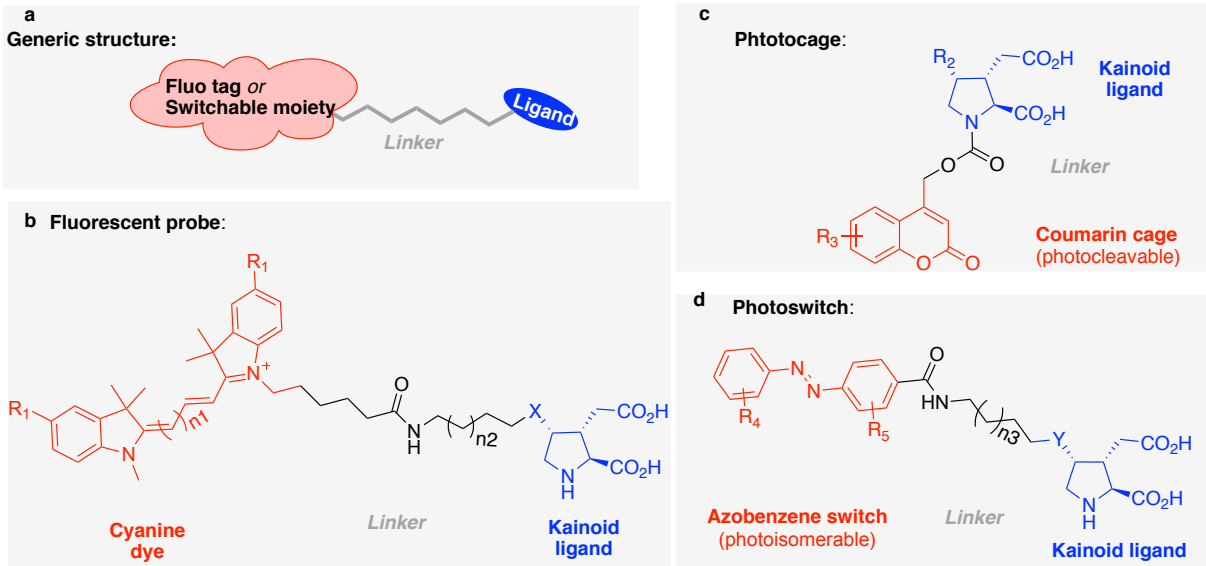

Figure 1–7. General structure of the proposed probes to study kainic acid receptors. (A). Generic structure of proposed probes. (B) The structure of fluorescent probe for KARs. (C). The structure of proposed photocage for KARs. (D). The structure of proposed photoswitch for KARs.

The first challenge in designing probes based on kainic acid required identification the most appropriate site for chemical modification that would still maintain a high binding affinity for KARs. Accordingly, I surveyed all the reported kainoid derivatives that have been tested for their biological activity. Then, I analyzed the relationship between their structure and their activity, and identified a set of guidelines for the best ligand design (Chapter 2). Structural features required for high affinity were extracted from over 100 KARs agonists, they revealed that modifications at C4 of the pyrrolidine ring is the best option. A complementary crystallographic analysis of iGluR proteins complexed with kainoid agonists supported the conclusions.

Next, a practical, scalable synthesis of kainic acid derivatives that can be easily modified at C4 had to be developed. While more than 50 syntheses of kainoids have been reported, none allow for late-stage modification of C4 substituents or are realistically scalable. Thus, I developed a unified synthetic strategy for C4 kainoids (Chapter 3). The synthesis begins with commercially available materials and can diverge into several C4 derivatives. Its effectiveness was demonstrated by preparing natural and unnatural kainoids.

The goal of creating novel chemical probes for KAR studies would be all the more powerful if any probe type could be assembled from a flexible kainoid precursor and the desired reporter tag or switch (Figure 1–7b). Since click chemistry provides a convenient option, I synthesized an alkynyl kainoid. This clickable kainoid was then utilized to construct fluorescent probes for KARs visualization in living cells (Chapter 4). A proof of concept was demonstrated using a red fluorescent probe with GluK2 expressed in model cells.

Finally, my synthetic efforts culminated with the creation of photo-active chemical probes to manipulate KARs function with visible light. Thus, I designed and synthesized photo-controllable KARs agonists (Chapter 5). A coumarin-caged kainoid was synthesized to control KARs with blue light (Figure 1–7c). Also, a photo-switchable kainoid was synthesized to reversibly control KARs (Figure 1–7d). The photo-induced kinetics of cleavage or switching of the probes were evaluated by extensive spectroscopic studies. At the moment of writing, these photoactive probes were being applied in living cells.

Chapter 2

A structure-activity relationship analysis of kainic acid-based agonists

A comprehensive survey is presented of all kainic acid analogs that have been tested for their biological activity. Specifically, this chapter: (1) gathers in a single location all structural variations of kainic acids reported thus far, (2) exposes design rules that must be met to optimize affinity for kainate receptors, and (3) suggests structural insights toward the design of next-generation KA analogs. The available structure-activity relationship (SAR) data were systematically analyzed and combined with the most recent crystallographic studies. From the exercise emerged a set of structural guidelines to help design high-affinity analogs. Given the renewed interest in neuroactive molecules, this chapter aims to guide the synthetic efforts of organic synthesis and facilitate the design of KAR probes.

2.1 Background

Due to KAR selective excitation by kainic acid, KARs were identified as a distinct family.[17] Besides KA, its natural analog-domoic acid (DA, **2**, Figure 2–1) also shows strong affinity with KARs.[39] Those kainoids were first isolated in the 1950s from the red algae.[43,44] Kainoids were initially used as anthelmintic for children in Japan, Southeastern Asia and Taiwan for decades.[40] Owing to the induced epilepsy and seizures by kainic acid and domoic acid,[41] they were abandoned for medicine use in the 1980s. However, their potent action on KARs made them widespread tools in neurobiology study.[3]

In neuro research, KA is utilized in tissue culture and animal to stimulate neurodegenerative models mediated by KARs.[42-44] It is also employed as an activator to validate their identity to distinguish other inotropic glutamate receptors (like AMPA and NMDA receptors). When binding to KARs, KA induces the influx of cellular Ca^{2+}, production of reactive oxygen species and

mitochondrial dysfunction, which leads to neuronal apoptosis and necrosis.[45] Although extensive studies have been conducted on KA induced models, their physiological functions in CNS is still obscure due to the lack of selective tools.[22]

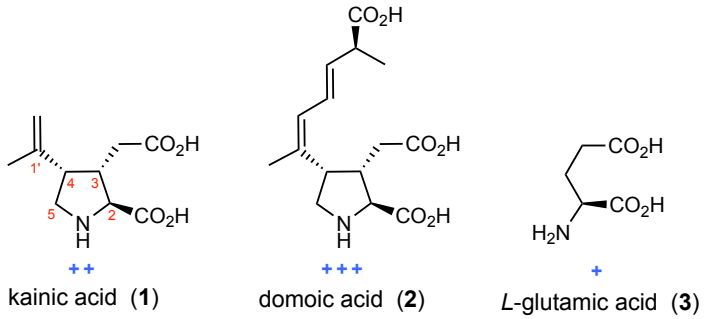

Figure 2–1. Natural kainoids and *L*-glutamic acid

As part of our research program on calcium signalling in glia, we needed to create a KARs–selective chemical probe. Opting to design a kainic acid analog, we looked to the literature to inform our structural design. However, we were surprised to find that, despite the wealth of SAR information that has been accumulated on kainic acid analogs over the past three decades, a systemic analysis of KA analogs' (kainoids) biological effects had never been reported.

In this analysis, we attempt to meet this need: we have gathered in one article, all the KA derivatives that have been biologically tested from natural or synthetic sources. We focus on the SAR of KA derivatives that have been tested for their biological activity. By juxtaposing this dense information, trends emerged in terms of SAR. These trends are supported by crystallographic data from recent reports.

2.2 Structural considerations

The unique activity of kainic acid (**1**) has led to several medicinal chemistry efforts aiming to create kainate analogs with improved potency and increased selectivity toward the KAR subset of glutamate receptors. This section summarizes how structural changes made to KA derivatives influence their biological activity. Results from over 50 studies were gathered and analyzed to identify correlations in structure-activity relationship.

2.2.1 The activity grading system

Direct comparisons between analogs can be difficult to make, as no standardized assay is used in the field. The biological data are reported from assays that use different techniques, different cells/tissue/organism, different iGluR proteins, etc. Consequently, we have opted for a qualitative

system indicating the activity of the compounds (Table 2–1). To enable a systematic comparison of analogs, a relative activity scale was calculated instead of using absolute values (see the original data in Table S2–1 and S2–2, Appendix A). The scale was normalized to positive controls used in each assay, i.e., glutamate, KA or DA. Calculations were always based on the most recent data for each compound. When available, priority was given to Ki or EC50 values with the most studied isoform GluK2 (also known as GluR6). Otherwise, [3H] displacement assays in cells, or activity in neurons were used. If more than one value was found for the same isoform, the average was used. All quantitative data and assay details are listed in a comprehensive table in the accompanying data analysis section (Tables 2–3).

Table 2–1. Qualitative scale used in this analysis

Relative Activity (RA)

Inactive	– –	Inactive		
0 < RA < 0.065	–	Less active than L-Glu		
0.065 ≤ RA < 1	+	Between L-Glu and KA	← *L*-Glu	0.065
1 ≤ RA < 2.89	+ +	Between KA and DA	← kainic acid	1
2.89 ≤ RA	+ + +	Equal or stronger than DA	← domoic acid	2.89

2.2.2 Early SAR studies on kainic acid

Before the age of elucidation of KARs' crystal structures, early SAR studies focused on direct derivatization of glutamic acid and kainic acid (Figure 2–2) to get insight into the features responsible for its binding activity. The acid and amine blocked kainoids (bisester **4** and amide **5**) showed no biological activity in crayfish opener muscle.[51,52] The natural occurring *allo*-kainic acid (**6**) differs from KA only by its epimeric C4 stereocenter and is essentially inactive when compared to the neurotoxin.[51,53] Similarly, inverting the configuration at C2 resulted in the loss of activity (kainoid **7**).[46] Together, these studies revealed that the amine, both carboxylic acids, and the stereocenters are all indispensable for receptor binding.

Interestingly, any steric bulk at C5 is not tolerated. For example, even the addition of a simple methyl group abolished the compounds' binding affinity, irrespective of the substituent's stereochemistry (kainoid **8** and **9**).[47] This suggested a closely nested interaction between KA's basic nitrogen and the protein's binding site. However, **10** and **11** lacking the C4 *iso*-propene are active for GluRs, but lost most of its activity on KARs.[55,56] It suggested that there is more to KA than simply being a rigid form of glutamic acid.

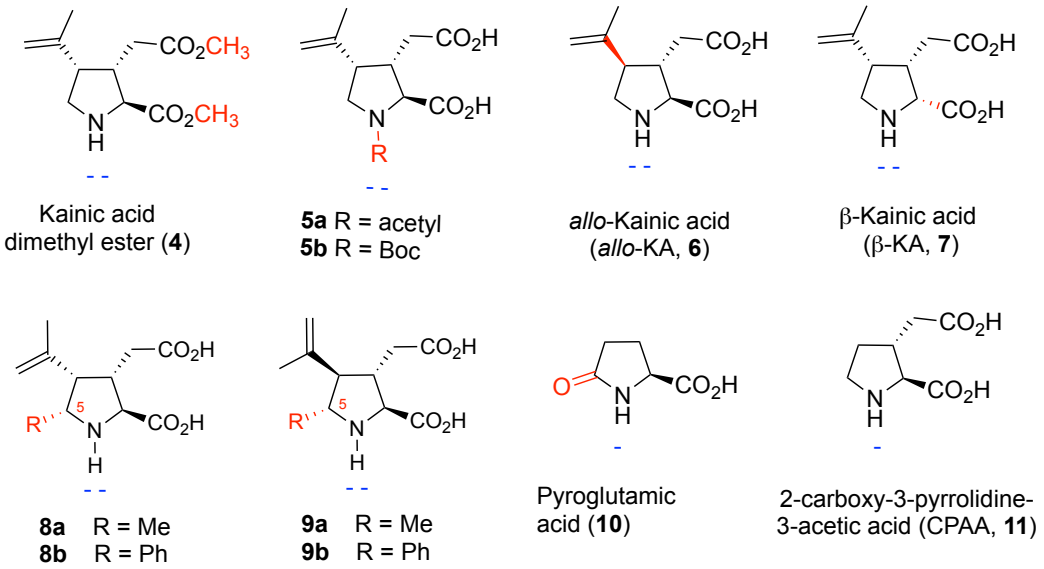

Figure 2–2. Kainiods for binding moiety study. Moieties different than KA are highlight as red.

2.2.3 Structural variation on the C4 position

Due to the necessity of C2 and C3 moieties, and the C5 being sterically intolerant, synthetic modification of kainoids focused on the C4 variations. Early medicinal chemistry research modified the C4 side-chain of kainic acid to provide more complex derivatives (Figure 2–3) for biological studies. These early kainoids share a common feature – they have same backbone with different C4 functional groups derived from functionalization on the *iso*-propenyl group of kainic acid. A C4 double bond retained kainoid **12a** exhibits comparable activity as KA, **14** which also shows the C4 tolerable feature for the binding. Surprisingly, the simple hydrogenation of the alkene led to an inactive DHKA (**13**).[57-59] Also, kainoids **14**, **15** and **17** lost almost all activity for the glutamate receptors.[48,49] And the more sterically demanding lactone **16** saw activity reduced by order of magnitude.[48] The fully oxidized carboxyl kainic acid **14a** and its C4 inverted acid **14b** were inactive because of the hydrophilic moiety on C4.[49] While ketone derivative **12a** is potent towards iGluRs, the C4 inverted derivative **12b** is inactive.[49] These observations point to the importance of maintaining an sp^2 hybridized centre on the C4 side-chain and C3,4-*cis* relative configuration.

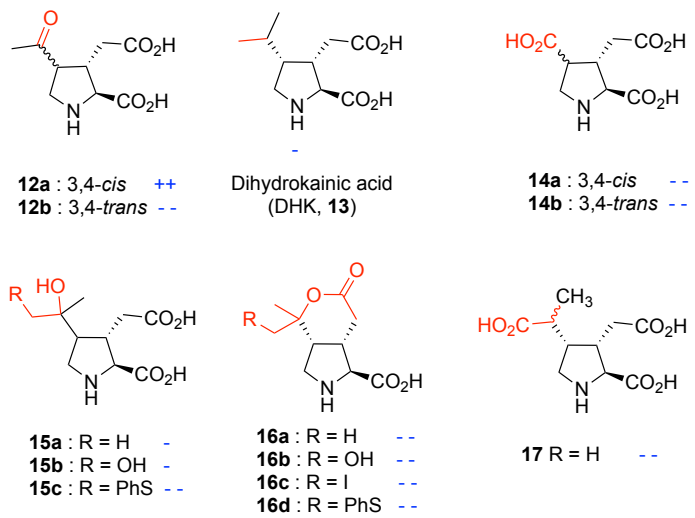

Figure 2–3. Early kainoids derivatized from KA

Perhaps the most intriguing analog is the homologated terminal alkene **18** (Figure 2-4). Similar to DHK, its poor potency **16** initially suggested that the steric constraints around the C4 side chain are very stringent since its hydrophobicity is essentially the same as KA. With extended sidechain kainoids,[50-52] higher potency was observed for the isomer bearing the C1'-C2' double bond in the *Z* configuration (kainoid **20**) than the *E* configuration isomer **21**.[49] Bulky substituents on or close to the C1' alkene (analog **22**, **23**, **24** and **25b**) decrease the activity greatly.[49,53-55] However, this argument does not hold up to the fact that **25a** possesses a bulky sidechain, and yet is more potent than KA,[55] which point to the potential contribution of the planar benzene-alkene conjugation system for the binding affinity.

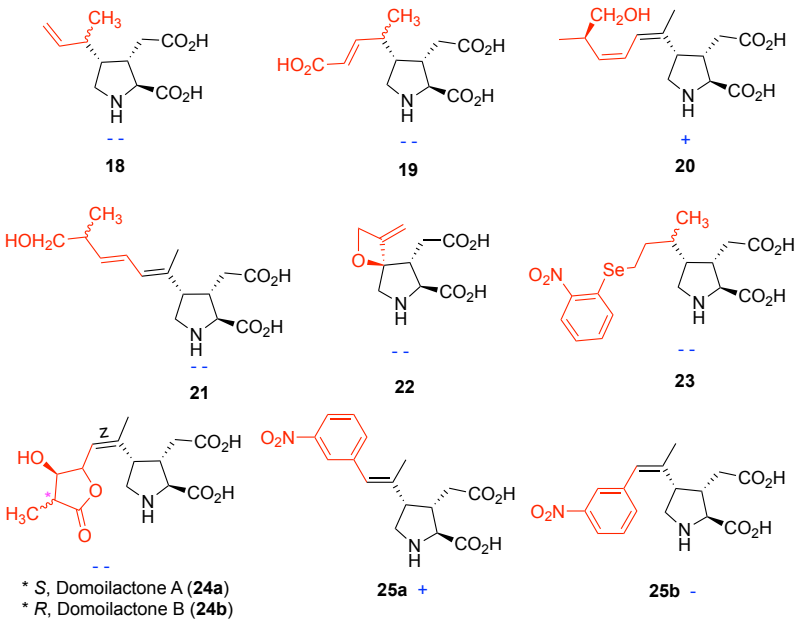

Figure 2-4. Early kainoids with C4 *sp*² substituents

2.2.4 C4 π - π stacking

With the advances of total synthesis, the more recently synthetic chemists were able to create more complex kainoids bearing various C4 sp^2 hybridized side chains (Figure 2–5). The activity of a series of congeners (**26-32**) were systemically measured by Shinozaki group.[56] While a general trend was that electron-poor analogs were more potent, a surprising number of variations were reported to be highly active: from the highly polar acromelate A and B (**26** and **27**) to the simple phenyl kainic acid (**32a**). All these kainoid bearing aromatic and heteroaromatic ring (**26-33**) displayed comparable or enhanced activities as KA.[56]

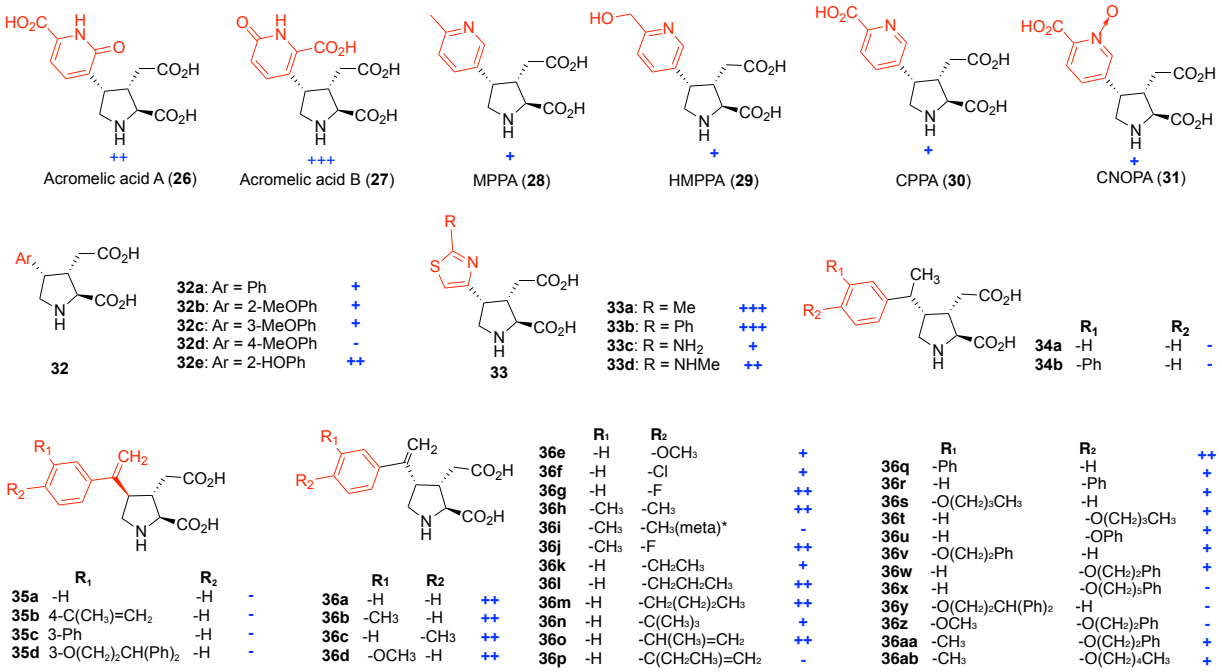

Figure 2–5. Aromatic kainoids obtained from total synthesis

A more comprehensive series of aryl kainoids and their activities were reported by Bleakman group (kainoids **34-36**).[57] Consistently with the rules we concluded from early kainoids, the C1' saturated (**34**) and C4 inverted analogs (**35**) were virtually inactive in the binding assays. Intriguingly, most of the C1' conjugation extended (alkene-benzene conjugation) kainoids **36** are potent agonist for KARs.[57] This may be due to the extended conjugation allowing for a better π– π overlap with the tyrosine residue in binding pockets (see Section 2.3, the crystal structure analysis). To some extent, the C4 side chain is bulkiness tolerable, eg. kainoids **36l**, **36m**, **36o** and **36q** (disubstituents on *meta* and *para* positions) with bulky substituents on benzene ring but still show equal affinity as KA. While disubstituents on *ortho* and *meta* position (kainoid **36i**) and oversized substituents (kainoid **36x** – **36z**) decrease the affinity significantly. Although the bulkiness effect for

approaching the binding sites of iGluRs, the substituents may also affect the electronic density of the conjugation system and further affect the non-covalent overlapping tyrosine residue in the binding site.

To better understand the electronic factors governing the binding affinity of kainoid **36** with iGluRs, we plotted the potency of derivatives 36 against their Hammett constants when they were available (Figure 2–6a).[58-60] While no clear electronic trend emerged from the plots, it can be noted that all compounds with lower Ki's than KA only have substituents in the *para* position; plotted compounds with meta-substituents were less potent than KA. Slightly lower activity for electron-rich aromatic compounds can arguably be observed (suggesting a potential electronic destabilization due to the electron-rich tyrosine)—however, this is admittedly a weak correlation. This weak correlation is also observed when we use the electrophilic constant parameters (Fig. 2–6b). Overall, this analysis does not invalidate a π - π stacking hypothesis, but it rules out a cation- π interaction.

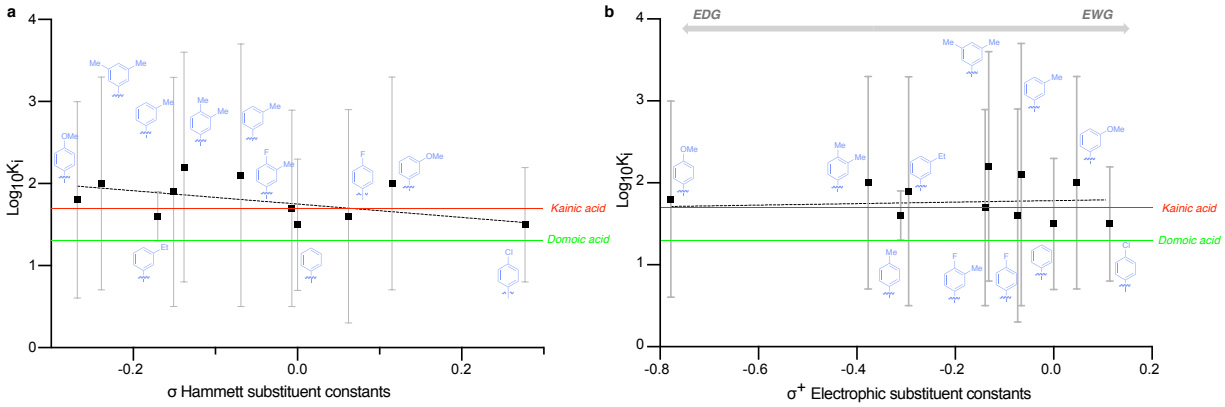

Figure 2–6. Plot of **36** kainoids as a function of K_i versus Hammett coefficients and the aromatic substitutents.

Taken together, the above observations converge toward a few structural features that are essential to the activity of KA derivatives. Both C1- and C2-carboxylic acids and the secondary amine must remain intact, and substitution at C5 is not tolerated. KA can be modified at C4 position, as long as: (1) the stereochemistry is kept *syn* relative to the C3 acetic acid side chain; (2) the C1' atom is sp^2 hybridized; and (3) if a substituted C1'–C2' alkene is present, that the cis geometry will facilitate the efficient binding. These "permissible" structural modifications are deduced from synthetic kainic acid analogs. They are further supported by the potent activity of the natural kainoid, domoic acid. The next section examines the effect of structural variation of DA on the GluR's activity.

2.2.5 Domoic acid derivatives

Domoic acid (**2**, DA) was first isolated in 1959 from the marine red algae, *Chondria armata*.[61] It is a natural toxin produced by marine diatoms (*Pseudo-nitzschia*). *Pseudo-nitzschia* was reported poisonous and the cause of the death of sea birds and sea lions.[62] The diatoms produced DAs can also bioaccumulate in marine organisms which feed on phytoplankton, such as shellfish, anchovies, and sardines.[63] Consumption of DAs contaminated seafood may eventually lead the neurotoxin accumulation in human body. In 1987, three deaths and over 100 illnesses outbroke in Princess Edward Island, the Canadian East coast as a result of the ingestion of DA contaminated blue mussels.[64] Those people suffered short-term memory loss (in addition to the normal clinical signs of food poisoning), which was later attributed to domoic acid.[64] In the brain, domoic acid destroys neuron cells by over-activating KARs, which leads to uncontrolled calcium influxes and causes neuron cells to degenerate.[39]

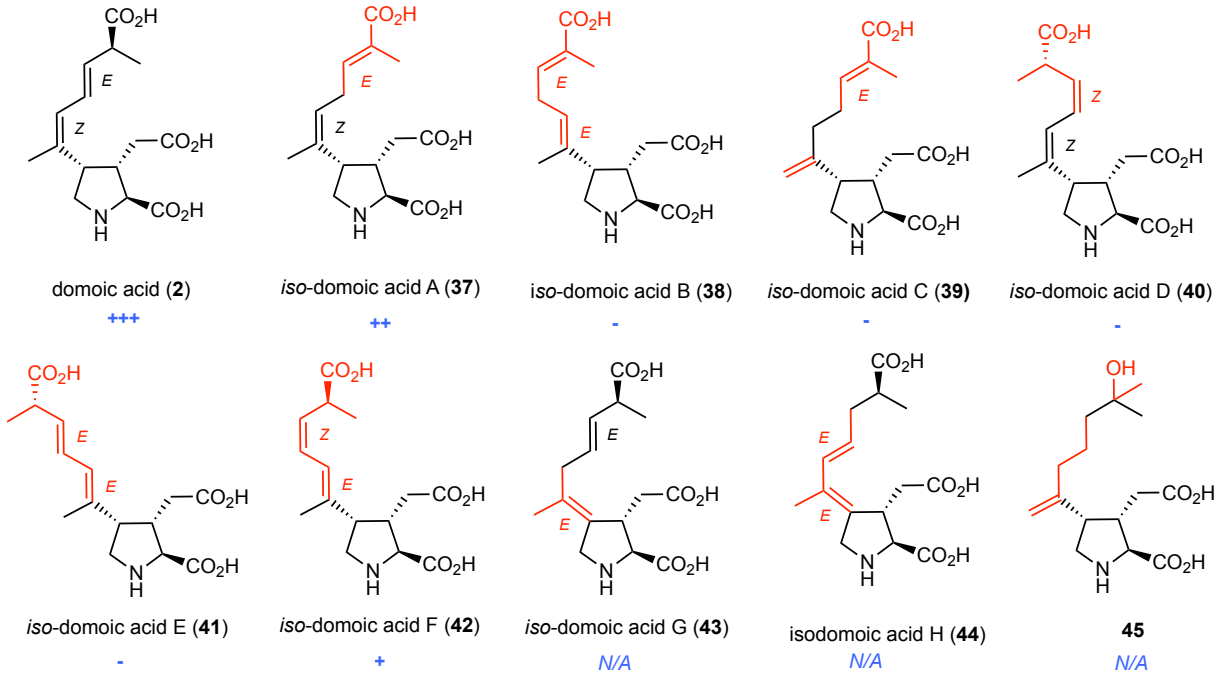

Figure 2–7. Domoic acid and *iso*-domoic acid derivatives. Compared to domioic acid, different moieties of *iso*-domoic acids were labeled as red.

Domoic acid is a KA analog, where the *iso*-propene sidechain is elongated by five carbons and bears a terminal carboxylic acid (Figure 2–7). DA's higher potency over KA shows not only that substituents on the alkene are tolerable, but that it is possible to increase the potency. While the structure of DA has been known since the 1950s, the first total synthesis was achieved by the Tomita group in 1982.[65] More recently, a comprehensive synthesis strategy of domoic acid and its isomers

B, C, E, F (38-42) were established by the Clayden and Baldwin groups. It remains the sole effort to prepare domoids to investigate the effect of DA's sidechain.

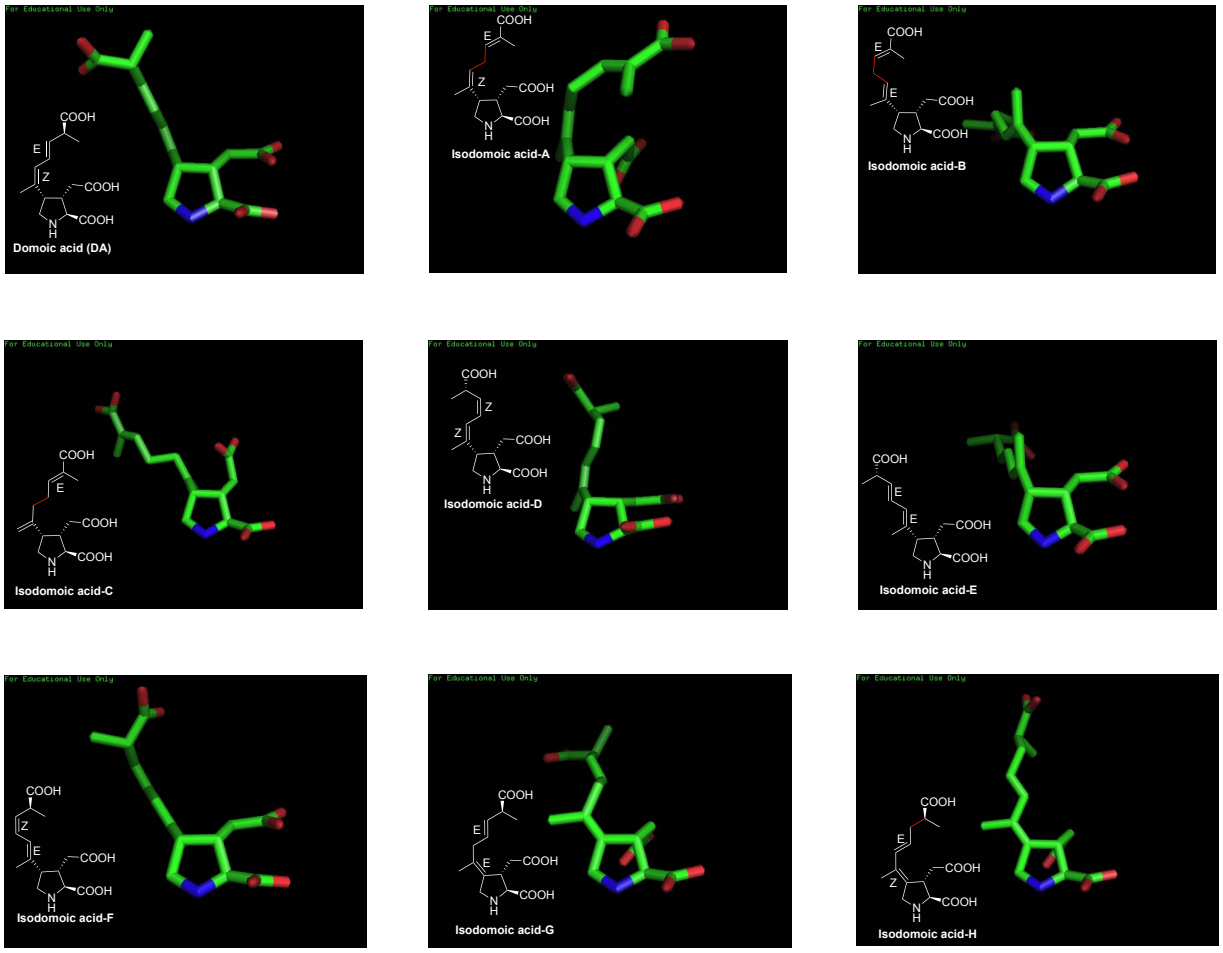

Figure 2-8. 3D structures of domoic acid and its analogues. (3D structures were produced by CORINA. The generated figures were processed by Pymol and Chemdraw.)

More recent biological studies revealed that the configuration of the C1'-alkene must be (Z) to maintain high affinity. Indeed, *iso*-domoic acid E (**41**) is 240 times less potent than DA—this recapitulates the observations made with KA derivatives **21**. Similarly, *iso*-domoic acids A and B (**37** and **38**) show that isomerizing the C1'-alkenes from *Z*- to *E*- resulted in a more than a 1000-fold decrease in K_i. This difference in activity is likely caused by an unfavourable interaction with the protein, as the exo C1'-alkene in the more flexible *iso*-domoic acid C (**39**) results in a K_i of 171 nM (close to Glu according to the grading system). This less dramatic loss than for **41** is most likely due to the ability of the sidechain to rotate around C1'-C2' position (Figure 2–8). For this reason, *iso*-domoic acid F (**42**) is active in binding with KARs. Overall, the most important sidechain parameter to maintain high potency appears to be the ability of the side chain to adopt a flexible (linear) conformation.

The position of the distal alkene at C4' or C5' does not appear to be critical. The regioisomer **37** shows virtually the same K_i as domoic acid. However, its configuration affects binding: the (Z)-C4'-alkene analog **40** is 250-fold less potent than domoic acid. In this case, the favoured *trans* configuration of the diene significantly increases the steric demand around the side chain compared that of domoic acid. This is supported by the (*E*, *Z*)-isomer **41** which is only ~30 times less potent than DA.

Interestingly, the configuration of the C6' centre does not appear to be important. Ablation of the stereocentre in *iso*-domoic acid A (**38**) still maintained activity. Two more diene isomers were synthesized by the Montgomery group (**43** and **44**), but their activity has not yet been reported. Given previous trials with KA analogs showing that stereogenicity at C4 is critical to its binding, we predict that their activity would be poor. Consistent with our prediction, another domoid **45** was reported with moderate activity for KARs (selective for KARs and non-active for NMDARs) by the Baldwin group.[66]

2.3 Protein–ligand interaction: the binding site of kainic acid

The KAR family consists of five proteins members: GluK1–GluK5. Like all glutamate receptors, individual GluK proteins assemble as tetramers to create a functional channel. The crystal structure of a full-length ionotropic glutamate receptor has remained elusive for over four decades due to their large size. However, progress in crystallization techniques has recently yielded structures for AMPA, NMDA, and KA receptors in rapid succession.[7,9] The structural features are then correlated with the SAR trends observed from the synthetic derivatives of KA and DA.

2.3.1 Crystallographic structures of glutamate receptors

Most knowledge about the binding site of glutamate and kainoid agonists has been gleaned from truncated proteins and chimera constructs. Indeed, close to 400 fragmentary structures of KA, AMPA, and NMDA receptors have been entered in the PDB since Gouaux's seminal report of the AMPA receptor GluA2's ligand binding domain (1GR2).[1] Subsequently, many fragments of kainate receptors have been reported, mostly about the ligand-binding domain (LBD).

In 2014, full-length structures of (truncated) ionotropic glutamate receptors were simultaneously reported for the first time: kainate receptor GluK2 by the Mayer lab (4UQQ, Fig. 2–9a, b),[67] and the AMPA receptor GluA2 by the Gouaux lab (4U1W, Fig. 2–9c, d). [7] Moreover, these structures provided long-awaited evidence confirming that structure-activity relationship deductions based on truncated LBD's closely matched the conformations of the complete receptors.

While it provided insight into how Glu (or KA) acts on the channel, the mechanism about how exactly it activates the channel to allow Ca^{2+} entry remains to be revealed.

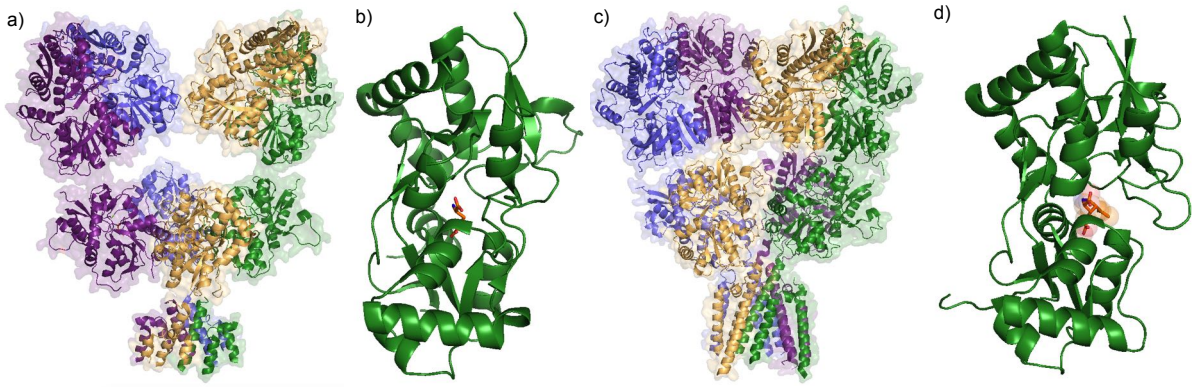

Figure 2–9. Structures of GluRs. (a) Kainate receptor GluK2 (iGluR6; 4UQQ). (b) Ligand-binding domain of kainate receptor iGluR6 for size comparison (4UQQ). (c) AMPA receptor GluA2 (iGluR2, 4U1W). (d) Zoomed-in portion of the full-length GluK2's LBD.

2.3.2 Structural analysis of GluK2-bound kainoids

Several truncated glutamate receptors have been cocrystallized with kainic acid. The LBDs have been reported for GluK1, GluK2, GluK3, and GluK5 as monomers, dimers, and trimers with typical resolutions ranging from 1.5 to 2.5 Å (~257, ~514, and ~790 aa, respectively).[68-72] From these structures, we know that KA's pyrrolidine basic nitrogen is involved in hydrogen bonding with residue Tyr764. Similarly, both C2 and C3 carboxylic acids make strong stabilizing electrostatic interactions with residues Arg523, Thr690, and Ser689. [73] This structural evidence explains and supports the empirical SAR data that arose from the early medicinal chemistry studies discussed in Section 2.2.

The LBD of all glutamate receptors has a flexible clam-like shape, with glutamate's binding pocket at the cleft's bottom. Binding of the ligand stabilizes a "closed" conformation of the clam-like domain, which induces the opening of the ion channel's pore, and allows the flow of Ca^{2+} ions through the cell's membrane.

Similarly, the structures also reveal why the alkene configuration of domoic acid's sidechain is crucial. For instance, it explains the difference in activity between *iso*-domoic acids A and B (**38** and **39**): the *Z* geometry of the C1'-alkene in **38** is required for the chain to extend in the cleft toward the solvent-exposed region. In contrast, the *E* alkene of **39** would force the aromatic system of tyrosine 488 within 3.9 Å distance. The residues making direct contact with the ligand are highlighted in green. Inset: full-length GluK2 tetramer displaying expanded LBD area (PDB 4uqq). The C4 sidechain of domoic acid extends into a space occupied by a semi-helical rigid portion of the protein (Figure 2–10). Interestingly, the geometry of the sidechain's past the C3' position seems

more forgiving as it lies in an outer region of the domain—a region mostly constituted of flexible loops. This is reflected in the affinity of domoic acids analogs **38**, **40**, and **43**: as long as the sidechain can adopt a somewhat extended linear conformation, the K_i remains in the low nanomolar range. And high affinity derivatives *iso*-domoic acid A (**37**) and F (**42**) can all adopt a conformation similar to domoic acid's C-4 side chain. Such orientation of the side chain is prevented for *iso*-domic acid B (**38**), C (**39**), D (**40**) and E (**41**) (Figure 2–8).

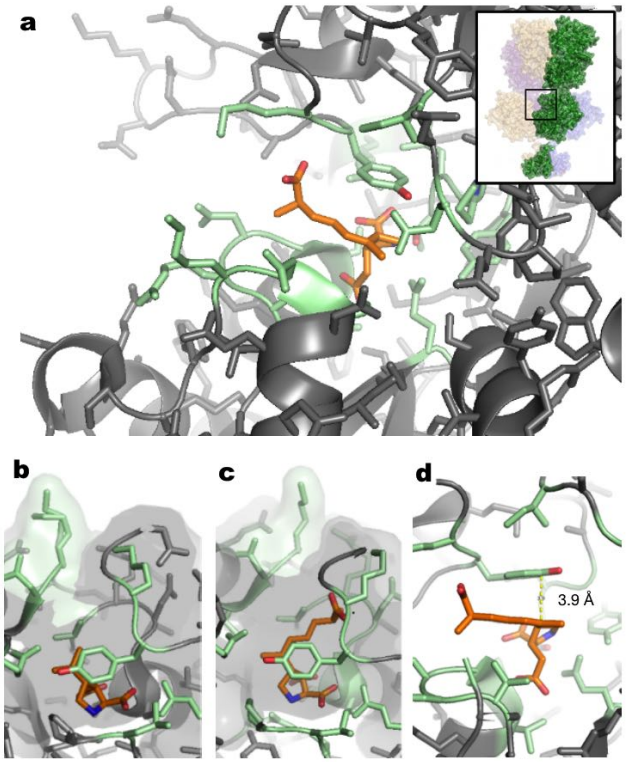

Figure 2–10. Kainic and domoic acids make a π–π interac-tion with Tyr488 in GluK receptors. (a) Side-view of GluK receptor cocrystallized with domoic acid (GluK1•DA; PDB 2pbw). (b,c) Top views of bound kainic acid and domoic acid; the alkene sidechain orientation is identical for both compounds (PDB 3c33, 2pbw, respectively). (d) Side-view of bound domoic acid shows perfect parallel alignment of the C4-alkene with the Try488.

It has been proposed that the carboxylic acid on domoic acid's sidechain participates in hydrogen bonding with an NH group from the receptor's main chain.[73] While this is a plausible interaction, structural analyses indicate it is unlikely to contribute much to the overall affinity of the compound. However, the hydrophilicity of the carboxylate may ensure proper orientation of the sidechain toward the protein surface. No terminal ester of DA (or an analog lacking the terminal carboxylic acid) has been reported to date.

From observing all crystal structure of iGluRs complexed to kainic acid or domoic acid, it is clear that the C4-isopropene engages in π − π stacking with tyrosine 488 (Fig. 2–10). Intriguingly,

Tyr488 is conserved in all three classes of GluR's despite it apparently not being involved in the binding of glutamate.

2.3.3 Notes on selectivity across KAR subtypes

The high level of homology between full sequences of kainate receptors GluK1–5 would seem to pose a tremendous challenge to design subtype-specific inhibitors (typically from 94% to 99.9% identity, Tables S2–4 – S2–7). However, close inspection of the agonist binding sites of KARs56-60 shows that variations exist within the binding pocket's residues (Figure 2–11). These differences may offer the possibility to design subtype-selective agonists.

```
                 ←————————— D1 —————————→          ←————————— D2 —————————→
                      *                  # #    #          *   ##                *#
GluK1   501   DGKYGAQNDK   528   AVAPLTITYVREK   700   VRDGSTMTFF   749   ALLMESTSIEY
GluK2   485   DGKYGAQDDV   513   AVAPLAITYVREK   685   VEDGATMTFF   734   AFLMESTTIEY
GluK3   488   DGKYGAQDDK   515   AVAPLTITHVREK   687   VKDGATMTFF   735   ALLMESTTIEY
GluK4   470   DGVYGVPEAN   497   AVAGLTITAEREK   670   IHGGSSMTFF   719   AFLLESTMNEY
GluK5   469   DGLYGAPEPN   496   AVAAFTITAEREK   669   IHAGSTMTFF   718   AFLLESTMNEY
```

Figure 2–11. Sequence homology of kainic acid's binding pocket for GluKs. Domains 1 and 2 provide two contact surfaces each with KA; residues involved in hydrogen bonding with kainic acid are indicated with a pound sign (#), and those contributing to van der Waals interactions with a star sign (*). Conserved residues are highlighted in green, similar residues in yellow (reference numbering: GRIK2/rat, P42260).

2.4 Molecular design rules for potent kainic acid analogs

In summary, we proposed the key factor for kainoids' affinity towards KARs are: (1) alkene group is necessary for activity due to the potential stacking with Try488 in the binding site; (2) bulky unsaturated or aromatic groups neighbouring the alkene would not affect the activity greatly; (3) configuration of *iso*-propene is very important for activity; (4) bulky group attached to distant group from KA core greatly decreases activity; (5) C4 side chains of high affinity domoids share a similar conformation as domoic acid, for instance analogue **45** compound (its flexible C4 side chain enables the rotation to a similar conformation as DA).

2.5 Summary

Kainic acid remains the most widespread tool in neuro research. With the systematic SAR analysis presented above, we hope it stimulates the creation of novel next-generation KAR agonists by synthetic scientists. We anticipate that those novel KA analogs will also offer the neurobiology community a convenient testing bed for KARs research.

Finally, as part of our research program in the mechanisms of synapse elimination, we have used these design rules to design and synthesize new agonists and molecular imaging probes to study iGluRs in living cells.

2.6 Data analysis

2.6.1 Calculation method

The literature values of binding, activity or affinity of KAR agonists are reported using a wide range of biochemical and biological assays. In order to compare the activity of kainic acid derivatives presented in different studies, a qualitative scale was established. Glutamate, kainic acid and domoic acid were set as benchmarks for this scale system.

Table 2–2. Qualitative scale

Relative Activity (RA)	Grade	Notes
Inactive	--	Inactive
$0 < RA < 0.065$	-	Weaker than L-Glu, but active
$0.065 \leq RA < 1$	+	Between L-Glu and KA
$1 \leq RA < 2.89$	++	Between KA and DA
$2.89 \leq RA$	+++	Being equal as or stronger than DA

The activity of each compound was first normalized to the positive control used in a given study (typically, glutamic acid or kainic acid). If needed, the resulting activity ratio was then further standardized to kainic acid. When a compound was tested in more than one assay, priority was given to data from GluRs binding assay (K_i or IC_{50}). Otherwise, data from [^{3}H]-KA displacement assays was used for calculations. If those data were not available, calculations were performed with the reported activity in neurons or in animal experiments. When multiple data were available for a single agonist, the most recent data is used.

Calculation methods:

1. Relative activity = K_i (or IC_{50}) of KA / K_i (or IC_{50}) of compounds
2. Relative activity = Effect of compounds / effect of KA
2. Relative activity (iso-DAs) = (K_i of DA / K_i of *iso*-DAs) × Ratio potency of DA

2.6.2 Calculated ratios and grades

The potency ratios of agonists are calculated according to the originally reported data (see Table S2-1 and S2–2, Appendix A). The calculated results are tabulated as following.

Table 2–3. Activity scales for kainoid analogues

Compound	Potency Ratio (Relative to KA)	RA Level	Ref.
Kainic acid (1) – *Reference*	1	++	51, 52, 62, 63, 65, 81-88
Domoic acid (2)	2.89	+++	75
***L*-Glu (3)**	0.065	+	76
4	Inactive	--	77
5a	Inactive	--	77
5b	Inactive	--	77
6	Inactive	--	78
7	Inactive	--	46
8a	Inactive	--	79
8b	Inactive	--	79
9a	Inactive	--	79
9b	Inactive	--	79
10	0.049	-	80
11	0.0063	-	81
12a	1	++	78
12b	0.299	+	78
13	0.00063	-	82
14a	Inactive	--	48
14b	Inactive	--	48
15a	0.013	-	52
15b	0.00065	-	52
15c	Inactive	--	48
16a	Inactive	--	48
16b	Inactive	--	48
16c	Inactive	--	52
16d	Inactive	--	83
17	Inactive	--	78
18	Inactive	--	78
19	Inactive	--	78
20	0.68	+	78
21	Inactive	--	78
22	Inactive	--	84
23	Inactive	--	78
24a	Inactive	--	54
24b	Inactive	--	54
25a	0.22	+	55
25b	0.043	-	55
Acro A (26)	2.2	++	76
Acro B (27)	7.2	+++	76
MPPA (28)	0.31	+	76
HMPPA (29)	0.68	+	76
CPPA (30)	0.87	+	76
CNOPA (31)	0.27	+	76
32a	0.34	+	74
32b	4.0	+	74
32c	0.85	+	74
32d	0.03	-	74
32e	1.6	++	74
33a	5.67	+++	74
33b	0.12	+	74
33c	6.8	+++	74
33d	2.13	++	74
34a	Inactive	--	57
34b	Inactive	--	57
35a	0.016	-	57
35b	0.023	-	57
35c	0.017	-	57
35d	0.001	-	57
36a	2.3	++	57
36b	1.7	++	57
36c	1.4	++	57
36d	1.1	++	57
36e	0.95	+	57
36f	0.95	+	57
36g	1.4	++	57
36h	1.6	++	57
36i	0.40	-	57
36j	1.94	++	57
36k	0.48	+	57
36l	1.02	++	57
36m	1.94	++	57
36n	0.20	+	57
36o	1.02	++	57
36p	0.41	-	57
36q	1.76	++	57
36r	0.41	+	57
36s	0.16	+	57
36t	1.32	+	57
36u	0.31	+	57
36v	0.21	+	57
36w	0.29	+	57
36x	0.029	-	57
36y	0.018	-	57
36z	0.041	-	57
36aa	0.41	+	57
36ab	0.08	+	57
***iso* DA A (37)**	1.62	++	81
***iso* DA B (38)**	0.001	-	81
***iso* DA C (39)**	0.040	-	81
***iso* DA D (40)**	0.004	-	81
***iso* DA E (41)**	0.004	-	81
***iso* DA F (42)**	0.10	+	81

Chapter 3

Synthesis of Kainoids and C4 Derivatives

Developing a general synthetic route to C4 kainoids is required as they are the most potent agonists of kainic acid receptors (KAR). While several syntheses of kainic acid and analogs have been reported since the discovery of this neurotoxin, none offers a practical route to kainic acid and its C4 derivatives simultaneously. This chapter describes a general synthesis of kainoids that allows access to C4 derivatives via late-stage divergence.

3.1 Background

Kainoids are a group of non-proteinogenic amino acids displaying strong neurological activity.[85] The title compound of the family, kainic acid (**1**) and its epimer *allo*-kainic acid (**6**) were isolated from the marine algae *Digenea simplex* in 1953 (Figure 3–1).[86] The unique selectivity of kainic acid for a subset of ionotropic glutamate receptors led to naming the class as kainate receptors (GluK1-5).[87] Kainic acid is now commonly used in neurobiology research to study conditions such as epilepsy, Huntington's, Parkinson's and Alzheimer's diseases.[45,88,89] As discussed in Chapter 2, biological testing of KA analogs revealed that the neuroactivity of KA is highly dependent on its C4 substituent. For instance, synthetic derivatives such as phenylkainic acid (**32a**),[46] acromelic acid A (**26**),[46] and thiazole analog **33c**[74] all display equal or higher potency than kainic acid.

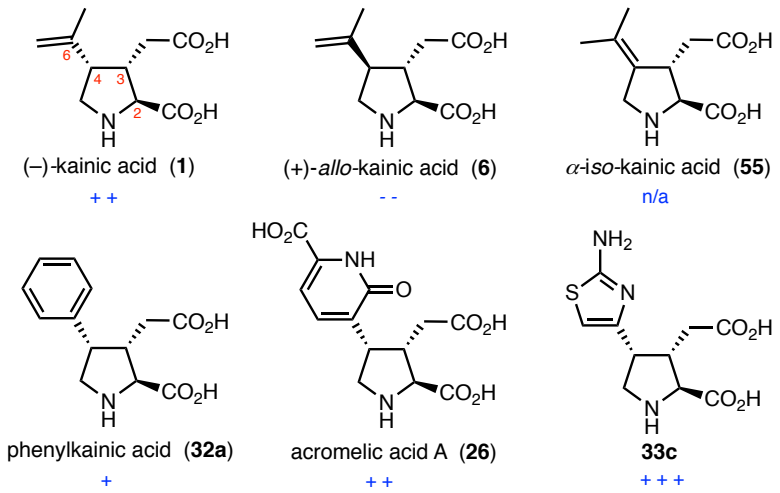

Figure 3–1. Naturally occurring (**1**, **6**, **55**, **26**) and synthetic kainoids (**32a**, **33c**). The affinity is indicated as "+" or "-" according to the grading system in Chapter 2.

Kainoids are a popular synthetic target: close to 70 syntheses of kainic acid, *allo*-kainic acid, *iso*-kainic acid, and phenylkainic acid have been reported.[85,86,90-95] The shortest synthesis of kainic acid was accomplished by Ohshima in six steps, however, it does not allow for ready variation of the C4 position.[96] Structure-activity relationship studies have confirmed that the C4 substituent of kainoids is the only position that can be exploited to enhance the activity of kainic acid (Chapter 2).[56,97] Moreover, these studies revealed that only sp^2-hybridized C4 substituents display a high affinity for GluK receptors.

As part of our research program in neuron-glia communication, we required a GluK chemical probe bearing a reporter tag at C4. We reasoned that an ideal approach would enable late-stage introduction of sp^2-hybridized nucleophiles at the C4 position. A route to phenylkainic acid reported by Baldwin in 1995 provided a potential framework that could be modified for our purpose.[98] Accordingly, we developed a pragmatic route that can deliver large amounts of C4 kainoid derivatives for cell and animal assays.[99]

3.2 Restrosynthetic analysis of 4-substituted kainoids

The proposed approach prioritizes the late-stage introduction of C4 substituents as sp^2-hybridized nucleophiles (Scheme 3–1). Installing C4 side chains was achieved via a sequence of stereoselective addition/reduction onto pyrrolidinone **56**, which is the pivotal intermediate of our strategy. Access to pyrrolidinone **57** from 4-hydroxyproline **58** was optimized from select precedents. This path would provide one of the shortest access to kainoid analogs.

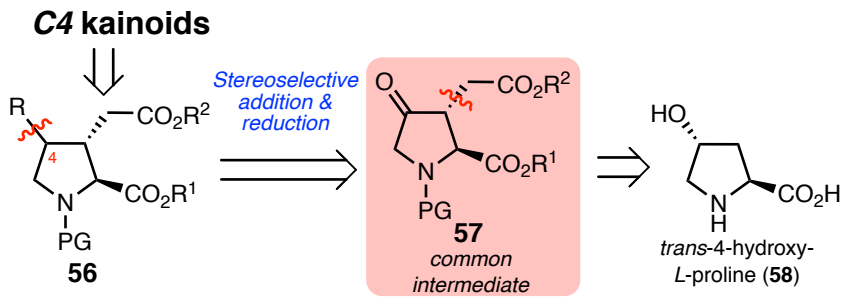

Scheme 3–1. Retrosynthesis analysis of 4-substituted kainoids

3.3 Optimization of C3 intermediate synthesis

The synthesis began with a two-step protection of *trans*-4-hydroxy-L-proline, followed by a Swern oxidation to obtain pyrrolidinone **61** (Scheme 3–2).[100-102] The choice of protecting group for the amine is crucial for the subsequent C3 alkylation leading to **62**.[101] Indeed, Lubell and Rapoport's phenylfluorenyl (Pf) protecting group[103,104] was unique in achieving enolate alkylation regioselectively at the more hindered alpha position of ketone **61**. Initial trials with Boc or Cbz were unproductive, leading to poor regioselectivity or stereoselectivity. While Pf's large steric bulk was essential to control selectivity, it would later offer its share of challenges.

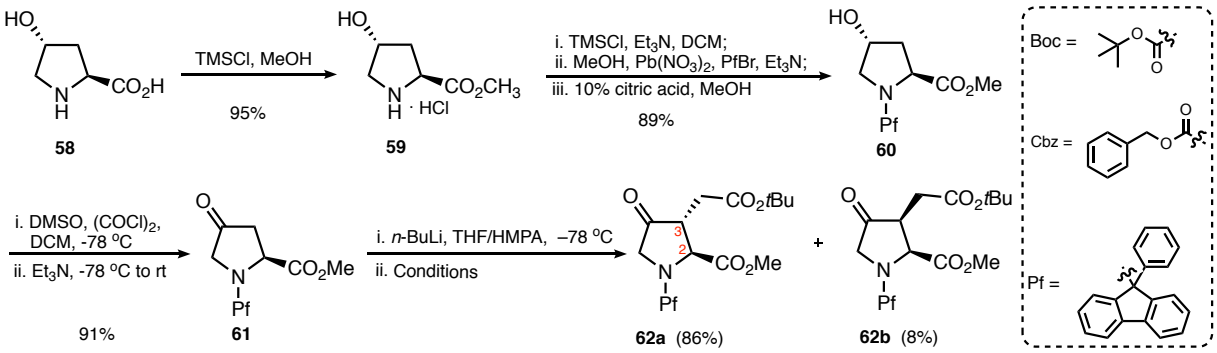

Scheme 3–2. Synthesis of pyrrolidin-4-one 62a.

Alkylation of the C3 ester side chain to obtain the desired *trans* diester **62a** is highly sensitive to reactions conditions (Table 3–1). We selected a *tert*-butyl ester because it allowed us to unambiguously assign the stereochemistry of subsequent compounds **63**–**65** (reduced conformational flexibility greatly enhances NOE). Adapting conditions for a related alkylation using a catalytic amount of NaI[101,102] yielded a 5:1 ratio when the reaction was performed on >5 grams scale using $BrCH_2CO_2tBu$ (entry 1). Instead, using *tert*-butyl iodoacetate directly, the ratio was improved to 14:1, although the conversion was sluggish (entry 4). Increasing equivalents and

temperature afforded an acceptable compromise in terms of conversion and selectivity (entries 2 and 3). The stereochemistry of **62a** and **62b** was determined by ^{1}H NMR analysis: the empirical $J_{H2\text{-}3}$ value for the 2,3-*trans* product **62a** is 6.1 Hz, and that of **62b** is 8.2 Hz (these C2,3 configurations were further confirmed by crystal structures of their derivatives in the reported studies). [100,102,105]

Table 3–1. Stereoselective alkylation of ketone 61

Entry	Halide	Conditions	Conversion (%)[a]	dr[a] **62a**:**62b**
1[b]	$BrCH_2CO_2tBu$ (3.5 eq)	–41 °C, 3h	100	5:1
2[c]	ICH_2CO_2tBu (5.0 eq)	–41 °C, 5.5 h	100	9:1[d]
3[c]	ICH_2CO_2tBu (6.0 eq)	–78 °C, 5 h	60	10:1
4[c]	ICH_2CO_2tBu (3.5 eq)	–78 °C, 5 h	50	14:1

[a] Determined by ^{1}H NMR analysis of crude products. [b] Reaction conditions: 1:5 HMPA/THF; 0.5 equiv. NaI, halide (Method B in supp. info.). [c] 1:10 HMPA/THF; halide (Method A in supp. info.). [d] After purification, the ratio of isolated products was 10.8:1.

3.4 Installation of C4 sidechain

3.4.1 Stereoselective addition of *sp*^{2} nucleophiles

Next, we turned to the key installation of side chains at the C4 position of **62a** (Scheme 3–3). When ketone **62a** was treated with alkenyl or aromatic Grignard reagents, only starting material **62a** epimerized at C3 was recovered. We explored less basic organocerium reagents to promote the addition. We found that using $CeCl_3{\cdot}2LiCl$ (1.3 equiv. for **62a**, 3.0 equiv. for **63b**) afforded alcohols **63** as single diastereomers with an almost quantitative yield.[106] The presence of LiCl is essential to full obtain conversion with **62a**, and the reaction worked equally well with *i*-Pr- and Ph-organometallic reagents (Table 3–2). Baldwin *et al.* reported a similar strategy using *N*-Bz proline ketone with PhMgBr and $CeCl_3$ that afforded a 52% yield.[98] However, the more sterically demanding *N*-Pf protected **62a** led to poor conversion with $CeCl_3$. For instance, using *i*-PrMgBr/$CeCl_3$ gave only 5% yield, and PhMgBr/$CeCl_3$ gave **63b** in 16% yield with C3 epimerized. NOE experiments confirmed the configuration of the C4 centers (Scheme 3–3).

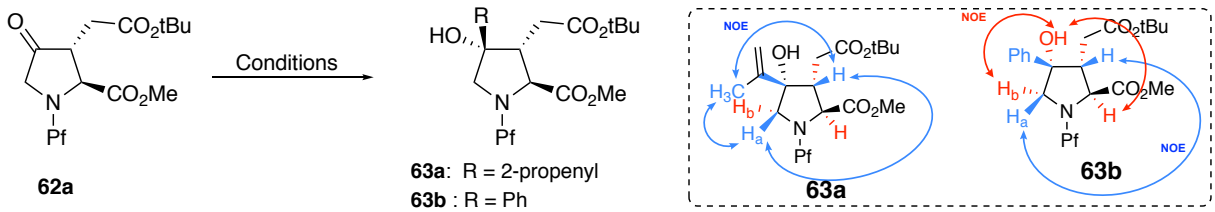

Scheme 3–3. Synthesis of C4 tertiary alcohols and NOE analyses

Table 3–2. Nucleophilic addition of ketone 11

Entry	Conditions	Conversion (%)
1	RMgBr, THF, rt	*NA*[a]
2	RMgBr (1.0 eq), $CeCl_3$ (1.0 eq), THF, 0 °C	**63a**: 5%; **63b**: 16%
3	RMgBr (3 eq), $CeCl_3 \cdot 2LiCl$ (1.5 eq), THF, -78 °C	**63a**: 98%; **63b**: 95%

[a] No desired conversion was observed.

3.4.2 Stereoselective deoxygenation of the C4 alcohol

Deoxygenation of tertiary alcohols **63a** and **63b** posed a significant challenge of chemoselectivity. Traditional radical-based deoxygenation methods failed, so we examined the reactivity of the parent carbonates (Scheme 3–4). Allylic carbonate **64a** was reduced via a catalytic transfer hydrogenation using ammonium formate and palladium acetate **64a** to afford a 3:1 regioisomeric mixture of *allo*–kainic acid precursor **65a** and *iso*–kainic acid precursor **65b**.[107] No conversion was observed on the **64b** with the same condition, which confirmed the limited application scope of this type reaction on allylic substrates.

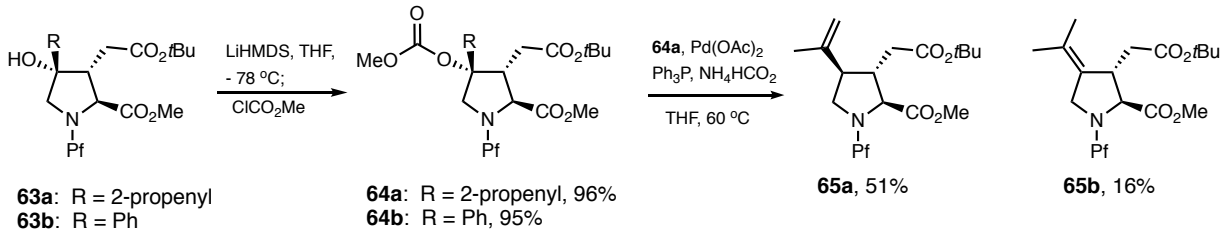

Scheme 3–4. Palladium-catalyzed allylic deoxygenation

The C3,4–*cis* diastereomer of **65** (precursor of kainic acid) was not observed under these reduction conditions. The steric bulk of the *N*-Pf protecting group likely prevents the catalyst from approaching the top face of the allylic carbonate (*viz.* path B, Scheme 3–5). We surmise that competing catalytic pathways take place. For instance, the sterically congested substrate **64a** may slow the antiperiplanar addition of Pd(0) to the allylic system, and a Pd(II) complex may act as Lewis acid toward the carbonate group. The resulting transient allylic carbocation then gets reduced from the same face as the leaving group.

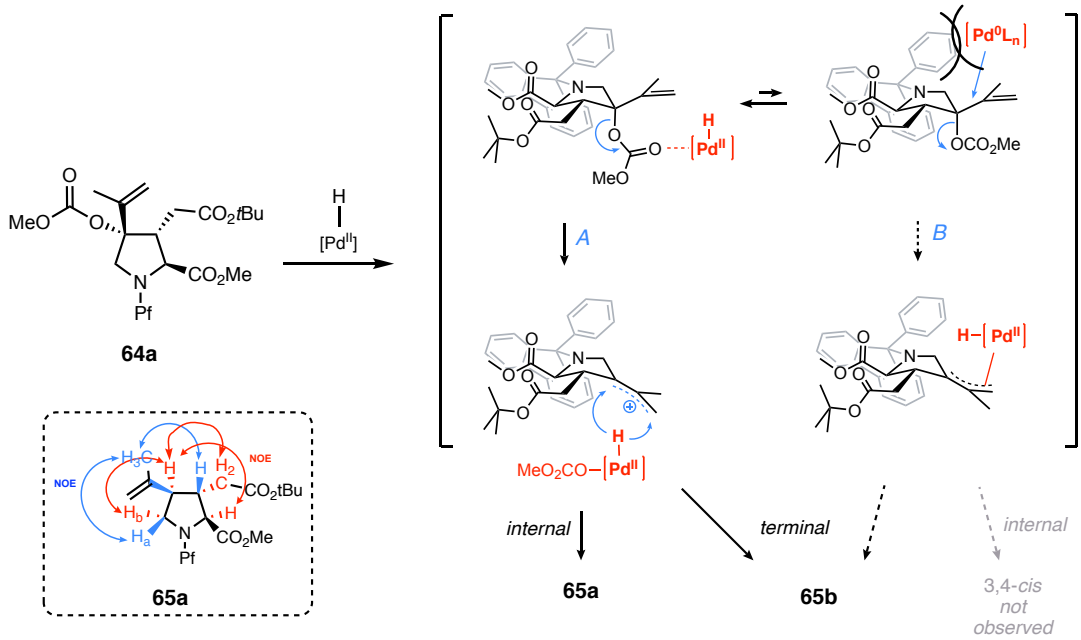

Scheme 3–5. Proposed mechanism for allylic deoxygenation

3.4.3 Protecting group swap: Pf for Boc

To change this stereoselectivity, the amine's Pf protecting group was replaced by a less bulky Boc. Extensive optimization was needed to selectively cleave the Pf group without losing the *tert*-butyl ester or epimerizing C3. We found buffered reductive conditions that are compatible with: tertiary alcohols, allylic carbonates, *tert*-butyl carbonates, and esters (summarized in Table 3–3). We settled on using Et_3SiH with TFA in dichloromethane, which led to quantitative removal of *N*-Pf (entries 2 and 3). Alternatively, Et_3SiH with I_2 in acetonitrile was also efficient, but led to the loss of the *tert*-butyl group (entry 4). Using Rapoport's original conditions (excess TFA)[108] removed the Pf group, however the *tert*-butyl ester was quite prone to elimination and high yields were difficult to reproduce (entry 1).

Table 3–3. Deprotection of *N*-phenylfluorenyl (*N*-Pf)

Entry	Cmpd	Conditions	Yield	Byproduct
1	**63a/b**	TFA (15 eq.), DCM, 1 h	90%[a]	PfOH
2	**63a/b**	Et_3SiH (3 eq.), TFA (5 eq.), DCM, 1 h	Quant.	PfH
3	**64a/b**	Et_3SiH (3 eq.), TFA (5 eq.), DCM, 1 h	Quant.	PfH
4	**64a/b**	Et_3SiH (2 eq.), I2 (1 eq.), MeCN, 10 min	Quant.[b]	PfH

(a) ~10% *tert*-Butyl ester was converted to the parent acid. (b) *tert*-Butyl ester was also deprotected under these conditions.

3.4.3 Deoxygenation to kainoids with modified selectivity

The pyrrolidine resulting from Pf deprotection of **64** was directly subjected to standard Boc protection conditions to afford carbamates **66a** and **66b** in excellent yields (Scheme 3–6). The catalytic hydrogenolysis of allylic carbonate **66a** with $Pd(OAc)_2$ and formate afforded **67a** and **67b** as a 1.1:1 mixture of C4 epimers. Improving the ratio for kainic acid precursor **67b** remained elusive, despite several attempts.

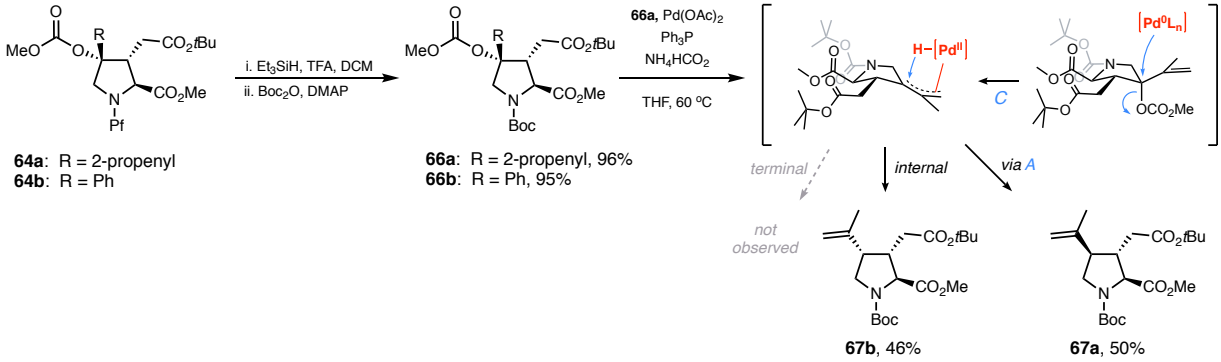

Scheme 3–6. Synthesis of *allo*-kainic acid and kainic acid precursors

Kainic acid (**1**), *allo*-kainic acid (**6**), and *iso*-kainic acid (**55**) were obtained via global deprotection of **67a**, **67b**, **65a** and **65b**, respectively (Scheme 3–7). A telescoped sequence was used for **67a** and **67b**: the reductive Pf deprotection was followed by a mildly alkaline hydrolysis. Natural products **6** and **55** were obtained in 78% and 79% yields respectively. Intriguingly, no epimer was observed in this ester hydrolysis reaction. **65** and **67** have epimerizable of C2 stereocentre, but the C3 and C4 stereocenters are not epimerizable under aqeous basic conditions. Due to thermodynamically favoured C2,3-*trans* configuration, it posts low probability for **65** and **67** to undergo C2 epimerization during the global deprotection. For this reason, aqeous basic conditions were employed to invert the C2 configuration when people obtained undesired C2,3-*cis* epimers.[109-111] Moreover, NMR spectra of **6** and **55** are consistent with reported data (Table S–1, Appendix C). The ~1:1 mixture of *N*-Boc protected diesters **67a** and **67b** was also deprotected with a telescoped sequence: alkaline hydrolysis followed by anhydrous TFA treatment led to kainic acid (**1**, 35%) and *allo*-kainic acid (**6**, 46%). Separation of **1** and **6** by crystallization and HPLC proved challenging. While it was possible to obtain analytically pure samples for characterization, the bulk of the products remained a mixture. Regardless, this mixture was useful to us—and we expect to others—as it enables the gram-scale synthesis of thiazole **33c** in four steps, currently the most potent GluK receptor agonist.[74]

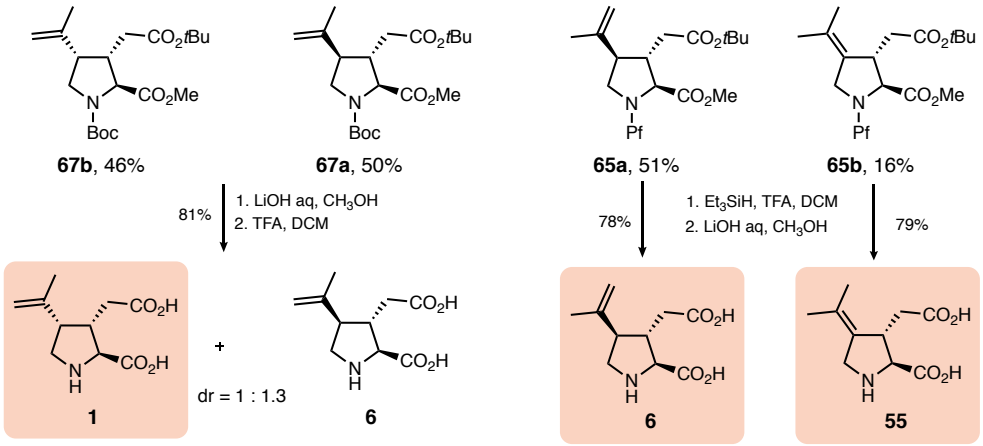

Scheme 3–7. Deprotection to kainic acid and isomers

3.5 Synthesis of phenylkainic acid & more C4 functionalization

Inspired by the lactone hydrogenolysis reaction developed by Baldwin *et al.*,[98] we attempted to invert the C4 stereocentre with a hydrogenation reaction (Scheme 3–8). Upon full deprotection, carbonate **64b** spontaneously cyclized to lactone **68** (sparingly soluble in DMSO). This lactone was then ring-opened with inversion of configuration under standard hydrogenation conditions using Pd/C. Phenylkainic acid (**32a**) was obtained as a single diastereomer in 90% yield from **68**.

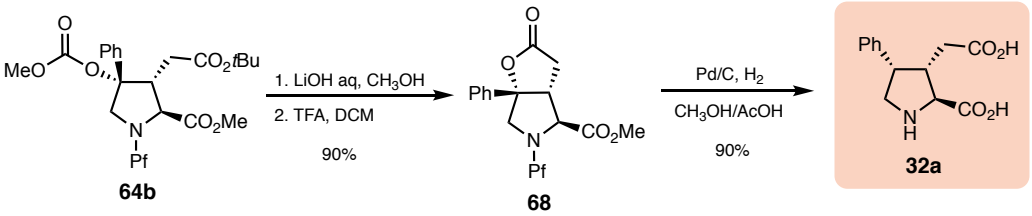

Scheme 3–8. First attempt at phenylkainic acid synthesis

Alternatively, we shortened the path above by directly cyclizing alcohol **63b** to lactone **69a** under excess of TFA. Lactone **69** was hydrogenolyzed to yield phenylkainic ester **70** as a single diastereomer (Scheme 3–9). Compared to Baldwin's synthesis of phenylkainic acid (9 steps, 11% overall yield),[98] our route fares well: **32a** is obtained in 8 steps with an overall yield of 54%. The configuration of C4 in **32a** was confirmed by ^{1}H NMR spectroscopic analyses and is consistent both with literature data (Table S3–1, Appendix B)[112] and with configuration assignment rules (Table

S3–2, Appendix B).[113] The C3,4–*cis* configuration was further confirmed by NOE analysis of the subsequent products **71a** and **71b** (Scheme 3–8).

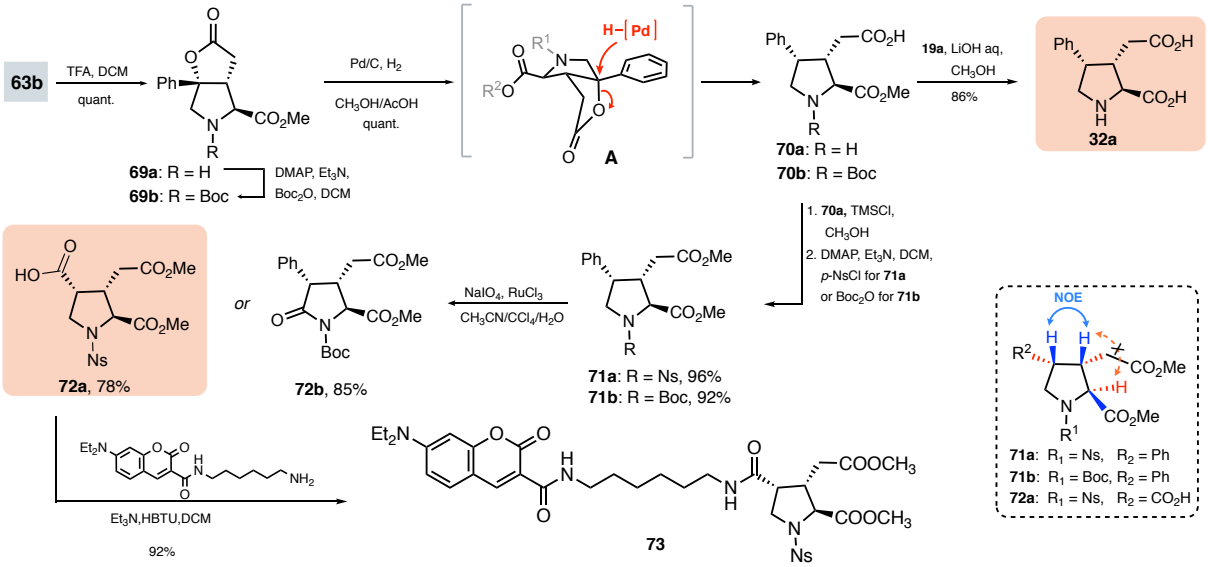

Scheme 3–9. Synthesis and Functionalization of Phenylkainic Acid. (*p*-Ns: *p*-nitrobenzenesulfonyl)

Our need for kainic acid-based chemical probes motivated us to exploit our most efficient route: that leading to intermediate **70a** in 7 steps (Scheme 3–9). Chemoselective oxidation of the C4-phenyl group to a carboxylic acid would provide a versatile synthetic handle to append any side chain at a late stage. Accordingly, diester amine **70a** was converted to the *N*- Boc diester **71b** in two steps. However, when **71b** was presented to $RuCl_3$ and $NaIO_4$, the phenyl group remained untouched and only the C5 position of the pyrrolidine was oxidized to pyrrolidinone **72b**. Instead of Boc, a *p*-nitrobenzenesulfonyl (Ns) protecting group was selected for its ability to deactivate the *N*-alpha position and its mild deprotection condition (ArSH, K_2CO_3, DMF).[114] Thus **70a** was converted to the *N*-Ns amide **71a** in two steps and almost quantitative yield. The phenyl group of **71a** was oxidized selectively and afforded the desired acid **72a** in 78% yield without epimerization (stereochemistry confirmed by NOE analysis).

The C4-acid kainoid **72a** provides easy access to a variety of kainoid derivatives. It enables the synthesis of numbers of heteroaromatic kainoids.[115] In addition, our work toward kainoid-based GluK imaging probes— presented in the following Chapters—confirms that **72a** can be readily coupled to fluorescent dyes.

3.6 Summary

In conclusion, a unified diastereoselective route to 4-substituted kainoids was demonstrated from commercially available *trans*-4-hydroxy-L-proline (Scheme 3–10). The sequence affords: kainic acid (11 steps, 19%), *allo*-kainic acid (9 steps, 24%), *iso*-kainic acid (9 steps, 8%), and phenylkainic acid (8 steps, 54%). In addition, a mild oxidation step has been developed for C4 derivatization from phenyl kainic acid. The novel acid **72a** (10 steps, 47%) is a readily modifiable intermediate that can give rapid access to non-natural kainoids via amide couplings, including KARs chemical probes. This report provides a general access to a range of biologically active 4-substituted kainoids.

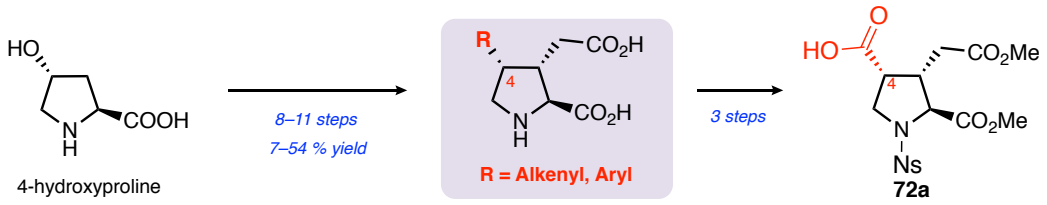

Scheme 3–10. A unified synthesis strategy of C4-kainoid derivatives

3.7 Experimental Section

3.7.1 General Experimental Procedures

Unless otherwise noted, reactions were carried out under an argon atmosphere, in flame-dried single-neck, round bottom flasks fitted with a rubber septum and with magnetic stirring. Air or water sensitive liquids and solutions were transferred via syringe or stainless-steel cannula. Organic solutions were concentrated by rotary evaporation at 25–45 °C at 50–200 torr. Thin layer chromatography (TLC) was performed on glass plates precoated with Silica gel F254, 250 µm, 60 Å, from EMD Chemicals Inc (EMD 5715-1). TLC plates were visualized under a 254 or 365 nm UV light source, then stained by immersion in either acidic aqueous-ethanolic vanillin solution, potassium permanganate, or acidic ethanolic ninhydrin, followed by heating using a heat gun. Purification was performed with 230-400 mesh silica gel from Silicycle, Quebec (SiliaFlash R12030B, P60, 40-63 µm, 60 Å).

3.7.2 Materials

Reagents and starting materials were purchased from: Sigma-Aldrich, Oakwood Chemicals, Alfa Aesar, Acros Organics, TCI America, or Fisher Scientific and were used as received unless otherwise noted. Tetrahydrofuran, dichloromethane, hexanes, toluene, and diethyl ether were purified on a glass contour solvent purification system under an argon atmosphere. Methanol was dried by allowing it to stand over freshly activated 4 Å molecular sieves for 48 h prior to use. Solvents used for chromatographic purifications were obtained from Fischer Scientific or VWR and used without further purification. All new compounds (**63-68**) and final products (**1**, **6**, **32a**, **26** and **73**) were characterized with 1D (^{1}H NMR and ^{13}C NMR) and 2D NMR (COSY, HSQC, HMBC) spectroscopic analyses.

3.7.3 Instruments

^{1} H and ^{13} C NMR spectra were recorded on a 400 MHz Varian NMR AS400 equipped with an ATB-400 probe at 25 °C. NMR spectra were analyzed with MestreNova version 10.0.2-15465 from Mestrelab Research. Chemical shifts are reported in parts per million (ppm, δ scale) downfield from tetramethylsilane and are referenced to residual proton signals in the NMR solvents ($CHCl_3$: δ 7.26, C 2 HD 5 SO: δ 2.50), for carbons ($CDCl_3$: δ 77.0, C $_2HD_5SO$: δ 39.5). Spectral data are listed as follows: chemical shift, integration, multiplicity (s = singlet, d = doublet, t = triplet, q = quartet, m = multiplet, br s= broad singlet), and coupling constant (*J*, Hz). Infrared spectra (IR) were obtained using a Nicolet 6700 FT-IR spectrometer as a neat film on a NaCl plate, or a Perkin-Elmer FT-IR Spectrum Two IR spectrometer. High resolution mass spectra were obtained from the UBC Mass Spectrometry Facility using a HCTultra PTM discovery system spectrometer (ESI), or from a Waters Micromass LCT Premier TOF Mass Spectrometer (ESI, Zandberg lab, UBCO). Melting points of solid samples were measured with a a IA9200 melting point apparatus (Electrothermal). The final products were purified HPLC on a C18 column (Eclipse Plus C18, 4.6 × 250mm, 5 µm, Agilent) with a Varian Prostar HPLC system (e.g., kainic acid and allo-kainic acid). HPLC condition for the purification was described in the corresponding procedure.

3.7.4 Experimental Procedures and Characterization

Synthesis of C2 precursors

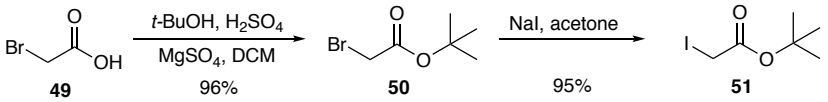

***tert*-Butyl bromoacetate (50).** To a rigorously stirred solution of magnesium sulfate (52.0 g, 432 mmol) in dichloromethane (300 mL) was slowly added concentrated sulfuric acid (3.8 mL, 72 mmol). After 10 min, bromoacetic acid (20.0 g, 144 mmol) was added at rt, followed by the addition of *tert*-butyl alcohol (41.2 mL, 432 mmol). After 24 h, a second portion of *tert*-butyl alcohol (20.5 mL, 216 mmol) was added to take the reaction to completion in an additional 24 h. The insoluble matter in the resulting reaction solution was removed by vacuum filtration. The filtrate was poured into water and extracted with dichloromethane (3 × 50 mL). The combined organic layer was washed with sodium bicarbonate solution, brine and dried over $MgSO_4$. The solvent was evaporated under reduced pressure to afford the crude *tert*-butyl bromoacetate as a light-yellow liquid (26.9 g, 96%), which was used for the following reaction without further purification.

^{1}**H NMR** (400 MHz, $CDCl_3$): δ 3.75 (s, 2H), 1.48 (s, 9H) ppm.

^{13}**C NMR** (101 MHz, $CDCl_3$): δ 166.2, 82.9, 27.8, 27.7 ppm.

***tert*-Butyl iodoacetate (51).** *tert*-Butyl bromoacetate (25.2 g, 128 mmol) was added at rt to a suspension of NaI (23.1 g, 154 mmol) in acetone (200 mL) under a nitrogen atmosphere; the resulting suspension was stirred for 5 h. The insoluble salt was removed by vacuum filtration, and the filtrate was concentrated under reduced pressure. The residue was redissolved in diethyl ether (150 mL) and washed with 100 mL of a basic $Na_2S_2O_3$ aqueous solution (5% wt in aqueous saturated sodium bicarbonate) and brine (100 mL). The organic layer was dried over $MgSO_4$ and filtered under a vacuum. The resulting solution was concentrated under reduced pressure to afford *tert*-butyl iodoacetate as a pale-yellow liquid (29.4 g, 95%). The crude *tert*-butyl iodoacetate, was dried over 4 Å molecular sieves to remove the trace water residue before use.

^{1}**H NMR** (400 MHz, $CDCl_3$): δ 3.61 (s, 2H), 1.46 (s, 9H) ppm.

^{13}**C NMR** (101 MHz, $CDCl_3$): δ 167.8, 82.3, 27.6, –2.6 ppm.

Preparation of a $CeCl_3$·2LiCl solution

The $CeCl_3$·2LiCl complex THF solution was prepared according to a literature procedure from Knochel et al.[106] A 50 mL Schlenk flask was charged cerium chloride heptahydrate (1.512 g, 4.1 mmol), anhydrous lithium chloride (0.345 g, 8.1 mmol—LiCl was pre-dried in oven at 100 °C for 5 hours) and a stir bar. The top joint was sealed, the side arm of the flask was connected to a vacuum line, and the flask was immersed in an oil bath (Figure 3–2a). The solids were stirred under high vacuum, and the temperature was increased slowly (+10 °C increases every 2 h). Finally, it was maintained at a temperature of 140 °C for 3 hours. The oil bath was removed and the mixture was allowed to cool to rt under vacuum. The vacuum was disconnected and replaced with argon inflow. Anhydrous THF (42 mL) was then added to the solids (Figure 3–2b) and stirred

for 72 hours, at which point the solution was colorless and transparent (~0.1 M, Figure 3–2c). *Note*: this solution is very hygroscopic and should be used up within 2 weeks.

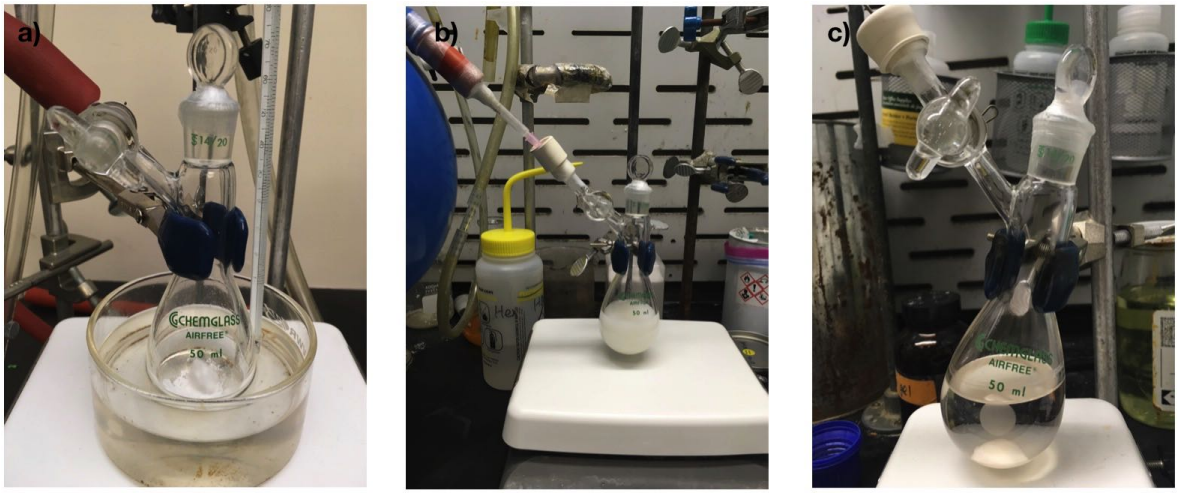

Figure 3–2. Preparation $CeCl_3 \cdot 2LiCl$ THF solution. (a) Drying of $CeCl_3 \cdot 2LiCl$ under hi-vac. (b) $CeCl_3 \cdot 2LiCl$ mixed with THF under argon. (c) $CeCl_3 \cdot 2LiCl$ is a colourless solution after 72 hours stirring at rt.

Synthesis of 9-bromo-9-phenylfluorene

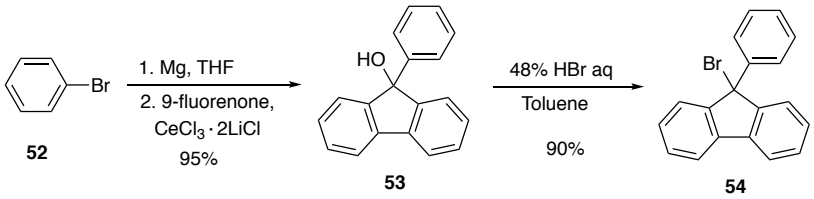

9-Hydroxyl-9-phenyluorene (**PfOH**, **53**). To a suspension of magnesium turnings (9.2 g, 382 mmol) in anhydrous THF (5 mL) under an argon atmosphere was added 0.5 mL of bromobenzene neat at rt in one portion to initiate the reaction. The reaction vessel was cooled to 0 °C on an ice bath, followed by the dropwise addition of a THF solution of bromobenzene (1.2 M, 270 mL) at 0 °C. The resulting reaction solution was allowed to reach rt and stirred vigorously for an additional 2 h. The exact concentration of the resulting phenyl magnesium bromide solution was determined by titration with salicylaldehyde phenylhydrazone. 25 This phenyl magnesium bromide solution (180 mL, 216 mmol) was transferred into a flame-dried single-neck flask by a syringe. To this solution were added $CeCl_3 \cdot 2LiCl$ (15 mL, 0.1 M) THF solution in one portion and 9-fluorenone (30.1 g, 186 mmol) by portions. After 15 min, TLC analysis showed full conversion. The reaction was quenched with diluted hydrochloric acid (1.0 M, 100 mL) at 0 °C. The resulting solution was extracted with Et_2O (3 × 150 mL). The combined organic layer was washed with brine, dried over $MgSO_4$, filtered, and concentrated under reduced pressure to yield PfOH as pale-yellow crystals (40.8 g, 95%).

Mp 108–109 °C.

FTIR (thin film): 3544, 3423, 3059, 1603, 1448, 774, 732, 701 cm^{-1}.

^{1}**H NMR** (400 MHz, $CDCl_3$): δ 7.75 (d, J = 7.5 Hz, 2H), 7.53–7.41 (m, 4H), 7.34 (dq, J = 15.1, 7.5 Hz, 7H), 2.79 (s, 1H) ppm.

^{13}C NMR (101 MHz, $CDCl_3$): δ 150.4, 143.2, 139.5, 129.0, 128.4, 128.2, 127.2, 125.4, 124.8, 120.1, 83.6 ppm.

9-Bromo-9-phenyluorene (PfBr, 54). PfBr was prepared according to the reported procedure. 26 The above PfOH (36.1 g, 140 mmol) was dissolved in toluene (150 mL), and aqueous HBr (48% w/w, 50 mL) was added at rt. This heterogeneous mixture was stirred vigorously at rt for 48 h, away from light. The mixture was then extracted with toluene (3 × 100 mL). The combined organic layer was washed with brine (6 × 150 mL), dried over $MgSO_4$, filtered, and concentrated under reduced pressure to afford the crude product as a light-yellow solid. Recrystallization with hexane afforded pale-yellow crystals (40.2 g, 90%).

Mp 100–101 °C.

FTIR (thin film): 3056, 1603, 837, 738, 694 cm^{-1}.

^{1}H NMR (400 MHz, $CDCl_3$): δ 7.67 (dt, J = 7.6, 0.9 Hz, 2H), 7.60–7.49 (m, 4H), 7.36 (td, J = 7.5, 1.2 Hz, 2H), 7.35–7.18 (m, 5H) ppm.

^{13}C NMR (101 MHz, $CDCl_3$): δ 149.6, 141.1, 138.1, 129.0, 128.5, 128.3, 128.0, 127.4, 126.1, 120.3, 67.5 ppm.

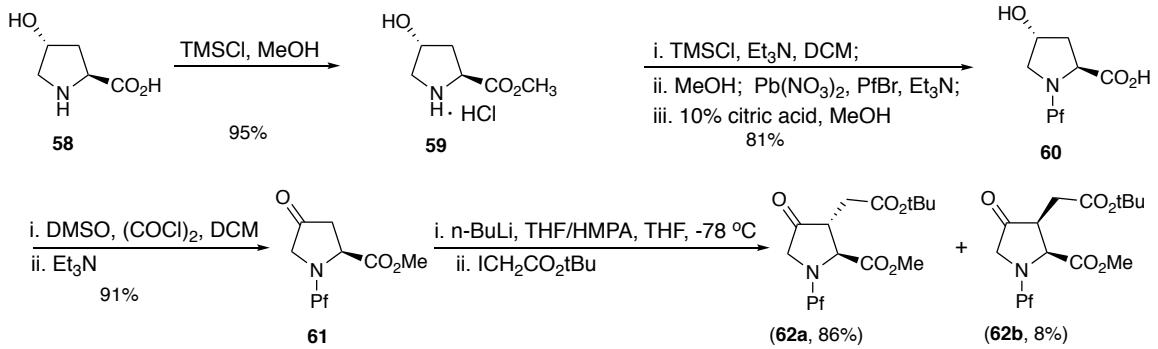

(2*S*,4*R*)-4-Hydroxypyrrolidine-2-carboxylic acid methyl ester hydrochloride (59). *trans*-4-Hydroxyl-L-proline (**58**, 10.0 g, 76 mmol) was suspended in methanol (150 mL) under argon. The suspension was cooled to 0 °C in an ice bath, followed by the dropwise addition of chlorotrimethylsilane (33.9 mL, 267 mmol). After 30 min, it was allowed to warm up to rt and stirred overnight. The solvent was removed under reduced pressure, the residue was triturated with Et_2O (100 mL), and ester **59** was obtained as white crystals (13.1 g, 95%).

^{1}H NMR (400 MHz, D_2O): δ 4.78–4.68 (m, 2H), 3.88 (s, 3H), 3.56 (dd, J = 12.6, 3.8 Hz, 1H), 3.44 (dt, J = 12.5, 1.6 Hz, 1H), 2.52 (ddt, J = 14.3, 7.8, 1.8 Hz, 1H), 2.32 (ddd, J = 14.5, 10.5, 4.3 Hz, 1H) ppm.

^{13}C NMR (101 MHz, D_2O): δ 170.2, 69.4, 58.1, 53.8, 53.4, 36.6 ppm.

HRMS (ESI-TOF) m/z: $[M + H]^+$ calcd for $C_6H_{12}NO_3$, 146.0817; found, 146.0817.

Methyl (2*S*)-4-oxo-1-(9-phenyl-9*H*-fluoren-9-yl) pyrrolidine-2-carboxylate (60). 60 was prepared according to the reported procedures.[100] The amine salt **59** (8.0 g, 44 mmol) was suspended in chloroform (300 mL) under argon. The reaction vessel was cooled to 0 °C in an ice bath, and trimethylamine (22.7 mL, 154 mmol) was added, followed by dropwise addition of chlorotrimethylsilane (14.7 mL, 110 mmol). The reaction was

stirred for 10 min at 0 °C, then allowed to warm up to rt, followed by heating to reflux for 2 h with vigorous stirring. The reaction mixture was cooled to 0 o C and methanol (2.7 mL, 66 mmol) was added to quench the excess TMSCl. The reaction was allowed to warm up to rt and stirred for 2 h. Anhydrous triethylamine (6.2 mL, 44 mmol) was added, followed 5 min. later by $Pb(NO_3)_2$ (11.9 g, 35 mmol) and **PfBr** (18.8 g, 57 mmol). The heterogeneous mixture was stirred vigorously at rt for 5 days. After full conversion, the reaction mixture was filtered and the filtrate was evaporated under reduced pressure. The residue was dissolved in a 10 % w/v solution of citric acid in methanol (250 mL), and allowed to react for an additional 1.5 h. The solvents were removed under reduced pressure. The residue was purified by column chromatography (25–50% acetone/hexane as elution gradient). The *N*-Pf-pyrrolidine **60** was recovered as a white foam-like solid (15.1 g, 89%).

Mp 85–86 °C.

FTIR (thin film): 3443, 3057, 2946, 1727 cm^{-1}.

^{1}**H NMR** (400 MHz, $CDCl_3$): δ 7.73 (dt, *J* = 7.5, 0.9 Hz, 1H), 7.64 (dt, *J* = 7.5, 1.0 Hz, 1H), 7.59 – 7.50 (m, 3H), 7.42 (td, *J* = 7.5, 1.1 Hz, 1H), 7.37 – 7.18 (m, 6H), 7.14 (td, *J* = 7.5, 1.2 Hz, 1H), 4.48 (q, *J* = 5.5 Hz, 1H), 3.56 (dd, *J* = 10.0, 5.3 Hz, 1H), 3.27 (dd, *J* = 8.9, 5.2 Hz, 1H), 3.23 (s, 3H), 2.90 (dd, *J* = 10.0, 5.0 Hz, 1H), 1.96 (dt, *J* = 12.8, 5.7 Hz, 1H), 1.77 (ddd, *J* = 13.0, 8.9, 6.0 Hz, 1H) ppm.

^{13} **C NMR** (101 MHz, $CDCl_3$): δ 175.9, 147.2, 146.1, 142.7, 141.4, 139.9, 128.7, 128.4, 128.3, 127.6, 127.3,127.3, 127.2, 127.1, 126.4, 120.1, 119.8, 70.3, 59.3, 56.8, 51.3, 39.9 ppm.

HRMS (ESI) m/z (M+H) + calcd. for $[C_{25}H_{23}NO_3+H]^+$ 386.1756, found 386.1750.

Methyl (2*S*)-4-oxo-1-(9-phenyl-9*H*-fluoren-9-yl)pyrrolidine-2-carboxylate (61). Preparation of ketone **61** was modified from a literature procedure.[102] Oxalyl chloride (5.7 mL, 66 mmol) was added to DCM (anhydrous, 150 mL) at - 78 °C under argon atmosphere, followed by dropwise addition of anhydrous DMSO (9.3 mL, 131 mmol). After 20 mins, a solution of **60** (10.1 g, 26 mmol) in DCM (50 mL) was added dropwise. The mixture was stirred for an additional 2 h. The reaction mixture was then treated with triethylamine (anhydrous, 60 mL) and allowed warm up to rt A saturated aqueous solution of $NaHCO_3$ (200 mL) was added, and the biphasic mixture was extracted with Et_2O (3 × 150 mL). The combined organic layer was washed with brine, dried over $MgSO_4$ and filtered. The solvent was evaporated under reduced pressure. The residue was purified by flash chromatography (25% acetone/hexane). Ketone **61** was recovered as a white crystalline solid (9.1 g, 91%).

Mp 128–129 °C.

FTIR (thin film): 3060, 2949, 2838, 1758, 1739 cm^{-1}.

^{1} **H NMR** (400 MHz, $CDCl_3$): δ 7.83–7.62 (m, 2H), 7.49–7.40 (m, 3H), 7.44–7.35 (m, 3H), 7.35 –7.16 (m, 5H), 3.76 (d, *J* = 17.8 Hz, 1H), 3.76 (dd, *J* = 8.6, 2.9 Hz, 1H), 3.48 (dt, *J* = 17.8, 1.2 Hz, 1H), 3.20 (s, 3H), 2.44 (dd, *J* = 18.1, 8.6 Hz, 1H), 2.29 (dd, *J* = 18.1, 2.9 Hz, 1H) ppm.

^{13}**C NMR** (101 MHz, $CDCl_3$): δ 212.9, 173.1, 146.5, 145.3, 141.8, 140.9, 140.3, 128.9, 128.9, 128.6, 128.0, 127.7, 127.6, 127.0, 126.9, 125.5, 120.3, 120.1, 76.0, 58.2, 55.2, 51.5, 51.5, 41.6 ppm.

HRMS (ESI) m/z (M+H) $^+$ calcd. for $[C_{25}H_{21}NO_3+H]^+$ 384.1600, found 384.1602.

Methyl (2*S*,3*R*)-3-[2-*tert*-butoxy]-2-oxoethyl]-4-oxo-1-(9-phenyl-9*H*-fluoren-9-yl)pyrrolidine-2-carboxylate (62a) and Methyl (2*S*,3*S*)-3-[2-(*tert*-butoxy)-2-oxoethyl]-4-oxo-1-(9-phenyl-9*H*-fluoren-9-yl)pyrrolidine-2-carboxylate (62b).

Method A. Ketone 10 (6.0 g, 16 mmol) was dissolved in THF (41.0 mL) and anhydrous HMPA (4.1 mL) in a single-neck □ask and under an Ar atmosphere. The solution was cooled to – 78 °C on a dry ice/acetone bath, followed by a dropwise addition of n-butyllithium (2.1 M in cyclohexane, 7.8 mL, 16 mmol). After 30 min, tert-butyl iodoacetate (18.9 g, 79 mmol) was added dropwise to the reaction. The solution was allowed to warm up to - 41 °C (dry ice/acetonitrile bath) and stirred for an additional 5.5 h. The reaction was quenched at - 41 °C by a quick addition of phosphoric acid (10% wt, 15 mL) and allowed to warm up to rt. Water (50 mL) was added, and the mixture was extracted with Et_2O (3 × 100 mL). The combined organic layers were washed with brine, dried over $MgSO_4$, and □ltered. The solvents were evaporated under reduced pressure to yield the alkylated products 11a and 11b. The diastereomeric ratio was determined with ^{1}H NMR of the crude product; dr = 9:1 with ketones 11a as the major isomer. The crude products from Method A were retaken in MeOH (5 mL) and stored at - 20 °C overnight in a freezer. The formed white solid was filtered and washed with cold methanol (5 mL) to yield 11a as a white solid (6.2 g). The mother liquor's solvents were removed, and the residue was purified by column chromatography on silica gel (15–25% EtOAc/ hexane as elution gradient) to yield 11a (525 mg) and 11b (621 mg, 8%) as a white foam-like solid.

Method B. This method was adapted from a reported procedure 14 using $BrCH_2COOtBu$ (3.5 equiv)/NaI (0.5 equiv). The alkylated ketones 11a and 11b were recovered with a dr = 5:1 (^{1}H NMR analysis of the crude).

trans-Ketodiester **62a** (Major, 6.725 g, 86%).

FTIR (thin film): 2974, 1758, 1730 cm^{-1}.

^{1}H NMR (400 MHz, $CDCl_3$): δ 7.70 (dd, *J* = 7.6, 1.0 Hz, 2H), 7.50 (dt, *J* = 7.6, 1.6 Hz, 3H), 7.43 (dt, *J* = 7.5, 0.8 Hz, 1H), 7.43–7.33 (m, 2H), 7.32–7.21 (m, 5H), 3.78 (d, *J* = 17.6 Hz, 1H), 3.45 (d, *J* = 17.6 Hz, 1H), 3.44 (d, *J* = 6.1 Hz, 1H), 3.10 (s, 3H), 2.82 (dd, *J* = 12.4, 6.2 Hz, 1H), 2.45–2.38 (m, 2H), 1.31 (s, 9H) ppm.

^{13}C NMR (101 MHz, $CDCl_3$): δ 211.8, 172.9, 169.6, 146.0, 144.4, 141.4, 141.1, 140.4, 128.9, 128.5, 127.9, 127.8, 127.7, 127.3, 127.0, 126.0, 120.2, 120.0, 81.4, 75.8, 63.7, 55.7, 51.5, 49.2, 34.2, 27.9 ppm.

HRMS (ESI-TOF) m/z: $[M + H]^+$ calcd for $C_{31}H_{32}NO_5$, 498.2280; found, 498.2278.

cis-Ketodiester **62b** (Minor, 621 mg, 8%).

FTIR (thin film): 2974, 1758, 1727 cm^{-1}.

^{1}H NMR (400 MHz, $CDCl_3$): δ 7.76–7.71 (m, 1H), 7.68 (d, *J* = 7.6 Hz, 1H), 7.41 (ddt, *J* = 9.0, 5.1, 1.6 Hz, 5H), 7.33 (dtd, *J* = 17.9, 7.4, 1.1 Hz, 3H), 7.24 (dt, *J* = 7.0, 1.1 Hz, 3H), 4.02 (d, *J* = 8.2 Hz, 1H), 3.80 (d, *J* = 17.6 Hz, 1H), 3.58 (dd, *J* = 17.6, 1.1 Hz, 1H), 3.15 (s, 3H), 3.11–3.01 (m, 1H), 2.57 (dd, *J* = 17.4, 5.2 Hz, 1H), 1.84 (dd, *J* = 17.4, 8.9 Hz, 1H), 1.34 (s, 9H) ppm.

^{13}C NMR (101 MHz, $CDCl_3$): δ 212.2, 171.7, 170.3, 146.9, 145.3, 141.7, 141.3, 139.8, 128.9, 128.8, 128.6, 128.1, 127.7, 127.6, 126.8, 126.7, 125.4, 120.1, 81.1, 75.4, 61.9, 53.7, 51.1, 48.0, 31.1, 28.0 ppm.

HRMS (ESI-TOF) m/z: $[M + H]^+$ calcd for $C_{31}H_{32}NO_5$, 498.2280; found, 498.2275.

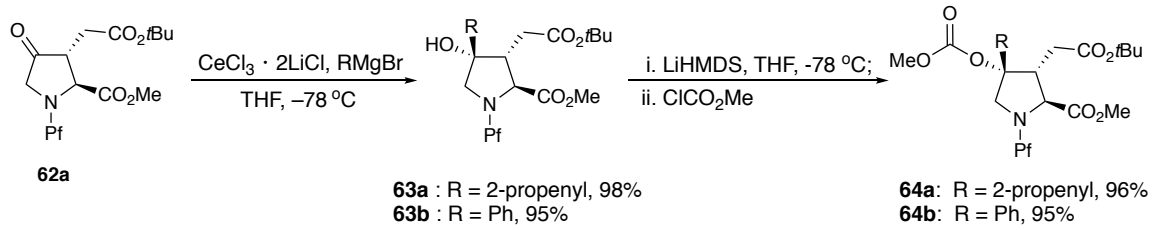

Methyl (2*S*,3*R*,4*S*)-3-(2-(*tert*-butoxy)-2-oxoethyl)-4-hydroxy-1-(9-phenyl-9*H*-fluoren-9-yl)-4-(prop-1-en-2-yl)pyrrolidine-2-carboxylate (63a). A single-neck flask was charged with magnesium turnings (322 mg, 13.1 mmol) and dry THF (20 mL) under an argon atmosphere, followed by the dropwise addition of 2-bromopropene (1.10 mL, 12.4 mmol) at rt. The suspension was stirred for 2 h and gradually turned to a pale-yellow solution. The resulting isopropenyl magnesium bromide solution was titrated using salicylaldehyde phenylhydrazone. To a single-neck flask was added ketone 11a (4.105 g, 8.25 mmol), purged with argon, and a $CeCl_3$·2LiCl solution in THF (107 mL, 0.1 M) was added via syringe at rt. The clear solution was cooled to –78 °C and stirred for 15 min. The *i*-PrMgBr solution (19.5 mL, 0.55 M) was added dropwise at –78 °C. After 2 h, the reaction was quenched at – 78 °C with a diluted 0.1 M HCl aqueous solution (10 mL). The biphasic mixture was extracted with Et_2O (2 × 100 mL), washed with brine, dried over $MgSO_4$, and filtered. The solvent was evaporated under reduced pressure to afford tertiary alcohol **63a** as a white foamlike solid (4.305 g, 98%), which was used without further purification.

FTIR (thin film): 3510, 3060, 2978, 2949, 2885, 1715, 1706 cm^{-1}.

^{1}H NMR (400 MHz, $CDCl_3$): δ 7.74 (d, J = 7.6 Hz, 1H), 7.67–7.50 (m, 4H), 7.44 (t, *J* = 7.5 Hz, 1H), 7.39–7.28 (m, 5H), 7.23–7.09 (m, 2H), 5.13 (s, 1H), 4.91 (s, 1H), 3.72 (d, *J* = 12.1 Hz, 1H), 3.18 (s, 3H), 3.07 (d, *J* = 3.9 Hz, 1H), 3.06 (d, *J* = 17.7 Hz, 1H), 2.85 (dt, *J* = 9.7, 6.2 Hz, 1H), 2.22 (dd, *J* = 16.3, 5.4 Hz, 1H), 1.99 (dd, *J* = 16.3, 6.7 Hz, 1H), 1.82 (s, 3H), 1.78 (s, 1H), 1.30 (s, 9H) ppm.

^{13}C NMR (101 MHz, $CDCl_3$): δ 174.9, 171.5, 146.8, 146.4, 144.6, 142.8, 141.7, 139.7, 129.0, 128.4, 128.3, 127.9, 127.7, 127.4, 127.3, 127.0, 126.2, 120.1, 119.7, 113.0, 81.9, 80.6, 66.3, 61.2, 51.3, 47.0, 32.3, 29.7, 27.9, 19.6 ppm.

HRMS (ESI-TOF) m/z: $[M + H]^+$ calcd for $C_{34}H_{38}NO_5$, 540.2744; found, 540.2730.

Methyl (2*S*,3*R*,4*S*)-3-(2-(*tert*-Butoxy)-2-oxoethyl)-4-hydroxy-4phenyl-1-(9-phenyl-9*H*-fluoren-9-yl) pyrrolidine-2-carboxylate (63b). This compound proceeded as described for **12a** with the following modifications: **62a** (2.530 g, 5.08 mmol), phenyl magnesium bromide (12 mL, 1.1 M), and $CeCl_3$·2LiCl (127 mL, 0.1 M). The crude product was purified by silica gel chromatography with ethyl acetate/hexanes as eluent (15–25% gradient). Alcohol **63b** was recovered as a white foam-like solid (2.780 g, 95%).

FTIR (thin film): 3506, 3059, 2977, 2946, 2879, 1729, 742, 704 cm^{-1}.

^{1}H NMR (400 MHz, $CDCl_3$): δ 7.75 (ddd, *J* = 7.5, 1.2, 0.6 Hz, 1H), 7.67–7.62 (m, 2H), 7.59–7.53 (m, 4H), 7.45 (dt, *J* = 7.5, 1.1 Hz, 1H), 7.40–7.36 (m, 2H), 7.35–7.28 (m, 4H), 7.25–7.24 (m, 1H), 7.24–7.22 (m, 1H), 7.22–7.19 (m, 1H), 7.19–7.16 (m, 1H), 3.86 (d, *J* = 12.1 Hz, 1H), 3.35 (d, *J* = 12.1 Hz, 1H), 3.22 (d, *J* = 12.0 Hz), 3.20 (s, 3H), 3.09–3.01 (m, 1H), 2.20 (dd, *J* = 16.3, 5.6 Hz, 1H), 2.08 (dd, *J* = 16.3, 6.7 Hz, 1H), 1.18 (s, 9H) ppm.

^{13}C NMR (101 MHz, $CDCl_3$): δ 174.9, 171.4, 146.7, 146.5, 142.8, 141.8, 141.6, 139.8, 129.0, 128.5, 128.4, 128.2, 127.9, 127.8, 127.4, 127.3, 127.1, 127.1, 126.1, 125.6, 120.2, 119.8, 81.1, 80.7, 66.4, 65.3, 51.4, 51.1, 32.5, 27.7 ppm.

HRMS (ESI-TOF) m/z: $[M + H]^+$ calcd for $C_{37}H_{38}NO_5$, 576.2744; found, 576.2738.

Methyl (2*S*,3*R*,4*S*)-3-(2-(*tert*-butoxy)-2-oxoethyl)-4-((methoxycarbonyl)oxy)-1-(9-phenyl-9*H*-fluoren-9-yl)-4-(prop-1-en-2-yl)pyrrolidine-2-carboxylate (64a). Allylic alcohol **63a** (3.8 g, 7.0 mmol) was dissolved in THF (40 mL) under an argon atmosphere, cooled to –78 °C. Lithium bis(trimethylsilyl)-amide solution (8.5 mL, 1.0 M) was added dropwise, and the reaction was stirred for 20 min. Methyl chloroformate (1.6 mL, 21.1 mmol) was added slowly, and the solution was allowed to react for 2 h. The reaction was quenched at –78 °C with a saturated ammonium chloride aqueous solution (20 mL) and extracted with Et_2O (2 × 100 mL). The combined organic layer was washed with brine, dried over $MgSO_4$, and filtered. The solvent was evaporated under reduced pressure to obtain carbonate 13a as a white foam-like solid. (4.1 g, 95%). Purity of the crude product was excellent, and **64a** was used as is for the next step.

FTIR (thin film): 2978, 2950, 1753, 1731 cm^{-1}.

^{1}H NMR (400 MHz, $CDCl_3$): δ 7.70 (d, *J* = 7.5 Hz, 1H), 7.62 (d, *J* = 7.5 Hz, 1H), 7.57–7.49 (m, 2H), 7.44 (d, *J* = 7.6 Hz, 1H), 7.41–7.34 (m, 2H), 7.33–7.26 (m, 1H), 7.24–7.09 (m, 5H), 4.96 (s, 1H), 4.87 (s, 1H), 3.98 (d, *J* = 12.9 Hz, 1H), 3.68 (s, 3H), 3.65–3.68 (m, 1H), 3.18 (d, *J* = 8.5 Hz, 1H), 3.15 (s, 3H), 2.80 (dt, *J* = 8.1, 4.7 Hz, 1H), 2.42 (dd, *J* = 16.8, 4.8 Hz, 1H), 2.07 (dd, *J* = 16.9, 7.8 Hz, 1H), 1.90 (s, 3H), 1.31 (s, 9H) ppm.

^{13}C NMR (101 MHz, $CDCl_3$): δ 174.0, 170.8, 153.6, 146.2, 146.1, 142.5, 141.9, 141.1, 140.1, 128.6, 128.4, 128.3, 128.1, 127.4, 127.4, 127.3, 126.9, 126.0, 120.0, 119.7, 90.1, 80.5, 66.0, 55.6, 54.4, 51.3, 48.2, 32.5, 27.9, 20.4 ppm.

HRMS (ESI-TOF) m/z: $[M + H]^+$ calcd for $C_{36}H_{40}NO_7$, 598.2805; found, 598.2797.

Methyl (2*S*,3*R*,4*S*)-3-(2-(*tert*-butoxy)-2-oxoethyl)-4((methoxycarbonyl)oxy)-4-phenyl-1-(9-phenyl-9*H*-fluoren-9-yl)pyrrolidine-2-carboxylate (64b). This compound proceeded as described for **64a**. Allylic alcohol (450 mg, 0.782 mmol) afforded carbonate **64b** (472 mg, 95%) as a foam-like solid.

FTIR (thin film): 3060, 2977, 2952, 1749, 1733 cm^{-1}.

^{1}H NMR (400 MHz, $CDCl_3$): δ 7.72 (ddd, *J* = 7.6, 1.1, 0.6 Hz, 1H), 7.65–7.58 (m, 3H), 7.52–7.48 (m, 1H), 7.45–7.30 (m, 7H), 7.30–7.24 (m, 4H), 7.24–7.15 (m, 2H), 4.34 (d, *J* = 13.0 Hz, 1H), 3.92 (d, *J* = 13.0 Hz, 1H), 3.67 (s, 3H), 3.28 (d, *J* = 8.2 Hz, 1H), 3.12 (s, 3H), 2.87 (dt, *J* = 8.0, 5.0 Hz, 1H), 2.38 (dd, *J* = 16.8, 5.0 Hz, 1H), 2.13 (dd, *J* = 16.8, 7.9 Hz, 1H), 1.22 (s, 9H) ppm.

^{13}C NMR (101 MHz, $CDCl_3$): δ 173.8, 170.3, 153.7, 146.2, 146.0, 142.4, 141.3, 140.1, 139.2, 128.7, 128.5, 128.4, 128.4, 128.1, 127.6, 127.5, 127.4, 127.3, 126.9, 126.1, 125.0, 120.1, 119.7, 89.5, 80.4, 66.4, 57.8, 54.5, 52.7, 51.3, 32.5, 27.9 ppm.

HRMS (ESI) m/z: $[M + H]^+$ calcd for $C_{39}H_{40}NO_7$, 634.2799; found, 634.2802.

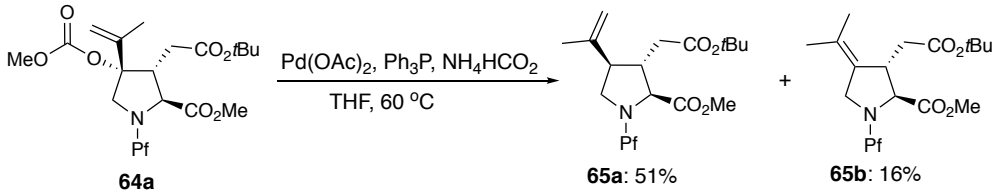

Methyl (2*S*,3*S*,4*R*)-3-(2-(*tert*-butoxy)-2-oxoethyl)-1-(9-phenyl-9*H*-fluoren-9-yl)-4-(prop-1-en-2-yl)pyrrolidine-2-carboxyl-ate (65a)

and **Methyl (2S,3S)-3-(2-(*tert*-butoxy)-2-oxoethyl)-1-(9-phenyl-9*H*-fluoren-9-yl)-4-(propan-2-ylidene)pyrrolidine-2-carboxylate (65b).**

Allylic carbonate 13a (621 mg, 1.36 mmol), palladium acetate (15 mg, 0.066 mmol), triphenyl phosphine (71 mg, 0.27 mmol), ammonium formate (427 mg, 6.78 mmol), and THF (10 mL) were charged into a single-neck flask equipped with a condenser. The flask was purged with three vacuum/argon cycles. The reaction vessel was heated at 60 °C with stirring until full conversion was observed by TLC (~5 h). The reaction mixture was filtered on a Celite pad and washed with Et_2O (20 mL). The filtrate was concentrated under reduced pressure to a brown oil. The crude oil was purified by silica gel chromatography with methyl tert-butyl ether/hexane as an eluent (15–25% gradient). The reduced diesters were recovered as white foam-like solids: 14a (263 mg, 51%) and 14b (82 mg, 16%).

Diester **65a**:

FTIR (thin film): 3059, 2977, 2930, 2855, 1728 cm^{-1}.

^{1}H NMR (400 MHz, $CDCl_3$): δ 7.74 (dd, *J* = 7.6, 1.1 Hz, 1H), 7.60 (d, *J* = 7.5 Hz, 1H), 7.58□ 7.48 (m, 3H), 7.44 (dt, *J* = 7.5, 1.1 Hz, 1H), 7.37–7.27 (m, 2H), 7.25–7.17 (m, 2H), 7.11 (dt, *J* = 7.5, 1.1 Hz, 1H), 4.75 (s, 2H), 3.43 (t, *J* = 11.1 Hz, 1H), 3.38–3.29 (m, 1H), 3.22 (s, 3H), 2.73–2.67 (m, 1H), 2.60 (dddd, *J* = 14.3, 8.9, 7.0, 5.2 Hz, 1H), 2.27 (dt, *J* = 11.0, 7.9 Hz, 1H), 2.07 (dd, *J* = 16.1, 5.2 Hz, 1H), 1.96 (dd, J = 16.1, 7.0 Hz, 1H), 1.69 (s, 3H), 1.29 (s, 9H) ppm.

^{13}C NMR (101 MHz, $CDCl_3$): δ 175.4, 170.7, 147.6, 146.8, 143.9, 142.7, 142.1, 139.3, 128.7, 128.3, 128.2, 128.0, 127.3, 127.2, 127.2, 127.1, 125.7, 120.0, 119.7, 113.5, 80.3, 67.5, 55.1, 52.2, 51.3, 43.9, 37.3, 27.9, 19.0 ppm.

HRMS (ESI) m/z: $[M + H]^+$ calcd for $C_{34}H_{38}NO_4$, 524.2801; found, 524.2805.

Diester **65b**:

FTIR (thin film): 3061, 2978, 2934, 2867, 1732 cm^{-1}.

^{1}H NMR (400 MHz, $CDCl_3$): δ 7.66 (dd, *J* = 12.5, 7.5 Hz, 2H), 7.53–7.42 (m, 3H), 7.42–7.27 (m, 4H), 7.25–7.16 (m, 5H), 4.01 (d, *J* = 12.5 Hz, 1H), 3.76 (d, *J* = 12.5 Hz, 1H), 3.38–3.25 (m, 1H), 3.02 (s, 3H), 2.93–2.81 (m, 1H), 2.44–2.23 (m, 2H), 1.62 (s, 3H), 1.57 (s, 3H), 1.33 (s, 9H) ppm.

^{13}C NMR (101 MHz, $CDCl_3$): δ 173.9, 171.2, 147.8, 146.1, 142.7, 140.9, 139.8, 133.2, 128.4, 128.3, 128.2, 127.7, 127.4, 127.3, 127.1, 126.9, 125.6, 123.4, 119.9, 119.7, 80.6, 65.0, 50.7, 49.2, 43.0, 40.1, 27.9, 21.3, 20.4 ppm.

HRMS (ESI) m/z: $[M + H]^+$ calcd for $C_{34}H_{38}NO_4$, 524.2801; found, 524.2809.

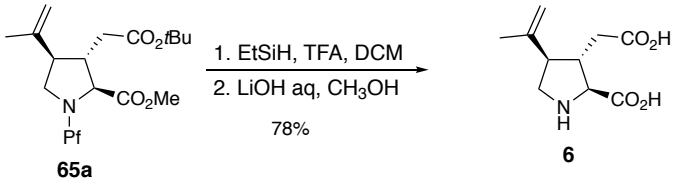

***allo*-Kainic Acid (6)**. *N*-Pf protected diester **65a** (103 mg, 0.197 mmol) was dissolved in dichloromethane (1 mL) at rt under argon. Triethyl silane (0.30 mL, 2.0 mmol) was added, followed by trifluoroacetic acid (0.19 mL, 3.0 mmol). The reaction was stirred at rt for 3 h, at which point a second portion of triethyl silane (0.63 mL, 3.9 mmol) and trifluoroacetic acid (0.39 mL, 5.9 mmol) was added. TLC showed full deprotection of the *N*-Pf group after an additional 4 h. The reaction was evaporated to dryness under reduced pressure. The residue was retaken in methanol (3 mL), a LiOH aqueous solution (1 mL, 2.5 M) was added, and the reaction was stirred at rt overnight. The reaction was then neutralized at 0 °C with a 1.0 M HCl aqueous solution, and the mixture was diluted with water (20 mL). The Pf-H byproduct was removed by extraction with petroleum ether (2 × 50 mL). The aqueous layer was concentrated to dryness under a high vacuum. The residue was retaken in water (5 mL) and purified by ion-exchange chromatography: ion-exchange resin Dowex 50WX4 100□200, eluting with 0.5 N aqueous ammonia. The eluting fractions were collected and analyzed by TLC for the presence of the desired product. (TLC plates were dried gently with a heat gun before being stained with ninhydrin; further heating revealed the presence of the amino acid 2 as yellow spots.) The fractions containing the product were combined and flash frozen, and the solvents were removed by lyophilization to yield a pale-yellow solid. This product was recrystallized with aqueous ethanol. The product was dissolved with minimal water, followed by the dropwise addition of ethanol until the crystal formed. It was then left standing at 0 °C, and *allo*-kainic acid was recovered after trituration as a white crystalline solid (33 mg, 78%).

Mp 239–242 °C.

FTIR (thin film): 3451, 2971, 1578 cm^{-1}.

^{1}H NMR (400 MHz, D_2O): δ 4.95 (bs, 1H), 4.94 (m, 1H), 3.92 (d, J = 8.1 Hz, 1H), 3.51 (dd, *J* = 11.8, 7.8 Hz, 1H), 3.33 (dd, *J* = 11.8, 10.6 Hz, 1H), 2.86 (dt, *J* = 10.5, 8.5 Hz, 1H), 2.72–2.59 (m, 2H), 2.41–2.32 (m, 1H), 1.73 (bs, 3H) ppm.

^{13}C NMR (101 MHz, D_2O): δ 179.3, 173.7, 140.6, 114.6, 64.9, 51.5, 48.2, 42.6, 39.7, 17.7 ppm. **HRMS** (ESI-TOF): m/z: $[M + H]^+$ calcd for $C_{10}H_{16}NO_4$, 214.1074; found, 214.1074.

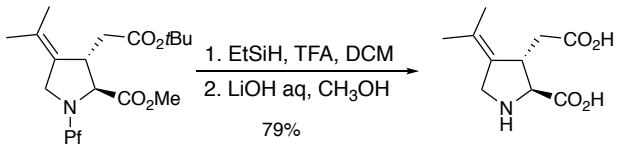

65b 55

***iso*–Kainic Acid (55)**. The compound proceeded as described for 2. Diester **65b** (50 mg, 0.95 mmol) was fully deprotected to afford *iso*–kainic **55** acid as a white crystalline solid (16 mg, 79%).

Mp 241–244 °C.

FTIR (thin film): 3421, 3182, 2920, 1732, 1554 cm^{-1}.

^{1}**H NMR** (400 MHz, D_2O): δ 4.16 (d, *J* = 1.6 Hz, 1H), 4.07 (d, *J* = 14.6, 1H), 3.96 (dd, *J* = 14.6, 1.9 Hz, 1H), 3.55 (t, *J* = 6.9 Hz, 1H), 2.51 (dd, *J* = 14.7, 6.9 Hz, 1H), 2.44 (dd, *J* = 14.6, 6.9 Hz, 1H), 1.74 (bs, 3H), 1.65 (bs, 3H) ppm.

^{13}**C NMR** (101 MHz, D_2O): δ 179.7, 173.7, 129.8, 125.7, 66.4, 46.7, 42.1, 41.2, 20.4, 20.3 ppm. **HRMS** (ESI-TOF) m/z: $[M + H]^+$ calcd for $C_{10}H_{16}NO_4$, 214.1074; found, 214.1075.

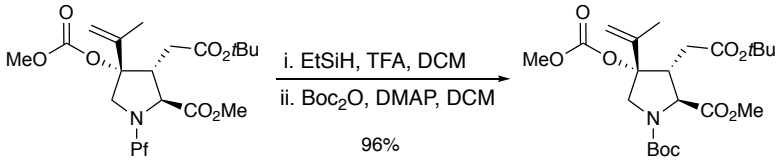

64a 66a

1-(*tert*-butyl)-2-methyl-(2*S*,3*R*,4*S*)-3-(2-(*tert*-butoxy)-2-oxo-ethyl)4-((methoxycarbonyl)oxy)-4-(prop-1-en-2-yl)pyrrolidine-1,2-dicarboxylate (66a). *N*-Pf protected allylic carbonate **64a** (3.010 g, 5.04 mmol) was dissolved in dichloromethane (50 mL) at rt under argon. Triethyl silane (2.4 mL, 15 mmol) was added, followed by the dropwise addition of trifluoroacetic acid (1.9 mL, 25 mmol). The reaction was stirred at rt for 1 h. Solvents were evaporated in vacuo; the TFA ammonium salt was recovered as a light-yellow waxy solid. The residue was retaken in dichloromethane (50 mL). Di-tert-butyl dicarbonate (1.8 g, 8.1 mmol) and 4-dimethylaminopyridine (1.5 g, 10 mmol) were added sequentially, and the reaction was allowed to stir at rt overnight. The reaction mixture was concentrated to dryness under reduced pressure. The residue was purified by column chromatography using ethyl acetate/hexanes as an eluent (15–25% gradient). *N*-Boc carbonate **66a** was recovered as a colorless oil (2.226 g, 97%).

FTIR (thin film): 2979, 1758, 1730, 1707 cm^{-1}.

^{1}**H NMR** (400 MHz, $CDCl_3$, two rotamers): δ 5.03 (s, 1H), 4.88 (s, 1H), 4.44 (d, *J* = 13.2 Hz, 1H), 4.00 (dd, *J* = 26.5, 9.6 Hz, 1H), 3.87–3.79 (m, 2H), 3.71 (s, 3H), 3.68 (s, 3H), 2.84–2.73 (m, 1H), 2.62 (dd, *J* = 17.5, 4.3 Hz, 1H), 2.39 (ddd, *J* = 17.6, 14.9, 7.6 Hz, 1H), 1.81 (s, 3H), 1.46–1.29 (m, 19H) ppm.

^{13}**C NMR** (101 MHz, $CDCl_3$, two rotamers): δ 172.5, 172.4, 170.7, 170.6, 154.2, 153.5, 153.4, 153.3, 139.5, 139.4, 114.1, 90.5, 89.7, 81.0, 80.7, 63.5, 63.0, 54.8, 54.7, 52.5, 52.3, 52.2, 52.1, 47.2, 46.6, 31.9, 31.6, 28.3, 28.1, 20.5, 20.4 ppm.

HRMS (ESI-TOF) m/z: $[M + Na]^+$ calcd for $C_{22}H_{35}NO_9Na$, 480.2204; found, 480.2221

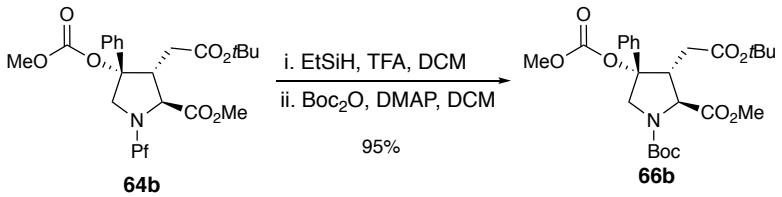

(2*S*,3*R*,4*S*)-1-(*tert*-Butyl)-2-methyl-3-(2-(*tert*-butoxy)-2-oxoethyl)4-((methoxycarbonyl)oxy)-4-phenyl-pyrrolidine-1,2-dicarboxylate (66b). This compound proceeded as described for **66a**. Allylic carbonate **64b** (451 mg, 0.712 mmol) afforded *N*-Boc carbonate **66b** as a colorless liquid (331 mg, 95%).

FTIR (thin film): 2974, 1755, 1727, 1705 cm^{-1}.

^{1}H NMR (400 MHz, $CDCl_3$): δ 7.41–7.35 (m, 2H), 7.34–7.28 (m, 3H), 4.66 (d, *J* = 13.3 Hz, 1H), 4.27 (t, *J* = 13.0 Hz, 1H), 4.16 (dd, *J* = 23.4, 9.5 Hz, 1H), 3.75 (s, 3H), 3.70 (s, 3H), 2.89 (ddd, *J* = 9.6, 7.8, 4.3 Hz, 1H), 2.61–2.43 (m, 2H), 1.45 (s, 9H), 1.31 (s, 9H) ppm.

^{13}C NMR (101 MHz, $CDCl_3$): δ 172.3, 172.2, 170.1, 170.0, 154.1, 153.5, 153.4, 153.3, 136.2, 128.8, 128.8, 128.2, 128.2, 124.7, 124.7, 90.0, 89.3, 80.9, 80.9, 80.7, 80.6, 64.0, 63.5, 54.8, 54.7, 53.9, 53.6, 52.4, 52.2, 52.0, 51.4, 31.7, 31.4, 30.9, 28.3, 28.2, 28.0, 27.9 ppm.

HRMS (ESI-TOF) m/z: $[M + H]^+$ calcd for $C_{25}H_{36}NO_9$, 494.2385; found, 494.2408.

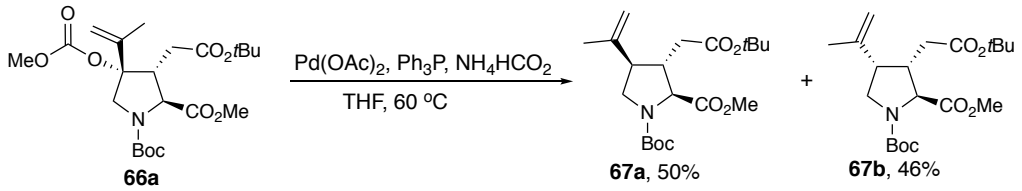

1-(*tert*-Butyl)-2-methyl-(2*S*,3*S*,4*R*)-3-(2-(tert-butoxy)-2-oxoethyl)4-(prop-1-en-2-yl)pyrrolidine-1,2-dicarboxylate (67a)

and **1-(*tert*-Butyl) 2-methyl (2*S*,3*S*,4*S*)-3-(2-(*tert*-butoxy)-2-oxoethyl)-4-(prop1-en-2-yl)pyrrolidine-1,2-dicarboxy-late (67b).**

These compounds proceeded as described for 14a and 14b. Allylic carbonate **66a** (2.010 g, 4.84 mmol) afforded a crude oil, which was purified by silica gel chromatography with ethyl acetate/hexane as an eluent (15–25% gradient). Diesters **67a** and **67b** were recovered as an inseparable mixture: colorless oil (1.592 g, 96%). The combined diastereomers were used as is for the next step.

HRMS (ESI) m/z: $[M + Na]^+$ calcd for $C_{20}H_{33}NO_6Na$, 406.2200; found, 406.2232.

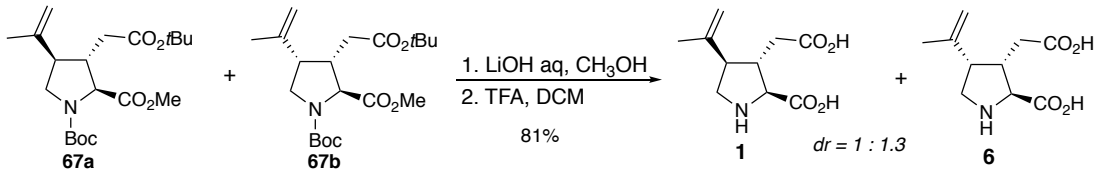

Kainic Acid (1) and ***allo*-kainic Acid (6)**. The diastereomeric mixture of **67a** and **67b** (605 mg, 1.46 mmol) was dissolved in methanol (20 mL), and a LiOH aqueous solution (2.5 N, 9.4 mL) was added. The mixture

was stirred at rt for 5 h. The reaction was neutralized at 0 °C with a diluted 1.0 N HCl aqueous solution and extracted with ethyl acetate (3 × 50 mL). The combined organic layer was dried over $MgSO_4$ and filtered. The solvents were evaporated under reduced pressure to obtain a colorless oil. The crude oil was retaken in dichloromethane (5.0 mL) under an argon atmosphere, and tri□uoroacetic acid (3.0 mL) was added at rt. The solution was stirred for 3 h and then was concentrated to dryness under reduced pressure to afford a light-yellow soild. This crude product was purified and recrystallized in methanol and water. The product was recovered as a white powder (273 mg, 81%) and consisted of kainic acid (**1**, 43%) and *allo*-kainic acid (**6**, 57%), as determined by ^{1}H NMR. The mixture of diastereomers proved to be inseparable with HPLC. The following data are for kainic acid (**1**).

^{1}H NMR (400 MHz, D_2O): δ 5.08 (bs, 1H), 4.78 (bs, 1H), 4.18 (d, J = 3.5 Hz, 1H), 3.67 (dd, J = 11.9, 7.3 Hz, 1H), 3.46 (t, J = 11.4 Hz, 1H), 3.18–3.00 (m, 2H), 2.53 (dd, J = 16.9, 6.3 Hz, 1H), 2.44 (dd, J = 16.8, 8.2 Hz, 1H), 1.78 (s, 3H) ppm.

HRMS (ESI-TOF) m/z: $[M + H]^+$ calcd for $C_{10}H_{16}NO_4$, 214.1074; found, 214.1076. MS analysis was conducted with the mixture of **1** and **6**.

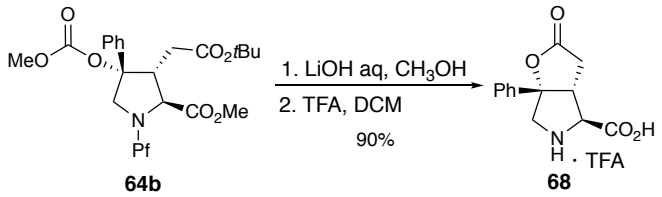

(3*R*,4*S*,6*S*)-4-Carboxy-2-oxo-6a-phenyl-5-(2,2,2-trifluoro-acetyl)hexahydro-2*H*-furo[2,3-c]pyrrol-5-ium (68). Benzylic carbonate **64b** (205 mg, 0.356 mmol) was dissolved in methanol (5 mL); a LiOH aqueous solution (1 mL, 2.5 N) was added at rt, and the mixture was stirred for 6 h. The reaction was neutralized at 0 °C with a diluted 1.0 N HCl aqueous solution and extracted with ethyl acetate (3 × 10 mL). The combined organic layer was dried over $MgSO_4$ and filtered. The solvents were evaporated under reduced pressure. This residue was retaken in dichloromethane (5 mL) under an argon atmosphere, trifluoroacetic acid (1 mL) was added, and the solution was stirred at rt for 3 h. The reaction mixture was concentrated to dryness under reduced pressure to obtain a light-yellow solid. This crude product was triturated with acetone (5 mL) and afforded lactone **68** as a white powder (90 mg, 90%). The solubility of lactone **68** is extremely poor in either H_2O, acetone, chloroform, or DMSO.

FTIR (thin film): 3521, 3017, 2983, 1783, 1605 cm^{-1}.

^{1}H NMR (400 MHz, D_2O): δ 7.59–7.46 (m, 5H), 4.36 (d, J = 4.8 Hz, 1H), 4.14 (d, J = 13.7 Hz, 1H), 3.92 (d, J = 13.7 Hz, 1H), 3.76–3.64 (m, 1H), 3.21 (dd, J = 19.1, 8.7 Hz, 1H), 2.98 (d, J = 19.2 Hz, 1H) ppm.

^{13}C NMR (101 MHz, DMSO-d_6): δ 175.5, 171.6, 139.5, 128.7, 128.2, 124.7, 95.0, 67.6, 58.1, 49.5, 34.7 ppm.

^{19}F NMR (376 MHz, DMSO-d_6): δ –73.45 ppm.

HRMS (ESI-TOF) m/z: $[M + H]^+$ calcd for $C_{13}H_{14}NO_4$, 248.0917; found, 248.0912.

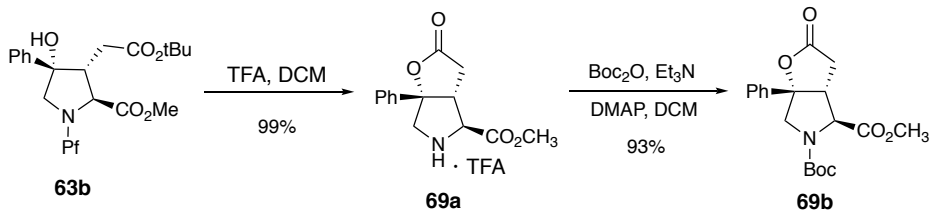

(3*R*,4*S*,6*S*)-4-(Methoxycarbonyl)-2-oxo-6a-phenyl-5-(2,2,2-trifluoroacetyl)hexahydro-2*H*-furo [2,3-c]pyrrol-5-ium (69a). To a stirred solution of allylic alcohol **63b** (2.268 g, 3.94 mmol) in dichloromethane (25 mL) was added trifluoroacetic acid (9.2 mL, 0.12 mol). After 3 h, TLC showed the full conversion. The reaction mixture was concentrated to dryness under reduced pressure. The residue was triturated in methanol (20 mL), and the insoluble byproduct (PfOH) was removed by filtration. The filtrate was concentrated to afford the trifluoroacetate salt of **69a** as a pale-yellow oil (1.465 g, 99%), which was used as is for the next step.

FTIR (thin film): 2955, 2914, 2847, 1777, 1733 cm^{-1}.

^{1}**H NMR** (400 MHz, CD_3OD): δ 7.27–7.21 (m, 4H), 7.21–7.15 (m, 1H), 4.50 (d, *J* = 6.6 Hz, 1H), 3.86 (d, *J* = 13.5 Hz, 1H), 3.69 (d, *J* = 13.5 Hz, 1H), 3.69 (s, 3H), 3.48 (ddd, *J* = 8.3, 7.1, 1.9 Hz 1H), 2.74 (dd, *J* = 18.7, 7.5 Hz, 1H), 2.67 (dd, *J* = 18.7, 2.0 Hz, 1H) ppm.

^{13}**C NMR** (101 MHz, CD_3OD): δ 175.0, 169.0, 137.3, 130.5, 130.3, 126.0, 94.4, 65.5, 57.6, 54.4, 50.4, 49.6, 49.4, 49.2, 49.0, 49.0, 48.6, 48.4, 34.2 ppm.

HRMS (ESI-TOF) m/z: $[M + H]^+$ calcd for $C_{14}H_{16}NO_4$, 262.1079; found, 262.1070.

5-(*tert*-Butyl)-4-methyl-(3*R*,4*S*,6*S*)-2-oxo-6a-phenylhexa-hydro-5*H*-furo[2,3-c]pyrrole-4,5-dicarboxylate (69b). To a solution of **69a** (TFA salt, 215 mg, 0.573 mmol) in dichloromethane (2 mL) was added DMAP (7 mg, 0.06 mmol), triethylamine (145 µL, 1.43 mmol), and Boc_2O (188 mg, 0.859 mmol). After 6 h, the reaction mixture was concentrated to dryness under reduced pressure. The crude residue was purified by column chromatography using dichloromethane/ methanol as an eluent (10–20% gradient). *N*-Boc-lactone **69b** was recovered as a colorless oil (192 mg, 93%).

FTIR (thin film): 2974, 2917, 1793, 1749, 1698 cm^{-1}.

^{1}**H NMR** (400 MHz, $CDCl_3$, two rotamers): δ 7.41 (m, 7.42–7.40, 4H), 7.39–7.33 (m, 4H), 4.41 (d, *J* = 4.6 Hz, 0.5H), 4.33–4.25 (m, 4H), 4.25–4.21 (m, 0.5H), 3.89 (dd, *J* = 13.0, 9.0 Hz, 1H), 3.83 (s, 3H), 3.23–3.17 (m, 1H), 2.90–2.62 (m, 2H), 1.44 and 1.46 (2s, 9H) ppm.

^{13}**C NMR** (101 MHz, $CDCl_3$, two rotamers): δ 174.2, 172.1, 172.0, 154.0, 153.0, 137.5, 137.2, 129.0, 128.9, 128.8, 124.8, 94.4, 93.4, 81.3, 81.2, 77.4, 77.2, 77.0, 76.7, 65.9, 65.8, 59.2, 58.6, 52.8, 52.6, 51.4, 50.5, 35.1, 34.9, 28.3, 28.2 ppm.

HRMS (ESI-TOF) m/z: $[M + Na]^+$ calcd for $C_{19}H_{23}NO_6Na$, 384.1423; found, 384.1455.

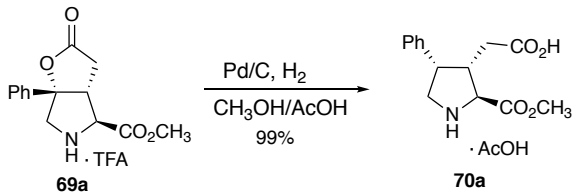

(2*S*,3*S*,4*S*)-1-Acetyl-3-(carboxymethyl)-2-(methoxycarbonyl)-4-phenylpyrrolidin-1-ium (**70a**).

To a solution of **69a** (TFA salt, 1.126 g, 2.97 mmol) in methanol (30 mL) were added acetic acid (0.71 mL) and Pd/C (56 mg). The reaction mixture was stirred under a hydrogen atmosphere (balloon) for 24 h. The resulting reaction mixture was filtered over a Celite pad. The filtrate was evaporated to dryness under reduced pressure and then a high vacuum to afford the acetate salt of **70a** as a pale-yellow powder (956 mg, 99%).

FTIR (thin film): 3390, 2521, 1739, 1673, 1635 cm^{-1}.

^{1}**H NMR** (400 MHz, CD_3OD): δ 7.42–7.31 (m, 4H), 7.29–7.22 (m, 2H), 4.59 (d, *J* = 6.2 Hz, 1H), 4.01–3.93 (m, 1H), 3.91 (s, 3H), 3.88–3.82 (m, 1H), 3.84–3.75 (m, 1H), 3.30–3.19 (m, 1H), 2.33 (ddd, *J* = 17.0, 7.8, 1.2 Hz, 1H), 2.22 (dd, *J* = 16.9, 6.1 Hz, 1H), 1.98 (s, 3H) ppm.

^{13}**C NMR** (101 MHz, CD_3OD): δ 173.8, 172.9, 168.9, 134.4, 128.6, 128.2, 127.7, 68.2, 58.1, 53.4, 53.1, 48.2, 48.0, 47.8, 47.6, 47.4, 47.2, 46.9, 43.9, 42.5, 33.0 ppm.

HRMS (ESI-TOF) m/z: $[M + H]^+$ calcd for $C_{14}H_{18}NO_4$, 264.1236; found, 264.1257.

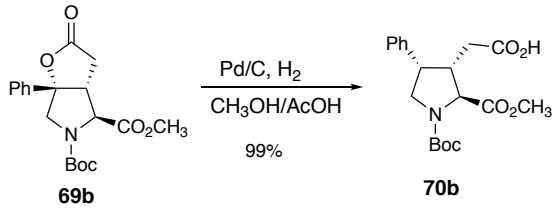

2-((2*S*,3*S*,4*S*)-1-(*tert*-Butoxycarbonyl)-2-(methoxycarbonyl)-4-phenylpyrrolidin-3-yl) acetic acid (**70b**). To a solution of lactone **69b** (175 mg, 0.484 mmol) in methanol (20 mL) was added Pd/C (25 mg). The reaction mixture was stirred under a hydrogen atmosphere (balloon) for 24 h. The resulting reaction solution was filtered over a celite pad. The filtrate was concentrated to dryness to under reduced pressure and afford **70b** as a colorless oil (174 mg, 99%).

FTIR (thin film): 2977, 2917, 1742, 1698 cm^{-1}.

^{1}**H NMR** (400 MHz, $CDCl_3$, two rotamers): δ 7.33–7.27 (m, 3H), 7.09–7.05 (m, 2H), 4.14 (d, *J* = 6.6 Hz, 0.4H), 4.02 (d, *J* = 6.7 Hz, 0.6H), 3.94 (ddd, *J* = 15.7, 10.9, 6.9 Hz, 1H), 3.84 (dd, *J* = 11.0, 4.7 Hz, 0.6H), 3.77 (d, *J* = 3.1 Hz, 3H), 3.74–3.73 (m, 0.4H), 3.71–3.65 (m, 1H), 2.99 (dt, *J* = 10.7, 6.9 Hz, 1H), 2.30 (ddd, *J* = 17.4, 14.7, 7.1 Hz, 1H), 2.14–2.02 (m, 1H), 1.45 and 1.49 (2s, 9H) ppm.

^{13}**C NMR** (101 MHz, $CDCl_3$): δ 176.8, 172.8, 172.5, 154.3, 153.5, 138.5, 138.4, 128.9, 127.7, 127.7, 127.4, 80.7, 80.6, 77.3, 77.0, 76.7, 63.3, 63.0, 52.5, 52.3, 50.8, 50.4, 45.2, 44.3, 44.1, 43.3, 33.1, 28.4, 28.3 ppm.

HRMS (ESI-TOF) m/z: $[M + Na]^+$ calcd for $C_{19}H_{25}NO_6Na$, 386.1580; found, 386.1556.

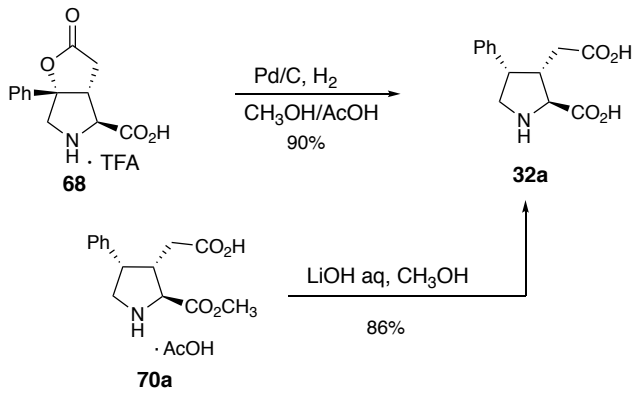

Phenyl kainic acid (4).

Synthetic Route from **68**. To a solution of lactone **68** (50 mg, 0.21 mmol), acetic acid (1 mL), and methanol (5 mL) was added Pd/C (5 mg). This reaction mixture was stirred under a hydrogen atmosphere (balloon) for 24 h. The resulting reaction mixture was filtered over a Celite pad, and the □ltrate was concentrated to dryness under reduced pressure. The residual acetic acid was removed under a high vacuum. The crude product was purified and recrystallized as described above for *allo*-kainic acid **6**. Phenylkainic acid (**32a**) was recovered as a white crystalline solid (45 mg, 90%).

Synthetic Route from **70a**. To a solution of methyl ester **70a** (386 mg, 1.21 mmol) in methanol (15 mL) was added a LiOH aqueous solution (8 mL, 2.5 N). Full conversion was observed after 4 h. The reaction was neutralized at 0 °C with 1.0 N aqueous HCl. The solvents were evaporated under a high vacuum. The resulting residue was purified and recrystallized as described above for **1**. Phenylkainic acid (**32a**) was recovered as a white crystalline solid (256 mg, 86%).

Mp 255–257 °C.

FTIR (thin film): 3429, 3185, 3042, 2920, 1736 cm^{-1}.

^{1}**H NMR** (400 MHz, D_2O): δ 7.49–7.34 (m, 3H), 7.27–7.18 (m, 2H), 4.05 (d, J = 7.3 Hz, 1H), 3.94 (dd, J = 11.4, 7.8 Hz, 1H), 3.87 (q, J = 7.8 Hz, 1H), 3.72 (dd, J = 11.4, 8.1 Hz, 1H), 3.15 (q, J = 7.2 Hz, 1H), 2.38 (dd, J = 16.3, 6.5 Hz, 1H), 2.02 (dd, J = 16.3, 8.7 Hz, 1H) ppm.

^{13}**C NMR** (101 MHz, D_2O): δ 178.5, 173.3, 136.2, 128.8, 128.2, 127.6, 65.1, 48.0, 44.8, 44.0, 35.7 ppm.

HRMS (ESI-TOF) m/z: $[M + H]^+$ calcd for $C_{13}H_{16}NO_4$, 250.1074; found, 250.1086.

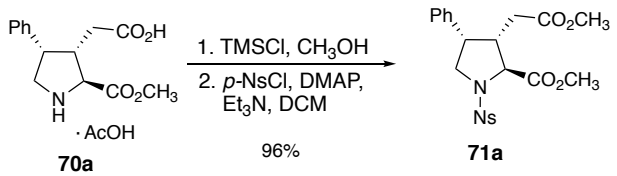

Methyl (2*S*,3*S*,4*S*)-3-(2-methoxy-2-oxoethyl)-1-((4-nitro-phenyl)sulfonyl)-4-phenylpyrrolidine-2-carboxylate (70a). To a solution of acid **70a** (acetate salt, 696 mg, 2.15 mmol) in methanol (5.0 mL) was added TMSCl (690 μL, 5.39 mmol). The solution was stirred at rt for 6 h. The reaction mixture was concentrated to dryness to afford the methyl ester as a white solid. This residue was retaken in dichloromethane (10 mL), and trimethylamine (746 μL, 5.39 mmol) was added, followed by DMAP (26 mg,

0.22 mmol) and *p*- NsCl (716 mg, 3.23 mmol). The reaction was stirred at rt overnight. The reaction concentrated to dryness. The resulting residue was purified by column chromatography using ethyl acetate/hexane as an eluent (10–30% gradient). *N*-Ns-protected diester **71a** was recovered as a white foam-like solid (953 mg, 96%).

FTIR (thin film): 3100, 2952, 1736, 1527 cm^{-1}.

^{1}**H NMR** (400 MHz, $CDCl_3$): δ 8.40 (d, *J* = 9.0 Hz, 1H), 8.13 (d, *J* = 9.1 Hz, 1H), 7.35–7.27 (m, 3H), 7.09–6.99 (m, 2H), 4.43 (d, *J* = 4.5 Hz, 1H), 3.81–3.78 (m, 3H), 3.78 (s, 3H), 3.60 (s, 3H), 3.10–2.99 (m, 1H), 2.02 (d, *J* = 1.8 Hz, 1H), 2.00 (d, *J* = 3.3 Hz, 1H) ppm.

^{13}**C NMR** (101 MHz, $CDCl_3$): δ 171.6, 171.4, 150.2, 144.5, 136.4, 129.0, 128.8, 127.7, 127.7, 124.2, 77.4, 77.0, 76.7, 65.2, 52.9, 51.9, 50.7, 45.2, 44.4, 32.5 ppm.

HRMS (ESI) m/z: $[M + H]^+$ calcd for $C_{21}H_{23}N_2O_8S$, 463.1175; found, 463.1174.

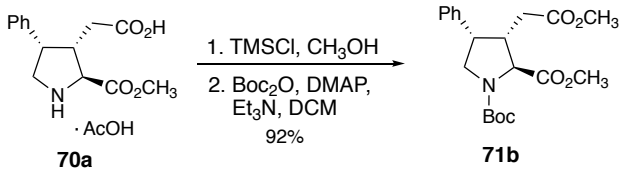

(2*S*,3*S*,4*S*)-1-(*tert*-Butyloxycarbonyl)-2-methoxycarbonyl-3-(methoxy-2'-oxoethyl)-4-phenylpyrrolidine (71b). To a solution of acid **70a** (acetate salt, 136 mg, 0.421 mmol) in methanol (2.5 mL) was added TMSCl (0.1 mL, 1 mmol) at rt. After 6 h, the reaction was concentrated to dryness to afford the methyl ester a white solid residue. This residue was retaken in dichloromethane (3 mL), and trimethylamine (150 μL, 1.08 mmol) was added, followed by DMAP (5 mg, 0.04 mmol) and Boc_2O (138 mg, 0.631 mmol). The white suspension was stirred overnight at rt. The solvent was evaporated under reduced pressure. The resulting residue was purified by column chromatography using ethyl acetate/hexane as an eluent (10–20% gradient) to afford Boc-protected diester **71b** as a colorless oil (146 mg, 92%).

FTIR (thin film): 2917, 2854, 1742, 1691 cm^{-1}.

^{1}**H NMR** (400 MHz, $CDCl_3$, two rotamers): δ 7.37–7.20 (m, 3H), 7.06 (dd, *J* = 7.9, 3.6 Hz, 2H), 4.07 (dd, *J* = 39.4, 6.4 Hz, 1H), 3.99–3.89 (m, 1H), 3.87–3.80 (m, 1H), 3.80–3.75 (m, 3H), 3.69 (q, *J* = 5.8 Hz, 1H), 3.65–3.58 (m, 3H), 3.01 (h, *J* = 7.2 Hz, 1H), 2.27 (dt, *J* = 17.7, 7.2 Hz, 1H), 2.04 (ddd, J = 17.2, 7.8, 4.9 Hz, 1H), 1.43 and 1.45 (2s, 9H) ppm.

^{13}**C NMR** (101 MHz, $CDCl_3$, two rotamers): δ 172.8, 172.5, 172.1, 172.1, 154.2, 153.5, 138.6, 138.4, 128.8, 127.7, 127.7, 127.3, 80.5, 77.3, 77.0, 76.7, 63.4, 63.1, 52.4, 52.2, 51.8, 51.7, 50.7, 50.2, 45.2, 44.3, 44.3, 43.5, 33.3, 33.2, 28.4, 28.3 ppm.

HRMS (ESI-TOF) m/z: $[M + Na]^+$ calcd for $C_{20}H_{27}NO_6Na$, 400.1736; found, 400.1717.

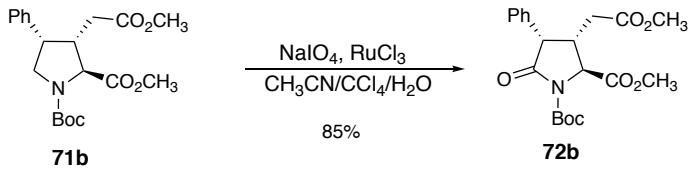

(2*S*,3*S*,4*S*)-1-(*tert*-Butyloxycarbonyl)-2-methoxycarbonyl-3-(methoxy-2'-oxoethyl)-5-oxo-4-phenylpyrrolidine (**72b**). *N*-Boc-protected diester **71b** (52 mg, 0.14 mmol) was dissolved in a solvent mixture composed of acetonitrile (0.5 mL), carbon tetrachloride (0.5 mL), and water (1 mL). Sodium metaperiodate (471 mg, 2.20 mmol) was added, followed by ruthenium trichloride monohydrate (2 mg, 0.009 mmol). After 8 h, TLC analysis showed only partial conversion. A second portion of metaperiodate (118 mg, 0.552 mmol) and ruthenium trichloride (1 mg, 0.04 mmol) was added. After an additional 24 h of reaction, the mixture was diluted with ethyl acetate (30 mL). The organic layer was washed with a 0.5 N HCl aqueous solution (5 mL) and brine (20 mL). It was then dried over $MgSO_4$ and filtered. The solvent was removed under reduced pressure. The resulting residue was purified by column chromatography using ethyl acetate/hexane as an eluent (10–30% gradient). *N*-Boc pyrrolidinone **72b** was recovered as a colorless oil (45 mg, 85%).

FTIR (thin film): 2950, 2912, 2851, 1796, 1743 cm^{-1}.

^{1}H NMR (400 MHz, $CDCl_3$): δ 7.36–7.29 (m, 3H), 7.17–7.10 (m, 2H), 4.43 (d, J = 3.3 Hz, 1H), 4.22 (d, J = 8.7 Hz, 1H), 3.86 (s, 3H), 3.57 (s, 3H), 3.08 (m, 1H), 2.30 (dd, J = 16.9, 8.8 Hz, 1H), 2.09 (dd, J = 16.9, 6.4 Hz, 1H), 1.53 (s, 9H) ppm.

^{13}C NMR (101 MHz, $CDCl_3$): δ 171.9, 171.3, 170.9, 149.5, 133.2, 129.5, 128.8, 127.9, 84.2, 62.0, 52.9, 51.9, 51.4, 37.0, 34.4, 27.9 ppm.

HRMS (ESI) m/z: $[M + Na]^+$ calcd for $C_{20}H_{25}NO_7Na$, 414.1529; found, 414.1492.

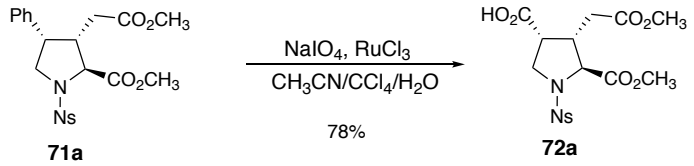

(2*S*,3*S*,4*S*)-1-((4'-Nitrophenyl)sulfonyl)-2-methoxycarbonyl-3-(methoxy-2'-oxoethyl)-4-phenylpyrrolidine-3-carboxylic acid (**72a**). This synthesis was proceeded according to the procedure described for **72b** and started with **71a** (901 mg, 1.95 mmol). The resulting reaction mixture was acidified with a 0.5 N aqueous HCl solution at 0 °C until the pH ~ 2. The resulting mixture was extracted with ethyl acetate (2 × 20 mL), followed by washing with brine (50 mL). The combined organic layers were then extracted with a saturated aqueous sodium bicarbonate solution (3 × 20 mL), and the desired product was thus extracted to the aqueous layers. The aqueous layers were combined and extracted with diethyl ether (3 × 20 mL) to remove impurities. The resulting aqueous layer was then acidified with a 0.5 N aqueous HCl solution at 0 °C until the pH ~ 2. It was then reextracted with ethyl acetate (3 × 30 mL) and washed with brine. The organic layer was dried over $MgSO_4$ and concentrated to dryness under reduced pressure. The residue was purified by column chromatography using methanol/dichloromethane as an eluent (5–10% gradient) to afford **72a** (652 mg, 78%) as a white foamy solid.

FTIR (thin film): 2914, 2851, 1723, 1591, 1524 cm^{-1}.

^{1}H NMR (400 MHz, $CDCl_3$): δ 8.37 (d, *J* = 9.1 Hz, 1H), 8.05 (d, *J* = 9.1 Hz, 1H), 4.14 (d, *J* = 7.0 Hz, 1H), 3.81 (s, 3H), 3.79–3.74 (m, 1H), 3.69 (s, 3H), 3.67–3.64 (m, 1H), 3.37–3.32 (m, 1H), 3.06–2.98 (m, 1H), 2.47 (dd, *J* = 17.0, 7.4 Hz, 1H), 2.36 (dd, *J* = 17.0, 7.5 Hz, 1H) ppm.

^{13}C NMR (101 MHz, $CDCl_3$): δ 175.8, 170.9, 170.8, 150.3, 143.3, 128.8, 124.2, 64.6, 53.1, 52.2, 49.2, 44.9, 42.0, 32.3 ppm.

HRMS (ESI-TOF) m/z: $[M + H]^+$ calcd for $C_{16}H_{19}N_2O_{10}S$, 431.0676; found, 431.0648.

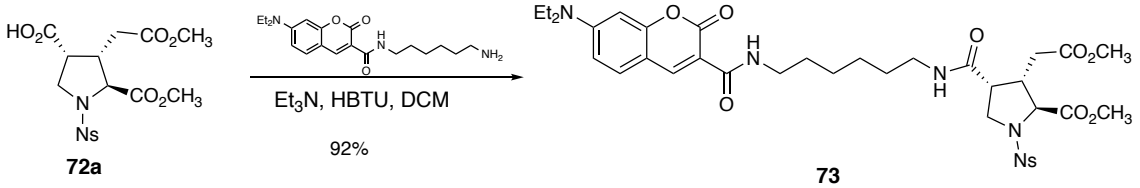

Methyl (2*S*,3*S*,4*R*)-4-((6-(7-(diethylamino)-2-oxo-2*H*-chromene3-carboxamido)hexyl) carbamoyl)-3-(2-methoxy-2-oxoethyl)-1-((4nitrophenyl)sulfonyl)pyrrolidine-2-carboxylate (73). To a stirred solution of **72a** (26 mg, 0.060 mmol) in dichloromethane (1 mL) were added triethylamine (13 μL, 0.090 mmol), HBTU (25 mg, 0.071 mmol), and the coumarin amine (33 mg, 0.091 mmol). After 1 h, **72a** was fully converted to **73**. The reaction mixture was poured into water and extracted with diethyl ether (3 × 15 mL). The combined ether layer was then washed with an ammonium chloride aqueous solution, sodium bicarbonate aqueous solution, and brine. The organic layer was then dried over $MgSO_4$, filtered, and concentrated to dryness under reduced pressure. The resulting residue was purified by column chromatography on silica gel (10-35% EtOAc/hexane as an elution gradient) to yield **73** (43 mg, 92%) as a yellow solid.

FTIR (thin film): 3452, 3338, 2923, 2851, 1672, 1616, 1581, 1533, 1515 cm^{-1}.

^{1}H NMR (400 MHz, $CDCl_3$): δ 8.83 (t, *J* = 6.0 Hz, 1H), 8.68 (s, 1H), 8.37 (d, *J* = 8.8 Hz, 2H), 8.06 (d, *J* = 8.8 Hz, 2H), 7.48 (d, *J* = 8.9 Hz, 1H), 6.66 (dd, *J* = 9.0, 2.5 Hz, 1H), 6.51 (d, *J* = 2.4 Hz, 1H), 6.24 (t, *J* = 5.6 Hz, 1H), 4.22 (d, *J* = 6.4 Hz, 1H), 3.74–3.78 (m, 4H), 3.68 (t, *J* = 4.9 Hz, 1H), 3.65 (s, 3H), 3.50–3.39 (m, 6H), 3.28 (td, *J* = 7.1, 5.2 Hz, 1H), 3.08 (dt, *J* = 15.0, 6.7 Hz, 2H), 3.03–2.95 (m, 1H), 2.42 (dd, *J* = 17.2, 8.2 Hz, 1H), 2.26 (dd, *J* = 17.2, 6.8 Hz, 1H), 1.60 (t, *J* = 6.7 Hz, 2H), 1.40 (d, *J* = 6.3 Hz, 2H), 1.37–1.30 (m, 4H), 1.25 (t, *J* = 7.1 Hz, 6H) ppm.

^{13}C NMR (101 MHz, $CDCl_3$): δ 172.0, 171.3, 169.3, 163.3, 162.9, 152.6, 150.2, 148.1, 143.4, 131.2, 129.0, 124.2, 110.0, 108.4, 96.5, 65.3, 52.9, 52.0, 50.0, 45.8, 45.1, 42.8, 38.7, 38.7, 32.3, 29.3, 28.8, 25.7, 25.6, 12.4 ppm.

HRMS (ESI-TOF) m/z: $[M + H]^+$ calcd for $C_{36}H_{46}N_5O_{12}S$, 772.2864; found, 772.2876.

Chapter 4

An Affinity-based Fluorescence Probe to Study Kainate Receptors

The expression of kainate receptors at the surface of neurons is crucial to healthy brain function.[16] Being able to visualize kainate receptors in living cells is currently a limitation in elucidating the mechanisms of neuron communication and their associated pathologies. In this chapter, a molecular fluorescence probe for kainate receptors is synthesized to enable the tracking of kainate receptors in model cells.

4.1 Background

In the brain, kainate receptors (KAR) play crucial regulatory roles in excitatory neurotransmission. KARs are concentrated at synapses—interface between two neurons—where they translate a chemical stimulus into ion fluxes, thereby creating electrical impulses. Their density at synaptic sites controls the efficiency of neuronal networks, and yet their surface expression is regulated by neuronal activity.[116] The mechanisms that govern this feedback-regulated localization are unclear.[117] A major challenge to studying these mechanisms is the technological limitations to localize functional KARs *in vivo*.

Current methods for tracking KARs in *living* cells rely on recombinant protein constructs like KAR fused to a fluorescent protein (e.g., green fluorescent protein, GFP).[116] This technique requires several genetic manipulations: cloning the KAR gene (if not available from other labs), fusing it to a GFP marker, inserting the construct in a transfection vector, then knocking down the native KAR in the cells/animal so that only the construct is the active one. An additional limitation is the size of GFP (25 kDa) compared to KARs (~100 kDa)[118] which can disturb: the protein's folding, its membrane trafficking, or its ion channel activity.[119] Alternative approaches with smaller tags, such as SNAP-, HA-, or Halo-tagged KARs have been used to minimize perturbations—but they all

require genetic modification of the protein, so their application is therefore limited to fully sequenced and cloned receptors.[120]

An ideal strategy to label KARs would be direct visualization without genetic manipulation. Immunochemistry (labelled antibodies) is the most common method to locate proteins, but it requires *fixed* cells—a process that kills the cell. Additional limitations include that: an antibody must exist for the targeted protein/animal; antibodies may not be selective;[121,122] cell permeability may be an issue.[123] Chemical labelling of proteins offers an alternative solution to biological methods.[124] Such chemical probes are generally based on a strong protein-ligand affinity to locate the POIs.[125] A POI can be labelled by its specific ligand and visualized by a fluorescence tag. The protein labelling event can involve a prolonged residence time of its ligand,[126] or a reaction between the POI and its ligand.[127,128]

I proposed to create an affinity-based fluorescence probe to study KARs in living cells. This method should alleviate drawbacks of conventional biological techniques. This probe is composed of a high affinity ligand, a linker of suitable length, and a fluorophore (Figure 4–1). In this chapter, I hypothesized that a KAR protein can bind a kainoid ligand modified with a cyanin dye and that KARs can be visualized by fluorescence microscopy. I expect that the high selectivity of kainoids for their native protein, KAR, will allow us to label selectively KARs in living cells. In addition, since the chemical probe is added *after* protein expression and it is small (< 1 kDa), it should allow the study of unperturbed receptors in living cells. This KAR-specific chemical probe should enable a broad scope of cellular applications without genetic manipulation.

4.2 Probe design

To ensure that the probe can bind to its receptor, I analyzed the crystal structure of the KAR protein complexed with domoic acid (Figure 4–1a, b). The binding site of domoic acid (DA) in GluK1 and GluK2 is conserved: (1) the protein residues interacting with the amine and carboxylic acid groups of DA are the same, (2) DA sits in the same orientation in both binding pockets, and (3) the C4 side chain extends out of the binding pocket. Therefore, the kainoid probe's C4 side chain should exhibit binding and activity similar to DA if the modification is appropriate.

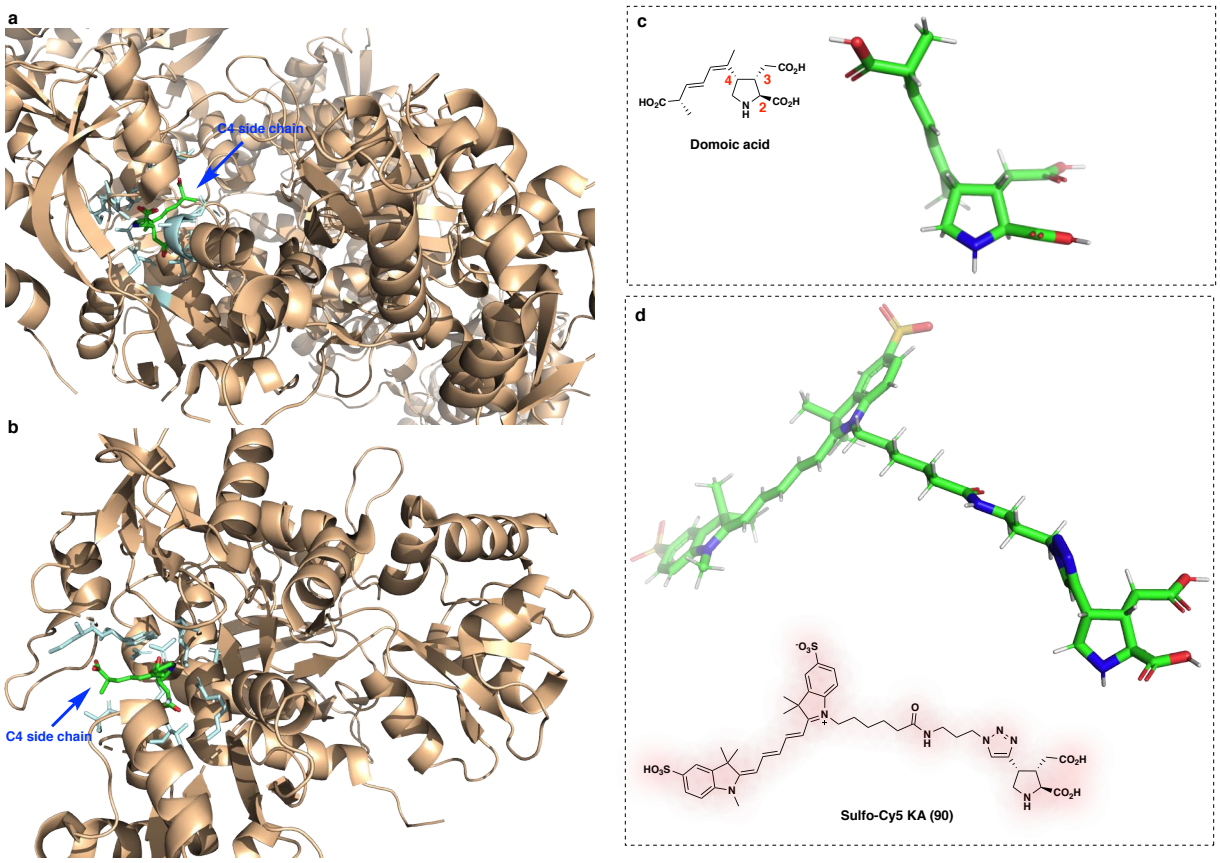

Figure 4–1. Structures of GluK receptors, domoic acid, and the proposed fluorescent probe. (**A**) Ribbon representation of the crystal structure of GluK2 protein complexed with domoic acid (PDB: 1YAE). (**B**) Ribbon representation of the crystal structure of GluK1 complexed with domoic acid (PDB: 2PBW). (**C**) 3D structure of domoic acid generated by CORINA. (**D**) 3D structure of proposed fluorescent probe **90**; generated by CORINA. The elements of domoic acid and **90** are shown in CHNOS colour mode. The protein main chains are shown in wheat tint; residues within 5 Å of **DA** are shown in pale cyan; images created with Pymol.

The proposed fluorescent probe, **Sulfo-Cy5-KA (90)**, is expected to mimic the binding of domoic acid with KARs and will be visualized by microscopy via its bis-sulfonylcyanine fluorescent moiety (Figure 4–1d). The length of the linker between the ligand and sulfo-Cy5 was selected to minimize interference of the fluorophore with the binding pocket of KARs. The fluorescent group sulfo-Cy5 was chosen because it was shown to minimize the amount of false positives due to self-embedding within the lipid bilayer of cells—a common issue with lipophilic fluorophores.[129] Moreover, sulfo-Cy5 is excited with wavelengths in the red visible range, and therefore does not damage cells, and allows for deep tissue penetration.

4.3 Probe synthesis

The synthesis began with the advanced intermediate **72a**, reported in the previous chapter. Acid **72a** was reduced to alcohol **85** via the one-pot formation of the activated hydroxybenzotriazole ester

72ab, followed by $NaBH_4$ reduction (Scheme 4–1). While extensive optimization was required for this reduction, only the productive conditions are summarized in Table 4–1. Conditions involving the (efficient) conversion of **72a** to carbonate **72aa**, only led to low yields when presented to the reducing agent (path a, Entry 1). Alternatively, a method using EDCI and HOBT developed more recently converted **72a** to the activated ester **72ab** smoothly, followed by a slightly more efficient reduction (path b, Entry 2).[130] The $NaBH_4$ reduction step was then modified by pre-activating with water *before* $NaBH_4$ adding to the activated ester, and it gave almost quantitative conversion (path b, Entry 3). Importantly, no epimerization was observed in this process, and NOE experiments confirmed the C3,4-*cis* configuration of alcohol **85**.

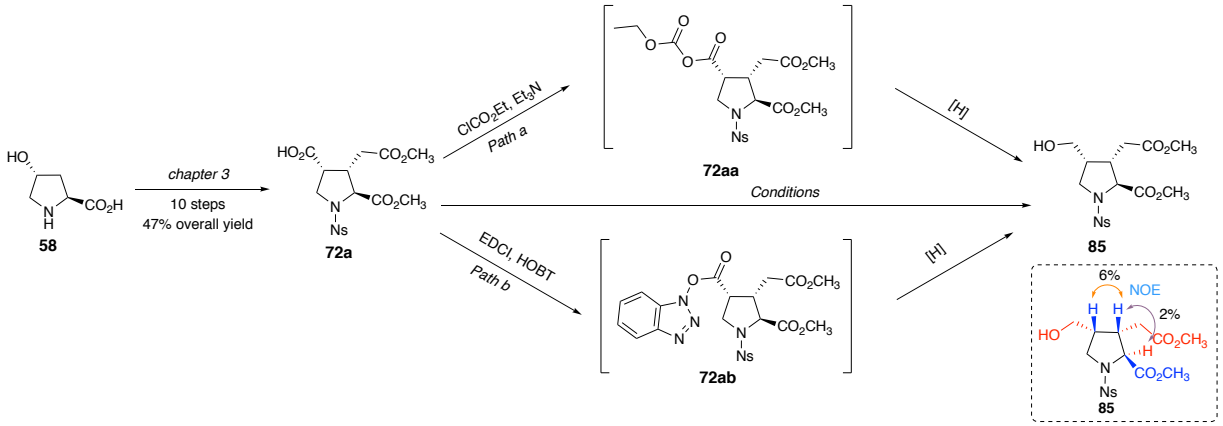

Scheme 4–1 Synthesis of kainoid alcohol 85

Table 4–1 Conditions for reduction of acid 72a to alcohol 85

Entry	Conditions	Yield
1	i. $ClCO_2Et/Et_3N$/THF, –10 °C; ii. $NaBH_4$/ MeOH	23%
2	i. EDCI/HOBT/DCM, rt; ii. $NaBH_4$, THF/H_2O , 0 °C	52%
3	i. EDCI/HOBT/DCM, rt; ii. $NaBH_4$ aq, THF/H_2O, 0 °C	95%

Next, alcohol **85** was oxidized to aldehyde **86a** with Dess-Martin periodinane (Scheme 4–2). It was necessary to use only 1.0 equivalent of DMP to obtain the desired C3,4-*cis* single diastereomer **86a** without C4 epimerization during the reaction. An excess of DMP (3–6 equiv.) gave the undesired **86b** C3,4-*trans* isomer of **86a**, which were inseparable by column chromatography. Epimerization of **86a** was also observed in presence of basic aqueous solutions, such as LiOH aq and NaOH aq.

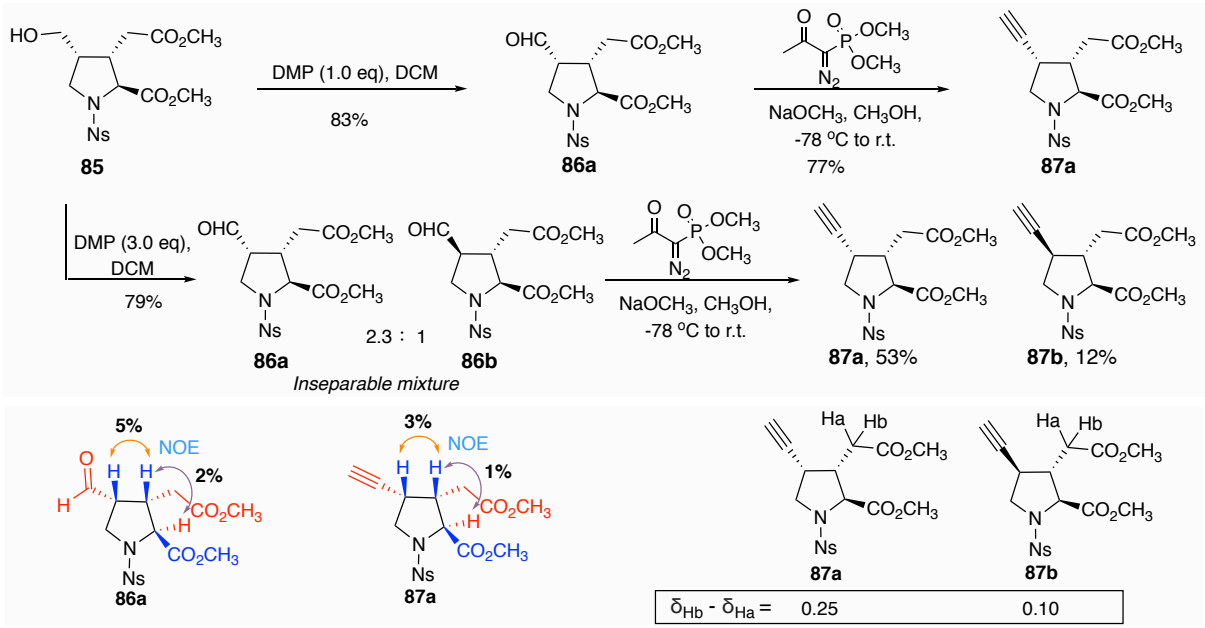

Scheme 4–2. Synthesis and stereochemistry assignment for aldehyde 87

Aldehyde **86a** subsequently underwent a one-carbon homologation to alkyne **87a** (Scheme 4–2). Bestmann-Ohira's diazophosphonate reagent converted the aldehyde into the alkyne under optimized mild conditions. Classical reaction conditions, e.g., $(MeO)_2P(O)C(N_2)COMe$; K_2CO_3; MeOH, only epimerized **86a** at C4 instead achieving the desired homologation. I optimized the reaction for milder conditions using $NaOCH_3$ at low temperature, which allowed the key ylide intermediate to form without epimerization.[131] Conveniently, the (undesired) diastereomeric mixture of **86a** and **86b** became separable at the alkyne stage. Alkynes **87a** and **87b** were essential to provide a characterization reference to assign the C3/C4 configuration unambiguously. NOE evidence supports the C3/C4-*cis* assignment for **86a** and **87a**. While NOE experiments aiming to confirm the C3/C4-*trans* configuration for **87b** were inconclusive due to chemical shifts overlap, the ^{1}H NMR spectra followed the reported "assignment rules": $(\delta_{Hb} - \delta_{Ha})$–*cis* > $(\delta_{Hb} - \delta_{Ha})$–*trans*.[113]

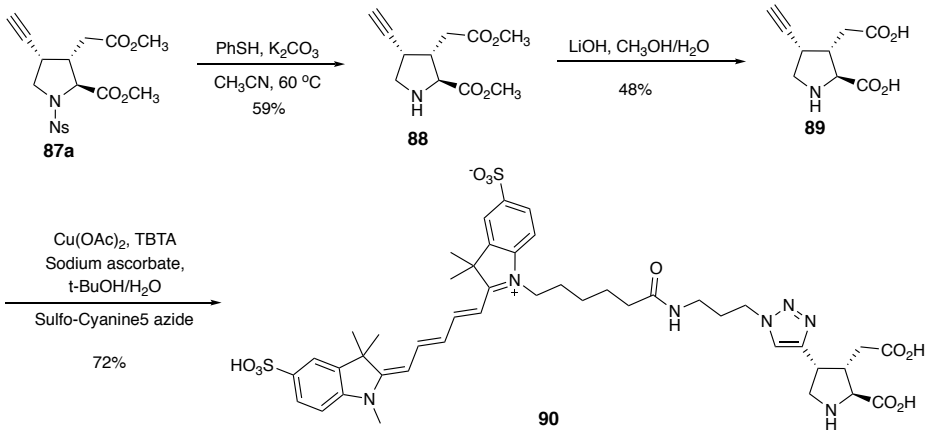

Scheme 4–3. Synthesis of novel alkynylkainic acid 89 and probe 90

Finally, alkyne **87a** was subjected to a sequence of global deprotection to yield a novel unnatural kainoid: alkynylkainic acid **89** (Scheme 4–3). The nosyl protecting group was removed with thiophenol and sodium bicarbonate, followed by a mild hydrolysis with LiOH. The modest yield of the bis-ester hydrolysis is partially due to the challenge of visualizing **88** and **89** during the purification process (silica-gel, followed by ion-exchange chromatography). NMR analysis of the crude product showed an otherwise clean conversion. With the obtained alkyne **89** in hand, the targeted fluorescent probe **90** was synthesized through a "click" reaction[132] coupling with the dye sulfo-cyanine-5-azide.

4.4 Preliminary imaging experiments of KAR with the Sulfo-Cy5-KA probe

The ultimate purpose of developing a KAR imaging probe is to label endogenous kainate receptors present at the surface of neurons (functional KARs). For our proof-of-concept experiments, I opted to test the imaging probe **Sulfo-Cy5-KA** in model cells that do not express kainate receptors natively, as a means to control for background signal. Thus, experiments were conducted with the human cell line HEK-293; these cells are robust to culture and do not natively express GluK proteins. Ironically, we had to resort to using genetic manipulations to test our fluorescent probe: we opted for a recombinant form of GluK2 accompanied by enhanced GFP (EGFP) as expression marker. Transfecting HEK-293 cells with recombinant pcDNA3-GRIK2-EGFP plasmids (Figure 4–2) enforces the exogenous expression of GluK2-EGFP. GluK2-positive cells can be identified by the fluorescence of EGFP. Transfected HEK cells were then subjected to probe **90**, **Sulfo-Cy5-KA**, for the fluorescence imaging.

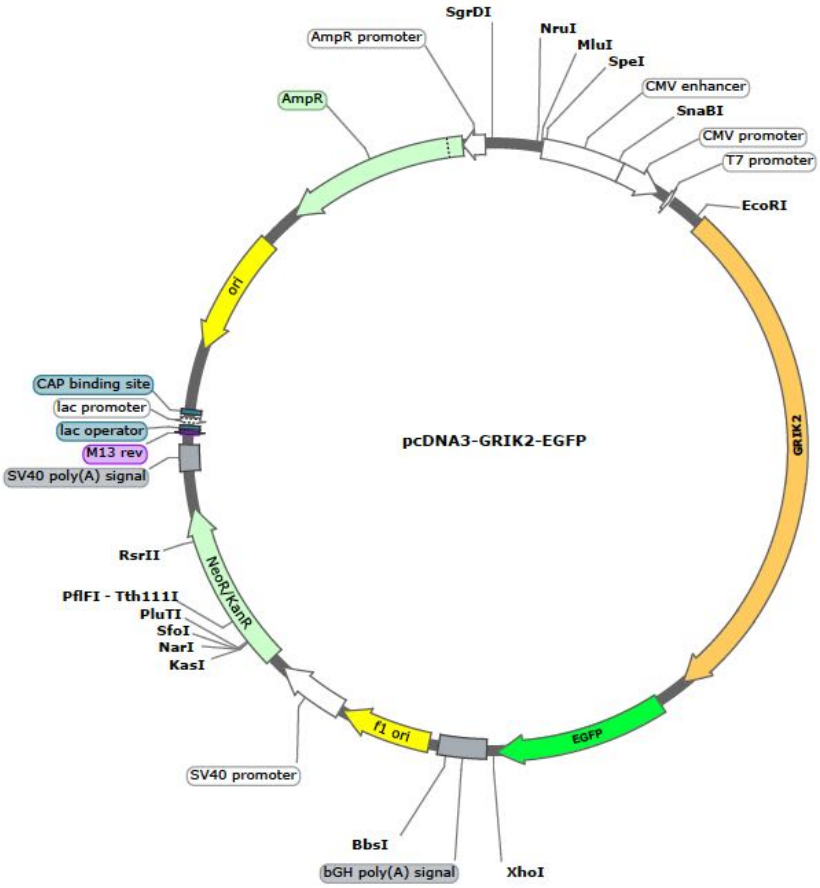

Figure 4–2. pcDNA3-GRIK2-EGFP plasmid gene map. The fluorescent protein gene for EGFP is downstream of GRIK2 and employed as a marker for GRIK2 gene expression. A spacer sequence separates GRIK2 and EGFP in this plasmid. The successful expression of GRIK2 in mammalian cells can be identified by the presence of EGFP, but they are not fused.

Assessing the labelling selectivity of the probe relied on the co-localization of green (EGFP) and red (**90**) fluorescence signals in the same cells. The colocalization protocol used to evaluate the probe **90** for GluK2 labelling is outlined in Figure 4–3. Briefly: HEK-293 cells were transfected with a plasmid encoding for both GluK2 and EGFP proteins (using calcium phosphate precipitate method); and the cells were allowed to incubate for 24-36 h. Typically, 40-60% of cells displayed positive green fluorescence. On a confocal microscope, a solution of the Sulfo-Cy5-KA probe was added to the cells medium and allowed to incubate for a given amount of time; then, the medium was removed and replaced with phosphate-buffered saline (PBS) solution. Cells were then imaged simultaneously in three channels: bright field, EGFP (green) field (488 nm excitation/ 505 nm emission) and Cy5 (far-red) field (635 nm excitation / 675 nm emission). The selectivity level of Gluk2 labelling was assessed by the colocalization of EGFP and probe **90** (Figure 4–3d).

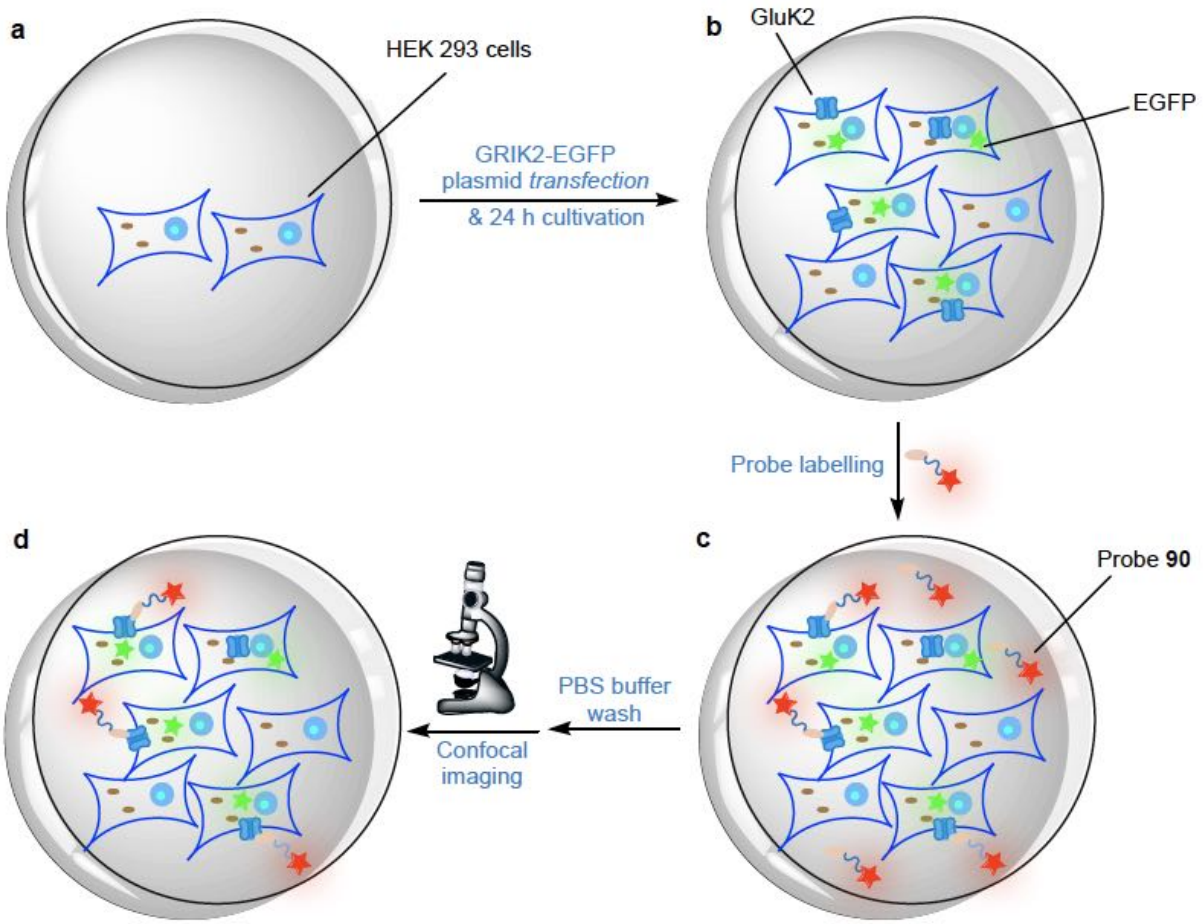

Figure 4–3. Fluorescence labelling experiments design with probe **90**. (A). HEK293 cells cultivation. (B). GRIK2 plasmid transfection and expression. (C) Fluorescence labelling with probe **90**. (D). Confocal imaging experiments.

The multiplexed fluorescence imaging experiments using confocal microscopy and HEK-293 cells confirmed that the labelling of GluK2 proteins by probe **90** is selective (Figure 4-4). No red

fluorescence signal in the Cy5 field was observed above background when probe **90** was applied to non-transfected HEK-293 cells (Figure 4–4a-c). When HEK293 cells transfected with the GRIK2-EGFP plasmid were subjected to probe **90**, the cells expressing the green EGFP marker (considered GluK2-positive) were found to exhibit significant red fluorescence (Figure 4–2e). Moreover, cells in the same dish that did not show GFP fluorescence—presumed to be non-transfected—did not display significant red fluorescence (Figure 4–4d-f).

This significant difference of signal in Cy5-associated red fluorescence between transfected and non-transfected cells strongly suggests that the probe **90** binds selectively to GluK2 proteins (Figure 4–2g). The fluorescence intensity measured at 675 nm (Cy5 field) in transfected cells was 30 times stronger than in GluK2-negative cells. Finally, the statistical significance difference was verified in repeated experiments of GluK2 transferred cells and control groups (Figure 4–2g) for the labelling probe **90**.

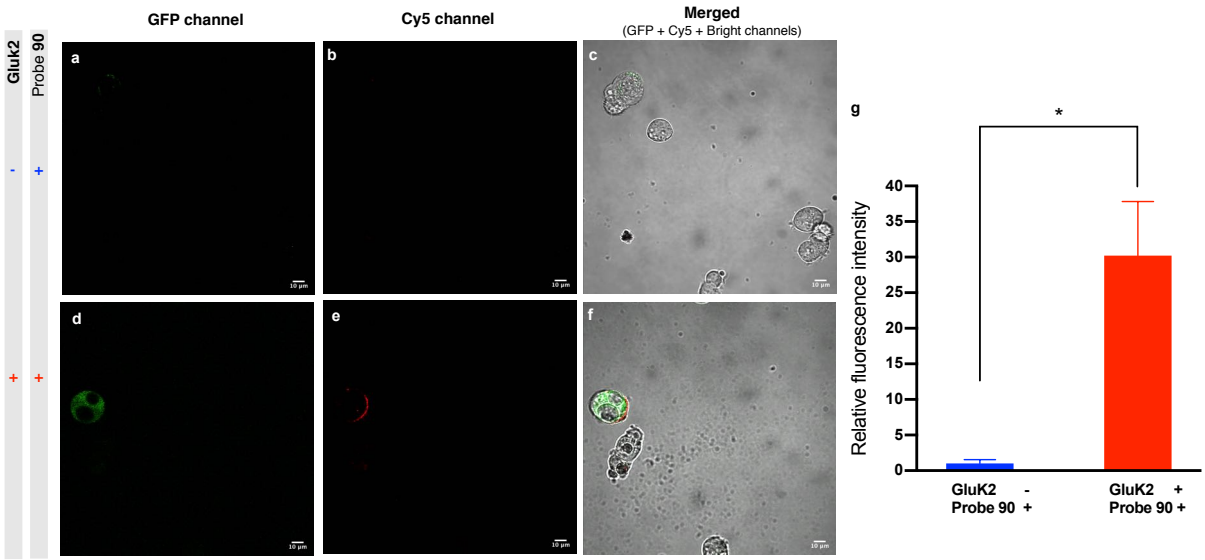

Figure 4–4. Representative images of HEK-293 cells after application of probe **90**. Cells were incubated with fluorescent probe **90** (**Sulfo-Cy5 KA**) (2.5 μM) for 10 mins at rt, then washed off with PBS buffer. Images were acquired by laser-scanning confocal fluorescence microscopy in green (exc.488 nm, em.505 nm), red (exc. 635 nm, em. 675 nm), and bright fields. Images of merged field were generated by merging images of GFP, Cy5 and bright fields (A–C) Non-transfected HEK-293 cells (control): no Cy5-related signal is discernable above background. (D–F) *GRIK2*-transfected HEK-293 cells: Cy5-fluorescence signal is observed only in cells that express the exogenous GluK2 protein as identified by presence of the green fluorescence EGFP expression marker. The probe's Cy5 fluorescence is highly localized to the cell membrane. Scale bar = 10 μM. (G) The fluorescence observed upon **Sulfo-Cy5 KA** treatment is significantly higher in cells that are GluK2-positive. The probe-labelled cells boundaries were defined manually in the bright field and chose as the region-of-interest (ROI). ROIs were measured in Fiji, and the obtained results were used to calculate the fluorescence intensities. The average fluorescence values were normalized to signal observed in the control cells. Values represent mean ± SD ($n_1 = 10$, $n_2 = 7$, $^*P < 0.0001$).

These preliminary imaging results in living cells demonstrate the potential of **Sulfo-Cy5-KA** as a KAR fluorescence probe. Two sets of experimental applications in fluorescence labelling are ongoing in the Menard lab; they include (1) unambiguously confirming the selectivity of **90** for KARs proteins by accurate fluorescence colocalization using a *fused* GRIK2-GFP recombinant chimera, and (2) exploring the use of **Sulfo-Cy5 KA** as an affinity quantification tool for KARs agonists screening. The results will be submitted for publication upon completion.

Despite the labelling efficiency of the **Sulfo-Cy5 KA**, its binding to the GluK receptors will trigger the opening of their ion channels. In other words, each protein that is visualized and *activated* by default, which perturbs the cell being observed. An ideal fluorescence probe would allow labelling GluK without perturbing their normal activity. With the general synthesis developed above, the next step will be to construct a *traceless* labelling probe—one that will label GluKs while leaving the binding site free for its native ligands.

4.5 Summary

An affinity-based fluorescent probe to label kainate receptors, **Sulfo-Cy5-KA** (**90**) was synthesized and applied in model cells. The synthesis of **Sulfo-Cy5-KA** was accomplished in 6 steps from the advanced intermediate **72a** in 12% yield. The overall synthesis yield from 4-hydroxyproline was 6% over 16 steps. Preliminary in *vitro* imaging of GluK2 expressed in HEK 293 cells demonstrated that **Sulfo-Cy5-KA** can be used to visualize membrane kainate receptors with confocal fluorescence microscopy. **Sulfo-Cy5-KA**'s far-red emission fluorescence is well suited for applications in neuronal tissue studies.

Importantly, the versatility of novel alkynylkainic acid **89** opens the door to the rapid synthesis of any KAR probe for neurobiology studies. It also expands the scope of accessible KAR agonists, e.g., new kainoid analogs **91**, via a one-step click reaction for medicinal chemistry research.

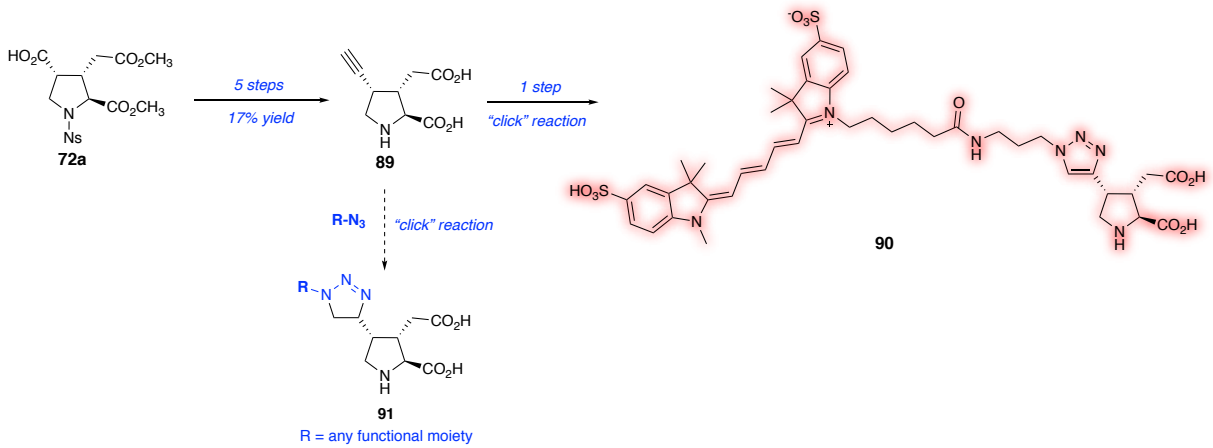

Scheme 4–4. Synthesis of a clickable kainoid and conjugated fluorescent probes

4.6 Experimental Section

4.6.1 General Experimental Procedures

Unless otherwise noted, reactions were carried out under an argon atmosphere, in flame-dried single-neck, round bottom flasks fitted with a rubber septum and with magnetic stirring. Air or water sensitive liquids and solutions were transferred via syringe or stainless-steel cannula. Organic solutions were concentrated by rotary evaporation at 25–45 °C at 50–200 torr. Thin layer chromatography (TLC) was performed on glass plates precoated with Silica gel F254, 250 µm, 60 Å, from EMD Chemicals Inc (EMD 5715-1). TLC plates were visualized under a 254 or 365 nm UV light source, then stained by immersion in either acidic aqueous-ethanolic vanillin solution, potassium permanganate, or acidic ethanolic ninhydrin, followed by heating using a heat gun. Purification was performed with 230-400 mesh silica gel from Silicycle, Quebec (SilicaFlash R12030B, P60, 40-63 µm, 60 Å).

4.6.2 Materials

Reagents and starting materials were purchased from: Sigma-Aldrich, Oakwood Chemicals, Alfa Aesar, Acros Organics, TCI America, or Fisher Scientific and were used as received unless otherwise noted. Sulfo-Cyanine 5 azide was purchased from Lumiprobe, US. Tetrahydrofuran, dichloromethane, hexanes, toluene, and diethyl ether were purified on a glass contour solvent purification system under an argon atmosphere. Methanol was dried by allowing it to stand over freshly activated 4 Å molecular sieves for 48 h prior to use. Solvents used for chromatographic purifications were obtained from Fischer Scientific or VWR and used without further purification. All new compounds were characterized with 1D (^{1}H NMR and ^{13}C NMR) and the protons and carbons are assigned by 2D NMR (COSY, HSQC, HMBC) spectroscopy.

4.6.3 Instruments

^{1}H and ^{13}C NMR spectra were recorded on a 400 MHz Varian NMR AS400 equipped with an ATB-400 probe at 25 °C. NMR spectra were analyzed with MestReNova version 10.0.2-15465 from Mestrelab Research. Chemical shifts are reported in parts per million (ppm, δ scale) downfield from tetramethylsilane and are referenced to residual proton signals in the NMR solvents ($CHCl_3$: δ 7.26, C_2HD_5SO: δ 2.50), for carbons ($CDCl_3$: δ 77.0, C_2HD_5SO: δ 39.5). Spectral data are listed as follows: chemical shift, integration, multiplicity (s = singlet, d = doublet, t = triplet, q = quartet, m = multiplet, br s= broad singlet), and coupling constant (*J*, Hz). Infrared spectra (IR) were obtained using a Perkin-Elmer FT-IR spectrometer. High resolution mass spectra were obtained from the McMaster Regional Centre for Mass spectrometry using a HCTultra PTM discovery system spectrometer (ESI), or from a Waters Micromass LCT Premier TOF Mass. The final product, Sulfo-Cy5 KA, was purified HPLC on a C18 column (Onyx™ Monolithic Semi-PREP C18, LC Column 100 x 10 mm) with a Varian Prostar HPLC system. HPLC condition for the purification was described in the corresponding procedure.

4.6.4 Statistical analysis and data processing

Crystal structures of KARs were downloaded from Protein Data Bank (PDB); the corresponding ID was shown in each figure. These PDB files were processed with PyMol (Education version, Schrödinger, Inc., New York, NY, USA). 3D models of DA and probe **90** were produced by Chemdraw 16.1 (PerkinElmer, Inc., Waltham, Massachusetts, US) and processed by PyMol. GraphPad Prism software (version 8.0, GraphPad Software Inc., La Jolla, CA, USA) was used to conduct statistical analyses.

4.6.5 Chemical synthesis procedures & characterization

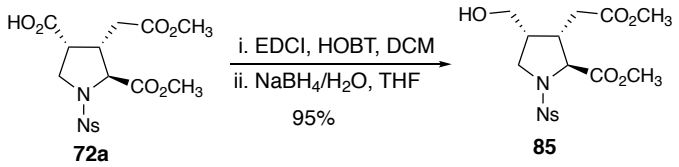

Methyl (2*S*,3*S*,4*R*)-4-(hydroxymethyl)-3-(2-methoxy-2-oxoethyl)-1-((4-nitrophenyl)sulfonyl)pyrrolidine-2-carboxylate (85). To a solution of acid **72a** (290 mg, 0.674 mmol) in dichloromethane (2 mL) were added EDCI (155 mg, 0.809 mmol) and HOBT (124 mg, 0.809 mmol) at rt. After 1.5 h, the solvent was removed under reduced pressure. The resulting residue was redissolved in THF (5 mL) and resulting a suspension. $NaBH_4$ (38 mg, 1.0 mmol) aqueous solution (1.0 mL) was added dropwise. After 30 mins, the reaction mixture was quenched with an ammonium chloride aqueous solution and extracted with ethyl acetate (3 × 10 mL). The combined organic layer was washed with brine, dried over $MgSO_4$ and filtered. The filtrate was concentrated under reduced pressure and afforded alcohol **85** as a colourless liquid without further purification.

FTIR (thin film): 3536, 3103, 2955, 1737, 1531 cm^{-1}.

^{1}**H NMR** (400 MHz, $CDCl_3$): δ 8.39 – 8.35 (m, 2H), 8.11 – 8.07 (m, 2H), 4.31 (d, *J* = 5.8 Hz, 1H), 3.74 (s, 3H), 3.70 (s, 3H), 3.59 (dd, *J* = 11.1, 6.3 Hz, 1H), 3.56 – 3.48 (m, 2H), 3.44 (dd, *J* = 10.0, 5.6 Hz, 1H), 2.91 (dq, *J* = 8.3, 6.3 Hz, 1H), 2.65 (dd, *J* = 12.5, 6.2 Hz, 1H), 2.58 (dd, *J* = 16.9, 8.4 Hz, 1H), 2.42 (dd, *J* = 16.9, 6.7 Hz, 1H) ppm.

^{13}**C NMR** (101 MHz, $CDCl_3$): δ 172.1, 171.4, 150.2, 144.5, 128.8, 124.2, 65.6, 60.4, 52.8, 52.2, 49.5, 42.1, 41.7, 32.4 ppm.

HRMS (ESI-TOF) m/z: $[M + Na]^+$ calcd for $C_{16}H_{20}N_2O_9SNa$, 439.0782; found, 439.0784.

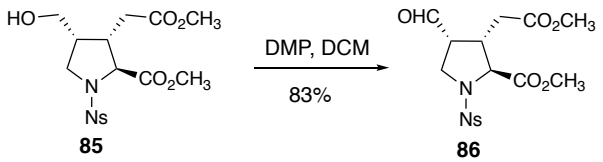

Methyl (2*S*,3*S*,4*R*)-4-formyl-3-(2-methoxy-2-oxoethyl)-1-((4-nitrophenyl)sulfonyl)pyrrolidine-2-carboxylate (86). To a solution of alcohol **85** (81 mg, 0.19 mmol) in DCM (2 mL) was added Dess-Martin periodinane (83 mg, 0.19 mmol) at rt. After 1 h, TLC show full conversion. The resulting solution was poured into sodium bicarbonate aqueous solution (5% wt, 20 mL) and extracted with ethyl acetate (3 × 10 mL). The combined organic layer was washed with sodium thiosulfate aqueous solution (5% wt, 10 mL) and brine. The resulting organic layer was then dried over $MgSO_4$. The filtrate was concentrated to dryness under reduced

pressure. The residue was purified by column chromatography using ethyl acetate / hexane as an eluent (20–40% gradient). Aldehyde product **86** was recovered as a white solid (202 mg, 83%).

FTIR (thin film): 3101, 2953, 1742, 1533 cm^{-1}.

^{1}**H NMR** (400 MHz, $CDCl_3$): δ 9.63 (s, 1H), 8.39 (d, *J* = 8.9 Hz, 2H), 8.06 (d, *J* = 8.9 Hz, 2H), 4.24 (d, *J* = 5.6 Hz, 1H), 3.84 (dd, *J* = 10.4, 5.5 Hz, 1H), 3.77 (s, 3H), 3.68 (s, 3H), 3.68 – 3.57 (m, 1H), 3.48 (tdd, *J* = 6.9, 5.3, 1.1 Hz, 1H), 3.12 (p, *J* = 6.8 Hz, 1H), 2.51 (dd, *J* = 17.1, 8.0 Hz, 1H), 2.39 (dd, *J* = 17.1, 7.1 Hz, 1H) ppm.

^{13}**C NMR** (101 MHz, $CDCl_3$): δ 198.3, 171.2, 170.7, 150.3, 143.8, 128.7, 124.3, 65.2, 53.0, 52.2, 51.4, 46.5, 41.5, 32.4 ppm.

HRMS (ESI-TOF) m/z: $[M + Na]^+$ calcd for $C_{16}H_{18}N_2O_9SNa$, 437.0625; found, 437.0620.

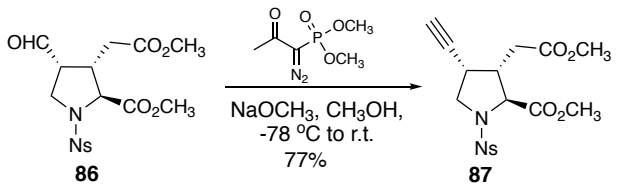

Methyl (*2S,3S,4S*)-4-ethynyl-3-(2-methoxy-2-oxoethyl)-1-((4-nitrophenyl)sulfonyl)pyrrolidine-2-carboxylate (87). To a single-neck flask charged with argon were added a solution of $NaOCH_3$ in methanol (1N, 0.78 mL, freshly prepared) and dry THF (10 mL). The resulting mixture was cooled to -78 °C using a dry ice/acetone bath. To this mixture was added the Bestmann-Ohira reagent (dimethyl-(1-azoacetonyl)phosphonate) in acetonitrile solution (10% wt, 2.1 mL) dropwise under vigorously stirring (slow stirring may lead a frozen solution due to the -45 °C melting point of acetonitrile). 10 mins later, the aldehyde **86** (202 mg, 0.487 mmol) in THF (2 mL) was added dropwise. After 30 mins, the solution was allowed to rt and maintained at rt for 15 mins. The reaction was quenched with ammonium chloride aqueous solution and extracted with ethyl acetate (3 × 10 mL). The combined organic layer was washed with sodium bicarbonate, brine, dried over $MgSO_4$ and filtered. The solvent was removed under reduced pressure and afforded a pale-yellow liquid residue. The crude was purified by column chromatography using ethyl acetate / hexane as an eluent (10–50% gradient). The alkyne product **87** was recovered as a white foam solid (153 mg, 77%).

FTIR (thin film): 3280, 3103, 3001, 1737, 1538 cm^{-1}.

^{1}**H NMR** (400 MHz, $CDCl_3$): δ 8.37 (d, *J* = 8.9 Hz, 2H), 8.07 (d, *J* = 8.9 Hz, 2H), 4.08 (d, *J* = 7.6 Hz, 1H), 3.79 (s, 3H), 3.73 (dd, *J* = 6.4, 3.2 Hz, 1H), 3.69 (s, 3H), 3.63 (dd, *J* = 10.3, 3.4 Hz, 1H), 3.31 (dh, *J* = 5.9, 2.6 Hz, 1H), 2.88 – 2.78 (m, 1H), 2.73 (dd, *J* = 17.0, 8.3 Hz, 1H), 2.46 (dd, *J* = 17.0, 6.0 Hz, 1H), 1.93 (d, *J* = 2.4 Hz, 1H) ppm.

^{13}**C NMR** (101 MHz, $CDCl_3$): δ 171.3, 171.0, 150.3, 143.8, 128.9, 124.2, 79.0, 64.1, 53.2, 53.0, 52.1, 43.3, 33.6, 32.9 ppm.

HRMS (ESI-TOF) m/z: $[M + Na]^+$ calcd for $C_{17}H_{18}N_2O_8SNa$, 433.0682; found, 433.0676.

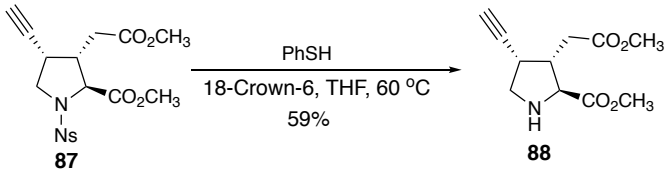

Methyl (2*S*,3*S*,4*S*)-4-ethynyl-3-(2-methoxy-2-oxoethyl)pyrrolidine-2-carboxylate (88). A single-neck flask was charged with alkyne **87** (153 mg, 0.372 mmol) in THF (5 mL), K_2CO_3 (77 mg, 0.56 mmol) and PhSH (115 μL, 1.12 mmol) at rt. The reaction was heated to 60 °C and maintained for 3 hrs. Then the reaction mixture was poured into water and extracted with ethyl acetate (3 × 10 mL). The combined organic layer was washed with sodium bicarbonate and brine. The resulting organic layer was dried over $MgSO_4$ and filtered. The filtrate was concentrated under reduced pressure and afforded a pale-yellow liquid. This crude was purified by column chromatography using ethyl acetate / hexane as an eluent (50-100% gradient). The diester product **88** was recovered as a colourless liquid (49 mg, 58%).

FTIR (thin film): 3270, 2996, 1738 cm^{-1}.

^{1}H NMR (400 MHz, $CDCl_3$): δ 3.75 (s, 4H), 3.70 (s, 3H), 3.57 (d, *J* = 7.6 Hz, 1H), 3.33 (dd, *J* = 10.6, 6.2 Hz, 1H), 3.20 (tdd, *J* = 6.3, 3.9, 2.5 Hz, 1H), 3.09 (dd, *J* = 10.6, 4.0 Hz, 1H), 2.89 – 2.79 (m, 1H), 2.72 (dd, *J* = 8.6, 5.6 Hz, 1H), 2.70 – 2.62 (m, 2H), 2.19 (d, *J* = 2.5 Hz, 1H) ppm.

^{13}C NMR (101 MHz, $CDCl_3$): δ 174.4, 172.5, 82.3, 63.8, 52.8, 52.4, 51.8, 43.2, 35.2, 34.7 ppm.

HRMS (ESI-TOF) m/z: $[M + H]^+$ calcd for $C_{11}H_{16}NO_4$, 226.1074; found, 226.1076.

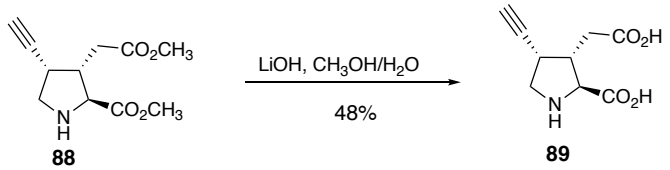

(2*S*,3*S*,4*S*)-3-(carboxymethyl)-4-ethynylpyrrolidine-2-carboxylic acid (89). To a single-neck flask were added diester (**88**) (43 mg, 0.07 mmol) in methanol (2 mL) and LiOH aqeous solution (2.5 N, 2 mL) at rt. The reaction was stirred at rt for 5 h. It was then neutralized with hydrochloric acid (1 N) at 0 °C. The resulting solution was concentrated under reduced pressure. The resulting residue was purified by ion-exchange chromotagraphy: ion-exchange resin Dowex 50WX4 100-200 mesh, eluting with 0.5 N aqeous ammonia. The elution fractions were collected and analyzed by TCL for the presence the desired product. (TLC plates were dried gently with a heat gun before being stained with ninhydrin; further heating revealed the presence of the amino acid **89** as yellow spots.) The fractions containing the product were combined and flash frozen, and the solvents were removed by lyophilization to yield **89** as a white solid (18 mg, 48%).

FTIR (thin film): 3272, 2996, 1730 cm^{-1}.

^{1}H NMR (400 MHz, D_2O): δ 3.86 (d, *J* = 9.2 Hz, 1H), 3.62 (dd, *J* = 11.8, 6.4 Hz, 1H), 3.59 – 3.52 (m, 1H), 3.56 – 3.48 (m, 1H), 2.82 – 2.76 (m, 1H), 2.76 – 2.68 (m, 2H), 2.68 – 2.63 (m, 1H) ppm.

^{13}C NMR (101 MHZ, D_2O): δ179.4, 173.0, 79.1, 75.5, 63.5, 50.3, 43.3, 37.3, 33.7 ppm.

HRMS (ESI-TOF) m/z: $[M - H]^-$ calcd for $C_9H_{10}NO_4$, 196.0615; found, 196.0612.

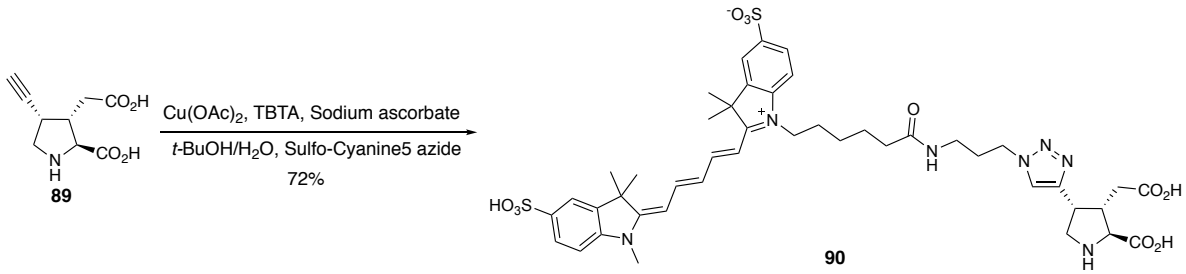

Sulfo-Cy5-trazole-KA (90). To a single-neck flask charged with argon was added KA alkyne **89** (2 mg, 0.006 mmol), Sulfo-Cy5-azide (7 mg, 0.009 mmol), sodium ascorbate aqueous solution (3.8 mM, 1.1 mL), TBTA aqueous solution (2 mM, 0.4 mL) and $CuSO_4$ aqueous solution (3.4 mM, 0.25 mL) and *t*-BuOH (1 mL). The temperature was increased to 60 °C and maintained for 24 h. The resulting mixture was concentrated under reduced pressure and purified by HPLC.

Sample (injection volume: 0.5 mL) was purified using a mobile phase composed of water/formic acid (0.02%) (solvent A) and acetonitrile/formic acid (0.02%) (solvent B), according to the following gradient steps (flow rate: 2.5 mL / min, detected by UV 235 nm), retention time = 3.6 min.

0 min 65% A- 35% B

10 min 65% A- 35% B

FTIR (thin film): 3392, 1702, 1640 cm^{-1}.

^{1}H NMR (400 MHz, D_2O): δ 8.07 (t, *J* = 13.1 Hz, 2H), 7.93 – 7.78 (m, 5H), 7.35 (d, *J* = 8.4 Hz, 2H), 6.58 (t, *J* = 12.5 Hz, 1H), 6.28 (dd, *J* = 13.6, 6.9 Hz, 2H), 4.33 (t, J = 6.7 Hz, 2H), 4.13 – 4.11 (m, 3H), 4.02 (q, *J* = 6.9 Hz, 1H), 3.80 (dd, J = 12.1, 7.4 Hz, 1H), 3.63 (d, *J* = 6.3 Hz, 1H), 3.60 (s, 3H), 3.20 – 3.09 (m, 1H), 3.01 (t, *J* = 6.8 Hz, 2H), 2.68 (dd, *J* = 17.2, 5.0 Hz, 1H), 2.27 – 2.08 (m, 3H), 2.00 – 1.79 (m, 4H), 1.75 – 1.56 (m, 12H), 1.51 – 1.20 (m, 4H) ppm.

HRMS (ESI-TOF) m/z: $[M - 2H]^{2-}$ calcd for $C_{44}H_{53}N_7O_{11}S_2$, 459.6628; found, 459.6633.

4.6.5 Biological experiments

Plasmid propagation

The GRIK2-GFP cDNA was prepared by Mellissa Hinderle (BSc Biochemistry 2016, UBC Okanagan, see cDNA preparation procedures in her thesis).

a. Transformation procedures:

The frozen DH10B competent cells were removed from the – 80°C freezer and thawed on ice. The competent cells were gently mixed by lightly flicking tube. 50 µl of cells were pipetted into a chilled falcon tube (Thermo Fisher, plolypylene, 14 mL). Unused cells were refrozen in a dry ice/ ethanol bath and stored in the – 80°C freezer.

cDNA solution (3 µl, 298 µg/µL) was added to cell suspension. The resulting mixture was gently swirled for a few seconds to mix, followed by incubation on ice for 30 minutes. The tube(s) was placed in 42°C water bath for 40 seconds without shaking (heat shock). Then the tube(s) was placed on ice for ~2 minutes. The transformation reaction(s) was diluted to 1 mL by addition of super optimal broth (SOC) media. (SOC. medium: 2% Tryptone, 0.5% Yeast Extract, 0.4% glucose, 10 mM NaCl, 2.5 mM KCl, 10 mM MgCl 2 & 10 mM $MgSO_4$.) The tube(s) was/were incubated in a shaking incubator at ~200 rpm for 1 hour at 37 °C.

The obtained bacteria medium was plated by spreading 30 µL of cell transformation mixture on LB agar plates containing ampicillin and incubated overnight at 37 °C. Single colonies were observed and picked for the subsequent propagation.

b. Propagation and cDNA purification procedures:

Single colonies were picked and transferred into individual falcon tubes containing 5 mL LB media and 0.5% ampicillin. Falcon tube(s) was/were incubated in a shaking incubator at ~200 rpm for 24 hours at 37°C. The

obtained medium was purified with Plasmid Mini Kit (Omega) by following the enclosed manual. The concentration of cDNA in each tube was determined by NanoPhotometer (Implen, NP80).

Cell culture and expression of GluR6. HEK-293T cells were cultured in Dulbecco's modified Eagle's medium (DMEM)-Glutamax (Invitrogen) supplemented with 10% fetal bovine serum (Invitrogen), penicillin (100 units/mL), streptomycin (100 μg/mL), and incubated in a 5% CO_2 humidified chamber at 37 °C. DMEM media with phenol red indicator was used for the culture. Non-phenol red DMEM media was used for the transfection in order to avoid background fluorescence in confocal imaging experiment.

HEK293 cells were transfected with the obtained cDNA plasmid. GFP was employed as transfection marker but not fused to the C- or N- terminal of GluK2.

Before the induction, the cells were passaged to a 2 mL petri dish with glass bottom (confluence: 20% – 40%). The petri dish was then put in the tissue incubator for 2 h to allow cells to attach to the glass bottom. 5 μL CaCl2 (2.5 M) was pipetted into a 1.5 mL micro centrifuge tube. To this tube was added the obtained plasmid (5 μL, 200–300 μg/μL). This mixture was then diluted with sterile water (50 μL) and mixed with cold HEPES buffer (50 μL). This obtained solution was added dropwise to the culture media of HEK-293 cells. After 24 h, transfection was confirmed by microscopy with the existence of GFP marker.

Chemical labelling of HEK-293 cells. The stock solution of probe **90** was prepared by dissolving probe in ultrapure water (prepared by a MilliporeSigma water systems) to the concentration of 100 μM. The fluorescent probe **90** (2.5 μM) was added to medium of HEK293 cells and incubated at rt for 5 mins. After this labeling, the cells were washed with PBS buffer (pH = 7.5) once with a micropipette.

Confocal imaging of labelled KAR (GluR6) in HEK-293 cells. Cell imaging was performed with a confocal microscope (FV1000, IX81, Olympus) equipped with a 60× numerical aperture (NA) = 1.35 oil objective. Fluorescence images were acquired using an argon laser for excitation of GFP and a red laser for excitation of Cy5. GluK2 transfected HEK293T cells were identified by the existence of GFP maker. The ROI measurement of fluorescence-labeled cells was performed with Fiji (opensource software).

$$\text{Relative fluorescence intensity} = \mathbf{F} / \mathbf{F_0}$$

F: fluorescence obtained from ROI measurement of GluR 6 transfected HEK293 cells

$\mathbf{F_0}$: fluorescence obtained from ROI measurement of non-transfected HEK293 cells

The data were analyzed by GraphPad Prism.

Chapter 5

Synthesis and Photochemistry of Light-Controllable Agonists for Kainate Receptors

Ion channel agonists and antagonists have been widely used in neurophysiological research over the past three decades. These studies rely on classical methods that lack temporal or spatial precision. In contrast, neurotransmitters that are photocaged or photoswitchable offer attractive alternatives as optically controllable tools for the precise manipulation of neurons. This chapter describes the synthesis and characterization of light-controllable agonists specifically designed to control kainate receptor activity.

5.1 Background

Optical control of biological processes is an emerging field, which permits bioactivity manipulations with spatiotemporal resolution.[31,133,134] The fundamental concept involves using light to activate or suppress a protein's activity. Biological approaches include optogenetics, pioneered by Deisseroth and Boyden; this technique controls neuronal activity with genetically encoded light-sensitive ion channels, i.e., channelrhodopsins.[135,136] With optogenetics, the gene of a light-gated ion channel is introduced locally into a rodent brain by viral infection. The infected mice subsequently displayed light-responsive behaviours upon blue light irradiation delivered to a brain region by fiber optic.[137] These powerful optogenetics tools have been applied to animals to elucidate nervous system functions, such as memory, neurological disorders, and neurodegenerative diseases.[138,139]

Optogenetic tools are spectacular, but they are restricted to genetically defined proteins and necessitate genetic manipulation for each organism investigated—a complication when studying the human brain. Photopharmacology was thus developed in parallel to optogenetics and offers a complementary set of tools (Figure 5–1).[31]

Photopharmacological tools are based on small molecules; they employ photochromic ligands combined with light irradiation to control an ion channel's conductance.[140] In the context of neurobiology, these photochromic ligands can be classified as photocaged and photoswitchable neurotransmitters (see Chapter 1.4).[34,140,141]

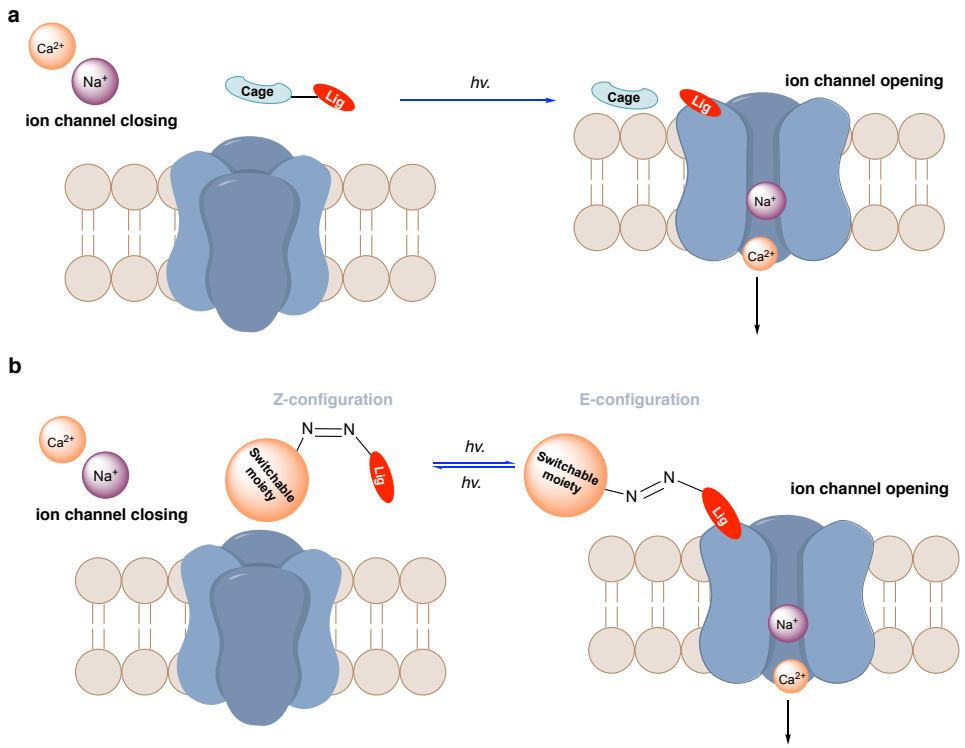

Figure 5–1. Cartoon examples of photopharmacology tools for the control of ion channels function. (A) Photocaged neurotransimitters: an agonist is made inactive with a light-cleavable protecting group (cage), upon light irradiation the "cage" releases the ligand that can now bind to its associated protein. (B) Photoswitchable neurotransmitters: an agonist is modified with a photo-isomerizable group that either prevents or allows binding to its associated protein, depending on the configuration of the molecule.

Photocaged neurotransmitters have two components: a neurotransmitter and the "cage", which is a photo-cleavable moiety (Figure 5–1a). The cage group must be suitably placed to prevent the neurotransmitter from binding to its receptor. When presented to the appropriate wavelength irradiation, the cage moiety is removed, thereby allowing the neurotransmitter to activate its associated protein receptors. Thus, neuroactivity, e.g. ion channel opening, can be triggered by simple light exposure.[142-144] However, this type of activation is irreversible due to the intrinsic nature of the decaging process – an irreversible chemical reaction.

Photoswitchable neurotransmitters were proposed as reversible regulators for ion channels (Figure 5–1b).[39,127,139-142] The labs of Woolley and Trauner utilized azobenzene groups combined with neurotransmitters to create such probes.[143,144] The probes undergo a configurational *cis*-to-*trans*

isomerization upon light irradiation, which gives access to two isomers of a neurotransmitter, with only one being a potent ligand for the receptor. Since the configurational change is reversible, the activation and deactivation of a POI can be reversibly regulated by light.

5.2 Research gap

The renewed interest in the role of glutamate receptors in neurodegenerative diseases has led to the recent creation of a number of photo-active tools for AMPA and NMDA receptors.[38,145-147] However, no photochromic ligand has been reported specifically for kainate receptors. This is likely due to the relative ease of chemical modification of ligands for AMPA and NMDA receptors.

In contrast, the only selective ligands reported for KA receptors are the complex family of kainoid natural products. Given our success in developing a synthesis that allows for easy C4-modification of kainoids, we are uniquely positioned to design new photoactive pharmacological tools to study the function of kainate receptors in neurons.

5.3 Design of photo-controllable agonists for KARs

The ideal photochromic ligand will selectively activate—or inhibit—a POI upon visible light irradiation, preferably with long wavelengths like far-red or near-IR (650–900 nm).[145,146] High selectivity of the ligand is crucial to minimize off-target effects, and visible light minimizes radical-based damages in living cells. With these considerations in mind, I hypothesized that a photocaged kainoid (DECM-PhKA, **100**) and a photoswitchable kainoid (TCAZKA, **103**) can be synthesized and will enable the photo-control of kainate receptors (Figure 5–2).

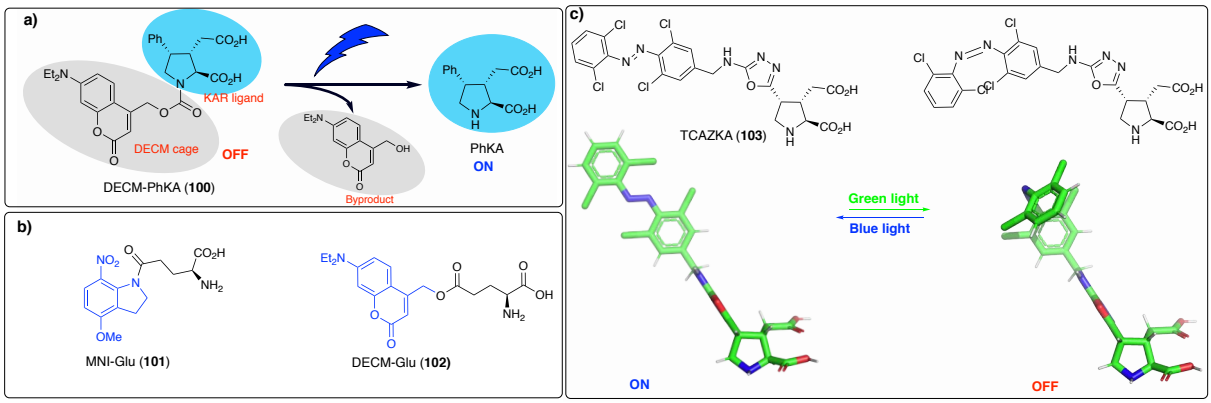

Figure 5–2. Examples of photocontrollable KAR agonists. (A) The proposed photocaged agonist for KAR: DECM-PhKA, **100**. (B) Simple photocaged glutamates have been reported with UV-cleavable amides or esters. (C) Proposed photoswitchable kainoid: TCAZKA, **103**.

Photocage Design. The proposed DECM-PhKA **100** is composed of phenylkainic acid and a coumarin "cage". Under blue light radiation, the coumarin cage should be cleaved, and the released phenylkainic acid (PhKA) will be available to bind and activate KARs (Figure 5–2a). The caged carbamate **100** was envisaged inert to KARs as we know from Chapter 2 that (1) the pyrrolidine's amine is essential to binding, and (2) there is no room in the binding pocket to accommodate the large coumarin group.

Since DECM-PhKA is inert when the coumarin cage is in place, the light irradiation will free phenylkainic acid which will exert a "turn-on" effect on the KARs channels. The specific 7-(*N,N*-diethylamino)coumaryl-3-methlyoxy (DECM) group was selected for its high quantum yield and maximum absorption in the visible blue region (390-410 nm). In order to have a comprehensive understanding on the decaging properties, the reported MNI-Glu (**101**) and DECM-Glu (**102**) will also be synthesized for comparison (Figure 5–2b). Since PhKA is at least 100-fold more active than glutamate for KARs, it is expected that DECM-PhKA will be amuch more rapid "turn-on" activator than MNI-Glu and DECM-Glu. This is important for neurobiology applications: intercellular communication in neurons occurs on the millisecond scale, therefore slow activation kinetics combined to diffusion can lead to undiscernable physiological responses. This proposed set of photocaged tools will allow the irreversible activation of GluRs.

Photoswitch Design. In contrast, the proposed photoswitch TCAZKA (**103**) can be reversibly isomerized between configurations that will fit, or not, in the binding site of KARs (Figure 5–2c). Consequently, a KAR probe like TCAZKA is expected to enable more elaborate experiments than photocages. Photoswitch **103** is comprised of a kainoid tethered to a tetracholoroazobenzene. Given that our synthesis makes the C4 position of kainoids easily modifiable (see chapter 4.1), we planned to introduce a tetrachloroazobenze moiety as part of the C4-side chain. Woolley's tetrachloroazobenze was chosen because it can be isomerized with visible light, at wavelengths that are not damaging to cells.[37,147] Indeed, the azo double bond of tetrachloroazobenze can isomerize between the *Z* (green light) and *E* (blue light) configuration. The bent *Z* configuration of the C4 side chain is expected to prevent the kainoid from fitting into the GluK channel's ligand-bining domain. In contrast, the linear *E* configuration of the group should allow binding (and possibly increase potency by decreasing K_{off}). Thus, we hypothesize that the photoswitch TCAZKA (**103**) can be isomerized reversibly using visible light. We also hypothesize that irradiating **103** with green (*Z*) light will have an OFF and blue light (*E*) will have an ON effect on the modulation of KARs channels in living cells.

5.4 Synthesis of photocaged agonists

5.4.1 Synthesis of MNI-Glu

MNI-Glu (**101**) was synthesized from 4-methoxyindole and glutamic acid in six steps according to literature precedents (Scheme 5–1).[143,148] 4-Methoxyindole (**104**) was converted to 4-methoxy-7-nitroindoline (**108**) via a sequence of reduction, *N*-Boc protection, nitration, and *N*-Boc deprotection. The resulting amine **108** was then coupled with *N*-Boc-Glu-O*t*Bu to give the fully protected amide **109**. Acidic conditions using TFA removed both the carbamate and the *tert*-butyl ester of **109** to afford MNI-Glu as the TFA salt (**101**).

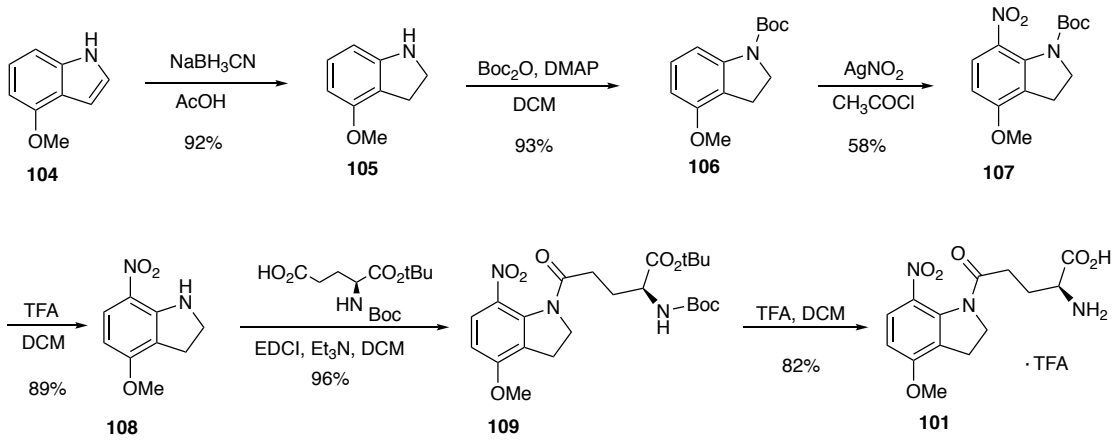

Scheme 5–1. Synthesis of MNI-Glu (101)

5.4.2 Synthesis of DECM-Glu and DECM-PhKA

The synthesis began with the preparation of a coumaryl cage precursor since both targets DECM-Glu (**102**) and DECM-PhKA (**100**) share this moiety (Scheme 5–2). The direct oxidation of **110**[149] to obtain aldehyde **112** with selenium dioxide never reached completion, even after overnight reflux in toluene. While a longer reflux time (3 to 5 days) did show consumption of coumarin **110**, it also created several impurities. A two-step procedure was thus adopted: coumarin **110** was first converted to enamine **111**, followed by a periodate oxidative cleavage to aldehyde **112**.[150] The aldehyde **112** was then smoothly reduced by $NaBH_4$ to alcohol **113**. Coumaryl alcohol **113** is the common fragment that will be used as cage component.

The unsymmetrical carbonate **114** was prepared as activated reagent for later amide couplings. This was accomplished by reacting alcohol **113** with 4-nitrophenyl chloroformate. 4-Susbtituted coumarins are highly sensitive to degradation when they bear a potential leaving group at the allylic

position. After several attempts, we found that the most stable acylating agent was the *para*-nitrophenol carbonate.

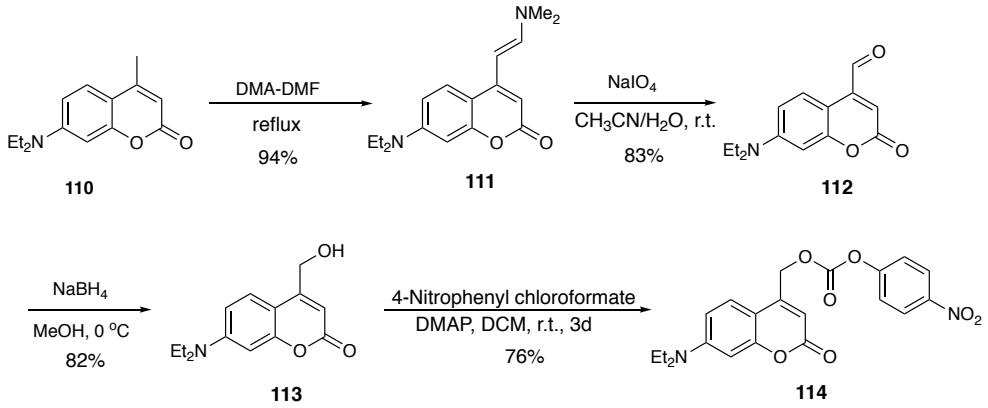

Scheme 5–2. Synthesis of DECM cage reagents

With alcohol **113** in hand, Boc-Glu-O*t*Bu was caged by esterification (Scheme 5–3). The *N*-Boc- and *t*-butyl ester groups of **116** were removed in a single deprotection step using TFA to afford DECM-Glu (**102**). We found that ester **102** was surprinsigly stable to daylight exposure (in the lab); enough to purify by column chromatography without requiring special precautions.

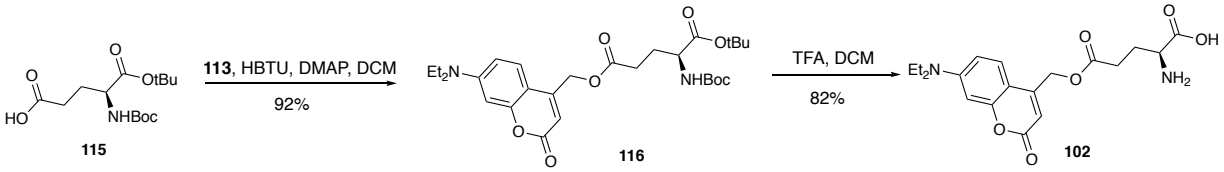

Scheme 5–3. Synthesis of DECM-Glu (102)

The synthesis of DECM-PhKA (**100**) took advantage of the advanced intermediate pyrrolidine **70a** described in Chapter 3 (Scheme 5–4). The carboxylic acid of pyrrolidine **70a** was esterified, then its amine was reacted with the unsymmetrical DECM carbonate **114** to give the fully protected **117**. However, hydrolysis of dimethyl ester **117** under conventional conditions (LiOH aq/CH_3OH) the DECM cage of **117** was cleaved as well. Turning to milder conditions—trimethyltin hydroxide—smoothly provided the desired caged phenylkainic **100**. However, the caged product **100** contained residual tin, even after column chromatography purification. Since tin is a concern in biological experiments due to its high cytotoxicity, I looked for an alternative sequence.

The successful sequence involved reacting the photoreactive carbonate **114** with PhKA directly. Thus, pyrrolidine **70a** was hydrolyzed first to obtain **32a**, followed by a direct carbamate

formation with **114**. This alternative route circumvented using heavy metal reagents and afforded the desired caged compound DECM-PhKA (**100**).

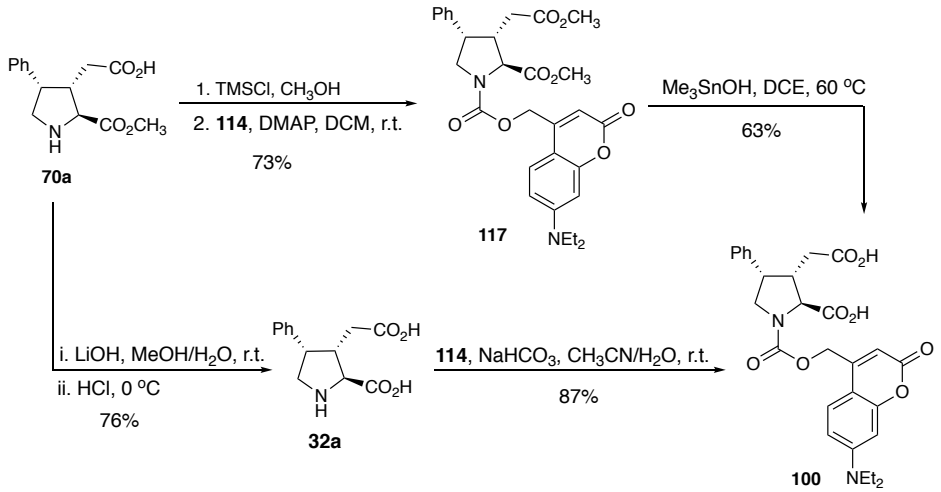

Scheme 5–4. Synthesis of DECM-PhKA (100)

5.5 Synthesis of photoswitchable kainoids

Inspired by the high affinity of C4 aromatic kainoids presented in Chapter 2, I planned to establish a route to new types of aromatic kainoids. Should it be successful, this strategy could be adapted to build kainoid photoswitches.

The photoisomerization of simple azobenzes can be realized UV light irradiation.[151] For this advantage, azobenzene derivatives have extensively utilized to construct molecular switches.[151] Moreover, the switching wavelengths can be extended to visible light region with the introduction substitutents onto the benzene ring, such as methoxyl, fluoro and chloro groups.[147,152,153] The tetrachloroazobenze used in this thesis was chosen due this visible-light switchable feature.[154]

5.5.1 Synthesis of a new heteroaromatic kainoid

In modern medicinal chemistry, the strategy of coupling a carboxylic acid to a thiosemi-carbazide[155,156] to prepare oxadiazoles in a single step has been widely used to create libraries of compounds.[157] This quick chemical assembly was adopted in my synthesis to construct C4 heteroaromatic kainoids and their parent photoswitch.

Aminooxazolyl kainoid **124** was selected as a class representative to develop the chemistry for two reasons: its strong electron-deficient quadrupole characteristics would enhance π - π stacking interactions with Tyr488 with the KAR binding site (see Chapter 2), and the 2-amino substituent

would allow easy attachment of different molecular cargo (e.g., fluorescent tags, biotin, photoswitch, etc.).

The synthesis of novel aminooxadiazolyl kainoid **124** began with the preparation of an *N*-protected thiosemicarbazide (Scheme 5–5). Benzylamine **118** was used to explore the synthesis route since it is removable under acidic conditions. This benzylamine **118** was converted to an isocyanate and then coupled with hydrazine to afford **120**. Thiosemicarbazide **120** was condensed with the EDCI-activated acid **72a** (Chapter 3) to obtain benzylamine **121**, which was surprisingly stable. *N*-Benzyl-protected kainoid **121** had to be refluxed in TFA to achieve the deprotection. The aminooxadiazolyl product **122** was fully deprotected with additional two steps to afford the desired oxadiazoyl kainic acid (OKA, **124**). The C4 configuration of **124** was confirmed by 2D ^{1}H NMR spectrocopy analysis using NOE experiments.

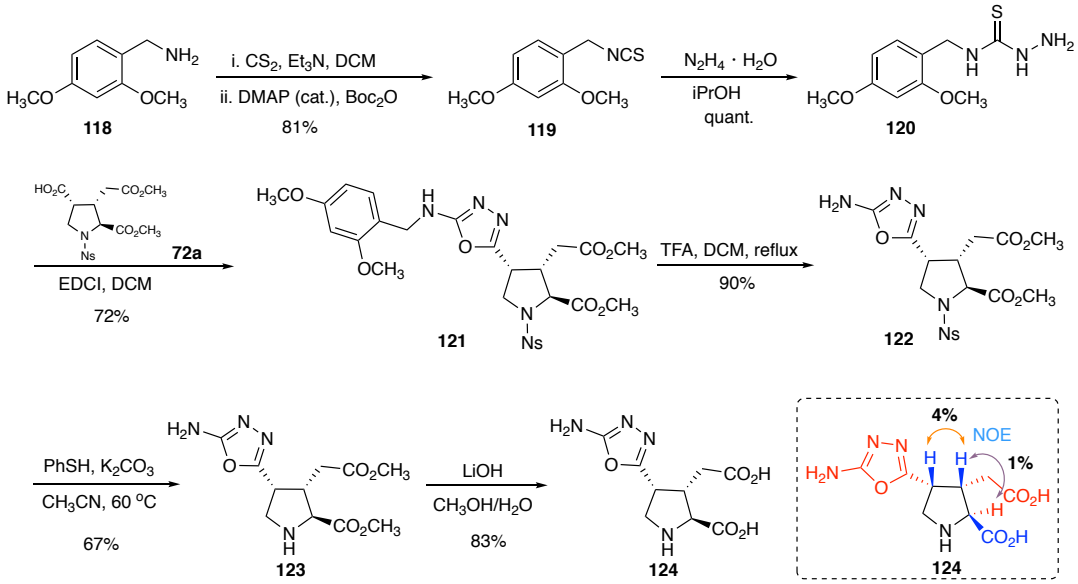

Scheme 5–5. Synthesis C4 kainoid derivative 124

5.5.2 Synthesis of an azobenzene kainoid photoswitch

The route to substituted oxadiazolyl kainic acid derivative **121** was exploited to create an azobenzene kainic photoswitch. This objective required us to synthesize the appropriate tetrachloroazobenzene precursor (Scheme 5–6). Accordingly, 4-aminobenzoic acid (**125**) was converted to 4-(phenylazo)benzoic acid **126** through a nitroso/amine condensation. Then a multi-chlorination selective for the *ortho* positions of **126** was realized via a palladium catalyzed C–H activation to afford tetrachlorinated acid **127** in 82% yield.[154]

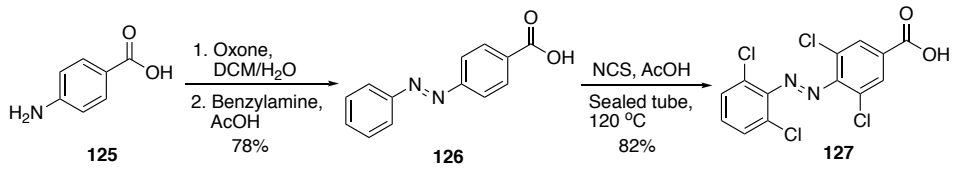

Scheme 5–6. Synthesis of a photoisomerizable tetracholoroazobenzoic acid.

The initial plan involved joining azobenzoic acid **127** with OKA diester **122** (Scheme 5–7). The acid **127** was transiently converted to the acyl chloride **127a**, and the poor nucleophilicity of the heteraromatic amine of oxadiazolyl **122** necessitated relative harsh conditions (reflux in pyridine) to provide the amide **133**. However, the deprotection of the *N*-nosyl group in presence of the unusually electrophilic amide **133** proved challenging. Indeed, the tetrachloroazobenzene moiety of **133** was cleaved when presented to PhSH (3.0 eq)/K_2CO_3 (2.0 eq)/CH_3CN at 60 °C. Although extensive optimizations were attempted—e.g., decreasing reagent amounts (1.0 eq PhSH, 1.0 eq K_2CO_3), decreasing reaction temperature (30 °C), or using additives (1.0 eq 18-crown-6)—the cleavage of tetratcholorobenzene was inevitable.

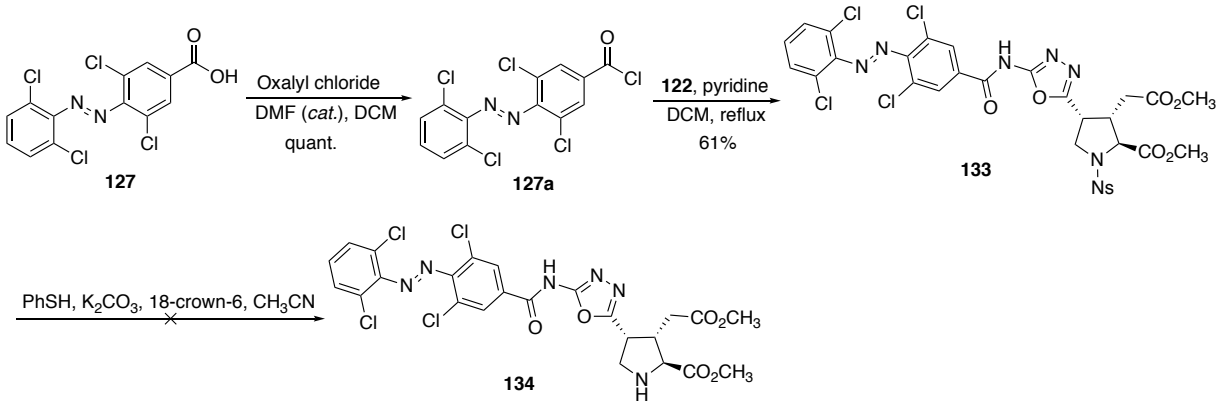

Scheme 5–7. First attempt at the synthesis of kainoid photoswitch 134

We then explored a direct coupling between kainoid acid **72a** and an azobenzene thiosemicarbazide to construct the oxadiazole as the coupling key reaction. While this strategy would add several synthetic steps, it was shown to be effective in the synthesis of **121** (Scheme 5–5).

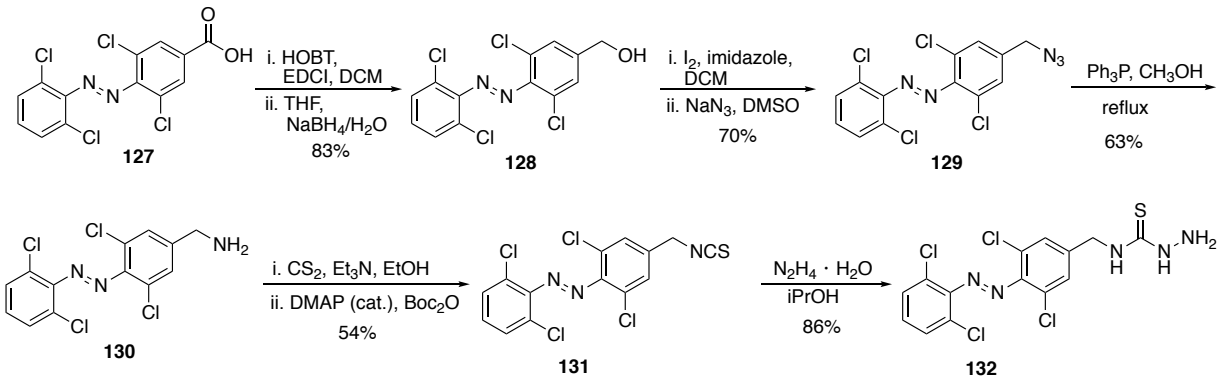

Scheme 5–8. Synthesis of a photoisomerizable tetracholoroazobenzene semicarbazide.

The required tetracholoroazobenzene semicarbazide presursor **132** was prepared from the azobenzoic acid **127** in seven transformations (Scheme 5–8). Acid **127** was reduced to alcohol **128** through a pre-activation with EDCI. Alcohol **128** was converted to the iodide, then to azide **129** in a one-pot sequence. A Staudinger reaction was used to reduce azide **129** to amine **130** via, which was then converted to thiosemicarbazide **132** by nucleophilic addition of hydrazine.

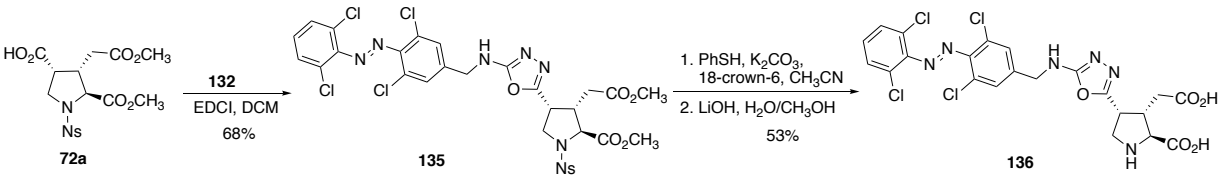

Scheme 5–9. Synthesis of kainoid photoswitch 136

The direct oxadiazole formation between acid **72a** and thiosemicarbazide **132** provided the alkylated aminooxadiazolyl kainoid **135** in an acceptable yield (Scheme 5–9). *N*-Nosyl deprotection of **135** using $PhSH/K_2CO_3/CH_3CN$ at 60 °C gave only a low yield of **136** (~23%) along with impurities. Using a lower temperature and an additive ($PhSH/K_2CO_3$/18-crown-6/CH_3CN at 30 °C) gave a cleaner reaction profile, and the crude product was telescoped for a methyl ester hydrolysis under basic aqueous condition to obtain the desired kainoid photoswitch **136**.

5.6 Photochemical characterization of photo-controllable kainoids

In order to use the photoactive chemical probes synthesized above in their physiologogical context adequately requires a comprehensive understanding of their behavior in solution. Measuring their spectral and kinetic properties was accomplished with a number of spectrophysical techniques.

5.6.1 Photochemical characterization of photocaged glutamates and kainoids

The photochemical properties of caged KAR agonists MNI-Glu (**101**), DECM-Glu (**102**) and DECM-PhKA (**100**) were measured first, followed by their photolysis rates. The photolysis experiments were carried out with two types of blue LED photochemical reactors (custom-made in our lab). One reactor had its maximum irradiation wavelength centered at 465 nm, and the other at 445 nm. Both lamps' irradiation range overlapped partially with the absorption ranges of DECM-Glu and DECM-PhKA, but there was almost no overlap with MNI-Glu (Figure 5–3).

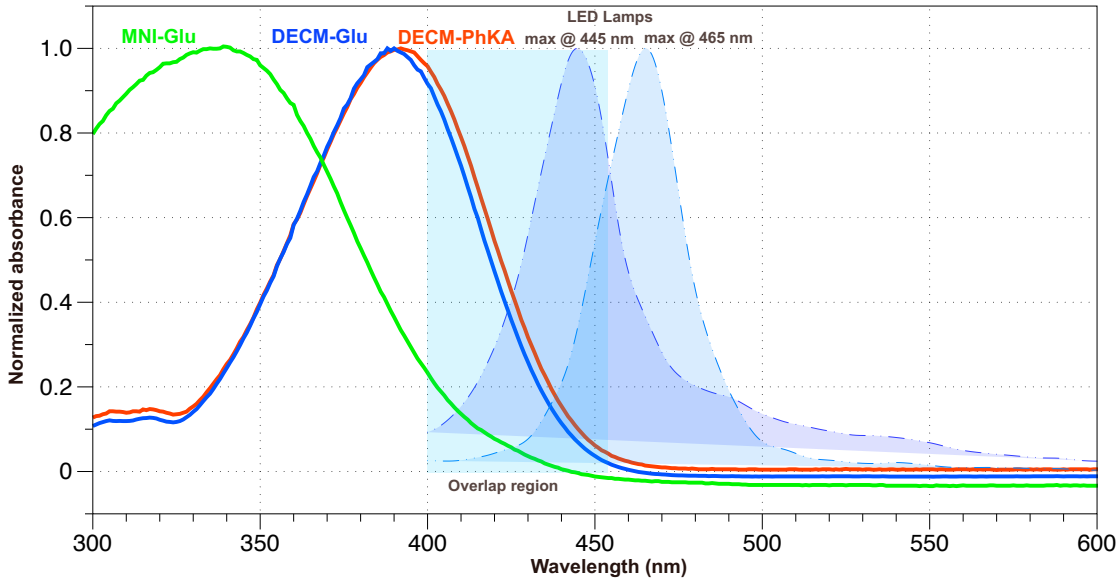

Figure 5–3. Overlay of the two photoreactors irradiadiation ranges (blue-shaded areas) of the absorption spectra of caged compounds **100-102**. The absorption of both molecules caged with a DECM coumaryl group overlap with the blue LED light sources. The smaller MNI cage group absorbs mostly in the UV range, and shows very little overlap with the light sources.

Photolysis reactions with the caged compounds **100-102** were performed in aqueous solutions to mimick physiological conditions (0.1% DMSO/H_2O). Indeed, photochemical reactions in water are notoriously inefficent from a quantum yield standpoint, therefore it was important to measure the efficiency of our photoreactive probes in an unbiased milieu, as close as possible to their intended applications. As expected from the data shown in Figure 5-3, MNI-Glu showed virtually no photolysis upon irradiation with the 445 nm blue LED light source (Figure 5–4a). In contrast, both DECM-Glu and DECM-PhKA showed effective cleavage under same conditions after only five minutes (Figure 5-4b and 4c).

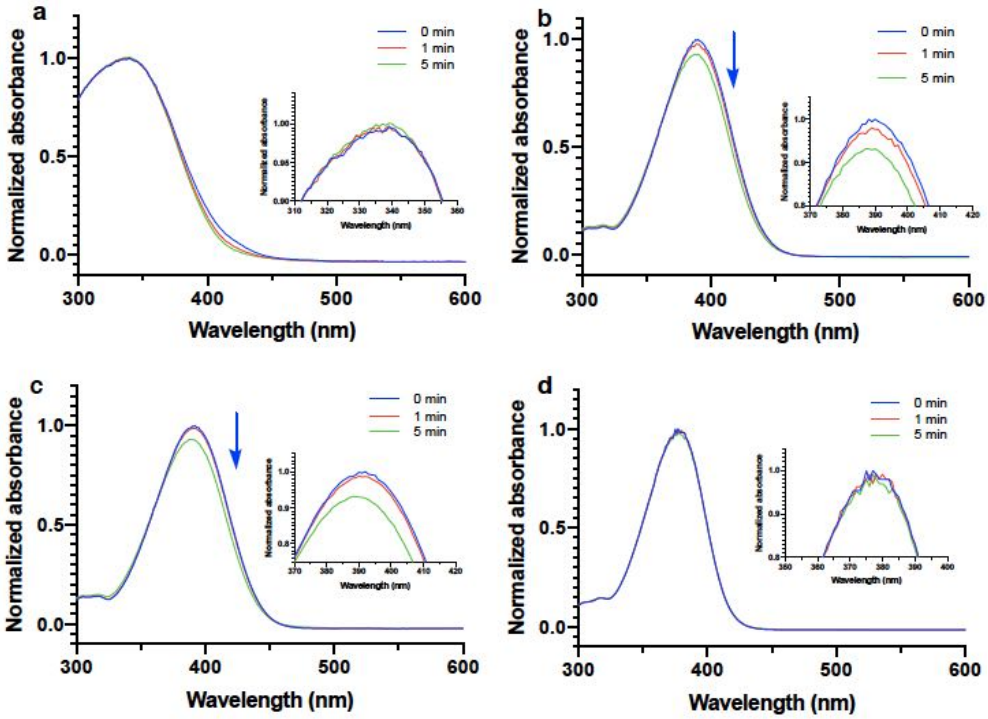

Figure 5–4. Time-dependent photolysis of caged compounds under blue LED light irradiation (445 nm): the absorbance of the compounds decrease as the photocage is released. (A) MNI-Glu in water containing 0.1% DMSO: no change in maximum absorbance is observed after 5 minutes irradiation. (B) DECM-Glu and (C) DEMC-PhKA in water containing 0.1% DMSO: both molecules display a ~10% change in absorbance after 5 minutes due to cleavage of the caged group. (D) DECM-PhKA in DMSO only: no photo-release takes place as water is required in the mechanism of photocehmical cleavage of the DECM coumarin.

As a control experiment, 445 nm irradiation of DECM-PhKA did not lead to uncaging in anhydrous DMSO (Figure 5-4d). This lack of reaction is explained by the necessity for a stoichiometric amount of water in the photolysis process (Figure 5–5). A successful lysis process involves the disassociation of [CM-A] to singlet ion pair [CM^+A^-] and subsequent combination with H_2O to yield CM-OH and A^-.[158] Without H_2O, the singlet ion pair [CM^+A^-] can undergo relaxation and recombine to the ground state of CMA.

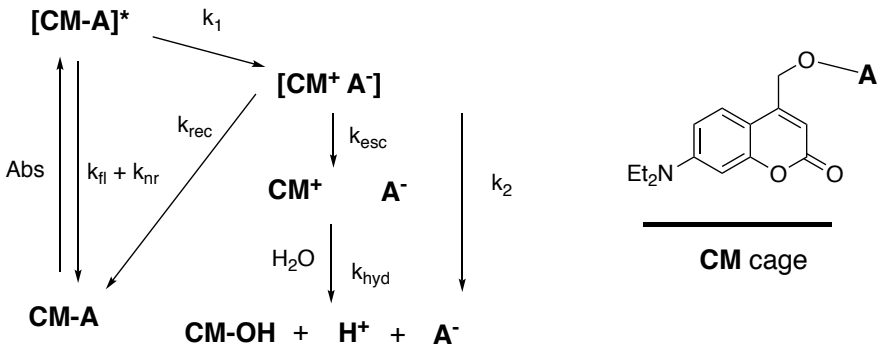

Figure 5–5. Proposed mechanism for the photolysis of the diethylcoumarin caged compounds under light radiation.

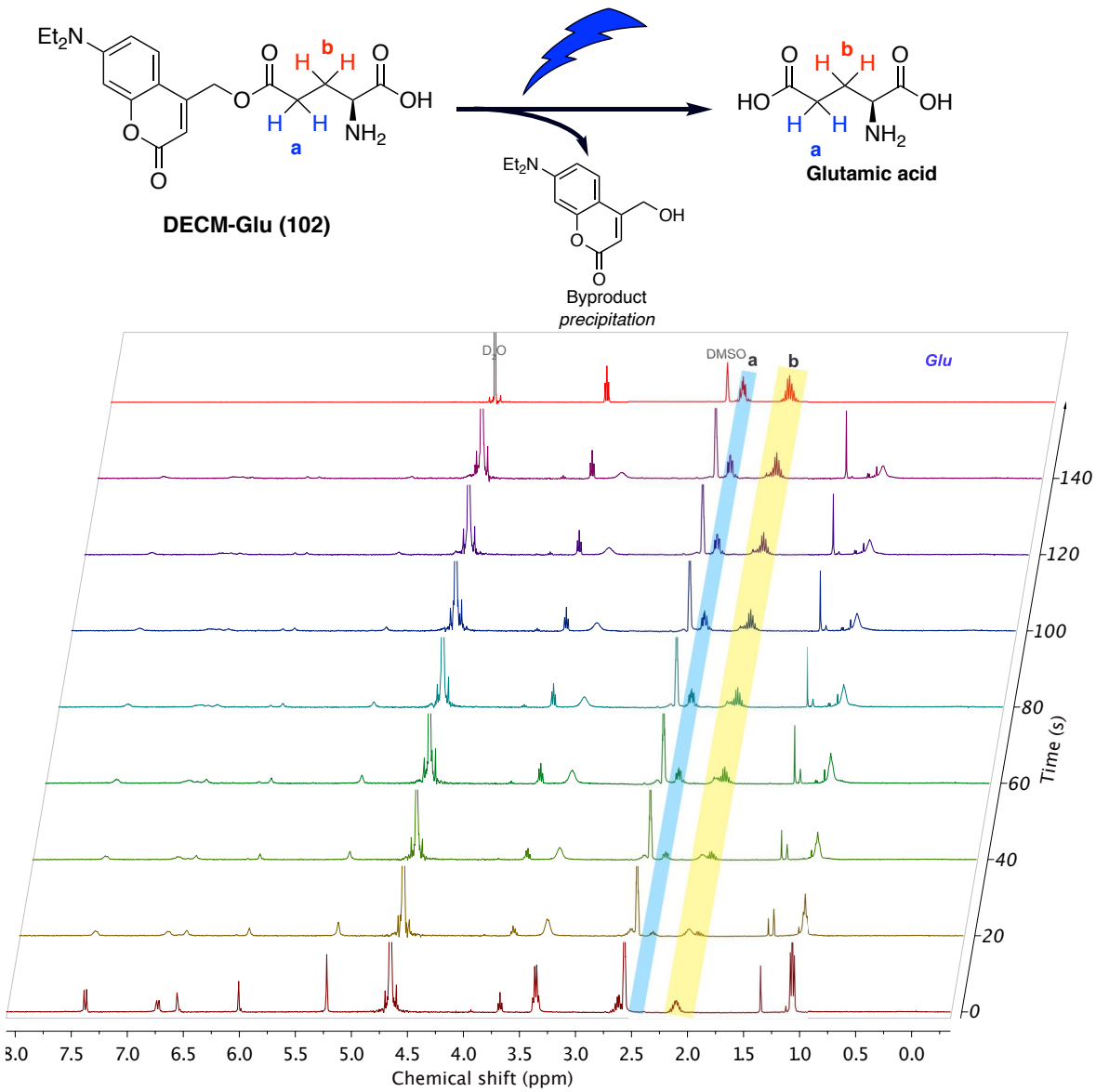

Figure 5–6. Overlaid ^{1}H NMR spectra for progressive photolysis of DECM-Glu (400 MHz, D_2O/DMSO-d_6: 5/1). The top spectrum is the glutamate standard in D_2O/DMSO. The cleaved coumarin byproduct is poorly soluble in aqueous solution; it precipitated out of solution and is therefore only visible in trace amount in the spectra.

The photolysis process can also be monitored by ^{1}H NMR spectroscopy (Figure 5–6). Initial trials for the uncaging of DECM-Glu (**102**) were conducted in a photoreactor equiped with a 445 nm or a 465 nm blue LED light source at room temperature. ^{1}H NMR spectra of the photolysis solution were measured at specific intervals. The overlaid ^{1}H NMR spectra presented in Figure 5–6 show that free glutamic acid was gradually released upon 445 nm irradiation (peaks a and b). However, DECM-Glu underwent photolysis much more slowly at 465 nm than at 445 nm (Figure S5–1, Appendix D). Under 445 nm irradiation, full cleavage was observed after 140 s (2:20 min). In

contrast, the 465 nm photoreactor required 16 mins irradiation to achieve only 80% conversion (Figure S5–2, Appendix D).

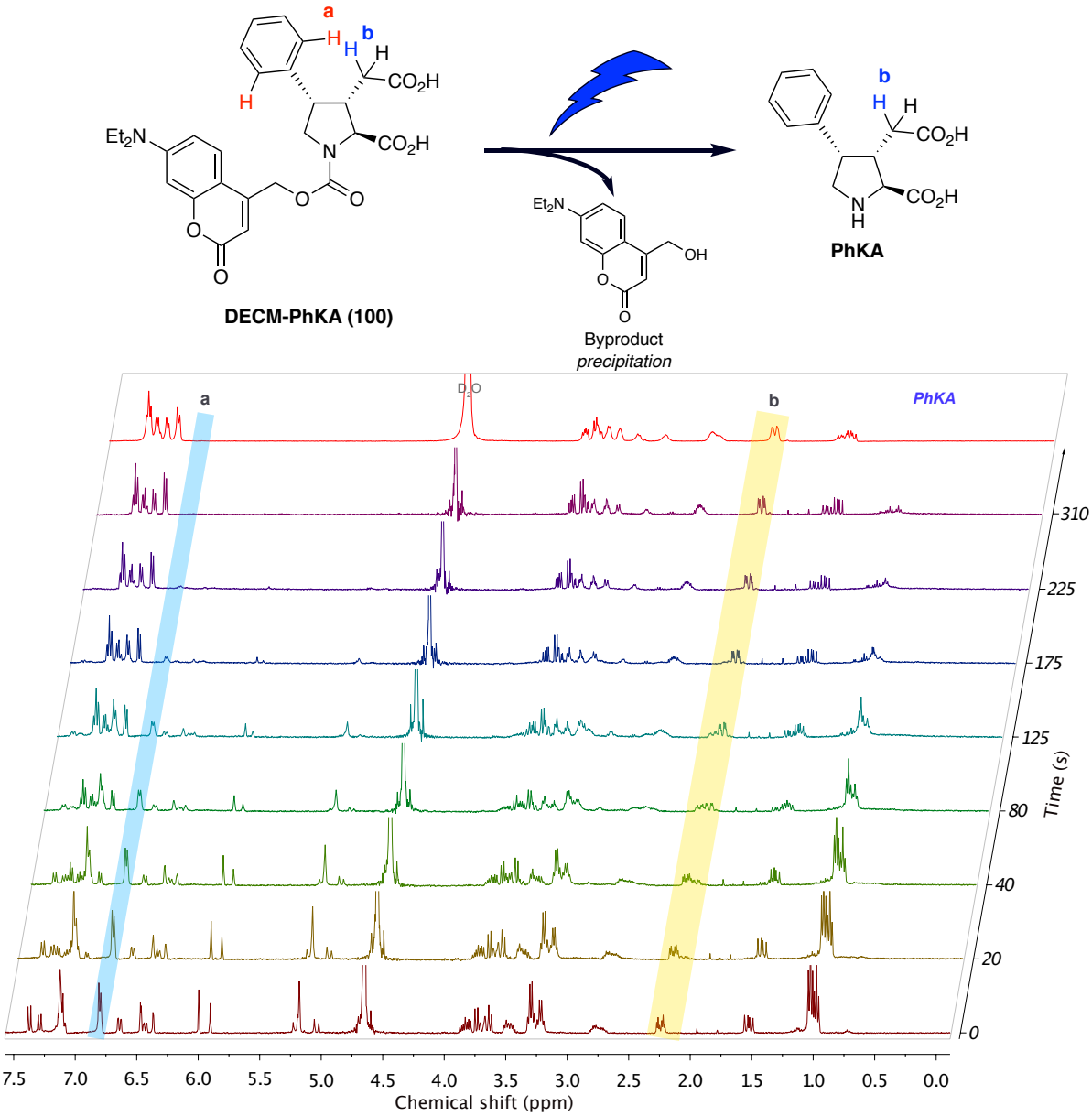

Figure 5–7. ^{1}H NMR (400 MHz, D_2O) spectra for progressive photolysis of DECM-PhKA. The top row is phenyl kainic acid standard in D_2O/DMSO. Since the low solubility of coumarin byproduct in aqueous solution, it gradually precipitated and exhibited low intensity in the spectra.

The photolysis of DECM-PhKA (**100**) was also studied by ^{1}H NMR spectroscopy in D_2O (Figure 5–7). The gradual release of free PhKA was found to be completed within 300 s (5:00 min). The CH_2 alpha to the carboxylic acid of PhKA (peak b) slightly shifted from 2.29 ppm to 2.20 ppm. Similarly, the *ortho* hydrogens on the phenyl group of DECM-PhKA shifted from 6.84 ppm to 7.03 ppm of the free PhKA and are key to assessing photolysis completion. The above kinetic

experiments confirmed the capabilities of releasing Glu and PhKA with visible light irradiation, in aqueous solution at neutral pH.

The ^{1}H NMR data presented above were used to determine photolysis rates (Figure 5–8). As expected, the photolysis of DECM cage exhibit an exponential kinetics[159](Figure 5–8a), which is also a feature of first-order reactions. DECM-Glu showed slightly faster lysis rate than DECM-PhKA (Figure 5–8a). DECM-Glu exhibits a half-life time of 33.4 s, while that of DECM-PhKA is 60.8 s. The slower lysis rate of DECM-PhKA may due to a the less favoured pathway upon radical cleavage of a carbamate *vs.* an ester. A similar trend was reported for the lysis of MNI caged glutamate: esters exhibited faster lysis rate than carbamate analogs.[160]

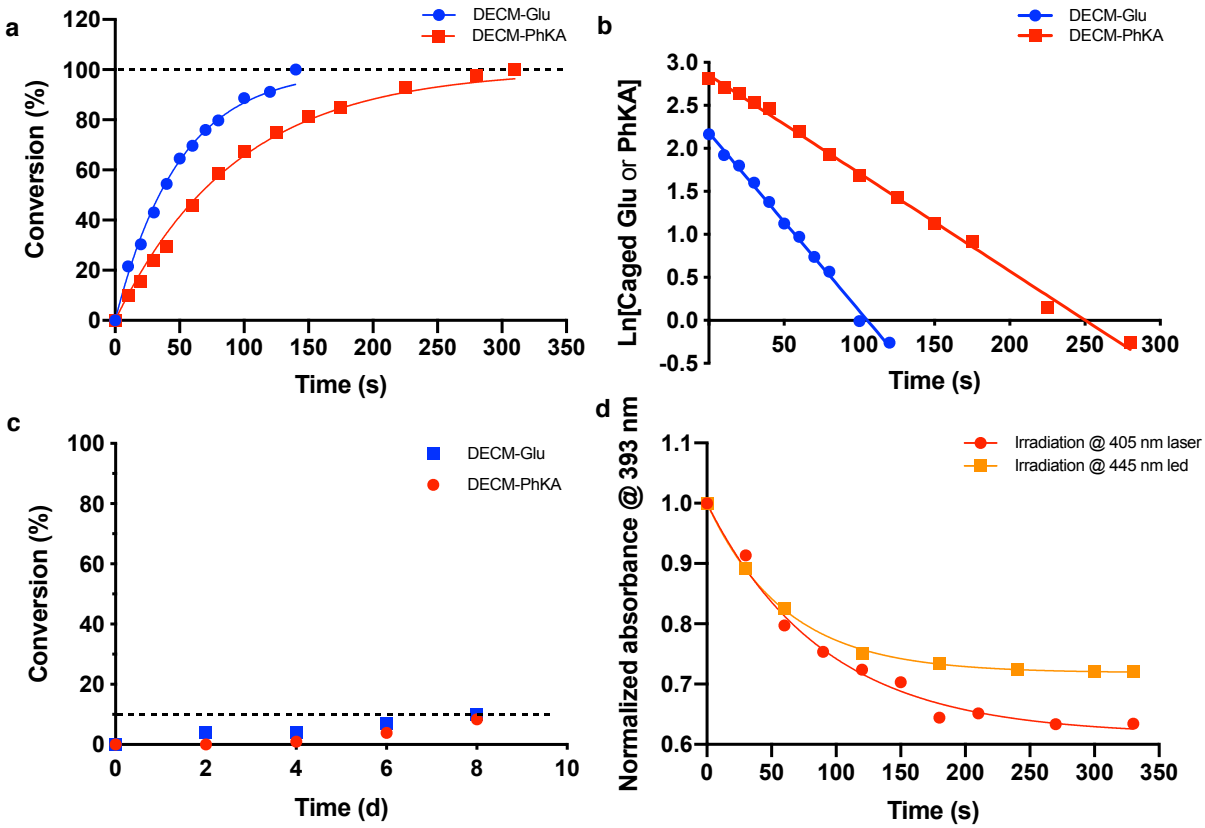

Figure 5–8. Photolysis rates of DECM-Glu (**102**) and DECM-PhKA (**100**). (A, B) DECM-Glu and DECM-PhKA photolysis rate upon 445 nm irradiation calculated from ^{1}H NMR integration data. The conversions versus time were fitted to exponential plateau curves with equations: $Y = 100 \times (1 - e^{-0.0202x})$, $r^2 = 0.994$ (DECM-Glu) and $Y = 100 \times (1 - e^{-0.0107x})$, $r^2 = 0.994$ (DECM-PhKA). The Ln[C] versus time were fitted to linear functions with equations: $Y = -0.0207x + 2.18$, $r^2 = 0.996$ (DECM-Glu) and $Y = -0.0114x + 2.85$, $r^2 = 0.997$ (DECM-PhKA). (C) DECM-Glu and DECM-PhKA photolysis rate under daylight in the lab: less than 10% uncaging occurs after 1 week. (D) Comparison of DECM-PhKA's photolysis rates by a 445 LED light and a 405 nm laser, the process was monitored by UV-Vis absorbance. Absorbances versus time were fitted to exponential plateau curves with equations: $Y = (1 - 0.616) \times e^{-0.0111x} + 0.616$ (DECM-Glu), $r^2 = 0.988$ and $Y = (1 - 0.719) \times e^{-0.0165x} + 0.719$, $r^2 = 0.999$ (DECM-PhKA). Uncaging rates are similar and cleavage is virtually complete after 5 minutes for both wavelengths.

The thermal stability of DECM-Glu and DECM-PhKA under normal lab light is vital to their practical use as biological tools: it is inevitable that they will get exposed to light during experiments. Gratifyingly, long-term tracking experiments suggest that they are stable to natural light exposure – only less than 10% cleavage occurred after 8 days of leaving a solution contained in an NMR tube standing in the lab (Figure 5–8c).

Finally, the intended release of DECM-PhKA by focal photolysis under 405 nm laser irradiation was evaluated (Figure 5–8d). Using a focused 405 nm laser beam for irradiation caused faster photolysis than a LED photoreactor (global sample irradiation). The photolysis rate was observed with a 405 nm laser was 1.5 times faster than with the LED reactor (Table 5–1). We note that this more efficient photocleavage could also partially be caused by a better spectral overlap with the absorption of DECM-PhKA; however for practical reasons, this aspect was not tested further.

Table 5–1. Photochemical properties of caged Glu and PhKA compounds

Compounds	Abs. λ_{max} (nm)	Light source	K (s^{-1})	$T_{1/2}$ (s)
MNI-Glu (101)	339	405, 445, or 465 nm	–	–
DECM-Glu (102)	390	465 nm LED lamp	1.66×10^{-3}	417
	390	445 nm LED lamp	2.07×10^{-2}	33.4
DECM-PhKA (100)	393	445 nm LED lamp	1.14×10^{-2}	60.8
	393	405 nm laser	1.65×10^{-2}	41.7

5.6.2 Photochemical characterization of kainoid photoswitch 136

The *cis / trans* isomerization of tetracholorazobenzene groups has been reported to be controllable via blue and green light irradiation.[145,155] In our case, it is important to prove that the isomerization of kainoid photoswitch **136** is possible, as well as to understand both the kinetics and thremodynamics of its *cis / trans* states under conditions that will be used in biological applications.

The *cis / trans* isomerization of photoswitch **136** was measured by UV-Vis spectrophotometirc analysis (Figure 5–9). Under a blue laser irradiation (405 nm), the photoswitch **136** prefers to exist in the *trans* configuration and showed a local absorbance maximum at ~400 nm. When presented to a green laser irradiation (532 nm), the absorbance of **136** at 400 nm decreased as anticipated. Although it demonstrates a spectral change (modified conjugation) due to configuration switching, a more precise technique than UV-Vis spectroscopy was used to quantify the level of *cis / trans* transformation.

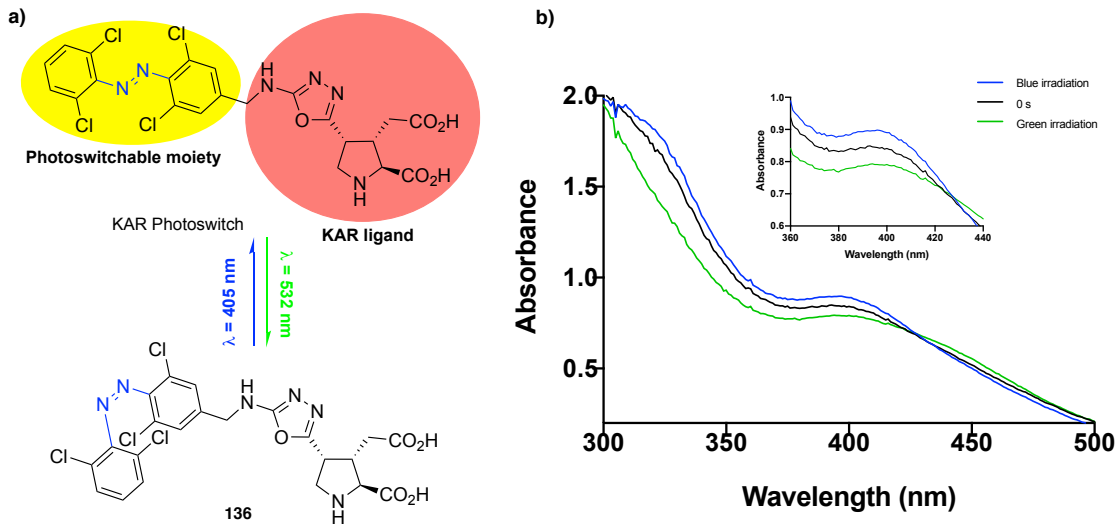

Figure 5–9. *Trans / cis-* isomerization of **136** and its UV-vis spectra. (A) *Trans / cis-* switching of **136**. (B) UV-vis spectra of **136** under irradiation. Blue line: irradiation with 405 nm laser for 3 mins; black line: sample kept in the dark for 24 h; green line: irradiation with 535 nm laser for 3 mins.

The mechanism of azobenzene *cis / trans* photoisomerization has been studied extensively, however its exact details remain controversial.[161] The two main proposals involve a bond breaking/rotation of the azobenzene group, or a direct inversion (Scheme 5–10).[162] The rotation mechanism involves a rupture of the N=N π bond via a light-generated diradical intermediate (π→π*), followed by a rotation around the N–N bond, terminating with the reformation of the N=N bond in the other configuration. In contrast, the direct inversion mechanism invokes a light-induced rehybridization of one nitrogen atom (n→π*) to form a N=N–C dihedral angle of 180°, followed by the inverted collapse of this dihedral angle to rehybridize the nitrogen in the opposite 120° configuration.[161]

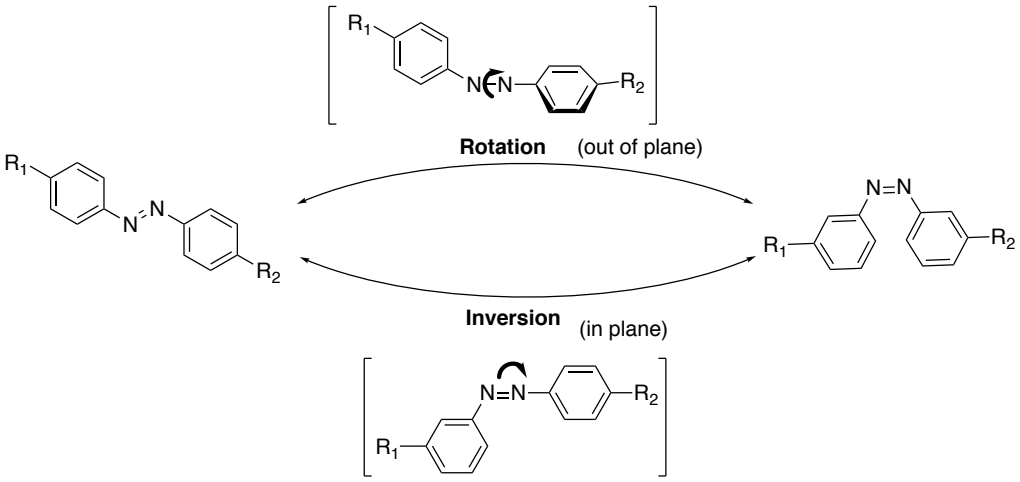

Scheme 5–10. Schematic diagram of photoisomerization mechanism of azobenzenes

In order to quantify the ratio of *cis* and *trans* isomers of switch **136** upon light irradiation, I turned to analysis of the compounds using ^{1}H NMR spectroscopy experiments (Figure 5–10). Interestingly, the benzylic hydrogens (*H13*) of the azobenzene **136** presented chemical shifts in the 4.57 to 4.27 ppm range when presented to blue or green light (blue box in Figure 5–10). Upon **green** light irradiation (Fig. 5-10a), the peak at 4.32 ppm decreased (red box *b*), while the overlapping 4.28–4.20 multiplets decreased (*band c*). At the same time, peaks at 4.52 and 4.45 ppm changed only slightly (*band a*). These shifts caused upon irradiation show *trans*-to-*cis* isomerization. The opposite changes were observed upon **blue** light irradiation (Figure 5–10b): the peaks in *band b* increased and the peaks in *band c* decreased. However, it was still challenging to conclusively determine the exact *cis* / *trans* ratio by this means, since the bands cannot be unambiguously assigned to the *cis* / *trans* isomers. Moreover, the relatively low solubility of **136** in water made it difficult to obtain the kinetic NMR data in D_2O; which is more appropriate to the aqueous solution of biological experiments.

The reversibility of the photoswitching was measured by UV-Vis spectroscopy analysis. When **136** was presented to alternating pulses of green and blue lasers, fast reversible switching was observed (Figure 5–11). Maximum isomerization from *trans* to *cis* was observed after 100 seconds, and quick relaxation from *cis* to *trans* was observed after 50 seconds. These isomers exhibited slow thermal relaxation in a dark place (>2 hours).

Figure 5–11 also shows that photobleaching of tetrachloroazobenzene **136** is not significant, even after multiple cycles of excitation. All the spectral characterization data presented above confirm that the configuration of photoswitch **136** can be controlled by visible light irradiation. However, none of the spectroscopic techniques could quantify whether a clean 100% conversion occurs between *cis* and *trans* isomer.

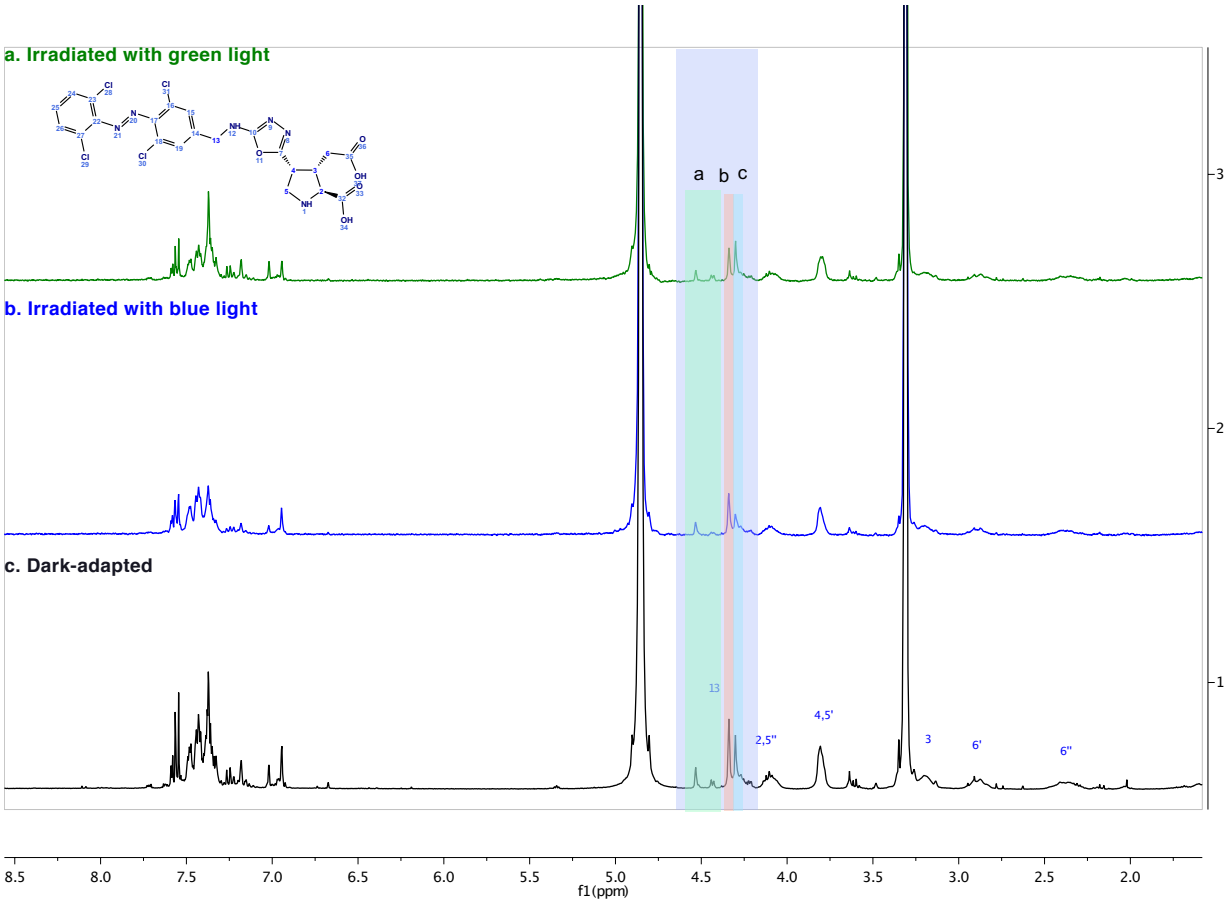

Figure 5–10. ^{1}H NMR spectra (CD_3OD) of **136** before and after light irradiation. (A). ^{1}H NMR spectrum of **136** after irradiation with a green laser for 10 mins; (B). ^{1}H NMR spectrum of **136** after irradiation with a laser blue for 10 mins; (C). ^{1}H NMR spectrum of **136** after dark-adaption overnight. All the hydrogens were assigned according to the gCOSY spectrum.

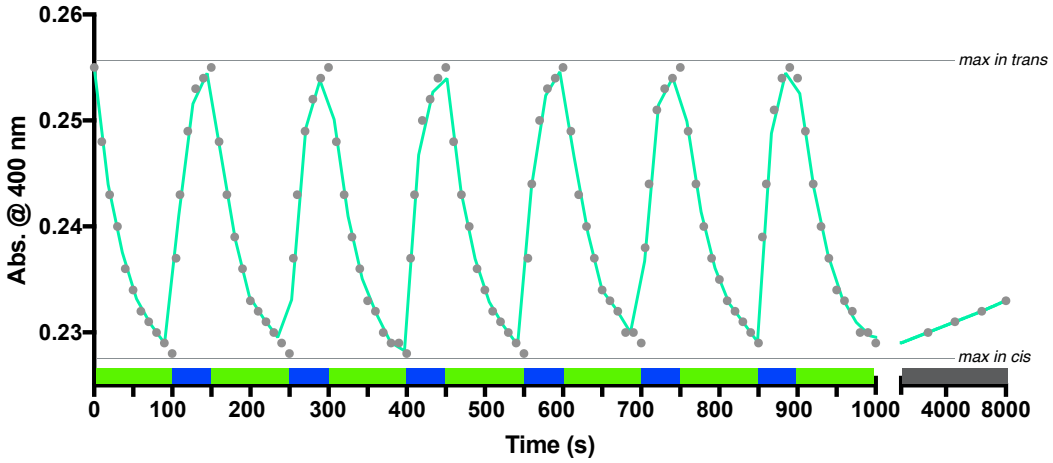

Figure 5–11. Sequential photoswitching of **136** using green (535 nm) and blue (405 nm) lasers, followed by an extended period of relaxation in the dark. The active kainoid (ON) is the thermodynamically favoured *trans*-**136** isomer and the inactive kainoid (OFF) is *cis*-136 isomer.

Importantly, it should be noted that the biological experiments where the kainoid photoswitch will be used do not require 100% conversion to the active isomer. As long as the concentration of active compound reaches the activation threshold of the kainate receptors, the calcium influx will be triggered in the cells, which will initiate the downstream propagation of the action potential in neurons. The application concentration and activation irradiation are thus expected to be optimized in biological experiments. Moreover, this incomplete—yet sufficient—photoisomerization is typically observed in other photoswitch activation of ion channels by other research groups.[152,163-165] Consequently, we expect that kainoid photoswitch **136** will control its phenotype control in biological experiments (currently being tested, but results were not complete at the time of writing).

5.7 Summary

In summary, a new heteroaromatic kainoid and two new types of pharmacological tools for kainate receptors were synthesized and characterized (Scheme 5–12). The photocaged kainoid DECM-PhKA (**100**) was obtained in one step with 87% yield from the phenyl kainic acid **32a**, which is an overall yield of 47% from 4-hydroxyproline over nine steps. Photoswitchable kainoid **136** was synthesized from crucial intermediate **72a** with 36% yield over three steps, which is an overall yield of 17% from 4-hydroxyproline over thirteen steps. The new heteroaromatic kainoid **124** was obtained from **72a** with 37%, which is an overall yield of 17% from hydroxyproline over fourteen steps.

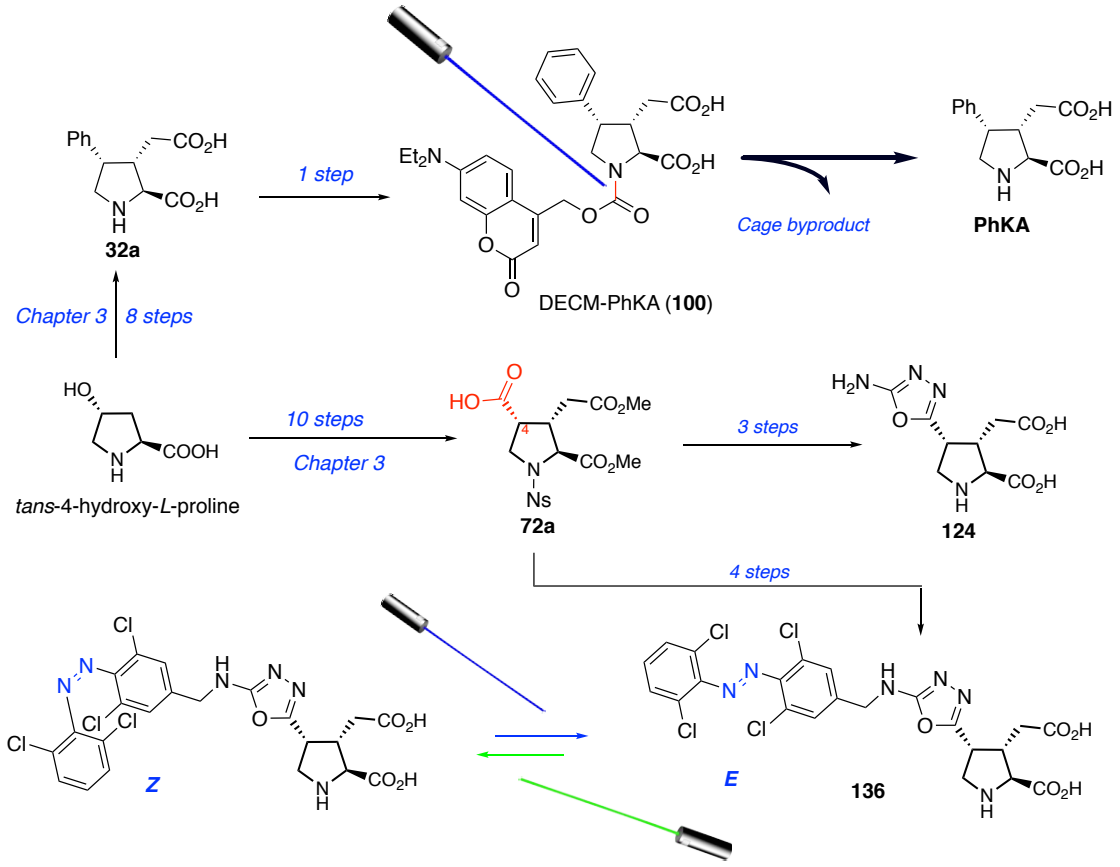

Scheme 5–12. Summary of synthesized new kainoids

The photochemical release of the highly active KAR agonist phenylkainic acid (PhKA, **32a**) from DECM-PhKA (**100**) was demonstrated upon blue light irradiation. The photocage DECM-PhKA displayed acceptable thermal stability under natural light. **100** exerted rapid release of PhKA with a half-life time of 41.7 seconds upon blue laser irradiation. This short time scale is essential for its application in living cells and neurobiology research.

The photoswitchable agonist **136** was demonstrated to undergo reversible *trans*/*cis* isomerization upon green and blue light irradiation. The photochemical characterization of tetrachloroazobenzene kainoid **136** confirmed that the *trans*/*cis* isomerization can manipulated repeatably without photobleaching, and it proved to be resistant to thermal relaxation on practical time scales.

From a medicinal chemistry standpoint, our new synthetic route to oxadiazolyl kainoid **124** provides an unprecedented access to a new class of kainoids. Synthesis and testing of this novel class of analogs are being explored, but they are beyond the scope of this thesis.

5.8 Experimental section

5.8.1 General Experimental Procedures

Unless otherwise noted, reactions were carried out under an argon atmosphere, in flame-dried single-neck, round bottom flasks fitted with a rubber septum and with magnetic stirring. Air or water sensitive liquids and solutions were transferred via syringe or stainless-steel cannula. Organic solutions were concentrated by rotary evaporation at 25–45 °C at 50–200 torr. Thin layer chromatography (TLC) was performed on glass plates precoated with Silica gel F254, 250 µm, 60 Å, from EMD Chemicals Inc (EMD 5715-1). TLC plates were visualized under a 254 or 365 nm UV light source, then stained by immersion in either acidic aqueous-ethanolic vanillin solution, potassium permanganate, or acidic ethanolic ninhydrin, followed by heating using a heat gun. Purification was performed with 230-400 mesh silica gel from Silicycle, Quebec (SiliaFlash R12030B, P60, 40-63 µm, 60 Å).

5.8.2 Materials

Reagents and starting materials were purchased from: Sigma-Aldrich, Oakwood Chemicals, Alfa Aesar, Acros Organics, TCI America, or Fisher Scientific and were used as received unless otherwise noted. Tetrahydrofuran, dichloromethane, hexanes, toluene, and diethyl ether were purified on a glass contour solvent purification system under an argon atmosphere. Methanol was dried by allowing it to stand over freshly activated 4 Å molecular sieves for 48 h prior to use. Solvents used for chromatographic purifications were obtained from Fisher Scientific or VWR and used without further purification.

5.8.3 Statistical analysis and data processing

GraphPad Prism software (version 8.0, GraphPad Software Inc., La Jolla, CA, USA) was used to conduct statistical analyses. Crystal structures of KARs were downloaded from Protein Data Bank (PDB); the corresponding ID was shown in each figure.3D models of compounds were produced by ChemDraw and CORINA and processed by PyMol (Education version, Schrödinger, Inc., New York, NY, USA). These PDB files were processed with PyMol.

5.8.4 Instruments

^{1}H and ^{13}C NMR spectra were recorded on a 400 MHz Varian NMR AS400 equipped with an ATB-400 probe at 25 °C. NMR spectra were analyzed with MestReNova version 10.0.2-15465 from Mestrelab Research. Chemical shifts are reported in parts per million (ppm, δ scale) downfield from tetramethylsilane and are referenced to residual proton signals in the NMR solvents ($CHCl_3$: δ 7.26, C 2 HD 5 SO: δ 2.50), for carbons ($CDCl_3$: δ 77.0, C $_2HD_5SO$: δ 39.5). Spectral data are listed as follows: chemical shift, integration, multiplicity (s = singlet, d = doublet, t = triplet, q = quartet, m = multiplet, br s= broad singlet), and coupling constant (*J*, Hz). Infrared spectra (IR) were obtained using a Nicolet 6700 FT-IR spectrometer as a neat film on a NaCl plate, or a Perkin-Elmer FT-IR Spectrum Two IR spectrometer. High resolution mass spectra were obtained

from the UBC Mass Spectrometry Facility using a HCTultra PTM discovery system spectrometer (ESI), or from a Waters Micromass LCT Premier TOF Mass Spectrometer (ESI, Zandberg lab, UBCO).
UV-VIS spectroscopy UV-VIS spectra were recorded on a Varian 50 Scan UV-Visible Spectropho- tometer. Illumination was provided by a blue laser (405 nm) and a green laser (535 nm) purchased from Armlaser, Quebec, Canada. The spectra were recorded after irradiation of the sample. The absorption is plotted as arbitrary units (A.U.) as a function of wavelength λ (nm).

5.8.5 Synthetic procedures & characterization

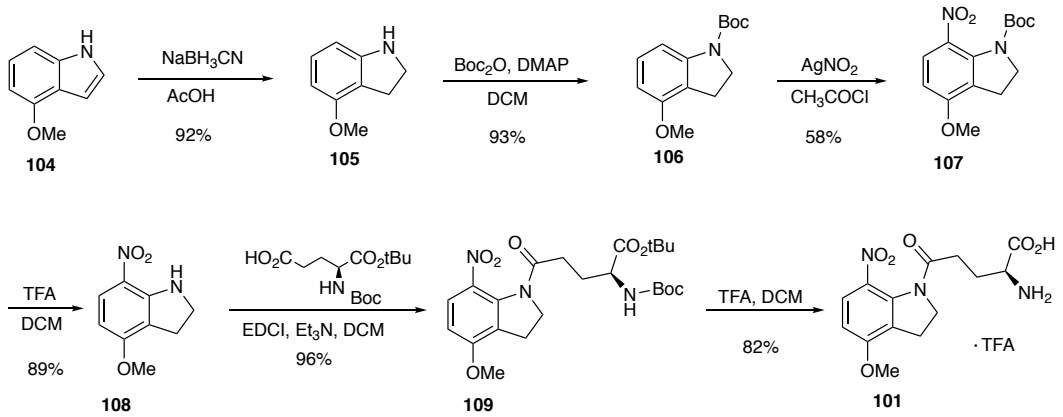

(*S*)-2-amino-5-(4-methoxy-7-nitroindolin-1-yl)-5-oxopentanoic acid, MNI-Glu (101) was prepared according to a modified literature procedure. Characterization data matched literature precedents.[148]

^{1}H NMR (400 MHz, D_2O): δ = 7.67 (d, *J* = 9.1 Hz, 1H), 6.78 (d, *J* = 9.2 Hz, 1H), 4.17 (t, *J* = 7.9 Hz, 2H), 3.81 (s, 3H), 3.65 (t, *J* = 6.3 Hz, 1H), 2.96 (t, *J* = 7.9 Hz, 2H), 2.64 (t, *J* = 7.5 Hz, 2H), 2.04 (q, *J* = 7.1 Hz, 2H) ppm.

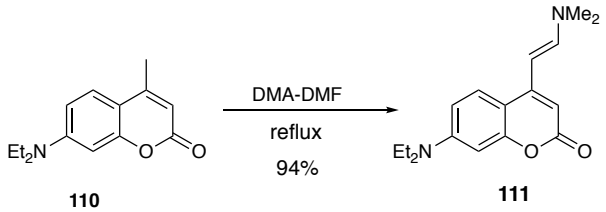

(*E*)-7-(diethylamino)-4-(2-(dimethylamino)vinyl)-2*H*-chromen-2-one (111). To a solution of coumarin **110** (10.00 g, 43.23 mmol) in dry DMF (50 mL) was added *N,N*-dimethylformamide dimethyl acetal (4.60 mL, 34.6 mmol). The reaction mixture was then refluxed overnight. The resulting mixture was poured to water. It resulted a large amount of brown precipitation, the solid product was collected by vaccum filtration. This solid product was further washed with ether (30 mL) to afford enamine **111** as a dark-yellow solid (11.64, 94%). The crude product was used as is directly for the next step.

FTIR (thin film): 2968, 2930, 2876, 2817, 1678, 1605, 1566 cm^{-1}.

^{1}H NMR (400 MHz, $CDCl_3$): δ 7.53 (d, *J* = 9.0 Hz, 1H), 7.22 (d, *J* = 13.0 Hz, 1H), 6.55 (dd, *J* = 9.0, 2.7 Hz, 1H), 6.49 (d, *J* = 2.6 Hz, 1H), 5.85 (s, 1H), 5.22 (d, *J* = 13.0 Hz, 1H), 3.40 (q, *J* = 7.1 Hz, 4H), 2.99 (s, 6H), 1.20 (t, *J* = 7.1 Hz, 6H) ppm.

^{13}C NMR (101 MHz, $CDCl_3$): δ 163.6, 156.4, 152.4, 150.1, 146.6, 124.8, 108.1, 107.9, 98.1, 93.4, 87.5, 44.7, 12.5 ppm.

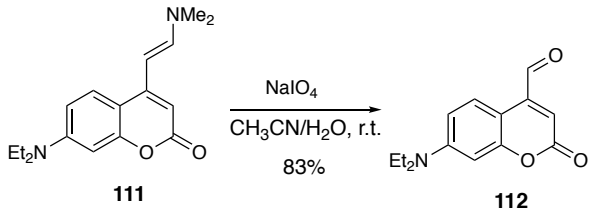

7-(diethylamino)-2-oxo-2*H*-chromene-4-carbaldehyde (112). Enamine **111** (2.0 g, 6.9 mmol) was dissolved in acetonitrile (5 mL). To this solution was added H_2O (5 mL) and $NaIO_4$ (1.6 g, 7.7 mmol). The resulting mixture was stirred at rt for 30 mins, TLC showed the full conversion. The reaction mixture was poured into water and extracted with ethyl acetate (3 × 50 mL). The combined organic layer was washed with brine, dried over $MgSO_4$ and filtered. The solvent was removed under reduced pressure. The residue was purified by column chromatography using ethyl acetate / hexane as an eluent (20-60% gradient). Aldehyde **112** was recovered as an orange solid (1.4 g, 83%).

^{1}H NMR (400 MHz, $CDCl_3$): δ 10.03 (s, 1H), 8.31 (d, *J* = 9.2 Hz, 1H), 6.63 (dd, *J* = 9.2, 2.6 Hz, 1H), 6.53 (d, *J* = 2.7 Hz, 1H), 6.45 (s, 1H), 3.43 (q, *J* = 7.1 Hz, 4H), 1.22 (t, *J* = 7.1 Hz, 6H) ppm.

^{13}C NMR (101 MHz, $CDCl_3$): δ 192.5, 161.9, 157.4, 151.0, 143.9, 127.0, 117.4, 109.5, 103.7, 97.6, 44.8, 12.5 ppm.

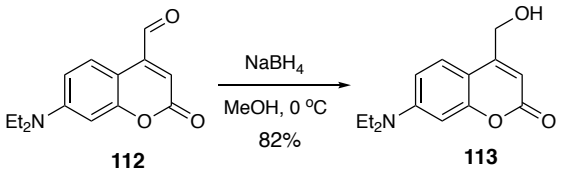

7-(diethylamino)-4-(hydroxymethyl)-2*H*-chromen-2-one (113). To a solution of aldehyde **112** (1.201 g, 4.89 mmol) in methanol (5 mL) was added sodium borohydride (93 mg, 2.5 mmol) at 0 ^{O}C. After 30 mins, TLC showed the full conversion. The mixture was quenched with ammonium chloride aqueous solution and extracted with ether (3 × 30 mL). The combined organic layer was washed with sodium bicarbonate aqueous solution and brine. The ether layer was dried over $MgSO_4$ and filtered. The filtrate was concentrated to dryness under reduced pressure to afford the alcohol **113** as a yellow solid (993 mg, 82%) without further purification.

FTIR (thin film): 3446, 2971, 1739, 1686 cm^{-1}.

^{1}H NMR (400 MHz, $CDCl_3$): δ 7.30 (d, *J* = 9.0 Hz, 1H), 6.55 (d, *J* = 9.0 Hz, 1H), 6.45 (s, 1H), 6.28 (s, 1H), 4.82 (s, 2H), 3.38 (q, *J* = 6.9 Hz, 4H), 1.18 (t, *J* = 7.3 Hz, 6H) ppm.

^{13}C NMR (101 MHz, $CDCl_3$): δ 163.1, 156.1, 155.5, 150.5, 124.4, 108.7, 106.4, 105.2, 97.6, 60.8, 44.7, 12.5 ppm.

HRMS (ESI) m/z: $[M + Na]^+$ calcd for $C_9H_{10}NO_4Na$, 270.1101; found, 270.1094.

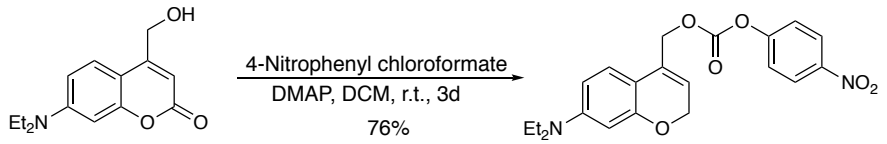

113 114

(7-(diethylamino)-2*H*-chromen-4-yl)methyl (4-nitrophenyl) carbonate (114). To a single-neck flask were added 4-nitrophenyl chloroformate (1.61 g, 7.99 mmol), alcohol **4** (659 mg, 2.66 mmol), DMAP (326 mg, 2.66 mmol) and dichloromethane (5 mL) at rt. The flask was then charged with argon and covered with tin foil to avoid light irradiation. After 2 d, the reaction mixture was poured into water and extracted with ethyl acetate (3 × 50 mL). The combined organic layer was then washed with brine and dried over $MgSO_4$. The organic solvent was removed under reduced pressure. The resulting residue was then washed with diethyl ether (50 mL) to remove excess alcohol and afforded the carbonate **114** (833 mg, 76%) as a yellow solid without further purification. The product was stored in a tin foil covered vial.

FTIR (thin film): 2972, 1774, 1711 cm^{-1}.

^{1}**H NMR** (400 MHz, $CDCl_3$): δ 8.31 (d, *J* = 9.1 Hz, 2H), 7.42 (d, *J* = 9.1 Hz, 2H), 7.32 (d, *J* = 9.0 Hz, 1H), 6.61 (dd, *J* = 9.0, 2.6 Hz, 1H), 6.54 (d, *J* = 2.6 Hz, 1H), 6.23 (s, 1H), 5.40 (d, *J* = 1.2 Hz, 2H), 3.43 (q, *J* = 7.1 Hz, 4H), 1.22 (t, *J* = 7.1 Hz, 6H) ppm.

^{13}**C NMR** (101 MHz, $CDCl_3$): δ 161.6, 156.4, 152.2, 150.9, 147.6, 125.4, 124.3, 121.7, 108.8, 107.0, 105.6, 98.0, 65.8, 44.8, 12.4 ppm.

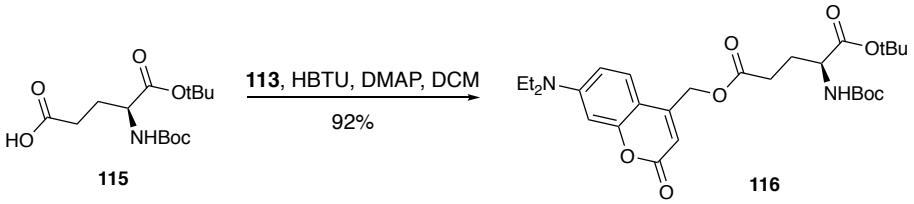

115 116

1-(*tert*-butyl) 5-((7-(diethylamino)-2-oxo-2*H*-chromen-4-yl)methyl) (*tert*-butoxycarbonyl)-*L*-glutamate (116). To a solution of Boc-Glu-OtBu (245 mg, 0.808 mmol) in dichloromethane (5 mL) were added alcohol **113** (241 mg, 0.972 mmol), HBTU (306 mg, 0.807 mmol) and triethylamine (115 μL, 0.808 mmol). The reaction was stirred under argon atmosphere at rt (the flask was cover with tin foil to avoid light irradiation) for 3 d. Then the reaction mixture was poured into water and extracted with ethyl acetate (3 × 20 mL). The combined organic layer was washed with ammonium chloride aqueous solution, sodium bicarbonate aqueous solution and brine. The resulting organic layer was dried over $MgSO_4$ and filtered. The filtrate was concentrated under reduced pressure (a tin foil was used to cover the flask when removing solvent on the rotavap). The resulting residue was purified by column chromatography using ethyl acetate / hexane as an eluent (10-60% gradient). Ester **116** was recovered as a yellow solid (395 mg, 92%).

^{1}**H NMR** (400 MHz, $CDCl_3$): δ 7.29 (d, *J* = 9.4 Hz, 1H), 6.58 (dd, *J* = 9.0, 2.5 Hz, 1H), 6.52 (d, *J* = 2.6 Hz, 1H), 6.12 (s, 1H), 5.23 (s, 2H), 5.10 (d, *J* = 8.3 Hz, 1H), 4.28 – 4.23 (m, 1H), 3.42 (q, *J* = 7.1 Hz, 4H), 2.64 – 2.44 (m, 2H), 2.27-2.16 (m, 1H), 1.99 -1.90 (m, 1H), 1.44 – 1.49 (m, 18H), 1.21 (t, *J* = 7.1 Hz, 6H) ppm.

^{13}C NMR (101 MHz, $CDCl_3$): δ 172.1, 161.8, 156.3, 150.7, 149.2, 124.4, 108.7, 106.6, 106.0, 97.8, 82.4, 79.9, 61.6, 53.2, 44.7, 30.1, 28.3, 28.1, 28.0, 12.4 ppm.

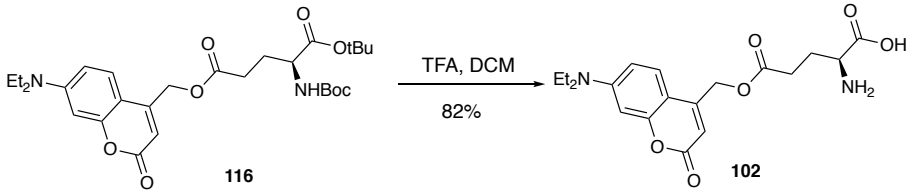

(*S*)-2-amino-5-((7-(diethylamino)-2-oxo-2*H*-chromen-4-yl)methoxy)-5-oxopentanoic acid (102). Ester **116** (395 mg, 0.742 mmol) was dissolved in dichloromethane (2.0 mL). Trifluoroacetic acid (1.7 mL, 22 mmol) was added dropwise. The resulting mixture was stirred at rt under argon. The flask was covered with tin foil and maintained for 4 h. The solvent was removed under reduced pressure (tin foil was used to cover the flask when removing solvent on the rotavap). The resulting residue was triturated in ether and yielded a yellow precipitation. It was filtered and solid precipitate was collected as the TFA salt of **102** (298 mg, 82%) without further purification.

FTIR (thin film): 3461, 3016, 2971, 1738 cm^{-1}.

^{1}H NMR (400 MHz, CD_3OD): δ 7.47 (d, *J* = 9.1 Hz, 1H), 6.74 (dd, *J* = 9.1, 2.6 Hz, 1H), 6.55 (d, *J* = 2.7 Hz, 1H), 6.06 (s, 1H), 5.40 – 5.28 (m, 2H), 3.80 (t, *J* = 6.5 Hz, 1H), 3.48 (q, *J* = 7.1 Hz, H), 2.84 – 2.67 (m, 2H), 2.21 (dtd, *J* = 18.3, 14.2, 12.8, 7.3 Hz, 2H), 1.21 (t, *J* = 7.1 Hz, 6H) ppm.

^{13}C NMR (101 MHz, CD_3OD): δ 156.1, 151.2, 151.1, 124.8, 109.0, 105.7, 104.7, 96.9, 61.4, 44.2, 29.2, 26.7, 25.6, 11.3 ppm.

^{19}F NMR (376 MHz, D_2O) δ -75.65.

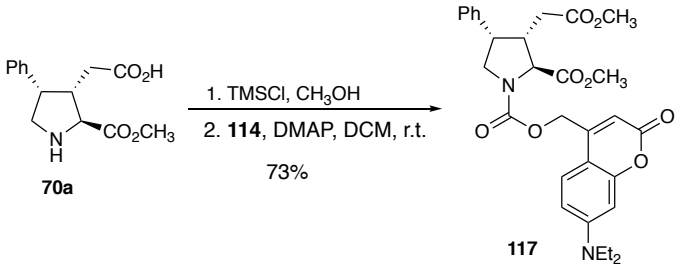

1-((7-(diethylamino)-2-oxo-2*H*-chromen-4-yl)methyl) 2-methyl (2*S*,3*S*,4*S*)-3-(2-methoxy-2-oxoethyl)-4-phenylpyrrolidine-1,2-dicarboxylate (117). To the solution of **70a** (25 mg, 95 μmol) in methanol (0.3 mL) was added TMSCl (30 μL, 0.24 mmol). The mixture was stirred at room temperature for 5 h. Then the solvent was removed under reduced pressure. To the resulting residue were added DMAP (17 mg, 0.14 mmol) and carbonate **114** (38 mg, 0.095 mmol). The mixture was stirred at rt under argon atmosphere for 24 h (tin foil was used to cover the whole flask during the reaction). The resulting mixture was concentrated to dryness. The residue was purified by column chromatography using ethyl acetate / hexane as an eluent (20-60% gradient). The carbamate **117** was recovered as a brown solid (47 mg, 92%).

^{1}H NMR (400 MHz, $CDCl_3$, two rotamers): δ 7.37 – 7.28 (m, 4H), 7.08 (d, *J* = 7.4 Hz, 2H), 6.59 (q, *J* = 8.5, 8.1 Hz, 1H), 6.51 (s, 1H), 6.12 (d, *J* = 37.2 Hz, 1H), 5.44 – 5.15 (m, 2H), 4.25 (t, *J* = 5.9 Hz, 1H), 4.07 (q, *J*

= 9.1 Hz, 1H), 3.98 – 3.87 (m, 1H), 3.82 (s, 1H), 3.77 (s, 2H), 3.63 (d, J = 3.9 Hz, 3H), 3.41 (d, J = 7.6 Hz, 1H), 3.14 – 3.06 (m, 1H), 2.35 – 2.25 (m, 1H), 2.14 – 2.04 (m, 1H), 1.21 (t, J = 6.7 Hz, 6H) ppm.

^{13}C NMR (101 MHz, $CDCl_3$, two rotamers): δ 172.1, 171.9, 171.9, 171.8, 162.1, 162.0, 161.8, 156.3, 156.2, 154.3, 153.9, 153.3, 150.8, 150.7, 150.7, 150.0, 149.9, 148.3, 129.0, 127.6, 127.5, 127.5, 126.1, 124.5, 124.3, 124.3, 115.7, 108.8, 108.7, 108.7, 106.9, 106.0, 105.9, 105.9, 105.8, 105.7, 97.8, 97.8, 65.3, 63.7, 63.2, 62.7, 52.7, 52.7, 51.9, 51.8, 50.7, 50.5, 45.1, 44.8, 44.7, 44.6, 44.2, 43.5, 33.2, 33.1, 12.4 ppm.

HRMS (ESI-TOF) m/z: $[M + Na]^+$ calcd for $C_{30}H_{34}N_2O_8Na$, 573.2207; found, 573.2204.

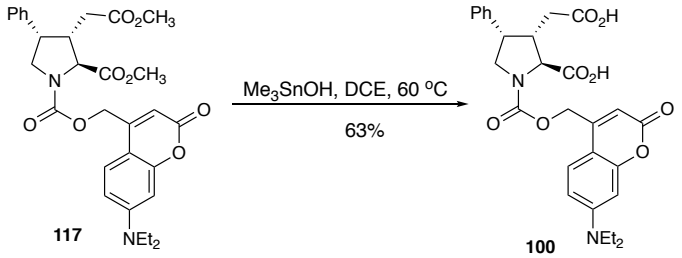

(2*S*,3*S*,4*S*)-3-(carboxymethyl)-1-(((7-(diethylamino)-2-oxo-2*H*-chromen-4-yl)methoxy)carbonyl)-4-phenylpyrrolidine-2-carboxylic acid (100). To a solution of carbamate **117** (30 mg, 55 μmol) in dichloroethane (2 mL) was added trimethyltin hydroxide (49 mg, 0.27 mmol). The mixture was refluxed overnight (the flask and condenser were covered with tin foil). The reaction mixture was poured into a hydrochloric acid (0.1 M, 10 mL) and extracted with ethyl acetate (3 × 10 mL). The combined organic layer was washed with brine, dried over $MgSO_4$ and filtered. The filtrate was concentrated and purified by column chromatography using methanol / dichloromethane as an eluent (5-20% gradient). Acid **100** was recovered as a yellow solid (18 mg, 88%) with trace tin residues. This method was thus abandoned due to the toxicity of tin for living cells.

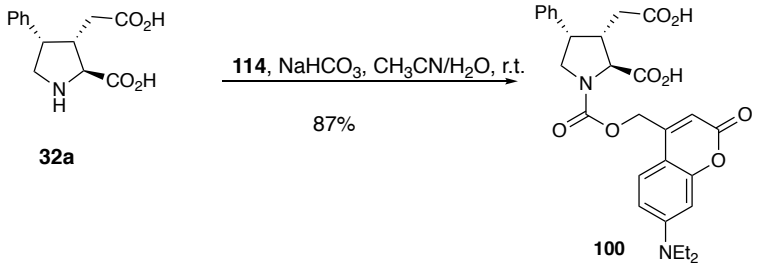

(2*S*,3*S*,4*S*)-3-(carboxymethyl)-1-(((7-(diethylamino)-2-oxo-2*H*-chromen-4-yl)methoxy)carbonyl)-4-phenylpyrrolidine-2-carboxylic acid (100). To a solution of PhKA (76 mg, 0.30 mmol) in H_2O (1.0 mL) and acetonitrile (2.0 mL) were added sodium bicarbonate (77 mg, 0.91 mmol) and carbonate **114** (125 mg, 0.30 mmol). The mixture was stirred at rt for 24 h (the whole flask was covered with tin foils). The resulting solution was then poured into a hydrochloric acid (0.1 M, 10 mL) solution and extracted with ethyl acetate (3 × 20 mL). The combined organic layer was washed with brine, dried over $MgSO_4$ and filtered. The filtrate was

concentrated under reduced pressure (tin foil was used to cover the flask when on the rotavap). The resulting residue was triturated in ether (30 mL) and filtered to afford **100** as a yellow solid.

FTIR (thin film): 3414, 2977, 1709, 1601 cm^{-1}.

^{1}**H NMR** (400 MHz, CD_3OD, two rotamers): δ 7.49 (t, *J* = 9.3 Hz, 1H), 7.32 (dt, *J* = 7.9, 4.1 Hz, 2H), 7.26 (t, *J* = 7.2 Hz, 1H), 7.13 (d, *J* = 7.2 Hz, 2H), 6.74 (ddd, *J* = 14.2, 9.1, 2.6 Hz, 1H), 6.55 (d, *J* = 2.5 Hz, 1H), 6.14 (d, *J* = 15.8 Hz, 1H), 5.47 – 5.28 (m, 2H), 4.31 – 4.09 (m, 1H), 4.07 – 3.84 (m, 1H), 3.77 (bs, 1H), 3.48 (qd, *J* = 7.0, 4.8 Hz, 4H), 3.07 (bs, 1H), 2.37 (bs, 1H), 2.06 – 1.90 (m, 1H), 1.21 (td, *J* = 7.1, 4.7 Hz, 6H) ppm.

^{13}**C NMR** (101 MHz, CD_3OD, two rotamers): δ 163.0, 156.1, 156.1, 154.0, 151.8, 151.1, 151.0, 138.5, 138.4, 128.5, 128.4, 127.5, 126.9, 124.8, 124.7, 109.1, 109.1, 105.7, 105.6, 104.8, 104.4, 96.8, 62.5, 45.0, 44.2, 31.3, 11.3 ppm.

HRMS (ESI-TOF) m/z: $[M - H]^-$ calcd for $C_{28}H_{29}N_2O_8$, 521.1929; found, 521.1906.

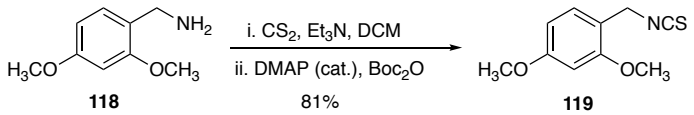

1-(isothiocyanatomethyl)-2,4-dimethoxybenzene (119). To a solution of benzylamine **118** (1.20 g, 7.18 mmol) and triethylamine (1.09 mL, 7.89 mmol) in dichloromethane (50 mL) was added carbon disulfide (4.34 mL, 71.7 mmol). The mixture was stirred at rt for 1 h. It resulted in a turbid solution. To this suspension were added Boc_2O (1.88 g, 8.61 mmol) and DMAP (87 mg, 0.72 mmol). The solution turned clear and was stirred at rt for another 30 mins. The mixture was poured into water and extracted with ether (3 × 50 mL). The combined organic layer was washed with 5% citric acid aqueous solution, brine, dried over $MgSO_4$ and filtered. The filtrate was concentrated under reduced pressure. The residue was purified by column chromatography using ethyl acetate / hexane as an eluent (5-10% gradient). The isocyanate product **119** was recovered as a colourless oil (1.221 g, 81%).

^{1}**H NMR** (400 MHz, $CDCl_3$): δ 7.19 (d, *J* = 8.1 Hz, 1H), 6.52 – 6.44 (m, 2H), 4.60 (s, 2H), 3.84 (s, 5H), 3.82 (s, 3H) ppm.

^{13}**C NMR** (101 MHz, $CDCl_3$): δ 161.3, 157.9, 129.4, 115.1, 104.1, 98.6, 55.5, 55.5, 44.1 ppm.

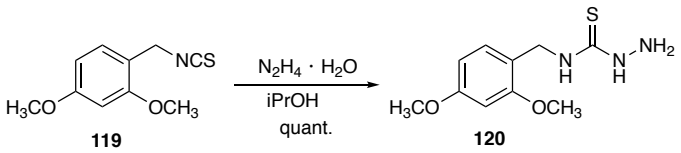

***N*-(2,4-dimethoxybenzyl)hydrazinecarbothioamide (120)**. To a solution of isocyanate **119** (987 mg, 4.72 mmol) in isopropanol (10 mL) was added hydrazine hydrate (432 μL, 60%, 5.19 mmol) dropwise. It resulted in a white precipitation right after the addition. The mixture was stirred for 20 min at rt. The solid product was recovered by vaccum filtration. It was further washed by ethanol and ether to afford the thiosemicarbozide **120** (1.132 g, 99%) as a white powder without further purification.

FTIR (thin film): 3342, 3280, 3188, 3152, 3004, 2938, 1557 cm^{-1}.

^{1}H NMR (400 MHz, DMSO-d_6): δ 8.70 (s, 1H), 7.94 (s, 1H), 7.08 (d, J = 8.3 Hz, 1H), 6.55 (d, J = 2.4 Hz, 1H), 6.46 (dd, J = 8.3, 2.3 Hz, 1H), 4.57 (d, J = 5.8 Hz, 2H), 4.49 (s, 2H), 3.80 (s, 3H), 3.74 (s, 3H) ppm.
^{13}C NMR (101 MHz, DMSO-d_6): δ 181.3, 159.8, 157.8, 129.0, 119.0, 104.2, 98.3, 55.5, 55.2, 41.6 ppm.
HRMS (ESI-TOF) m/z: [M + Na]$^+$ calcd for $C_{10}H_{15}N_3O_2SNa$, 264.0777; found, 264.0786.

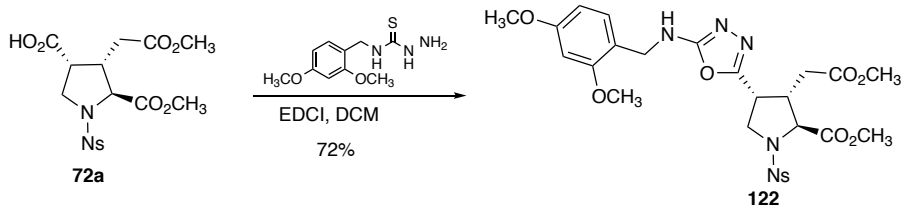

Methyl (2*S*,3*S*,4*R*)-4-(5-((2,4-dimethoxybenzyl)amino)-1,3,4-oxadiazol-2-yl)-3-(2-methoxy-2-oxoethyl)-1-((4-nitrophenyl)sulfonyl)pyrrolidine-2-carboxylate (122). To a solution of acid **72a** (369 mg, 0.857 mmol) in dichloromethane (5 mL) was added thiosemicarbozide **120** (310 mg, 1.29 mmol) and EDCI (575 mg, 3.00 mmol). The mixture was stirred at rt for 24 h. The solvent was removed under reduced pressure. The product was purified by column chromatography using ethyl acetate / hexane as an eluent (10-50% gradient). The oxodiazole product **122** was recovered as a white solid (385 mg, 72%).
FTIR (thin film): 3013, 2951, 1742 cm^{-1}.
^{1}H NMR (400 MHz, $CDCl_3$): δ 8.26 (d, J = 8.8 Hz, 2H), 7.91 (d, J = 8.7 Hz, 2H), 7.20 (d, J = 8.2 Hz, 1H), 6.49 (d, J = 2.3 Hz, 1H), 6.45 (dd, J = 8.2, 2.4 Hz, 1H), 5.27 (s, 1H), 4.42 – 4.21 (m, 3H), 3.91– 3.83 (m, 1H), 3.86 (s, 3H), 3.80 (s, 6H), 3.79 – 3.70 (m, 2H), 3.60 (s, 3H), 3.07 (p, J = 6.9 Hz, 1H), 2.62 (dd, J = 17.4, 8.1 Hz, 1H), 2.35 (dd, J = 17.5, 6.8 Hz, 1H) ppm.
^{13}C NMR (101 MHz, $CDCl_3$): δ 171.3, 171.0, 163.5, 161.1, 158.6, 156.5, 150.3, 143.3, 130.7, 128.4, 124.3, 117.9, 103.8, 98.8, 64.5, 55.5, 55.4, 53.0, 52.0, 50.7, 43.5, 42.6, 37.8, 32.0 ppm.
HRMS (ESI-TOF) m/z: [M + Na]$^+$ calcd for $C_{26}H_{29}N_5O_{11}SNa$, 642.1476; found, 642.1483.

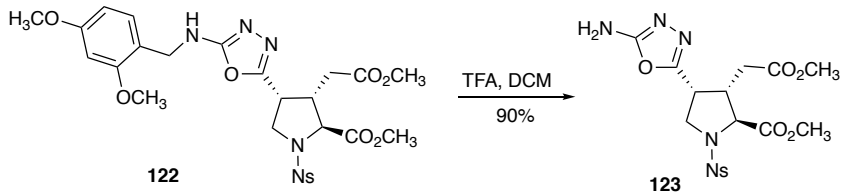

Methyl (2*S*,3*S*,4*R*)-4-(5-amino-1,3,4-oxadiazol-2-yl)-3-(2-methoxy-2-oxoethyl)-1-((4-nitrophenyl)sulfonyl)pyrrolidine-2-carboxylate (123). To the solution of oxodiazole (342 mg, 0.426 mmol) in dichloromethane (5 mL) was added trifluoroacetic acid (0.163 mL, 2.13 mmol). The mixture was stirred at 50 °C. After 3 h, TLC showed full conversion. The solvent was removed under reduced pressure. The product was purified by column chromatography using ethyl acetate / hexane as an eluent (10-50% gradient). Oxodiazole **123** was recovered as a white solid (181 mg, 90%).
FTIR (thin film): 3423, 3363, 3102, 2953, 1733, 1656 cm^{-1}.

^{1}H NMR (400 MHz, $CDCl_3$): δ 8.36 (d, *J* = 8.8 Hz, 2H), 8.01 (d, *J* = 8.8 Hz, 2H), 5.27 (s, 2H), 4.34 (d, *J* = 6.9 Hz, 1H), 3.94 – 3.86 (m, 1H), 3.84 – 3.78 (m, 1H), 3.81 (s, 3H), 3.64 (s, 3H), 3.35 (s, 1H), 3.09 (p, *J* = 6.7 Hz, 1H), 2.59 (dd, *J* = 17.4, 8.3 Hz, 1H), 2.40 (dd, *J* = 17.4, 6.7 Hz, 1H) ppm.

^{13}C NMR (101 MHz, $CDCl_3$): δ 171.2, 171.0, 150.4, 143.5, 128.6, 124.3, 64.5, 56.0, 53.1, 52.1, 50.5, 42.7, 37.8, 32.1, 29.7 ppm.

HRMS (ESI-TOF) m/z: $[M + Na]^+$ calcd for $C_{17}H_{19}N_5O_9Na$, 492.0796; found, 492.0792.

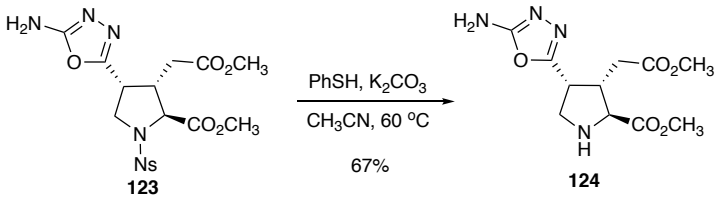

Methyl (2*S*,3*S*,4*R*)-4-(5-amino-1,3,4-oxadiazol-2-yl)-3-(2-methoxy-2-oxoethyl)pyrrolidine-2-carboxylate (124). To a solution of oxodiazole **124** (165 mg, 0.351 mmol) in acetonitrile (3 mL) were added thiophenol (54 μL) and potassium carbonate (73 mg). The mixture was stirred at 60 °C for 3 h. The reaction mixture poured into water and extracted ethyl acetate (3 × 10 mL). The combined organic layer was washed with brine, dried over $MgSO_4$ and filtered. The filtrate was concentrated under reduced pressure and the resulting residue was by column chromatography using methanol / dichloromethane as an eluent (5-20% gradient). Oxodiazole amine **124** was recovered as a white solid (67 mg, 67%).

FTIR (thin film): 3401, 2931, 2856, 1738, 1659 cm^{-1}.

^{1}H NMR (400 MHz, $CDCl_3$): δ 5.51 (s, 2H), 3.76 (s, 3H), 3.72 (d, *J* = 7.9 Hz, 1H), 3.71 – 3.66 (m, 1H), 3.65 (s, 3H), 3.43 (dd, *J* = 11.3, 6.5 Hz, 1H), 3.31 (dd, *J* = 11.3, 4.1 Hz, 1H), 2.97 (dtd, *J* = 9.0, 7.7, 6.0 Hz, 1H), 2.73 (s, 1H), 2.64 (dd, *J* = 17.0, 6.0 Hz, 1H), 2.49 (dd, *J* = 17.0, 9.0 Hz, 1H) ppm.

^{13}C NMR (101 MHz, $CDCl_3$): δ 174.1, 172.1, 163.2, 159.9, 64.0, 52.5, 51.9, 50.1, 43.5, 39.8, 34.0 ppm.

HRMS (ESI-TOF) m/z: $[M + H]^+$ calcd for $C_{11}H_{17}N_4O_5$, 285.1193; found, 285.1194.

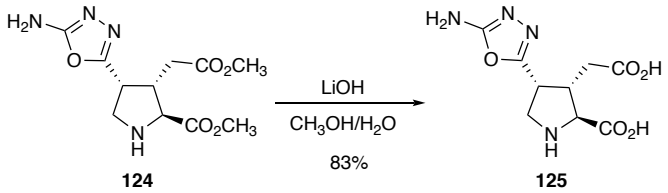

(2*S*,3*S*,4*R*)-4-(5-amino-1,3,4-oxadiazol-2-yl)-3-(carboxymethyl)pyrrolidine-2-carboxylic acid (125). To a solution of oxadiazole amine **124** (63 mg, 0.22 mmol) in methanol (1 mL) was added LiOH aqueous solution (2.5 M, 2.7 mL). The resulting mixture was stirred at rt for 5 h. The solution was neutralized by addition of hydrochloric acid (0.5 M) at 0 °C. The mixture was concentrated under reduced pressure. The residue was dissolved in water (2 mL) and purified by ion-exchange chromatography: ion-exchange resin Dowex 50WX4 100-200 mesh, eluting with 0.5 N aqueous ammonia. The eluting fractions were collected and analyzed by TLC for the presence of the desired product. (TLC plates were dried gently with a heat gun before being stained with ninhydrin; further heating revealed the presence of the amino acid **125** as yellow spots.) The

fractions containing the product were combined and flash frozen, and the solvents were removed by lyophilization to yield a pale-yellow solid. This product was recrystallized with aqueous ethanol to afford the final product **125** as a white solid (47 mg, 83%).

FTIR (thin film): 3395, 2951, 1742, 1727 cm^{-1}.

^{1}**H NMR** (400 MHz, D_2O): δ 4.03 (q, *J* = 6.9 Hz, 1H), 3.93 (d, *J* = 8.9 Hz, 1H), 3.88 (dd, *J* = 12.4, 7.7 Hz, 1H), 3.77 (dd, *J* = 12.5, 5.2 Hz, 1H), 3.08 (td, *J* = 11.3, 10.7, 5.3 Hz, 1H), 2.69 (dd, *J* = 16.8, 4.6 Hz, 1H), 2.09 (dd, *J* = 16.8, 10.8 Hz, 1H) ppm.

^{13}**C NMR** (101 MHz, D_2O): δ 178.0, 172.4, 164.7, 158.2, 64.4, 46.5, 43.1, 37.7, 36.3 ppm.

HRMS (ESI-TOF) m/z: $[M + H]^+$ calcd for $C_{11}H_{17}N_4O_5$, 257.0868; found, 257.0868.

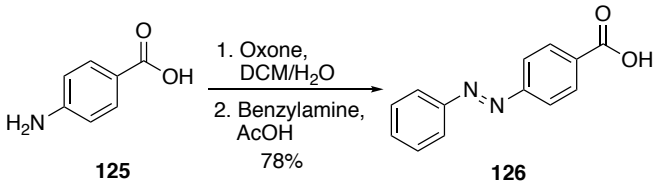

(*E*)-4-(phenyldiazenyl)benzoic acid (**126**). To a solution of 4-aminobenzoic acid (8.1 g, 59.1 mmol) in dichloromethane (30 mL) and water (30 mL) was added oxone (21.8 g, 70.9 mmol). The mixture was stirred vigorously at rt for 2 h. It resulted a suspension mixture. The mixture was filtered, the solid was further washed with water and afforded a dark yellow solid (8.3 g, 93%) product without further purification. The obtained 4-nitrosobenzoic acid (8.3 g, 54.9 mmol) was added to a single-neck flask. To this flask were added benzylamine (6.1 mL, 65.9 mmol) and acetic acid 50 mL. The mixture was stirred at 50 °C overnight. The resulting mixture was poured into water and resulted in a large amount of brown precipitation. The solid precipitation was recovered by vaccum filtration. This obtained solid was then recrystallized in ethanol and gave the 4-(phenylazo)benzoic acid **126** as a red solid (10.5 g, 84%).

FTIR (thin film): 3464, 3010, 1739, 1680 cm^{-1}.

^{1}**H NMR** (400 MHz, DMSO-d_6): δ 13.23 (s, 1H), 8.19 – 8.08 (m, 2H), 8.00 – 7.86 (m, 4H), 7.68 – 7.53 (m, 3H) ppm.

^{13}**C NMR** (101 MHz, DMSO-d_6): δ 166.7, 154.3, 151.9, 132.9, 132.2, 130.7, 129.6, 122.8, 122.6 ppm.

HRMS (ESI-TOF) m/z: $[M - H]^+$ calcd for $C_{13}H_9N_2O_2$, 225.0670; found, 225.0666.

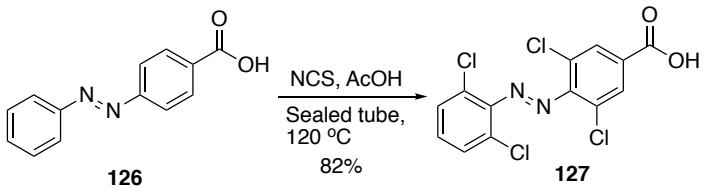

(*E*)-3,5-dichloro-4-((2,6-dichlorophenyl)diazenyl)benzoic acid (**127**). 4-(phenylazo)benzoic acid (5.1 g, 22.5 mmol), *N*-chlorosuccinimide (15.1 g, 112.7 mmol), palladium acetate (101 mg, 0.451 mmol) and acetic acid (50 mL) was added to a pressure tube. The mixture was degassed by argon and sealed, followed by heating to 120 °C. After 2 days, the tube was cooled to rt and opened. The mixture was poured into water and yielded a

large amount of precipitation. The suspension was filtered. The solid product was recrystallized in methanol and yield **127** as a red solid (6.7 g, 82%) without further purification.

FTIR (thin film): 3467, 3016, 2945, 1739 cm^{-1}.

^{1}**H NMR** (400 MHz, acetone-d_6): δ 12.04 (bs, 1H), 8.17 (s, 2H), 7.69 (dd, J = 8.1, 0.6 Hz, 2H), 7.55 (dd, J = 8.7, 7.5 Hz, 1H) ppm.

^{13}**C NMR** (101 MHz, acetone-d_6): δ 164.7, 151.3, 147.8, 133.3, 132.2, 131.24, 130.9, 127.9, 127.4 ppm.

HRMS (ESI-TOF) m/z: $[M - H]^-$ calcd for $C_{13}H_5Cl_4N_2O_2$, 360.9111; found, 360.9111.

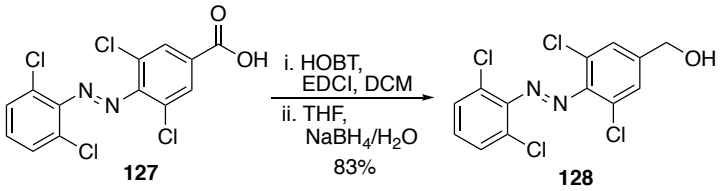

(*E*)-(3,5-dichloro-4-((2,6-dichlorophenyl)diazenyl)phenyl)methanol (**128**). To a solution of acid **127** (3.5 g, 9.6 mmol) in dichloromethane (10 mL) were added HOBT (1.6 g, 11 mmol) and EDCI (2.0 g, 11 mmol). The mixture was stirred at rt for 1 h. The solvent was then removed under reduced pressure. The resulting mixture was resuspended in THF (10 mL). A solution of sodium borohydride (437 mg, 11.5 mmol) in water (2 mL) was added dropwise into the reaction mixture. After the addition, the mixture was stirred at rt for 30 mins. It resulted in a clear mixture. This mixture was poured into water and extracted with ethyl acetate (3 × 20 mL). The combined organic layer was washed with ammonium chloride aqueous solution, brine and dried over $MgSO_4$. It was filtered and the filtrate was concentrated under reduced pressure. The resulting residue was purified by column chromatography using ethyl acetate / hexane as an eluent (10-30% gradient). The alcohol product **128** was recovered as a red oil (2.8 g, 83%).

FTIR (thin film): 3370, 3070, 1724, 1562 cm^{-1}.

^{1}**H NMR** (400 MHz, $CDCl_3$): δ 7.44 (bs, 3H), 7.31 – 7.20 (m, 2H), 4.71 (s, 2H) ppm.

^{13}**C NMR** (101 MHz, $CDCl_3$): δ 147.7, 146.3, 143.5, 129.6, 129.4, 127.6, 127.2, 127.2, 63.4 ppm.

HRMS (ESI-TOF) m/z: $[M + H]^+$ calcd for $C_{13}H_9Cl_4N_2O$, 348.9464; found, 348.9459.

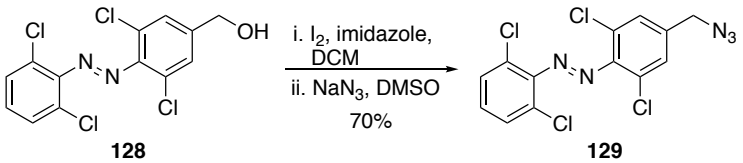

(*E*)-1-(4-(azidomethyl)-2,6-dichlorophenyl)-2-(2,6-dichlorophenyl)diazene (**129**). To a solution of alcohol **128** (1.6 g, 4.6 mmol) in dichloromethane (30 mL) triphenylphosphine (1.4 g, 5.5 mmol), iodine (1.4 g, 5.5 mmol), imidazole (373 mg, 5.5 mmol) were added. The reaction mixture was stirred at rt for 2 h. Then TLC showed full conversion of the alcohol to iodide. To the resulting mixture were added DMSO (20 mL) and sodium azide (357 mg, 5.5 mmol). After 15 min, TLC showed full conversion of iodide to azide. The resulting mixture was poured into water and extracted with ethyl acetate (3 × 20 mL). The combined organic layer was

purified by column chromatography using ethyl acetate / hexane as an eluent (10-20% gradient). The azide **129** was recovered as a red oil (1.2 g, 70%).

FTIR (thin film): 3072, 2105, 1562 cm^{-1}.

^{1}**H NMR** (400 MHz, $CDCl_3$): δ 7.48 – 7.41 (m, 4H), 7.29 – 7.24 (m, 1H), 4.40 (s, 2H) ppm.

^{13}**C NMR** (101 MHz, cdcl$_3$): δ 147.6, 147.2, 138.0, 129.7, 129.4, 128.6, 127.8, 127.3, 53.2 ppm.

HRMS (ESI-TOF) m/z: $[M + H]^+$ calcd for $C_{13}H_8Cl_4N_5$, 373.9528; found, 373.9526.

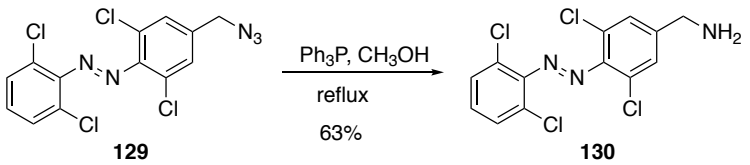

(*E*)-(3,5-dichloro-4-((2,6-dichlorophenyl)diazenyl)phenyl)methanamine (**130**).To a solution of azide **129** (1.1 g, 2.9 mmol) in methanol (10 mL) was added triphenylphosphine (1.5 g, 5.9 mmol). The mixture was refluxed for 4 h. The solvent was removed under reduced pressure. The resulting mixture was purified by column chromatography using ether / chloroform (25%) as first eluent to remove triphenylphosphine and triphenylphosphine oxide byproduct, and using chloroform / methanol (10%) to afford the amine **130** as a red liquid (645 mg, 63%).

^{1}**H NMR** (400 MHz, $CDCl_3$, *trans* and *cis* mixture): δ 7.49 – 7.42 (m, 3H), 7.29 – 7.21 (m, 2H), 3.93 (s, 2H), 1.66 (s, 2H) ppm.

^{13}**C NMR** (101 MHz, $CDCl_3$, *trans* and *cis* mixture): δ 148.2, 147.9, 146.6, 146.0, 145.8, 129.5, 129.4, 129.4, 129.3, 129.3, 129.1, 128.0, 128.0, 127.7, 127.6, 127.2, 126.0, 126.0, 45.2, 44.9 ppm.

HRMS (ESI-TOF) m/z: $[M + H]^+$ calcd for $C_{13}H_{10}Cl_4N_3$, 347.9623; found, 347.9622.

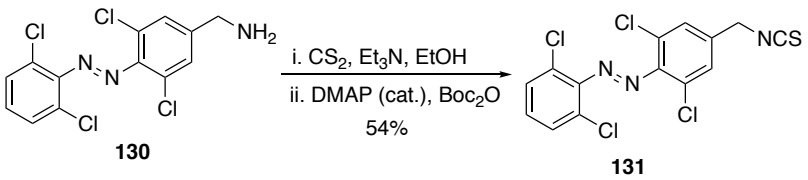

(*E*)-1-(2,6-dichloro-4-(isothiocyanatomethyl)phenyl)-2-(2,6-dichlorophenyl)diazene (**131**). To a solution of amine **130** (580 mg, 1.66 mmol) in methanol (20 mL) were added triethylamine (0.276 mL, 1.99 mmol) and carbon disulfide (1.0 mL, 16.6 mmol). The mixture was stirred at rt for 1 h. It resulted in a turbid solution. To this suspension were added Boc_2O (435 mg, 8.61 mmol) and DMAP (10 mg, 0.083 mmol). The solution then turned to clear solution and was stirred at rt for another 30 mins. The mixture was poured into water and extracted with ether (3 × 20 mL). The combined organic layer was washed with 5% citric acid aqueous solution, brine, dried over $MgSO_4$ and filtered. The filtrate was concentrated under reduced pressure. The residue was purified by column chromatography using ethyl acetate / hexane as an eluent (10-20% gradient). The isocyanate **131** was recovered as a red liquid (353 mg, 54%).

^{1}**H NMR** (400 MHz, $CDCl_3$): δ 7.49 – 7.42 (m, 4H), 7.31 – 7.25 (m, 1H), 4.78 (t, J = 0.7 Hz, 1H) ppm.

^{13}C NMR (101 MHz, $CDCl_3$): δ 147.6, 147.4, 136.4, 129.8, 129.5, 128.0, 127.6, 127.4, 47.4 ppm.

HRMS (ESI-TOF) m/z: $[M + H]^+$ calcd for $C_{14}H_8Cl_4N_3S$, 389.9188; found, 389.9189.

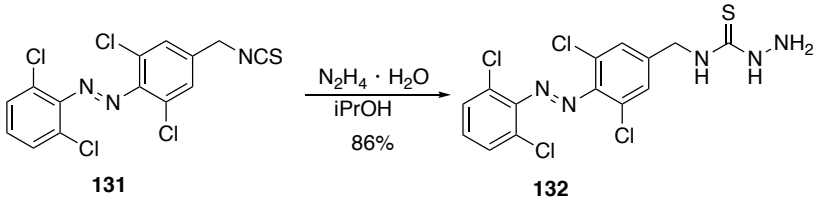

(*E*)-N-(3,5-dichloro-4-((2,6-dichlorophenyl)diazenyl)benzyl)hydrazinecarbothioamide (132). To a solution of isocyanate **131** (238 mg, 0.608 mmol) in isopropanol (3 mL) was added hydrazine hydrate (101 μL, 60%, 1.22 mmol) dropwise. It resulted yellow in precipitation right after the addition. The mixture was stirred for 20 mins at rt. The solid product was recovered by vaccum filtration. It was further washed by ether and ethanol to afford the thiosemicarbozide **132** (221 mg, 86%) as a yellow powder without further purification.

FTIR (thin film): 3402, 2940, 2254, 1660 cm^{-1}.

^{1}H NMR (400 MHz, DMSO-d_6): δ 8.90 (bs, 1H), 8.59 (bs, 1H), 7.69 (d, J = 8.1 Hz, 2H), 7.58 (s, 2H), 7.50 (t, J = 8.2 Hz, 1H), 4.76 (d, J = 5.3 Hz, 2H), 4.59 (bs, 2H) ppm.

^{13}C NMR (101 MHz, DMSO-d_6): δ 146.8, 144.7, 144.6, 131.1, 129.9, 128.4, 126.1, 125.9, 45.0 ppm.

HRMS (ESI-TOF) m/z: $[M + H]^+$ calcd for $C_{14}H_{12}Cl_4N_5S$, 421.9562; found, 421.9572.

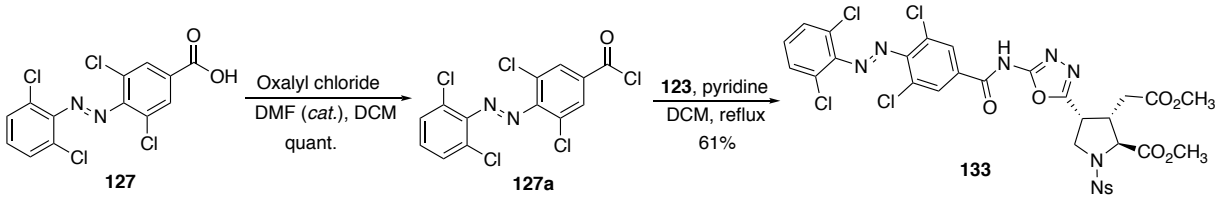

Methyl (2*S*,3*S*,4*R*)-4-(5-(3,5-dichloro-4-((*E*)-(2,6-dichlorophenyl)diazenyl)benzamido)-1,3,4-oxadiazol-2-yl)-3-(2-methoxy-2-oxoethyl)-1-((4-nitrophenyl)sulfonyl)pyrrolidine-2-carboxylate (133). To a suspension of acid **127** (50 mg, 0.14 mmol) in dichloromethane (1 mL) was added oxalyl cholide (35 μL, 0. 42 mmol) at rt. Then a drop of dry DMF was added to the mixture to accelerate the reaction. The reaction mixture turned to a clear dark red solution. After 1 h, the solvent was removed under reduced pressure and yielded a brown solid. The resulting solid was redissolved in dichloromethane (2 mL). To this mixture were added amine **123** (65 mg, 0.14 mmol) and pyridine (11 μL, 0.14 mmol). The resulting mixture was heated to reflux overnight. The resulting mixture was concentrated under reduced pressure. The crude product was purified by column chromatography using ethyl acetate / hexane as an eluent (10-50% gradient). The oxadiazole product **133** was recovered as a red solid (68 mg, 61%).

^{1}H NMR (400 MHz, CD_3CN): δ 8.31 (d, J = 8.9 Hz, 2H), 8.25 (s, 2H), 7.99 (d, J = 8.8 Hz, 2H), 7.60 (d, J = 8.2 Hz, 2H), 7.43 (dd, J = 8.6, 7.6 Hz, 1H), 4.31 (d, J = 6.7 Hz, 1H), 3.96 – 3.83 (m, 3H), 3.79 – 3.73 (m, 1H), 3.72 (s, 3H), 3.54 (s, 3H), 3.13 (p, J = 6.9 Hz, 1H), 2.46 (dd, J = 17.2, 6.7 Hz, 1H), 2.31 (dd, J = 17.3, 7.8 Hz, 1H) ppm.

^{13}C NMR (101 MHz, CD_3CN): δ 172.1, 171.9, 151.3, 149.8, 148.0, 144.4, 131.8, 130.9, 130.8, 129.5, 127.8, 127.3, 125.5, 65.8, 53.5, 52.6, 50.9, 43.4, 39.1, 33.1 ppm.

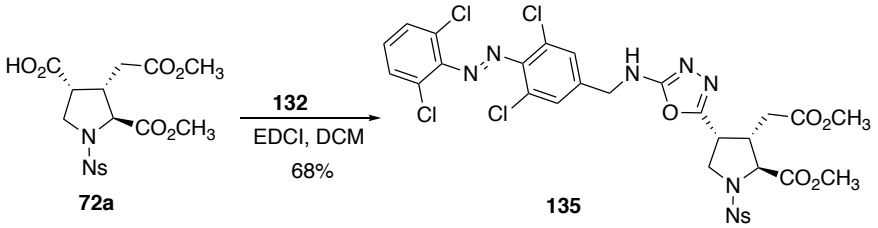

Methyl (2*S*,3*S*,4*R*)-4-(5-((3,5-dichloro-4-((*E*)-(2,6-dichlorophenyl)diazenyl)benzyl)amino)-1,3,4-oxadiazol-2-yl)-3-(2-methoxy-2-oxoethyl)-1-((4-nitrophenyl)sulfonyl)pyrrolidine-2-carboxylate (135). To a solution of acid **72a** (24 mg, 56 μmol) in dichloromethane (2 mL) were added thiosemicarbazide (28 mg, 67 μmol) and EDCI (37 mg, 0.19 mmol). The resulting mixture was stirred at rt for 48 h. The mixture was concentrated under reduced pressure. The resulting mixture was purified by column chromatography using ethyl acetate / hexane as an eluent (10-50% gradient). The oxodiazole amine product was recovered as an orange solid (30 mg, 68%).

FTIR (thin film): 3333, 2970, 1739, 1637, 1532 cm^{-1}.

^{1}H NMR (400 MHz, $CDCl_3$): δ 8.36 (d, *J* = 9.1 Hz, 2H), 8.03 (d, *J* = 9.1 Hz, 2H), 7.50 – 7.43 (m, 4H), 7.30 – 7.26 (m, 1H), 5.41 (t, *J* = 6.2 Hz, 1H), 4.51 (d, *J* = 5.6 Hz, 2H), 4.36 (d, *J* = 6.5 Hz, 1H), 3.87 – 3.80 (m, 3H), 3.78 (s, 3H), 3.61 (s, 3H), 3.08 (dt, *J* = 12.4, 4.9 Hz, 1H), 2.53 (dd, *J* = 17.4, 8.2 Hz, 1H), 2.38 (dd, *J* = 17.4, 6.7 Hz, 1H) ppm.

^{13}C NMR (101 MHz, $CDCl_3$): δ 171.1, 171.0, 163.1, 157.3, 150.4, 147.6, 147.1, 143.8, 139.6, 129.8, 129.5, 129.2, 128.6, 128.6, 128.4, 127.8, 127.3, 124.3, 64.6, 53.0, 52.1, 50.2, 46.2, 42.7, 37.9, 32.4 ppm.

HRMS (ESI-TOF) m/z: $[M + Na]^+$ calcd for $C_{30}H_{25}Cl_4N_7O_9SNa$, 822.0081; found, 822.0074.

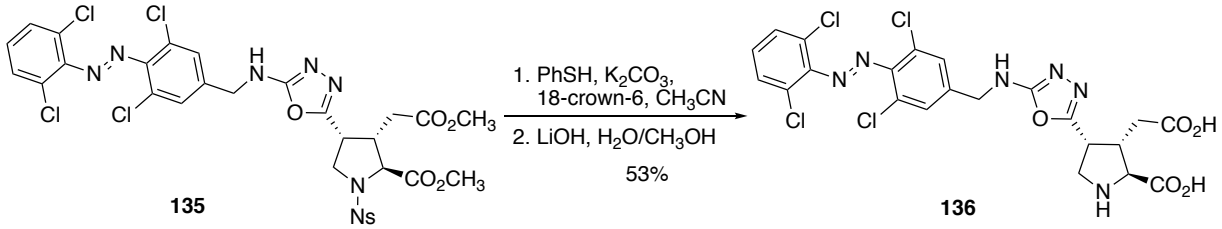

(2*S*,3*S*,4*R*)-3-(carboxymethyl)-4-(5-((3,5-dichloro-4-((*E*)-(2,6-dichlorophenyl)diazenyl)benzyl)amino)-1,3,4-oxadiazol-2-yl)pyrrolidine-2-carboxylic acid (136). To a solution of oxodiazole **135** (28 mg, 35 μmol) in acetonitrile (2 mL) were added thiophenol (10 μL, 0.10 mmol), 18-crown-6 (14 mg) and potassium carbonate (7 mg). The mixture was heated to 40 °C. After 3 h, the reaction mixture was poured into water and extracted with ethyl acetate (3 × 10 mL). The combined organic layer was washed with brine, dried over $MgSO_4$ and filtered. The filtrate was concentrated under reduced pressure. The resulting mixture was purified by column chromatography using ethyl acetate / hexane as an eluent (10-100% gradient). The oxodiazole amine product was recovered as an orange solid (16 mg, 74%). The obtained solid was redissolved in methanol (1 mL). To this solution was added LiOH aqueous solution (2.5 M, 0.32 mL). The resulting mixture was

stirred at rt for 6 h. The solution was neutralized by addition of hydrochloric acid (0.5 M) at 0 °C, precipitations formed after the neutralization. The solution was centrifuged. The aqueous solution was removed by pipette, the obtained solid was re-suspended in water (3 mL) and re-centrifuged. The aqueous solution was removed and the solid product was dried under high vaccum. It afforded the orange solid (11 mg, 56%) as the azo product **136** without further purification.

FTIR (thin film): 3352, 2948, 1643 cm^{-1}.

^{1}**H NMR** (400 MHz, CD_3OD): δ 7.50 – 7.42 (m, 1H), 7.42 – 7.29 (m, 2H), 7.31 – 7.19 (m, 2H), 4.45 – 4.15 (m, 2H), 4.08 – 3.86 (m, 2H), 3.73 – 3.62 (m, 2H), 3.06 – 2.97 (m, 1H), 2.92 – 2.72 (m, 1H), 2.36 – 2.10 (m, 1H) ppm.

^{13}**C NMR** (101 MHz, CD_3OD): δ 172.8, 172.5, 168.7, 168.5, 135.5, 129.6, 129.3, 129.1, 129.0, 128.2, 128.0, 127.0, 61.6, 45.4, 40.7, 32.4 ppm.

HRMS (ESI-TOF) m/z: $[M - H]^-$ calcd for $C_{22}H_{17}Cl_4N_6O_5$, 585.0026; found, 585.0020.

Chapter 6

General Conclusion

From a chemical biology perspective, an overarching objective of this thesis is the design of chemical probes to study kainate receptors (KAR) using light. The underlying foundation of this work, however, is the creation and exploitation of synthetic strategies to obtain novel C4 kainoids. The robust synthetic routes presented herein have enabled us to obtain these C4 kainoids on a practical scale. Some C4 kainoid intermediates have been further derivatized to create a number of photoactive KAR probes. Figure 6-1 provides an overview of the synthetic strategies and target molecules developed.

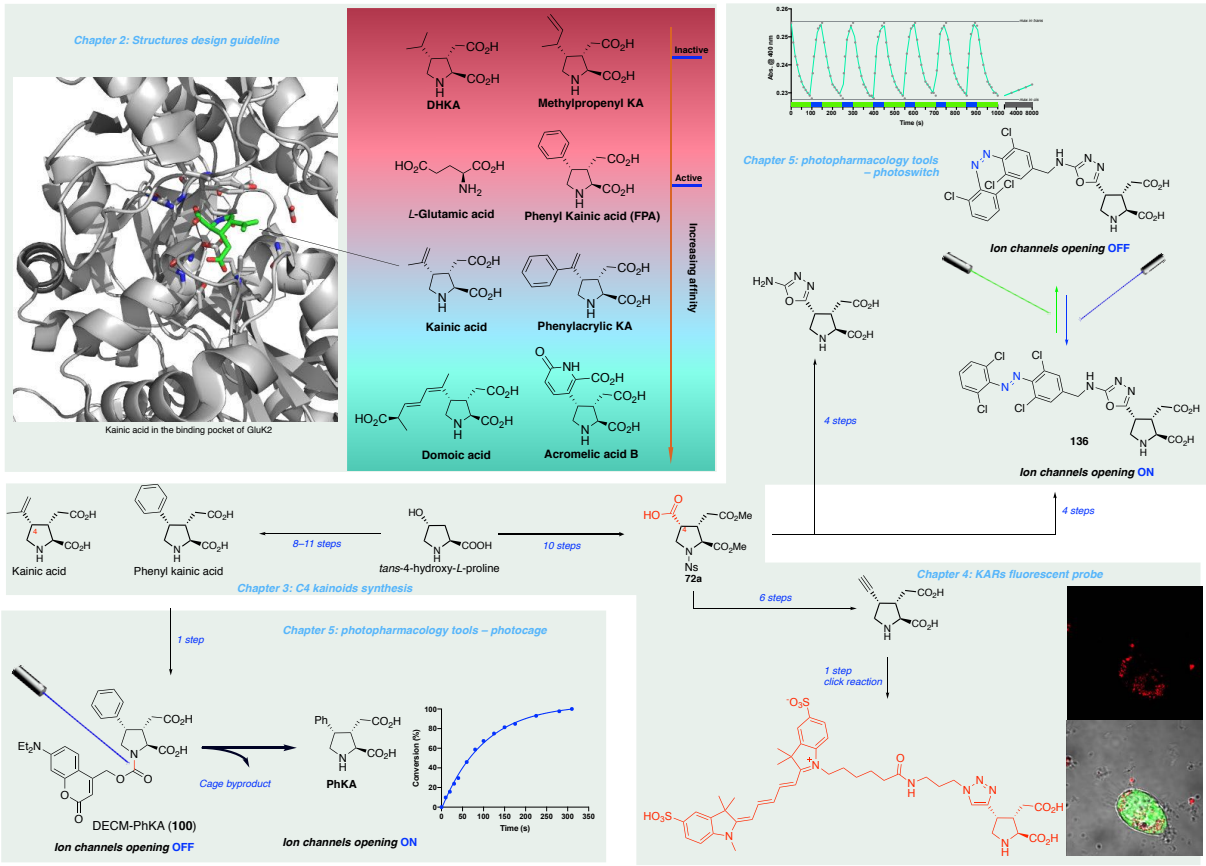

Figure 6–1. Overview of the SAR analysis, probes synthesis, and their application.

Chapter 2 described a comprehensive survey of kainic acid analogs that have been tested for their biological activity. The available activity data of kainoids were systematically analyzed and combined with the most recent crystallographic studies. From the exercise emerged a set of structural guidelines to help design high-affinity analogs. We have used this analysis to design the suite of molecules presented in subsequent chapters. We expect it will also help guide the synthetic efforts of organic synthesis and medicinal chemistry research in view of the renewed interest in neuroactive molecules. In our hands

In Chapter 3, a unified stereoselective synthesis of 4-substituted kainoids is presented. Four kainic acid analogues were obtained in 8–11 steps with up to 54% overall yields. Starting from *trans*-4-hydroxy-L-proline, the sequence enables a late-stage modification of C4 substituents with sp^2 nucleophiles. Stereoselective steps include a cerium-promoted nucleophilic addition and a palladium-catalyzed reduction. A 10-step route to acid **21a** was also established to enable ready functionalization of the C4 position.

A versatile alkynyl kainoid was synthesized in Chapter 4 that capitalized on our C4 kainoid synthesis. The easily modifiable nature of the alkyne functional group via "click" chemistry enabled the synthesis of several chemical probes via one-step coupling reaction with azides. A red fluorescent probe was synthesized (sulfoCy5-KA, **90**), and confocal microscopy imaging experiments in living cells demonstrated its use for KARs visualization. Biological experiments with this probe are still ongoing in our lab, including binding affinity measurements with biophysical experiments. This probe offers neurobiologists a tool to visualize KARs and study their trafficking that complements genetic methods.

Finally, Chapter 5 described two sets of photopharmacology tools for KARs – photocaged and photoswitchable kainoids. The photocaged kainoid, DECM-PhKA is derived from phenyl kainic acid – a selective agonist for KARs. Photochemical studies on DECM-PhKA confirmed the release of the active PhKA upon blue light irradiation, DECM-PhKA is relatively stable under natural light. It will provide a new tool to enable the temporal and spatial activation of KARs by blue light. Moreover, a reversible agonist – photoswitchable kainoid **136** was developed. Photochemical studies of **136** demonstrated the reversible *trans*/*cis* isomerization upon blue and green light irradiation. It offers one more reversible modulation tool for KARs with temporal and spatial precision using visible light. The further electrophysiology experiments on these novel tools are still ongoing in our lab.

Kelowna
July 2, 2019

Appendix A

Biological data for kainoids collected from reported studies

Table S2–1. Original literature data for the activity of kainic acid analogs in functional assays

Compound	Potency								
	Potency relative to L-Glu[80]	Mimimum effective concentration (μM)[46]		Potency relative to KA neurotoxicity (%)[166]			Potency relative to L-Glu[52] (inducing Na^+ efflux from preloaded rat striatum slices)	Effect in rat cerebellar slices[48,83]	
		Depolarization	Potentiation	Retina	Striatum	Electrophysiology		EC_{50} (mM)	KA Antagonist IC_{50} (mM) (KA 1 mM)
L-Glu (**3**)	1	0.03	Inactive[a]	0.3	< 0.1	1.0	1.0		
Pyroglutamic acid (**10**)	0.7 – 0.8								
CPAA (**11**)									
KA (**1**)	8 - 80						8.0	1.0	
allo – KA (**6**)		Inactive[a]	Inactive[a]						
DHK (**13**)	0.06 - 0.6	Inactive[a]	Inactive[a]	< 1.0	< 2.0	Inactive[a]			
β-KA (**7**)		Inactive[a]	Inactive[a]						
N-acetyl kainic acid (**5a**)		Inactive[a]	Inactive[a]	< 1.0	< 2.0	Inactive[a]			
Kainic acid dimethyl ester (**4**)		Inactive[a]	Inactive[a]	< 1.0	< 2.0	Inactive[a]			
Carboxyl kainic acid (**14a**)							2.5	Inactive	Inactive
Carboxyl *allo* – kainic acid (**14b**)							2.3	Inactive	Inactive
Kainic acid methyl ketone (**12a**)		0.01	0.003				5.2		
allo – kainic acid methyl ketone (**12b**)							4.6		
Hydroxyl kainic acid (**15a**)							0.2		
Dihydroyl kainic acid (**15b**)							0.1		
Phenylthio-hydroxyl kainic acid (**15c**)							0.1	Inactive	Isomer A 0.3 Isomer B 0.5
Kainic acid lactone (**16a**)		Inactive[a]	Inactive[a]					--	3 (KA 0.1 mM)[6]
Kainic acid hydroxy-lactone (mixed isomers) (**16b**)								Inactive[b]	2.0[b]
Kainic acid iodolactone (**16c**)								Isomer A Very weak Isomer B Inactive	Isomer A Inactive Isomer B 0.3
Domoic acid (**2**)		0.006	0.003						

Table S2–2. Original literature data for the activity of kainic acid analogs in functional assays. (Continued)

Compound	Potency															
	IC50 (Displacement by kainate analogue of bound [3H] KA (20 nm))[51] (μ M)	Effect on neurons[52-53]		Insecticidal Activity[54]	IC_{50} for KA receptors[55] (μ M)	Mean molar potency ratios, relative to KA[76]		Binding to GluR 6[79]	[3H] kainate binding Ki[57] (nM)		[3H] kainate binding to KA Receptors Ki (μ M)[167]	Binding to GluR6 Ki[168](nM)	In vivo potencies[169]			Synaptosomal KA BRA Ki[81](nM)
		Minimum effective or used concentration (μ M)	Effects			Dorsal root fibers	Motoneurones		HumGluR 6 receptors	Rat forebrain receptors			Spike amplitude EC50 (nM)	Spike area EC50 (nM)	GluR6 binding assay Ki (nM)	
L-Glu (3)		0.68	No effect			0.11 ±0.01	0.02 ±0.003									
KA (1)	17.8	0.3 - 0.03	Effective			1	1		53.0 ± 23.6	3.7 ± 0.20	0.01					
allo-KA (6)		0.47	No effect													
KA methylketone (12a)		0.3 - 0.03	Effective													
allo-KA methylketone (12b)		0.47	No effect													
DA (2)		0.3 – 0.03	Effective			34 ± 2.4	2.2 ± 0.08		18.3 ±10.2			4.9 ± 0.29	228	237	3.35	2.4
DHK (13)	645.6	0.47	No effect			< 0.01	< 0.01				16					
CPAA (11)											1.6					
25a	79.4															
25b	416.8															
17		0.28	No effect													
18		0.26	No effect													
19		0.2	No effect													
21		0.24	No effect													
20		0.24	Effective													
23		0.19	No effect													
Domoilactone A (24a)				Inactive												
Domoilactone B (24b)				Inactive												
22					> 100											
Acro A (26)						1.7 ± 0.08	2.7 ± 0.1									
Acro B (27)						13 ± 0.7	1.4 ± 0.04									
MPPA (28)						0.045 ± 0.006	0.57 ± 0.05									
HMPPA (29)						0.45 ± 0.04	0.91 ± 0.04									
CPPA (30)						0.91 ± 0.12	0.82 ± 0.04									
CNOPA (31)						0.29 ± 0.06	0.22 ± 0.02									
32a						0.22 ± 0.03	0.45 ± 0.33									
32b						4.2 ± 0.29	3.8 ± 0.12									
32c						1.3 ± 0.13	1.9 ± 0.12									
9a								No effect								
9b								No effect								
34a									> 100,000	NA						
34b									> 100,000	NA						
36a									29.8 ± 6.9	1.6 ± 0.25						
36b									122.5 ± 40.9	2.2 ± 0.25						
36c									41.1 ±1.8	2.6 ±0.87						
36d									93.5 ± 21.5	3.5 ± 0.45						
36e									57.4 ± 15.4	3.9 ±1.61						

36f									31.7 ± 5.4	3.9 ± 0.41						
36g									38.4 ± 21.7	2.7 ± 0.49						
36h									107.8 ± 20.4	2.3 ± 0.90						
36i									169.3 ± 23.6	9.5 ± 1.43						
36j									54.3 ± 16.2	1.9 ± 0.63						
36k									82.2 ± 24.3	7.7 ± 3.02						
36l									146.8 ±46.4	3.6 ±2.80						
36m									145.6 ± 26.2	1.9 ±0.63						
36n									262.7 ± 59.7	18.5 ± 12.75						
36o									131.5 ± 46.2	3.6 ± 0.59						
36p									288.0 ± 105.0	9.0 ± 0.83						
36q									90.6 ± 10.9	2.1 ± 0.57						
36r									130.6 ± 29.8	9.1 ± 3.18						
36s									275.3 ± 498.5	23.3 ± 0.47						
36t									146.6 ± 52.0	2.8 ± 0.64						
36u									209.6 ± 60.9	11.9 ± 2.29						
36v									667.0 ± 259.8	16.0 ± 6.52						
36w									126.2 ± 40.3	6.2 ± 1.10						
36x									1295.7 ± 272.2	126.0 ± 34.9						
36y									2423.3 ± 300.2	210.3 ± 59.3						
36z									1284 ± 131.5	NA						
36aa									129.3 ± 13.6	NA						
36ab									663.3 ± 300.1	NA						
35a									6969.0 ± 1330.8	230.0 ± 38.3						
35b									2303.3 ± 802.5	5400 and 2400						
35c									3109.2 ± 934.3	NA						
35d									> 100, 000	3000 ±100						
Iso-DA A (37)				Effective									887	939	130	4.4
Iso-DA B (38)				Effective												5000
Iso-DA C (39)				Effective								1176 ± 70	3712	4626	1176	171
Iso-DA D (40)																600
Iso-DA E (41)																600
Iso-DA F (42)																67

Table S2-3. Correlation of the binding affinity of analogs of compounds **34**, **35**, and **36** with the Hammett constants of their aromatic substituents.

Compound	∑ σ (Hammett substituent constants)	∑ σ^+ (Electrophilic substituent constants)	[^{3}H] Kainate binding K_i (nM)	$Log_{10}Ki$
1	-	-	53 ± 23.6	1.7 ± 1.4
2	-	-	18.3 ± 10.2	1.3 ± 1.0
34a	-	-	>100,000	> 5
34b	-	-	>100,000	> 5
35a	-	-	6,969 ± 1331	3.8 ± 3.1
35b	-	-	2,303 ± 802	3.4 ± 2.9
35c	-	-	3,109 ± 934	3.5 ± 3.0
35d	-	-	>100,000	
36a	0	0	29.8 ± 6.9	1.5 ± 0.8
36b	-0.069	-0.066	122.5 ± 40.9	2.1 ± 1.6
36c	-0.170	-0.311	41.1 ± 1.8	1.6 ± 0.3
36d	0.115	0.047	93.5 ± 21.5	2.0 ± 1.3
36e	-0.268	-0.778	57.4 ± 15.4	1.8 ± 1.2
36f	0.277	0.114	31.7 ± 5.4	1.5 ± 0.7
36g	0.062	-0.073	38.4 ± 21.7	1.6 ± 1.3
36h	-0.239	-0.377	107.8 ± 20.4	2.0 ± 1.3
36i	-0.138	-0.132	169.3 ± 23.6	2.2 ± 1.4
36j	-0.007	-0.139	54.3 ± 16.2	1.7 ± 1.2
36k	-0.151	-0.295	82.2 ± 24.3	1.9 ± 1.4
36l	-	-	146.8 ± 46.4	2.2 ± 1.7
36m	-	-	145.6 ± 26.2	2.2 ± 1.4
36n	-	-	262.7 ± 59.7	2.4 ± 1.8
36o	-	-	131.5 ± 46.2	2.1 ± 1.7
36p	-	-	288.0 ± 105.0	2.5 ± 2.0
36q	-0.010	0.109	90.6 ± 10.9	2.0 ± 1.0
36r	0.060	-0.179	130.6 ± 29.8	2.1 ± 1.5
36s	0.100	-	275.3 ± 598.5	2.4 ± 2.8
36t	-0.320	-	146.6 ± 52.0	2.2 ± 1.7
36u	-0.320	-0.500	209.6 ± 60.9	2.3 ± 1.8
36v	-	-	667 ± 259	2.8 ± 2.4
36w	-	-	126.2 ± 40.3	2.1 ± 1.6
36x	-	-	1,296 ± 272	3.1 ± 2.4
36y	-	-	2,423 ± 300	3.4 ± 2.5
36z	-	-	1,284 ± 131	3.1 ± 2.1
36aa	-	-	129.3 ± 13.6	2.1 ± 1.1
36ab		-	663 ± 300	2.8 ± 2.5

Table S2–4. Kainate receptors reference sequences for the most commonly used organisms (mouse, rat, and humans).

Ionotropic glutamate receptor	*organism*	Catalogued name	Accession number	Protein size (# a.a.)
GluK1	*mus musculus*	m.m.	Q60934.2	836
(GluR5)		m.m. isoform a	NP_666184.2	934
		m.m. isoform b	NP_034478.1	905
		m.m. isoform c	NP_001333893.1	903
	rattus norvegicus	r.n.	P22756.3	949
		r.n. isoform 1	NP_001104587.1	949
		r.n. isoform 2	NP_058937.1	920
		r.n. isoform 3	NP_001104584.1	905
	homo sapiens	h.s.	P39086.1	918
		h.s. isoform 1	NP_000821.1	918
		h.s. isoform 2	NP_783300.1	905
		h.s. isoform 3	NP_001307545.1	920
		h.s. isoform 4	NP_001307547.1	781
		h.s. isoform 5	NP_001307550.1	763
		h.s. isoform 7	NP_001317922.1	934
		h.s. isoform 8	NP_001317923.1	949
GluK2	*mus musculus*	m.m. isoform 1	NP_001104738.1	908
(GluR6)		m.m. isoform 2	NP_034479.2	869
	ratus norvegicus	r.n.	P42260.2	908
		r.n.	NP_062182.1	908
	homo sapiens	h.s. isoform 1	NP_068775.1	908
		h.s. isoform 2	NP_786944.1	869
		h.s. isoform 3	NP_001159719.1	892
GluK3	*mus musculus*	m.m.	NP_001074566.1	919
(GluR7)	*rattus norvegicus*	r.n.	P42264.1	919
		r.n. isoform 1	NP_001106187.1	919
		r.n. isoform 2	NP_852038.2	910
	homo sapiens	h.s.	NP_000822.2	919
GluK4	*mus musculus*	m.m	NP_780690.2	956
(KA1)	*rattus norvegicus*	r.n.	Q01812.1	956
		r.n.	NP_036704.1	956
	homo sapiens	h.s. isoform 1	NP_001269399.1	956
		h.s. isofrom 2	NP_001269402.1	956
GluK5	*mus musculus*	m.m.	NP_032194.2	979
(KA2)	*rattus norvegicus*	r.n.	NP_113696.1	979
	homo sapiens	h.s. isoform 1	NP_001287959.1	981
		h.s. isoform 2	NP_002079.3	980

Table S2–5. Homology analysis of GluK1 between mouse, rat, and human isoforms.

Homology Analysis of **GluK1** between mouse, rat, and human isoforms

GluK1	*mus musculus*				*rattus norvegicus*				*homo sapiens*							
	m.m. Q60934.2 836 aa	m.m. isoform a NP_666184.2 934 aa	m.m. isoform b NP_034478.1 905	m.m. isoform c NP_001333893.1 903	r.n. P22756.3 949 aa	r.n. isoform 1 NP_001104587.1 949	r.n. isoform 2 NP_058937.1 920	r.n. isoform 3 NP_001104584.1 905	h.s. P39086.1 918 aa	h.s. isoform 1 NP_000821.1 918	h.s. isoform 2 NP_783300.1 905	h.s. isoform 3 NP_001307545.1 920	h.s. isoform 4 NP_001307547.1 781	h.s. isoform 5 NP_001307550.1 763	h.s. isoform 7 NP_001317922.1 934	h.s. isoform 8 NP_001317923.1 949
Q60934.2		89.2% (89.4%)	86.1% (86.3%)	88.3% (88.4%)	86.5% (87.5%)	86.9% (87.8%)	84.0% (84.8%)	85.3% (86.2%)	85.2% (86.8%)	85.2 (86.8%)	84.7% (86.2%)	83.4% (84.8%)	71.5% (72.9%)	81.9% (83.0%)	87.4% (89.1%)	86.0% (87.7%)
NP_666184.2	89.2% (89.4%)	*numbering reference*	96.9% (96.9%)	91.4% (91.4%)	96.9% (97.9%)	97.4% (98.2%)	94.4% (95.3%)	95.9% (96.8%)	96.1% (98.2%)	96.1% (98.2%)	94.8% (96.8)	93.3% (95.3%)	81.6% (83.5%)	94.4% (96.1%)	97.4% (9.7%)	95.9% (98.1%)
NP_034478.1	86.1% (86.3%)	96.9% (96.9%)		99.7% (99.8%)	94.0% (94.9%)	94.4% (95.3%)	97.4% (98.3%)	99.0% (99.9%)	95.8% (97.9%)	95.8% (97.9%)	97.8% (99.9%)	96.2% (98.3%)	84.2% (86.2%)	98.2% (100.0%)	94.8% (96.8%)	93.3% (95.3%)
NP_001333893.1	88.3% (88.4%)	91.4% (91.4%)	99.7% (99.8%)		96.8% (97.8%)	97.2% (98.2%)	96.9% (97.9%)	98.6% (99.7%)	95.8% (98.0%)	95.8% (98.0%)	97.4% (99.7%)	95.8% (97.9%)	83.1% (85.2%)	97.8% (99.7%)	97.8% (99.9%)	96.1% (98.2%)
P22756.3	86.5% (87.5%)	96.9% (97.9%)	94.0% (94.9%)	96.8% (97.8%)		99.6% (99.7%)	96.5% (96.6%)	94.9% (95.0%)	96.7% (99.4%)	96.7% (99.4%)	92.3% (94.8%)	93.8% (96.4%)	79.5% (81.8%)	91.7% (93.8%)	95.0% (97.8%)	96.5% (99.4%)
NP_001104587.1	86.9% (87.8%)	97.4% (98.2%)	94.4% (95.3%)	97.2% (98.2%)	99.6% (99.7%)		**96.9%** (96.9%)	95.4% (95.4%)	**97.1%** (99.8%)	97.1% (99.8%)	92.7% (95.2%)	**94.2%** (96.7%)	79.8% (82.1%)	92.2% (94.1%)	95.5% (98.1%)	**96.9%** (99.7%)
NP_058937.1	84.0% (84.8%)	94.4% (95.3%)	97.4% (98.3%)	96.9% (97.9%)	96.5% (96.6%)	96.9% (96.9%)		98.4% (98.4%)	**96.8%** (99.5%)	96.8% (99.5%)	95.7% (98.2%)	**97.2%** (99.8%)	82.3% (84.7%)	95.8% (97.8%)	92.7% (95.2%)	**94.2%** (96.7%)
NP_001104584.1	85.3% (86.2%)	95.9% (96.8%)	99.0% (99.9%)	98.6% (99.7%)	94.9% (95.0%)	95.4% (95.4%)	98.4% (98.4%)		95.2% (97.8%)	95.2% (97.8%)	97.2% (99.8%)	95.7% (98.2%)	83.6% (86.1%)	97.8% (99.9%)	94.2% (96.7%)	92.7% (95.2%)
P39086.1	85.2% (86.8%)	96.1% (98.2%)	95.8% (97.9%)	95.8% (98.0%)	96.7% (99.4%)	97.1% (99.8%)	96.8% (99.5%)	95.2% (97.8%)		21.9% (62.5%) ???	97.9% (98.1%)	99.7% (99.8%)	83.7% (83.8%)	95.0% (95.9%)	98.3% (98.3%)	100.0% (100.0%)
NP_000821.1	85.2 (86.8%)	96.1% (98.2%)	95.8% (97.9%)	95.8% (98.0%)	96.7% (99.4%)	97.1% (99.8%)	96.8% (99.5%)	95.2% (97.8%)	21.9% (62.5%) ???		97.9% (98.1%)	99.7% (99.8%)	83.7% (83.8%)	95.0% (95.9%)	98.3% (98.3%)	100.0% (100.0%
NP_783300.1	84.7% (86.2%)	94.8% (96.8)	97.8% (99.9%)	97.4% (99.7%)	92.3% (94.8%)	92.7% (95.2%)	95.7% (98.2%)	97.2% (99.8%)	97.9% (98.1%)	97.9% (98.1%)		98.4% (98.4%)	86.3% (86.3%)	97.6% (98.4%)	96.9% (96.9%)	95.4% (95.4%)
NP_001307545.1	83.4% (84.8%)	93.3% (95.3%)	96.2% (98.3%)	95.8% (97.9%)	93.8% (96.4%)	94.2% (96.7%)	97.2% (99.8%)	95.7% (98.2%)	99.7% (99.8%)	99.7% (99.8%)	98.4% (98.4%)		84.9% (84.9%)	95.7% (96.5%)	95.4% (95.4%)	96.9% (96.9%)
NP_001307547.1	71.5% (72.9%)	81.6% (83.5%)	84.2% (86.2%)	83.1% (85.2%)	79.5% (81.8%)	79.8% (82.1%)	82.3% (84.7%)	83.6% (86.1%)	83.7% (83.8%)	83.7% (83.8%)	86.3% (86.3%)	84.9% (84.9%)		81.9% (81.9%)	83.6% (83.6%)	82.3% (82.3%)
NP_001307550.1	81.9% (83.0%)	94.4% (96.1%)	98.2% (100.0%)	97.8% (99.7%)	91.7% (93.8%)	92.2% (94.1%)	95.8% (97.8%)	97.8% (99.9%)	95.0% (95.9%)	95.0% (95.9%)	97.6% (98.4%)	95.7% (96.5%)	81.9% (81.9%)		94.0% (94.7%)	92.2% (92.9%)
NP_001317922.1	87.4% (89.1%)	97.4% (9.7%)	94.8% (96.8%)	97.8% (99.9%)	95.0% (97.8%)	95.5% (98.1%)	92.7% (95.2%)	94.2% (96.7%)	98.3% (98.3%)	98.3% (98.3%)	96.9% (96.9%)	95.4% (95.4%)	83.6% (83.6%)	94.0% (94.7%)		98.4% (98.4%)
NP_001317923.1	86.0% (87.7%)	95.9% (98.1%)	93.3% (95.3%)	96.1% (98.2%)	96.5% (99.4%)	96.9% (99.7%)	94.2% (96.7%)	92.7% (95.2%)	100.0% (100.0%)	100.0% (100.0%	95.4% (95.4%)	96.9% (96.9%)	82.3% (82.3%)	92.2% (92.9%)	98.4% (98.4%)	

Table S2–6. Homology analysis of GluK2, GluK3, GluK4, and GluK5 between mouse, rat, and human isoforms.

Homology Analysis of **GluK2** between mouse, rat, and human isoforms

GluK2	*mus musculus* **m.m. isoform 1** NP_001104738.1 908	**m.m. isoform 2** NP_034479.2 869	*ratus norvegicus* **r.n.** P42260.2 908	**r.n.** NP_062182.1 908	*homo sapiens* **h.s. isoform 1** NP_068775.1 908	**h.s. isoform 2** NP_786944.1 869	**h.s. isoform 3** NP_001159719.1 892
NP_001104738.1	*numbering reference*	99.9% (100.0%)	99.6% (99.9%)	99.9% (100.0%)	98.7% (99.6%)	98.5% (99.5%)	98.5% (99.5%)
NP_034479.2	99.9% (100.0%)		99.4% (99.9%)	99.8% (100.0%)	98.5% (99.5%)	98.6% (99.5%)	97.7% (99.0%)
P42260.2	99.6% (99.9%)	99.4% (99.9%)	*numbering reference*	99.7% (99.9%)	99.1% (99.7%)	98.9% (99.6)	98.9% (99.6%)
NP_062182.1	99.9% (100.0%)	99.8% (100.0%)	99.7% (99.9%)		98.8% (99.6%)	98.6% (99.5%)	98.6% (99.5%)
NP_068775.1	98.7% (99.6%)	98.5% (99.5%)	99.1% (99.7%)	98.8% (99.6%)		99.9% (100.0%)	99.9% (100.0%)
NP_786944.1	98.5% (99.5%)	98.6% (99.5%)	98.9% (99.6)	98.6% (99.5%)	99.9% (100.0%)	*numbering reference*	99.9% (100.0%)
NP_001159719.1	98.5% (99.5%)	97.7% (99.0%)	98.9% (99.6%)	98.6% (99.5%)	99.9% (100.0%)	99.9% (100.0%)	

Note: The amino acid numbering reference used in this review is highlighted in yellow (GluK2_rat, P42260).

Homology Analysis of **GluK3** between mouse, rat, and human isoforms

GluK3	*mus musculus* **m.m.** NP_001074566.1 919	*rattus norvegicus* **r.n.** P42264.1 919	**r.n. isoform 1** NP_001106187.1 919	**r.n. isoform 2** NP_852038.2 910	*homo sapiens* **h.s.** NP_000822.2 919
NP_001074566.1		99.5% (99.7%)	99.8% (100.0%)	99.8% (100.0%)	99.0% (99.9%)
P42264.1	99.5% (99.7%)		99.7% (99.7%)	99.6% (99.6%)	98.7% 99.6%
NP_001106187.1	99.8% (100.0%)	99.7% (99.7%)	[REF]	100.0% (100.0%)	99.0% 99.9%
NP_852038.2	99.8% (100.0%)	99.6% (99.6%)	100.0% (100.0%)		99.2% (99.9%)
NP_000822.2	99.0% (99.9%)	98.7% 99.6%	99.0% 99.9%	99.2% (99.9%)	

Homology Analysis of **GluK4** between mouse, rat, and human isoforms

GluK4	*mus musculus* **m.m** NP_780690.2 956	*rattus norvegicus* **r.n.** Q01812.1 956	**r.n.** NP_036704.1 956	*homo sapiens* **h.s. isoform 1** NP_001269399.1 956	**h.s. isofrom 2** NP_001269402.1 956
NP_780690.2		99.5% (99.9%)	99.6% (100.0%)	97.9% (99.7%)	98.3% (99.6%)
Q01812.1	99.5% (99.9%)		99.9% (99.9%)	97.8% (99.6%)	98.2% (99.5%)
NP_036704.1	99.6% (100.0%)	99.9% (99.9%)		97.9% (99.7%)	98.3% (99.6%)
NP_001269399.1	97.9% (99.7%)	97.8% (99.6%)	97.9% (99.7%)		99.5% (99.6%)
NP_001269402.1	98.3% (99.6%)	98.2% (99.5%)	98.3% (99.6%)	99.5% (99.6%)	

Homology Analysis of **GluK5** between mouse, rat, and human isoforms

GluK5	*mus musculus* **m.m.** NP_032194.2 979	*rattus norvegicus* **r.n.** NP_113696.1 979	*homo sapiens* **h.s. isoform 1** NP_001287959.1 981	**h.s. isoform 2** NP_002079.3 980
NP_032194.2		100.0% (100.0%)	99.5% (99.9%)	98.9% (99.6%)
NP_113696.1	100.0% (100.0%)		99.5% (99.9%)	98.9% (99.6%)
NP_001287959.1	99.5% (99.9%)	99.5% (99.9%)		100.0% (100.0%)
NP_002079.3	98.9% (99.6%)	98.9% (99.6%)	100.0% (100.0%)	

Table S2–7. Reported crystallized protein structures of ionotropic glutamate receptors: kainate receptors (GluK1-5), AMPA receptors (GluA1-4), and NMDA receptors (GluN1-2B).

			PDB #	Amino acids	Resolution (Å)	Year	Lab	Citation
KAINATE receptors								
GluK1	*h*	iGluR5 + drug	4YMB	514	1.93	2015	Kastrup	
	h	iGluR5 + drug	4QF9	771	2.28	2015	Kastrup	
	h	iGluR5 + drug	4MF3	522	3.00	2014	Ornstein	
		iGluR5 + drug	4MF3	522	3.00	2013	Clawson	
		iGluR5 + KA	4EOX	514	2.00	2012	Kastrup	
	h	iGluR5 + drug	4DLD	514	2.00	2012	Kastrup	
		iGluR5 + drug	3s2v	514	2.50	2011	Kastrup	
	h	iGluR5 + toxin	3QXM	516	1.65	2011	Ikeda-Saito	
	h	iGluR5 + drug	3FVO	512	1.50	2010	Ikeda-Saito	
	h	iGluR5 + drug	3FVN	512	1.50	2010	Ikeda-Saito	
	h	iGluR5 + drug	3FVK	512	1.50	2010	Ikeda-Saito	
	h	iGluR5 + drug	3FVG	512	1.50	2010	Ikeda-Saito	
	h	iGluR5 + toxin	3FV2	512	1.50	2010	Ikeda-Saito	
	h	iGluR5 + toxin	3FV1	512	1.50	2010	Ikeda-Saito	
	h	iGluR5 + toxin	3FUZ	512	1.65	2010	Ikeda-Saito	
		iGluR5 + drug	3gbb	514	2.10	2009	Kastrup	
		iGluR5 + toxin	3gba	1028	1.35	2009	Kastrup	
	h	iGluR5 + toxin	2ZNU	256	1.80	2009	Ikeda-Saito	
	h	iGluR5 + toxin	2ZNT	256	1.60	2009	Ikeda-Saito	
	h	iGluR5 + glu	2ZNS	256	2.00	2009	Ikeda-Saito	
		iGluR5 + drug	2wky	516	2.20	2009	Kastrup	
		iGluR5 + NH4	3C36	516	1.68	2008	Mayer	
		iGluR5 + Cs	3C35	516	1.97	2008	Mayer	
		iGluR5 + Ru	3C34	516	1.82	2008	Mayer	
		iGluR5 + K	3C33	516	1.72	2008	Mayer	
		iGluR5 + Na	3C32	516	1.72	2008	Mayer	
		iGluR5 + Li	3C31	516	1.49	2008	Mayer	
		iGluR5 + drug	2qs4	1032	1.58	2008	Mayer	
		iGluR5 + drug	2qs3	516	1.76	2008	Mayer	
		iGluR5 + drug	2qs2	516	1.80	2008	Mayer	
		iGluR5 + drug	2qs1	516	1.80	2008	Mayer	
		iGluR5 + DA	2PBW	514	2.50	2007	Kastrup	J. Biol. Chem. 2007, 25726
		iGluR5 + drug	1VSO	257	1.85	2007	Kastrup	J. Biol. Chem. 2007, 25726
		iGluR5 + drug	2f36	1032	2.11	2006	Mayer	
		iGluR5 + drug	2f35	516	1.87	2006	Mayer	
		iGluR5 + drug	2f34	516	1.74	2006	Mayer	
		iGluR5 + drug	1ycj	514	1.95	2005	Kastrup	

		PDB #	Amino acids	Resolution (Å)	Year	Lab	Citation
KAINATE receptors							
GluK2	iGluR6 full length + glu	4UQQ	3528	7.60	2014	Mayer	Nature 2014, 514, 328
	iGluR6 mut + glu	4BDL	522	1.75	2013	Green	
	iGluR6 mut + KA	4BDM	1044	3.40	2013	Green	
	iGluR6 mut + KA	4BDN	1044	2.50	2013	Green	
	iGluR6 mut + KA	4BDO	1044	2.55	2013	Green	
	iGluR6 mut + glu	4BDQ	522	1.90	2013	Green	
	iGluR6 mut + glu	4BDR	522	1.65	2013	Green	
	iGluR6 + glu-AZO	4H8I	518	2.00	2013	Trauner / Schiefer	
	h iGluR6 + toxin	3QXM	516	1.65	2011	Ikeda-Saito	
	iGluR6 + glu	2XXR	522	1.60	2011	Green	J. Neurosci. 2011, 2916
	iGluR6 + KA	2XXT	522	1.90	2011	Green	J. Neurosci. 2011, 2916
	iGluR6 mut + glu	2XXU	522	1.50	2011	Green	J. Neurosci. 2011, 2916
	iGluR6 mut + KA	2XXV	522	1.70	2011	Green	J. Neurosci. 2011, 2916
	iGluR6 mut + glu	2XXW	522	2.30	2011	Green	J. Neurosci. 2011, 2916
	iGluR6 mut + glu	2XXX	522	2.10	2011	Green	J. Neurosci. 2011, 2916
	iGluR6 mut + KA	2XXY	1044	3.00	2011	Green	J. Neurosci. 2011, 2916
	iGluR6 / KA dimer	3ql4	1576	2.91	2011	Mayer	
	iGluR6	3QLT	790	2.99	2011	Mayer	
	iGluR6 / KA dimer	3qlu	1576	2.91	2011	Mayer	
	iGluR6 / KA tetramer	3qlv	3940	3.94	2011	Mayer	
	h iGluR6 + toxin	3FUZ	512	1.65	2010	Ikeda-Saito	
	h iGluR6 + toxin	3FV1	512	1.50	2010	Ikeda-Saito	
	h iGluR6 + toxin	3FV2	512	1.50	2010	Ikeda-Saito	
	h iGluR6 + drug	3FVG	512	1.50	2010	Ikeda-Saito	
	h iGluR6 + drug	3FVK	512	1.50	2010	Ikeda-Saito	
	h iGluR6 + drug	3FVN	512	1.50	2010	Ikeda-Saito	
	h iGluR6 + drug	3FVO	512	1.50	2010	Ikeda-Saito	
	h iGluR6 + glu	2ZNS	256	2.00	2009	Ikeda-Saito	
	h iGluR6 + toxin	2ZNT	256	1.60	2009	Ikeda-Saito	
	h iGluR6 + toxin	2ZNU	256	1.80	2009	Ikeda-Saito	
	iGluR6 + glu	3g3f	518	1.38	2009	Mayer	
	iGluR6 mut + glu	3g3g	518	1.30	2009	Mayer	
	iGluR6 mut + glu	3g3h	518	1.50	2009	Mayer	
	iGluR6 mut + glu	3g3i	518	1.37	2009	Mayer	
	iGluR6 mut + glu	3g3j	518	1.32	2009	Mayer	
	iGluR6 mut + glu	3g3k	518	1.24	2009	Mayer	
	iGluR6	3h6g	790	2.70	2009	Mayer	
	iGluR6	3h6h	790	2.90	2009	Mayer	
	iGluR6 mut	2I0B	777	1.96	2007	Mayer	
	iGluR6 mut	2I0C	518	2.25	2006	Mayer	
	iGluR6 + glu	1s50	259	1.65	2005	Mayer	
	iGluR6 + glu	1s7y	518	1.75	2005	Mayer	
	iGluR6 + drug	1s9t	518	1.80	2005	Mayer	
	iGluR6 + glu	1sd3	518	1.80	2005	Mayer	
	iGluR6 mut + DA	1tt1	518	1.93	2005	Mayer	
	iGluR6 + glu	1txf	528	2.10	2005	Mayer	
	iGluR6 mut + DA	1YAE	1872	3.11	2005	Heinemann	PNAS 2005, 102, 1708

		PDB #	Amino acids	Resolution (Å)	Year	Lab	Citation
KAINATE receptors							
GluK3	iGluR7 + drug	4NWC	258	2.01	2014	Kastrup	ChemMedChem 2014, 2254
	iGluR7 + drug	4NWD	258	2.60	2014	Kastrup	
	iGluR7 + glu	4MH5	258	1.65	2013	Kastrup	
	iGluR7 + drug	4IGR	258	2.65	2013	Kastrup	
	iGluR7 + KA	3U92	514	1.90	2012	Mayer	
	iGluR7 + glu	3U93	514	1.88	2012	Mayer	
	iGluR7 + glu	3U94	1028	1.96	2012	Mayer	
	iGluR7 + drug	4G8N	258	2.30	2012	Kastrup	
	iGluR7 + KA	4eow	258	2.35	2012	Kastrup	
	iGluR7 + glu	3s9e	516	1.60	2011	Kastrup	
	iGluR7	3olz	796	2.75	2010	Mayer	
GluK5	KA2 / iGluR6 dimer	3ql4	1576	2.91	2011	Mayer	
	KA2 / iGluR6 dimer	3qlu	1576	2.91	2011	Mayer	
	KA2 / iGluR6 tetramer	3qlv	3940	3.94	2011	Mayer	
	KA2	3om0	393	1.40	2010	Mayer	
	KA2	3om1	786	1.68	2010	Mayer	

			PDB #	Amino acids	Resolution (Å)	Year	Lab	Citation
AMPA receptors								
GluA1	*h*	iGluR1 + drug	3ua8	263	1.90	2012	Kallen	
GluA2	*um*	iGluR2 + drug	5h8s	789	1.70	2016	Lupardus	
		iGluR2 full length	4u1w	3296	3.25	2014	Gouaux	Cell 2014, 778
		iGluR2 full length + KA	4u2q	3296	3.52	2014	Gouaux	Cell 2014, 778
	hum	iGluR2	3rn8	840	1.70	2011	Timm	
	hum	iGluR2	3rnn	876	1.75	2011	Timm	
	hum	iGluR2	3r7x	526	2.10	2011	Kallen	
		iGluR2 mut + KA	3t9h	774	2.02	2011	Oswald	
	rat	iGluR2 + drug	2xx8	789	1.55	2011	Yusaf	
	rat	iGluR2 + drug	2xx7	873	2.20	2011	Yusaf	
	rat	iGluR2 + drug	2xx9	789	1.97	2011	Yusaf	
	rat	iGluR2 + drug	2xxh	789	1.50	2011	Yusaf	
	rat	iGluR2 + drug	2xxi	789	1.60	2011	Yusaf	
	hum	iGluR2 + drug	2xhd	526	1.80	2010	Yusaf	
	hum	iGluR2	2wjx	1164	4.10	2009	Clayton	
	hum	iGluR2	2wjw	388	1.80	2009	Clayton	
		iGluR2 mut	2gfe	786	1.54	2006	Mayer	
		iGluR2 + glu	2cmo	526	2.65	2006	Kastrup	
		iGluR2 **TYR** mut + KA	2anj	263	2.10	2005	Kastrup	J. Biol. Chem. 2005, 35469
		iGluR2 mut Y702 + drug	1SYH	263	1.80	2005	Kastrup	
		iGluR2 mut Y702 + drug	1SYI	526	2.10	2005	Kastrup	
		iGluR2 mut Y702 + KA	1XHY	263	1.85	2005	Kastrup	
		iGluR2 + AMPA	1MS7	789	1.97	2003	Kastrup / Gouaux	
		iGluR2 mut + KA	1P1N	263	1.60	2003	Mayer / Gouaux	
		iGluR2 mut + drug	1p1o	263	1.60	2003	Mayer / Gouaux	
		iGluR2 mut + AMPA	1p1q	789	2.00	2003	Mayer / Gouaux	
		iGluR2 mut + AMPA	1p1u	526	2.00	2003	Mayer / Gouaux	
		iGluR2 mut + AMPA	1p1w	526	1.80	2003	Mayer / Gouaux	
		iGluR2 + drug	1NNP	526	1.90	2003	Kastrup / Gouaux	
		iGluR2 + drug	1N0T	1052	2.10	2003	Kastrup / Gouaux	
		iGluR2 + ATPA	1NNK	263	1.85	2003	Kastrup / Gouaux	
		iGluR2 mut + drug	1lb9	526	2.30	2002	Mayer / Gouaux	
		iGluR2 mut + KA	1LBB	263	2.10	2002	Mayer / Gouaux	
		iGluR2 mut + drug	1lbc	789	1.80	2002	Mayer / Gouaux	
		iGluR2 + AMPA	1m5b	789	1.85	2002	Kastrup / Mayer / Gouaux	
		iGluR2 + AMPA	1m5c	263	1.65	2002	Kastrup / Mayer / Gouaux	
		iGluR2 + AMPA	1m5d	263	1.73	2002	Kastrup / Mayer / Gouaux	
		iGluR2 + AMPA	1m5e	789	1.46	2002	Kastrup / Mayer / Gouaux	
		iGluR2 + drug	1m5f	789	1.95	2002	Kastrup / Mayer / Gouaux	
		iGluR2 + KA	1fw0	263	1.90	2000	Gouaux	
		iGluR2 + KA	1ftk	279	1.60	2000	Gouaux	
		iGluR2 + glu	1ftj	789	1.90	2000	Gouaux	
		iGluR2 + glu	1ftl	526	1.80	2000	Gouaux	
		iGluR2 + AMPA	1ftm	789	1.70	2000	Gouaux	
		iGluR2	1fto	526	2.00	2000	Gouaux	
		iGluR2 + KA	1gr2	279	1.90	1998	Gouaux	Nature 1998, 913

		PDB #	Amino acids	Resolution (Å)	Year	Lab	Citation
NMDA receptors							
GluN1	*h* iGluN1 / GluN2A	5h8q	578	1.90	2016	Lupardus	
	h iGluN1 / GluN2A	5h8r	578	2.09	2016	Lupardus	
GluN2A	*h* iGluN1 / GluN2A	5h8q	578	1.90	2016	Lupardus	
	h iGluN1 / GluN2A	5h8r	578	2.09	2016	Lupardus	
	` NR2A	5h8h	578	2.23	2016	Lupardus	
	h NR2A	5h8n	578	2.50	2016	Lupardus	
	h NR2A	5h8f	578	1.81	2016	Lupardus	
	h NR2A	5i1j	578	2.44	2016	Lupardus	
	h NR2A	5i1k	578	2.86	2016	Lupardus	
	h NR2A	5i1n	578	2.12	2016	Lupardus	
	h NR2A	3nfl	492	1.91	2011	Wolff	
GluN2B	*h* GluN2B	5ewj	1508	2.77	2016	Pandit	
	h GluN2B	5ewL	1508	2.98	2016	Pandit	
	h GluN2B	5ewm	1508	2.76	2016	Pandit	

Appendix B

NMR data of kainoids and comparison

Table S3–1. NMR comparison between obtained kainoids and reported data

Compound	NMR	This work	Ref
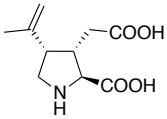 **1, kainic acid**	^{1}H NMR (D_2O)	(400 MHz) δ 5.08 (bs, 1H), 4.78 (bs, 1H), 4.18 (d, *J* = 3.5 Hz, 1H), 3.67 (dd, *J* = 11.9, 7.3 Hz, 1H), 3.46 (t, *J* = 11.4 Hz, 1H), 3.18 – 3.00 (m, 2H), 2.53 (dd, *J* = 16.9, 6.3 Hz, 1H), 2.44 (dd, *J* = 16.8, 8.2 Hz, 1H), 1.78 (s, 3H).	(300 MHz) δ 5.11 (s, 1H), 4.82 (s, 1H), 4.15 (d, *J* = 3.1 Hz, 1H), 3.70 (dd, *J* = 11.7, 7.4 Hz, 1H) 3.50 (dd, *J* = 11.7, 10.5 Hz, 1H), 3.18−3.03 (m, 2H), 2.45 (dd, *J* = 15.6, 6.4 Hz, 1H), 2.34 (dd, *J* = 15.6, 8.2 Hz, 1H), 1.83 (s, 3H).
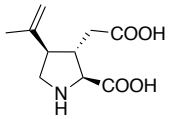 **2, *allo*-kainic acid**	^{1}H NMR (D_2O)	(400 MHz) δ 4.95 (bs, 1H), 4.94 (m, 1H), 3.92 (d, *J* = 8.1 Hz, 1H), 3.51 (dd, *J* = 11.8, 7.8 Hz, 1H), 3.33 (dd, *J* = 11.8, 10.6 Hz, 1H), 2.86 (dt, *J* = 10.5, 8.5 Hz, 1H), 2.72 – 2.59 (m, 2H), 2.41 – 2.32 (m, 1H), 1.73 (bs, 3H).	(500 MHz) δ 4.99 (bs, 1H), 4.98 (bs, 1H), 3.93 (d, *J* = 8.7 Hz, 1H), 3.57 (dd, *J* = 11.8, 8.1 Hz, 1H), 3.36 (t, *J* = 11.2 Hz, 1H), 2.89 (dt, *J* = 10.0, 8.1 Hz, 1H), 2.70 (dd, *J* = 15.0, 4.4 Hz, 1H), 2.68-2.65 (m, 1H), 2.45 (dd, *J* = 14.8, 7.2 Hz, 1H), 1.75 (s, 3H).
	^{13}C NMR (D_2O)	(101 MHz) δ 179.3, 173.7, 140.6, 114.6, 64.9, 51.5, 48.2, 42.6, 39.7, 17.7.	(125 MHz) δ 178.0, 173.6, 140.5, 115.1, 65.0, 51.5, 48.3, 42.4, 38.9, 18.0.
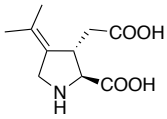 **3, *iso*-kainic acid**	^{1}H NMR (D_2O)	(400 MHz) δ 4.16 (d, *J* = 1.6 Hz, 1H), 4.07 (d, *J* = 14.6, 1H), 3.96 (dd, *J* = 14.6, 1.9 Hz, 1H), 3.55 (t, *J* = 6.9 Hz, 1H), 2.51 (dd, *J* = 14.7, 6.9 Hz, 1H), 2.44 (dd, *J* = 14.6, 6.9 Hz, 1H), 1.74 (bs, 3H), 1.65 (bs, 3H).	(250 MHz) 4.15 (d, *J* = 1.2 Hz, 1H), 4.06 (d, *J* = 14.9 Hz, 1H), 3.94 (d, *J* = 14.9 Hz, 1H), 3.55 (td, *J* = 6.8, 1.2 Hz, 1H), 2.54 (dd, *J* = 14.8, 6.8 Hz, 1H), 2.46 (dd, *J* = 14.8, 6.8 Hz, 1H), 1.71 (s, 3H), 1.62 (s, 3H).
	^{13}C NMR (D_2O)	(101 MHz) δ 179.7, 173.7, 129.8, 125.7, 66.4, 46.7, 42.1, 41.2, 20.4, 20.3.	(126 MHz) δ 178.1, 174.1, 131.0, 126.0, 66.7, 47.4, 42.2, 39.8, 21.2, 20.9.
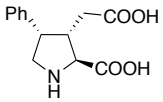 **(+)-Phenylkainic acid, 4**	^{1}H NMR (D_2O)	(400 MHz) δ 7.49 – 7.34 (m, 3H), 7.27 – 7.18 (m, 2H), 4.05 (d, *J* = 7.3 Hz, 1H), 3.94 (dd, *J* = 11.4, 7.8 Hz, 1H), 3.87 (q, *J* = 7.8 Hz, 1H), 3.72 (dd, *J* = 11.4, 8.1 Hz, 1H), 3.15 (q, *J* = 7.2 Hz, 1H), 2.38 (dd, *J* = 16.3, 6.5 Hz, 1H), 2.02 (dd, *J* = 16.3, 8.7 Hz, 1H).	(500 MHz) δ 7.43-7.33 (m, 3H), 7.23 (d, *J* = 7.5 Hz, 2H), 4.00 (d, *J* = 6.9 Hz, 1H), 3.91 (dd, *J* = 12.0, 8.0 Hz, 1H), 3.83 (q, *J* = 8.0 Hz, 1H), 3.69 (dd, *J* = 12.0, 8.0 Hz, 1H), 3.09 (ddt, *J* = 8.6, 8.0, 6.9 Hz, 1H), 2.29 (dd, *J* = 16.0, 6.9 Hz, 1H), 1.91 (dd, *J* = 16.0, 8.6 Hz, 1H).
	^{13}C NMR (D_2O)	(101 MHz) δ 178.5, 173.3, 136.2, 128.8, 128.2, 127.6, 65.1, 48.0, 44.8, 44.0, 35.7.	(126 MHz) δ 181.9, 176.2, 139.1, 131.2, 131.0, 130.4, 67.9, 50.9, 47.6, 47.0, 38.9.

Table S3–2 Rules for assigning C3,4 configuration of Kainoids[113]

	C3,4–*cis* kainoid	C3,4-*trans* kainoid
	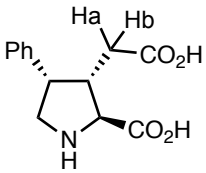 C3,4–*cis*	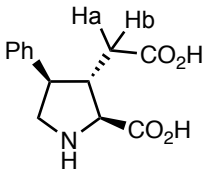 C3,4–*trans*
Rules	δH_a–δH_b (3,4-*cis*) > δH_a–δH_b (3,4-*trans*)	
Reported data (300 MHz, D_2O)	δ $H_{a\text{-}b}$ (3,4-*cis*) = 0.37 ppm	δ $H_{a\text{-}b}$ (3,4-*cis*) = 0.18 ppm
Experimental data in this work (400 MHz, D_2O)	δ $H_{a\text{-}b}$ = 0.36 ppm	–

1D NOE Experiments and Spectra

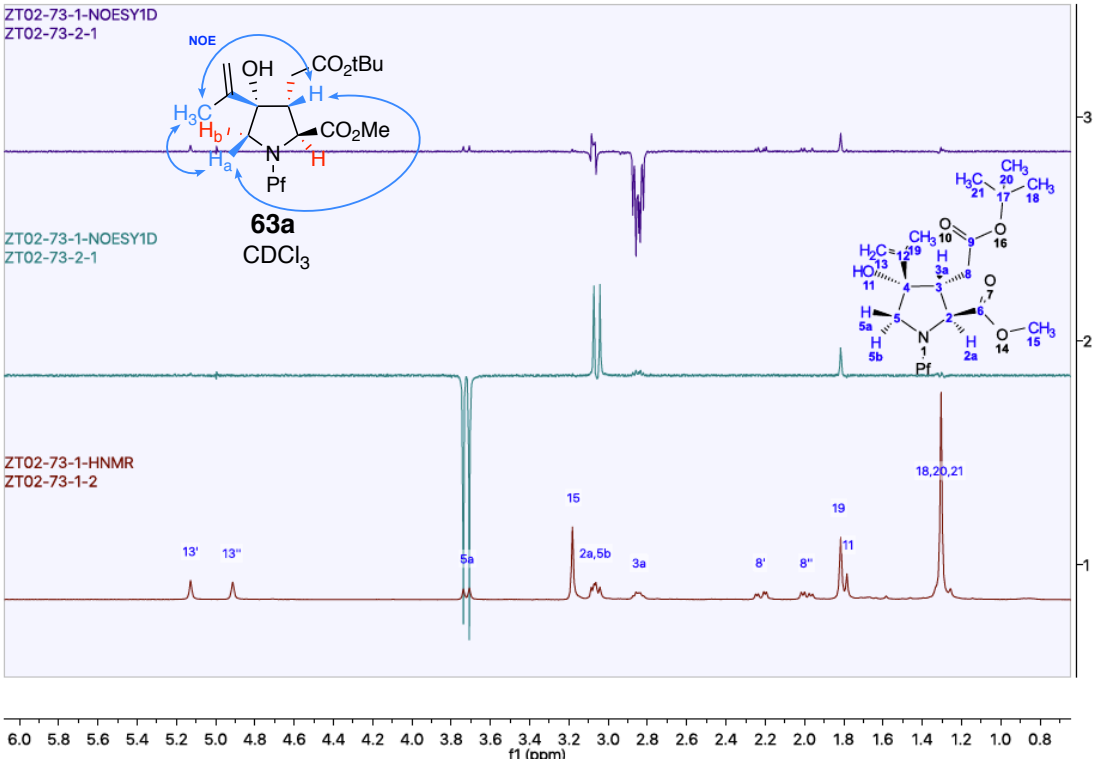

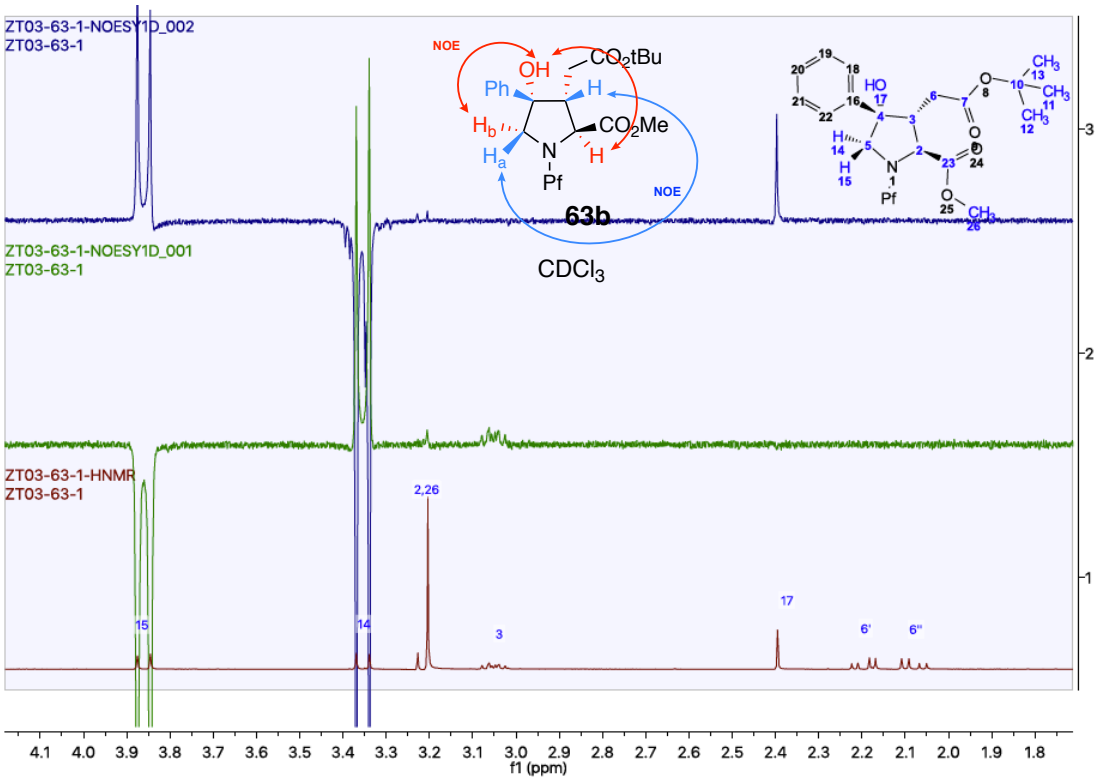

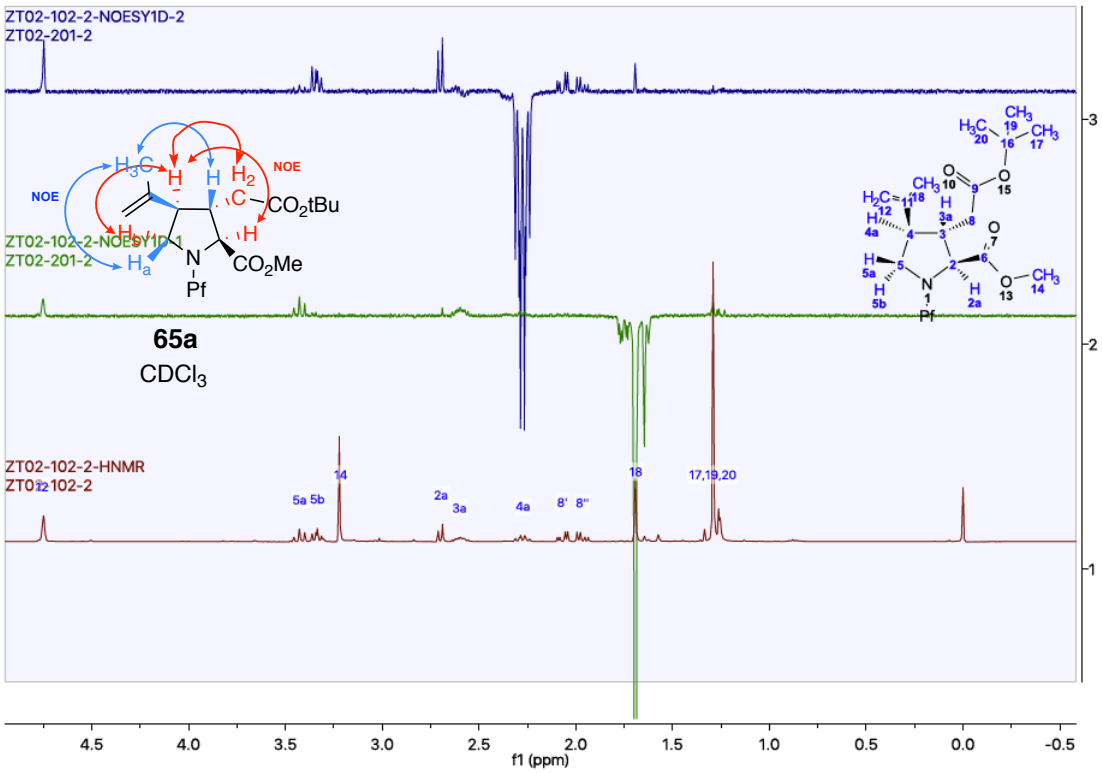
ZT02-102-2-NOESY1D-2
ZT02-201-2
NOE
NOE
CO2tBu
CO2Me
Pf
ZT02-102-2-NOESY1D-1
ZT02-201-2
65a
CDCl3
ZT02-102-2-HNMR
ZT02-102-2
5a 5b
14
2a
3a
4a
8' 8''
18
17,19,20
4.5
4.0
3.5
3.0
2.5
2.0
1.5
1.0
0.5
0.0
-0.5
f1 (ppm)

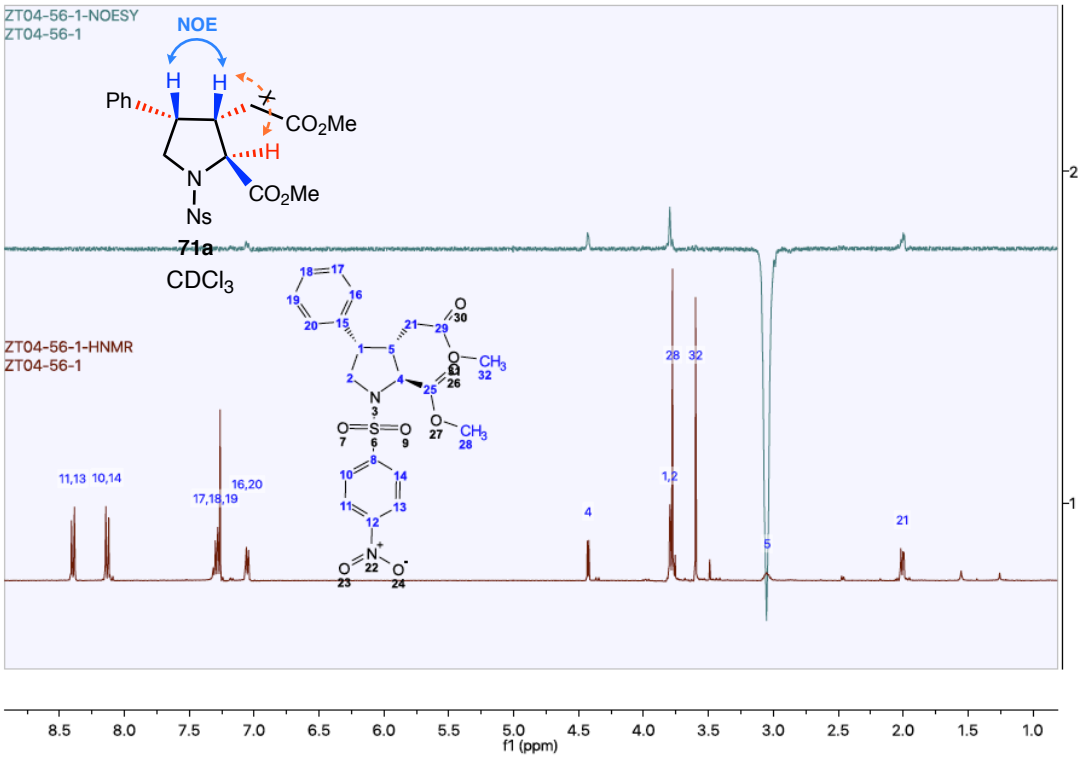
ZT04-56-1-NOESY
ZT04-56-1
NOE
Ph
CO2Me
CO2Me
Ns
71a
CDCl3
ZT04-56-1-HNMR
ZT04-56-1
11,13
10,14
17,18,19
16,20
4
1,2
28
32
5
21
8.5
8.0
7.5
7.0
6.5
6.0
5.5
5.0
4.5
4.0
3.5
3.0
2.5
2.0
1.5
1.0
f1 (ppm)

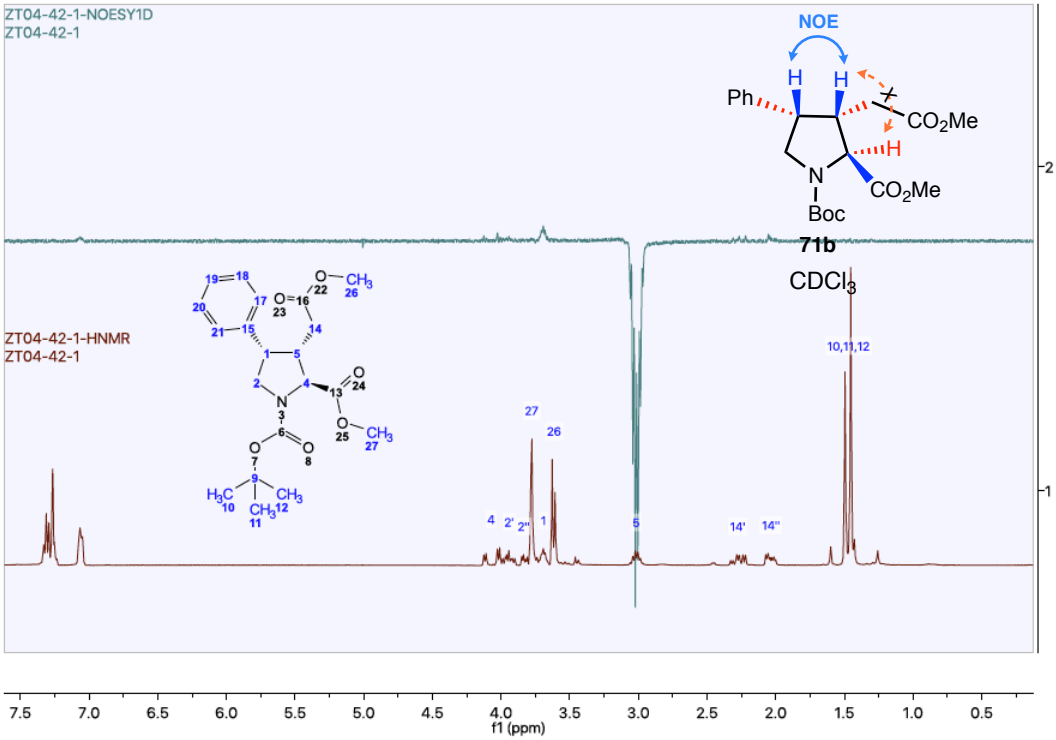
ZT04-42-1-NOESY1D
ZT04-42-1
NOE
Ph
H
H
CO2Me
H
N
Boc
CO2Me
71b
CDCl3
ZT04-42-1-HNMR
ZT04-42-1
10,11,12
27
26
4
2'
2"
1
5
14'
14"
f1 (ppm)

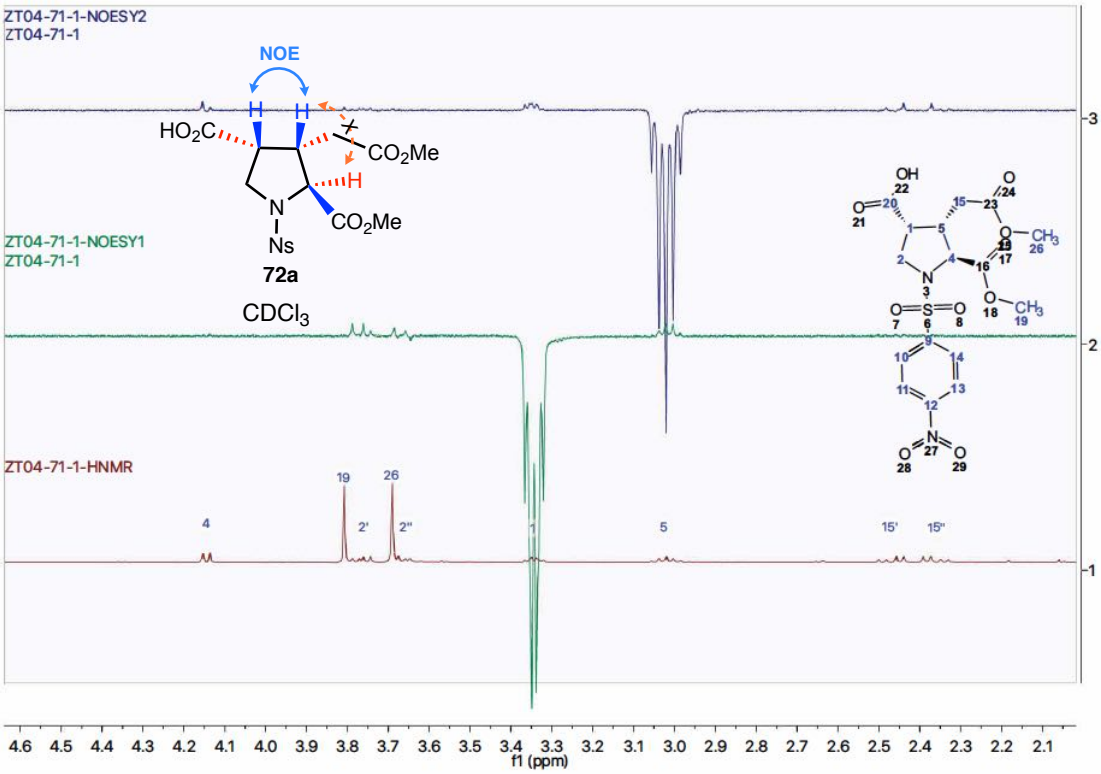
ZT04-71-1-NOESY2
ZT04-71-1
NOE
HO2C
H
H
CO2Me
H
N
Ns
CO2Me
72a
CDCl3
ZT04-71-1-NOESY1
ZT04-71-1
ZT04-71-1-HNMR
19
26
4
2'
2"
1
5
15'
15"
f1 (ppm)

NMR spectra

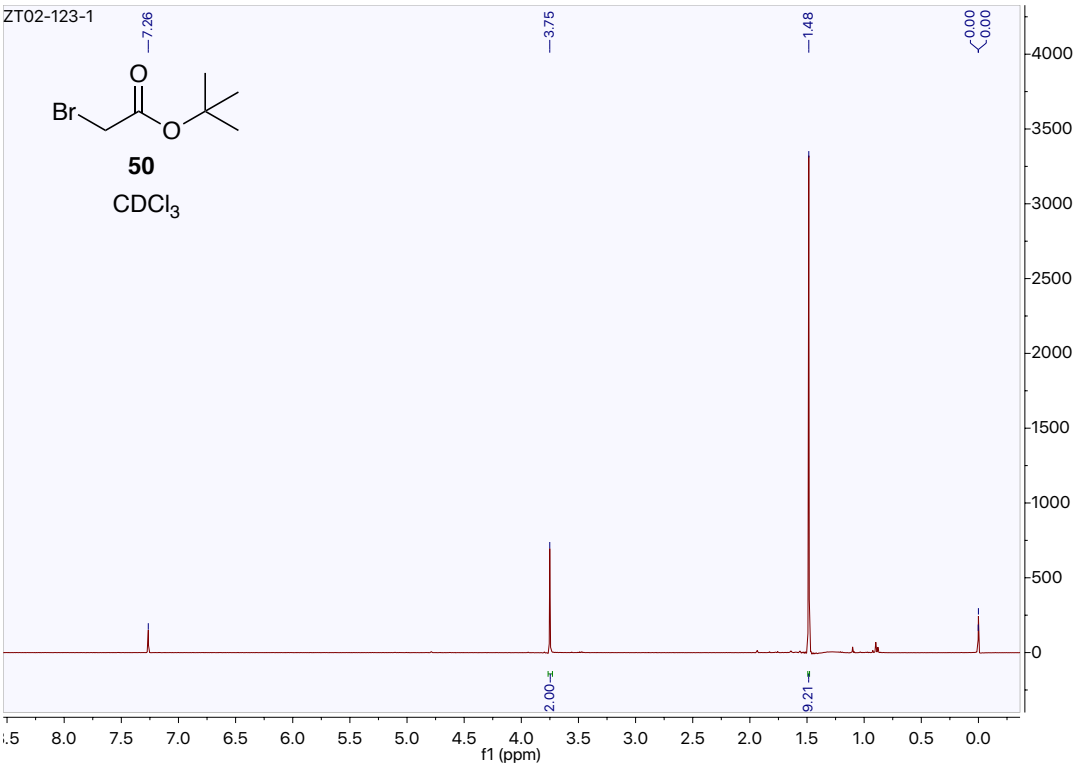
ZT02-123-1
7.26
3.75
1.48
0.00
0.00
Br
O
O
50
CDCl3
2.00
9.21
f1 (ppm)

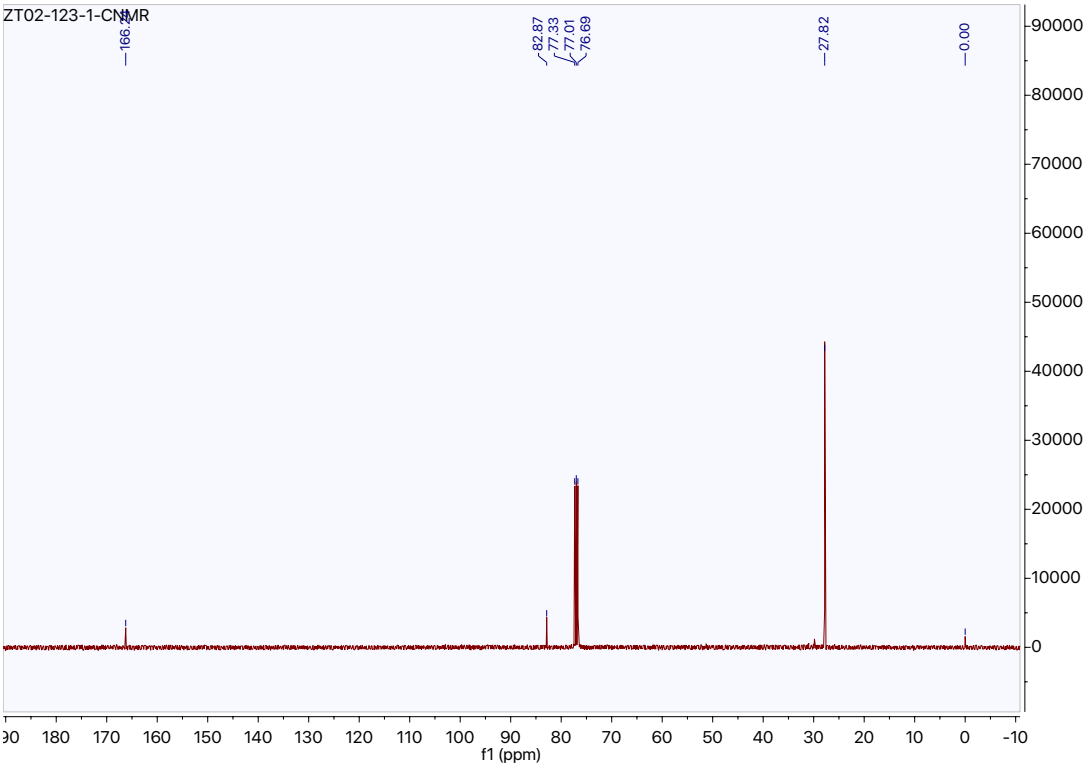
ZT02-123-1-CNMR
166.7
82.87
77.33
77.01
76.69
27.82
0.00
f1 (ppm)

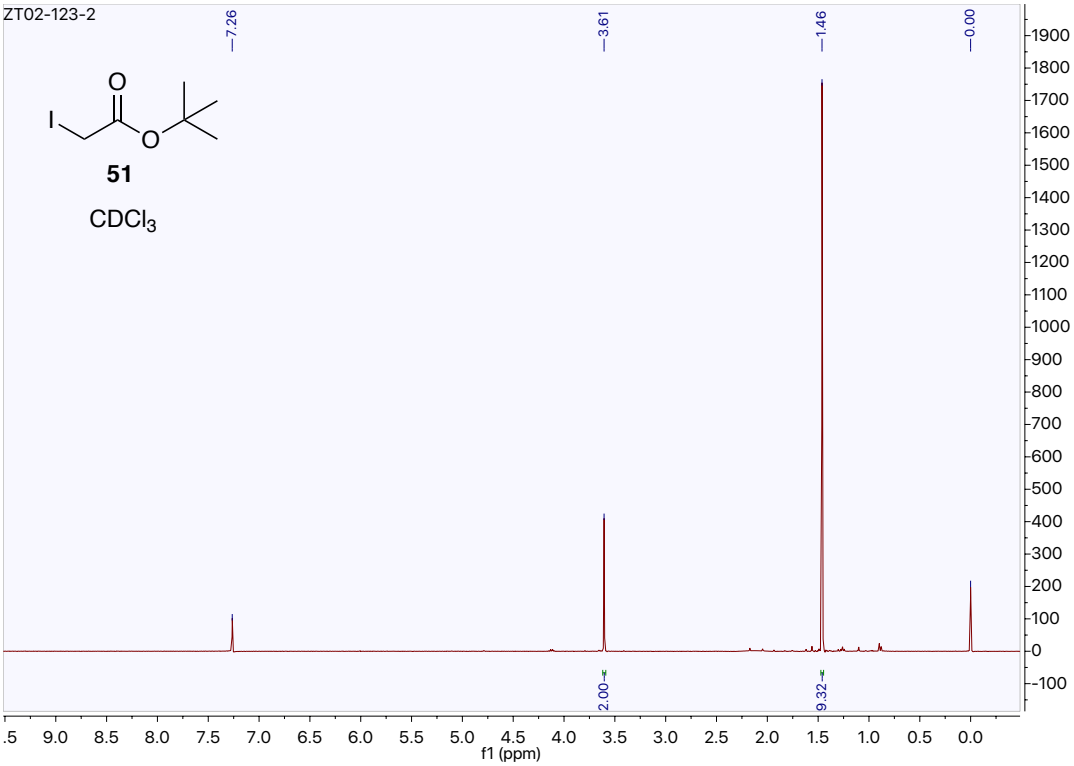
ZT02-123-2
7.26
3.61
1.46
0.00
I
O
O
51
CDCl3
2.00
9.32
f1 (ppm)

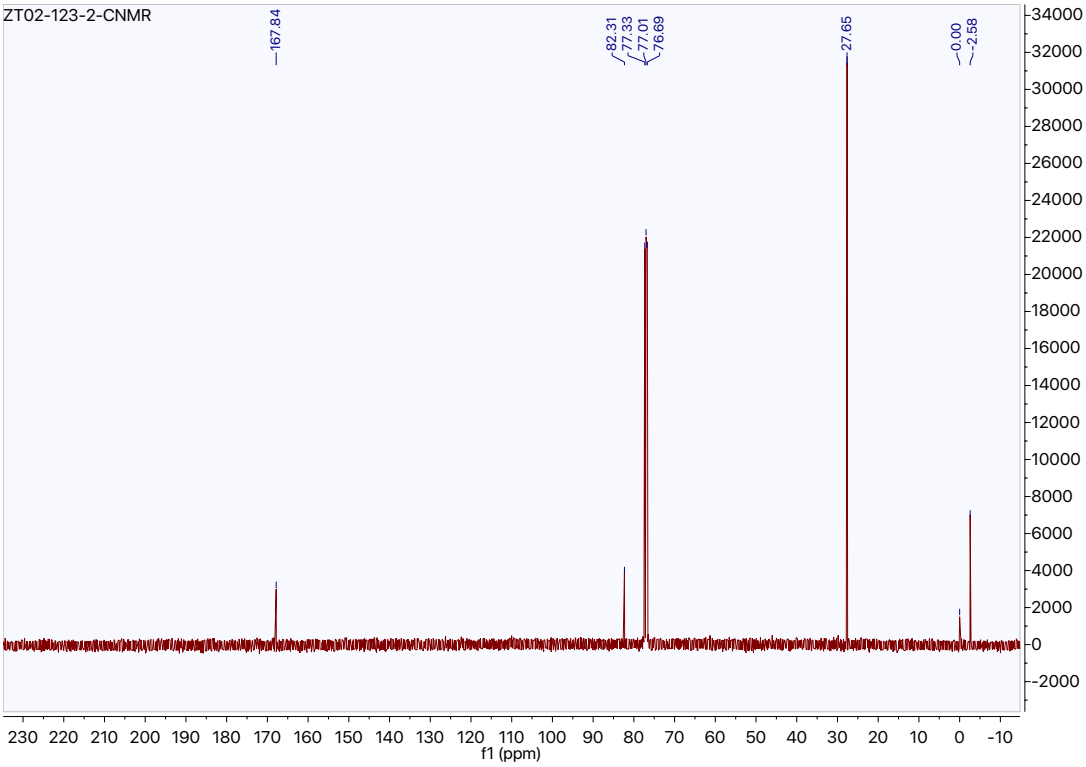
ZT02-123-2-CNMR
167.84
82.31
77.33
77.01
76.69
27.65
0.00
-2.58
f1 (ppm)

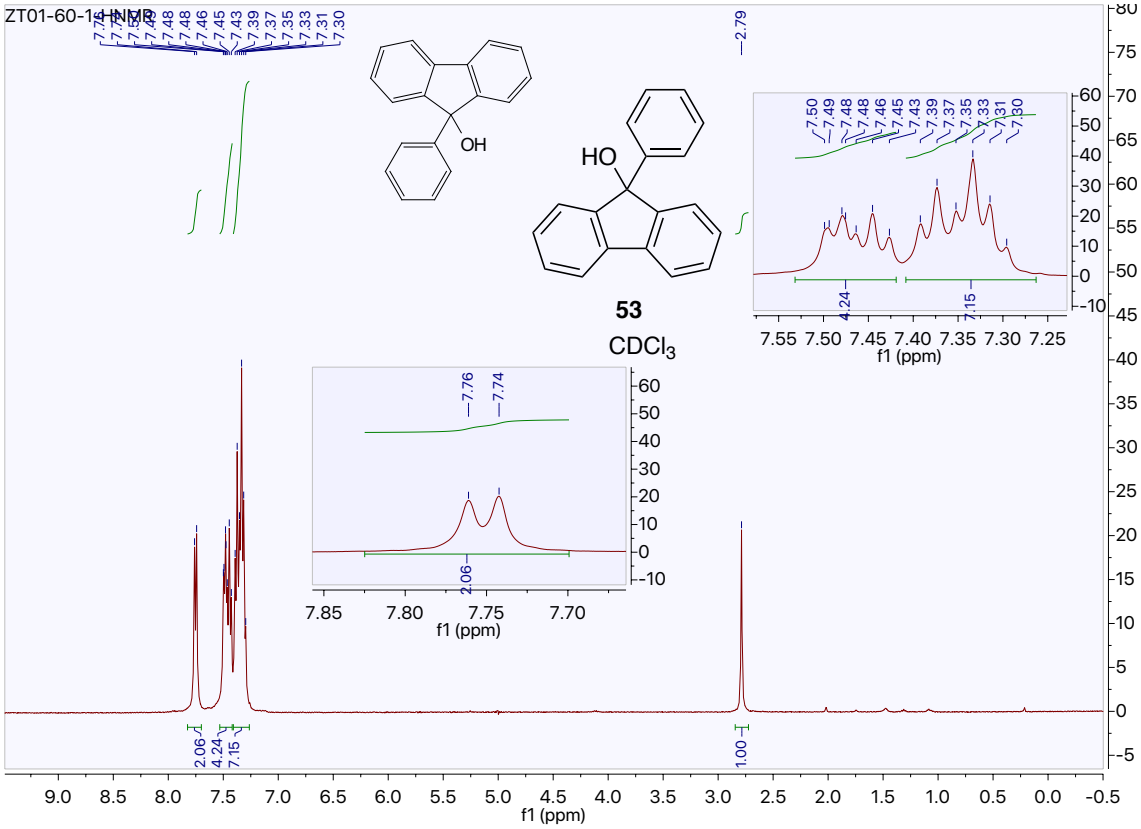
ZT01-60-1-1H NMR
OH
HO
53
CDCl3
f1 (ppm)

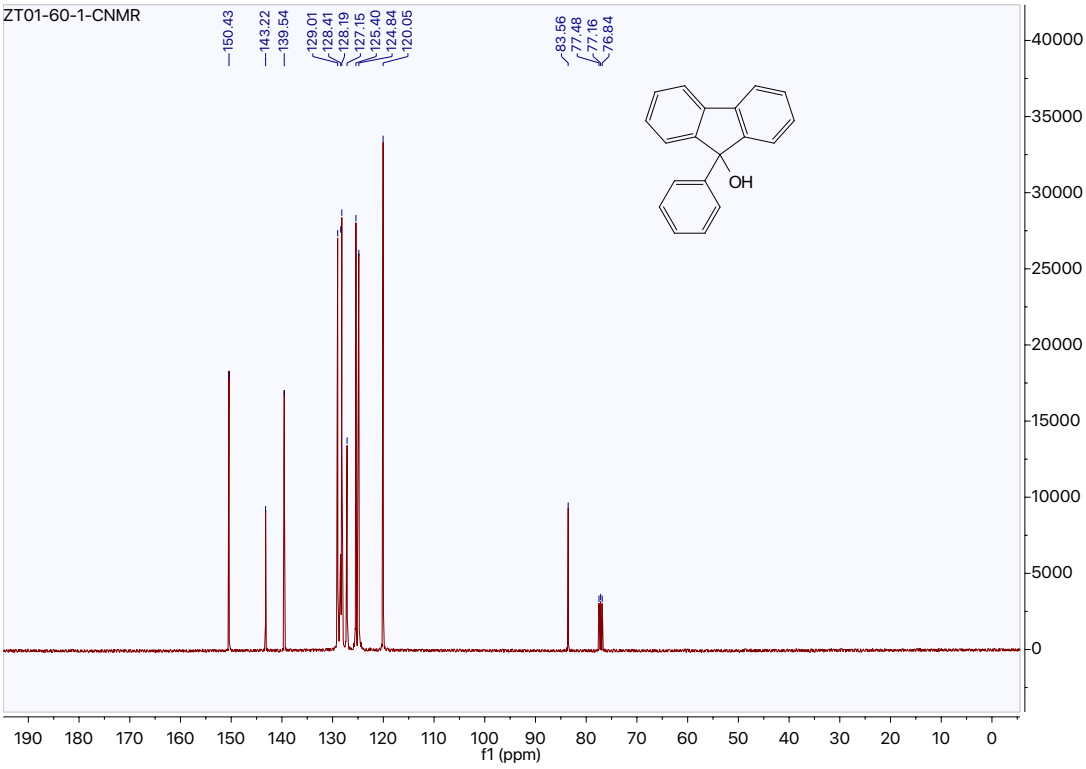
ZT01-60-1-CNMR
OH
f1 (ppm)

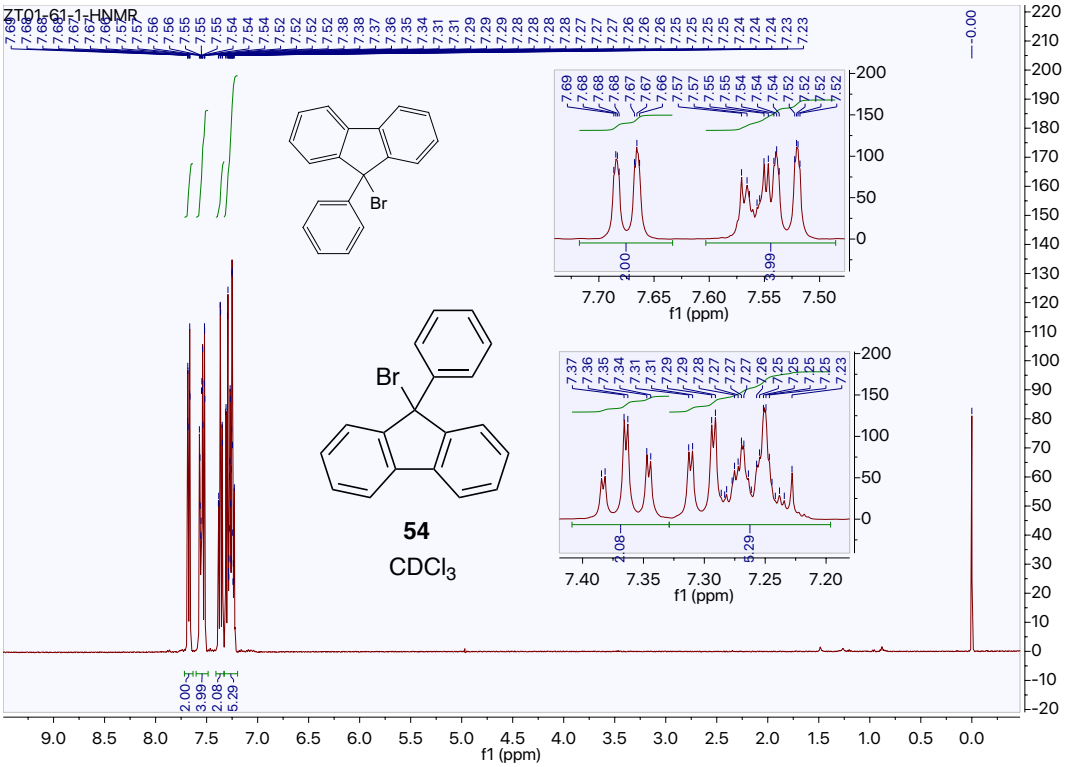
ZT01-61-1-HNMR
Br
Br
54
CDCl3
f1 (ppm)

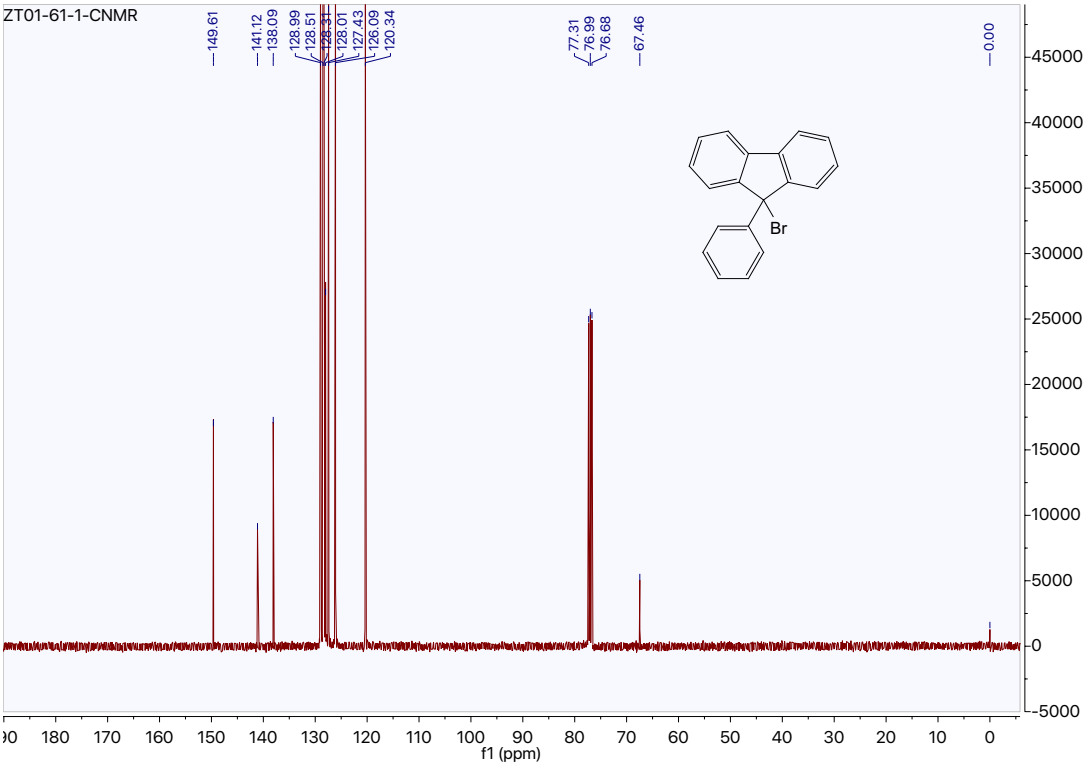
ZT01-61-1-CNMR
149.61
141.12
138.09
128.99
128.51
128.31
128.01
127.43
126.09
120.34
77.31
76.99
76.68
67.46
0.00
Br
f1 (ppm)

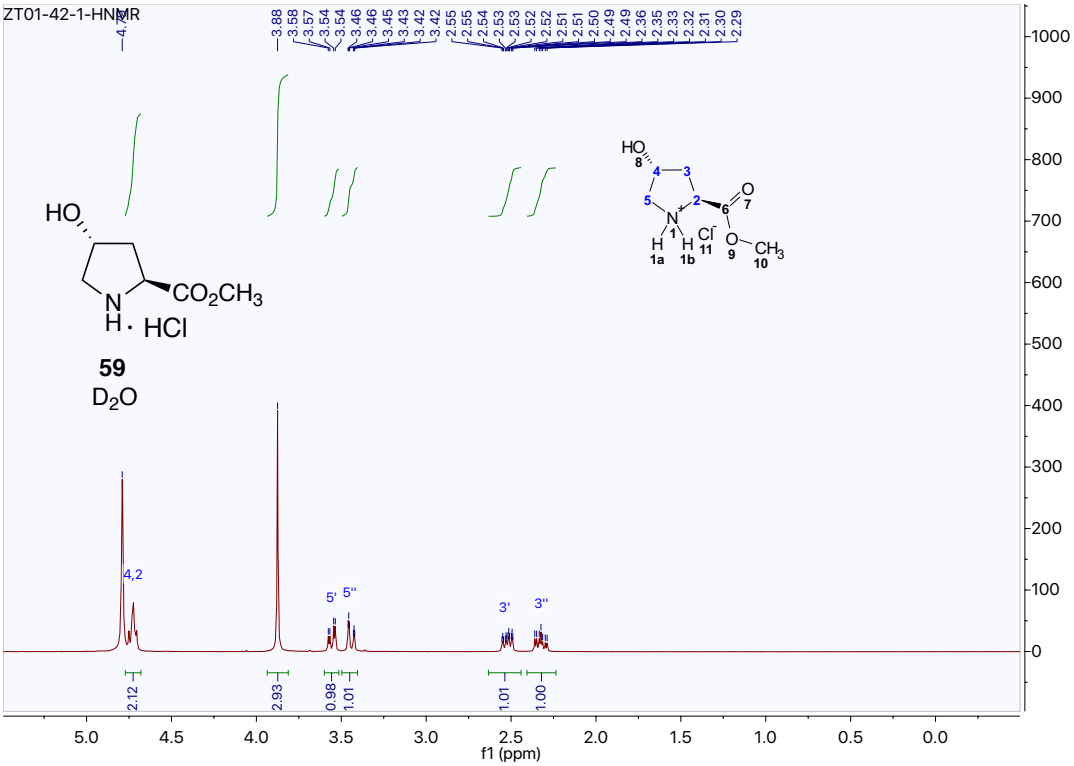
ZT01-42-1-HNMR
HO
CO2CH3
N
H · HCl
59
D2O
4,2
5'
5''
3'
3''
2.12
2.93
0.98
1.01
1.01
1.00
f1 (ppm)

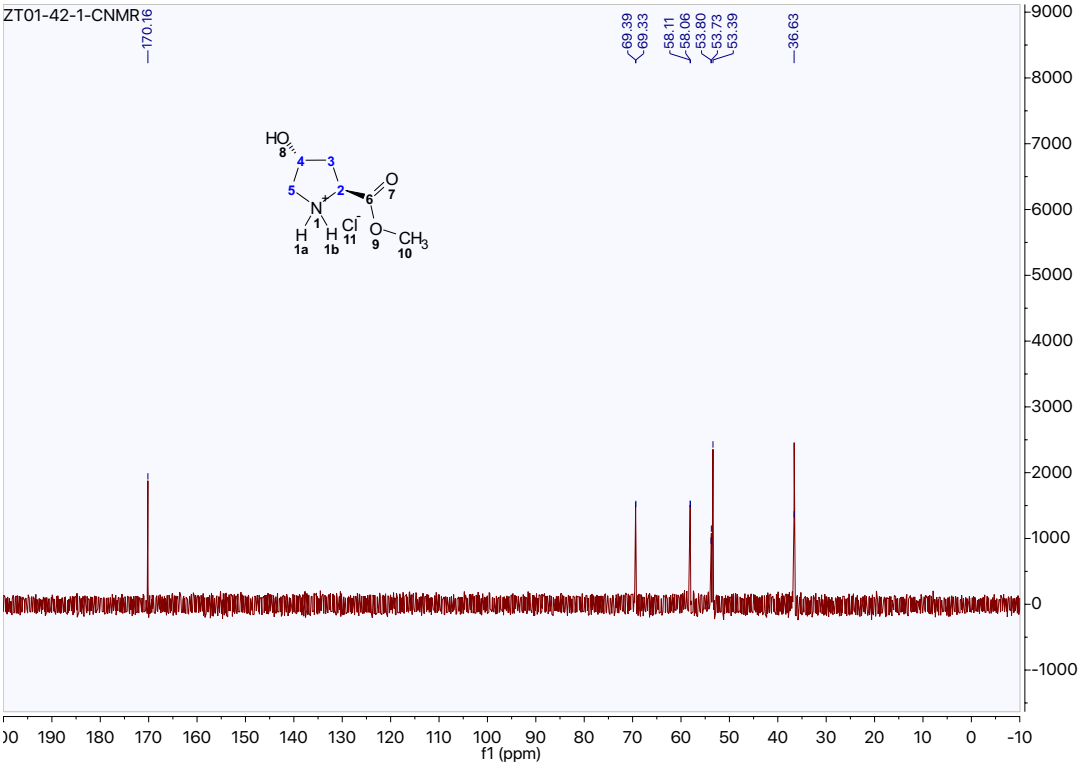
ZT01-42-1-CNMR
170.16
69.39
69.33
58.11
58.06
53.80
53.73
53.39
36.63
f1 (ppm)

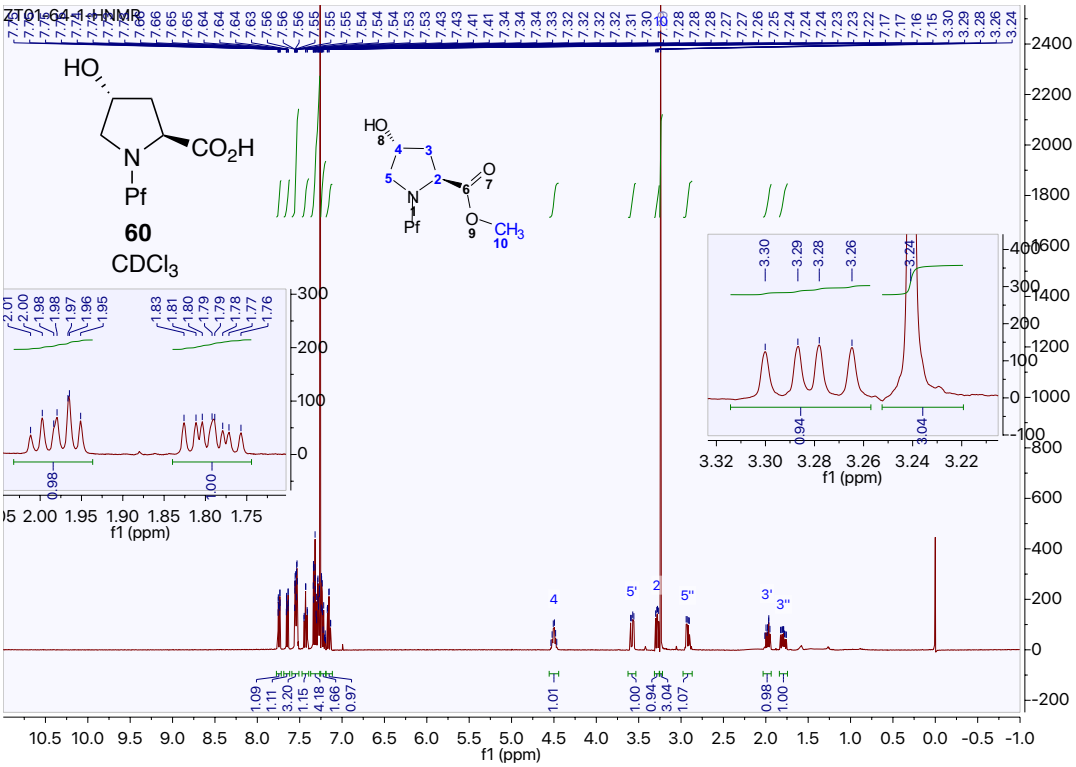
ZT01-64-1-1HNMR
HO
CO2H
N
Pf
60
CDCl3
f1 (ppm)

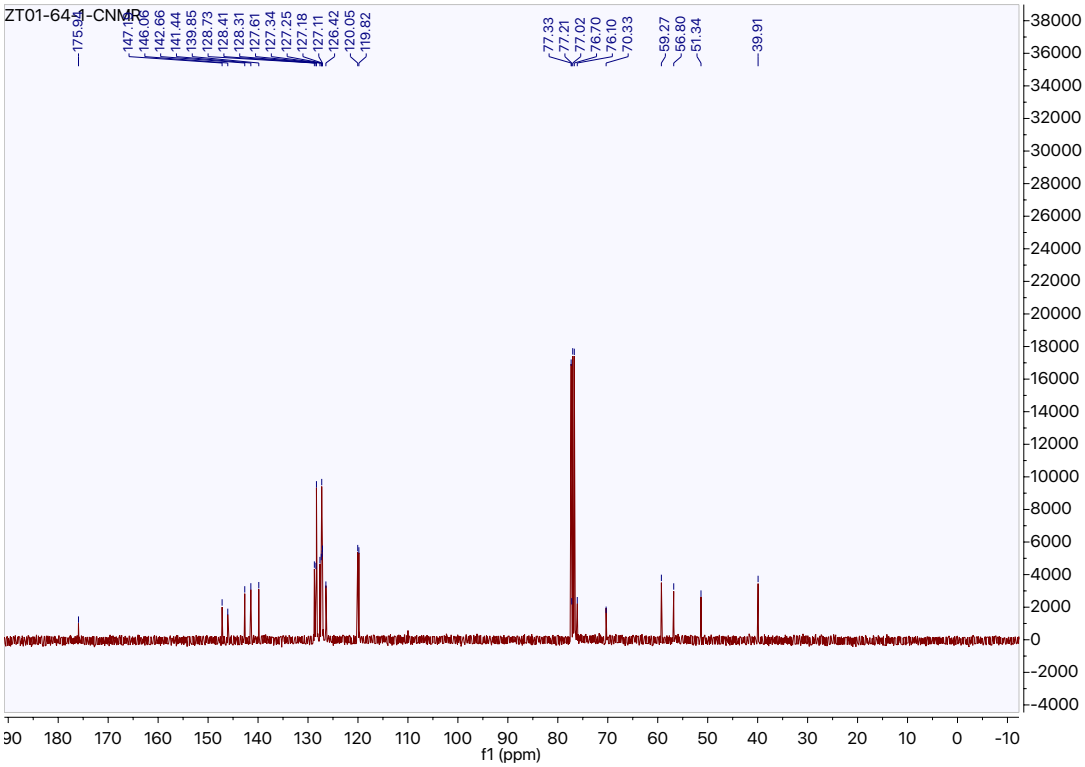
ZT01-64-1-CNMR
f1 (ppm)

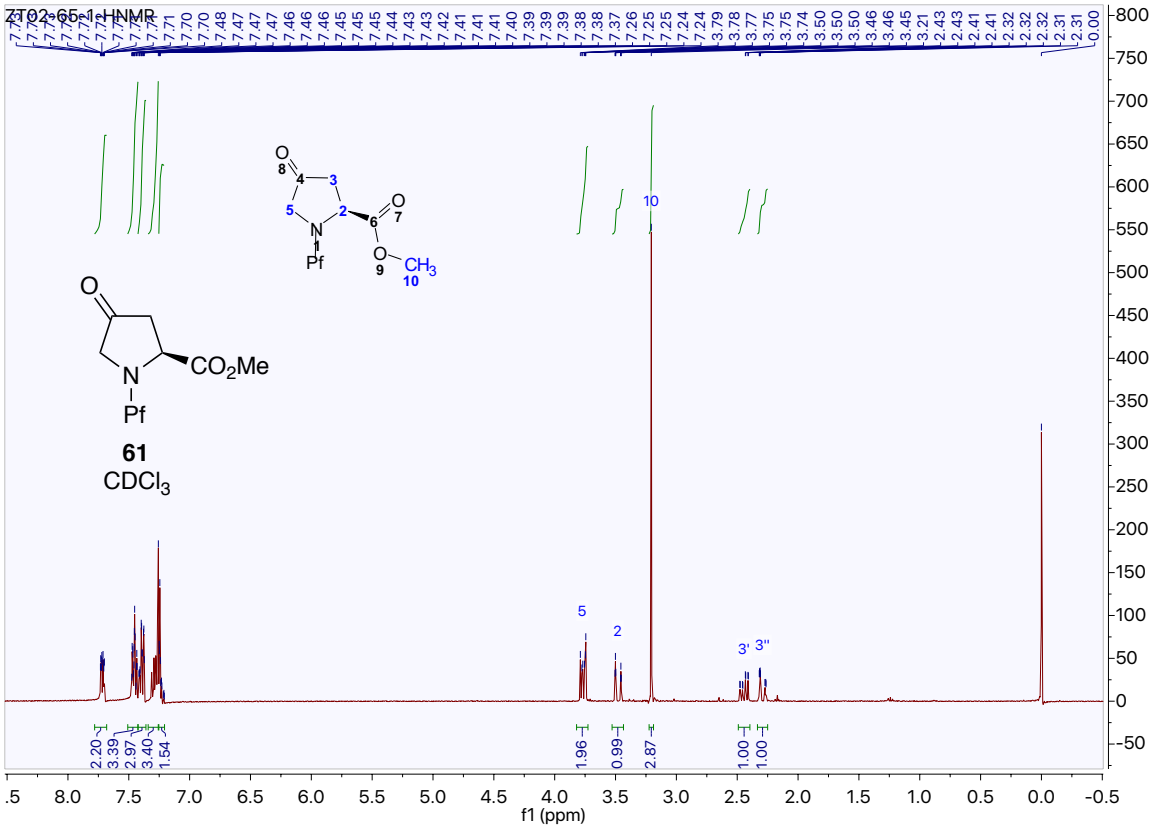
ZT02-65-1-1HNMR
61
CDCl3
CO2Me
Pf
f1 (ppm)

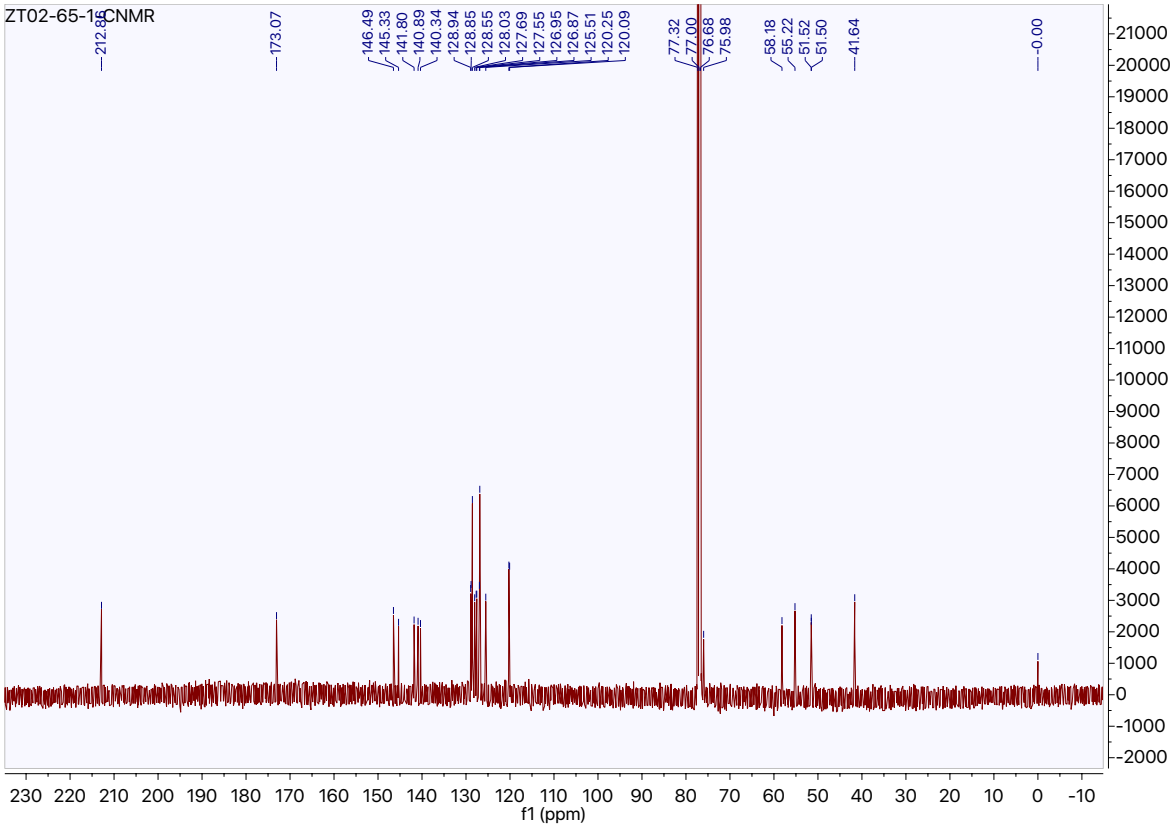
ZT02-65-1-13CNMR
f1 (ppm)

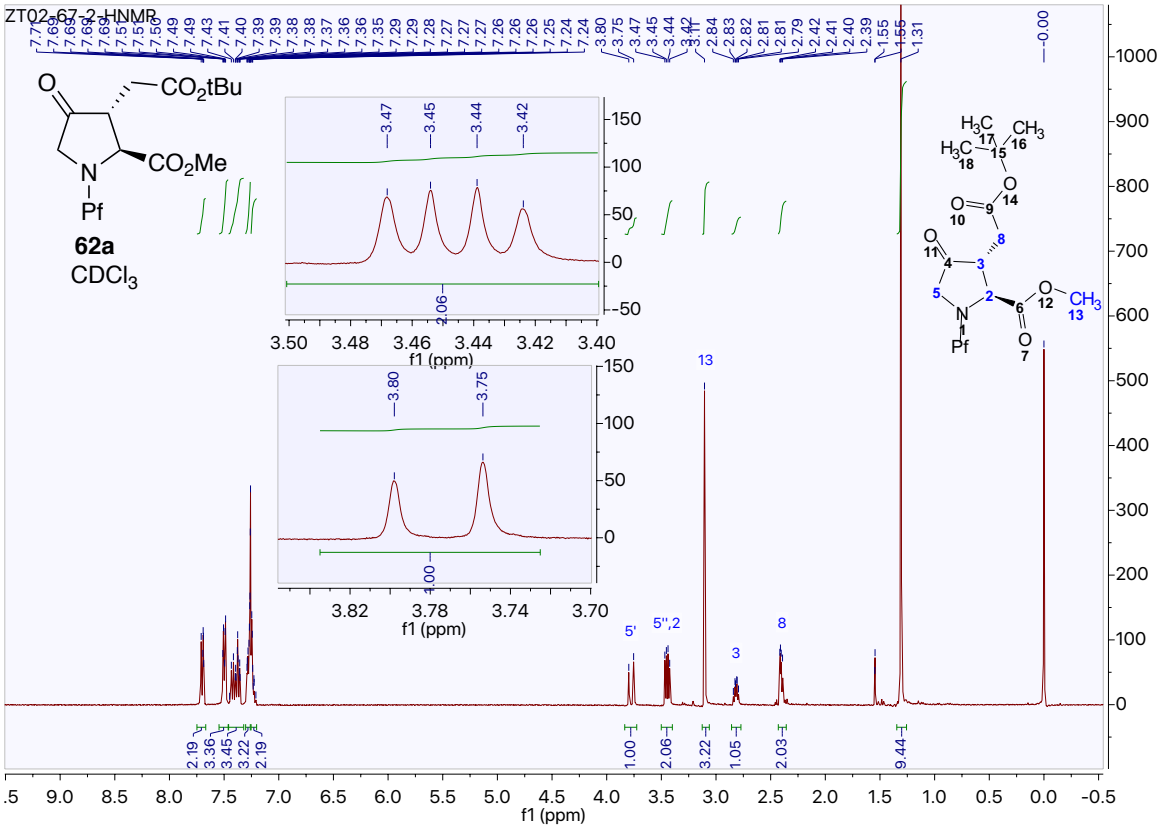
ZT02-67-2-HNMR
CO_2tBu
CO_2Me
Pf
62a
$CDCl_3$
f1 (ppm)

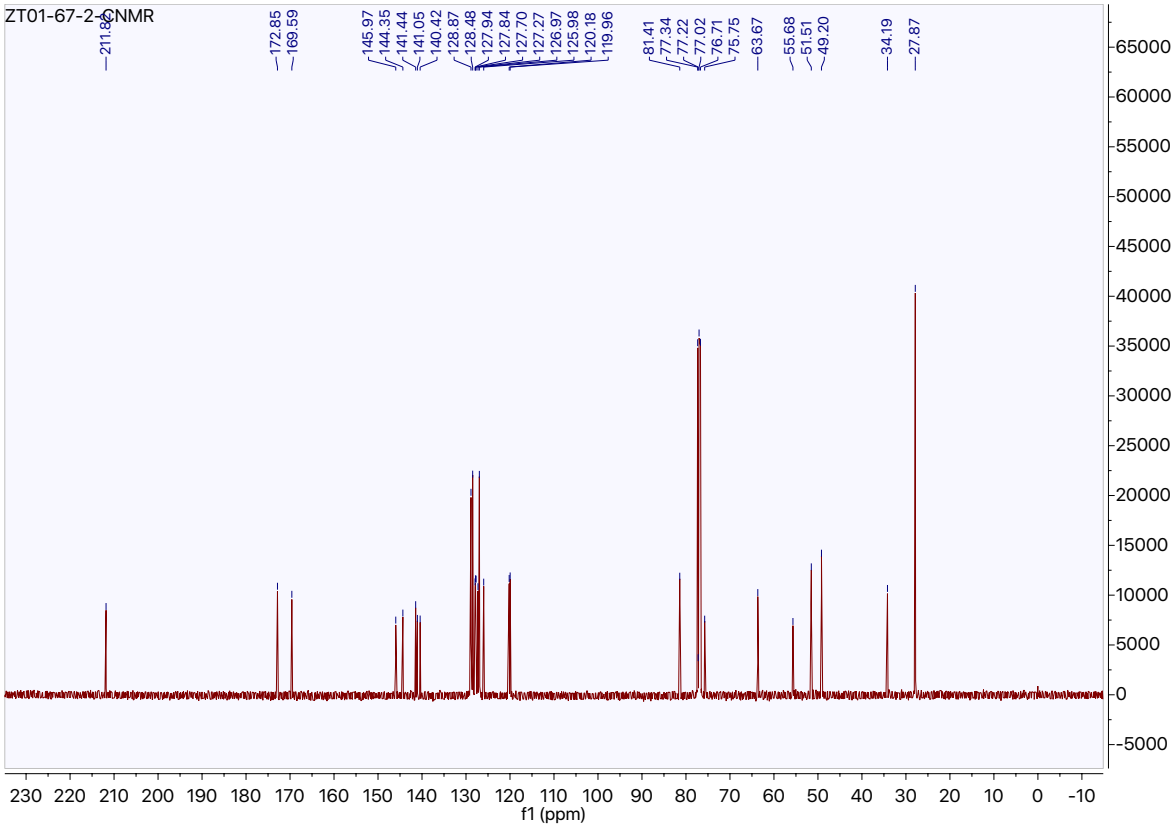
ZT01-67-2-CNMR
f1 (ppm)

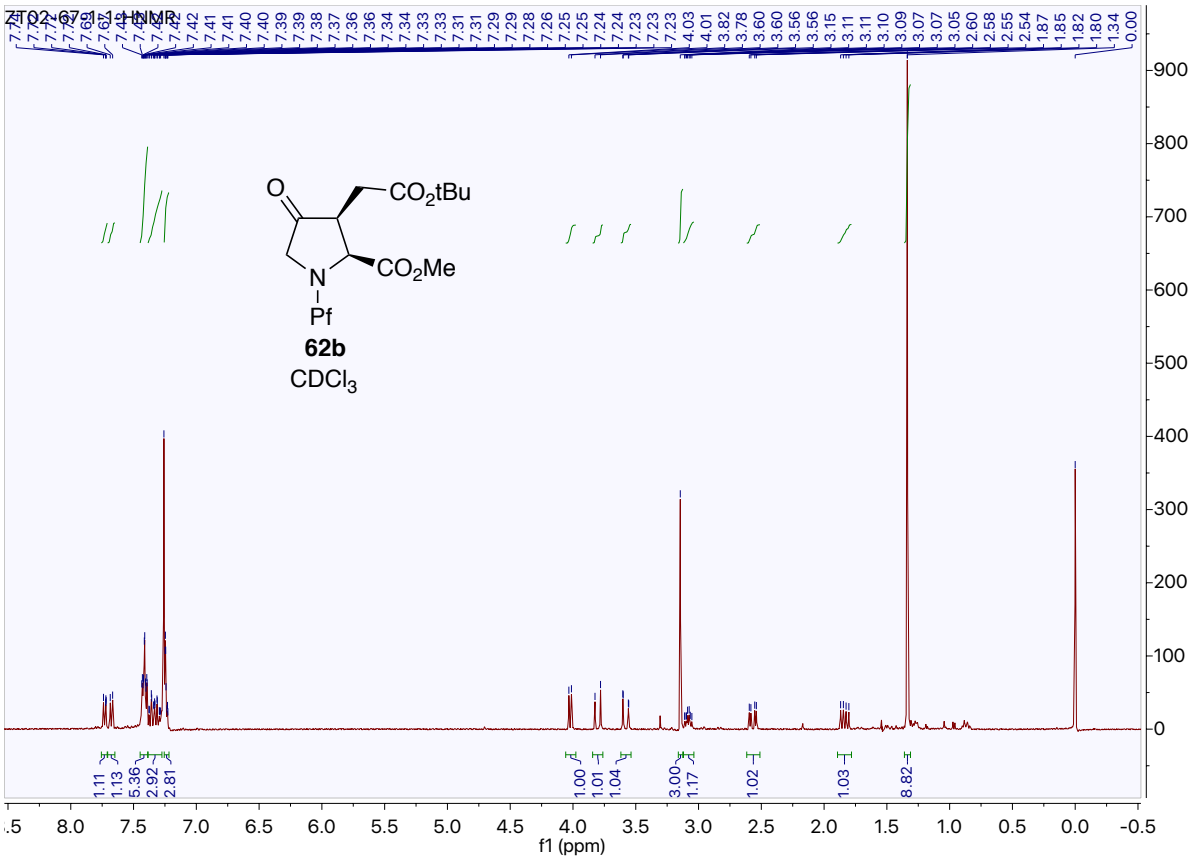
ZT02-67-1-1-HNMR
CO2tBu
CO2Me
N
Pf
62b
CDCl3
f1 (ppm)

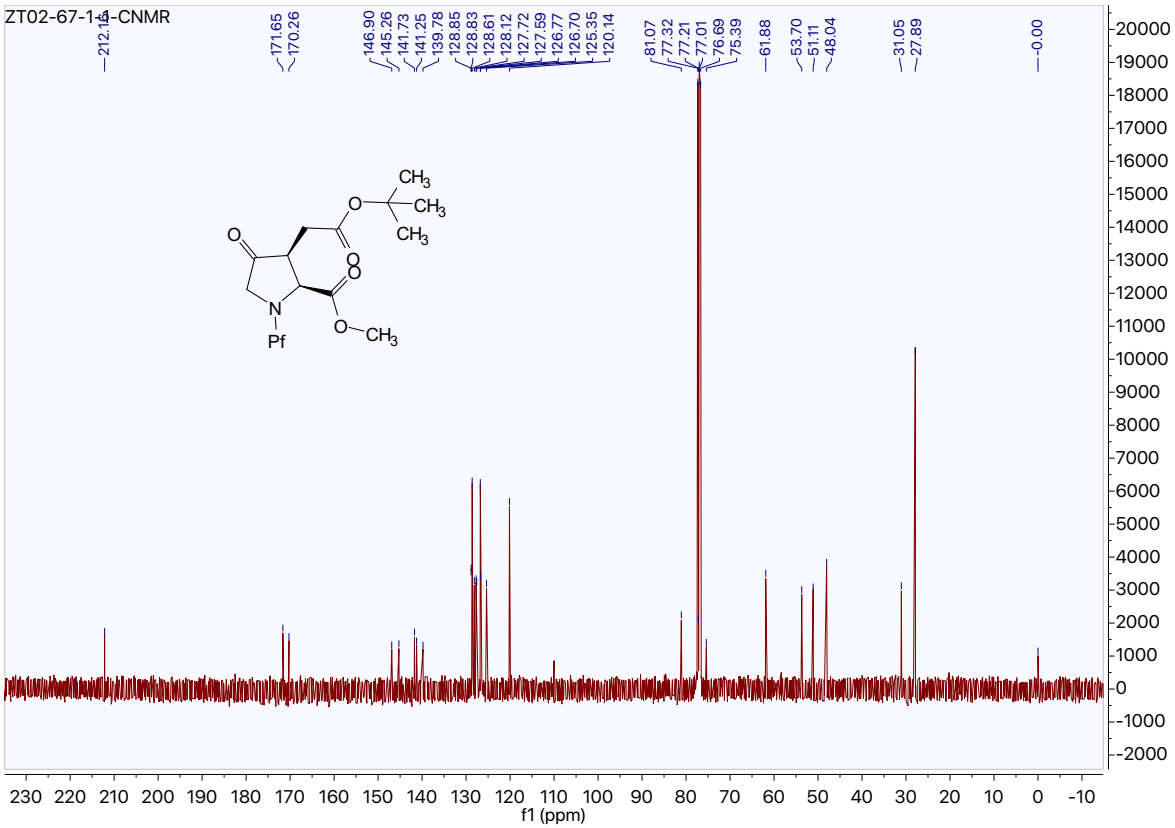
ZT02-67-1-4-CNMR
CH3
CH3
CH3
O
N
Pf
CH3
f1 (ppm)

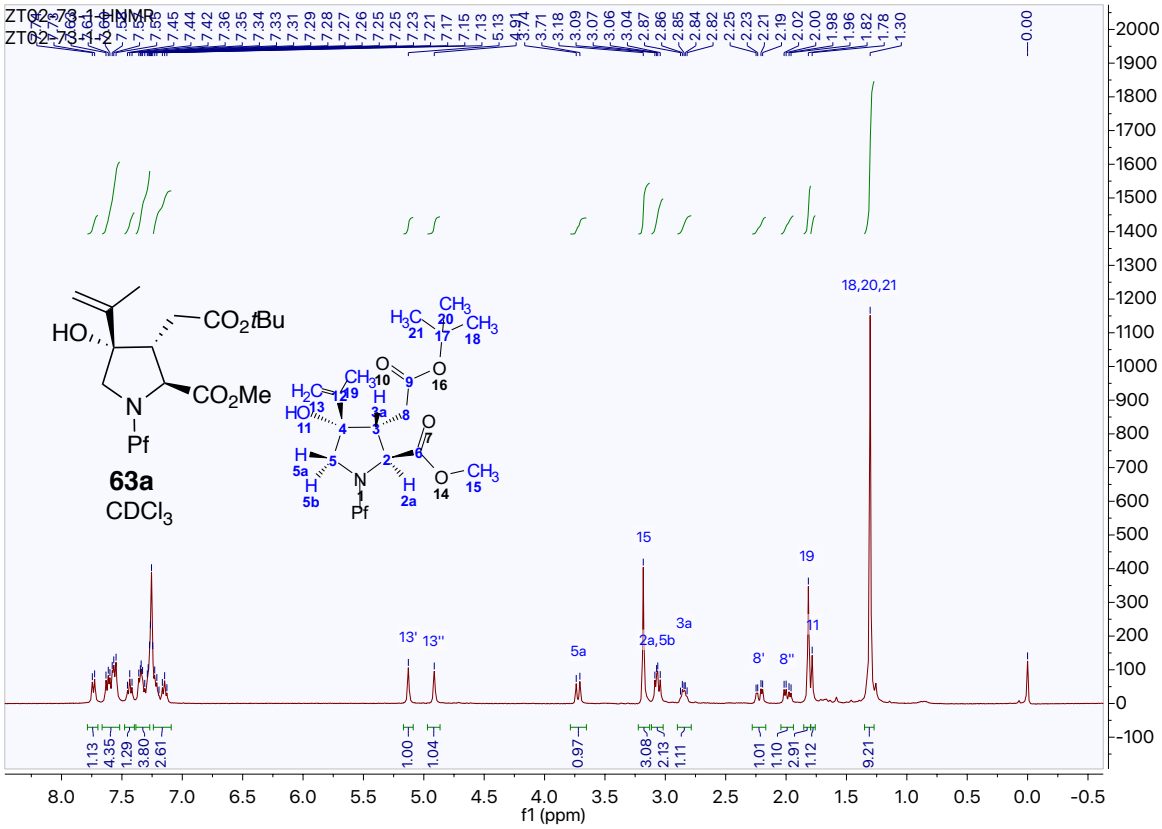
ZT02-73-1-HNMR
ZT02-73-1-2
63a
CDCl3
f1 (ppm)

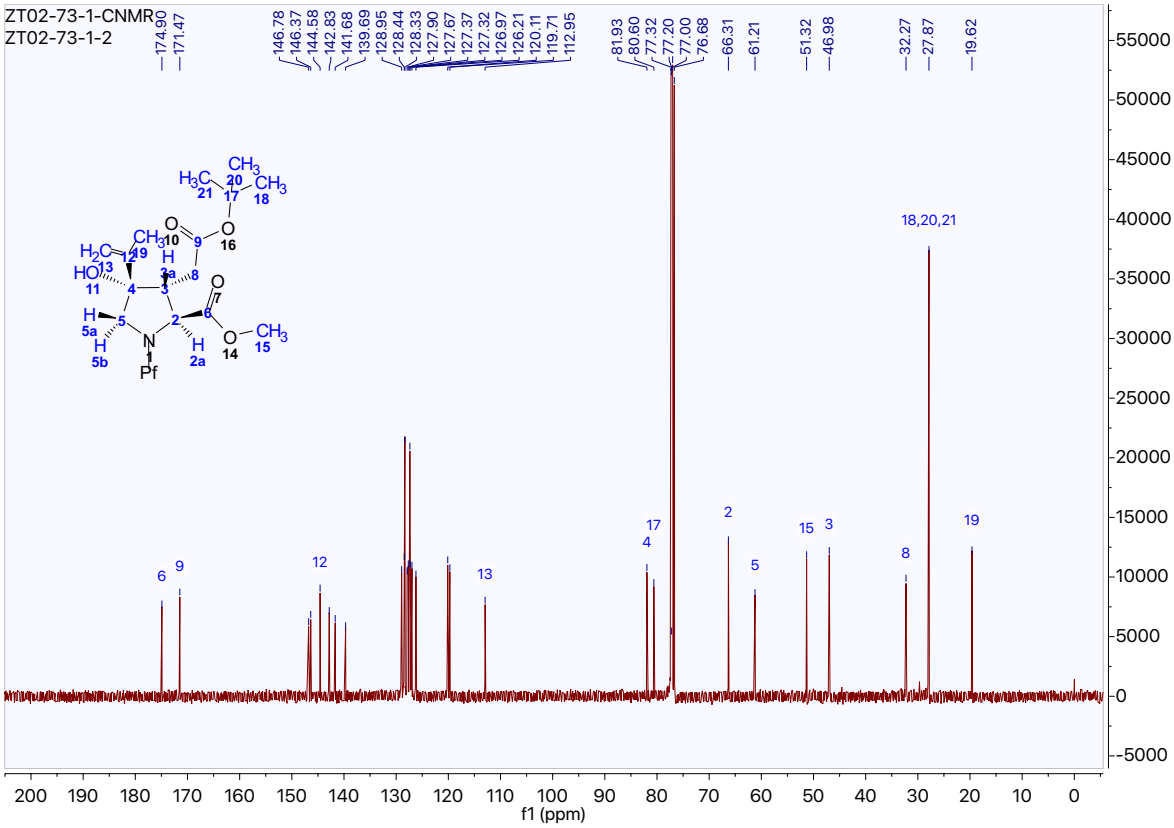
ZT02-73-1-CNMR
ZT02-73-1-2
f1 (ppm)

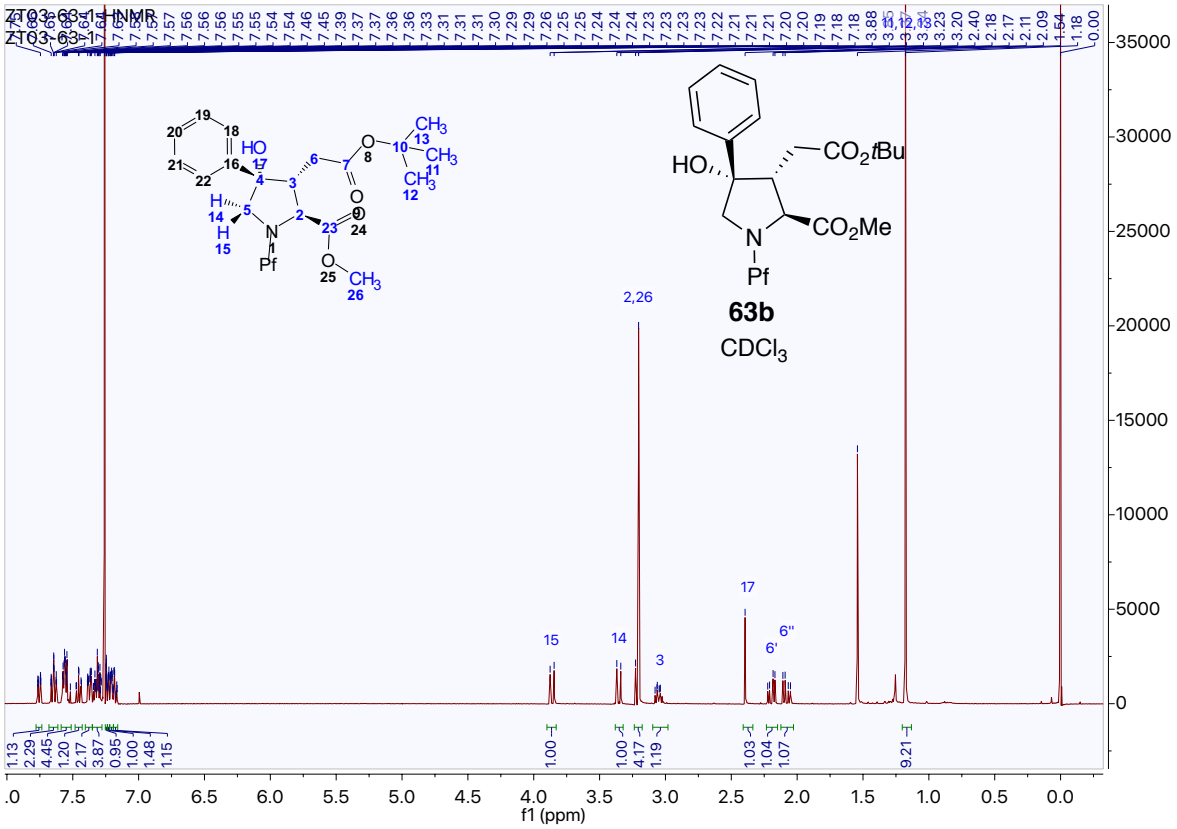
ZT03-63-1-HNMR
ZT03-63-1
63b
CDCl3
f1 (ppm)

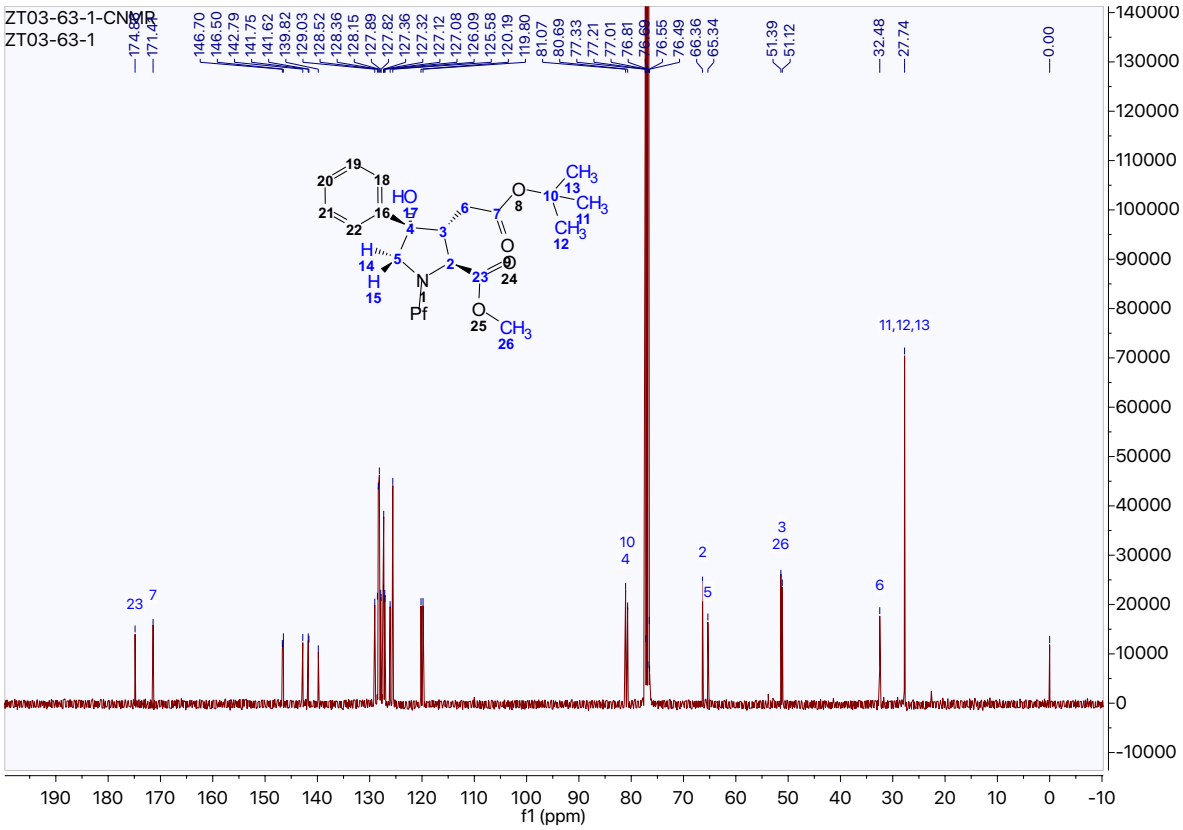
ZT03-63-1-CNMR
ZT03-63-1
f1 (ppm)

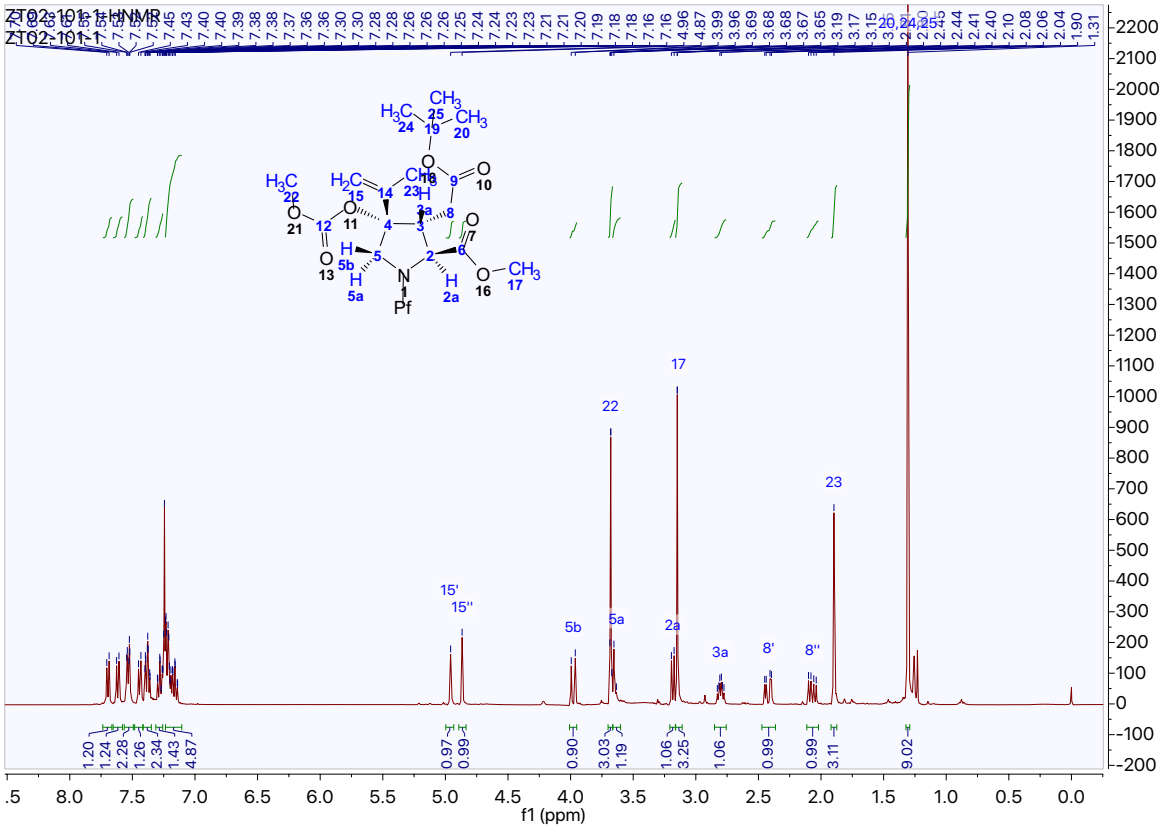
ZT02-101-1-HNMR
ZT02-101-1
f1 (ppm)

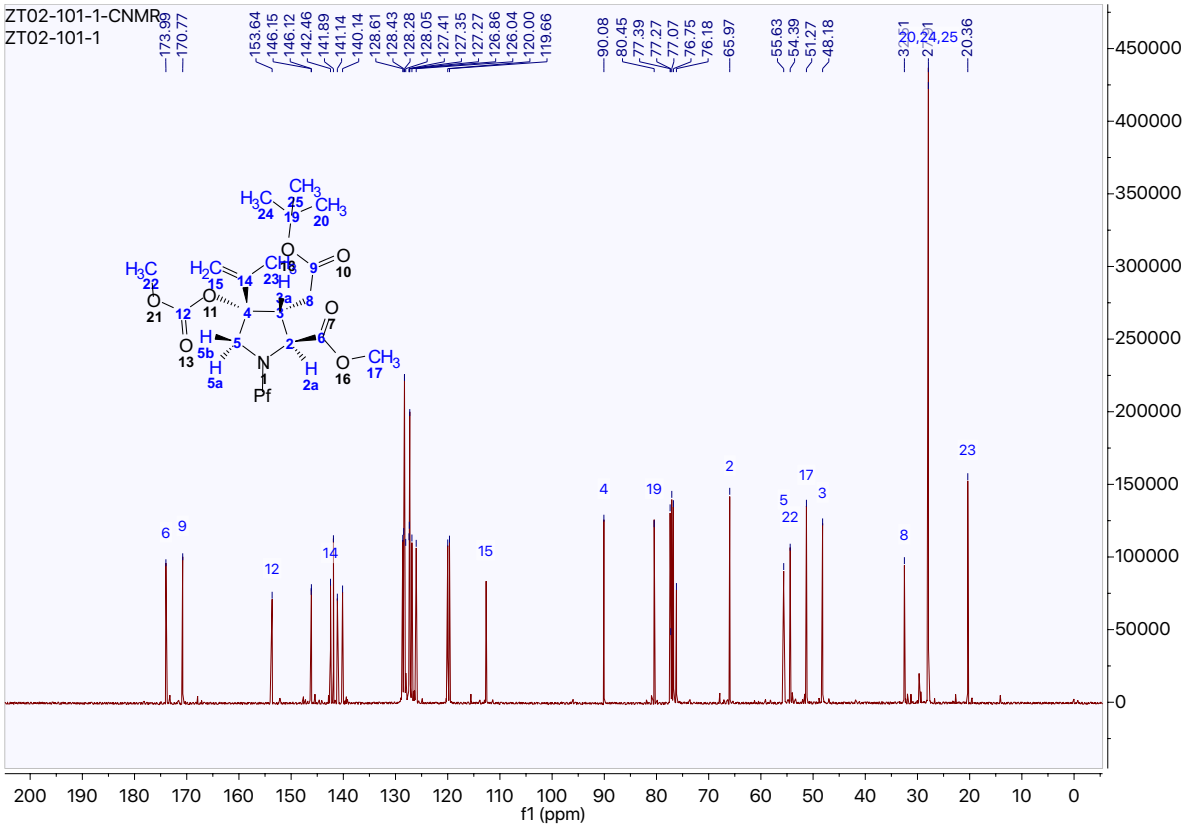
ZT02-101-1-CNMR
ZT02-101-1
f1 (ppm)

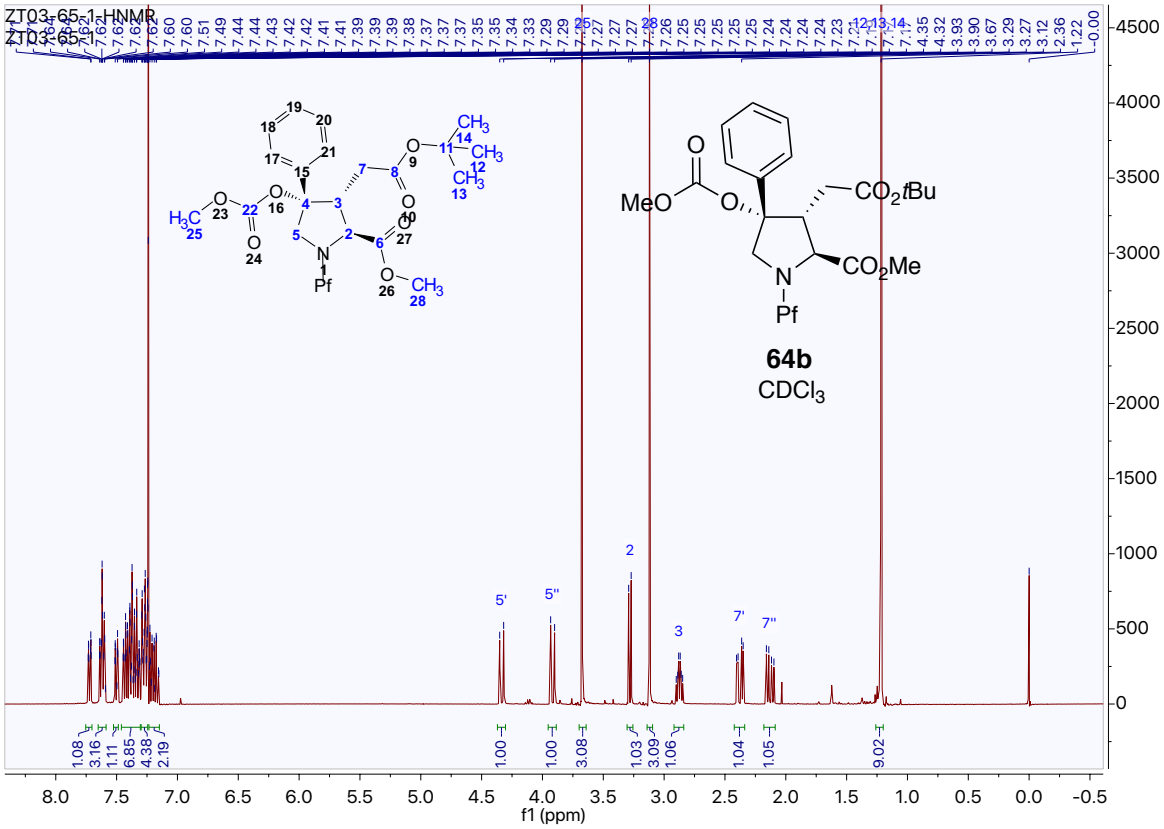
ZT03-65-1-HNMR
ZT03-65-1
64b
CDCl3
f1 (ppm)

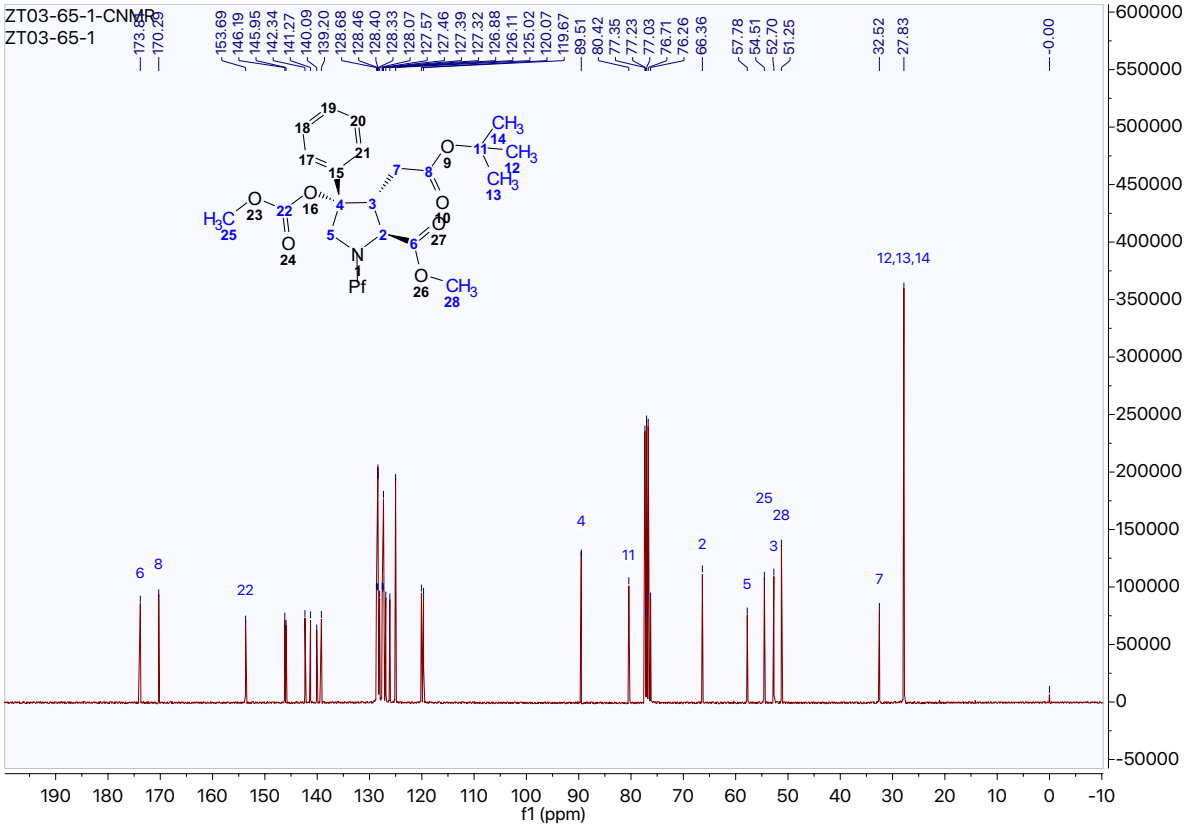
ZT03-65-1-CNMR
ZT03-65-1
f1 (ppm)

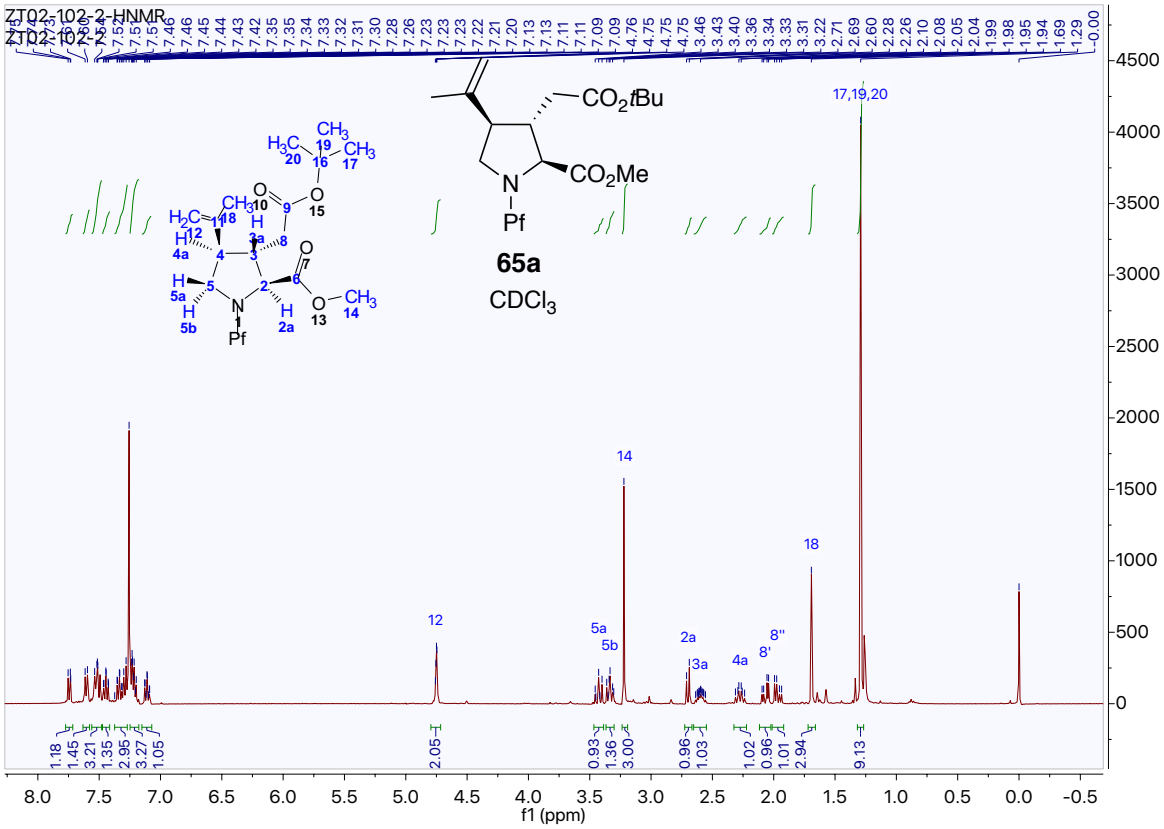
ZT02-102-2-HNMR
ZT02-102-2
65a
CDCl3
f1 (ppm)

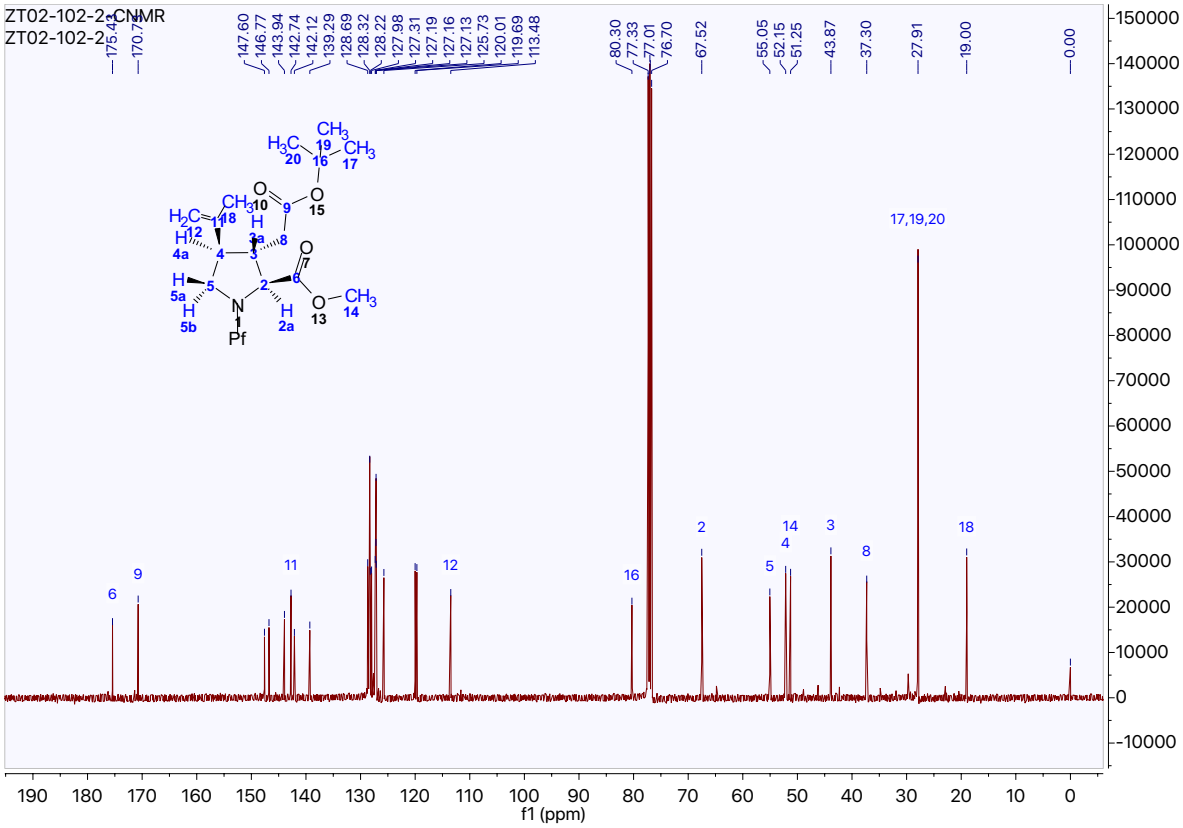
ZT02-102-2-CNMR
ZT02-102-2
f1 (ppm)

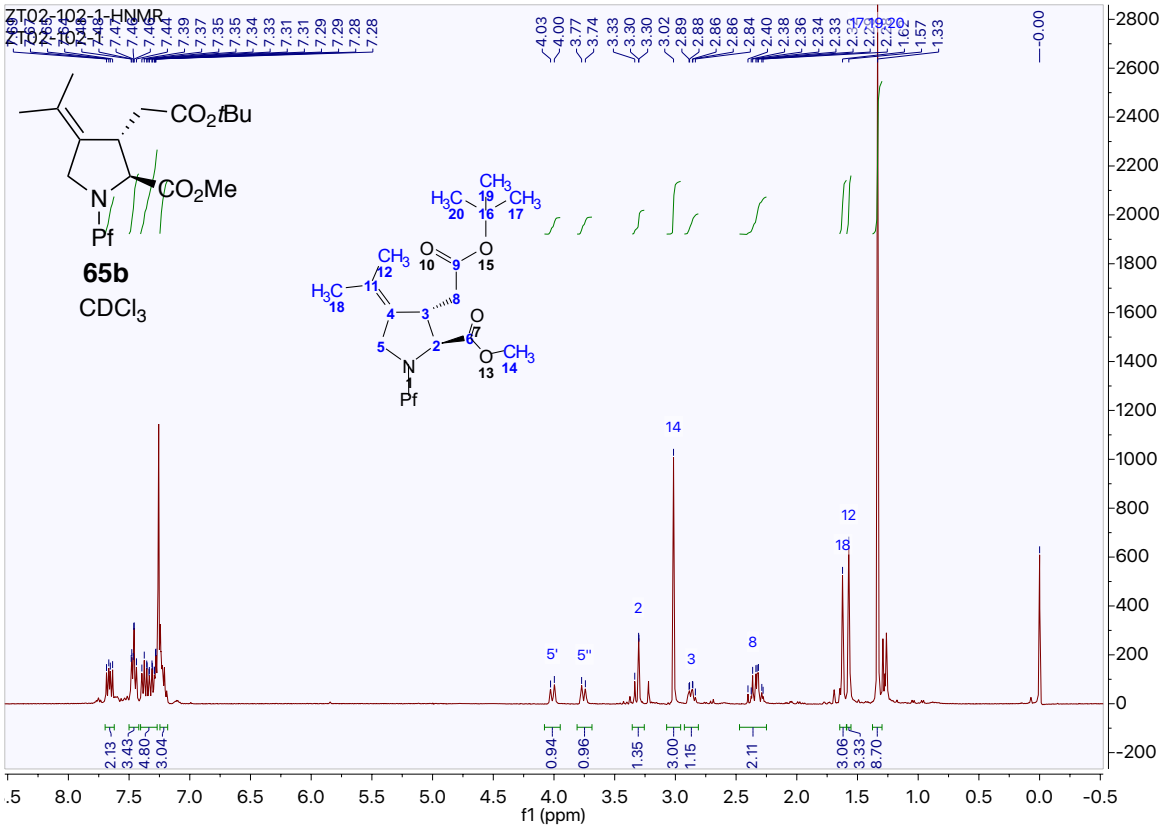
ZT02-102-1-HNMR
ZT02-102-1
CO2tBu
CO2Me
N
Pf
65b
CDCl3
f1 (ppm)

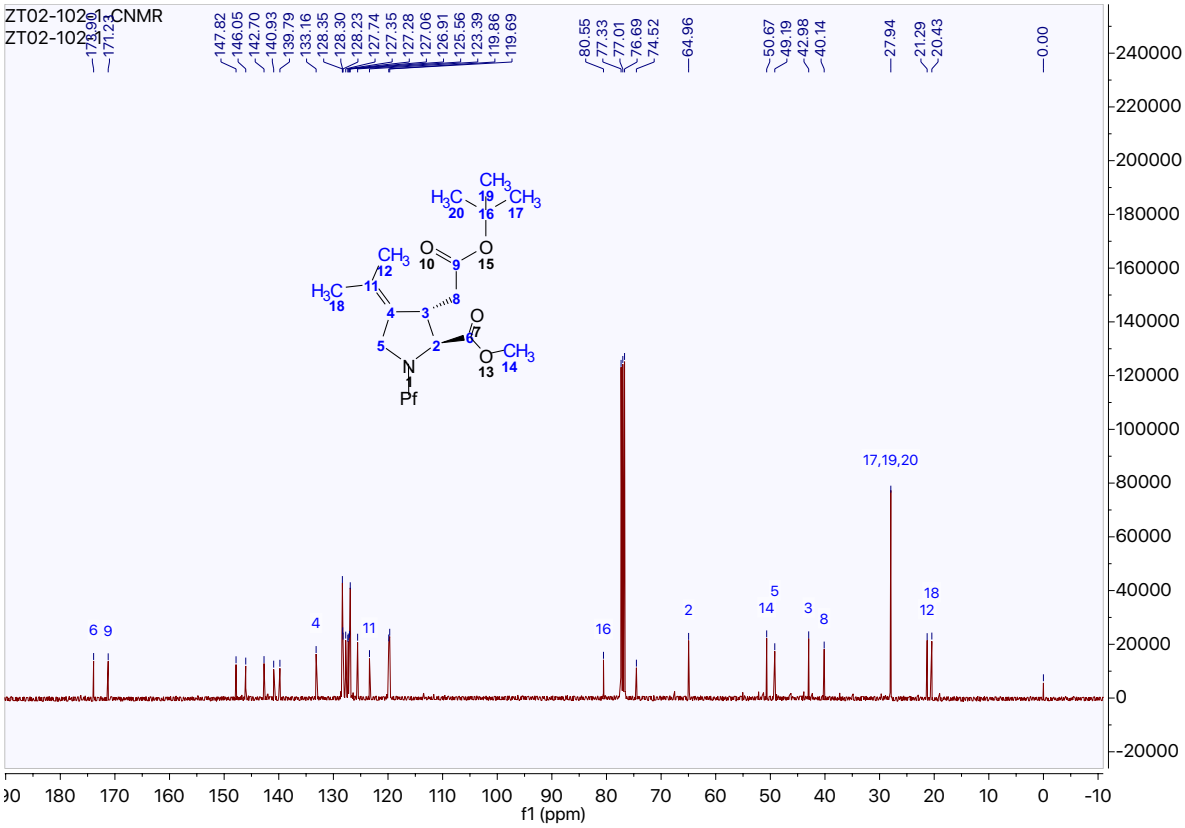
ZT02-102-1-CNMR
ZT02-102-1
f1 (ppm)

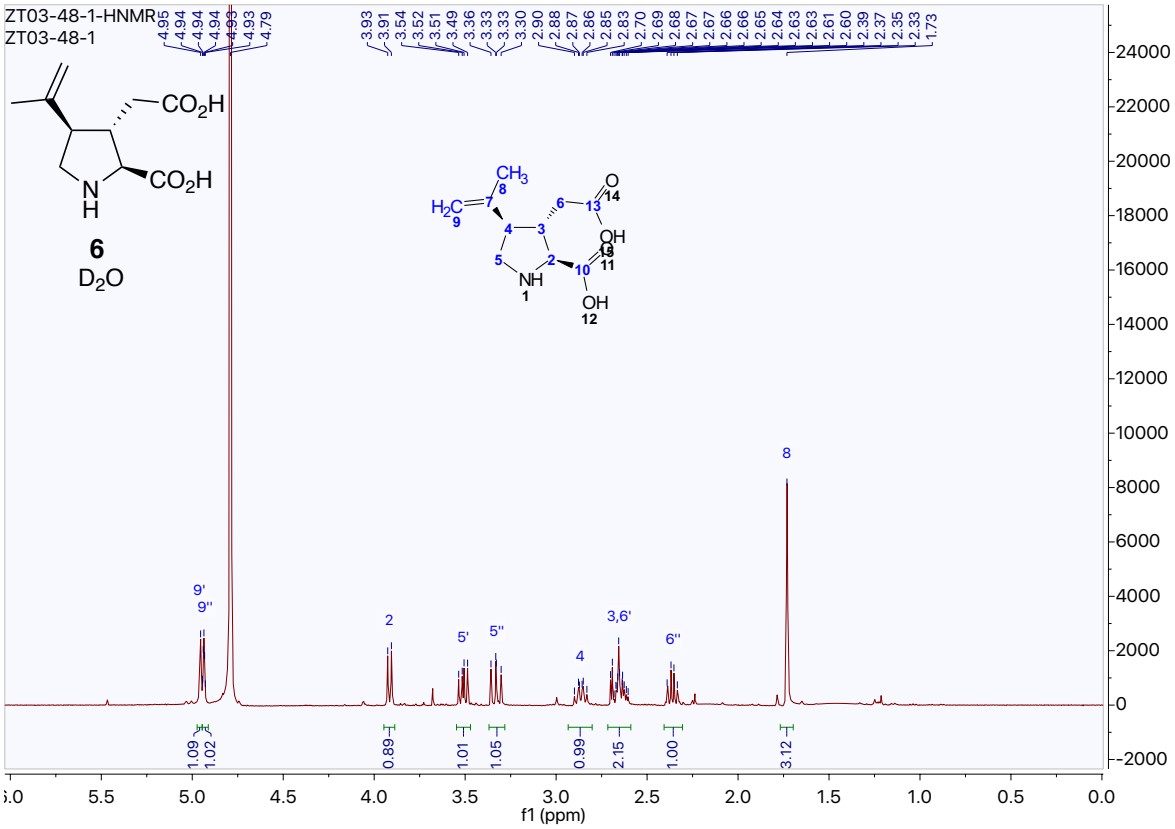
ZT03-48-1-HNMR
ZT03-48-1
6
D2O
f1 (ppm)

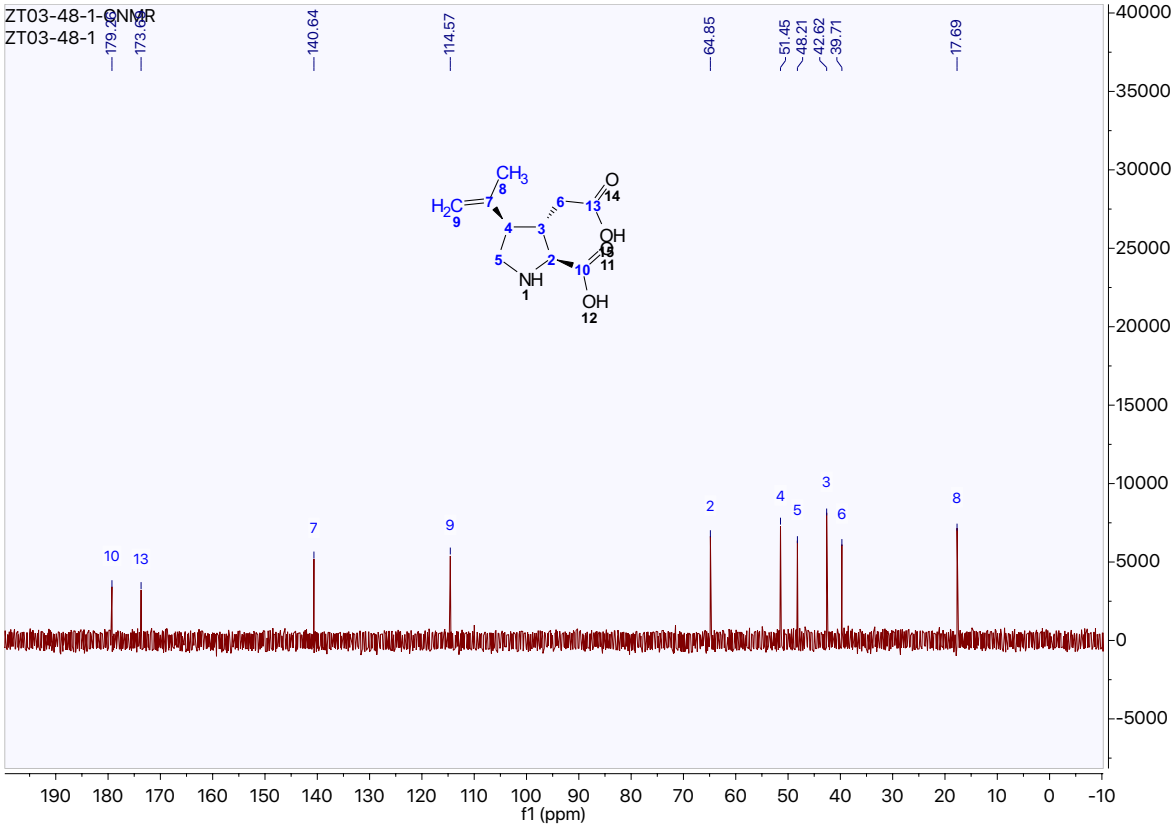
ZT03-48-1-CNMR
ZT03-48-1
f1 (ppm)

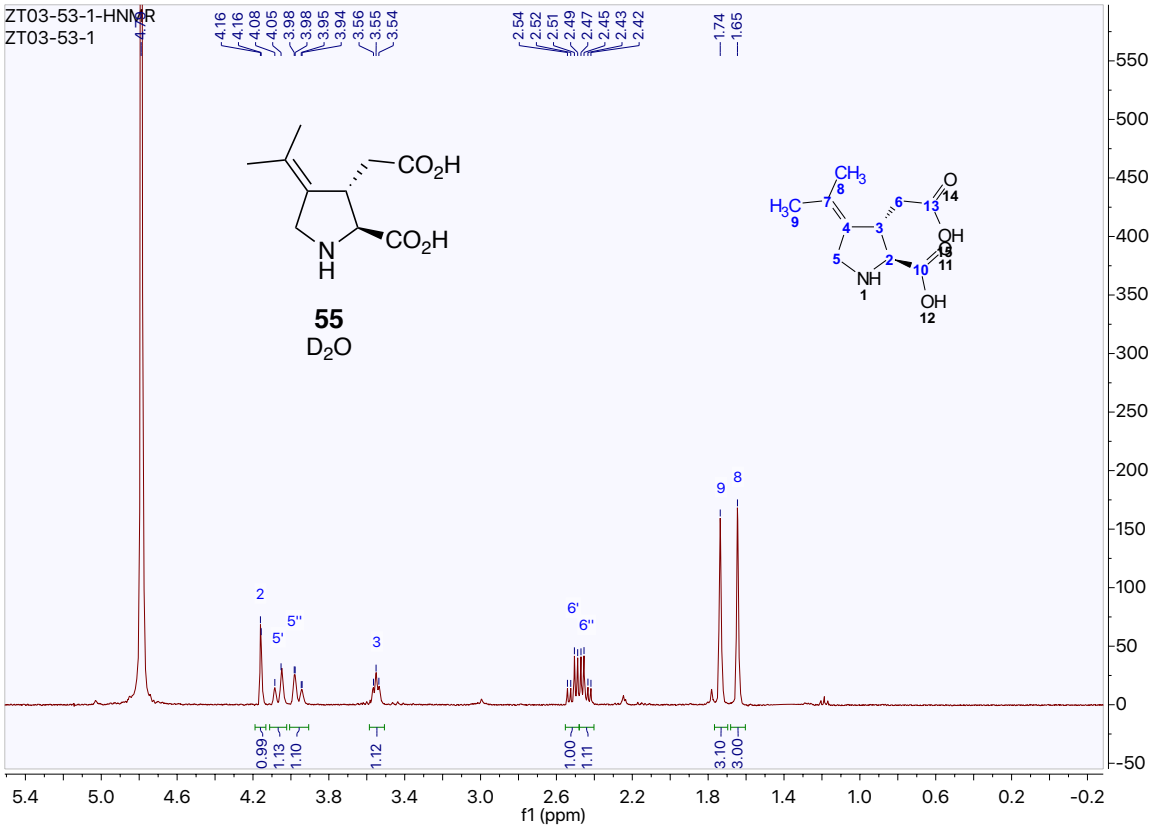
ZT03-53-1-HNMR
ZT03-53-1
55
D2O
f1 (ppm)

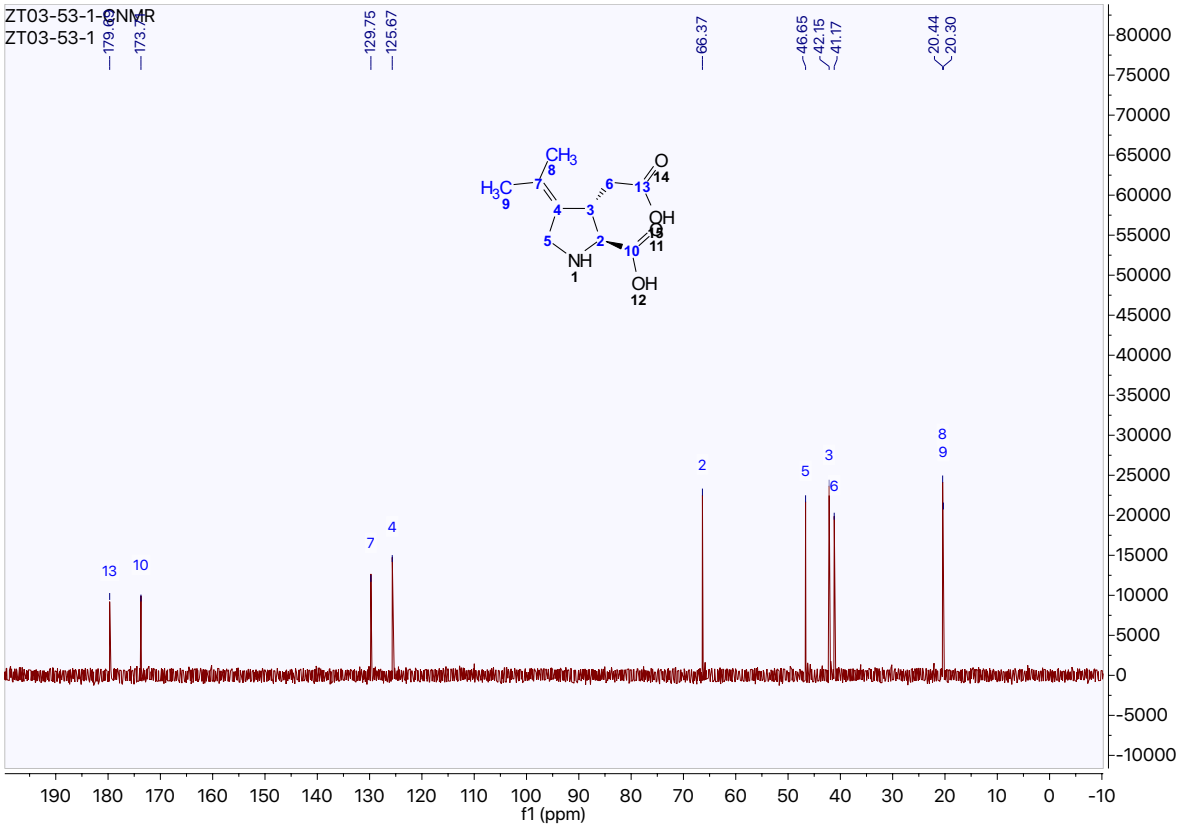
ZT03-53-1-CNMR
ZT03-53-1
f1 (ppm)

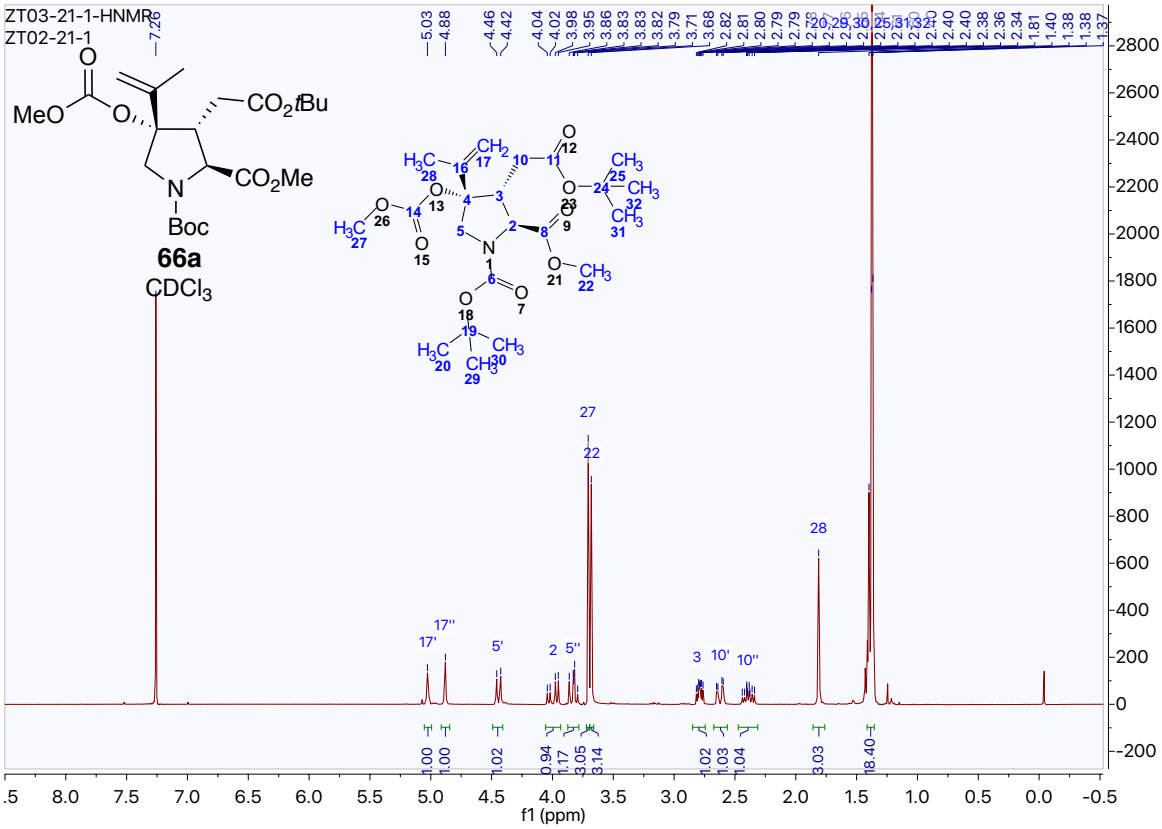
ZT03-21-1-HNMR
ZT02-21-1
MeO
O
CO_2tBu
CO_2Me
N
Boc
66a
$CDCl_3$
f1 (ppm)

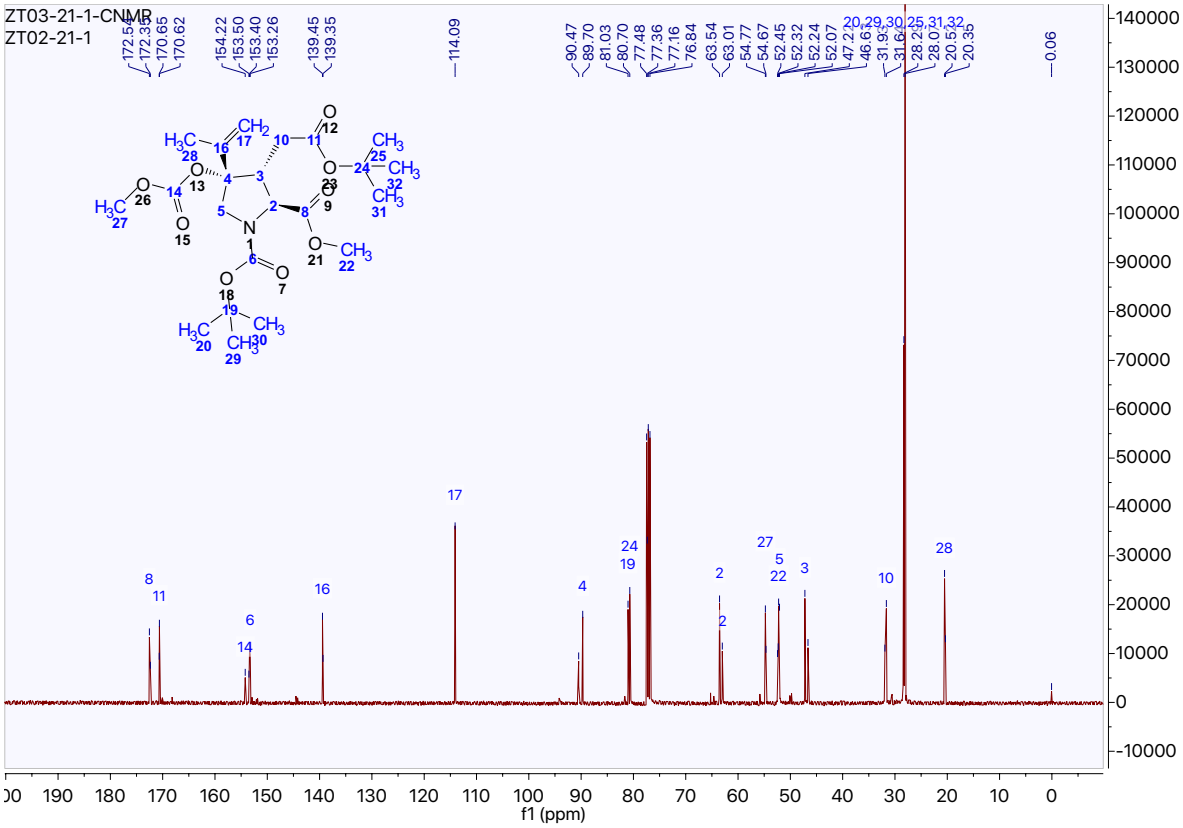
ZT03-21-1-CNMR
ZT02-21-1
f1 (ppm)

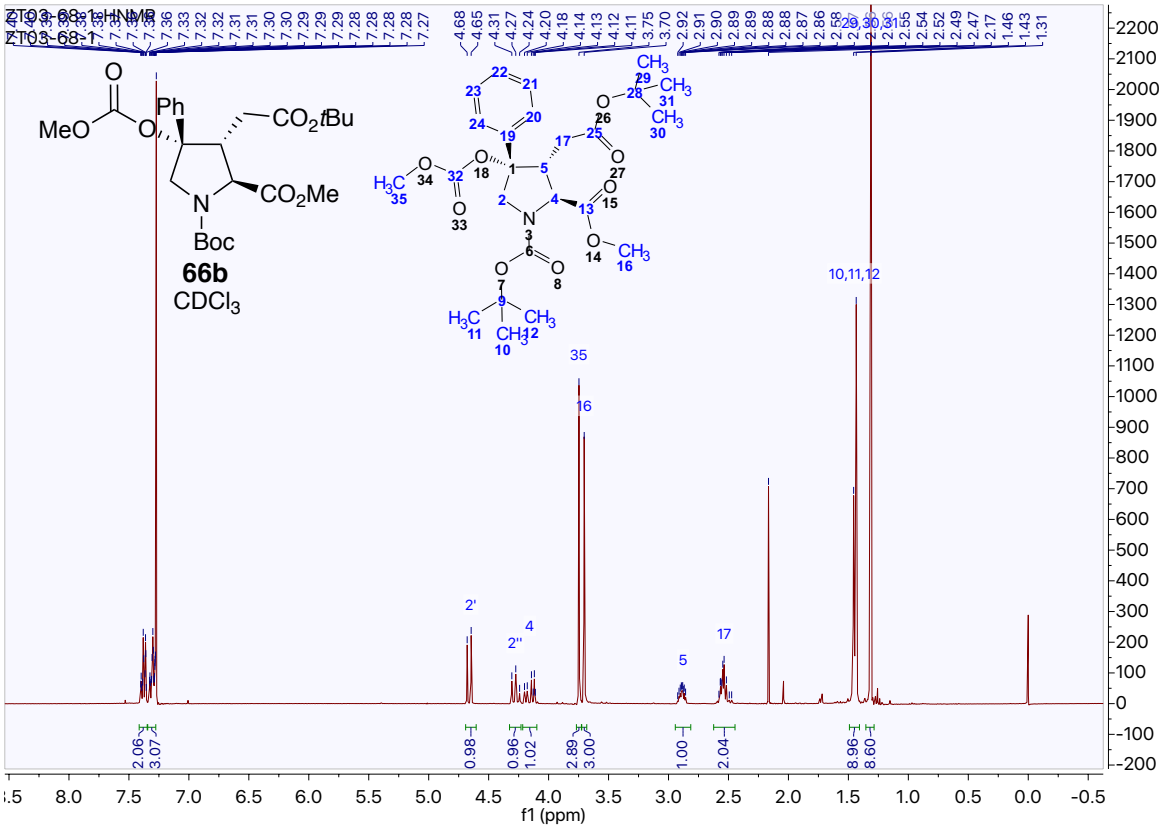
ZT03-68-1-HNMR
ZT03-68-1
66b
CDCl3
f1 (ppm)

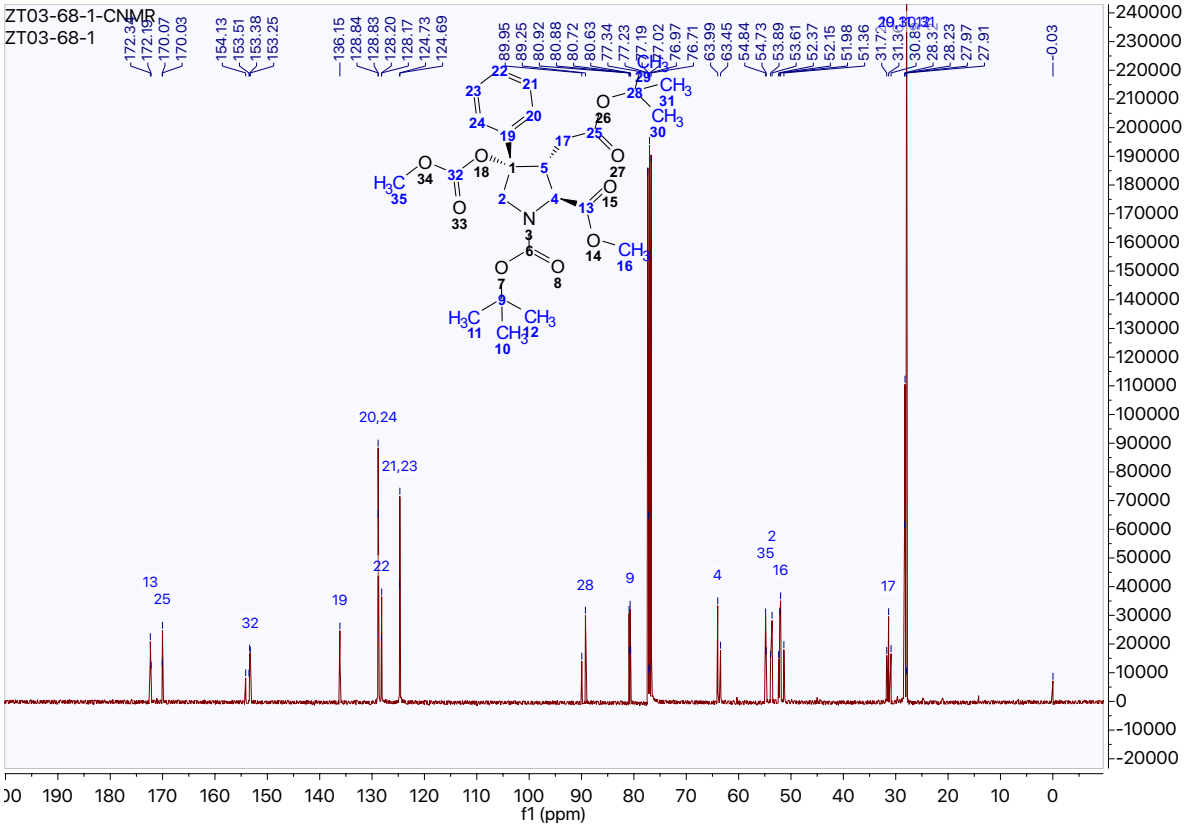
ZT03-68-1-CNMR
ZT03-68-1
f1 (ppm)

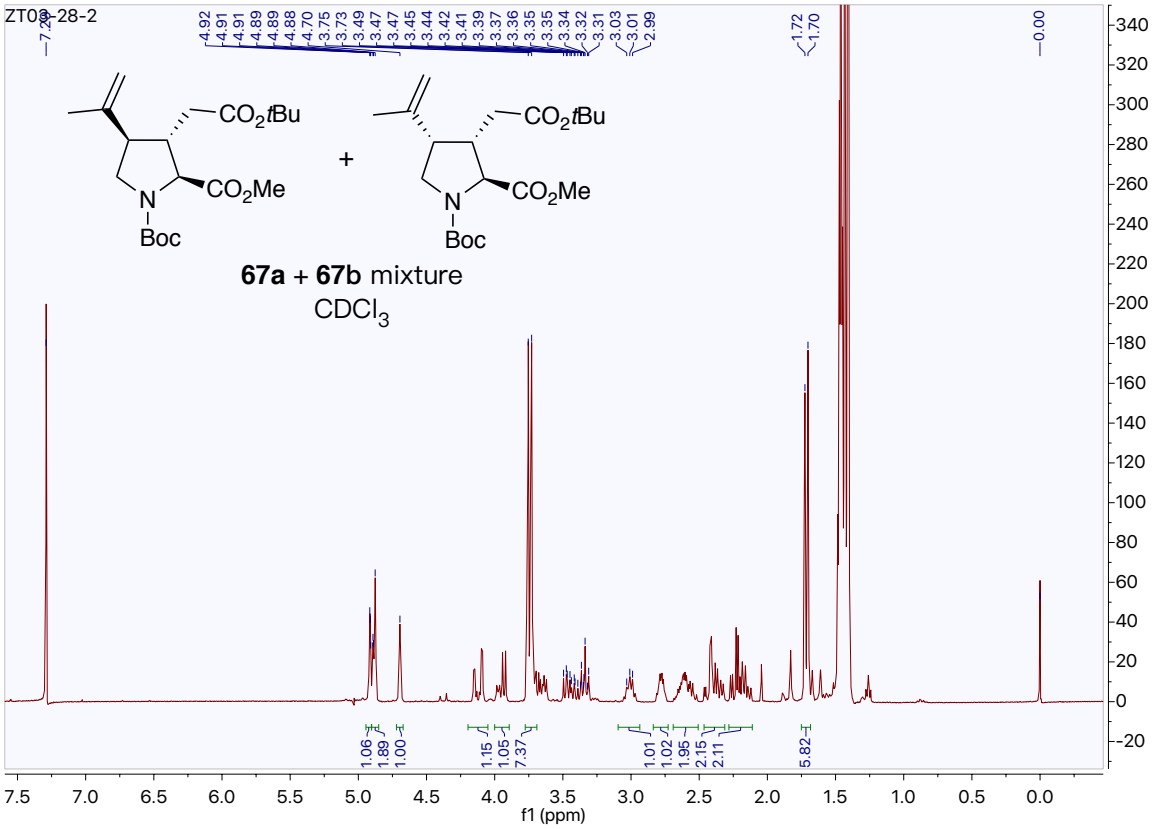
ZT03-28-2
CO2tBu
CO2Me
N
Boc
+
67a + 67b mixture
CDCl3
f1 (ppm)

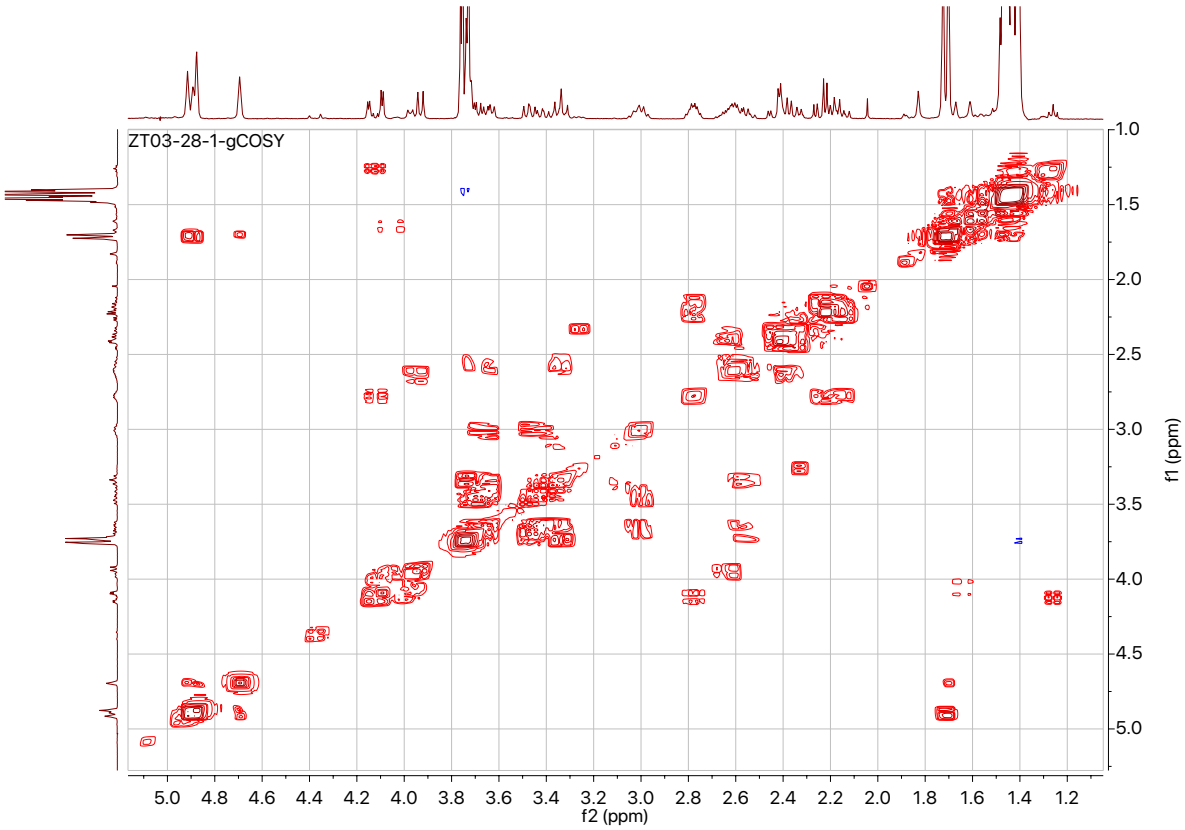
ZT03-28-1-gCOSY
f1 (ppm)
f2 (ppm)

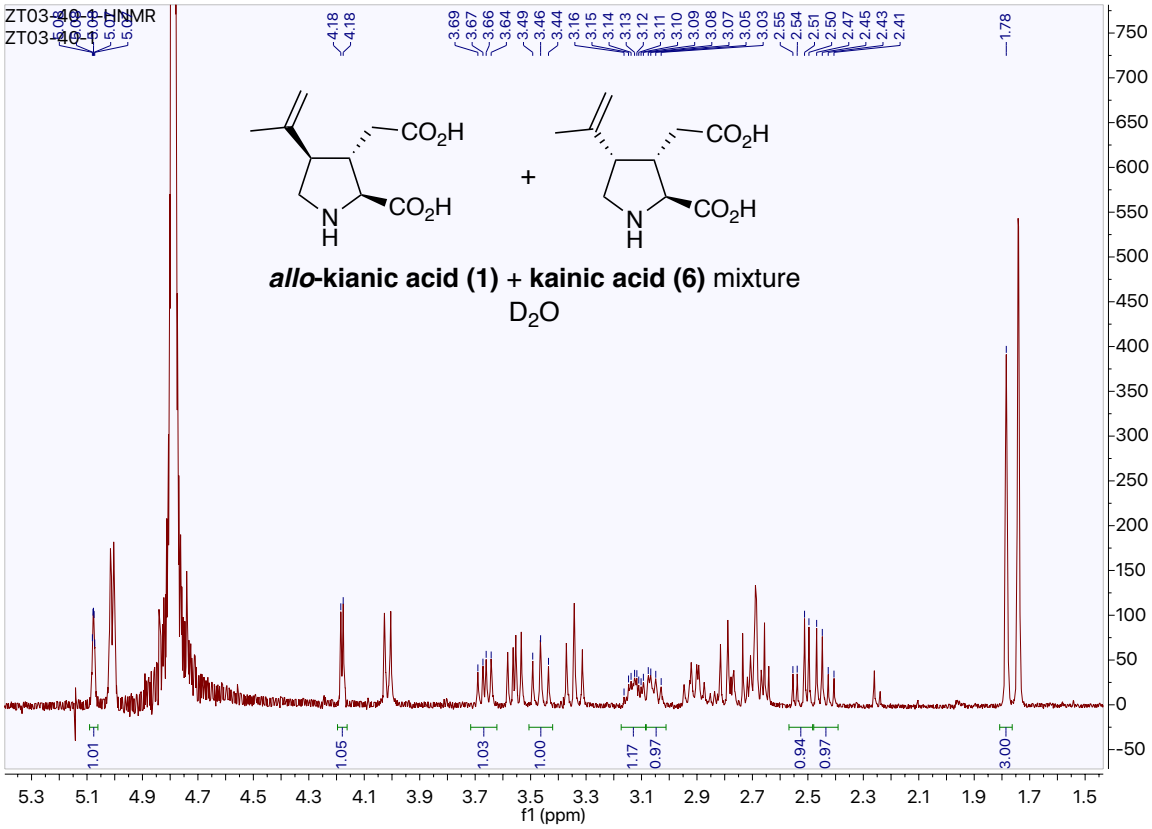
ZT03-40-1-1HNMR
ZT03-40-1
CO2H
CO2H
N
H
+
CO2H
CO2H
N
H
allo-kianic acid (1) + kainic acid (6) mixture
D2O
f1 (ppm)

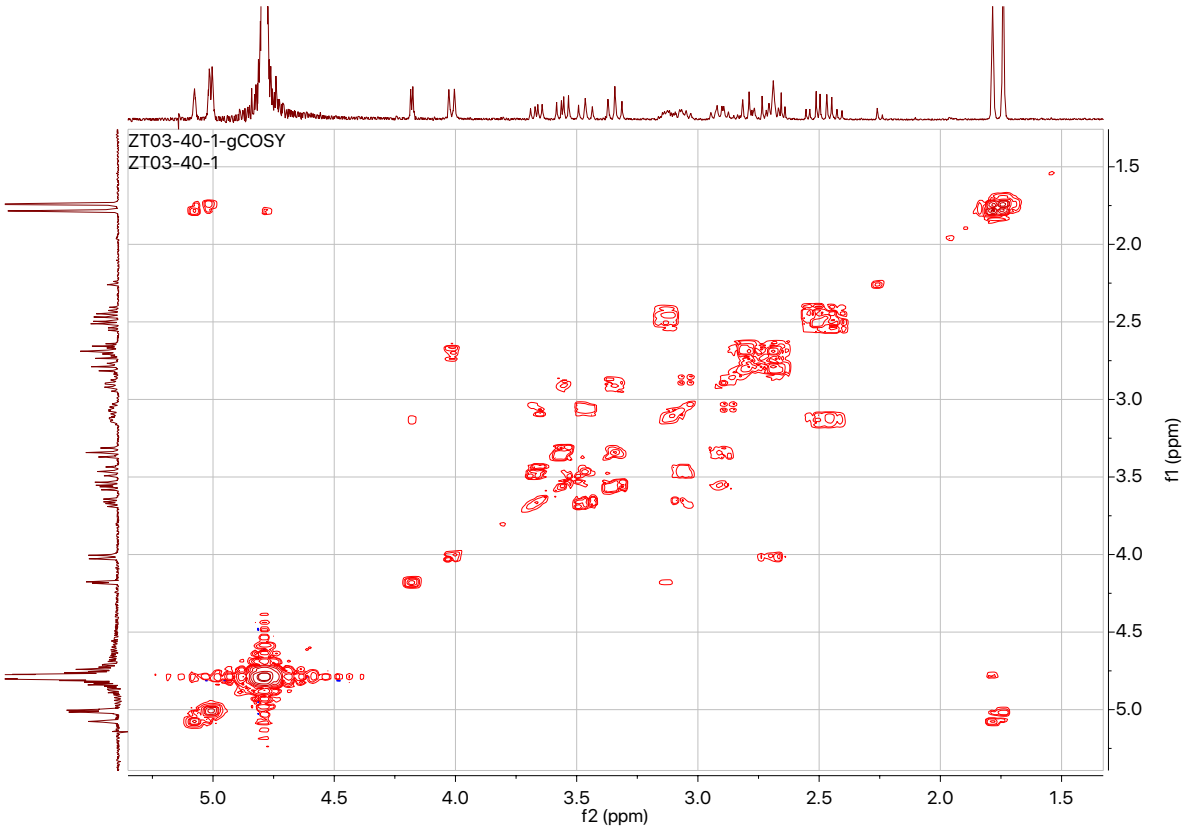
ZT03-40-1-gCOSY
ZT03-40-1
f2 (ppm)
f1 (ppm)

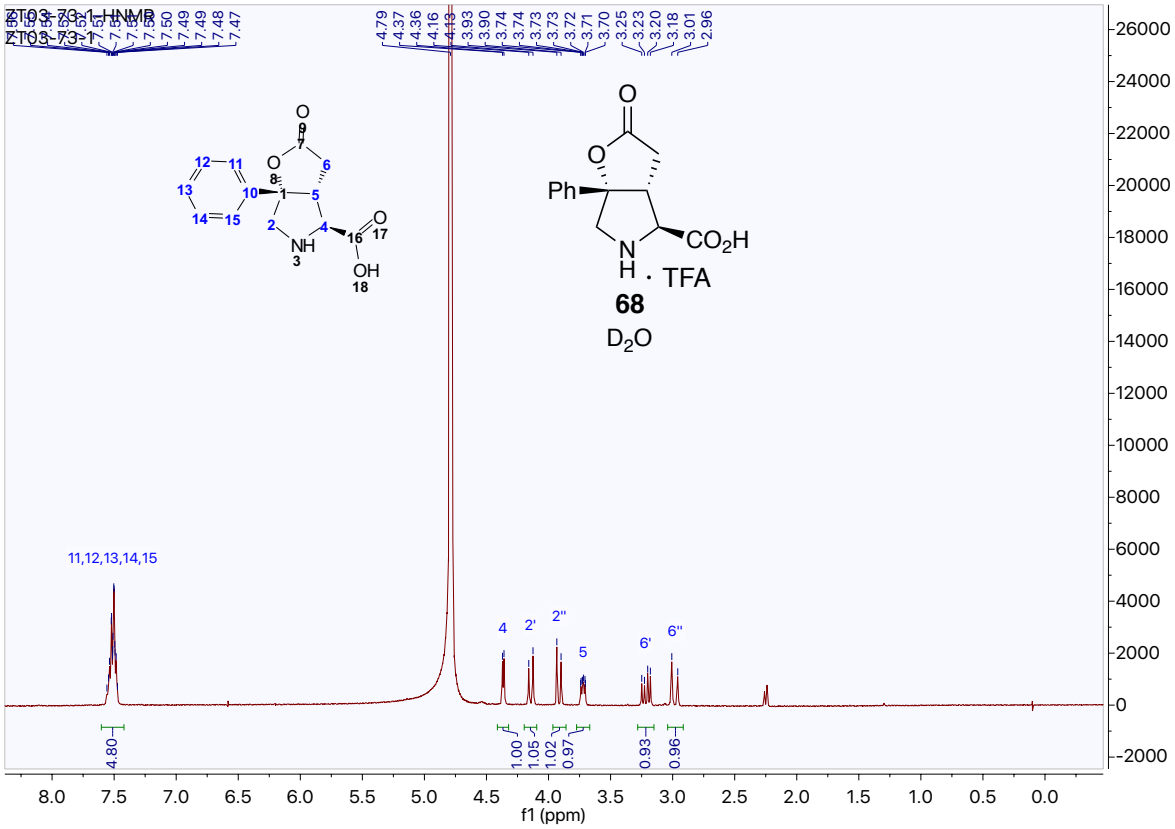
ZT03-73-1-HNMR
ZT03-73-1
Ph
CO2H
N
H · TFA
68
D2O
11,12,13,14,15
4
2'
2''
5
6'
6''
4.80
1.00
1.05
1.02
0.97
0.93
0.96
f1 (ppm)

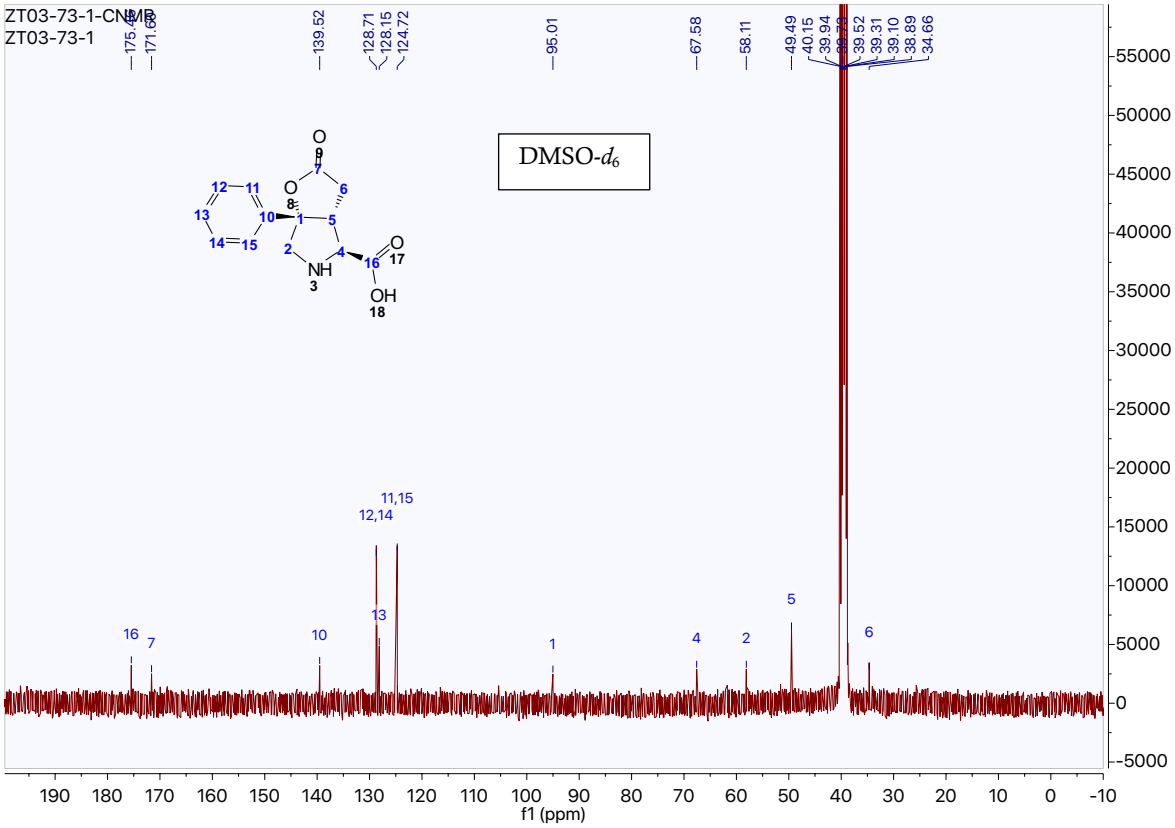
ZT03-73-1-CNMR
ZT03-73-1
DMSO-d6
11,15
12,14
13
16
7
10
1
4
2
5
6
f1 (ppm)

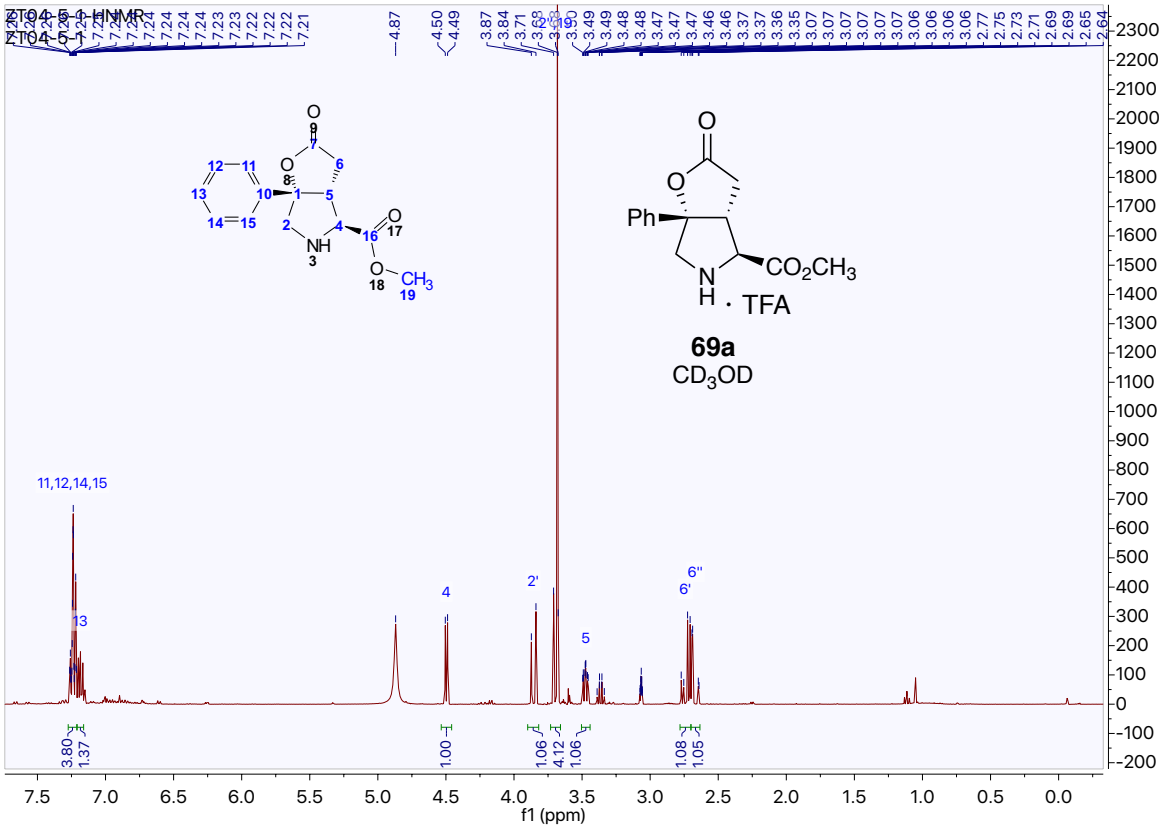
ZT04-5-1-HNMR
ZT04-5-1
69a
CD3OD
Ph
CO2CH3
N
H · TFA
11,12,14,15
13
4
2'
5
6''
6'
3.80
1.37
1.00
1.06
4.12
1.06
1.08
1.05
f1 (ppm)

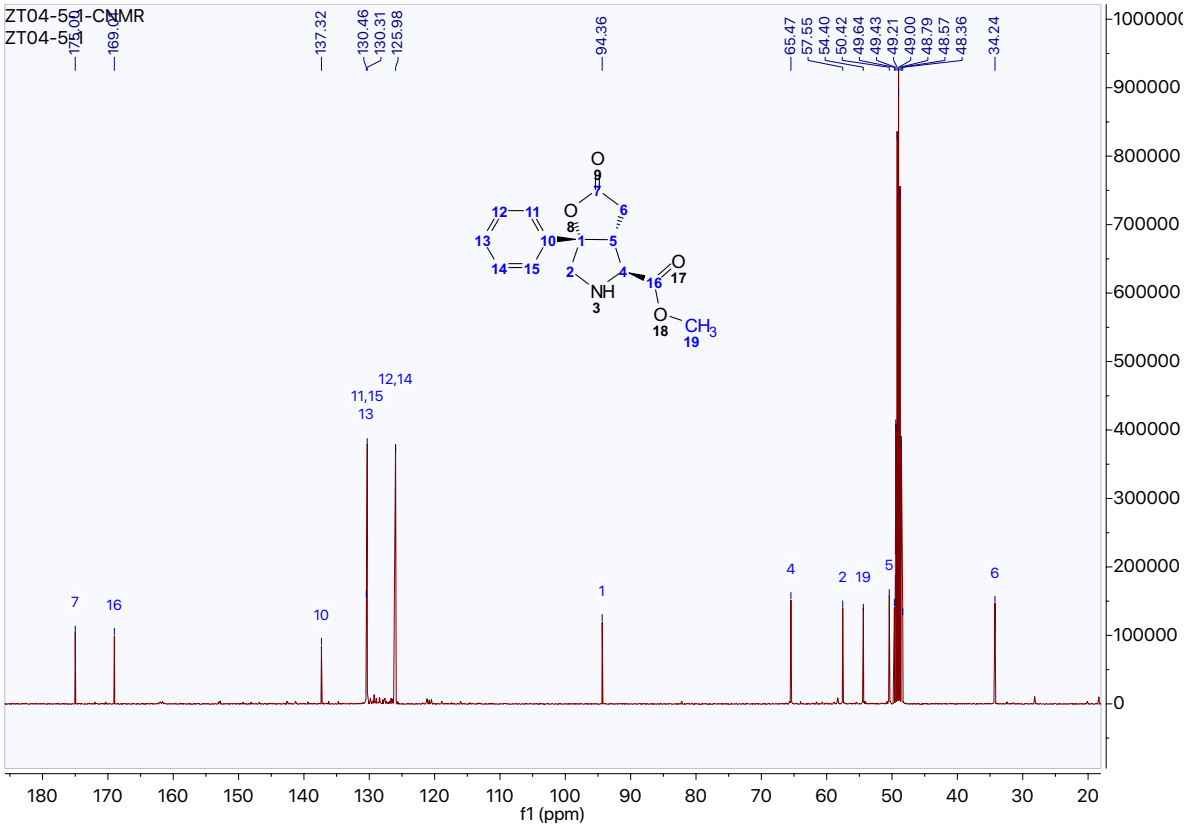
ZT04-5-1-CNMR
ZT04-5-1
175.00
169.03
137.32
130.46
130.31
125.98
94.36
65.47
57.55
54.40
50.42
49.64
49.43
49.21
49.00
48.79
48.57
48.36
34.24
12,14
11,15
13
7
16
10
1
4
2
19
5
6
f1 (ppm)

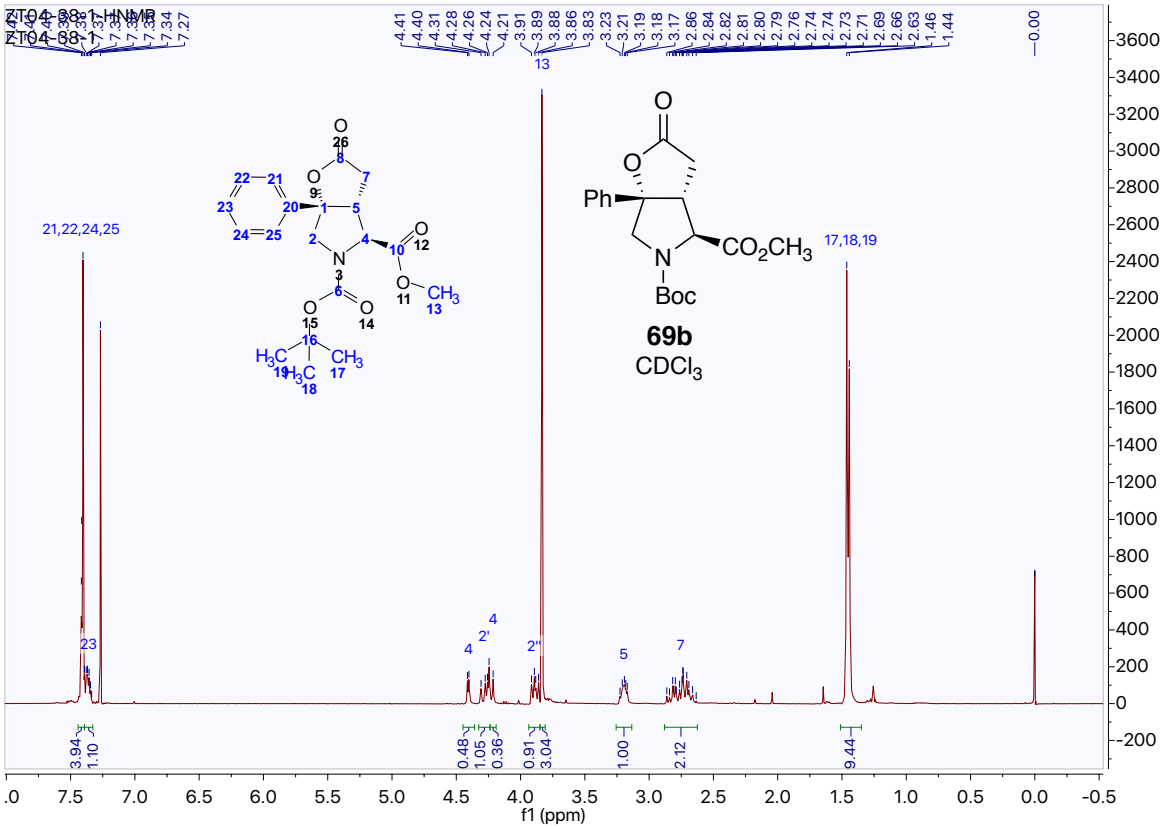
ZT04-38-1 HNMR
ZT04-38-1
69b
CDCl3
Ph
CO2CH3
Boc
21,22,24,25
17,18,19
f1 (ppm)

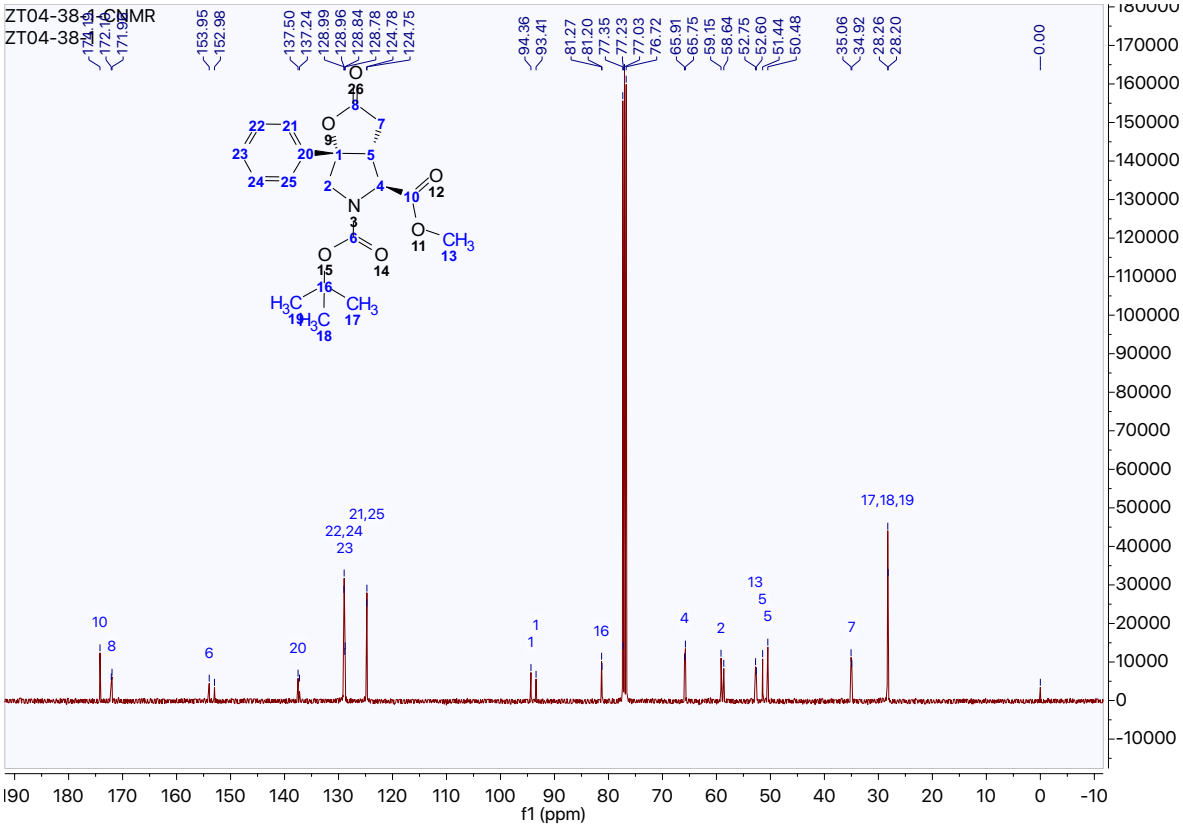
ZT04-38-1 CNMR
ZT04-38-1
17,18,19
21,25
22,24
23
f1 (ppm)

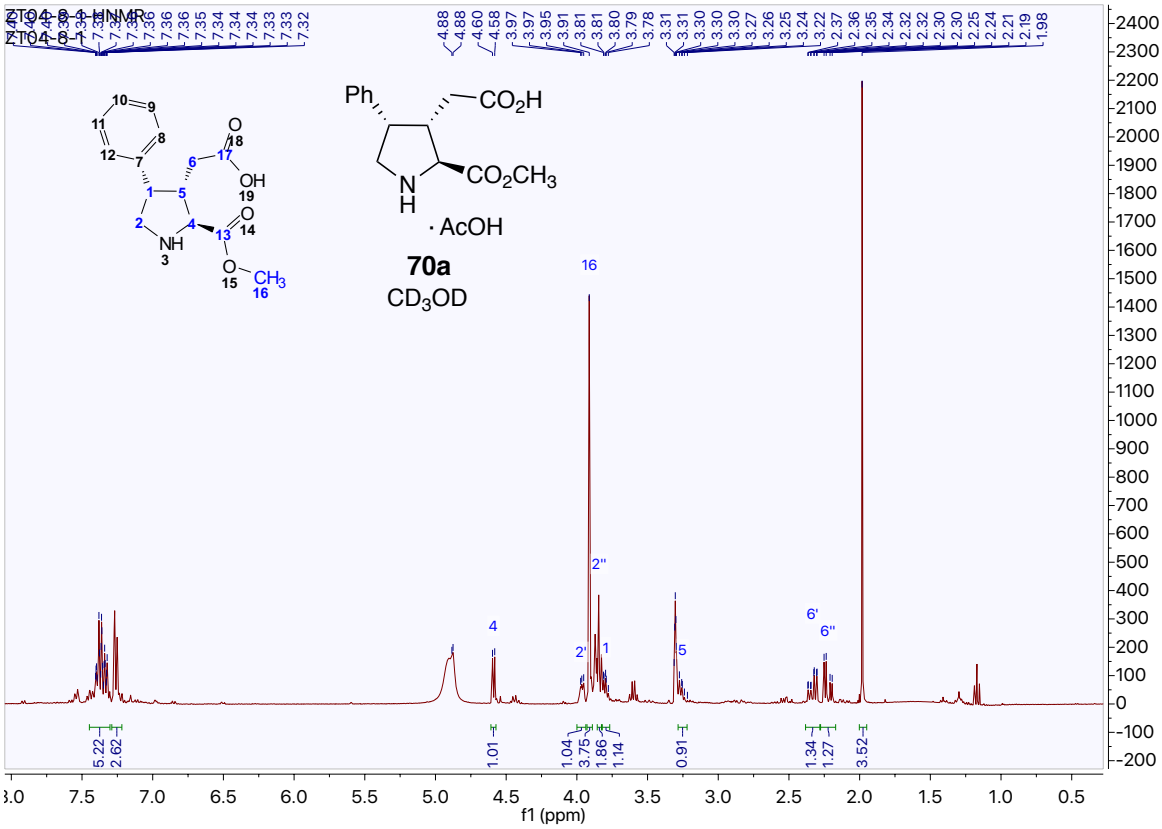
ZT04-8-1 HNMR
ZT04-8-1
Ph
CO2H
CO2CH3
N
H
· AcOH
70a
CD3OD
f1 (ppm)

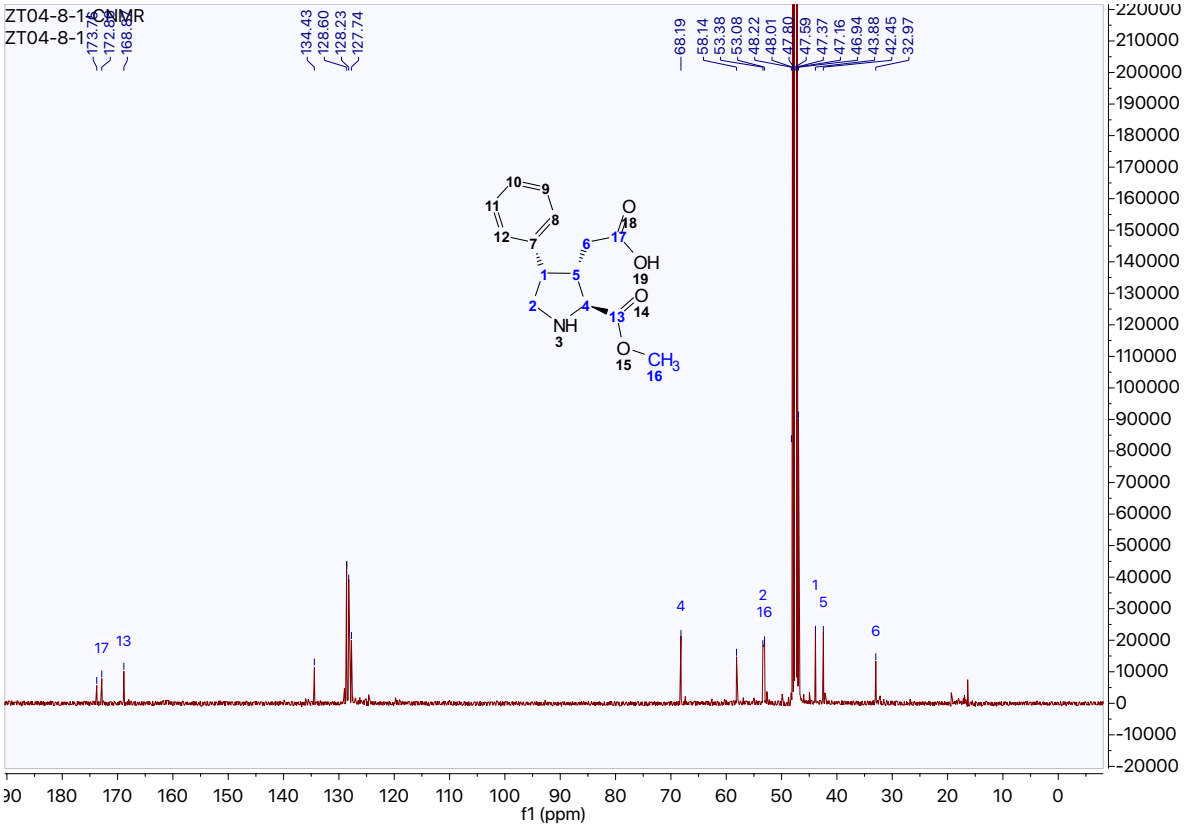
ZT04-8-1 CNMR
ZT04-8-1
f1 (ppm)

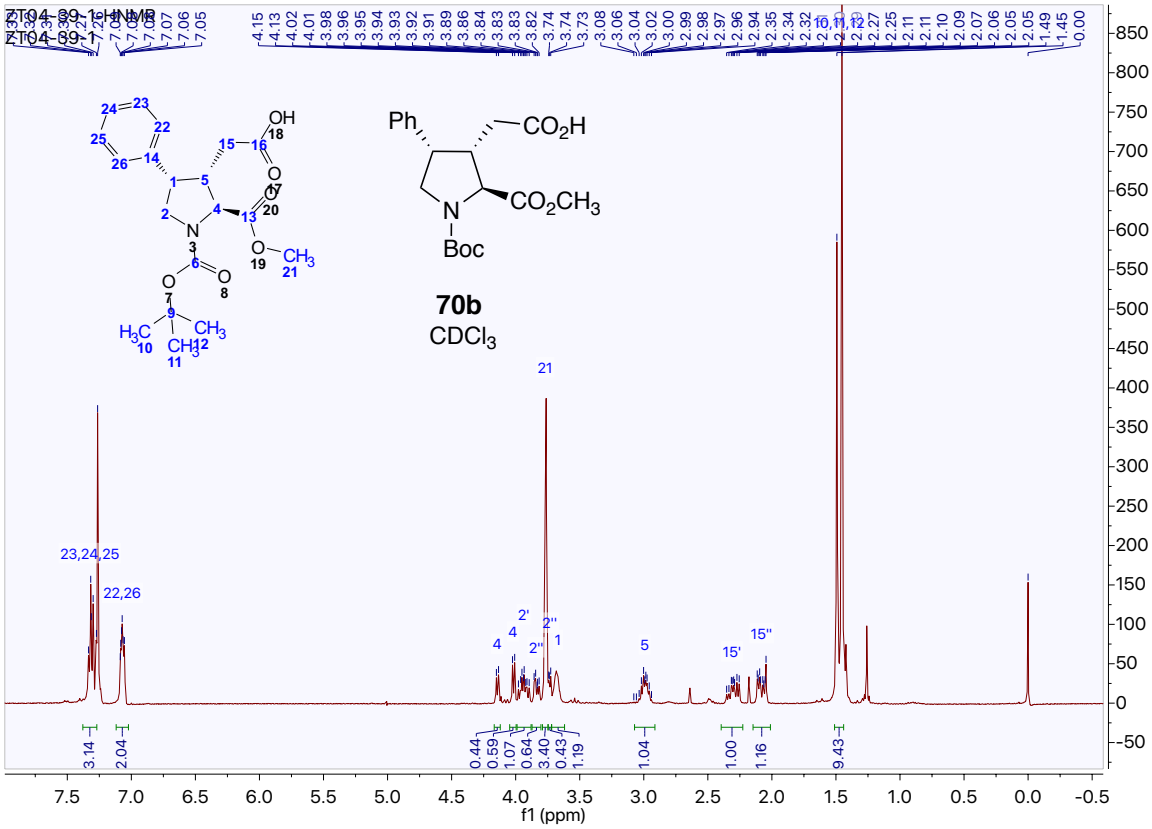
ZT04-39-1-HNMR
ZT04-39-1
70b
CDCl3
Ph
CO2H
CO2CH3
N
Boc
OH
O
CH3
H3C
CH3
23,24,25
22,26
21
4
2'
2''
1
5
15'
15''
10,11,12
3.14
2.04
0.44
0.59
1.07
0.64
3.40
0.43
1.19
1.04
1.00
1.16
9.43
f1 (ppm)

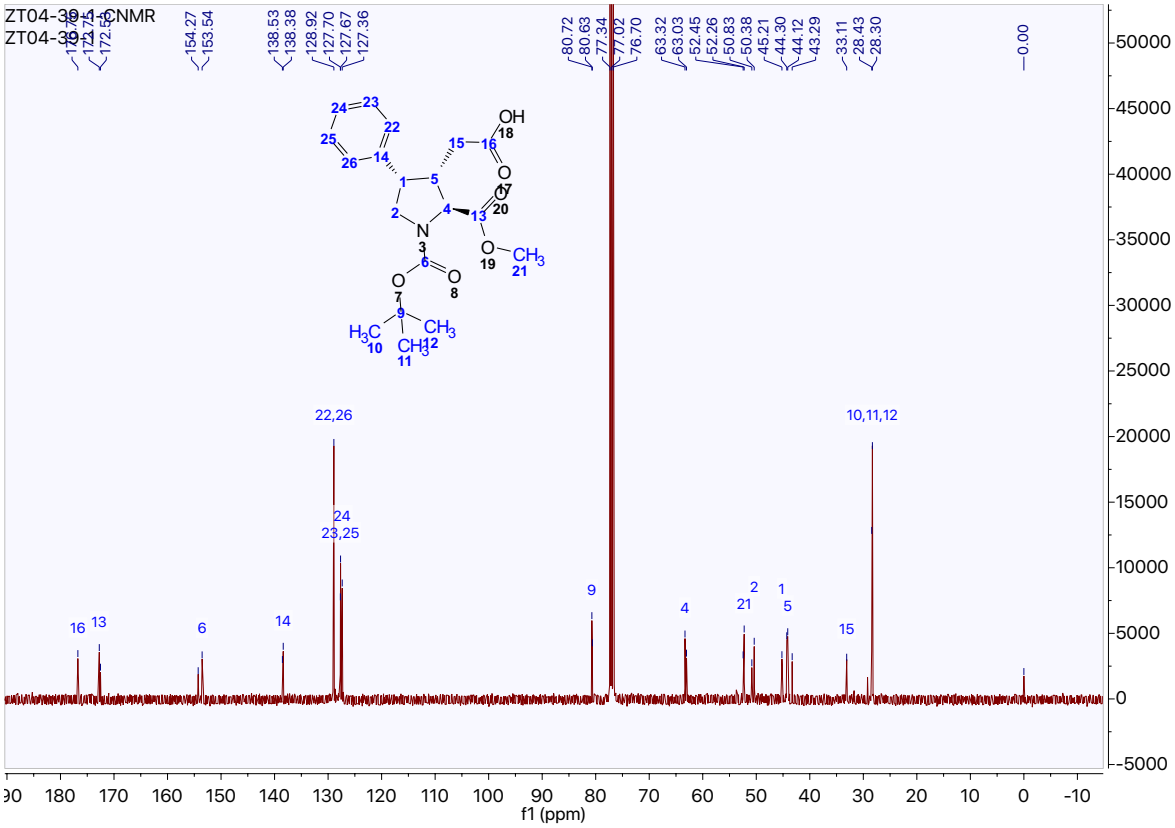
ZT04-39-1-CNMR
ZT04-39-1
OH
O
CH3
H3C
CH3
22,26
24
23,25
10,11,12
16
13
6
14
9
4
2
21
1
5
15
f1 (ppm)

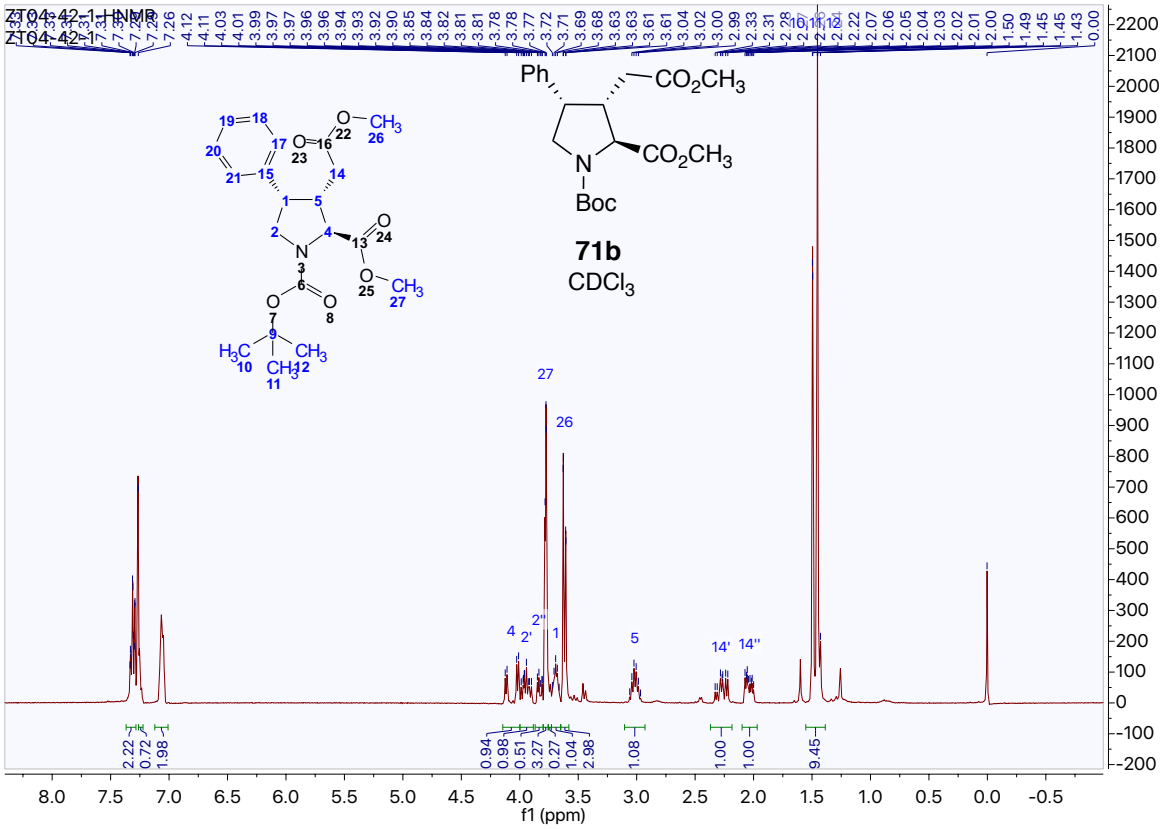
ZT04-42-1-HNMR
ZT04-42-1
Ph
CO2CH3
CO2CH3
N
Boc
71b
CDCl3
f1 (ppm)

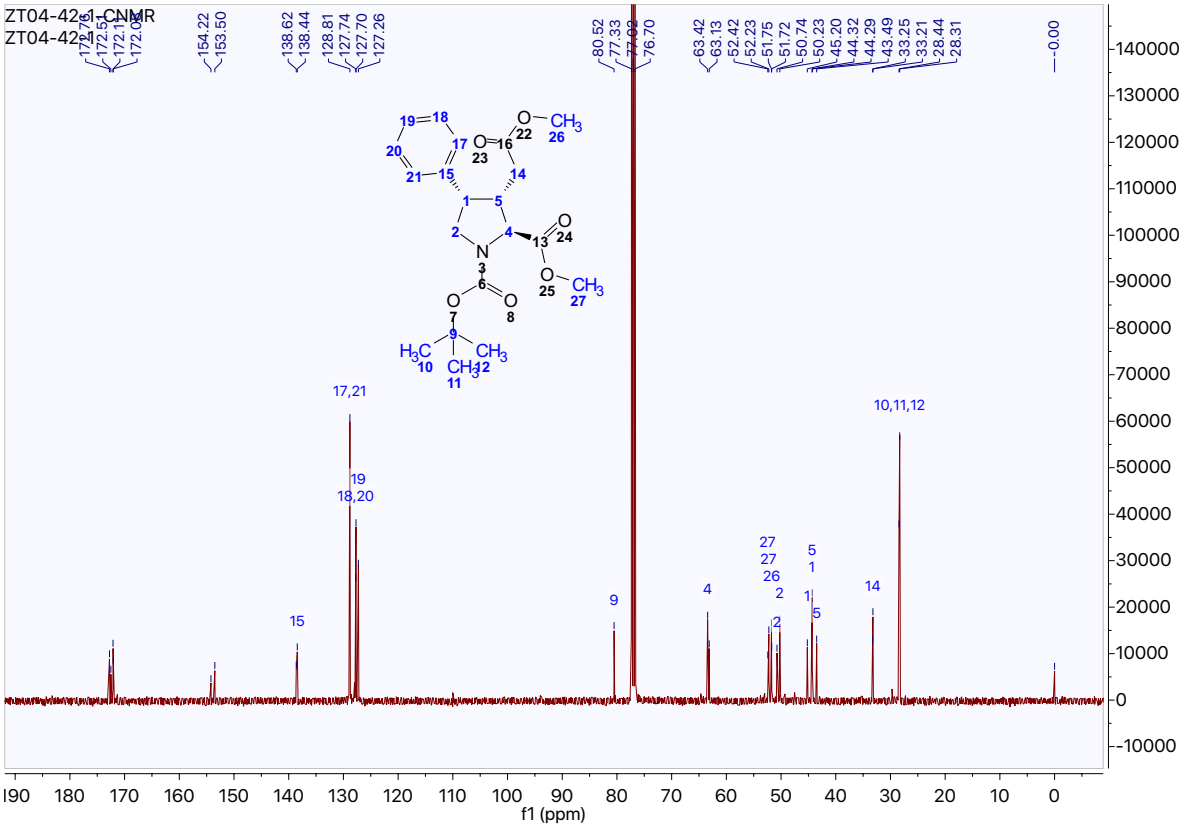
ZT04-42-1-CNMR
ZT04-42-1
f1 (ppm)

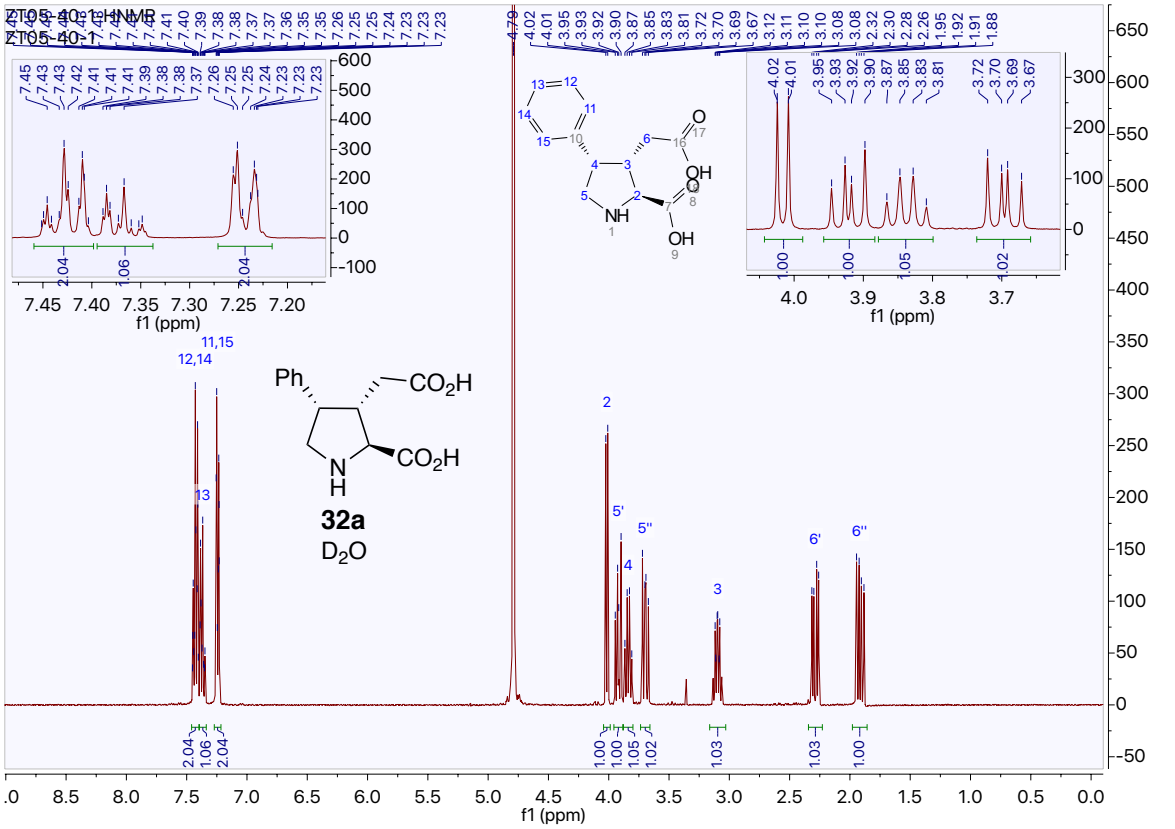
ZT05-40-1-HNMR
ZT05-40-1
f1 (ppm)
Ph
CO2H
CO2H
N
H
32a
D2O

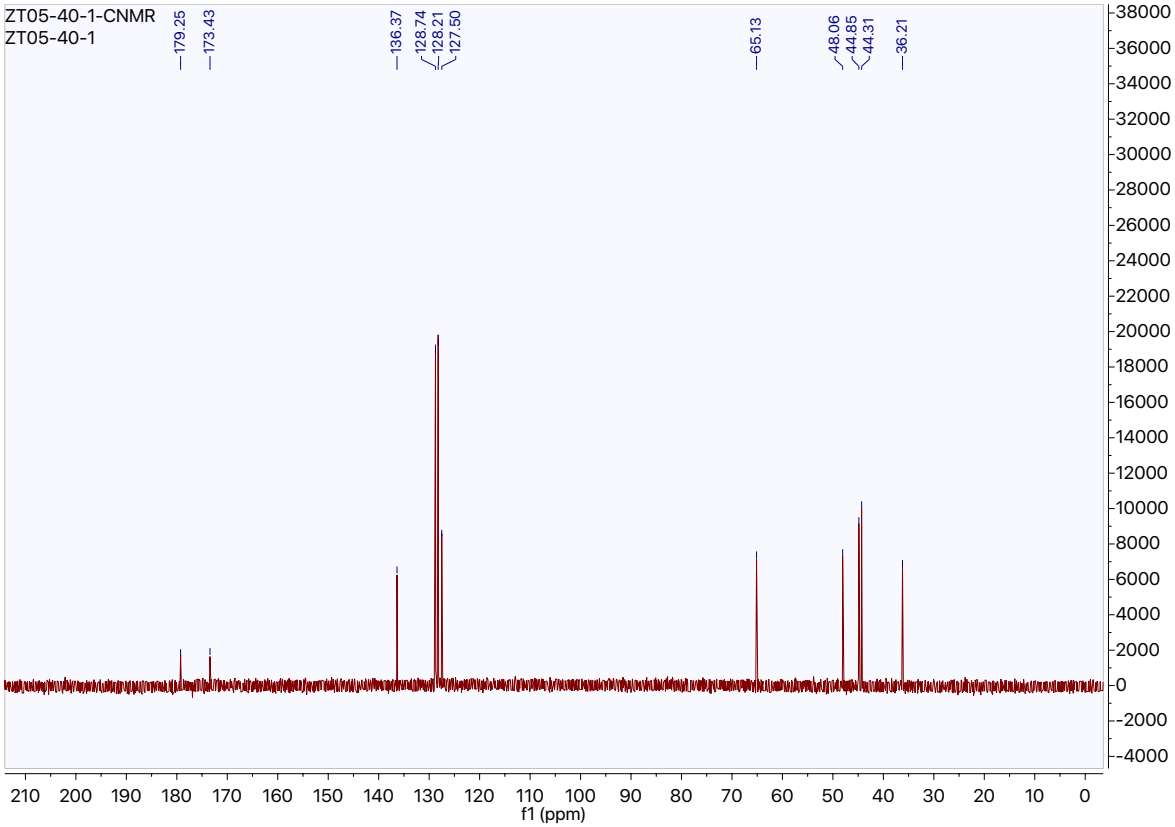
ZT05-40-1-CNMR
ZT05-40-1
179.25
173.43
136.37
128.74
128.21
127.50
65.13
48.06
44.85
44.31
36.21
f1 (ppm)

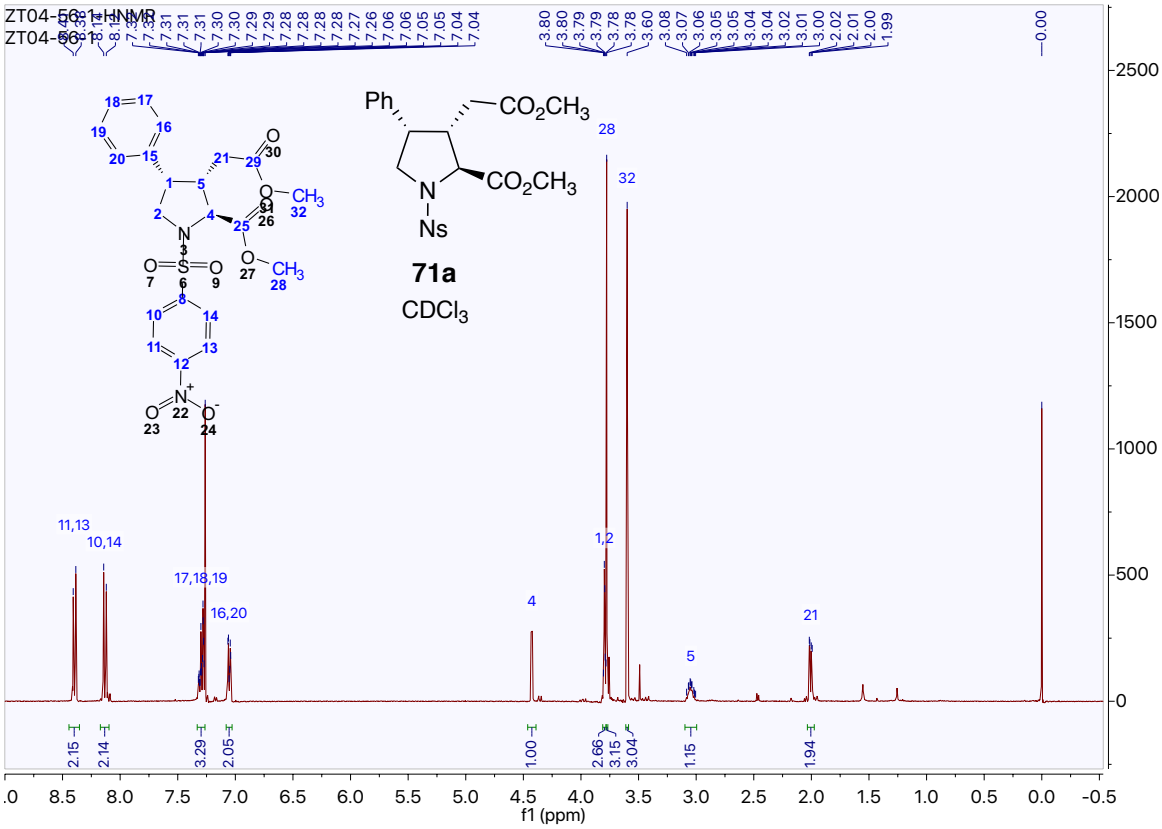
ZT04-56-1-HNMR
ZT04-56-1
71a
CDCl3
f1 (ppm)

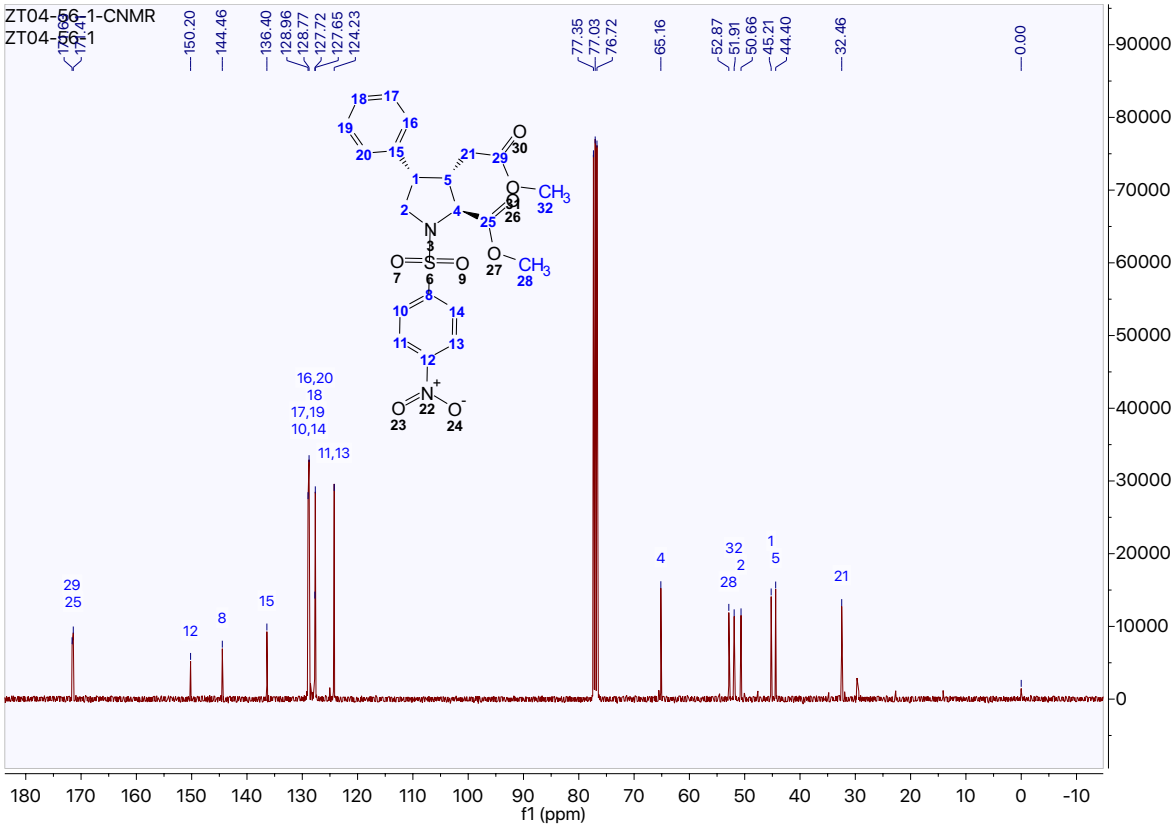
ZT04-56-1-CNMR
ZT04-56-1
f1 (ppm)

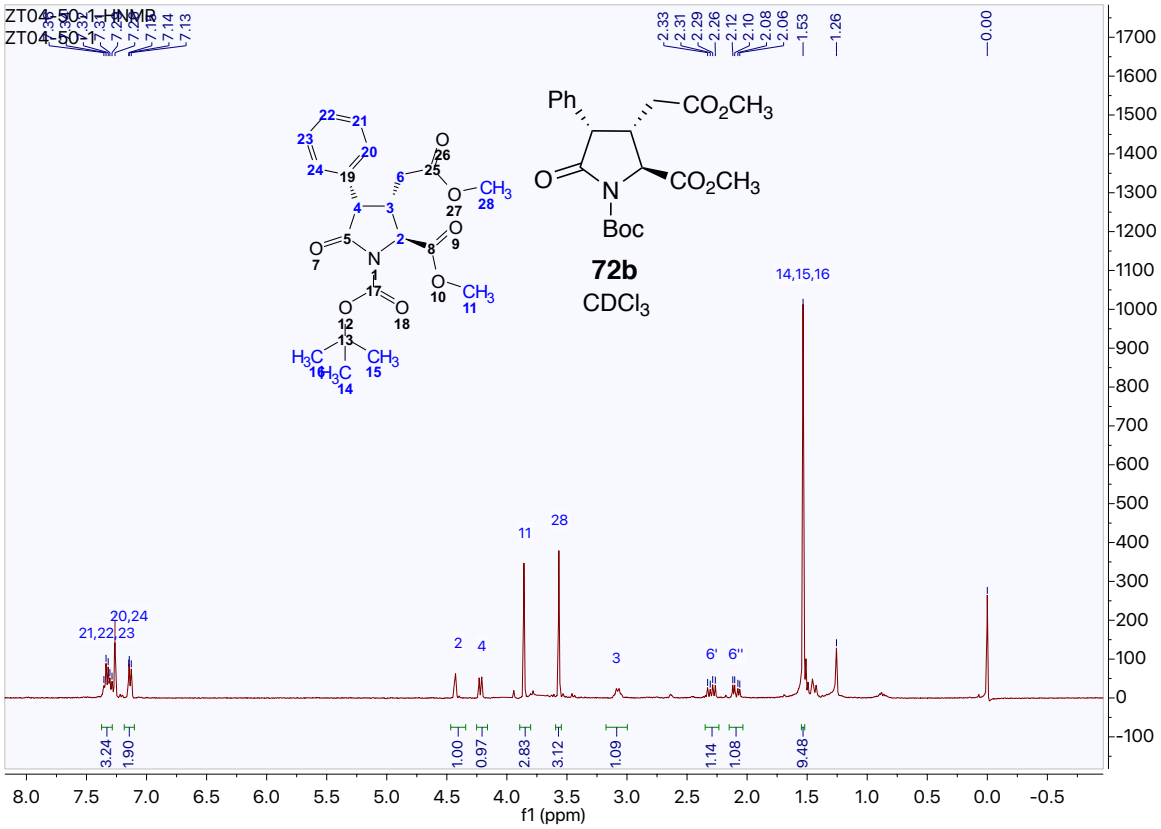
ZT04-50-1-1HNMR
ZT04-50-1
72b
CDCl3
Ph
CO2CH3
CO2CH3
Boc
14,15,16
11
28
20,24
21,22,23
2
4
3
6'
6''
f1 (ppm)

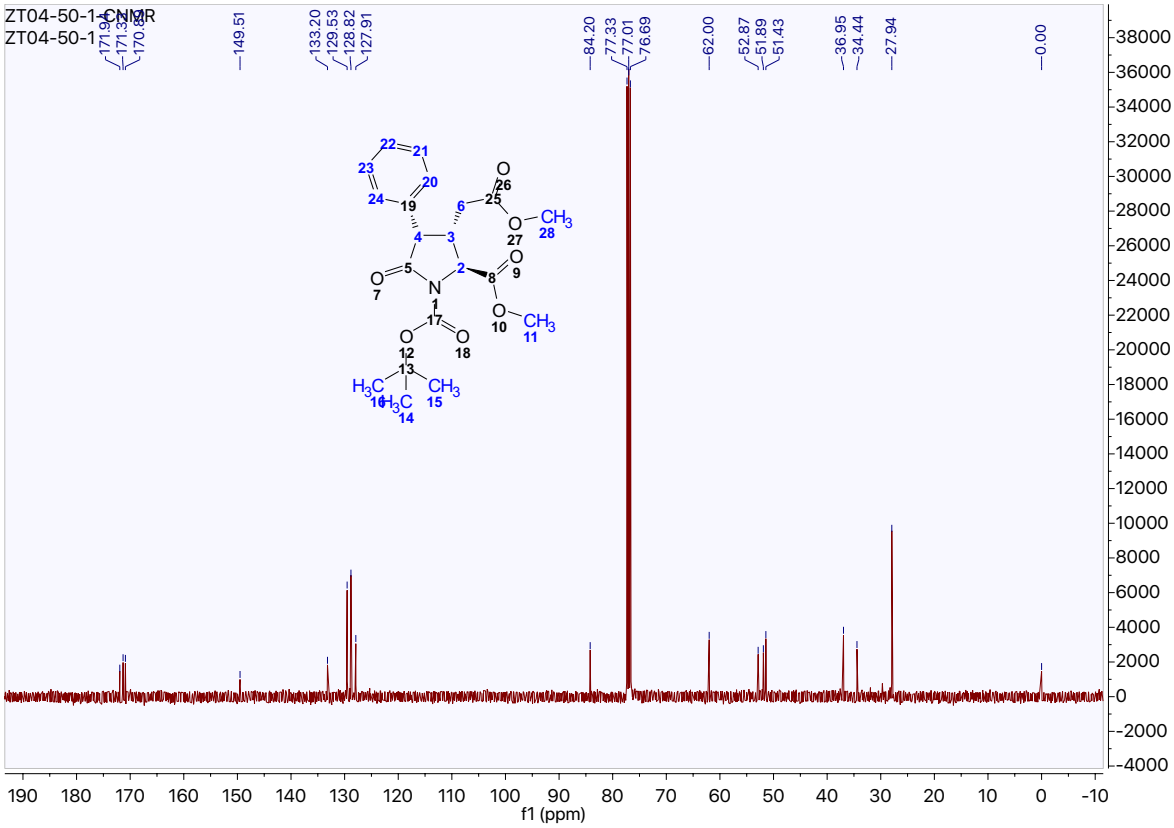
ZT04-50-1-CNMR
ZT04-50-1
149.51
133.20
129.53
128.82
127.91
84.20
77.33
77.01
76.69
62.00
52.87
51.89
51.43
36.95
34.44
27.94
0.00
f1 (ppm)

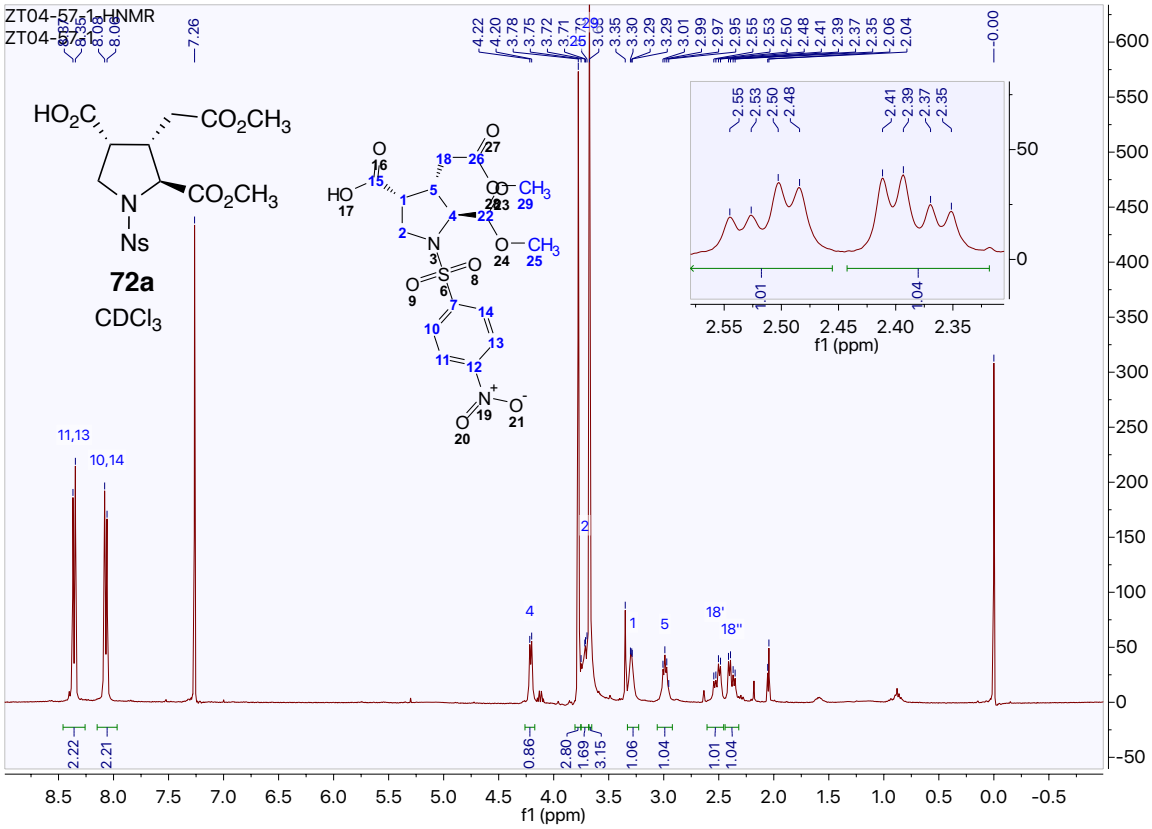
ZT04-57-1-HNMR
72a
CDCl3
f1 (ppm)

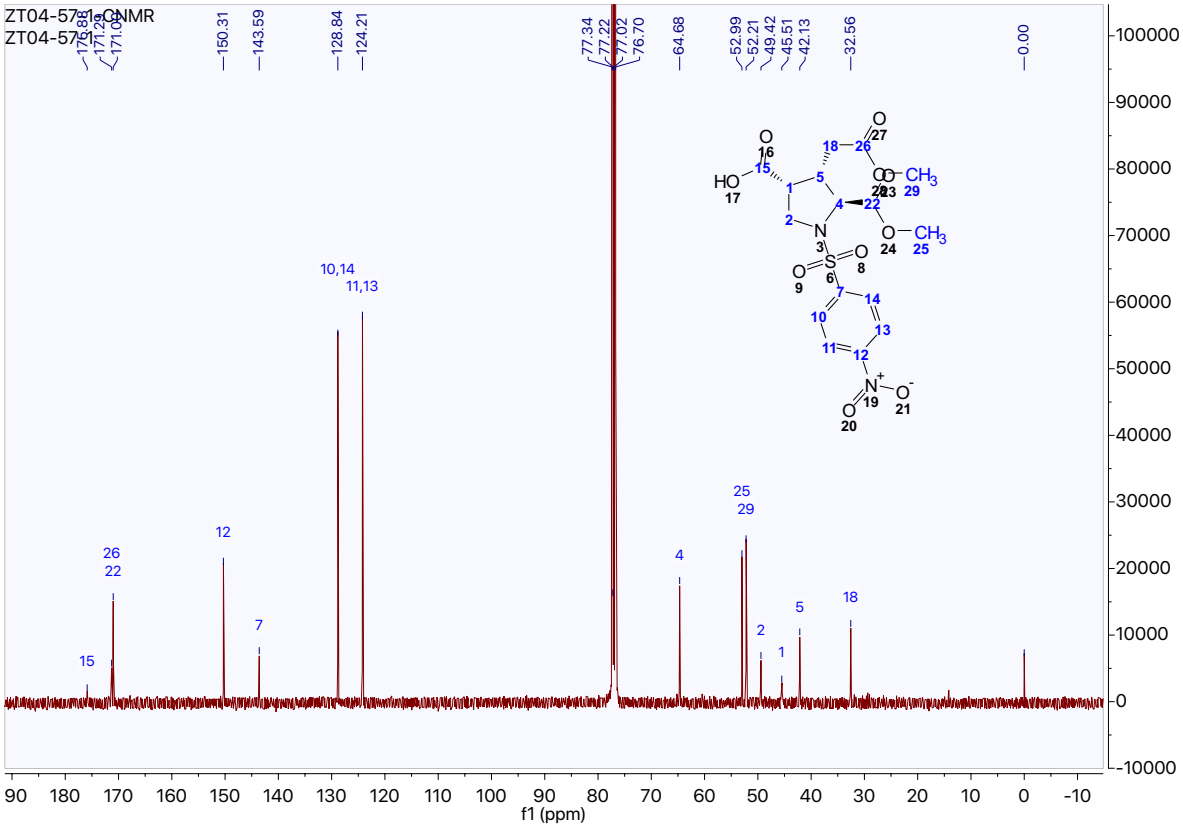
ZT04-57-1-CNMR
f1 (ppm)

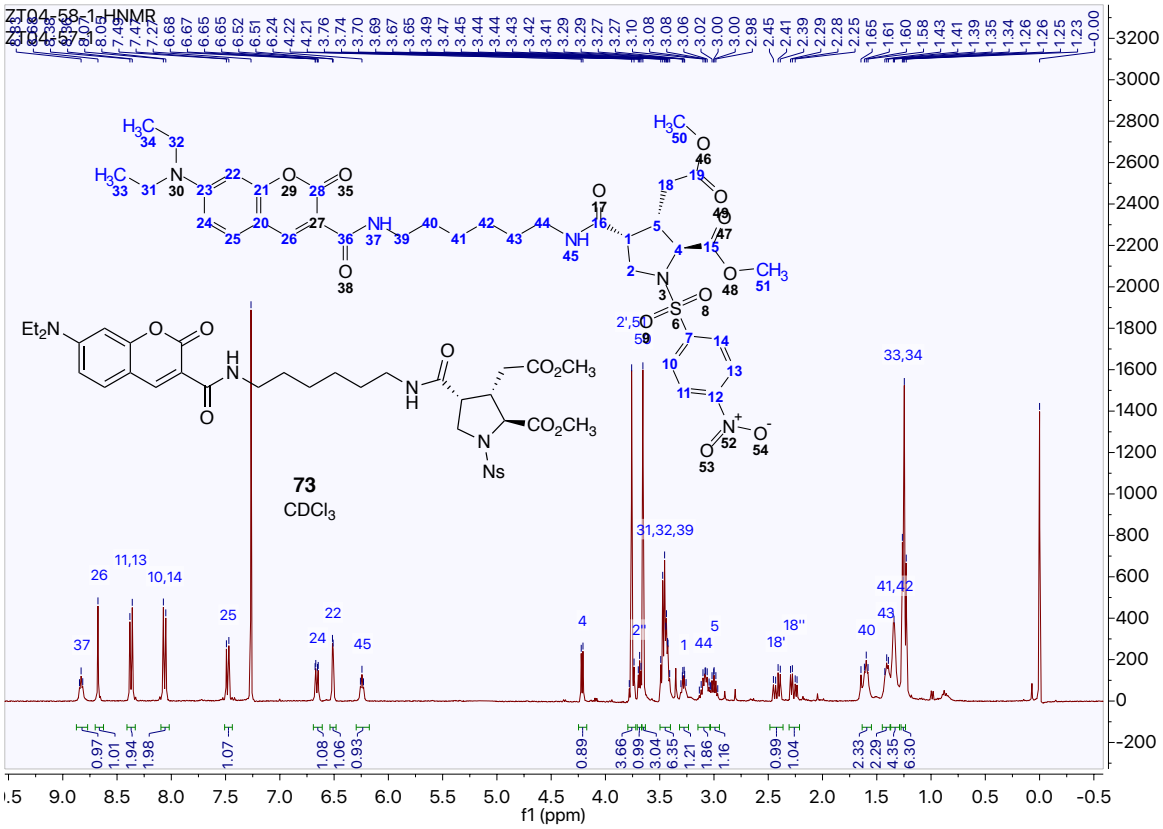
ZT04-58-1 HNMR
ZT04-57-1
73
CDCl3
f1 (ppm)

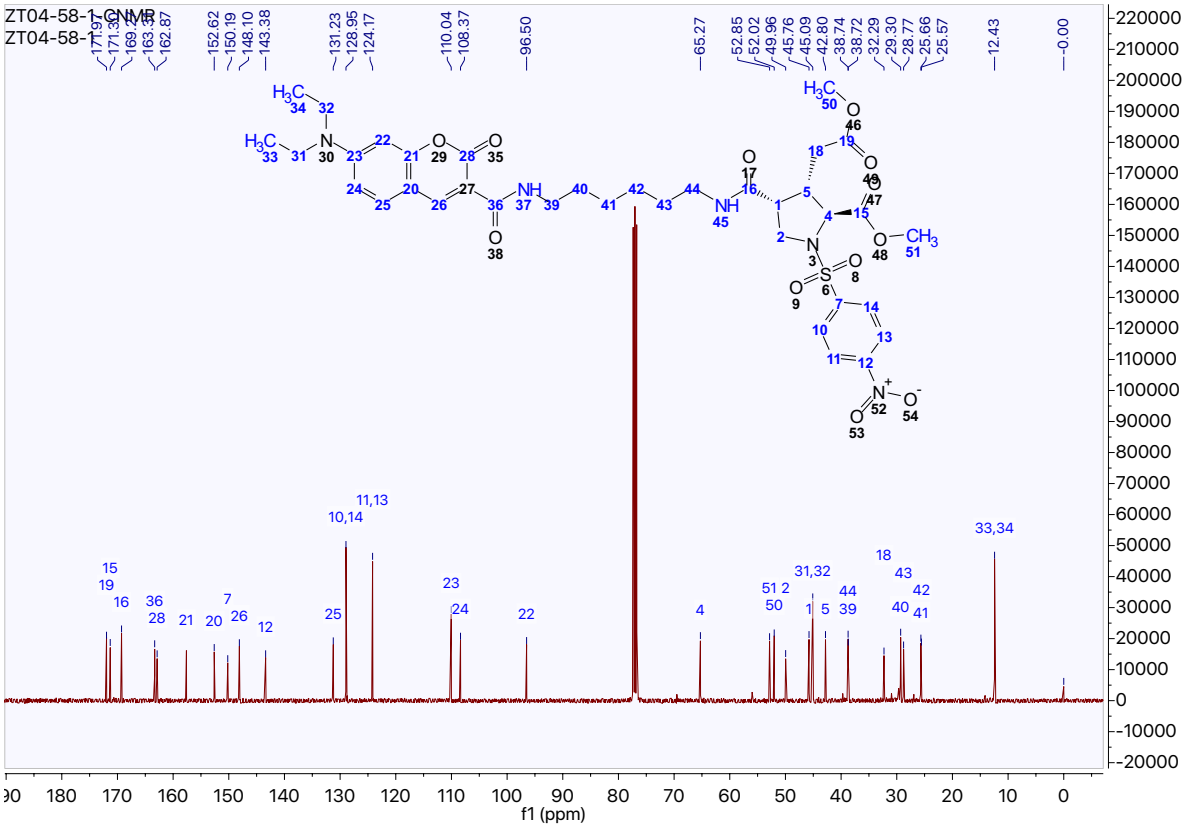
ZT04-58-1 CNMR
ZT04-58-1
f1 (ppm)

Appendix C

1D NOE spectra of compounds in Chapter 4

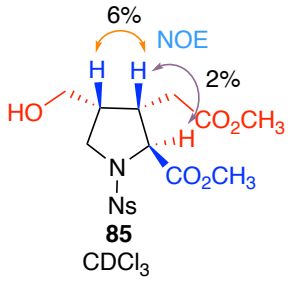

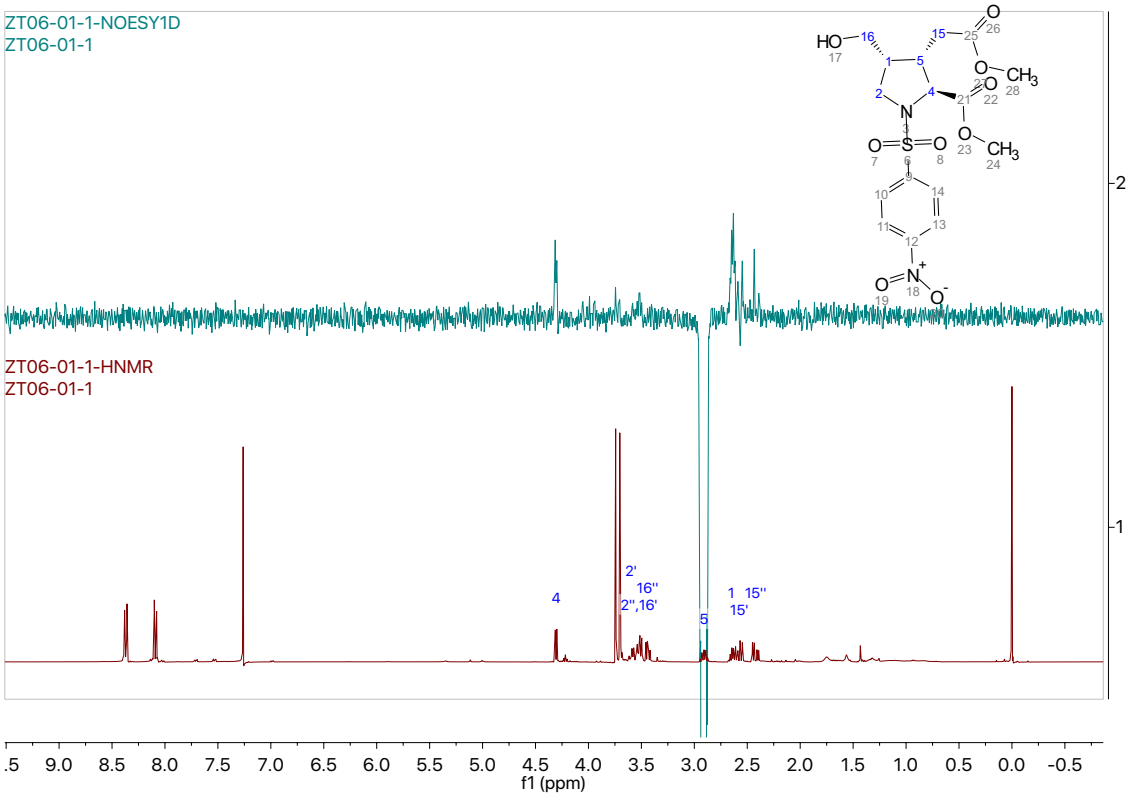

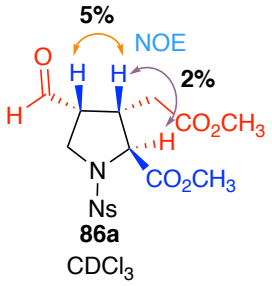
5%
NOE
2%
O
H
H
H
CO2CH3
H
N
CO2CH3
Ns
86a
CDCl3

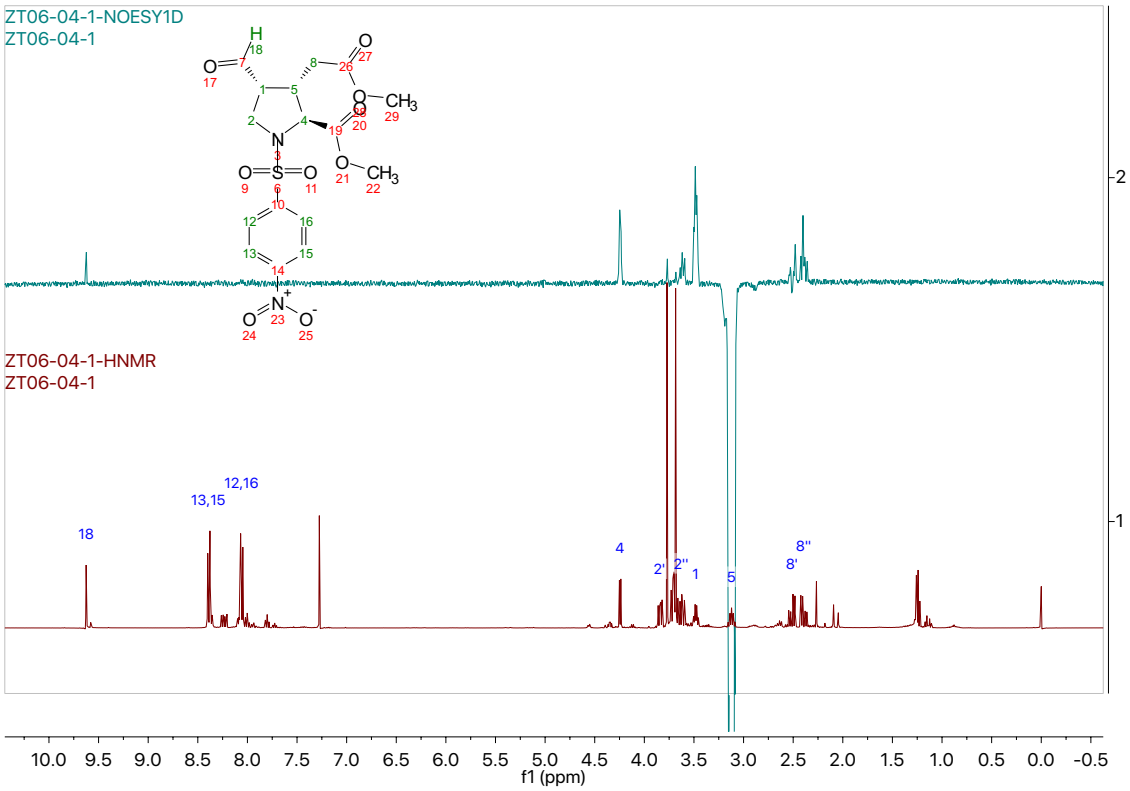
ZT06-04-1-NOESY1D
ZT06-04-1
ZT06-04-1-HNMR
ZT06-04-1
18
13,15
12,16
4
2'
2''
1
5
8''
8'
-2
-1
10.0 9.5 9.0 8.5 8.0 7.5 7.0 6.5 6.0 5.5 5.0 4.5 4.0 3.5 3.0 2.5 2.0 1.5 1.0 0.5 0.0 -0.5
f1 (ppm)

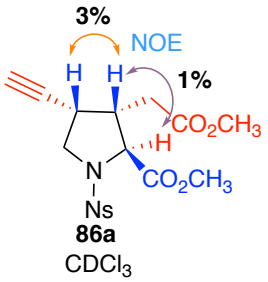
3%
NOE
1%
H
H
CO2CH3
H
N
CO2CH3
Ns
86a
CDCl3

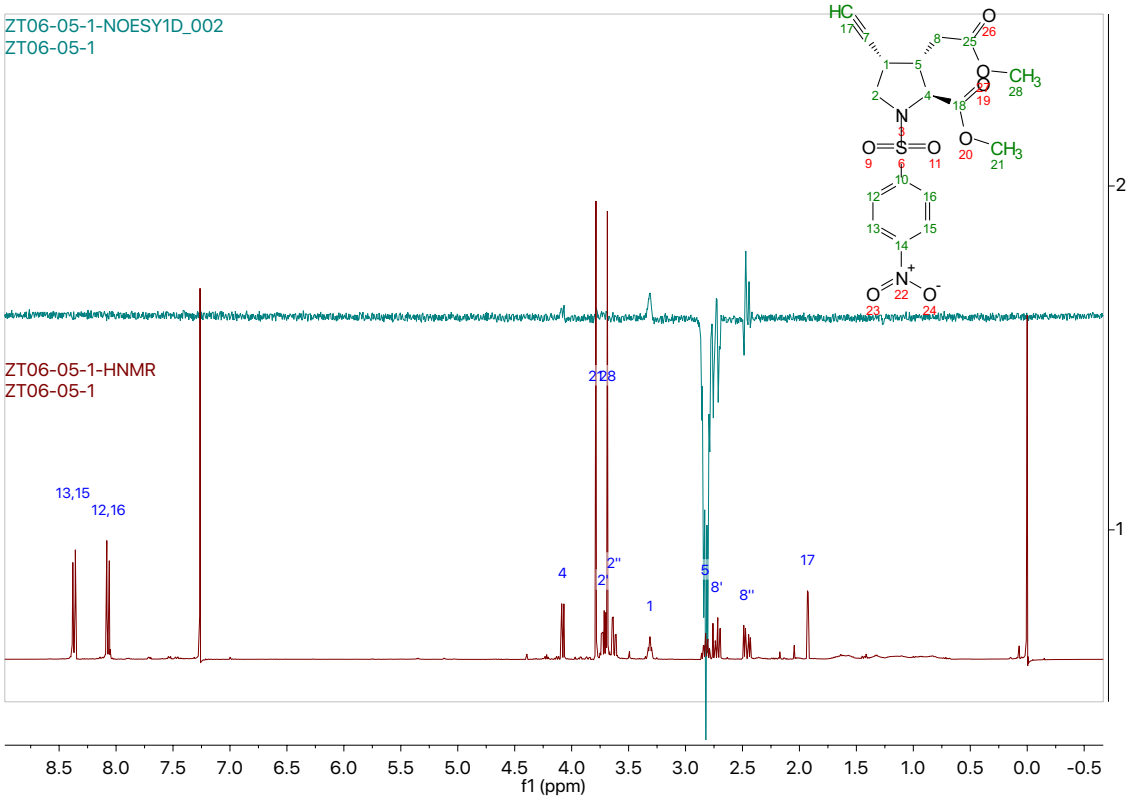
ZT06-05-1-NOESY1D_002
ZT06-05-1
ZT06-05-1-HNMR
ZT06-05-1
13,15
12,16
4
2'
2''
2
28
1
5
8'
8''
17
-2
-1
8.5
8.0
7.5
7.0
6.5
6.0
5.5
5.0
4.5
4.0
3.5
3.0
2.5
2.0
1.5
1.0
0.5
0.0
-0.5
f1 (ppm)

NMR spectra of compounds in Chapter 4

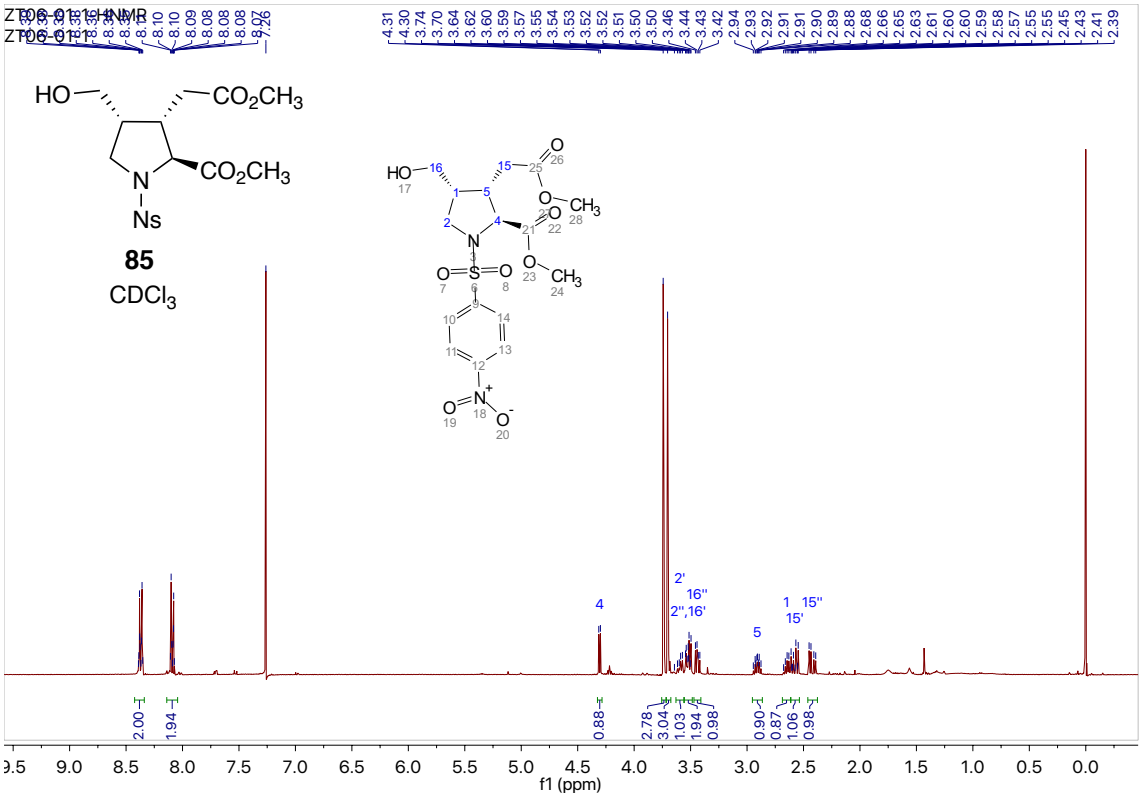

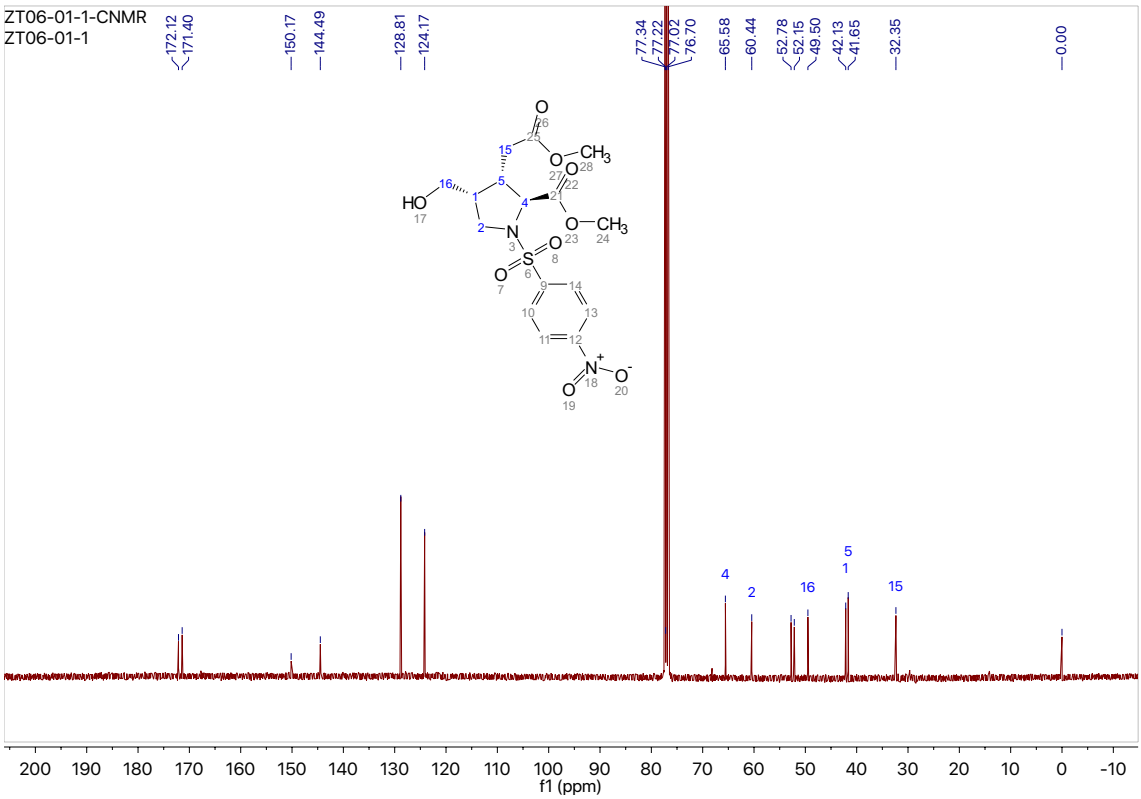

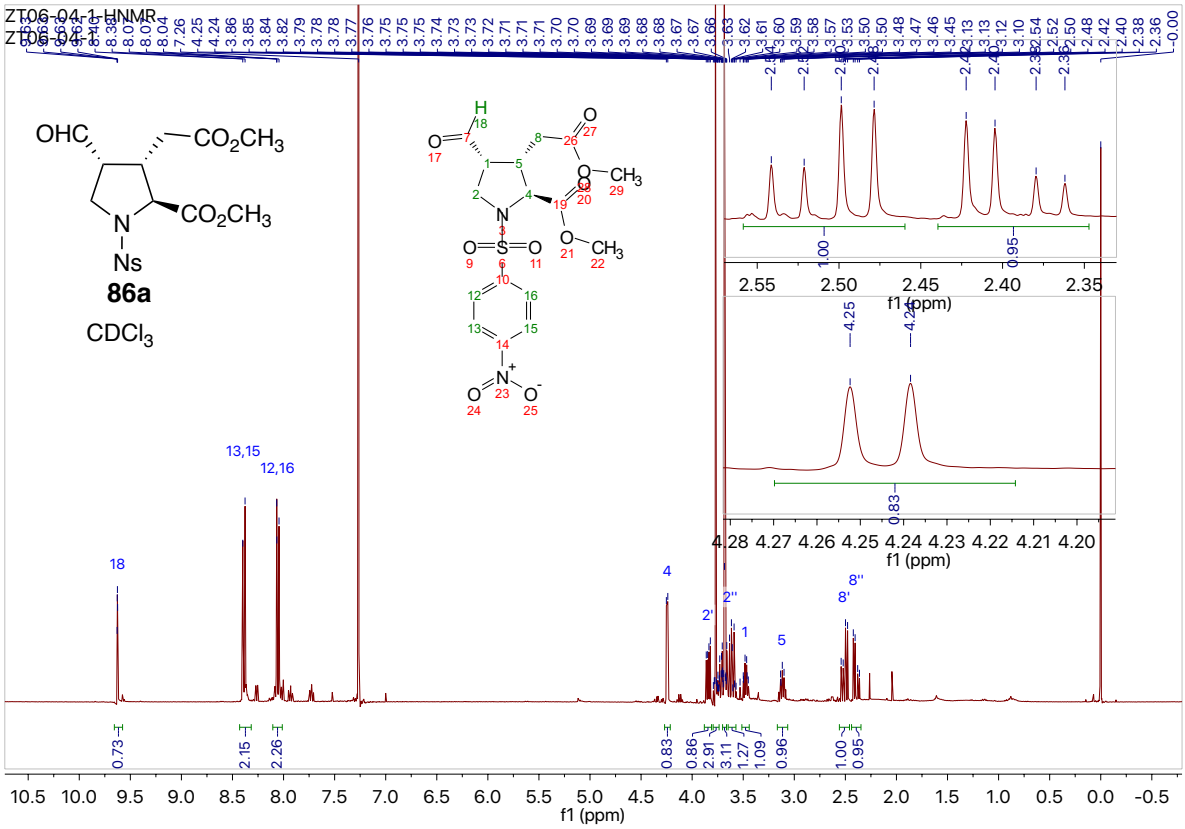
ZT06-04-1-HNMR
ZT06-04-1
OHC
CO2CH3
CO2CH3
N
Ns
86a
CDCl3
13,15
12,16
18
4
2'
2''
1
5
8'
8''
f1 (ppm)

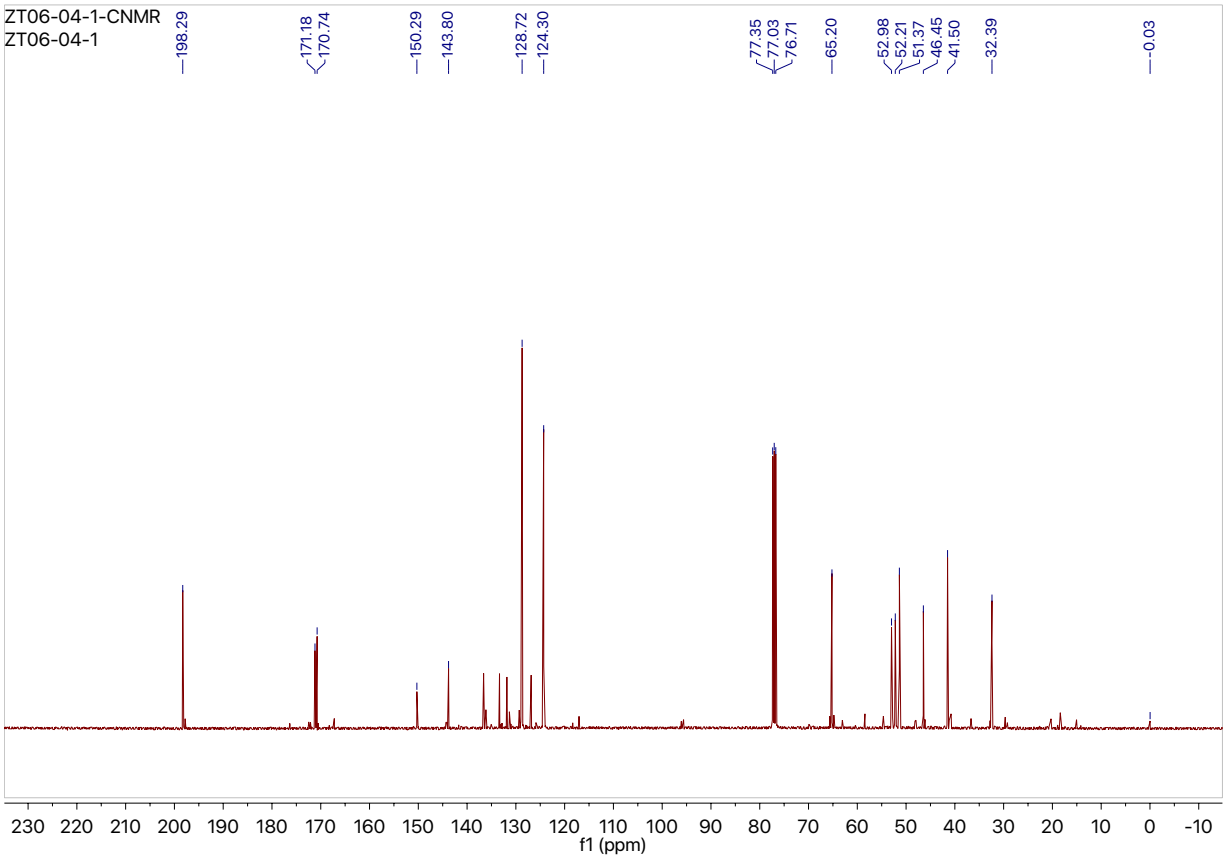
ZT06-04-1-CNMR
ZT06-04-1
198.29
171.18
170.74
150.29
143.80
128.72
124.30
77.35
77.03
76.71
65.20
52.98
52.21
51.37
46.45
41.50
32.39
-0.03
f1 (ppm)

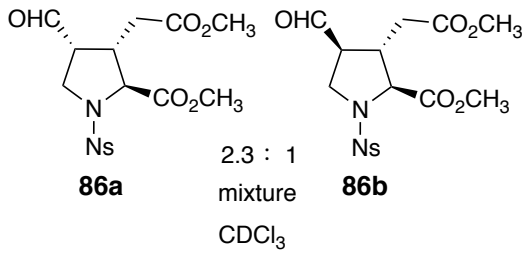
OHC
CO2CH3
CO2CH3
N
Ns
86a
2.3 : 1
mixture
CDCl3
OHC
CO2CH3
CO2CH3
N
Ns
86b

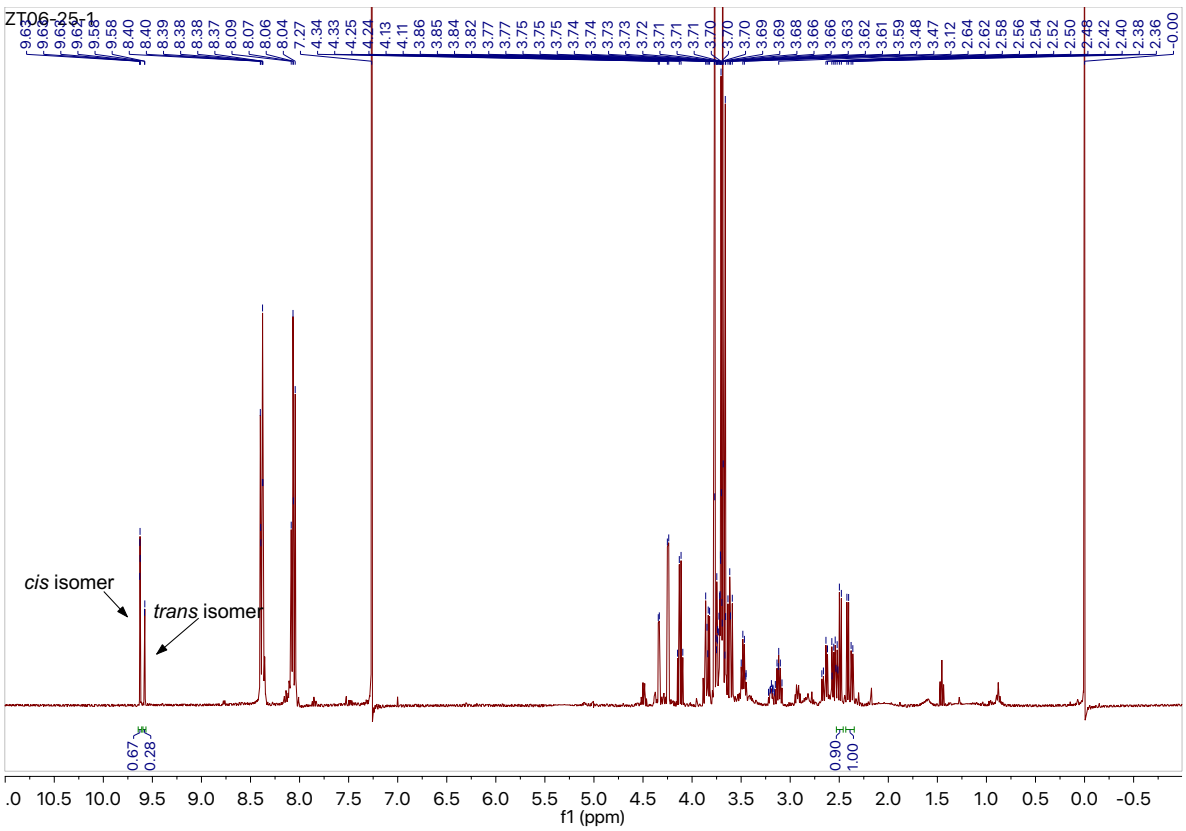
ZT06-25-1
cis isomer
trans isomer
0.67
0.28
0.90
1.00
f1 (ppm)

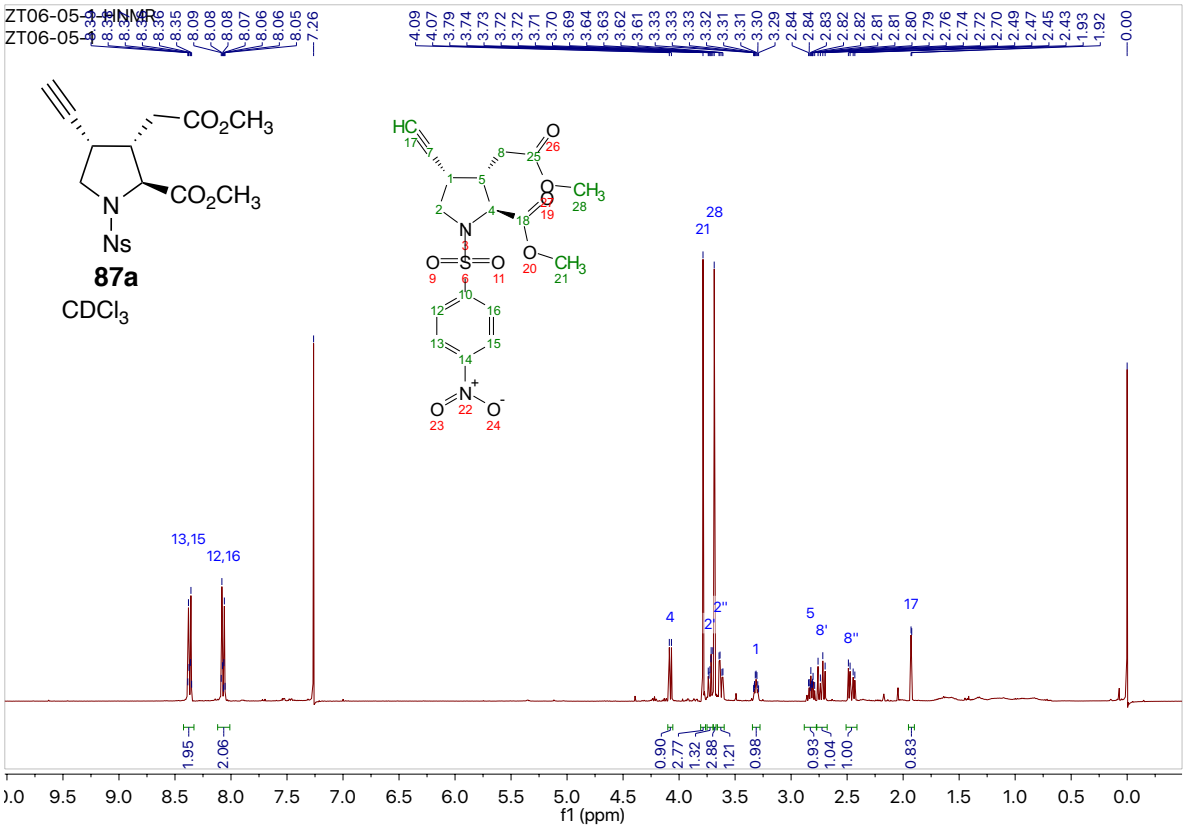
ZT06-05-1-HNMR
ZT06-05-1
87a
CDCl3
f1 (ppm)

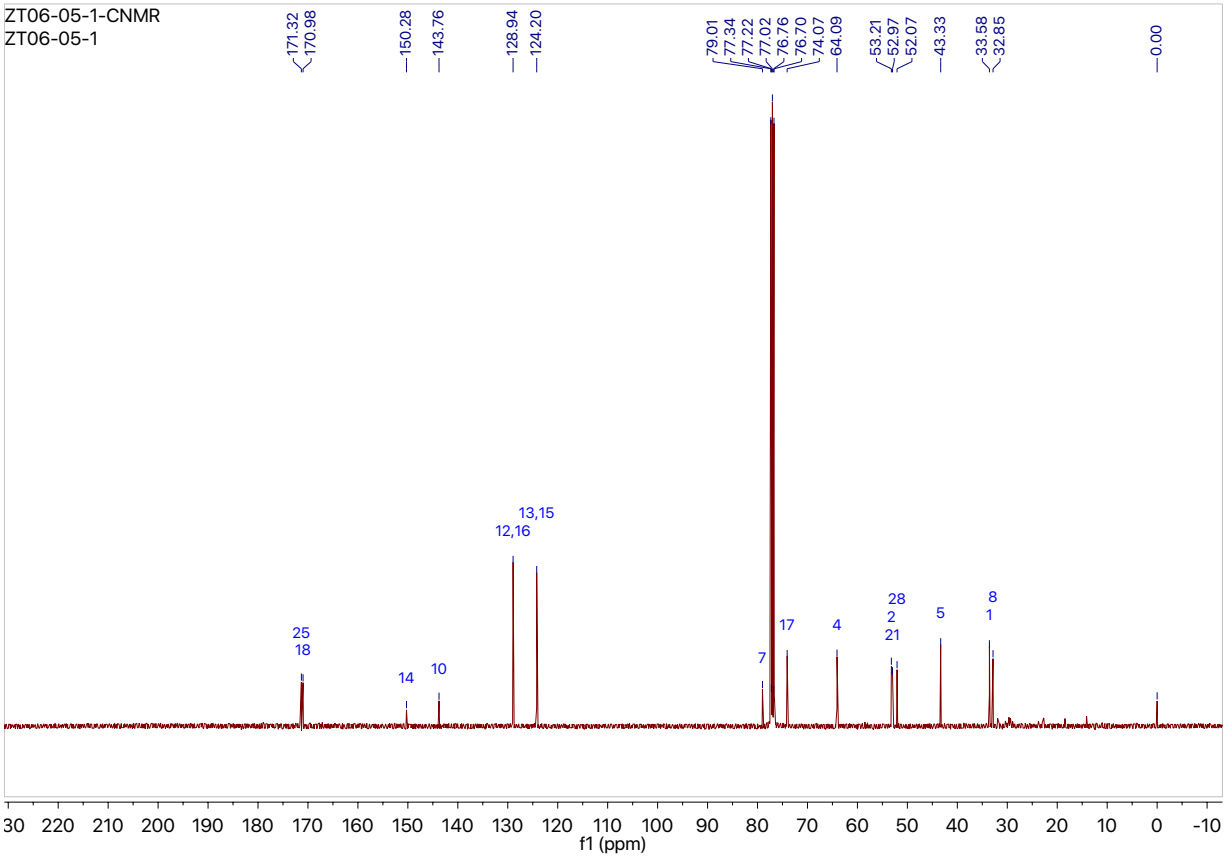
ZT06-05-1-CNMR
ZT06-05-1
f1 (ppm)

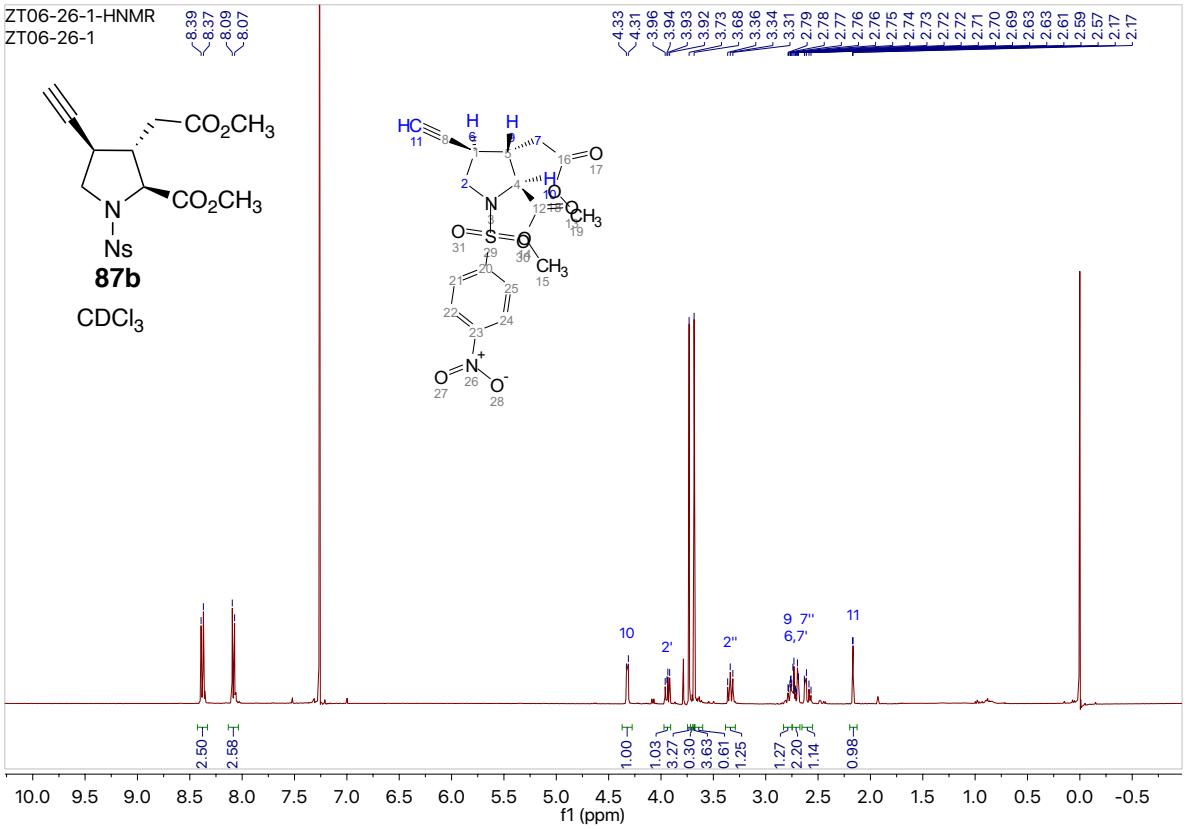
ZT06-26-1-HNMR
ZT06-26-1
87b
CDCl3
f1 (ppm)

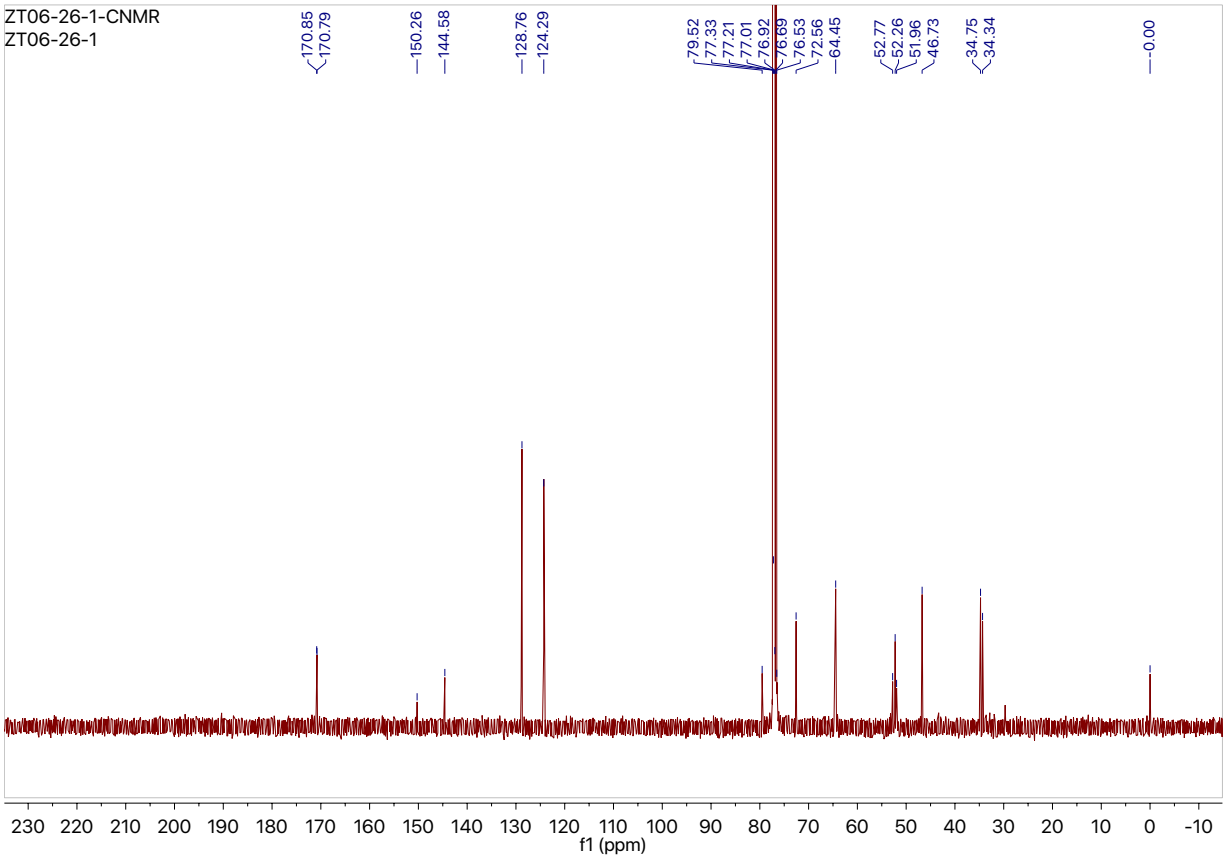
ZT06-26-1-CNMR
ZT06-26-1
f1 (ppm)

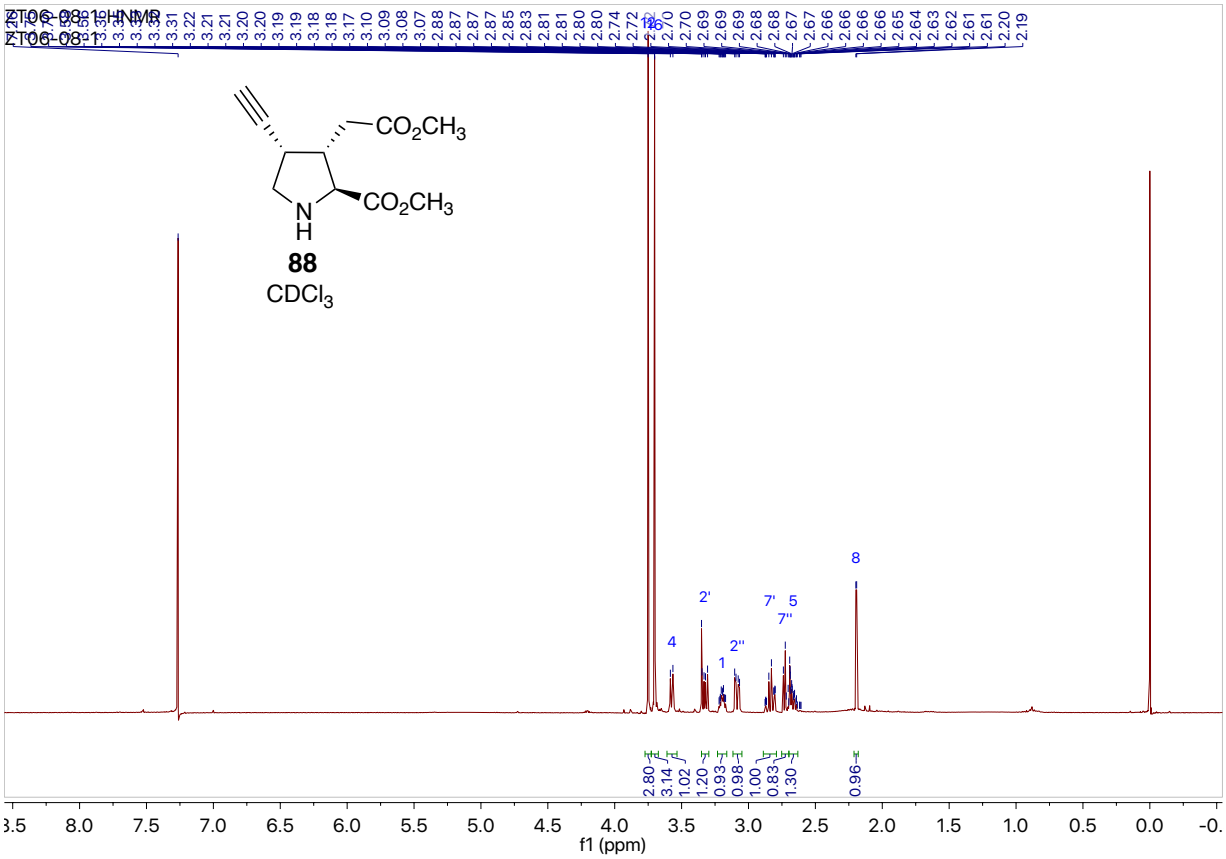
ZT06-08-1-HNMR
ZT06-08-1
CO2CH3
CO2CH3
N
H
88
CDCl3
4
2'
1
2''
7'
7''
5
8
2.80
3.14
1.02
1.20
0.93
0.98
1.00
0.83
1.30
0.96
f1 (ppm)

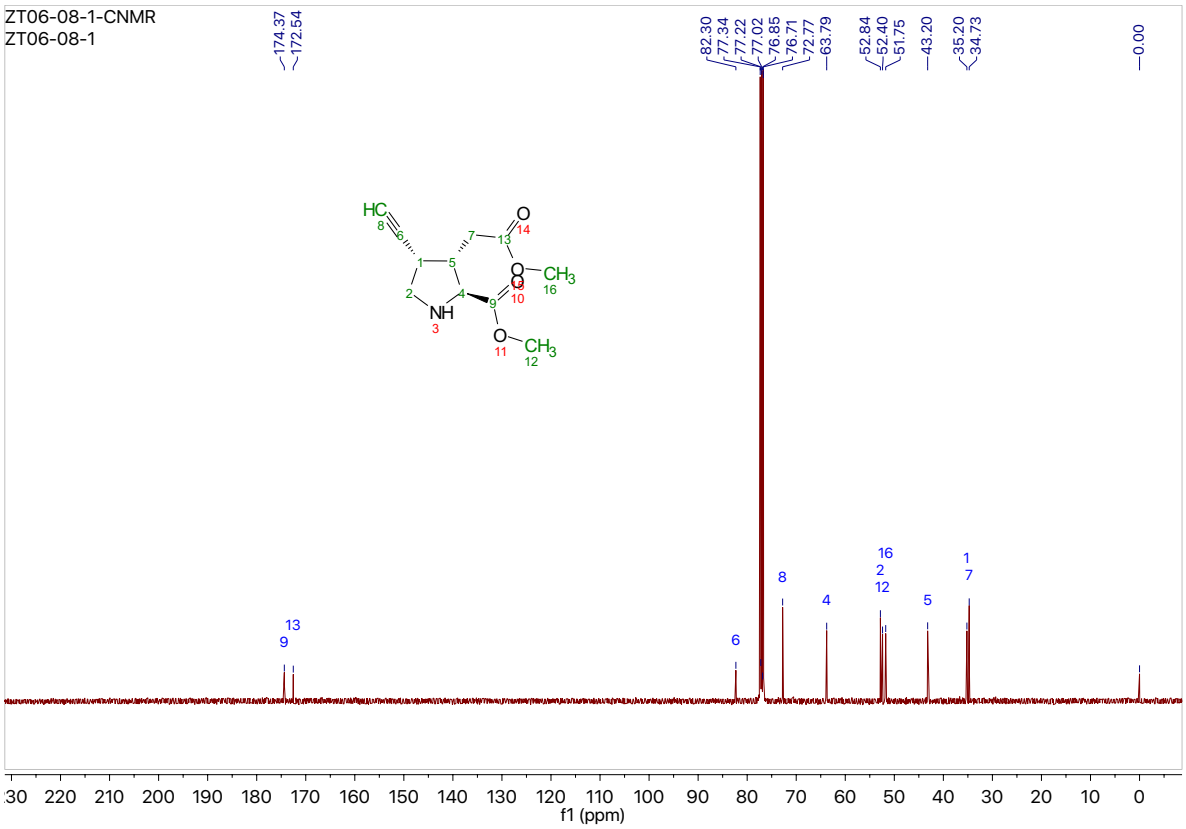
ZT06-08-1-CNMR
ZT06-08-1
174.37
172.54
82.30
77.34
77.22
77.02
76.85
76.71
72.77
63.79
52.84
52.40
51.75
43.20
35.20
34.73
0.00
HC
NH
CH3
CH3
13
9
6
8
4
16
2
12
5
1
7
f1 (ppm)

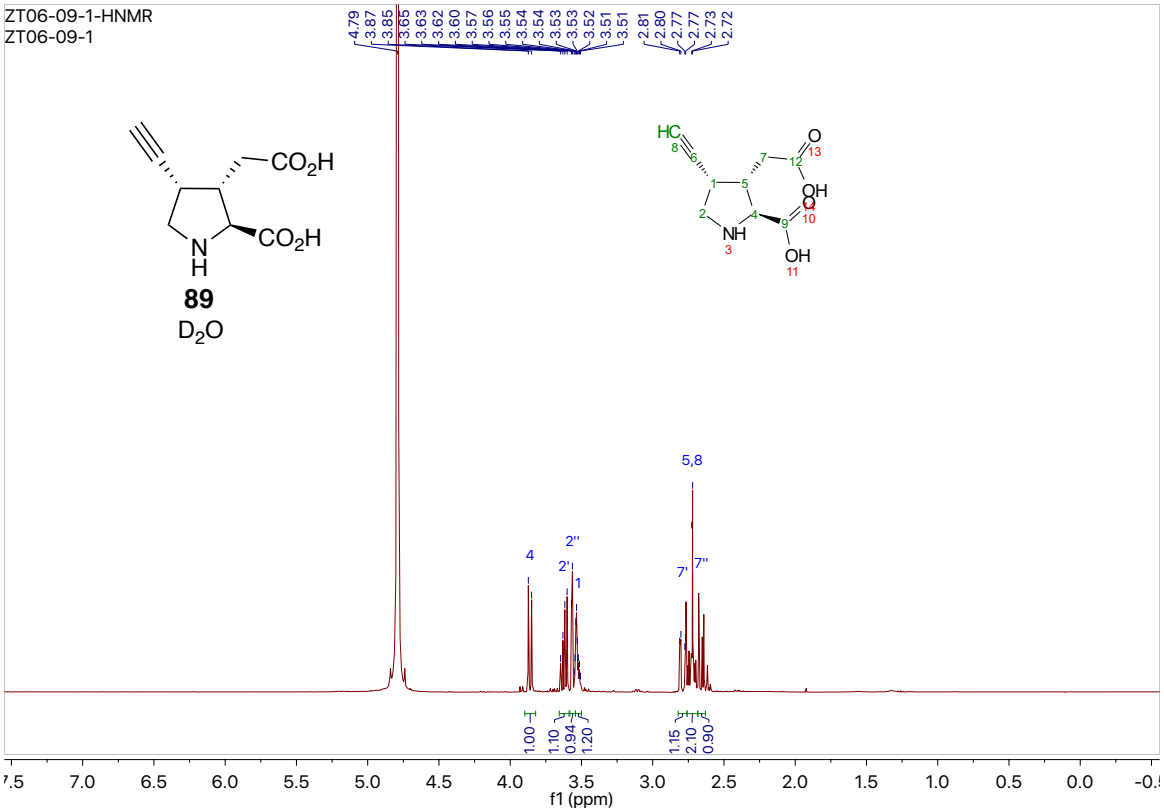
ZT06-09-1-HNMR
ZT06-09-1
4.79
3.87
3.85
3.65
3.63
3.62
3.60
3.57
3.56
3.55
3.54
3.54
3.53
3.53
3.52
3.51
3.51
2.81
2.80
2.77
2.77
2.73
2.72
CO2H
CO2H
N
H
89
D2O
HC
O
OH
NH
OH
5,8
4
2''
2'
1
7'
7''
1.00
1.10
0.94
1.20
1.15
2.10
0.90
f1 (ppm)

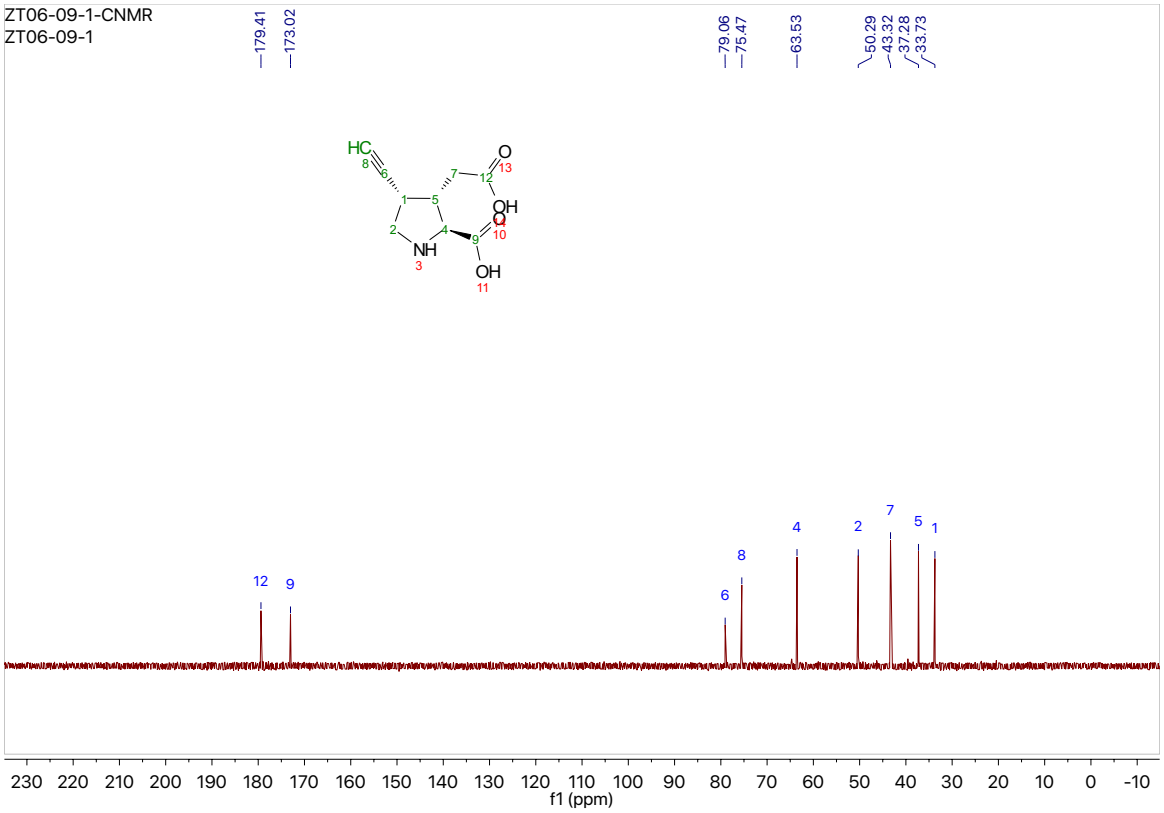
ZT06-09-1-CNMR
ZT06-09-1
179.41
173.02
79.06
75.47
63.53
50.29
43.32
37.28
33.73
HC
O
OH
NH
OH
12
9
6
8
4
2
7
5
1
f1 (ppm)

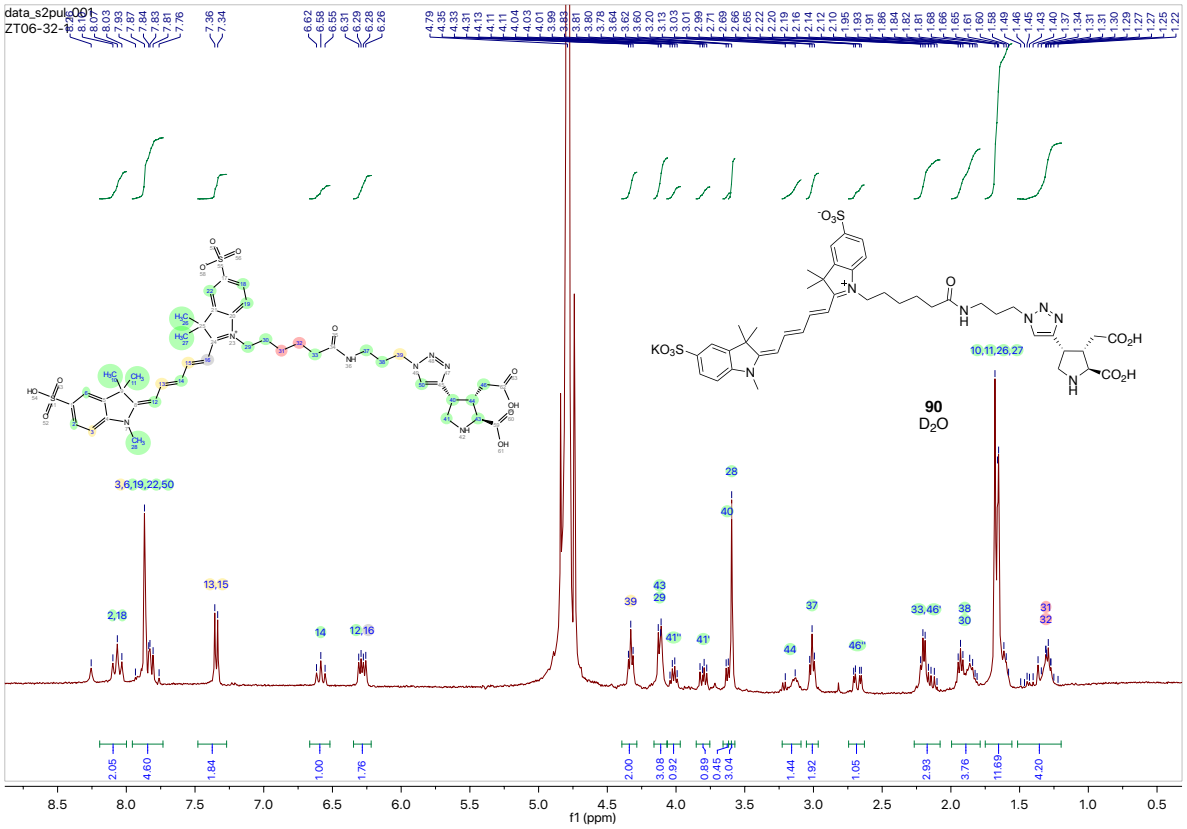
data_s2pulse_001
ZT06-32-
90
D_2O
f1 (ppm)

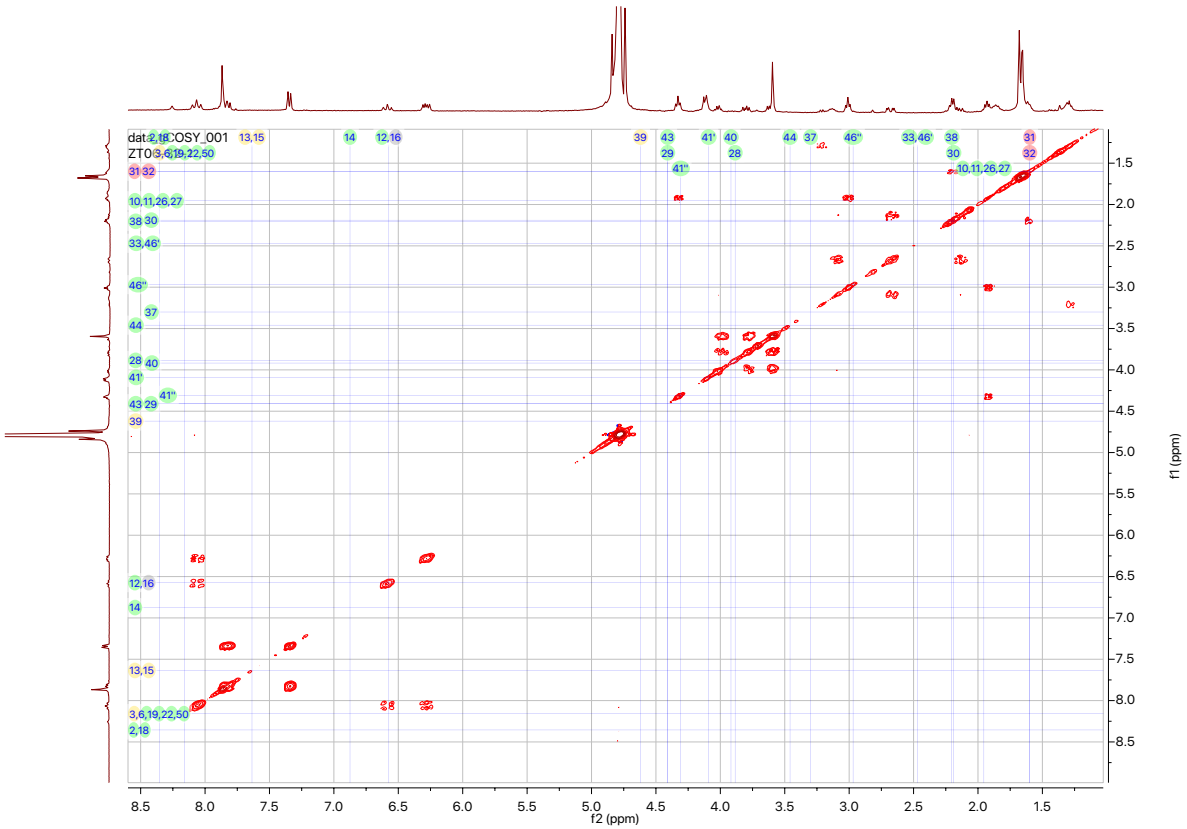
dat 2,tBCOSY_001
ZT0
f2 (ppm)
f1 (ppm)

Appendix D

NMR spectra of photolysis

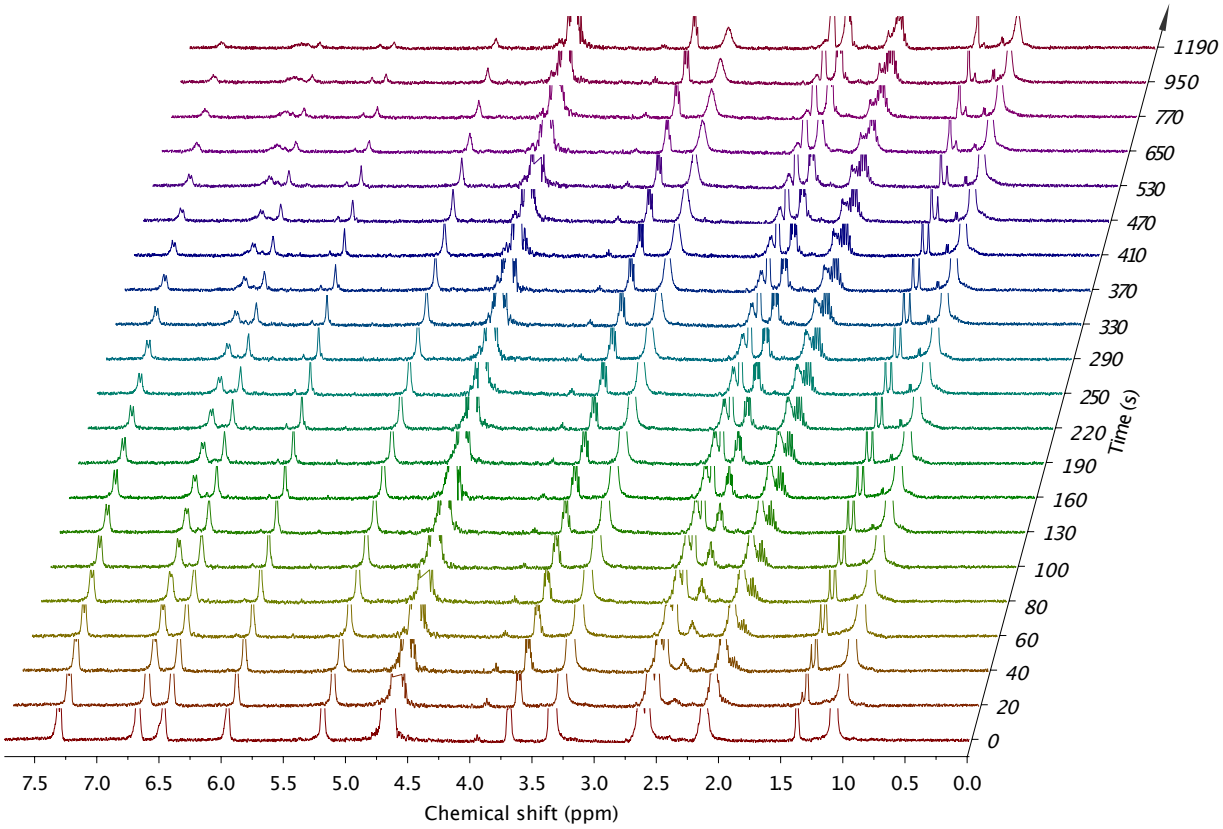

Figure S5–1. ^{1}H NMR spectra for progressive photolysis of DECM-Glu by 465 nm photoreactor

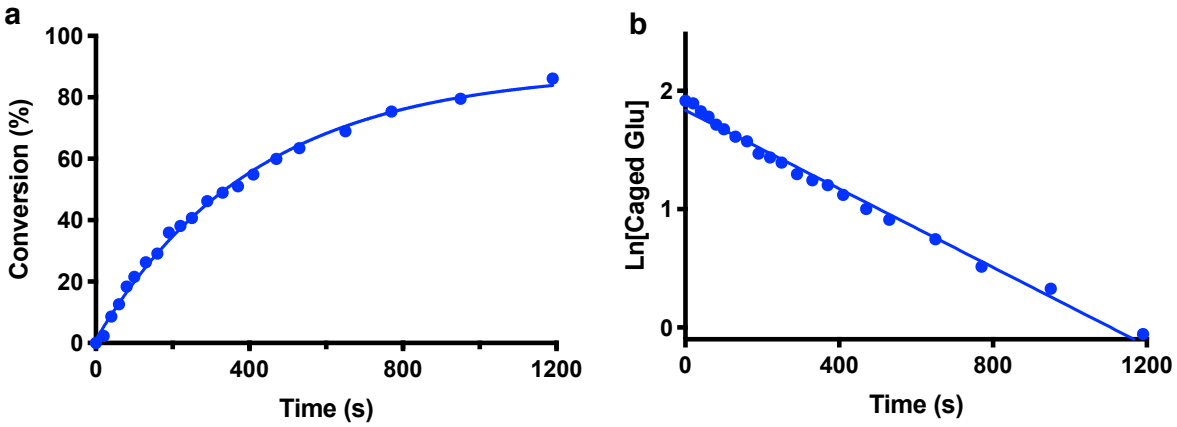

Figure S5–2. Photolysis rate of DECM-Glu under 465 nm photoreactore

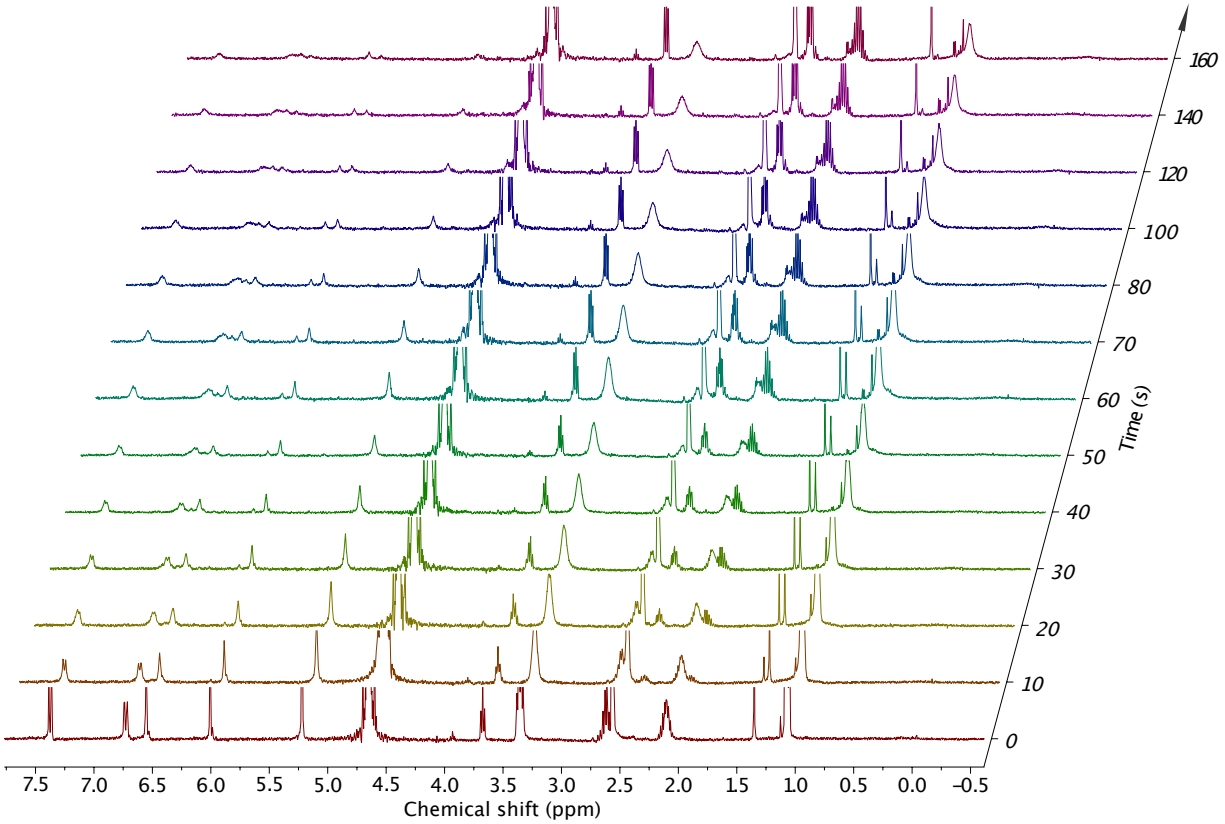

Figure S5–3. ^{1}H NMR spectra for progressive photolysis of DECM-Glu by 445 nm photoreactor

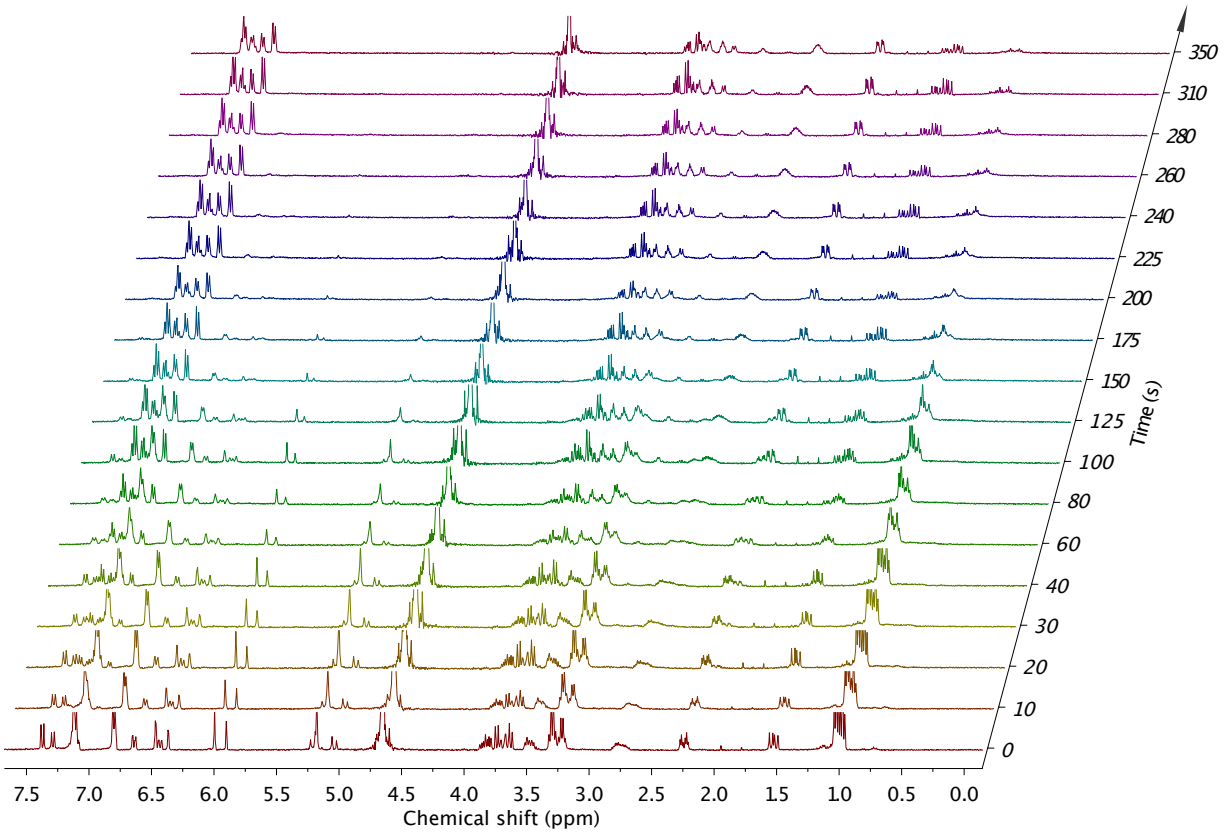

Figure S5–4. 1H NMR spectra for progressive photolysis of DECM-PhKA by 445 nm photoreactor

1D NOE spectra of compounds in Chapter 5

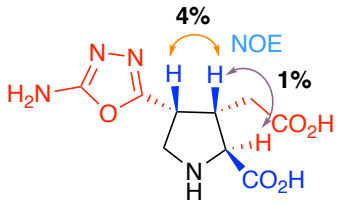

124

D_2O

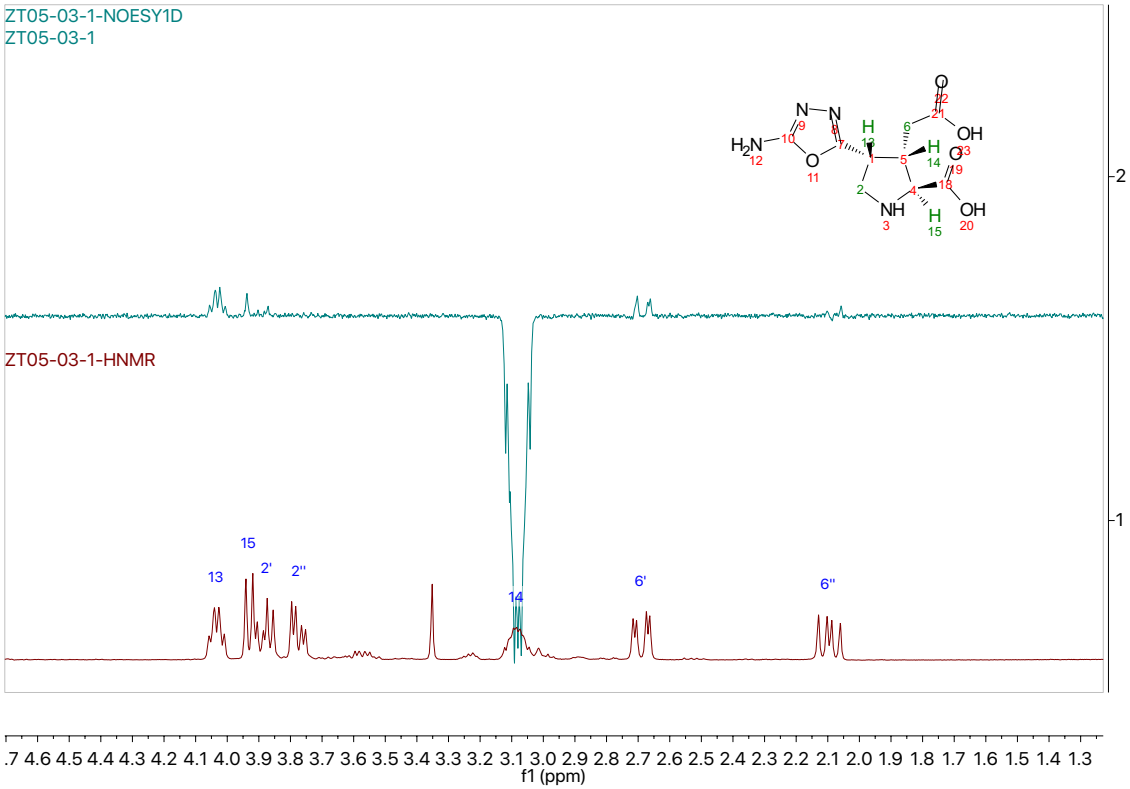

NMR spectra of compounds in Chapter 5

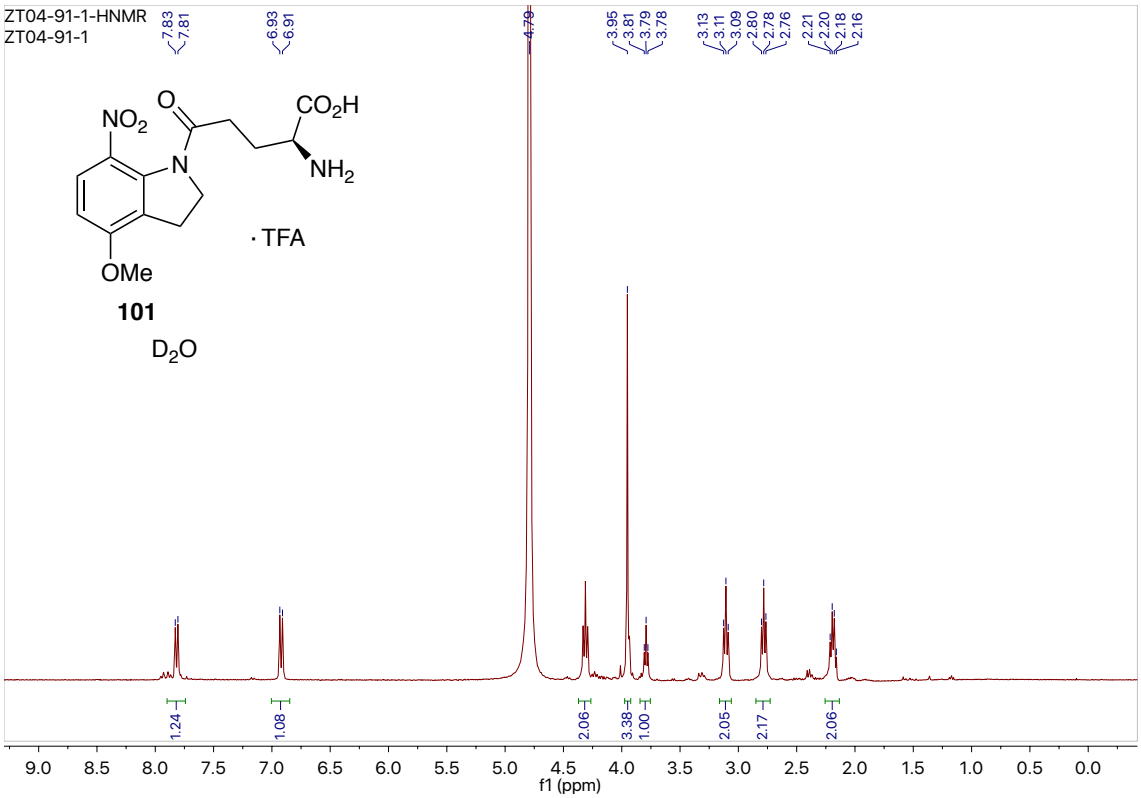

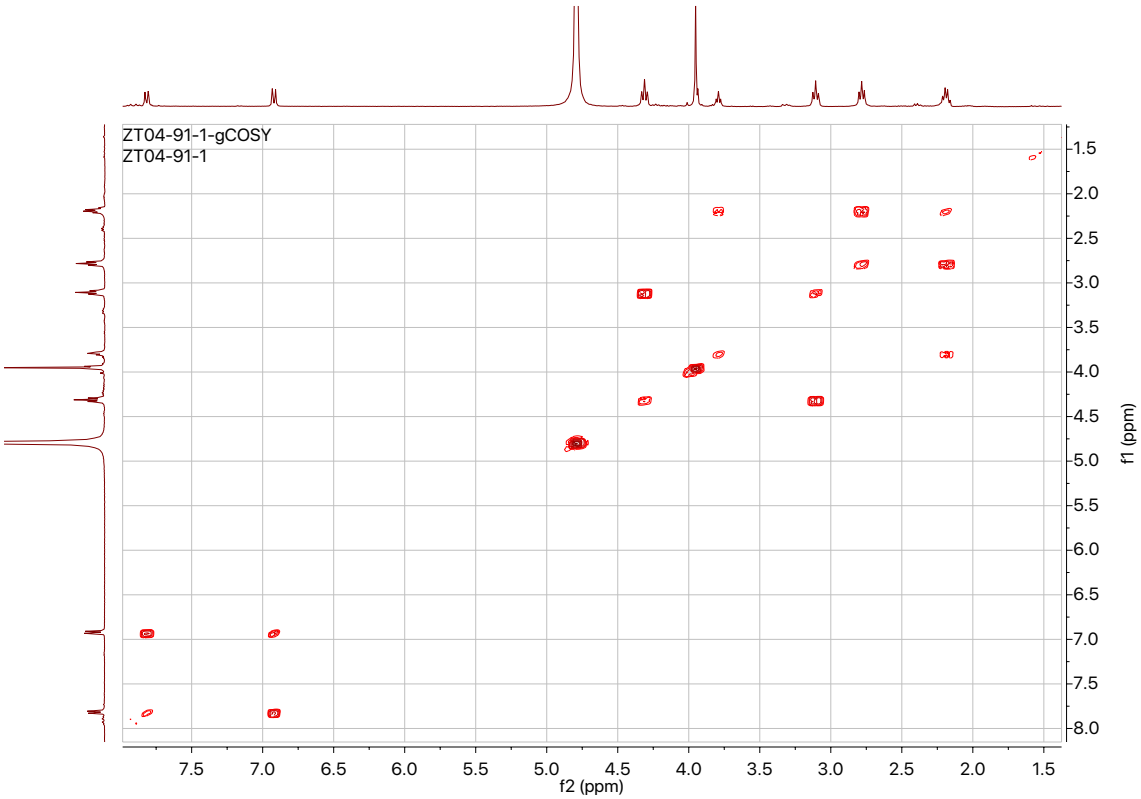

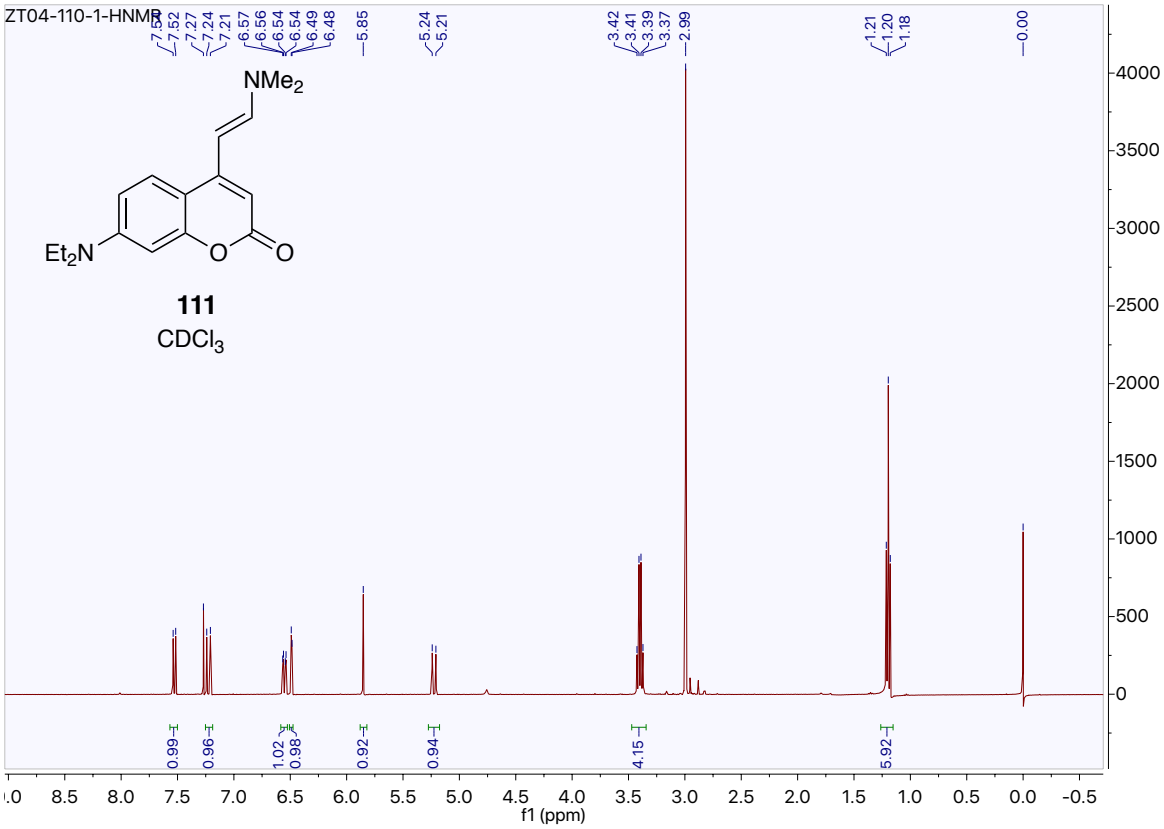
ZT04-110-1-HNMR
7.55
7.52
7.27
7.24
7.21
6.57
6.56
6.54
6.54
6.49
6.48
5.85
5.24
5.21
3.42
3.41
3.39
3.37
2.99
1.21
1.20
1.18
0.00
NMe2
Et2N
O
O
111
CDCl3
0.99
0.96
1.02
0.98
0.92
0.94
4.15
5.92
f1 (ppm)

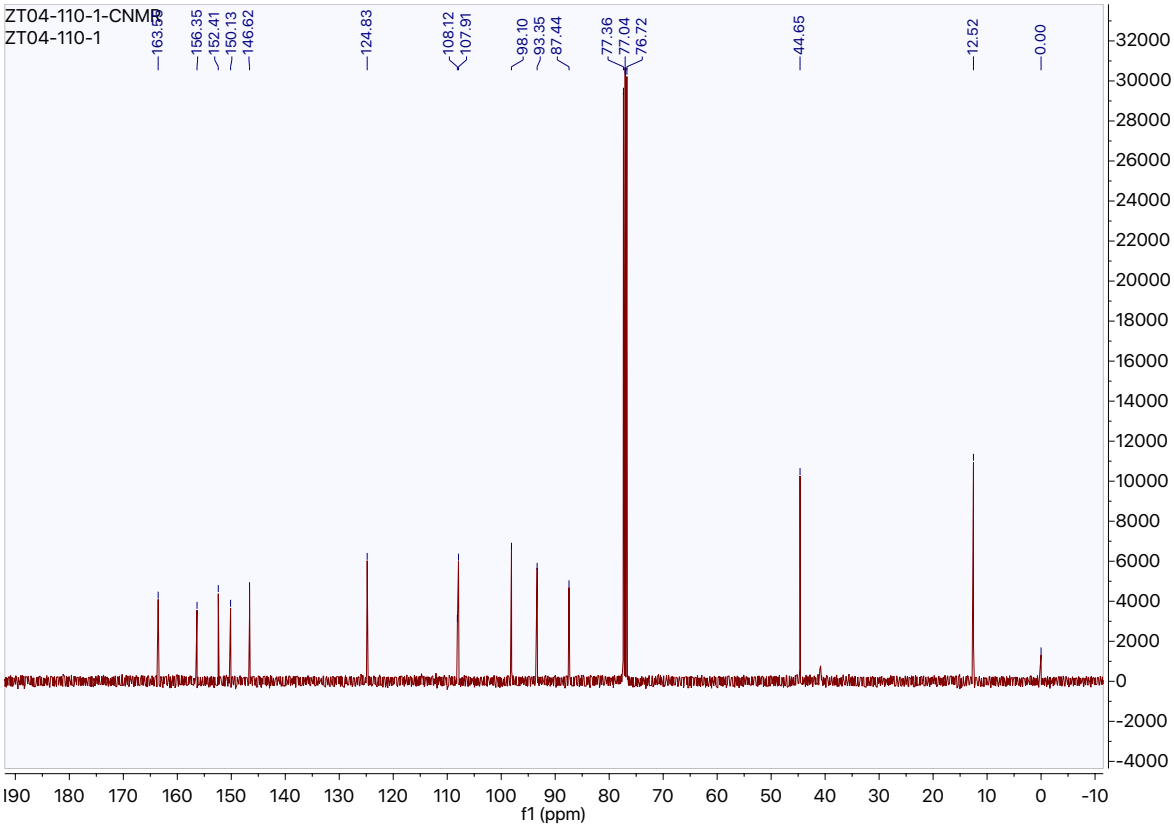
ZT04-110-1-CNMR
ZT04-110-1
163.55
156.35
152.41
150.13
146.62
124.83
108.12
107.91
98.10
93.35
87.44
77.36
77.04
76.72
44.65
12.52
0.00
f1 (ppm)

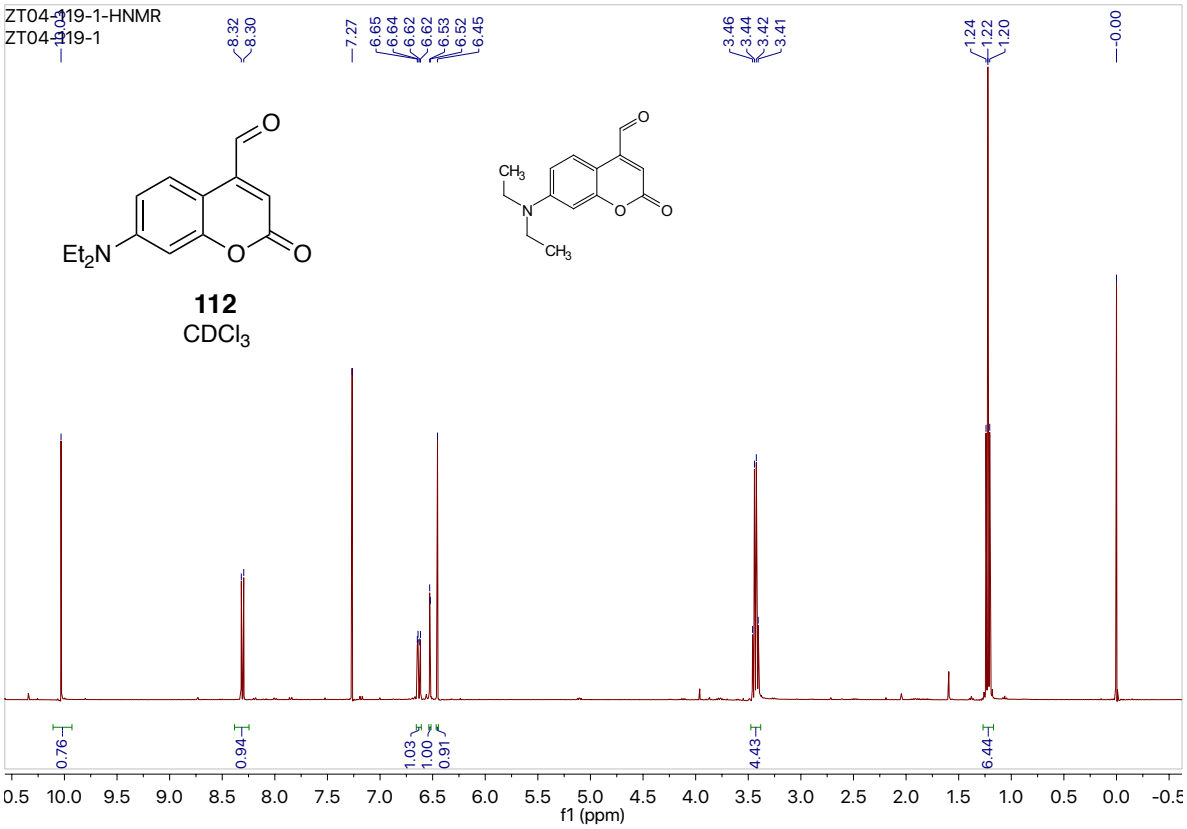
ZT04-119-1-HNMR
ZT04-119-1
10.04
8.32
8.30
7.27
6.65
6.64
6.62
6.62
6.53
6.52
6.45
3.46
3.44
3.42
3.41
1.24
1.22
1.20
0.00
Et2N
112
CDCl3
0.76
0.94
1.03
1.00
0.91
4.43
6.44
f1 (ppm)

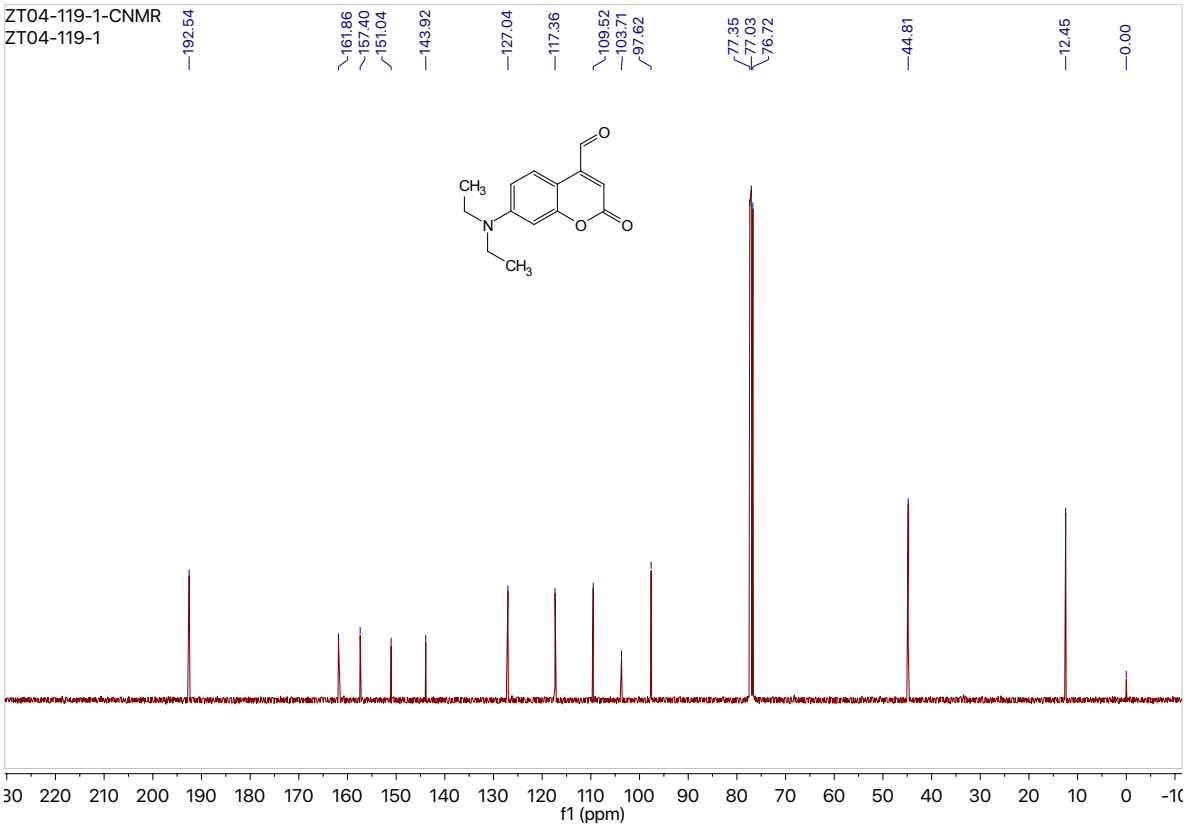
ZT04-119-1-CNMR
ZT04-119-1
192.54
161.86
157.40
151.04
143.92
127.04
117.36
109.52
103.71
97.62
77.35
77.03
76.72
44.81
12.45
0.00
f1 (ppm)

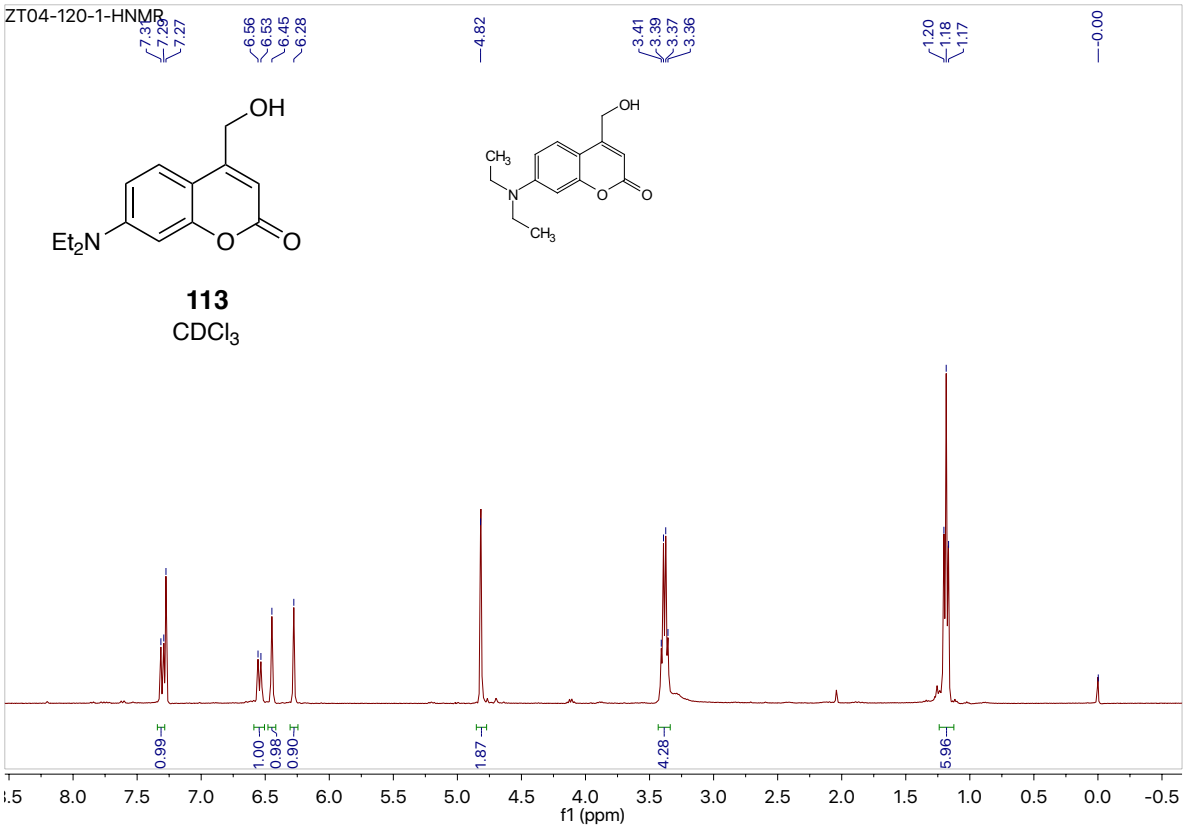
ZT04-120-1-HNMR
7.31
7.29
7.27
6.56
6.53
6.45
6.28
4.82
3.41
3.39
3.37
3.36
1.20
1.18
1.17
0.00
OH
Et2N
O
O
113
CDCl3
CH3
N
CH3
0.99
1.00
0.98
0.90
1.87
4.28
5.96
8.0
7.5
7.0
6.5
6.0
5.5
5.0
4.5
4.0
3.5
3.0
2.5
2.0
1.5
1.0
0.5
0.0
-0.5
f1 (ppm)

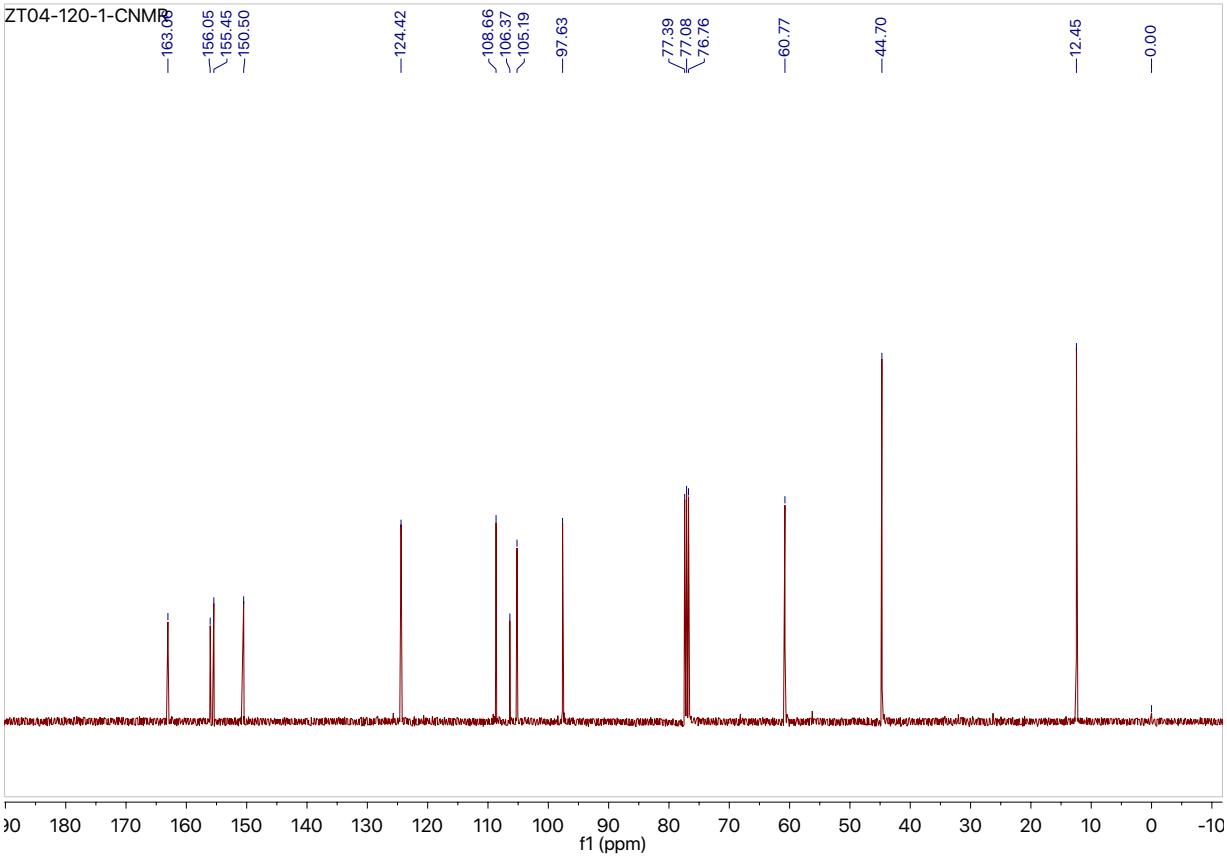
ZT04-120-1-CNMR
163.06
156.05
155.45
150.50
124.42
108.66
106.37
105.19
97.63
77.39
77.08
76.76
60.77
44.70
12.45
0.00
180
170
160
150
140
130
120
110
100
90
80
70
60
50
40
30
20
10
0
-10
f1 (ppm)

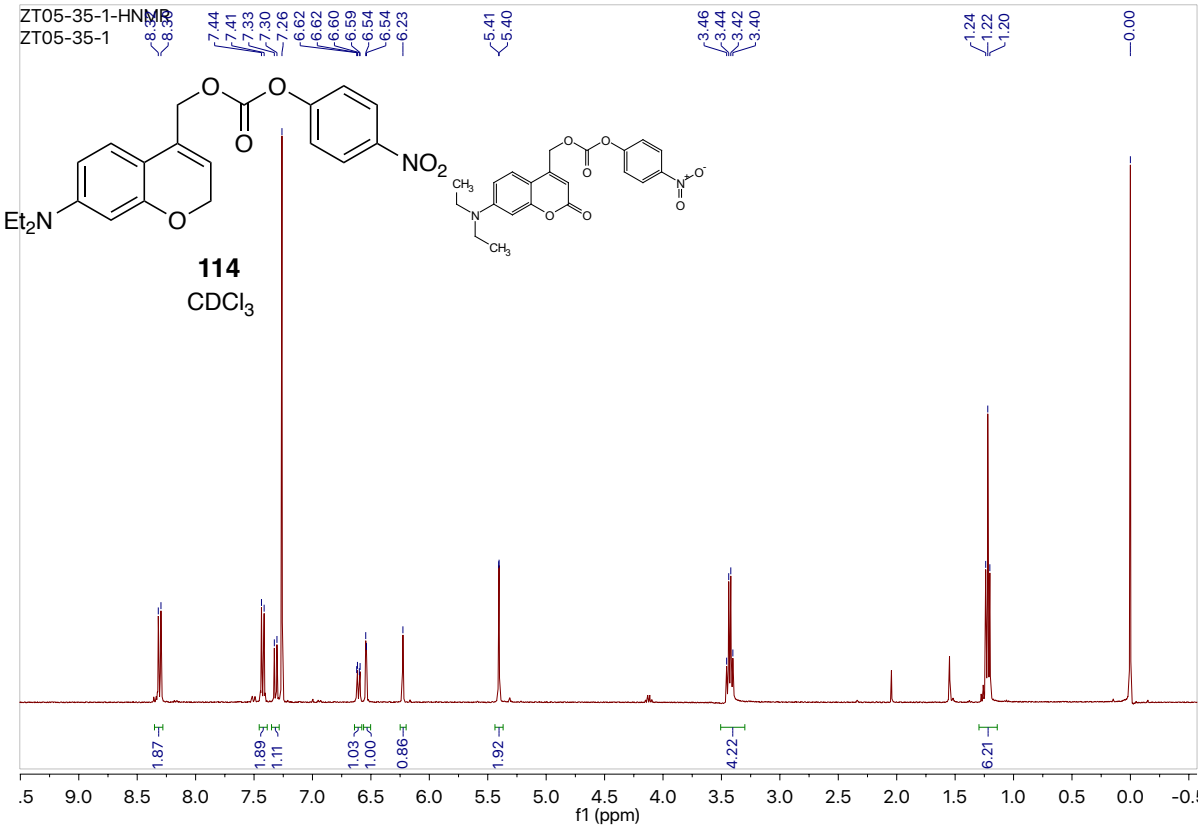
ZT05-35-1-HNMR
ZT05-35-1
8.33
8.32
7.44
7.41
7.33
7.30
7.26
6.62
6.62
6.60
6.59
6.54
6.54
6.23
5.41
5.40
3.46
3.44
3.42
3.40
1.24
1.22
1.20
0.00
1.87
1.89
1.11
1.03
1.00
0.86
1.92
4.22
6.21
114
CDCl3
f1 (ppm)

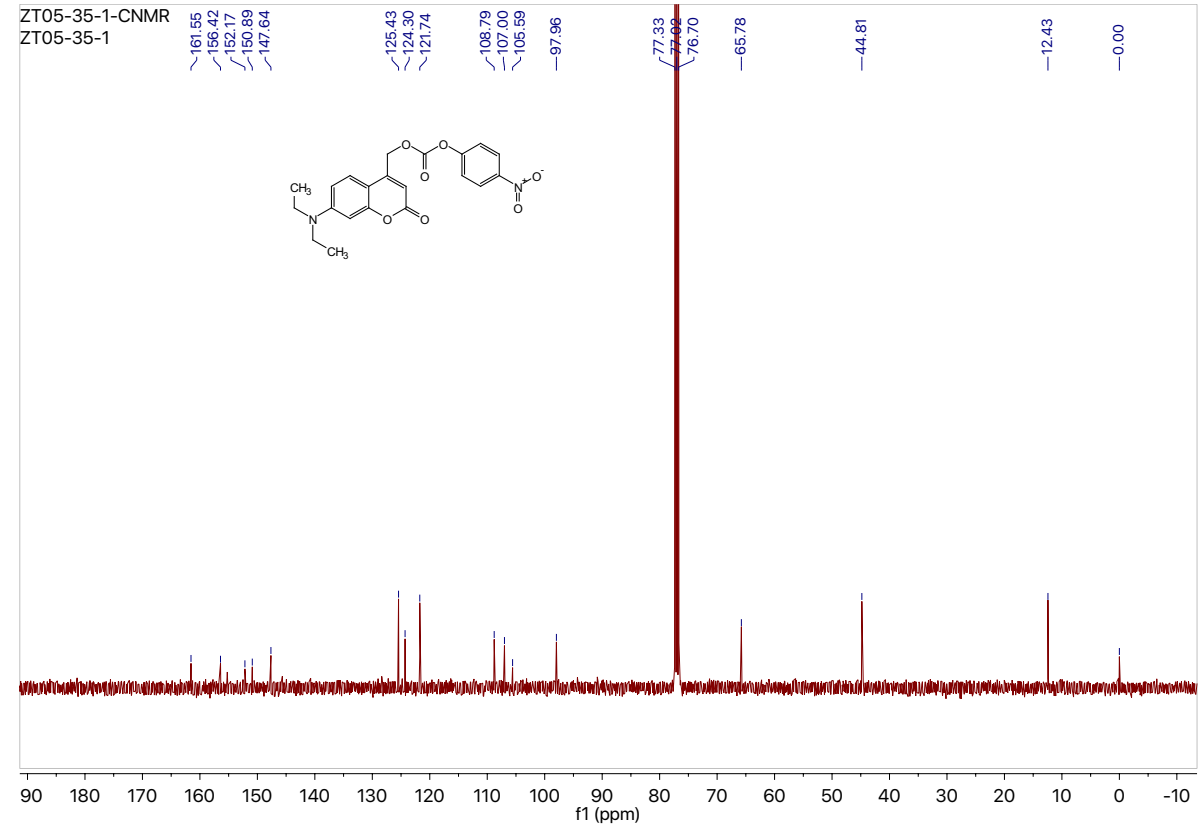
ZT05-35-1-CNMR
ZT05-35-1
161.55
156.42
152.17
150.89
147.64
125.43
124.30
121.74
108.79
107.00
105.59
97.96
77.33
77.02
76.70
65.78
44.81
12.43
0.00
f1 (ppm)

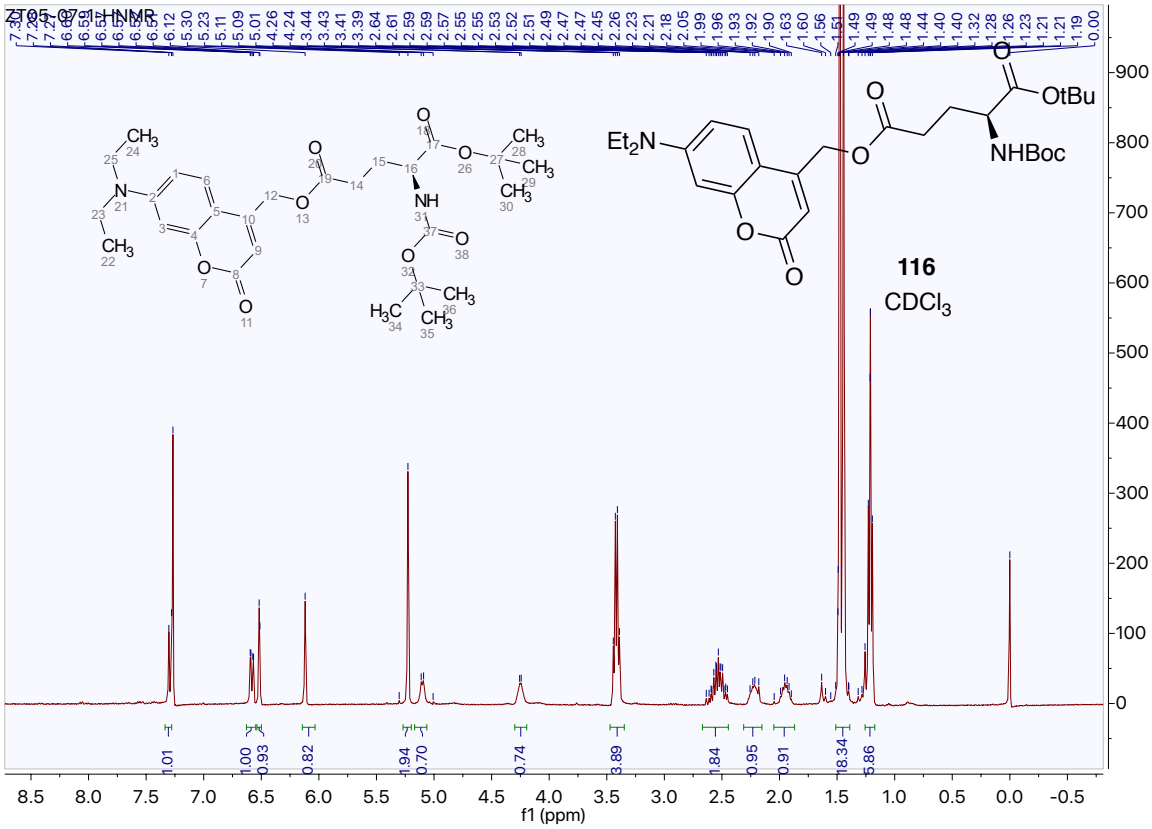
ZT05-07-1-HNMR
116
CDCl3
f1 (ppm)

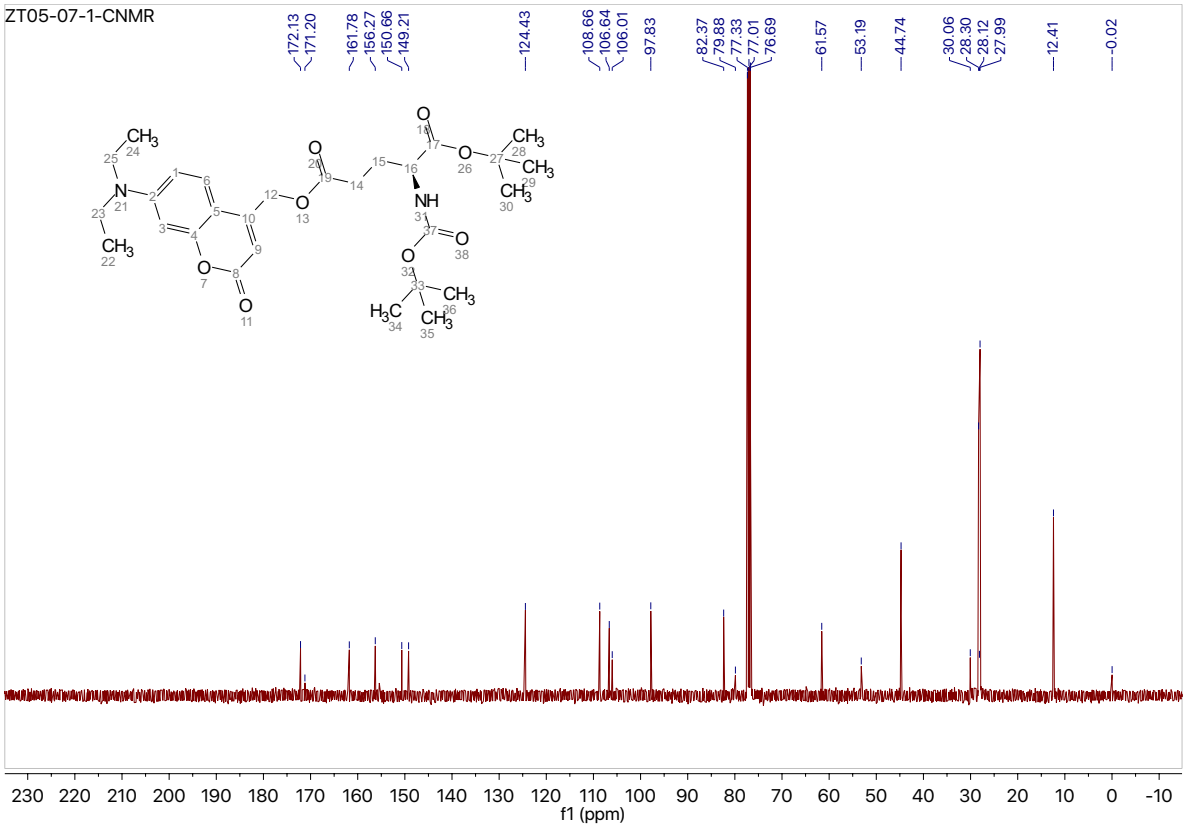
ZT05-07-1-CNMR
f1 (ppm)

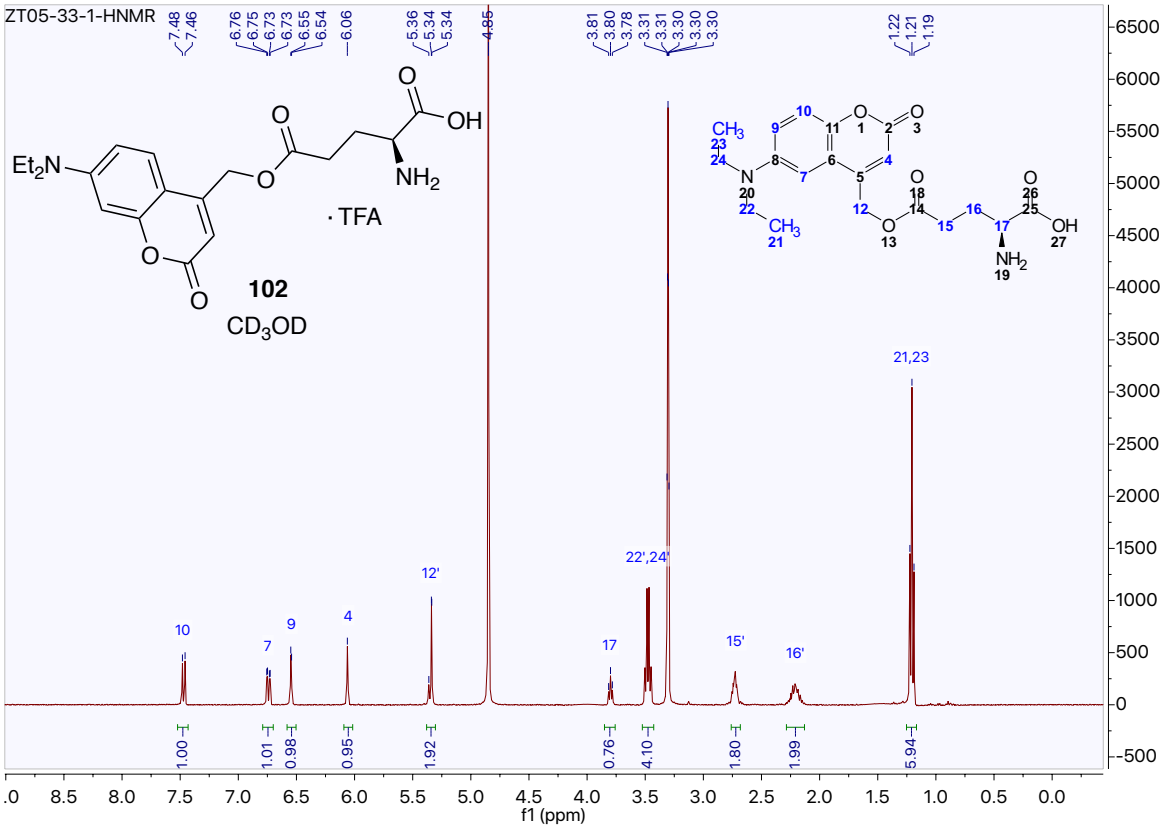
ZT05-33-1-HNMR
102
CD3OD
· TFA
f1 (ppm)

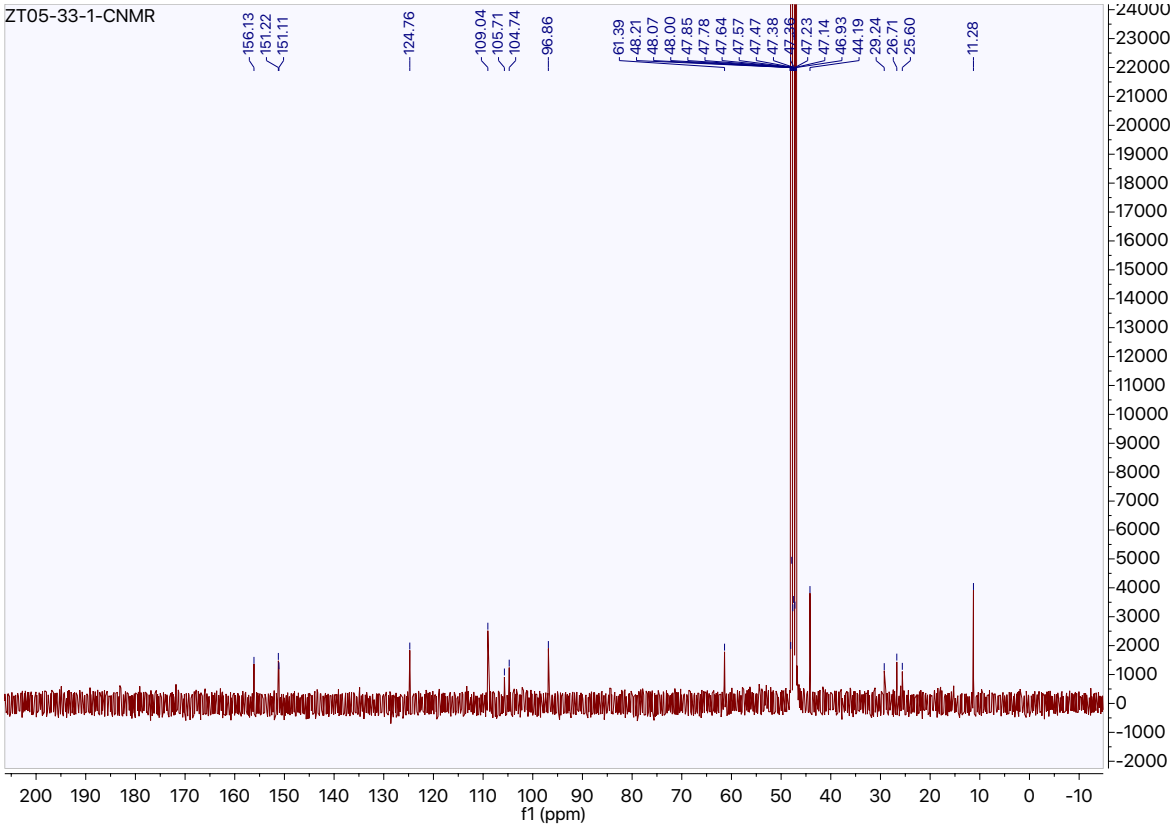
ZT05-33-1-CNMR
f1 (ppm)

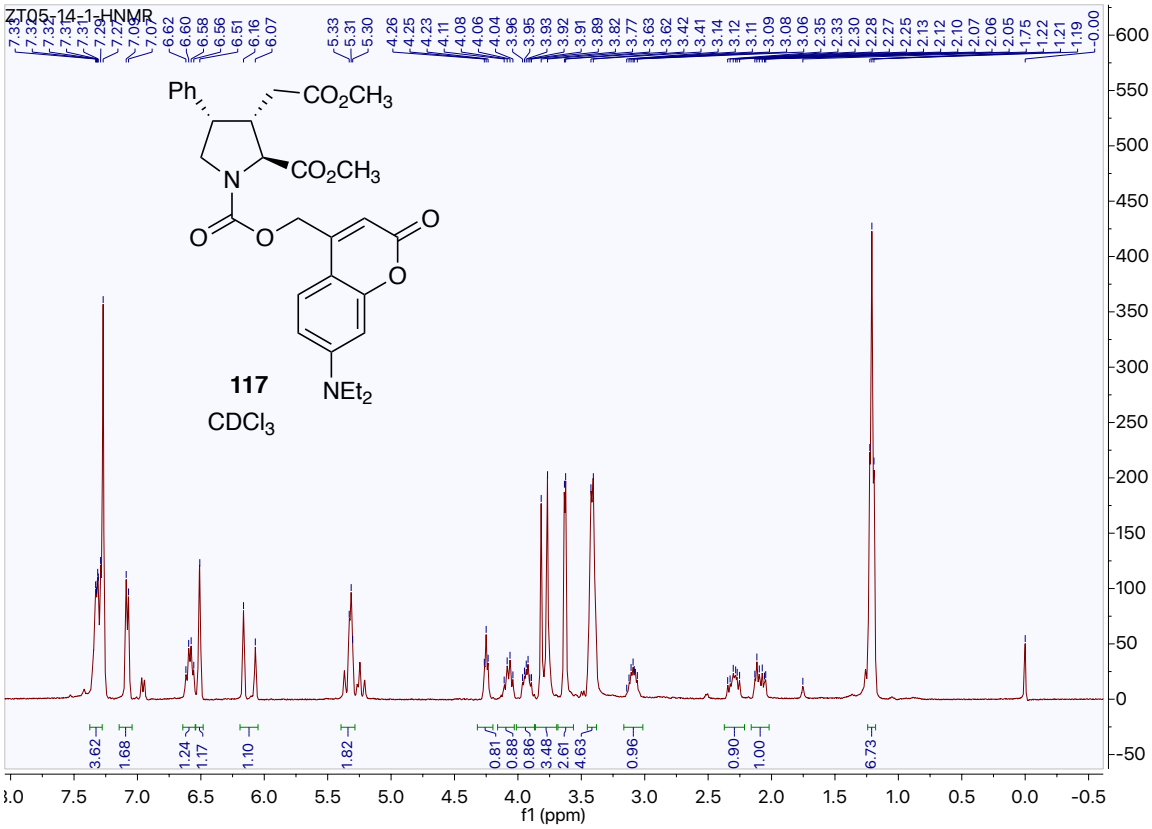
ZT05-14-1-HNMR
Ph
CO2CH3
CO2CH3
N
O
O
O
O
NEt2
117
CDCl3
f1 (ppm)

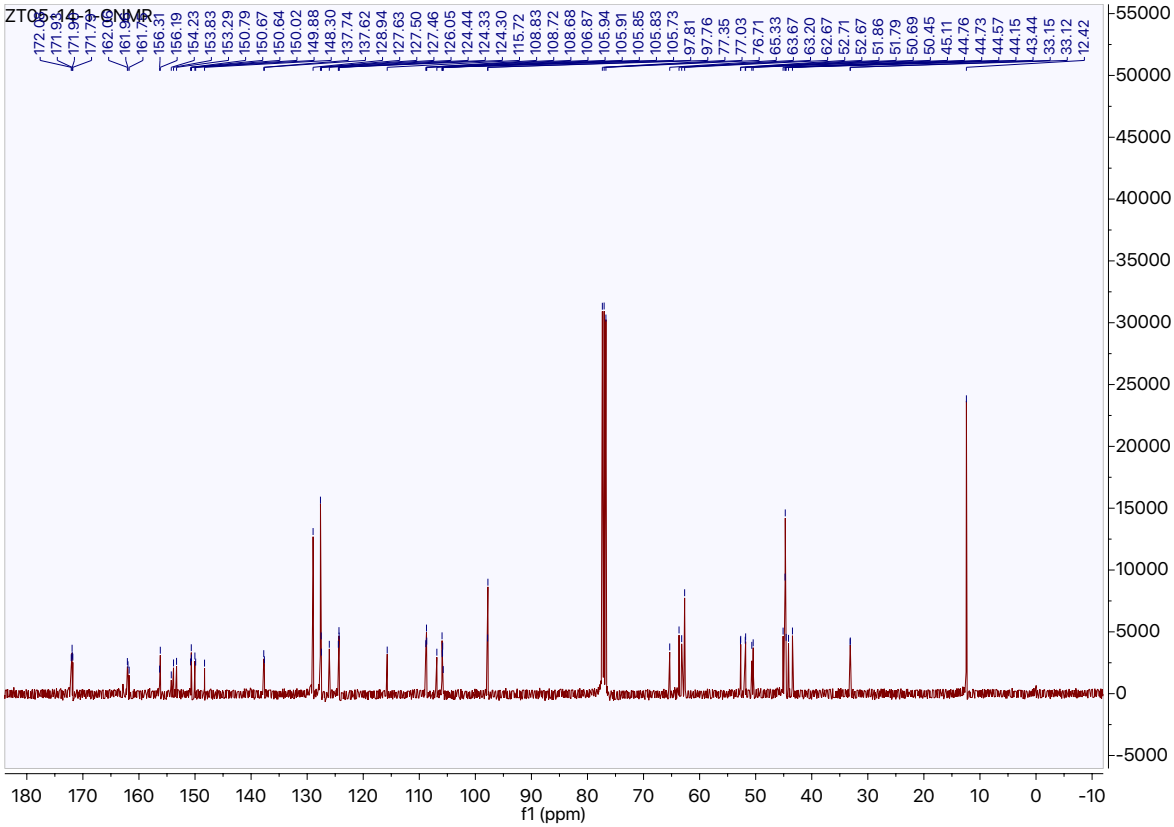
ZT05-14-1-CNMR
f1 (ppm)

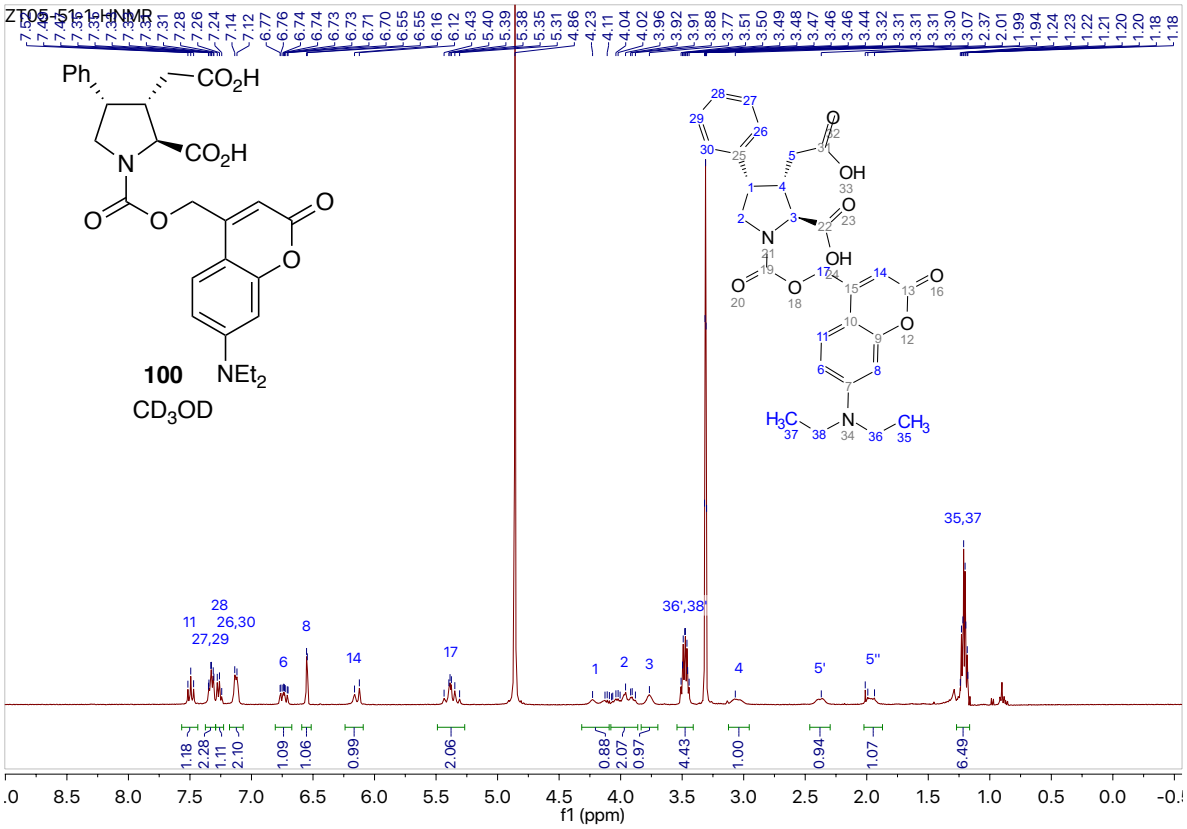
ZT05-51-1-HNMR
Ph
CO2H
CO2H
N
O
O
O
O
100
NEt2
CD3OD
35,37
28
11
26,30
27,29
8
6
14
17
1
2
3
36',38'
4
5'
5''
f1 (ppm)

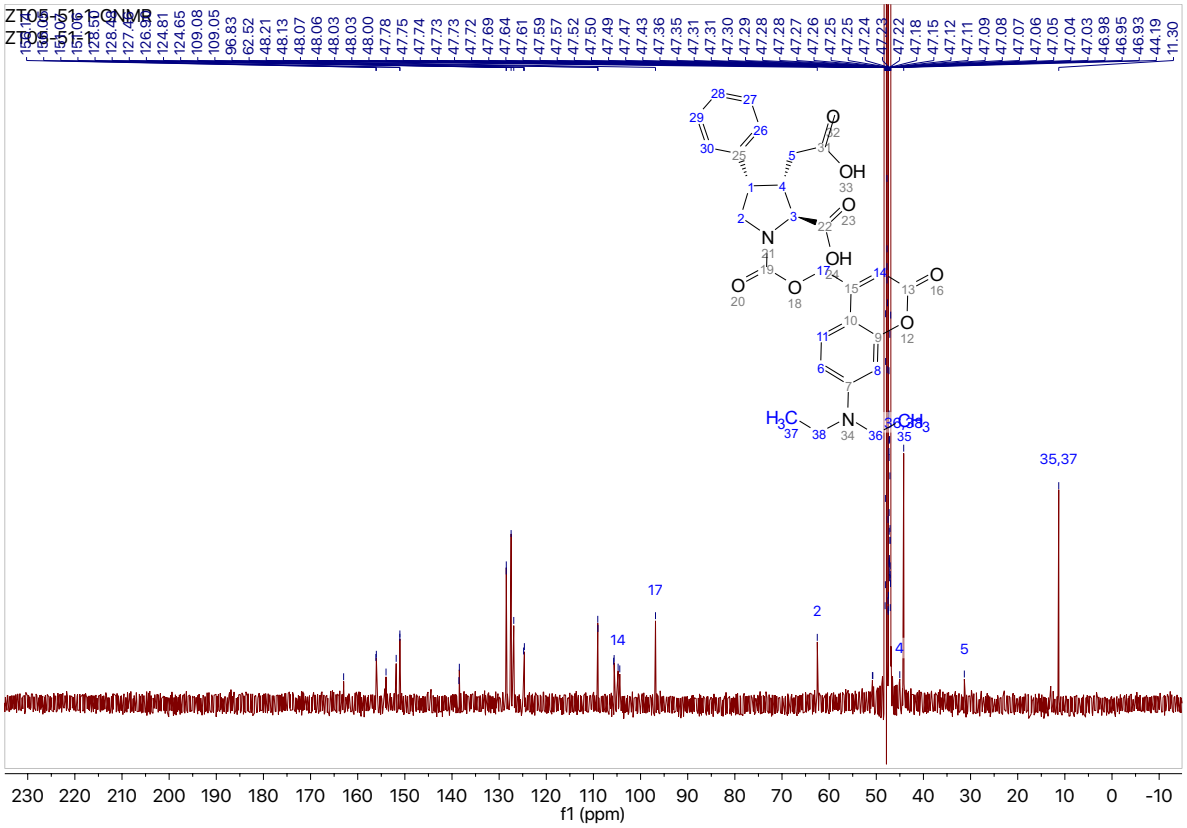
ZT05-51-2-CNMR
35,37
17
14
2
4
5
f1 (ppm)

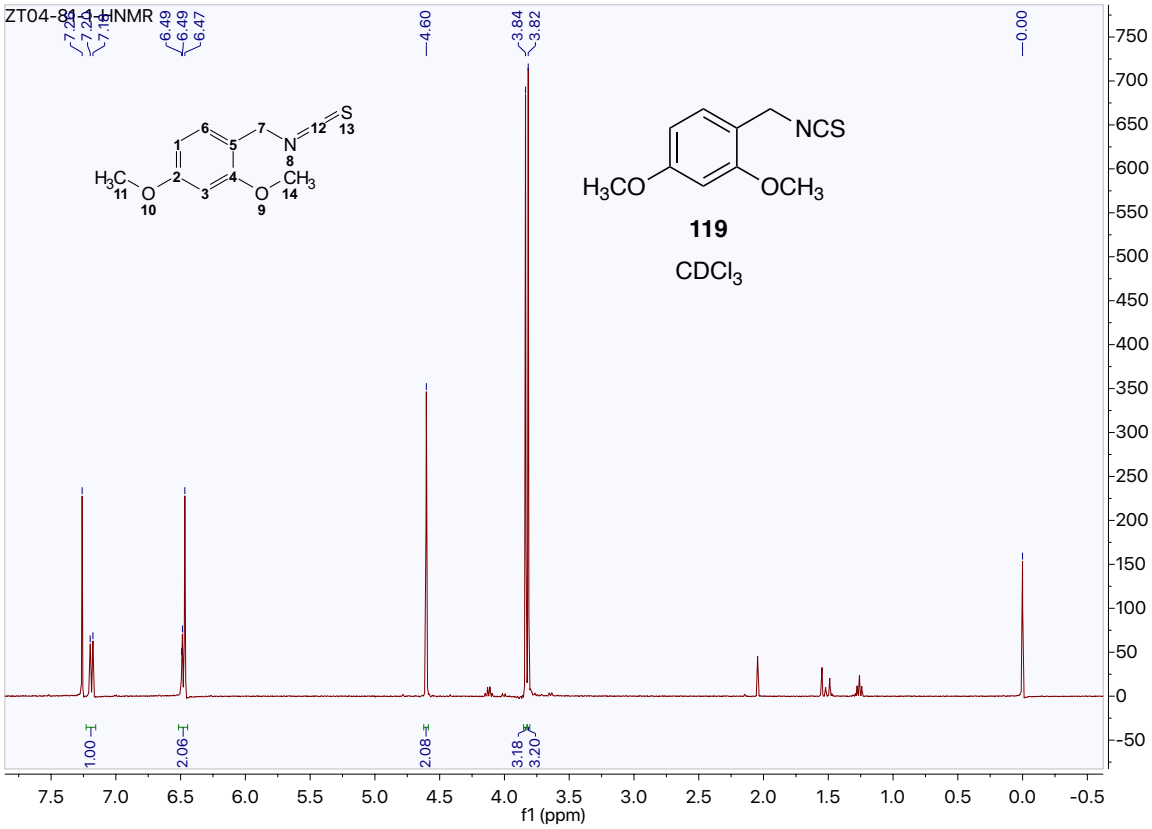
ZT04-81-1-1HNMR
7.22
7.21
7.19
6.49
6.49
6.47
4.60
3.84
3.82
0.00
NCS
H3CO
OCH3
119
CDCl3
1.00
2.06
2.08
3.18
3.20
f1 (ppm)

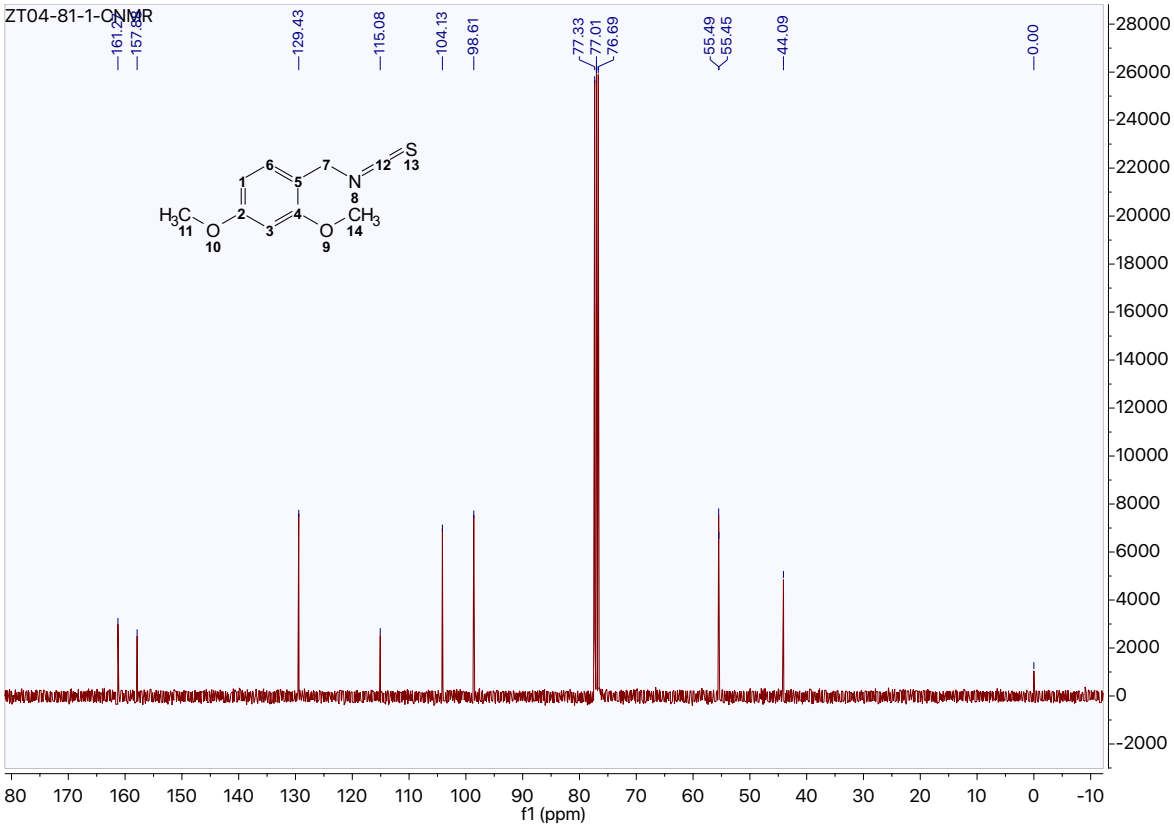
ZT04-81-1-CNMR
161.27
157.84
129.43
115.08
104.13
98.61
77.33
77.01
76.69
55.49
55.45
44.09
0.00
f1 (ppm)

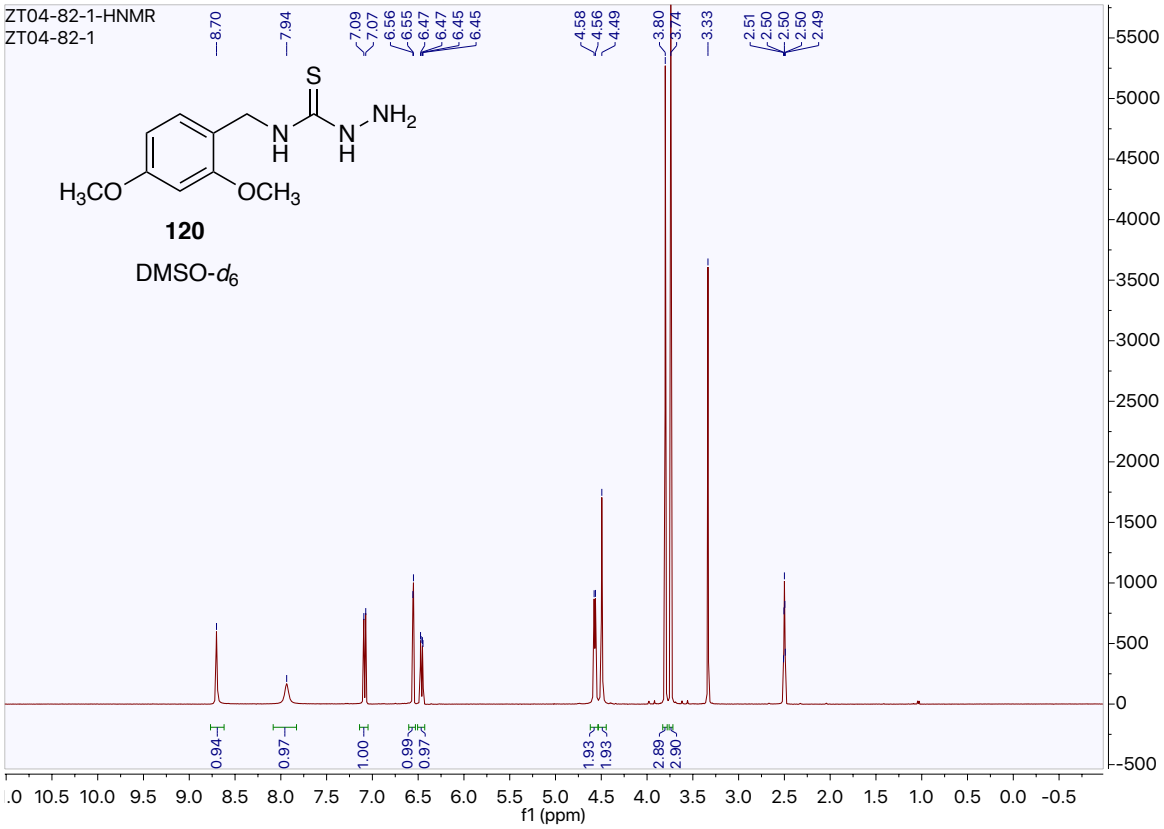
ZT04-82-1-HNMR
ZT04-82-1
8.70
7.94
7.09
7.07
6.56
6.55
6.47
6.47
6.45
6.45
4.58
4.56
4.49
3.80
3.74
3.33
2.51
2.50
2.50
2.50
2.49
S
NH2
N
H
N
H
H3CO
OCH3
120
DMSO-d6
0.94
0.97
1.00
0.99
0.97
1.93
1.93
2.89
2.90
f1 (ppm)

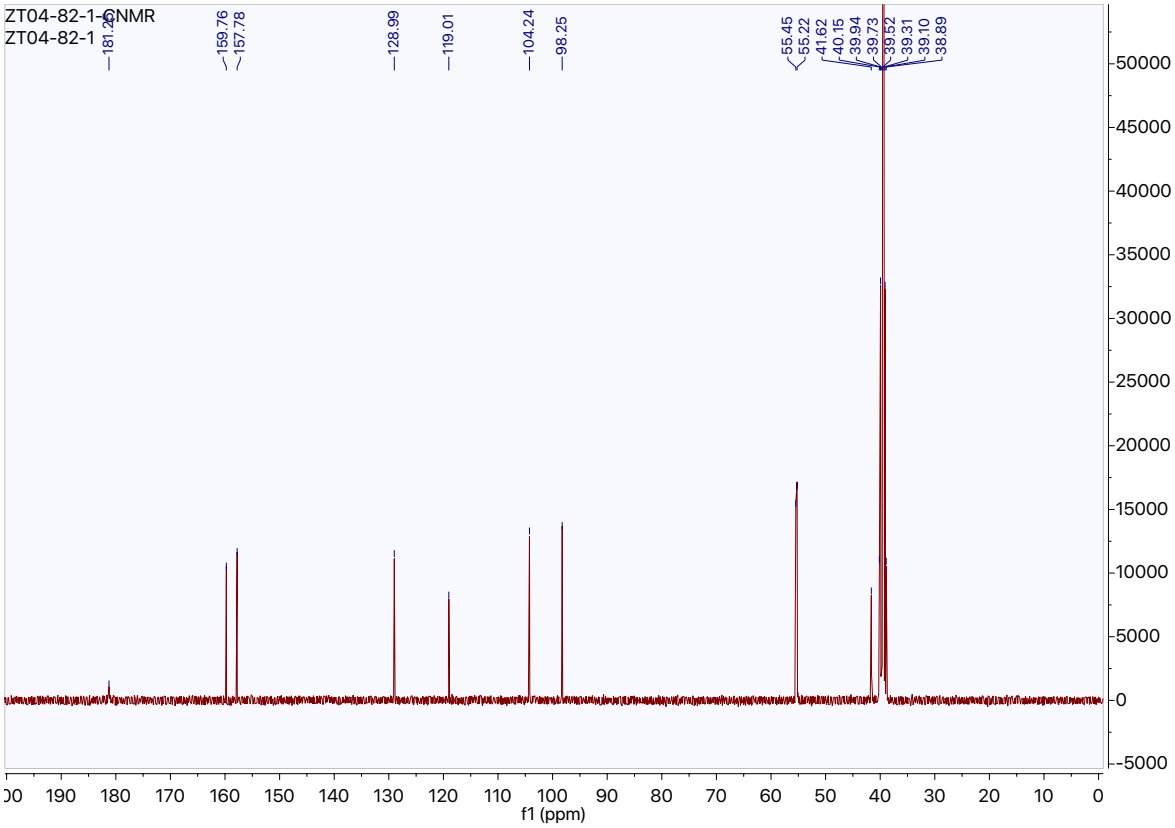
ZT04-82-1-CNMR
ZT04-82-1
181.20
159.76
157.78
128.99
119.01
104.24
98.25
55.45
55.22
41.62
40.15
39.94
39.73
39.52
39.31
39.10
38.89
f1 (ppm)

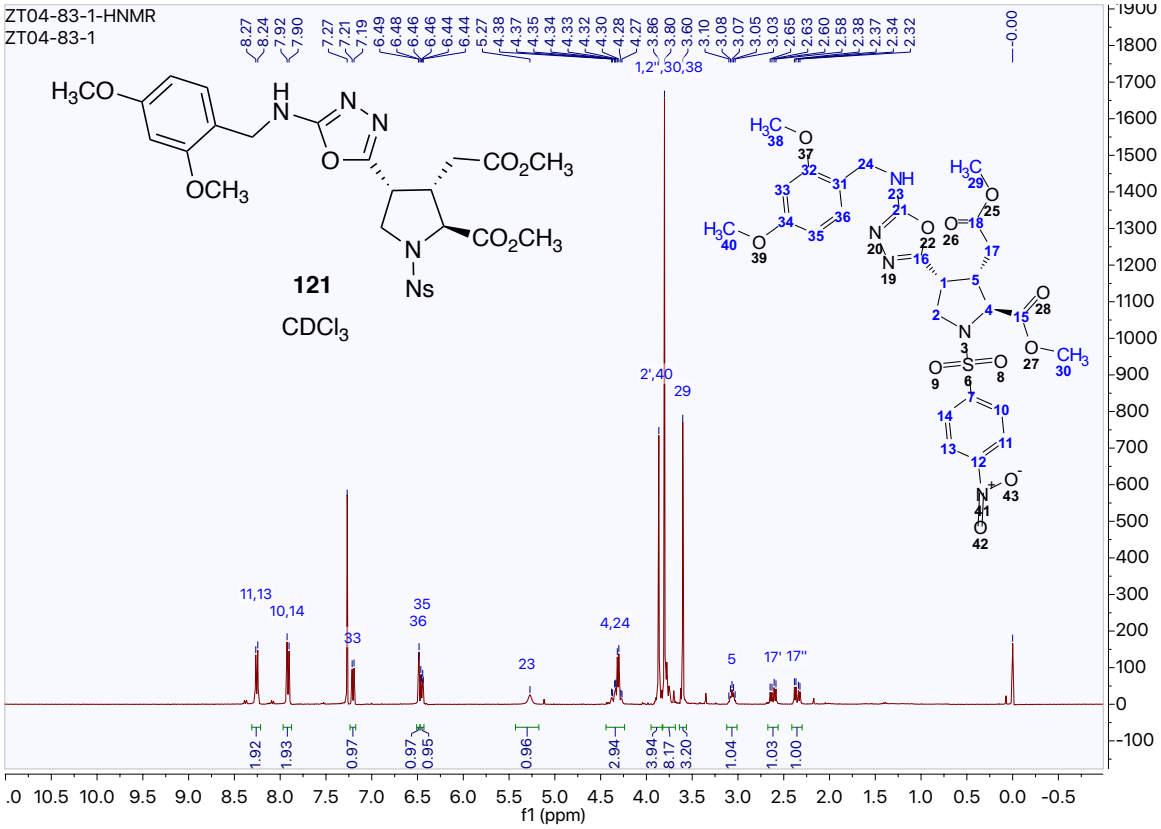
ZT04-83-1-HNMR
ZT04-83-1
121
CDCl3
f1 (ppm)

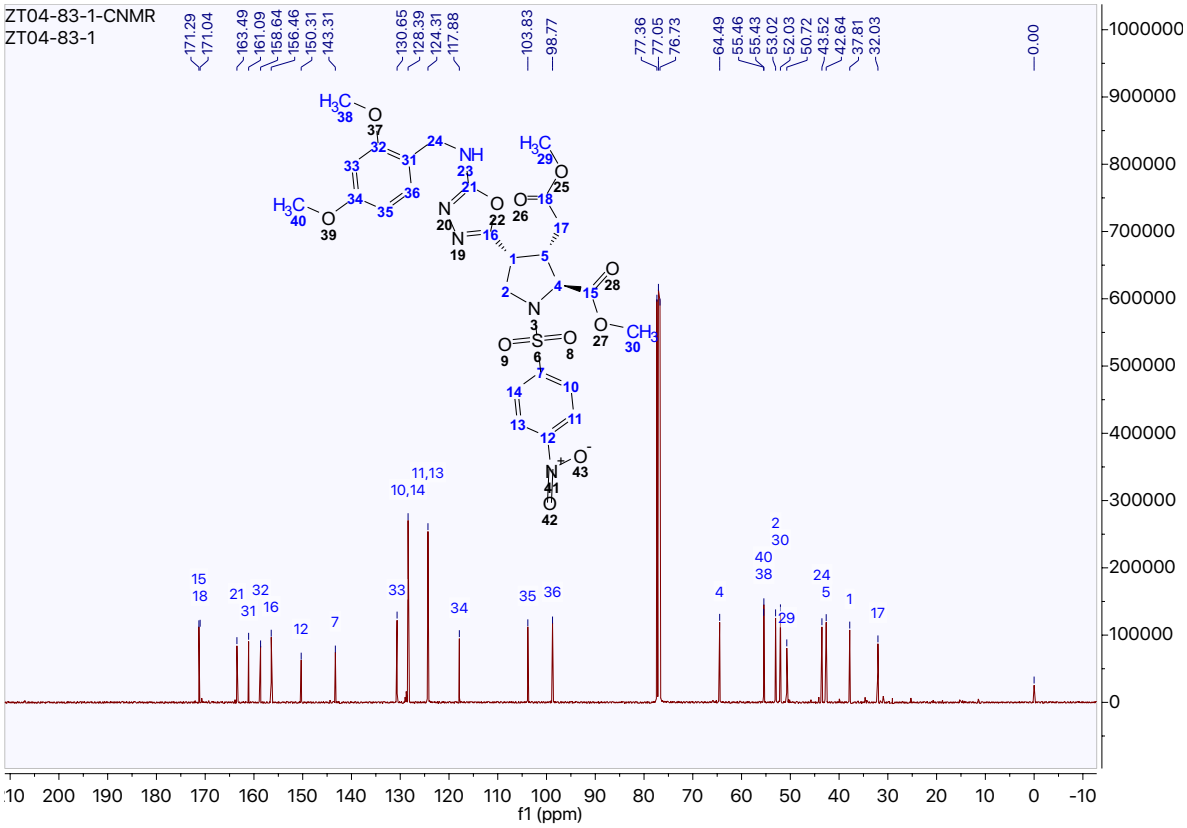
ZT04-83-1-CNMR
ZT04-83-1
f1 (ppm)

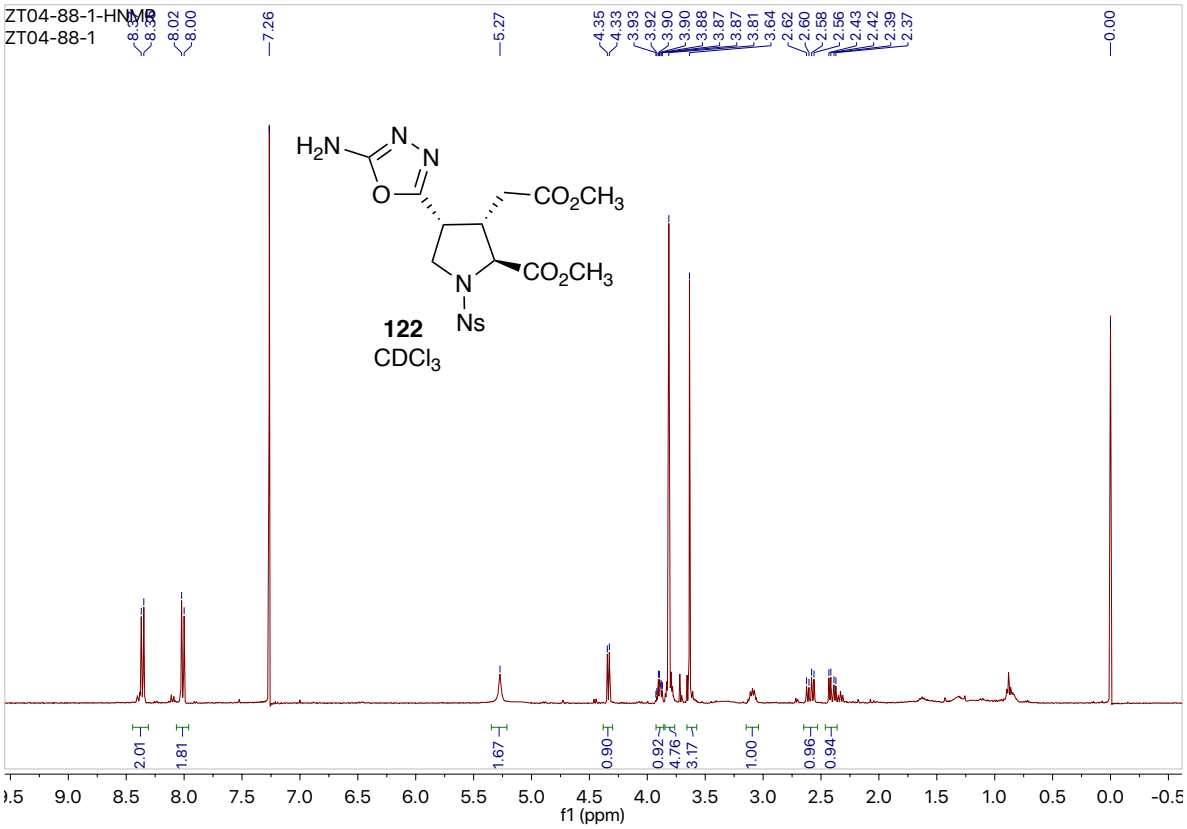
ZT04-88-1-HNMR
ZT04-88-1
8.37
8.35
8.02
8.00
7.26
5.27
4.35
4.33
3.93
3.92
3.90
3.90
3.88
3.87
3.87
3.81
3.64
2.62
2.60
2.58
2.56
2.43
2.42
2.39
2.37
0.00
H2N
N
N
O
CO2CH3
CO2CH3
N
Ns
122
CDCl3
2.01
1.81
1.67
0.90
0.92
4.76
3.17
1.00
0.96
0.94
9.0 8.5 8.0 7.5 7.0 6.5 6.0 5.5 5.0 4.5 4.0 3.5 3.0 2.5 2.0 1.5 1.0 0.5 0.0
f1 (ppm)

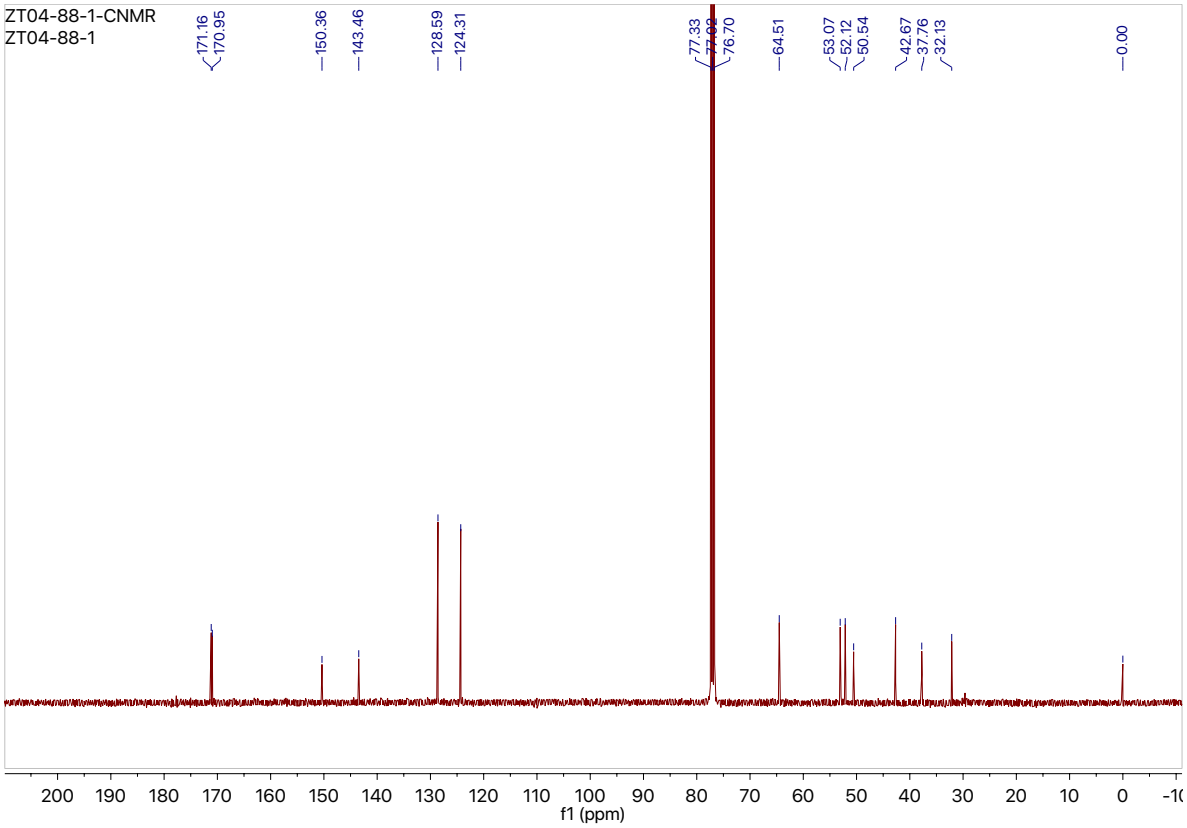
ZT04-88-1-CNMR
ZT04-88-1
171.16
170.95
150.36
143.46
128.59
124.31
77.33
77.02
76.70
64.51
53.07
52.12
50.54
42.67
37.76
32.13
0.00
200 190 180 170 160 150 140 130 120 110 100 90 80 70 60 50 40 30 20 10 0
f1 (ppm)

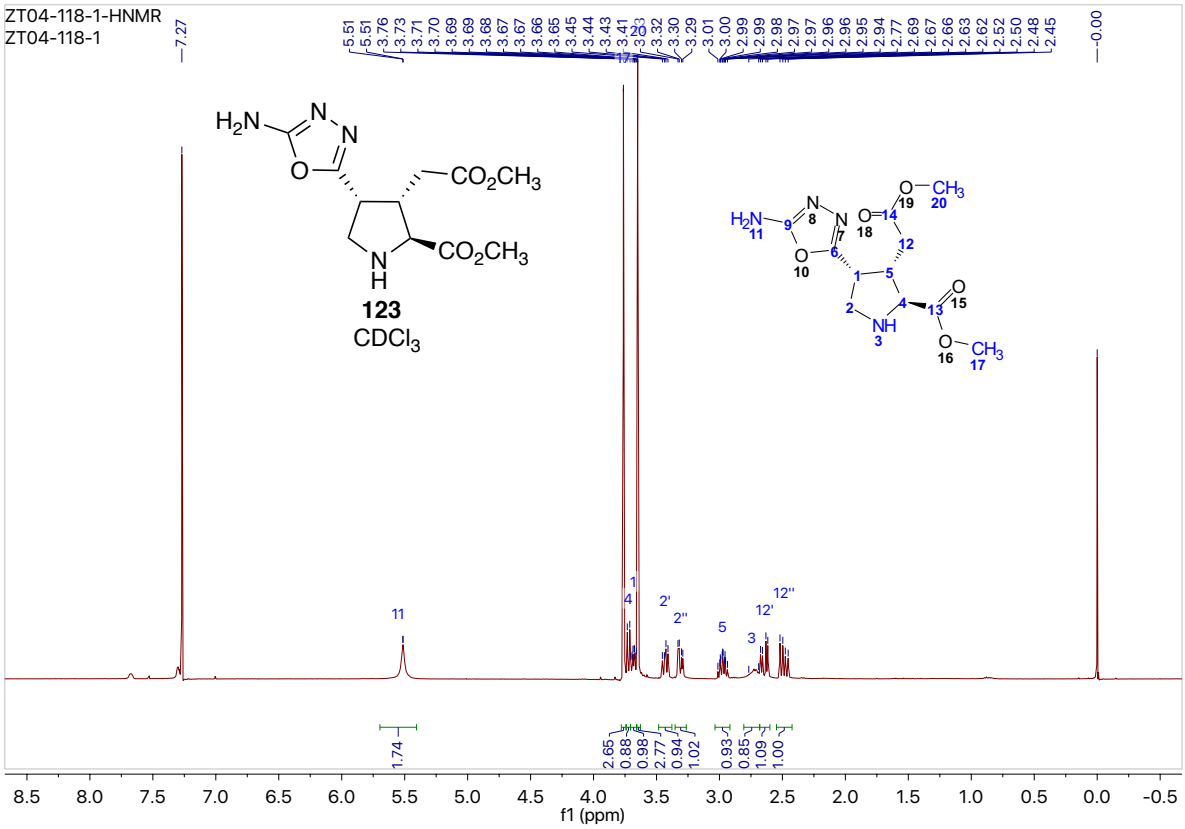
ZT04-118-1-HNMR
ZT04-118-1
123
CDCl3
f1 (ppm)

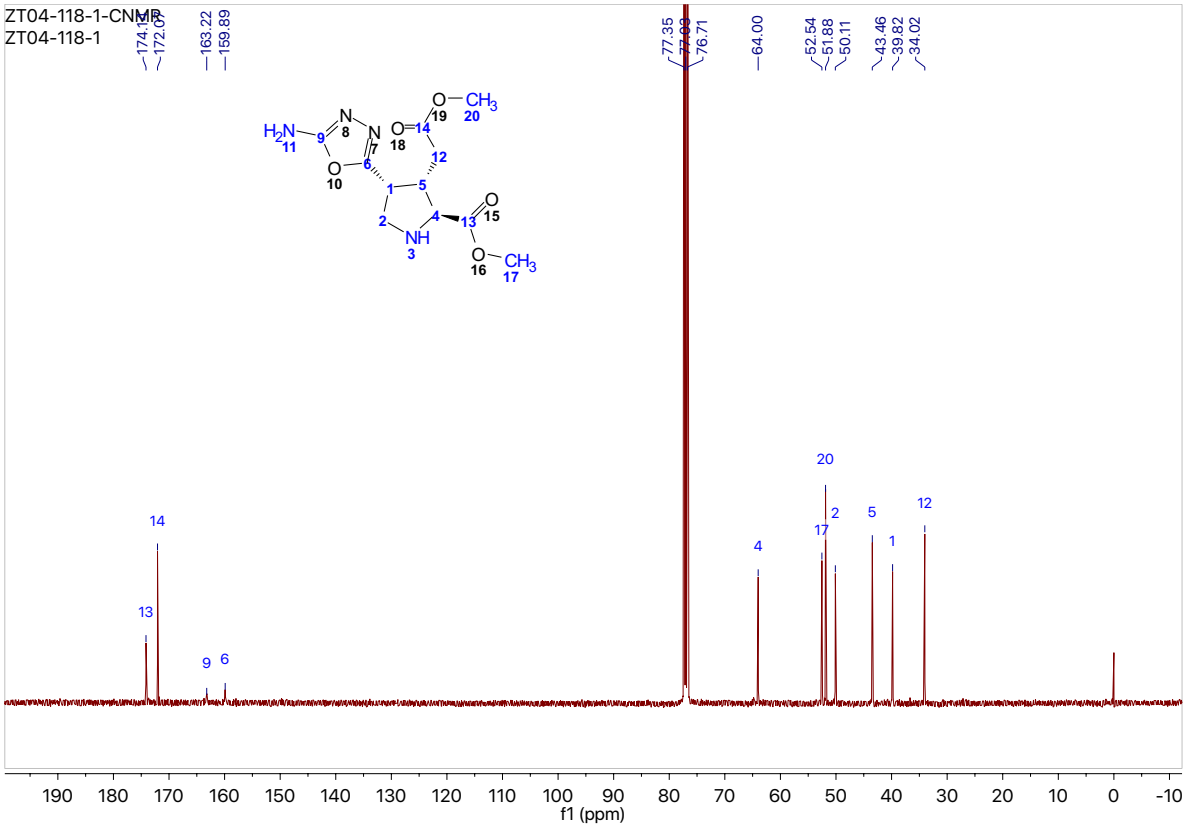
ZT04-118-1-CNMR
ZT04-118-1
f1 (ppm)

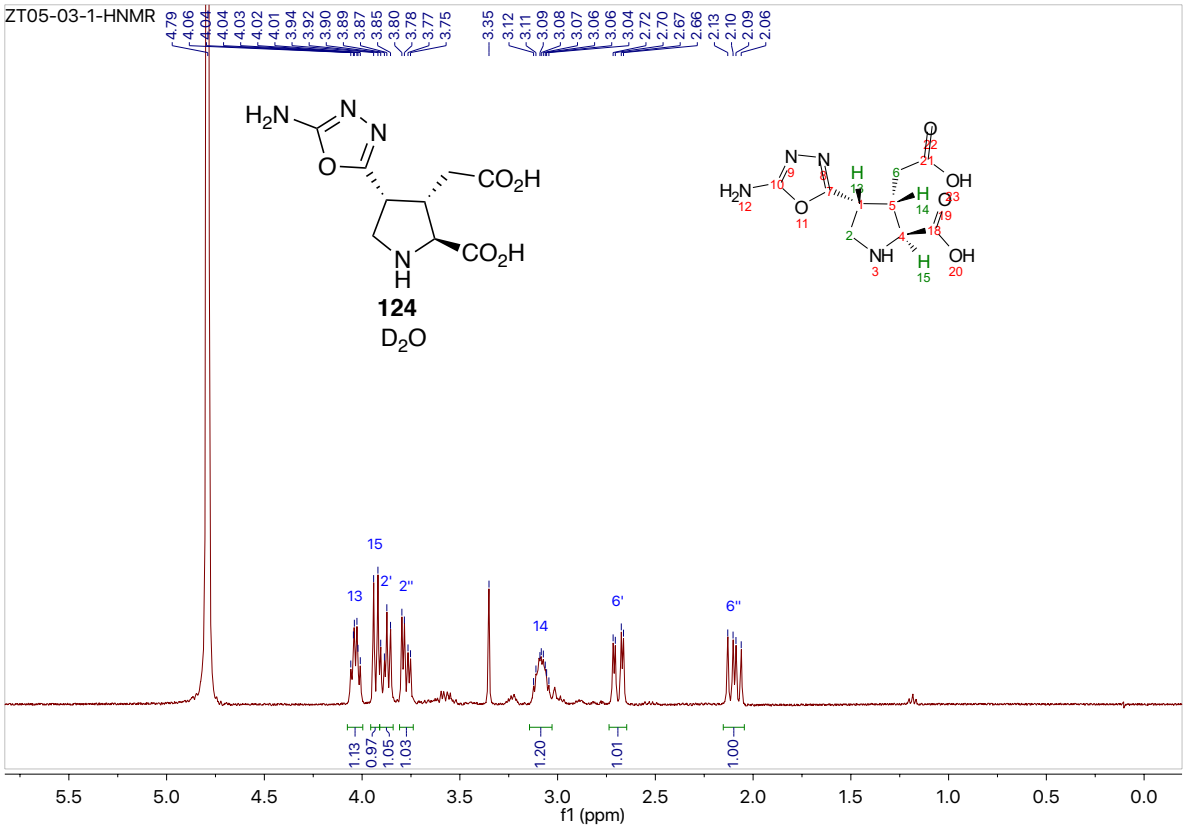
ZT05-03-1-HNMR
4.79 4.06 4.04 4.04 4.03 4.02 4.01 3.94 3.92 3.90 3.89 3.87 3.85 3.80 3.78 3.77 3.75
3.35 3.12 3.11 3.09 3.08 3.07 3.06 3.06 3.04 2.72 2.70 2.67 2.66 2.13 2.10 2.09 2.06
124
D_2O
15
13
2'
2''
14
6'
6''
1.13 0.97 1.05 1.03 1.20 1.01 1.00
5.5 5.0 4.5 4.0 3.5 3.0 2.5 2.0 1.5 1.0 0.5 0.0
f1 (ppm)

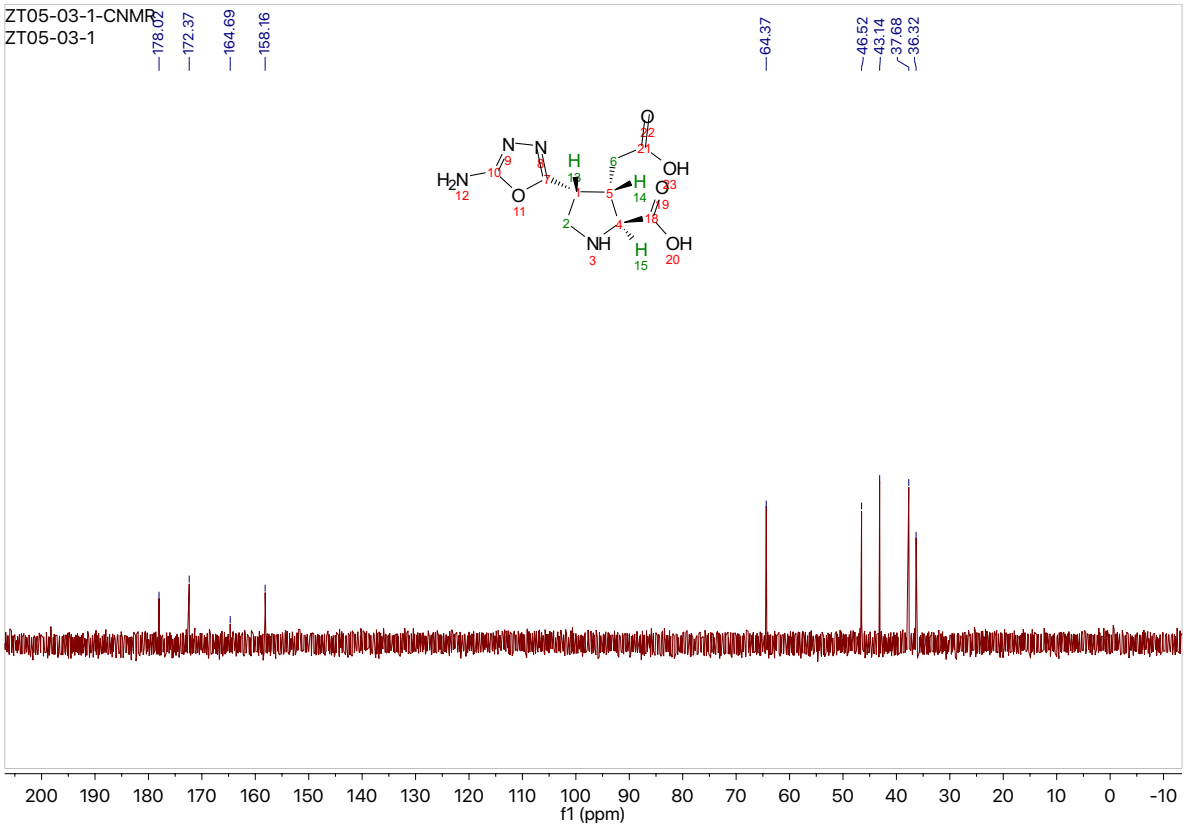
ZT05-03-1-CNMR
ZT05-03-1
178.02 172.37 164.69 158.16
64.37
46.52 43.14 37.68 36.32
200 190 180 170 160 150 140 130 120 110 100 90 80 70 60 50 40 30 20 10 0 -10
f1 (ppm)

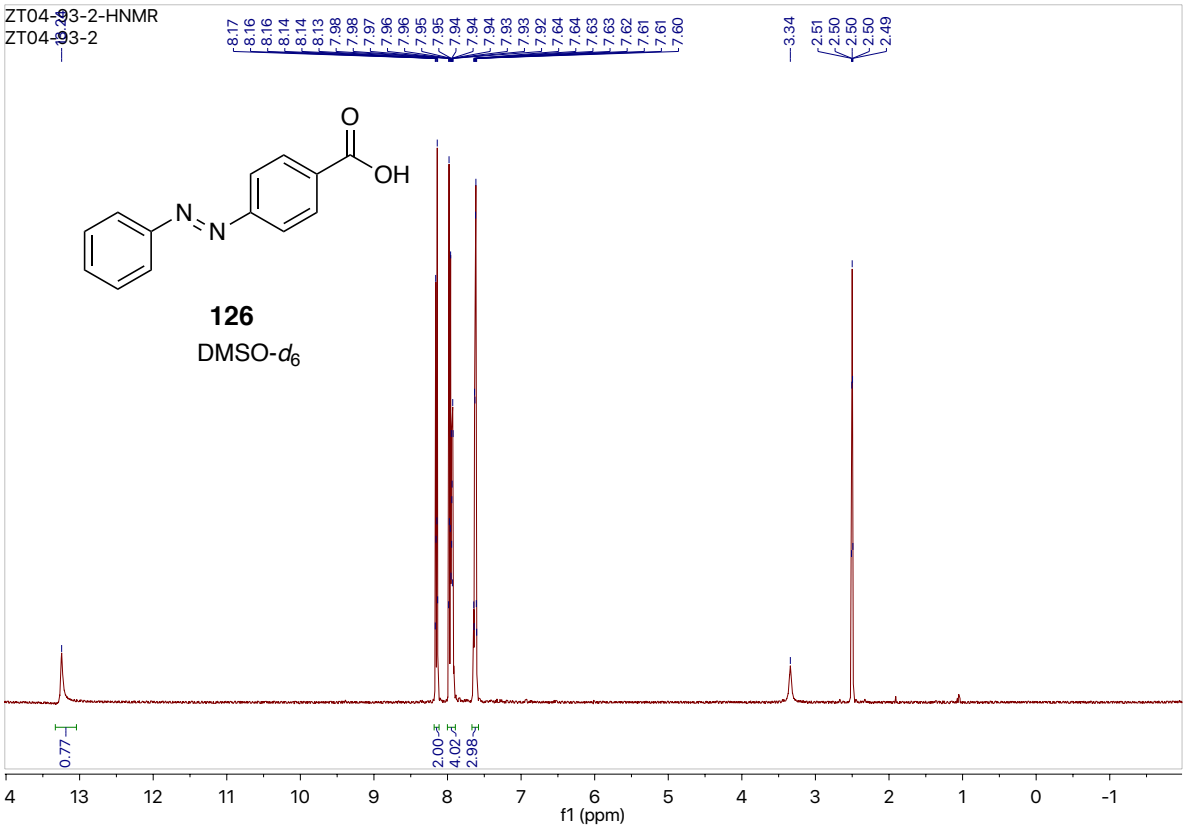
ZT04-93-2-HNMR
ZT04-93-2
13.24
8.17
8.16
8.16
8.14
8.14
8.13
7.98
7.98
7.97
7.96
7.96
7.95
7.95
7.94
7.94
7.94
7.93
7.93
7.92
7.64
7.64
7.63
7.63
7.62
7.61
7.61
7.60
3.34
2.51
2.50
2.50
2.50
2.49
O
OH
N
N
126
DMSO-d_6
0.77
2.00
4.02
2.98
f1 (ppm)

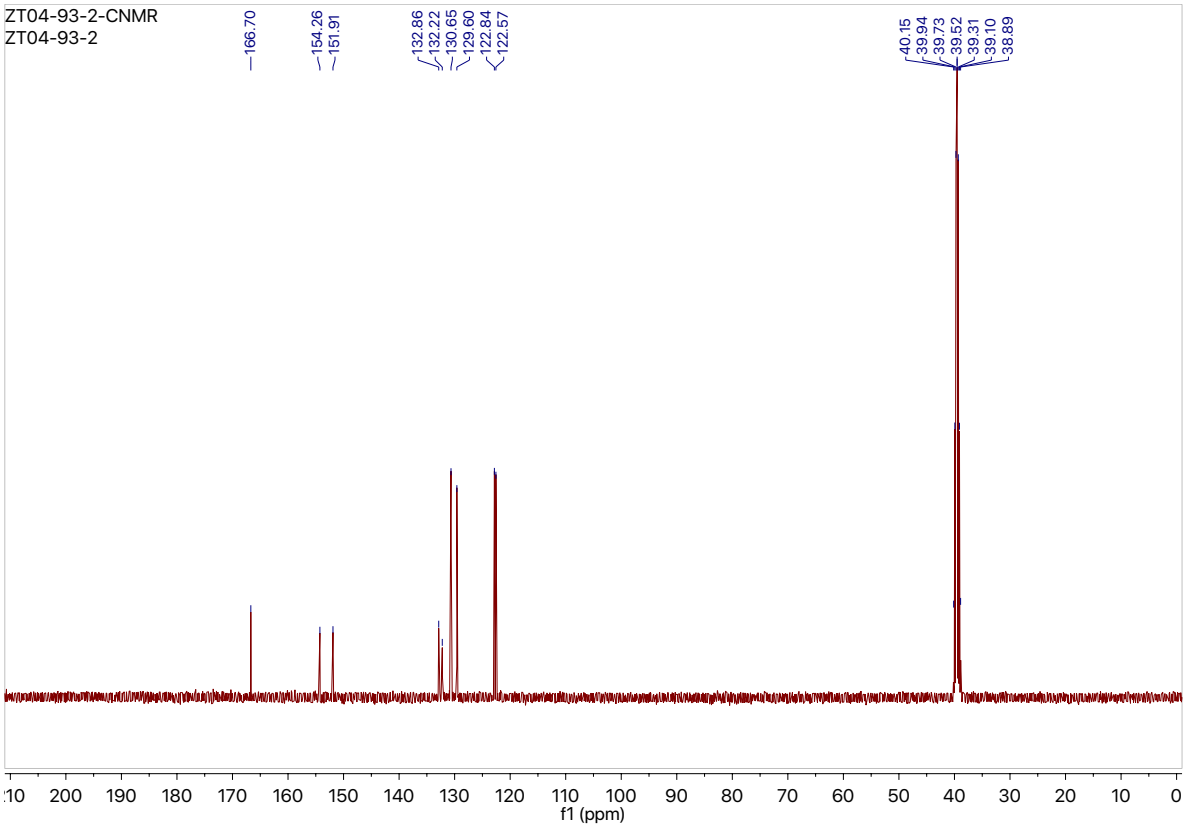
ZT04-93-2-CNMR
ZT04-93-2
166.70
154.26
151.91
132.86
132.22
130.65
129.60
122.84
122.57
40.15
39.94
39.73
39.52
39.31
39.10
38.89
f1 (ppm)

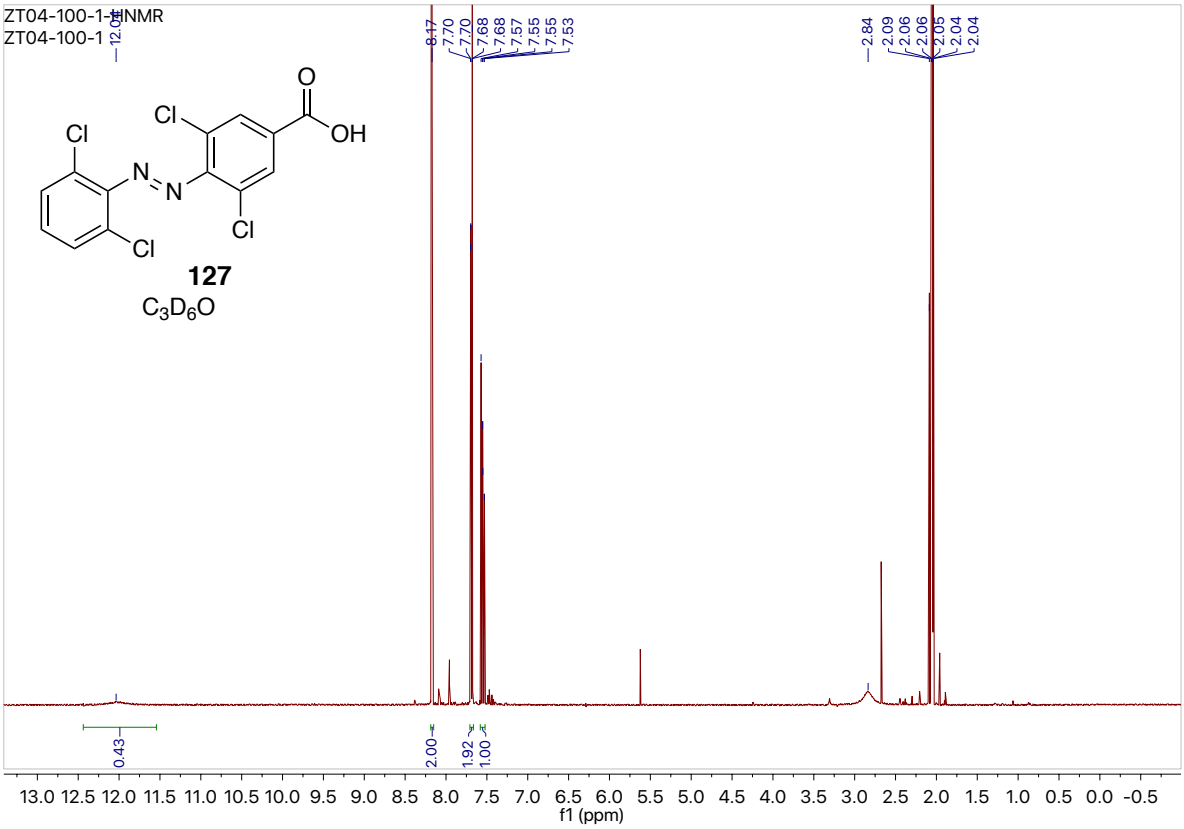
ZT04-100-1-HNMR
ZT04-100-1
12.04
8.17
7.70
7.70
7.68
7.68
7.57
7.55
7.55
7.53
2.84
2.09
2.06
2.06
2.05
2.04
2.04
Cl
Cl
Cl
Cl
N
N
O
OH
127
C_3D_6O
0.43
2.00
1.92
1.00
13.0 12.5 12.0 11.5 11.0 10.5 10.0 9.5 9.0 8.5 8.0 7.5 7.0 6.5 6.0 5.5 5.0 4.5 4.0 3.5 3.0 2.5 2.0 1.5 1.0 0.5 0.0 -0.5
f1 (ppm)

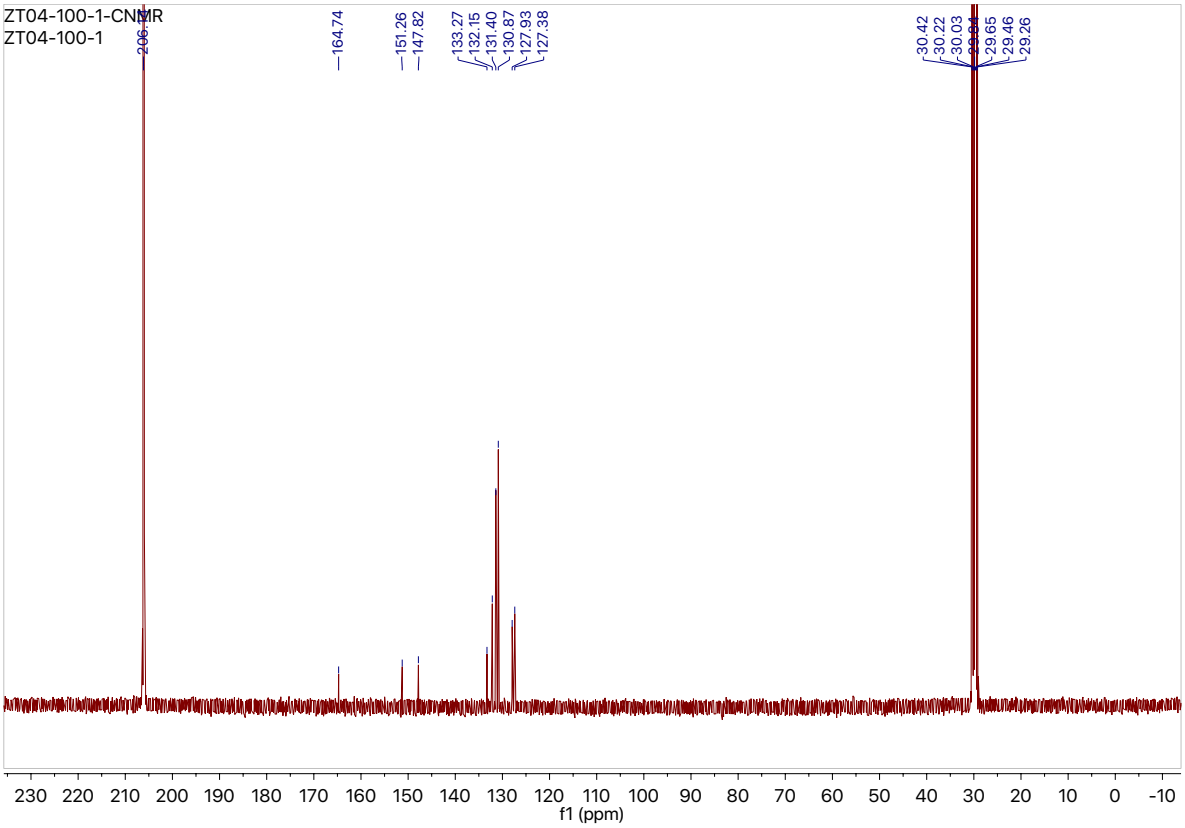
ZT04-100-1-CNMR
ZT04-100-1
206.7
164.74
151.26
147.82
133.27
132.15
131.40
130.87
127.93
127.38
30.42
30.22
30.03
29.84
29.65
29.46
29.26
230 220 210 200 190 180 170 160 150 140 130 120 110 100 90 80 70 60 50 40 30 20 10 0 -10
f1 (ppm)

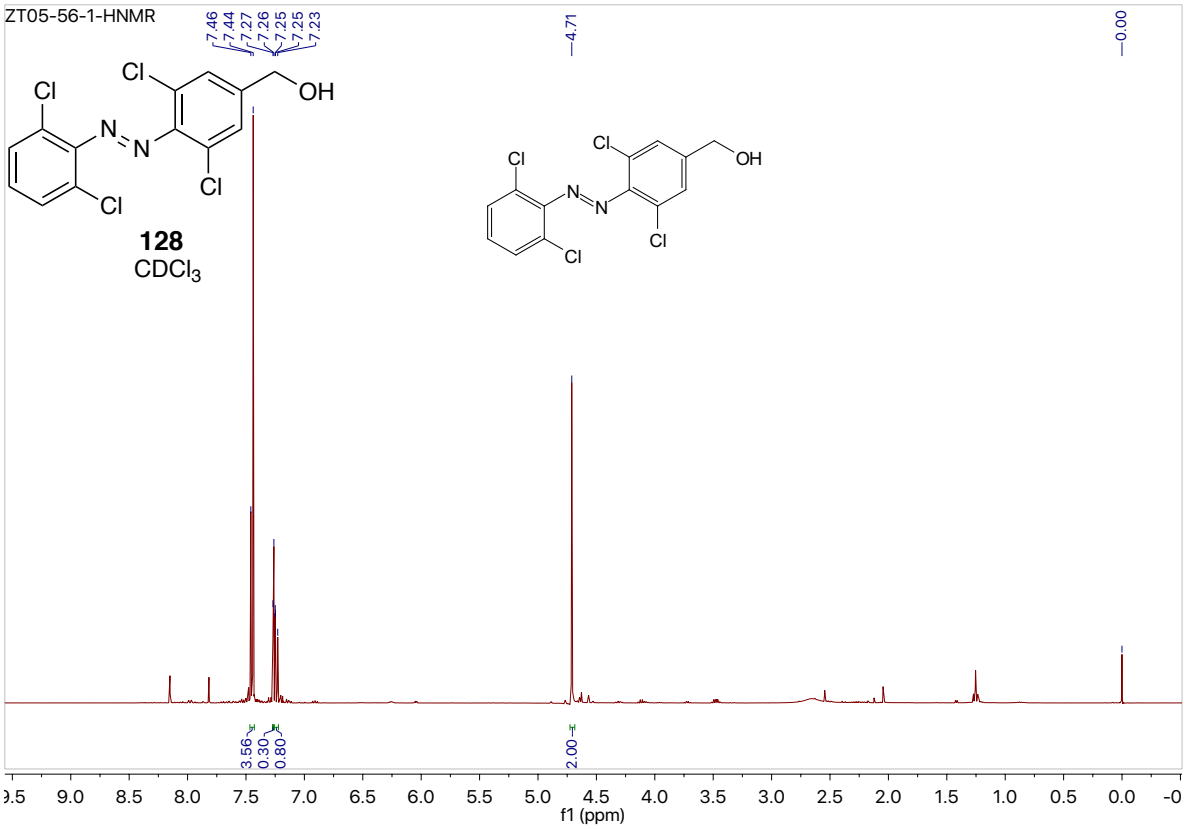
ZT05-56-1-HNMR
7.46
7.44
7.27
7.26
7.25
7.25
7.23
4.71
0.00
Cl
Cl
N
N
Cl
OH
Cl
Cl
128
CDCl3
3.56
0.30
0.80
2.00
f1 (ppm)

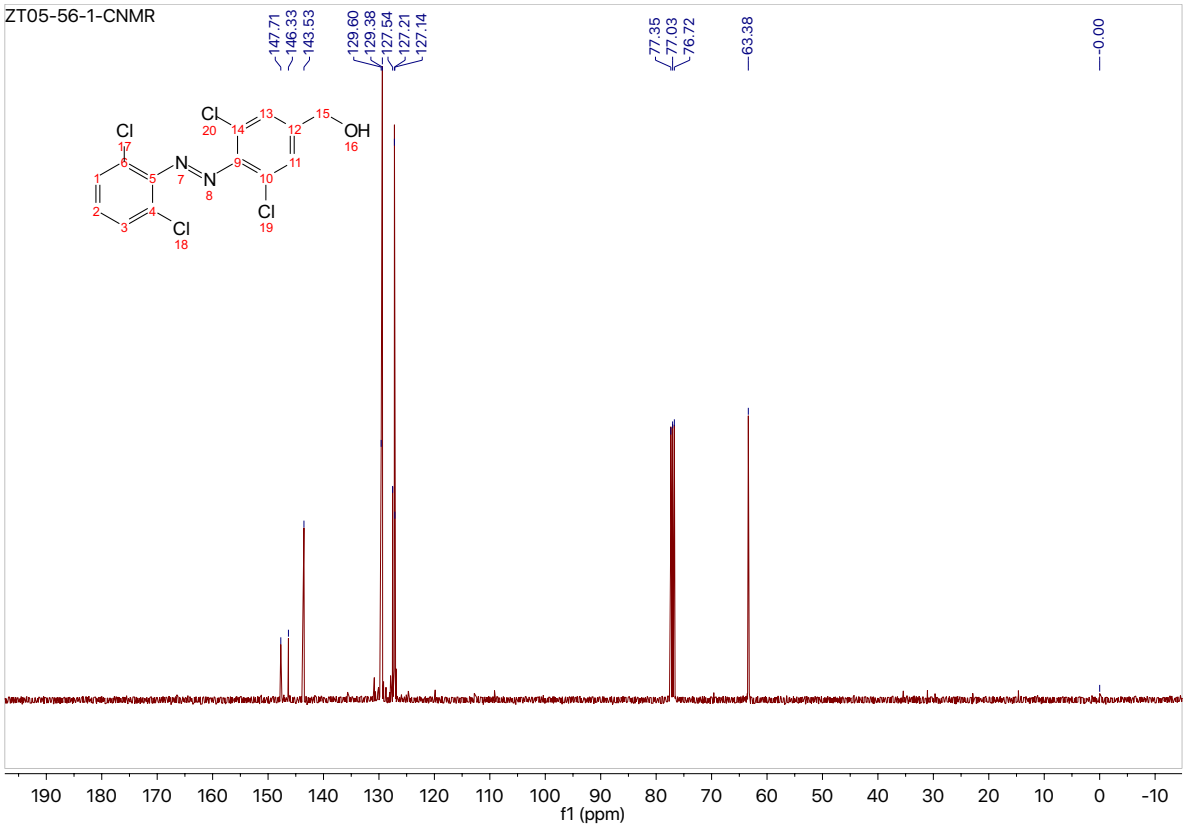
ZT05-56-1-CNMR
147.71
146.33
143.53
129.60
129.38
127.54
127.21
127.14
77.35
77.03
76.72
63.38
0.00
Cl
Cl
OH
N
N
Cl
Cl
f1 (ppm)

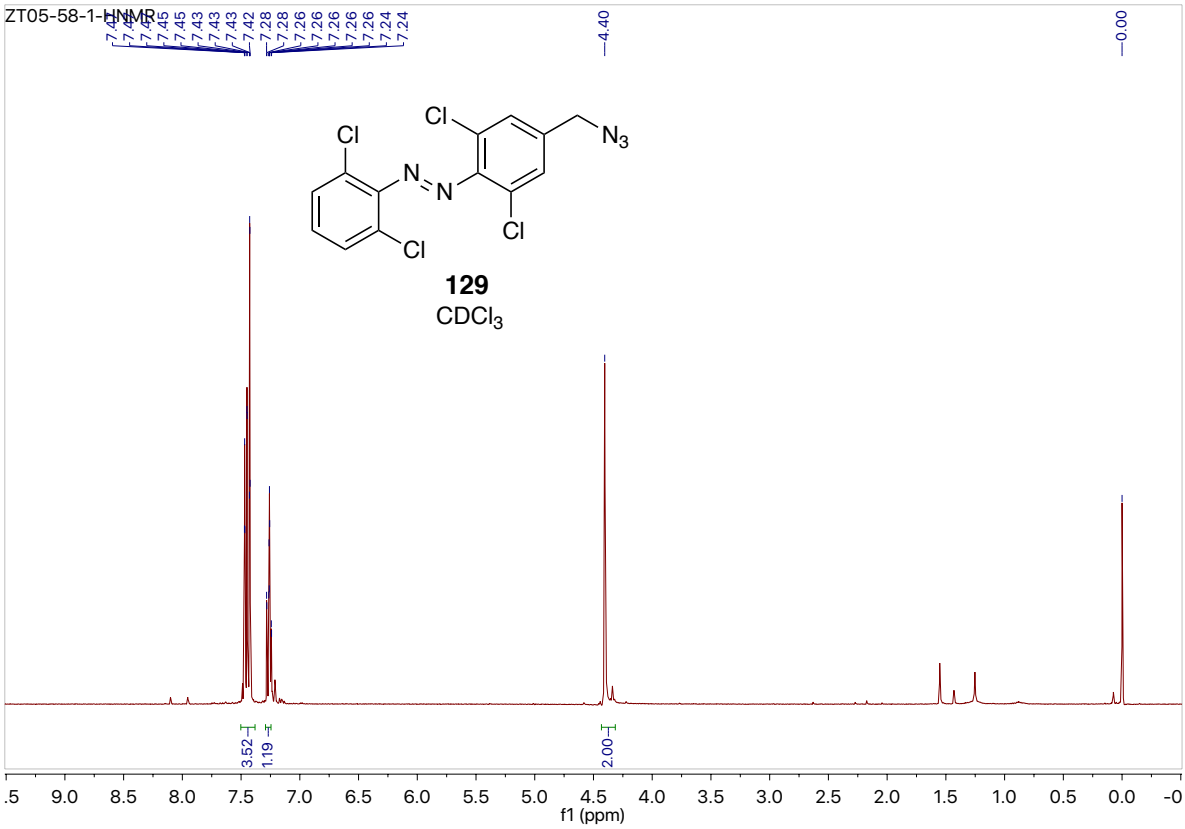
ZT05-58-1-HNMR
7.46
7.45
7.43
7.42
7.28
7.26
7.24
4.40
0.00
Cl
Cl
N
N
Cl
Cl
N3
129
CDCl3
3.52
1.19
2.00
f1 (ppm)

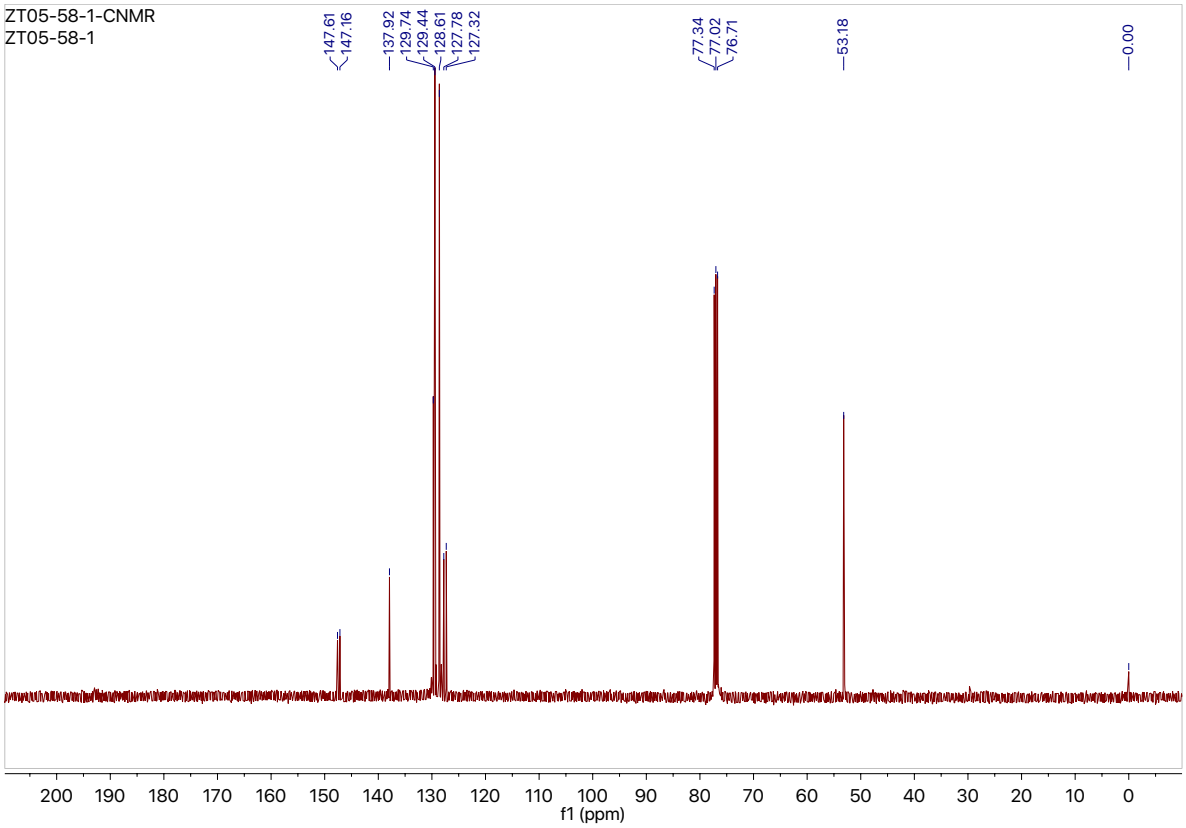
ZT05-58-1-CNMR
ZT05-58-1
147.61
147.16
137.92
129.74
129.44
128.61
127.78
127.32
77.34
77.02
76.71
53.18
0.00
f1 (ppm)

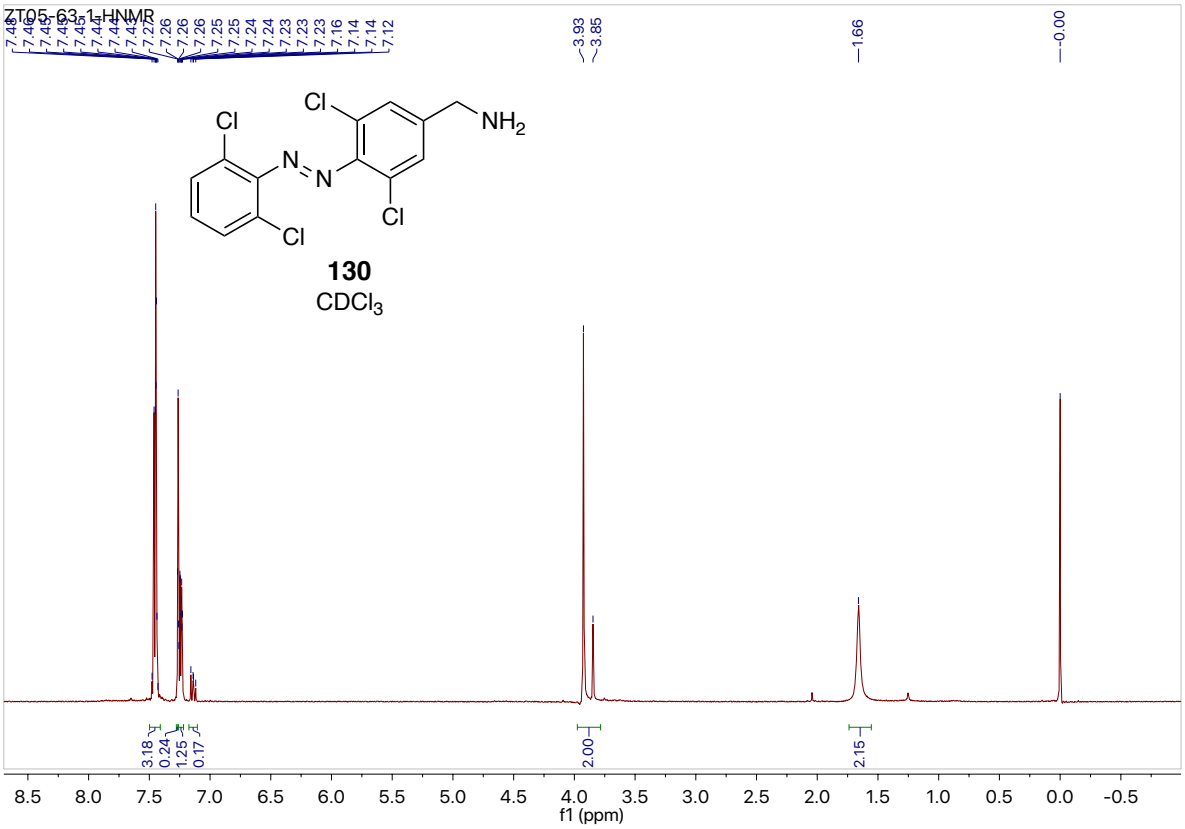
ZT05-63-1-HNMR
7.46 7.46 7.45 7.45 7.44 7.44 7.44 7.43 7.27 7.26 7.26 7.26 7.25 7.25 7.24 7.24 7.23 7.23 7.23 7.16 7.14 7.14 7.12
3.93
3.85
1.66
0.00
Cl
Cl
Cl
Cl
N
N
NH2
130
CDCl3
3.18
0.24
1.25
0.17
2.00
2.15
8.5 8.0 7.5 7.0 6.5 6.0 5.5 5.0 4.5 4.0 3.5 3.0 2.5 2.0 1.5 1.0 0.5 0.0 -0.5
f1 (ppm)

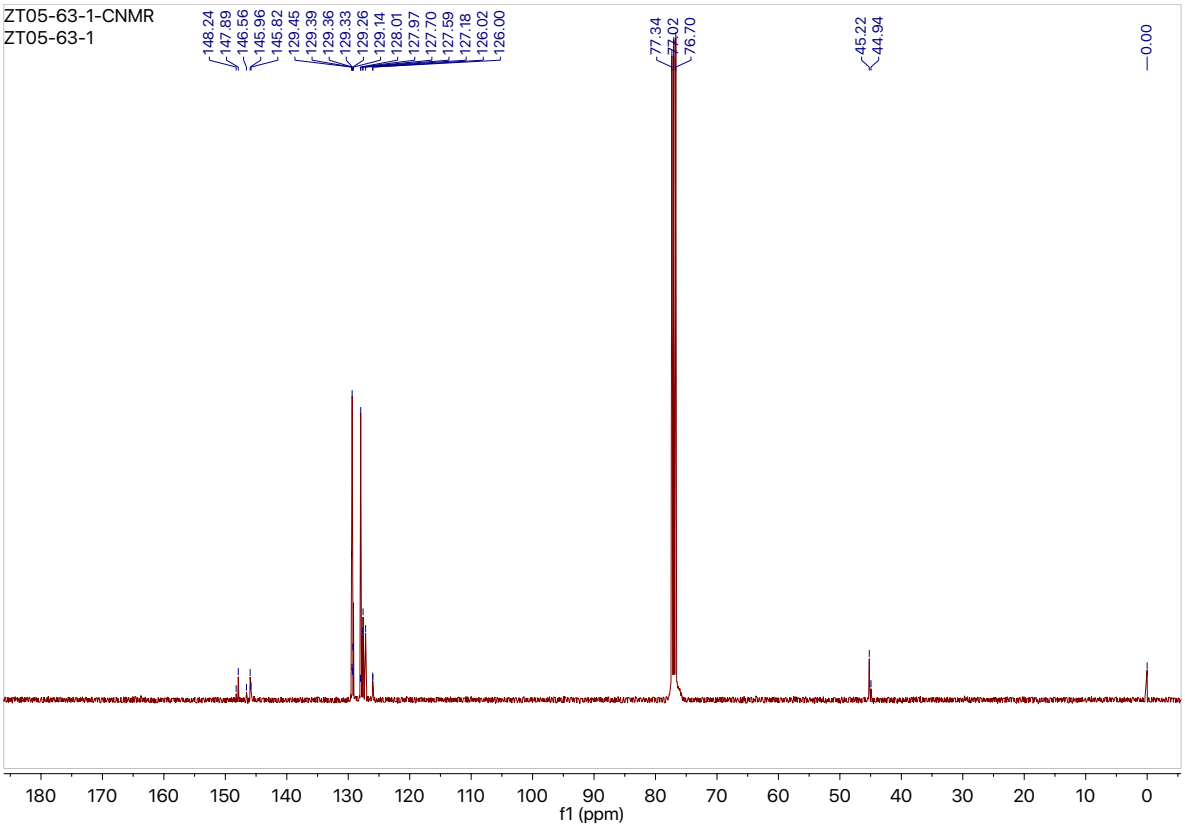
ZT05-63-1-CNMR
ZT05-63-1
148.24
147.89
146.56
145.96
145.82
129.45
129.39
129.36
129.33
129.26
129.14
128.01
127.97
127.70
127.59
127.18
126.02
126.00
77.34
77.02
76.70
45.22
44.94
0.00
180 170 160 150 140 130 120 110 100 90 80 70 60 50 40 30 20 10 0
f1 (ppm)

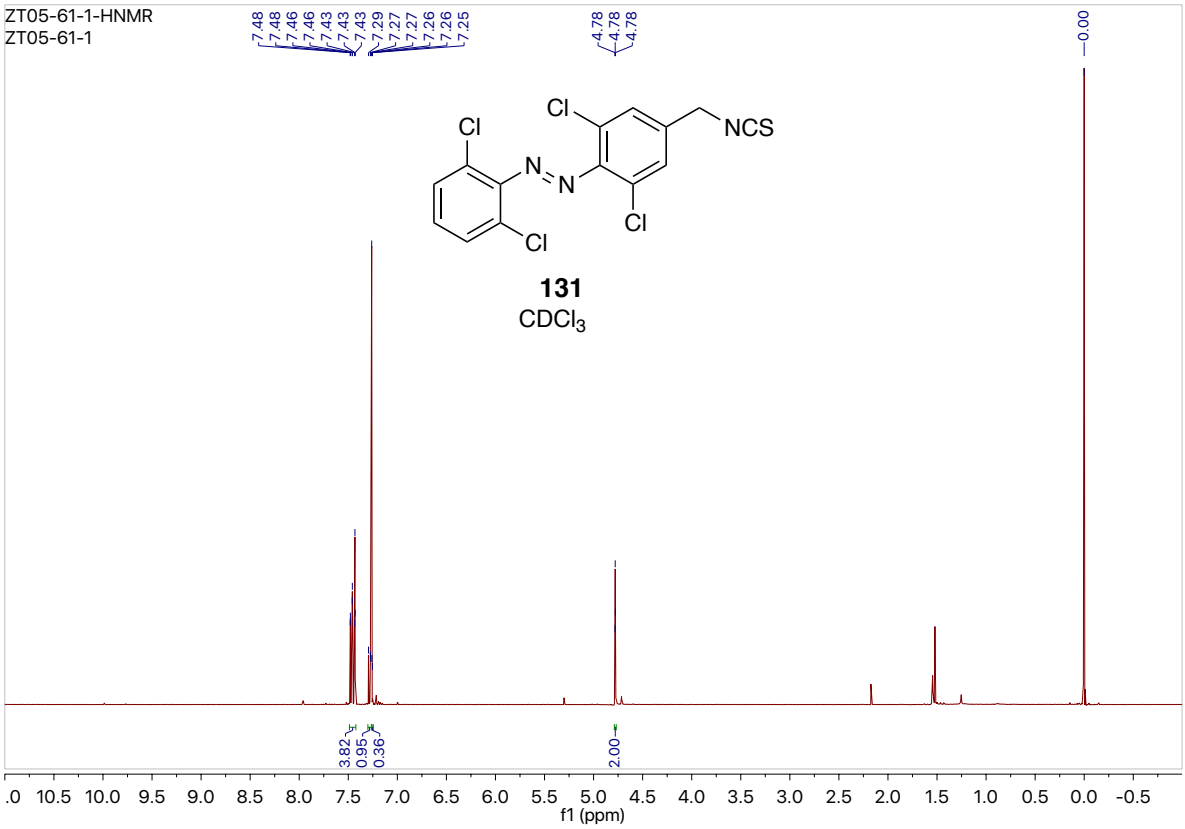
ZT05-61-1-HNMR
ZT05-61-1
7.48
7.48
7.46
7.46
7.43
7.43
7.43
7.29
7.27
7.27
7.26
7.26
7.25
4.78
4.78
4.78
0.00
Cl
Cl
Cl
Cl
N
N
NCS
131
CDCl3
3.82
0.95
0.36
2.00
.0 10.5 10.0 9.5 9.0 8.5 8.0 7.5 7.0 6.5 6.0 5.5 5.0 4.5 4.0 3.5 3.0 2.5 2.0 1.5 1.0 0.5 0.0 -0.5
f1 (ppm)

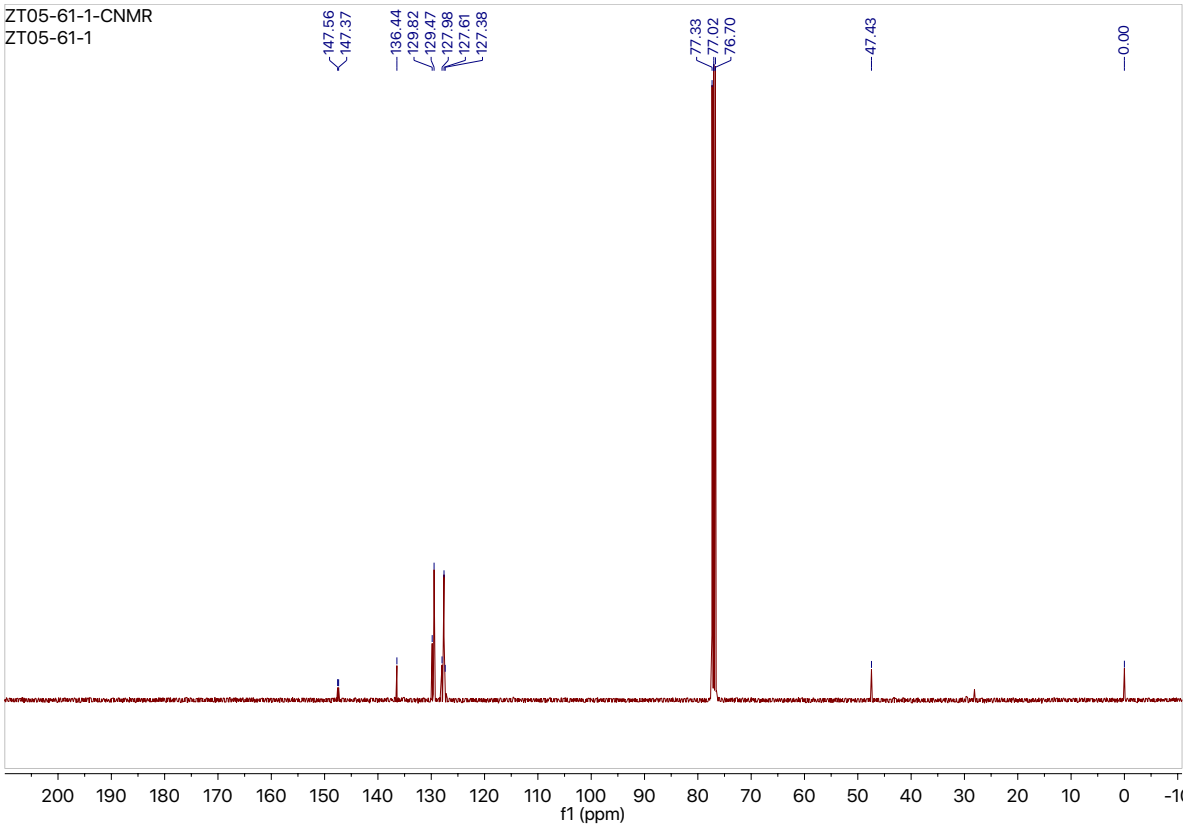
ZT05-61-1-CNMR
ZT05-61-1
147.56
147.37
136.44
129.82
129.47
127.98
127.61
127.38
77.33
77.02
76.70
47.43
0.00
200 190 180 170 160 150 140 130 120 110 100 90 80 70 60 50 40 30 20 10 0 -10
f1 (ppm)

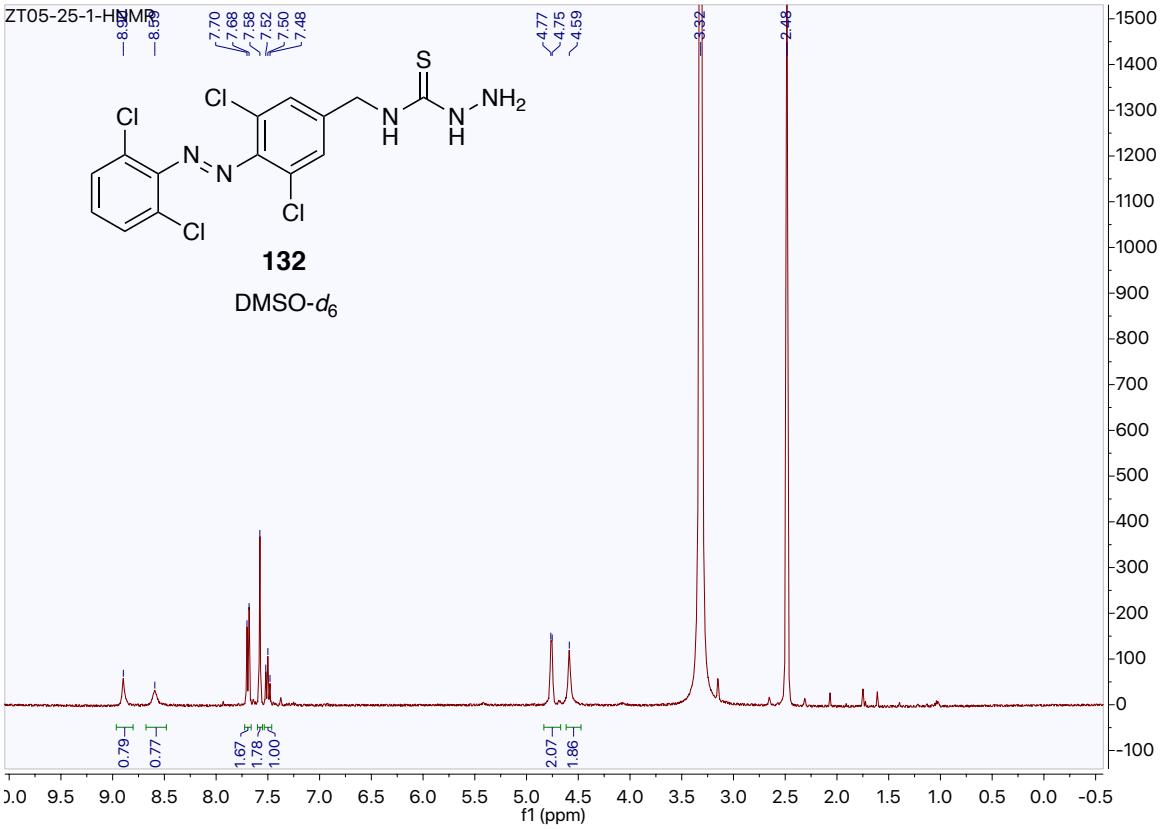
ZT05-25-1-HNMR
8.99
8.59
7.70
7.68
7.58
7.52
7.50
7.48
4.77
4.75
4.59
3.32
2.48
Cl
Cl
Cl
Cl
N
N
S
N
H
N
H
NH2
132
DMSO-d6
0.79
0.77
1.67
1.78
1.00
2.07
1.86
f1 (ppm)

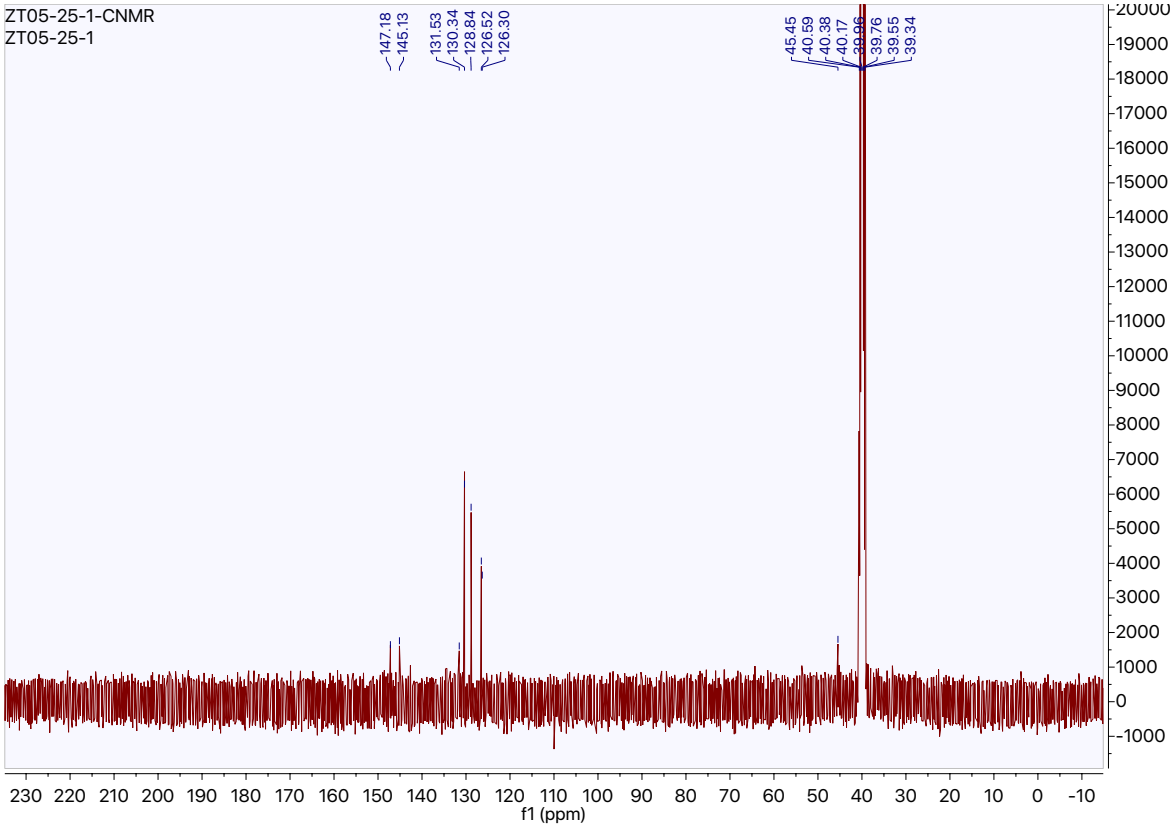
ZT05-25-1-CNMR
ZT05-25-1
147.18
145.13
131.53
130.34
128.84
126.52
126.30
45.45
40.59
40.38
40.17
39.96
39.76
39.55
39.34
f1 (ppm)

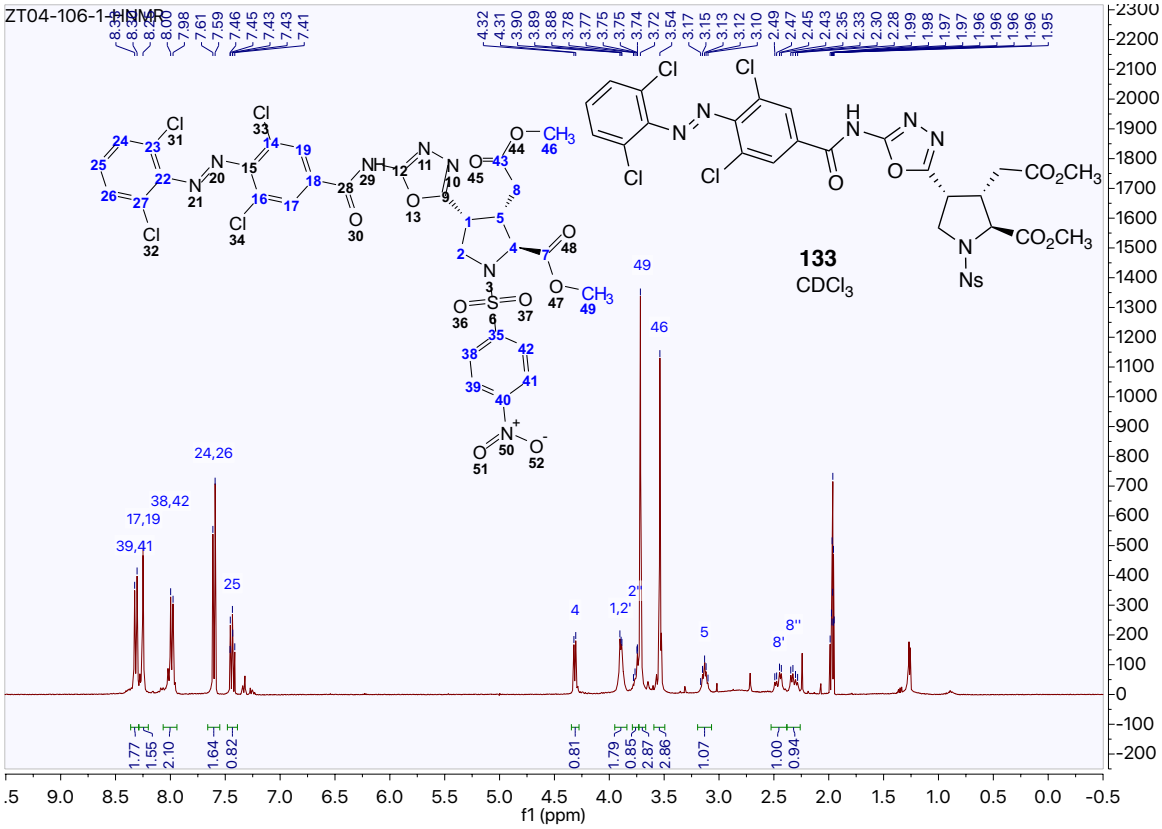
ZT04-106-1-HNMR
133
CDCl3
f1 (ppm)

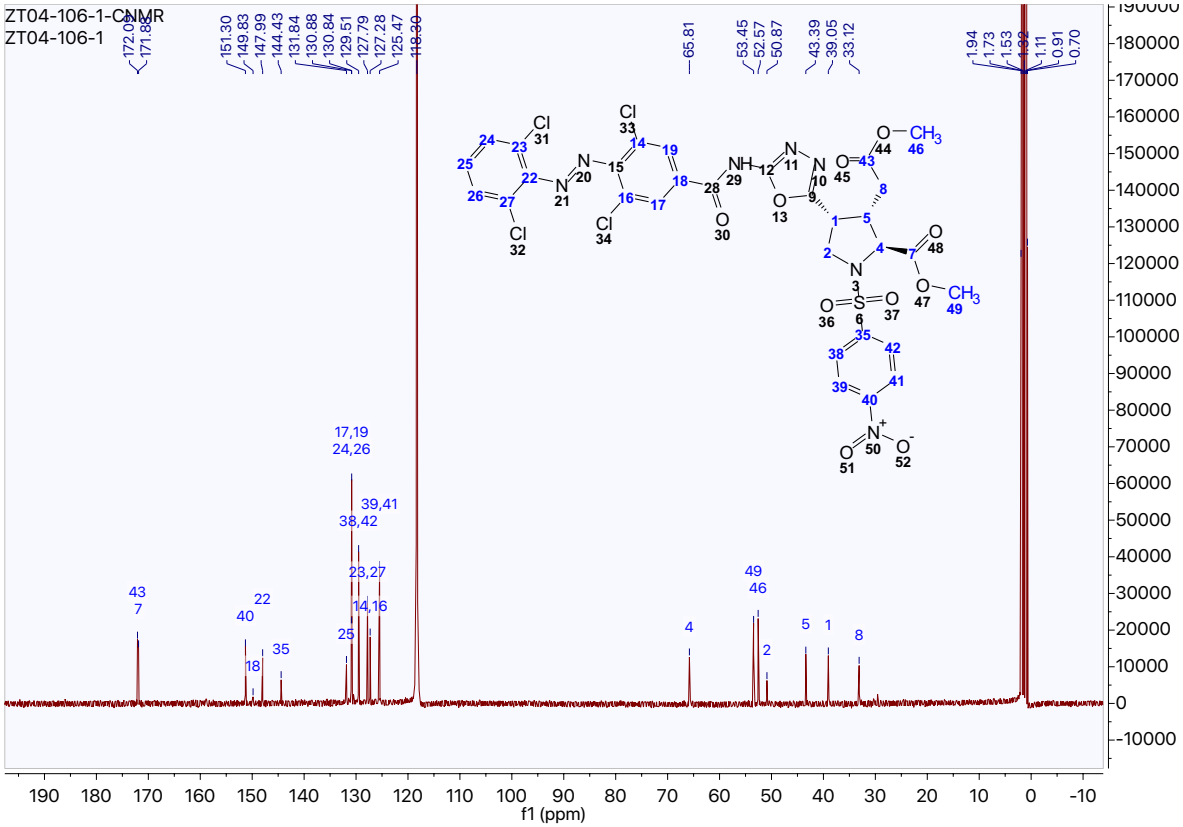
ZT04-106-1-CNMR
ZT04-106-1
f1 (ppm)

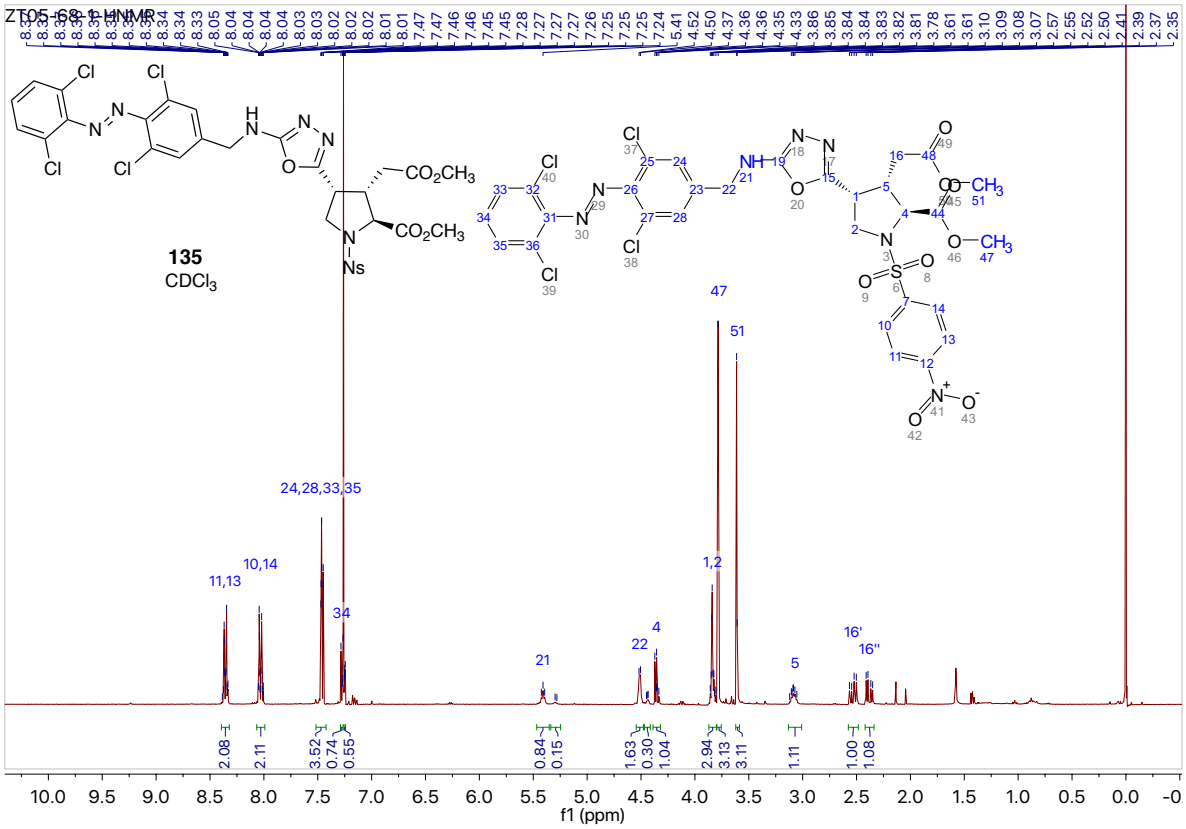
ZT05-68-1-HNMR
135
CDCl3
f1 (ppm)

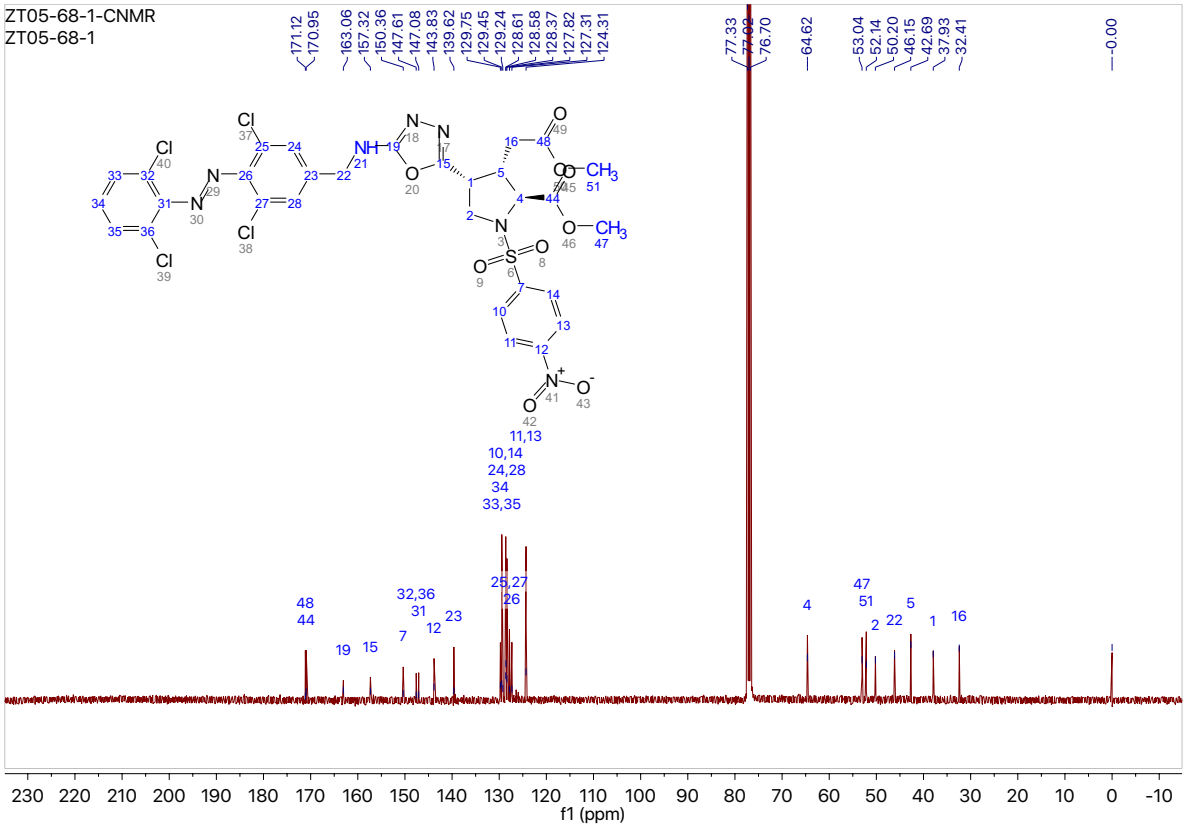
ZT05-68-1-CNMR
ZT05-68-1
f1 (ppm)

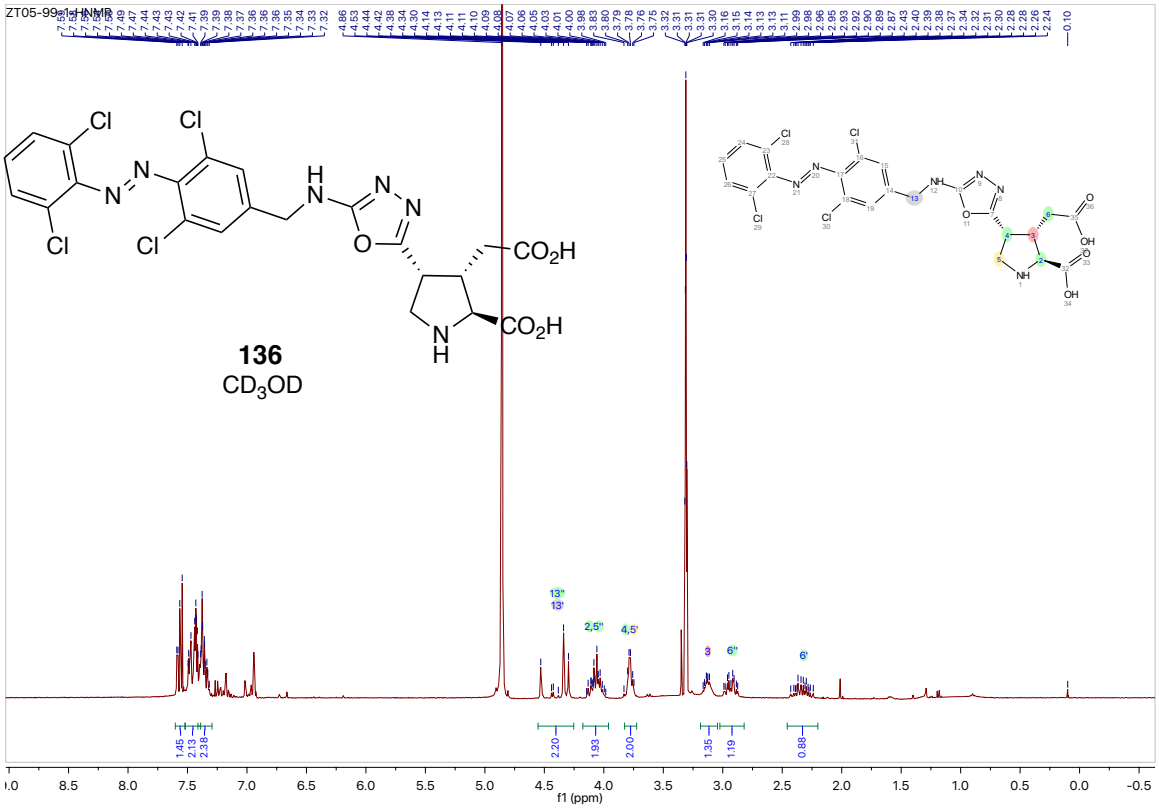
ZT05-99-1-1HNMR
136
CD3OD
f1 (ppm)

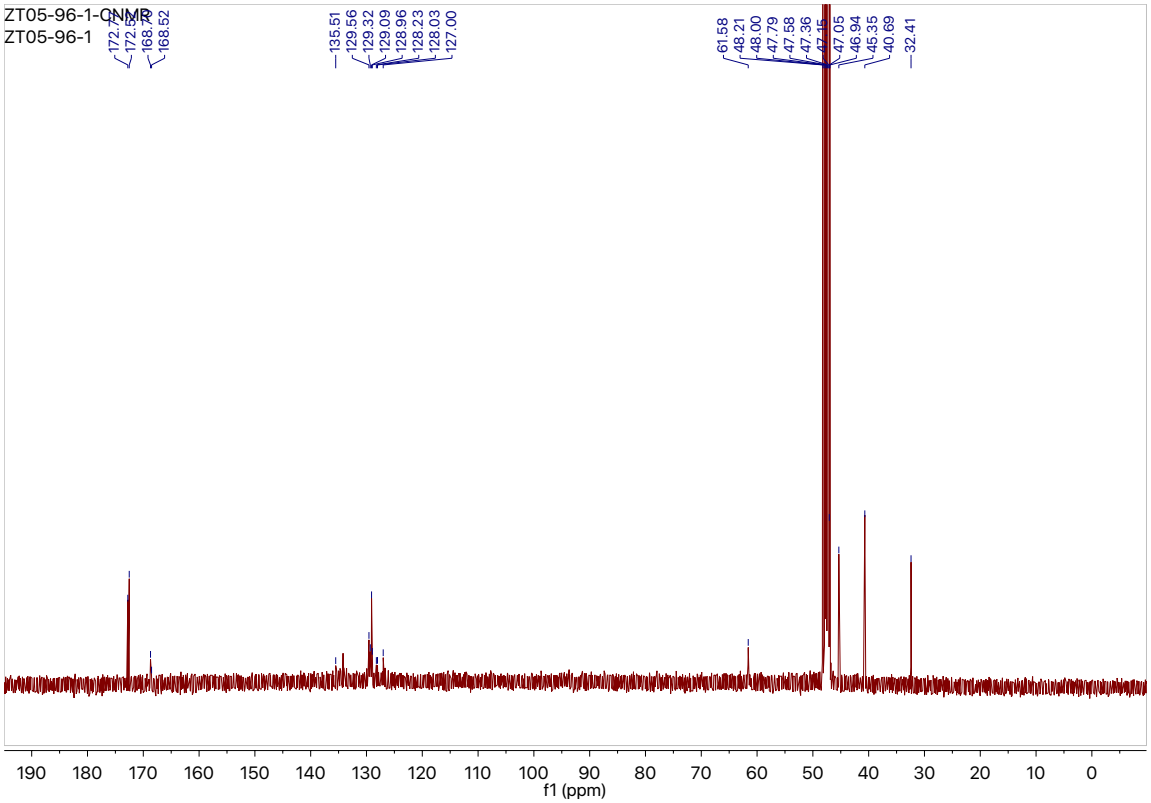
ZT05-96-1-CNMR
ZT05-96-1
f1 (ppm)

References

(1) Armstrong, N.; Sun, Y.; Chen, G.-Q.; Gouaux, E. *Nature* **1998**, *395* (6705), 913.
(2) Karakas, E.; Regan, M. C.; Furukawa, H. *Trends Biochem. Sci.* **2015**, *40* (6), 328.
(3) Lerma, J. *Nat. Rev. Neurosci.* **2003**, *4* (6), 481.
(4) Sobolevsky, A. I.; Rosconi, M. P.; Gouaux, E. *Nature* **2009**, *462* (7274), 745.
(5) Contractor, A.; Heinemann, S. F. *Science Signaling* **2002**, *2002* (156), re14.
(6) Mayer, M. L. *Neuron* **2005**, *45* (4), 539.
(7) Dürr, K. L.; Chen, L.; Stein, R. A.; De Zorzi, R.; Folea, I. M.; Walz, T.; Mchaourab, H. S.; Gouaux, E. *Cell* **2014**, *158* (4), 778.
(8) Meyerson, J. R.; Chittori, S.; Merk, A.; Rao, P.; Han, T. H.; Serpe, M.; Mayer, M. L.; Subramaniam, S. *Nature* **2016**, *537* (7621), 567.
(9) Meyerson, J. R.; Kumar, J.; Chittori, S.; Rao, P.; Pierson, J.; Bartesaghi, A.; Mayer, M. L.; Subramaniam, S. *Nature* **2014**, *514* (7522), 328.
(10) Liao, D.; Hessler, N. A.; Malinow, R. *Nature* **1995**, *375* (6530), 400.
(11) Isaac, J. T. R.; Nicoll, R. A.; Malenka, R. C. *Neuron* **1995**, *15* (2), 427.
(12) Durand, G. M.; Kovalchuk, Y.; Konnerth, A. *Nature* **1996**, *381* (6577), 71.
(13) Liu, X. J.; Salter, M. W. *Eur. J. Neurosci.* **2010**, *32* (2), 278.
(14) Contractor, A.; Mulle, C.; Swanson, G. T. *Trends Neurosci.* **2011**, *34* (3), 154.
(15) Collingridge, G. L.; Olsen, R. W.; Peters, J.; Spedding, M. *Neuropharmacol.* **2009**, *56* (1), 2.
(16) Lerma, J. *Nat. Rev. Neurosci.* **2003**, *4* (6), 481.
(17) Sihra, T. S.; Flores, G.; Rodríguez-Moreno, A. *Neuroscientist* **2014**, *20* (1), 29.
(18) Weisskopf, M. G.; Nicoll, R. A. *Nature* **1995**, *376* (6537), 256.
(19) Lerma, J.; Marques, J. M. *Neuron* **2013**, *80* (2), 292.
(20) Lerma, J.; Marques, J. M. *Neuron* **2013**, *80* (2), 292.
(21) Wyeth, M. S.; Pelkey, K. A.; Petralia, R. S.; Salter, M. W.; McInnes, R. R.; McBain, C. J. *J. Neurosci.* **2014**, *34* (2), 622.
(22) Matute, C. *CNS Neurosci. Ther.* **2010**, *17* (6), 661.
(23) Lévesque, M.; Avoli, M. *Neuroscience & Biobehavioral Reviews* **2013**, *37* (10), 2887.
(24) Zheng, X.-Y.; Zhang, H.-L.; Luo, Q.; Zhu, J. *J. Biomed. Biotechnol.* **2011**, *2011* (1–3), 457079.
(25) Wang, Q.; Yu, S.; Simonyi, A.; Sun, G. Y.; Sun, A. Y. *Mol Neurobiol* **2005**, *31* (1-3), 3.
(26) Jalil, E. C.; Dalain, Al, S. M.; Castillo, R.; Martínez, G.; Fernández, O. S. L. *Journal of Applied Toxicology* **2001**, *21* (5), 403.
(27) Lerma, J. *Curr. Opin. Pharmacol.* **2006**, *6* (1), 89.
(28) Wakayama, S.; Kiyonaka, S.; Arai, I.; Kakegawa, W.; Matsuda, S.; Ibata, K.; Nemoto, Y. L.; Kusumi, A.; Yuzaki, M.; Hamachi, I. *Nat. Commun.* **2017**, *8*, 14850.
(29) Kiyonaka, S.; Sakamoto, S.; Wakayama, S.; Morikawa, Y.; Tsujikawa, M.; Hamachi, I. *ACS Chem. Biol.* **2018**, *13* (7), 1880.
(30) Nørager, N. G.; Jensen, C. B.; Rathje, M.; Andersen, J.; Madsen, K. L.; Kristensen, A. S.; Strømgaard, K. *ACS Chem. Biol.* **2013**, *8* (9), 2033.
(31) Broichhagen, J.; Frank, J. A.; Trauner, D. *Acc. Chem. Res.* **2015**, *48* (7), 1947.
(32) Papageorgiou, G.; Ogden, D.; Kelly, G.; Corrie, J. E. T. *Photochem. Photobio. Sci.* **2005**, *4* (11), 887.

(33) Vishakha R Shembekar; Yongli Chen; Barry K Carpenter, A.; George P Hess. *Biochemistry* **2005**, *44* (19), 7107.
(34) Ellis-Davies, G. C. R. *Nat. Methods* **2007**, *4* (8), 619.
(35) Laprell, L.; Hull, K.; Stawski, P.; Schön, C.; Michalakis, S.; M, B.; Sumser, M. P.; Trauner, D. *ACS Chem. Neurosci.* **2015**, *7* (1), 15.
(36) Barber, D. M.; Liu, S.-A.; Gottschling, K.; Sumser, M.; Hollmann, M.; Trauner, D. *Chem. Sci.* **2017**, *8* (1), 611.
(37) Kienzler, M. A.; Reiner, A.; Trautman, E.; Yoo, S.; Trauner, D.; Isacoff, E. Y. *J. Am. Chem. Soc.* **2013**, *135* (47), 17683.
(38) Gómez-Santacana, X.; Pittolo, S.; Rovira, X.; Lopez, M.; Zussy, C.; Dalton, J. A. R.; Faucherre, A.; Jopling, C.; Pin, J.-P.; Ciruela, F.; Goudet, C.; Giraldo, J.; Gorostiza, P.; Llebaria, A. *ACS Cent. Sci.* **2017**, *3* (1), 81.
(39) Lefebvre, K. A.; Robertson, A. *Toxicon* **2010**, *56* (2), 218.
(40) TREMBLAY, J.-F. *Chem. Eng. News* **2000**, *78* (1), 14.
(41) Costa, L. G.; Giordano, G.; Faustman, E. M. *NeuroToxicol.* **2010**, *31* (5), 409.
(42) COYLE, J. T.; SCHWARCZ, R. *Nature* **1976**, *263* (5574), 244.
(43) Leite, J. P.; Garcia-Cairasco, N.; Cavalheiro, E. A. *Epilepsy research* **2002**, *50* (1), 93.
(44) Zheng, X.-Y.; Zhang, H.-L.; Luo, Q.; Zhu, J. *J. Biomed. Biotechnol.* **2011**, *2011* (1–3), 457079.
(45) Wang, Q.; Yu, S.; Simonyi, A.; Sun, G. Y.; Sun, A. Y. *Mol. Neurobiol.* **2005**.
(46) Shinozaki, H.; Shibuya, I. *Neuropharmacol.* **1976**, *15* (2), 145.
(47) Iván Collado; Jesús Ezquerra; Ana I Mateo, A.; Rubio, A. *J. Org. Chem.* **1998**, *63* (6), 1995.
(48) Goldberg, O.; Luini, A.; Teichberg, V. I. *J. Med. Chem.* **1983**, *26* (1), 39.
(49) Takeuchi, H.; Watanabe, K.; Nomoto, K.; Ohfune, Y.; Takemoto, T. *Eur. J. Pharmacol.* **1984**, *102* (2), 325.
(50) Wang, W.; Simovic, D. D.; Di, M.; Fieber, L.; Rein, K. S. *Bioorg. Med. Chem. Lett.* **2013**, *23* (7), 1949.
(51) Johnston, G. A. R.; Kennedy, S. M. E.; Twitchin, B. *J. Neurochem.* **1979**, *32* (1), 121.
(52) Teichberg, V. I.; Goldberg, O.; Luini, A. *Mol. Cell. Biochem.* **1981**, *39* (1), 281.
(53) Kozikowski, A. P.; Fauq, A. H. *Tetrahedron Lett.* **1990**, *31* (21), 2967.
(54) Maeda, M.; Kodama, T.; Tanaka, T.; Yoshizumi, H.; Takemoto, T.; Nomoto, K.; Fujita, T. *Tetrahedron Lett.* **1987**, *28* (6), 633.
(55) Conway, G. A.; Park, J. S.; Maggiora, L.; Mertes, M. P.; Galton, N.; Michaelis, E. K. *J. Med. Chem.* **1984**, *27* (1), 52.
(56) Ishida, M.; Shinozaki, H. *Br. J. Pharmacol.* **1991**, *104* (4), 873.
(57) Cantrell, B. E.; Zimmerman, D. M.; Monn, J. A.; Kamboj, R. K.; Hoo, K. H.; Tizzano, J. P.; Pullar, I. A.; Farrell, L. N.; Bleakman, D. *J. Med. Chem.* **1996**, *39* (19), 3617.
(58) Brown, H. C.; Okamoto, Y. *J. Am. Chem. Soc.* **1958**, *80* (18), 4979.
(59) Leffler, J. E.; Grunwald, E. *Rates and equilibria of organic reactions: as treated by statistical, thermodynamic and extrathermodynamic methods*; 2013.
(60) Lewis, M.; Bagwill, C.; Hardebeck, L. K. E.; Wireduaah, S. *Comput. Struct. Biotec. J.* **2012**, *1* (1), e201204004.
(61) Govenkar, M. B.; Wahidulla, S. *Phytochem.* **2000**, *54* (8), 979.
(62) Scholin, C. A.; Gulland, F.; Doucette, G. J.; Benson, S.; Busman, M.; Chavez, F. P.; Cordaro, J.; DeLong, R.; De Vogelaere, A.; Harvey, J.; Haulena, M.; Lefebvre, K.; Lipscomb, T.; Loscutoff, S.; Lowenstine, L. J.; Marin, R., III; Miller, P. E.; McLellan, W. A.; Moeller, P. D. R.; Powell, C. L.; Rowles, T.; Silvagni, P.; Silver, M.; Spraker, T.; Trainer, V.; Van Dolah, F. M. *Nature* **2000**, *403* (6765), 80.

(63) Wright, J. L. C.; Boyd, R. K.; de Freitas, A. S. W.; Falk, M.; Foxall, R. A.; Jamieson, W. D.; Laycock, M. V.; McCulloch, A. W.; McInnes, A. G.; Odense, P.; Pathak, V. P.; Quilliam, M. A.; Ragan, M. A.; Sim, P. G.; Thibault, P.; Walter, J. A.; Gilgan, M.; Richard, D. J. A.; Dewar, D. *Can. J. Chem.* **2011**, *67* (3), 481.

(64) Wright, J. L. C.; Boyd, R. K.; de Freitas, A. S. W.; Falk, M.; Foxall, R. A.; Jamieson, W. D.; Laycock, M. V.; McCulloch, A. W.; McInnes, A. G.; Odense, P.; Pathak, V. P.; Quilliam, M. A.; Ragan, M. A.; Sim, P. G.; Thibault, P.; Walter, J. A.; Gilgan, M.; Richard, D. J. A.; Dewar, D. *Can. J. Chem.* **1989**, *67* (3), 481.

(65) Ohfune, Y.; Tomita, M. *J. Am. Chem. Soc.* **1982**.

(66) Baldwin, J. E.; Moloney, M. G.; Parsons, A. F. *Tetrahedron* **1990**, *46* (20), 7263.

(67) Meyerson, J. R.; Chittori, S.; Merk, A.; Rao, P.; Han, T. H.; Serpe, M.; Mayer, M. L.; Subramaniam, S. *Nature* **2016**, *537* (7621), 567.

(68) Krogsgaard-Larsen, N.; Storgaard, M.; Møller, C.; Demmer, C. S.; Hansen, J.; Han, L.; Monrad, R. N.; Nielsen, B.; Tapken, D.; Pickering, D. S.; Kastrup, J. S.; Frydenvang, K.; Bunch, L. *J. Med. Chem.* **2015**, *58* (15), 6131.

(69) Møllerud, S.; Pinto, A.; Marconi, L.; Frydenvang, K.; Thorsen, T. S.; Laulumaa, S.; Venskutonytė, R.; Winther, S.; Moral, A. M. C.; Tamborini, L.; Conti, P.; Pickering, D. S.; Kastrup, J. S. *ACS Chem. Neurosci.* **2017**, *8* (9), 2056.

(70) Venskutonytė, R.; Frydenvang, K.; Hald, H.; Rabassa, A. C. de; Gajhede, M.; Ahring, P. K.; Kastrup, J. S. *Neurochem. Int.* **2012**, *61* (4), 536.

(71) Nayeem, N.; Mayans, O.; Green, T. *J. Neurosci.* **2011**, *31* (8), 2916.

(72) Kumar, J.; Mayer, M. L. *J. Mol. Biol.* **2010**, *404* (4), 680.

(73) Hald, H.; Naur, P.; Pickering, D. S.; Sprogøe, D.; Madsen, U.; Timmermann, D. B.; Ahring, P. K.; Liljefors, T.; Schousboe, A.; Egebjerg, J.; Gajhede, M.; Kastrup, J. S. *J. Biol. Chem.* **2007**, *282* (35), 25726.

(74) Jack E Baldwin; Andrew M Fryer, A.; Pritchard, G. J. *J. Org. Chem.* **2001**, *66* (8), 2588.

(75) Holland, P. T.; Selwood, A. I.; Mountfort, D. O.; Wilkins, A. L.; McNabb, P.; Rhodes, L. L.; Doucette, G. J.; Mikulski, C. M.; King, K. L. *Chem. Res. Toxicol.* **2005**, *18* (5), 814.

(76) Ishida, M.; Shinozaki, H. *Br. J. Pharmacol.* **1991**, *104* (4), 873.

(77) Schwarcz, R.; Scholz, D.; Coyle, J. T. *Neuropharmacol.* **1978**, *17* (2), 145.

(78) King, A. E.; Wheal, H. V. *Eur. J. Pharmacol.* **1984**, *102* (1), 129.

(79) Collado, I.; Ezquerra, J.; Mateo, A. I.; Pedregal, C.; Rubio, A. *J. Org. Chem.* **1999**, *64* (12), 4304.

(80) Johnston, G. A.; Curtis, D. R.; Davies, J.; McCulloch, R. M. *Nature* **1974**, *248* (5451), 804.

(81) Sawant, P. M.; Tyndall, J. D. A.; Holland, P. T.; Peake, B. M.; Mountfort, D. O.; Kerr, D. S. *Neuropharmacol.* **2010**, *59* (3), 129.

(82) Sonnenberg, J. D.; Koch, H. P.; Willis, C. L.; Bradbury, F.; Dauenhauer, D.; Bridges, R. J.; Chamberlin, A. R. *Bioorg. Med. Chem. Lett.* **1996**, *6* (13), 1607.

(83) Foster, G. A.; Roberts, P. J.; Teichberg, V. I.; Goldberg, O. *Neurosci. Lett.* **1982**, *29* (2), 169.

(84) Collado, I.; Ezquerra, J.; Mateo, A. I.; Rubio, A. *J. Org. Chem.* **1998**, *63* (6), 1995.

(85) Stathakis, C. I.; Yioti, E. G.; Gallos, J. K. *Eur. J. Org. Chem.* **2012**, *2012* (25), 4661.

(86) Parsons, A. F. *Tetrahedron* **1996**, *52* (12), 4149.

(87) Werner, P.; Voigt, M. *Nature* **1991**.

(88) Greenamyre, J. T.; Young, A. B. *Neurobiol. Aging* **1989**, *10* (5), 593.

(89) Stein, B. A.; Sapolsky, R. M. *Brain Res.* **1988**, *473* (1), 175.

(90) Moloney, M. G. *Nat. Pro. Rep.* **2002**, *19* (5), 597.

(91) Fujii, M.; Yokoshima, S.; Fukuyama, T. *Eur. J. Org. Chem.* **2014**, *2014* (22), 4823.

(92) Bhat, C.; Kumar, A. *Asian J. Org. Chem.* **2015**, *4* (2), 102.

(93) Clayden, J.; Read, B.; Hebditch, K. R. *Tetrahedron* **2005**, *61* (24), 5713.

(94) Lei, H.; Xin, S.; Qiu, Y.; Zhang, X. *Chem. Commun.* **2018**, *54* (7), 727.

(95) Sasaki, S.; Suzuki, H.; Ouchi, H.; Asakawa, T.; Inai, M.; Sakai, R.; Shimamoto, K.; Hamashima, Y.; Kan, T. *Org. Lett.* **2014**, *16* (2), 564.

(96) Zhang, M.; Watanabe, K.; Tsukamoto, M.; Shibuya, R.; Morimoto, H.; Ohshima, T. *Chem. Eur. J.* **2015**, *21* (10), 3937.

(97) Chevliakov, M. V.; Montgomery, J. *Angew. Chem. Int. Ed.* **1998**, *37* (22), 3144.

(98) Baldwin, J. E.; Rudolph, M. *Tetrahedron Lett.* **1994**, *35* (33), 6163.

(99) Takita, S.; Yokoshima, S.; Fukuyama, T. *Synthesis* **2011**, *2011* (23), 3848.

(100) Blanco, M. A.-J. S.; Sardina, F. J. *J. Org. Chem.* **1996**, *61* (14), 4748.

(101) Poisson, J.-F.; Orellana, A.; Greene, A. E. *J. Org. Chem.* **2005**, *70* (26), 10860.

(102) Zanato, C.; Watson, S.; Bewick, G. S.; Harrison, W. T. A.; Zanda, M. *Org. Biomol. Chem.* **2014**, *12* (47), 9638.

(103) Supernant, S. and Lubell, W. D. *J. Org. Chem.* **2005**, *71* (2), 848.

(104) Gill, P.; Lubell, W. D. *J. Org. Chem.* **1995**, *60* (9), 2658.

(105) Dietrich E., Lubell, W.D., *J. Org. Chem.* **2003**, *68* (18), 6988.

(106) Krasovskiy, A.; Kopp, F.; Knochel, P. *Angew. Chem. Int. Ed.* **2006**, *45* (3), 497.

(107) Ma, D.; Wu, W.; Deng, P. *Tetrahedron Lett.* **2001**, *42* (39), 6929.

(108) Jamison, T. F.; Rapoport, H. *(S) - N - (9 - Phenylfluoren - 9 - yl)Alanine and (S) - Dimethyl N - (9 - Phenylfluoren - 9 - yl)Aspartate*; John Wiley & Sons, Inc.: Hoboken, NJ, USA, 1993; Vol. 109, pp 226–226.

(109) Campbell, A. D.; Taylor, R. J. K.; Raynham, T. M. *Chem. Commun.* **1999**, *0* (3), 245.

(110) Rubio, A.; Ezquerra, J.; Escribano, A.; Remuiñán, M. J.; Vaquero, J. J. *Tetrahedron Lett.* **1998**, *39* (15), 2171.

(111) Takita, S.; Yokoshima, S.; Fukuyama, T. *Org. Lett.* **2011**, *13* (8), 2068.

(112) Jack E Baldwin; Andrew M Fryer, A.; Pritchard, G. J. *J. Org. Chem.* **2001**, *66* (8), 2597.

(113) Baldwin, J. E.; Fryer, A. M.; Pritchard, G. J. *J. Org. Chem.* **2001**, *66* (8), 2597.

(114) Matoba, M.; Kajimoto, T.; Node, M. *Synth. Commun.* **2008**, *38* (8), 1194.

(115) Layton, M. E.; Kelly, M. J. I.; Rodzinak, K. J.; Sanderson, P. E.; Young, S. D.; Bednar, R. A.; DiLella, A. G.; Mcdonald, T. P.; Wang, H.; Mosser, S. D.; Fay, J. F.; Cunningham, M. E.; Reiss, D. R.; Fandozzi, C.; Trainor, N.; Liang, A.; Lis, E. V.; Seabrook, G. R.; Urban, M. O.; Yergey, J.; Koblan, K. S. *ACS Chem. Neurosci.* **2011**, *2* (7), 352.

(116) Ren, Z.; Riley, N. J.; Needleman, L. A.; Sanders, J. M.; Swanson, G. T.; Marshall, J. *J. Biol. Chem.* **2003**, *278* (52), 52700.

(117) González, I. M. G.; Henley, J. M. *Traffic* **2013**, *14* (7), 810.

(118) Sun, H.; Lu, L.; Zuo, Y.; Wang, Y.; Jiao, Y.; Zeng, W.-Z.; Huang, C.; Zhu, M. X.; Zamponi, G. W.; Zhou, T.; Xu, T.-L.; Cheng, J.; Li, Y. *Nat. Commun. 2014 5:null* **2014**, *5* (1), 4980.

(119) Coutinho, V.; Kavanagh, I.; Sugiyama, H.; Tones, M. A.; Henley, J. M. *Mol. Cell. Neurosci.* **2001**, *18* (3), 296.

(120) Yan, S.; Sanders, J. M.; Xu, J.; Zhu, Y.; Contractor, A.; Swanson, G. T. *J. Neurosci.* **2004**, *24* (3), 679.

(121) Harvey, D. M.; Calkins S, D. J. *Vis. Neurosci.* **2002**, *19* (5), 681.

(122) Dietrich, M. O.; Mantese, C. E.; Porciuncula, L. O.; Ghisleni, G.; Vinade, L.; Souza, D. O.; Portela, L. V. *Brain Res.* **2005**, *1065* (1-2), 20.

(123) Chen, X.; Cho, D.-B.; Yang, P.-C. *N. Am. J. Med. Sci.* **2010**, *2* (5), 241.

(124) Ueno, T. and Nagano T., *Nat. Methods*, **2011**, 8, 642.

(125) Jing, C.; Cornish, V. W. *Acc. Chem. Res.* **2011**, *44* (9), 784.
(126) Wakayama, S.; Kiyonaka, S.; Arai, I.; Kakegawa, W.; Matsuda, S.; Ibata, K.; Nemoto, Y. L.; Kusumi, A.; Yuzaki, M.; Hamachi, I. *Nat. Commun.* **2017**, *8*, 14850.
(127) Chabot, N.; Moreau, S.; Mulani, A.; Moreau, P.; Keillor, J. W. *Chem. Biol.* **2010**, *17* (10), 1143.
(128) Chen, Y.; Tsao, K.; Acton, S. L.; Keillor, J. W. *Angew. Chem. Int. Ed.* **2018**, *130* (38), 12570.
(129) Hughes, L. D.; Rawle, R. J.; Boxer, S. G. *PLoS ONE* **2014**, *9* (2), e87649.
(130) Morales-Serna, J.; Garcia-Rios, E.; Bernal, J.; Paleo, E.; Gavino, R.; Cardenas, J. *Synthesis* **2011**, *2011* (09), 1375.
(131) Lemiere, G.; Sedehizadeh, S.; Toueg, J.; Fleary-Roberts, N.; Clayden, J. *Chem. Commun.* **2011**, *47* (13), 3745.
(132) Yamada, Y. M. A.; Sarkar, S. M.; Uozumi, Y. *J. Am. Chem. Soc.* **2012**, *134* (22), 9285.
(133) Schönberger, M.; Althaus, M.; Fronius, M.; Clauss, W.; Trauner, D. *Nat. Chem.* **2014**, *6* (8), 712.
(134) Hüll, K.; Morstein, J.; Trauner, D. *Chem. Rev.* **2018**, *118* (21), 10710.
(135) Pama, E. A. C.; Colzato, L. S.; Hommel, B. *Front. Psychol.* **2013**, *4*, 610.
(136) Fiala, A.; Suska, A.; Schlüter, O. M. *Curr. Biol.* **2010**, *20* (20), R897.
(137) Pama, E. A. C.; Colzato, L. S.; Hommel, B. *Front. Psychol.* **2013**, *4*, 610.
(138) Kramer, R. H.; Mourot, A.; Adesnik, H. *Nat. Neurosci.* **2013**, *16* (7), 816.
(139) Li, D.; Hérault, K.; Isacoff, E. Y.; Oheim, M.; Ropert, N. *J. Physiol.* **2012**, *590* (4), 855.
(140) Hüll, K.; Morstein, J.; Trauner, D. *Chem. Rev.* **2018**, *118* (21), 10710.
(141) Ellis-Davies, G. C. R. *Nat Protoc* **2011**, *6* (3), 314.
(142) Olson, J. P.; Kwon, H.-B.; Takasaki, K. T.; Chiu, C. Q.; Higley, M. J.; Sabatini, B. L.; Ellis-Davies, G. C. R. *J. Am. Chem. Soc.* **2013**, *135* (16), 5954.
(143) Fedoryak, O. D.; Sul, J.-Y.; Haydon, P. G.; Ellis-Davies, G. C. R. *Chem. Commun.* **2005**, *1* (29), 3664.
(144) Huang Y. H.; Sinha S.R.; Fedoryak O.D.; Ellis-Davies G. C. R.; Bergles D.E. *Biochemistry* **2005**, *44* (9), 3316.
(145) Olson, J. P.; Kwon, H.-B.; Takasaki, K. T.; Chiu, C. Q.; Higley, M. J.; Sabatini, B. L.; Ellis-Davies, G. C. R. *J. Am. Chem. Soc.* **2013**, *135* (16), 5954.
(146) Hoppmann, C.; Maslennikov, I.; Choe, S.; Wang, L. *J. Am. Chem. Soc.* **2015**, *137* (35), 11218.
(147) Samanta, S.; Beharry, A. A.; Sadovski, O.; McCormick, T. M.; Babalhavaeji, A.; Tropepe, V.; Woolley, G. A. *J. Am. Chem. Soc.* **2013**, *135* (26), 9777.
(148) Wang, X.; Gao, Y.; Xu, Y.; Li, L.; Zhang, Z.; Liu, J. *Synth. Commun.* **2009**, *39* (22), 4030.
(149) Brimioulle, R.; Guo, H.; Bach, T. *Chem. Eur. J.* **2012**, *18* (24), 7552.
(150) Weinrich, T.; Gränz, M.; Grünewald, C.; Prisner, T. F.; Göbel, M. W. *Eur. J. Org. Chem.* **2017**, *2017* (3), 491.
(151) Zhu, M.; Zhou, H. *Org. Biomol. Chem.* **2018**, *16* (44), 8434.
(152) Wegener, M.; Hansen, M. J.; Driessen, A. J. M.; Szymanski, W.; Feringa, B. L. *J. Am. Chem. Soc.* **2017**, *139* (49), 17979.
(153) Hansen, M. J.; Lerch, M. M.; Szymanski, W.; Feringa, B. L. *Angew. Chem. Int. Ed.* **2016**, *55* (43), 13514.
(154) Konrad, D. B.; Frank, J. A.; Trauner, D. *Chem. Eur. J.* **2016**, *22* (13), 4364.
(155) Patel, K. D.; Prajapati, S. M.; Panchal, S. N.; Patel, H. D. *Synth. Commun.* **2014**, *44* (13), 1859.
(156) Yang, S.-J.; Lee, S.-H.; Kwak, H.-J.; Gong, Y.-D. *J. Org. Chem.* **2012**, *78* (2), 438.

(157) Boström, J.; Hogner, A.; Llinàs, A.; Wellner, E.; Plowright, A. T. *J. Med. Chem.* **2012**, *55* (5), 1817.
(158) Schmidt, R.; Geissler, D.; Hagen, V.; Bendig, J. *J. Phys. Chem. A* **2007**, *111* (26), 5768.
(159) Schmidt, R.; Geissler, D.; Hagen, V.; Bendig, J. *J. Phys. Chem. A* **2005**; 109 (23), 5000.
(160) Guruge, C.; Ouedraogo, Y. P.; Comitz, R. L.; Ma, J.; Losonczy, A.; Nesnas, N. *ACS Chem. Neurosci.* **2018**, *9* (11), 2713.
(161) Diau, W. E. *J. Phys. Chem. A* **2004**, *108* (6), 950.
(162) Crecca C.R.; Roitberg, A. E. *J. Phys. Chem. A* **2006**; 110 (26), 8188.
(163) Donthamsetti, P. C.; Winter, N.; Schönberger, M.; Levitz, J.; Stanley, C.; Javitch, J. A.; Isacoff, E. Y.; Trauner, D. *J. Am. Chem. Soc.* **2017**, *139* (51), 18522.
(164) Gómez-Santacana, X.; Pittolo, S.; Rovira, X.; Lopez, M.; Zussy, C.; Dalton, J. A. R.; Faucherre, A.; Jopling, C.; Pin, J.-P.; Ciruela, F.; Goudet, C.; Giraldo, J.; Gorostiza, P.; Llebaria, A. *ACS Cent. Sci.* **2017**, *3* (1), 81.
(165) Barber, D. M.; Liu, S.-A.; Gottschling, K.; Sumser, M.; Hollmann, M.; Trauner, D. *Chem. Sci.* **2017**, *8* (1), 611.
(166) Köhler, C.; Schwarcz, R. *Neuroscience* **1983**, *8* (4), 819.
(167) Tsai, C.; Schneider, J. A.; Lehmann, J. *Neurosci. Lett.* **1988**, *92* (3), 298.
(168) Holland, P. T.; Selwood, A. I.; Mountfort, D. O.; Wilkins, A. L.; McNabb, P.; Rhodes, L. L.; Doucette, G. J.; Mikulski, C. M.; King, K. L. *Chem. Res. Toxicol.* **2005**, *18* (5), 814.
(169) Sawant, P. M.; Weare, B. A.; Holland, P. T.; Selwood, A. I.; King, K. L.; Mikulski, C. M.; Doucette, G. J.; Mountfort, D. O.; Kerr, D. S. *Toxicon* **2007**, *50* (5), 627.